3.3 COMPARISON OF EXPERTS' MODELS AND ASSESSMENTS

3.3.1 Spatial and Temporal Models

Table 3.3-1 lists the various spatial modeling approaches used by each of the eight experts and, where relevant, the geology data sets used by each. Each of the three experts not using geology data quantitatively in their models did use the information qualitatively in defining their zones.

Table 3.3-1. Spatial Modeling Approaches and Geology Data Used by Each Expert

	Expert							
Spatial Modeling Approach	**CC**	**BC**	**WH**	**MK**	**AM**	**MS**	**FS**	**GT**
Locally homogenous zones		x		x	x			x
Parametric spatial density function: Bivariate Gaussian field shape						x		
Non-parametric spatial density function: Kernel density estimation	x		x	x	x		x	
Modification of basic models with interpretation of geology data	x		x	x		x	x	
Lithostatic pressure			x	x		x	x	
Mean crustal density	x							
Tomography			x	x			x	
Cumulative extension			x					

Table 3.3-2 lists the various temporal modeling approaches used by each of the eight experts.

Table 3.3-2. Temporal Modeling Approaches Used by Each Expert

	Expert							
Temporal Modeling Approach	**CC**	**BC**	**WH**	**MK**	**AM**	**MS**	**FS**	**GT**
Homogenous Poisson with rate estimated from identified past events	x		x	x	x	x		x
Homogenous Poisson with expert-specified distribution on rate		x						
Time-volume rate model			x	x	x		x	x
Temporal clustering model						x		
Explicit modeling of alternative conceptual models for rate (e.g., a steady-state rate model , an increased rate model, and a decreased rate model)	x	x						

Section 3.2 includes a table for each expert describing how they interpret past events in the YMR, including the various alternative interpretations considered. Most of the spatial and temporal models specified by the experts use the identified past events directly: both parametric and non-parametric spatial density estimates are created based on the locations (and expert-assigned weighting) of past events, and in most cases, the experts specified that the rate for either the homogenous Poisson or the time-volume rate models be estimated based on past events they identified. Table 3.3-3 lists the events in the YMR with a summary of how they were interpreted by each expert.

Table 3.3-3. Experts' Interpretation of Past Events and Magnetic Anomalies

	Expert Interpretation (number of events)							
Past Event or Anomaly	**CC**	**BC**	**WH**	**MK**	**AM**	**MS**	**FS**	**GT**
Lathrop Wells	1	1	1	1	1	1	1	1
Sleeping Buttes	1	1	2	1 to 2	2	NA	2	2*
Quaternary Crater Flat	1	1 to 2	4 to 5	1 to 4	5	2 to 5	1 to 5	1 to 4
Buckboard Mesa	1	1	1	1	1		1	
Pliocene Centers	3	1	7	1 or 3+	5 to 7	7	3	1 to 4
Pliocene basalt of Crater Flat	1		3	1	3	3	1	1
Anomaly B	1		1	1	1	1	1	1
Anomaly F	1		1	1	1 to 3	1 to 3	1	1 to 3
Anomaly G			1					
Anomaly H			1					
Thirsty Mesa	1	1	1	1	1	NA	1	1
Anomalies C&D	2	1	2	1 to 2	0 to 2	0 to 2	0 to 1	
Jackass Flats			1 to 2	1				
Dome Mountain			1 to 3	1				
Western Crater Flat (RQ4T)			2 to 5	1 to 4				
Solitario Canyon			1 to 2	1 to 2				
Anomaly A				1				
Little Skull Mountain			3 or 6					
Anomaly E	1		1		0 to 1			
Anomaly K			0 to 1		0 to 1			
Anomalies 3 and J			0 to 1					
Anomaly 2			0 to 1					
Anomaly 1			0 to 1					
V1, V2, V3			3					

* For GT's models, the Sleeping Buttes events lie in the background zone.
+ All Pliocene centers listed below may be considered a single event. If they are not a single event, they are interpreted as shown in the rows below.

Mean Rate Density

The best summary measure of the impacts of the various spatial and temporal models used by the different experts, and their varying interpretation of past events, is the mean rate density map for each. Figure 3.3-1 shows the mean rate density maps for all eight experts to facilitate comparisons (note that larger versions of these maps are included in the individual model discussions in Section 3.2). In each map, the color-shaded area represents the model domain. For several experts (Crowe, Hackett, Kuntz, and Spera), this domain is defined by the expert-specified region of interest. For experts whose model includes a background rate (McBirney, Sheridan, and Thompson), the rate everywhere outside the shaded area is equal to the background rate. For those experts and for Connor, the domain was selected for modeling convenience to be no larger than the geographic extent of the data used in the spatial models, and to encompass the region where the conditional probability of intersection of an event is non-zero.

Several important similarities across the mean rate density maps are apparent: for all experts, the highest mean rate density occurs in the vicinity of the Crater Flat events, and experts who

included some explicit weighting of events by age (Hackett, Kuntz, McBirney, and Spera) exhibit somewhat higher rate density contours encompassing the Lathrop Wells event and, for Hackett, the Quaternary Crater Flat cones.

The use of the "geology-informed" models appears to lead to a smoother rate density map in general, and allows for areas of higher rate density where events have not occurred in the past. As an example, see the 1e-10 contour on the mean rate density map for Sheridan, which is driven by the consideration of lithostatic pressure and Sheridan's estimate of the relevance of those data to the locations of future events. The effect is not seen in parametric or non-parametric spatial density estimates alone, where higher rate density always appears where past events have occurred.

Recurrence Rate

It is typical in volcanic hazard analysis to discuss a mean recurrence rate or recurrence interval for events. In the context of PVHA-U it is to difficult compare recurrence rates across experts. For example, each expert has a uniquely-defined region of interest, and those regions have different areas. So even if two experts had otherwise identical models, with different regions of interest their mean recurrence rates (expressed as the number of events per year in their region of interest) would be different. Further, the rate within a region of interest is spatially varying, as shown in the mean rate density plots of Figure 3.3-1, so even if the regions of interest of all experts were of similar areas, an "average" recurrence rate across the region of interest is not meaningful in term of the events that are of the most interest (intersecting events).

The mean recurrence rate for each expert's model, within their defined region of interest, was presented in the subsections of Section 3.2. To allow for some comparison of the recurrence rate across experts, the mean recurrence rate for each expert was calculated for a region that all experts included in their model, termed the "intersecting ROI." Figure 3.3-2 illustrates this intersecting region of interest, and Table 3.3-4 presents the mean recurrence rate in this ROI for each expert. The table also includes the mean recurrence interval associated with the mean recurrence rate for each expert. Uncertainty exists in the recurrence interval associated with a specific recurrence rate: give a Poisson model, the time between events (the recurrence interval) is defined by an exponential distribution with mean equal to the recurrence rate, and the mean of this distribution (the inverse of the rate) is typically referred to as the "mean recurrence interval." Table 3.3-4 also shows the uncertainty in this recurrence interval, representing the range of time-between-events that might be seen given the mean recurrence rate.

The best comparison of hazard models across experts is the actual frequency of intersection, and those results are presented in Section 4.

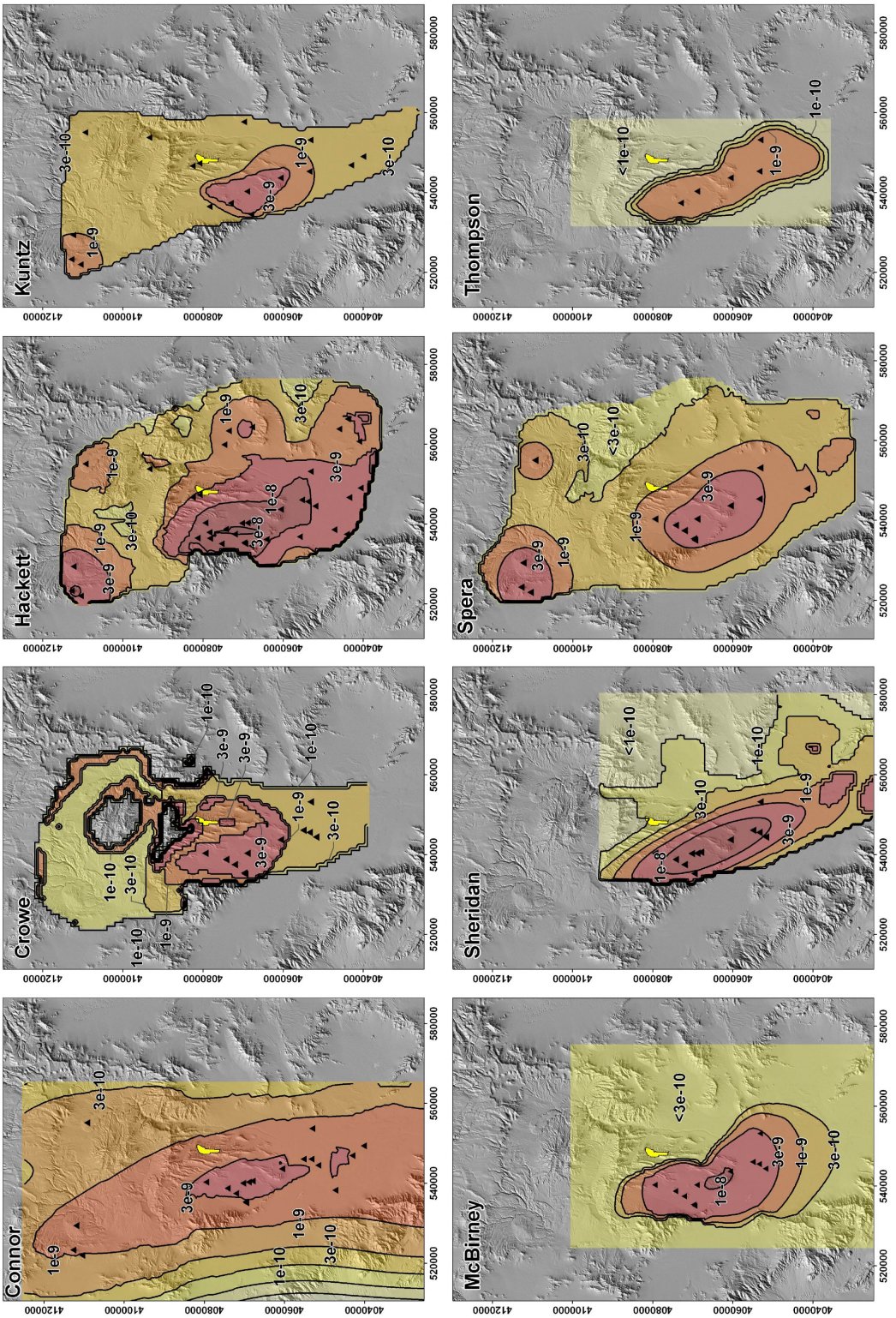

NOTE: Mean rate density is in units of events per year per km^2. Yellow polygon represents the repository footprint; black triangles represent past events judged relevant by each expert (their most likely event set is depicted). Color-shaded area indicates the model domain. Map grid ticks are UTM meters; tick intervals are 20 km.

Figure 3.3-1. Mean Rate Density Maps for the 10,000-Year Assessment for Each Expert

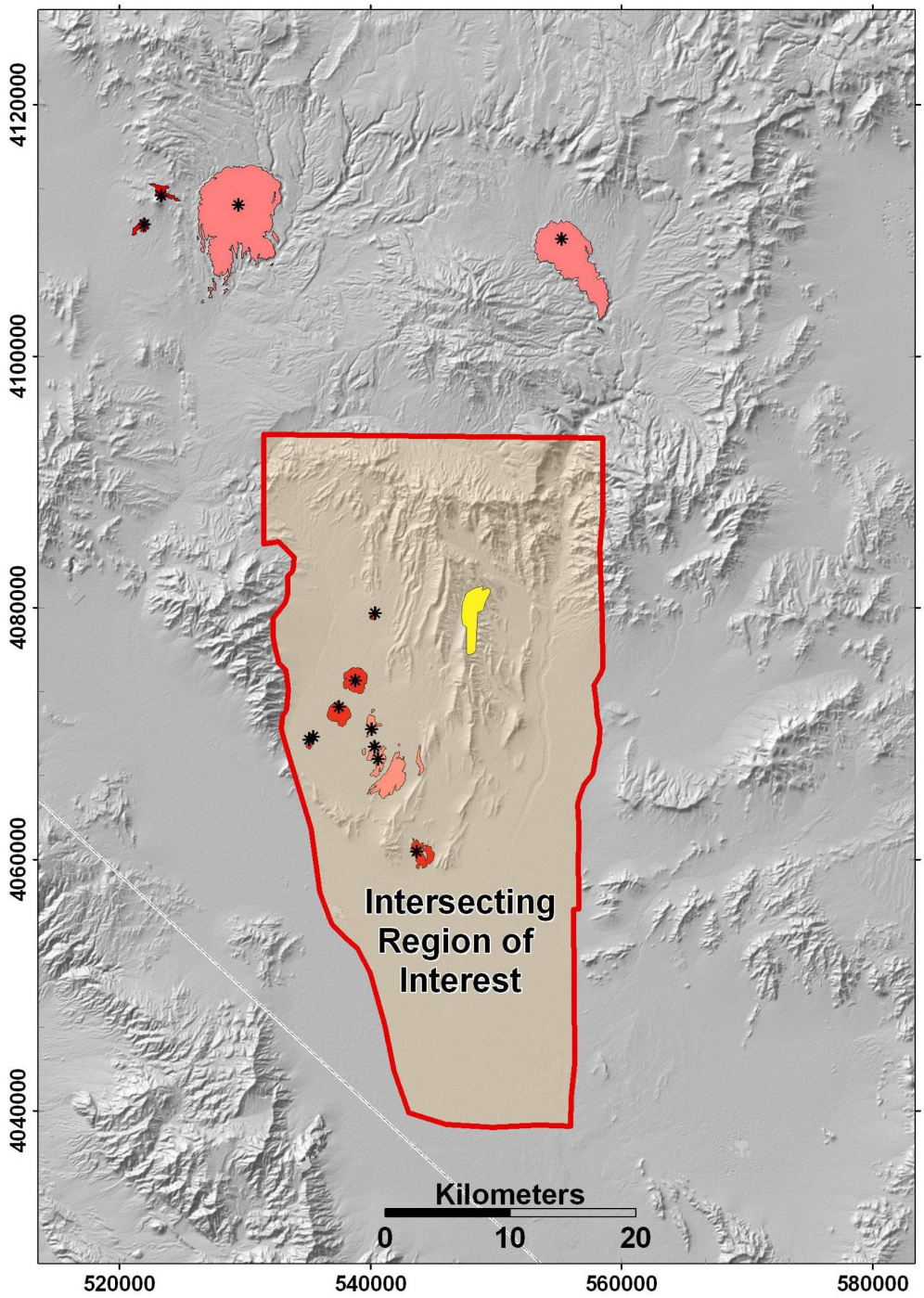

Note: Pink outcrop patterns represent Pliocene volcanic centers; red outcrop patterns represent Quaternary volcanic centers. Asterisks represent volcanic vents. Map grid ticks are UTM meters; tick intervals are 20 km.

Figure 3.3-2. Intersection of the Regions of Interests and Model Domains for All Experts

Table 3.3-4. Mean Recurrence Rates and Associated Recurrence Intervals for All Experts for the Intersecting Region of Interest

Expert	Mean Recurrence Rate in the Intersecting ROI (events/year)	Mean Recurrence Interval Associated with the Mean Recurrence Rate (thousands of years)	5th to 95th Percentiles of the Recurrence Interval Given the Mean Recurrence Rate (thousands of years)
CC	2.64e-6	378	19 to 1,130
BC	2.85e-6	351	18 to 1,050
WH	9.46e-6	106	5.4 to 317
MK	1.38e-6	735	37 to 2,170
AM	3.48e-6	287	15 to 861
MS	5.54e-6	181	9.3 to 541
FS	2.45e-6	408	21 to 1,223
GT	1.04e-6	961	49 to 2,880

3.3.2 Event descriptions

As described in detail in the subsections of Section 3.2, each expert has a unique definition of an igneous event, just as they have unique spatial and temporal models. No "standard" approaches for defining or modeling the characteristics of individual igneous events exist, so there may appear to be greater variety of event descriptions than there are spatial and temporal models.

While the variance among experts in event descriptions is significant, each expert includes some common features that can be compared. All experts defined events as including the potential for at least dikes, column-producing conduits, and non-column-producing vents. Six of the eight experts also included the potential for sills in their event descriptions, with much lower probability than the other features.

Figure 3.3-3 illustrates the distribution of the number of dikes in an event for each expert's event definition. Some experts specified a distribution on the number of dikes directly, and others defined it as a function of other parameters. The distributions shown in the figure are from the event simulation results with 100,000 iterations, for each expert. As described previously, both CC and BC specified alternative event definitions. Figure 3.3-3 shows the number of dikes associated with the event definition they assigned the highest probability for the 10,000-year assessment. The differences in the distribution of the number of dikes between these models and their alternative models are small. The most likely number of dikes in an event is one or two. Two experts (CC and GT) allow for the possibility of more than 9 dikes in an event.

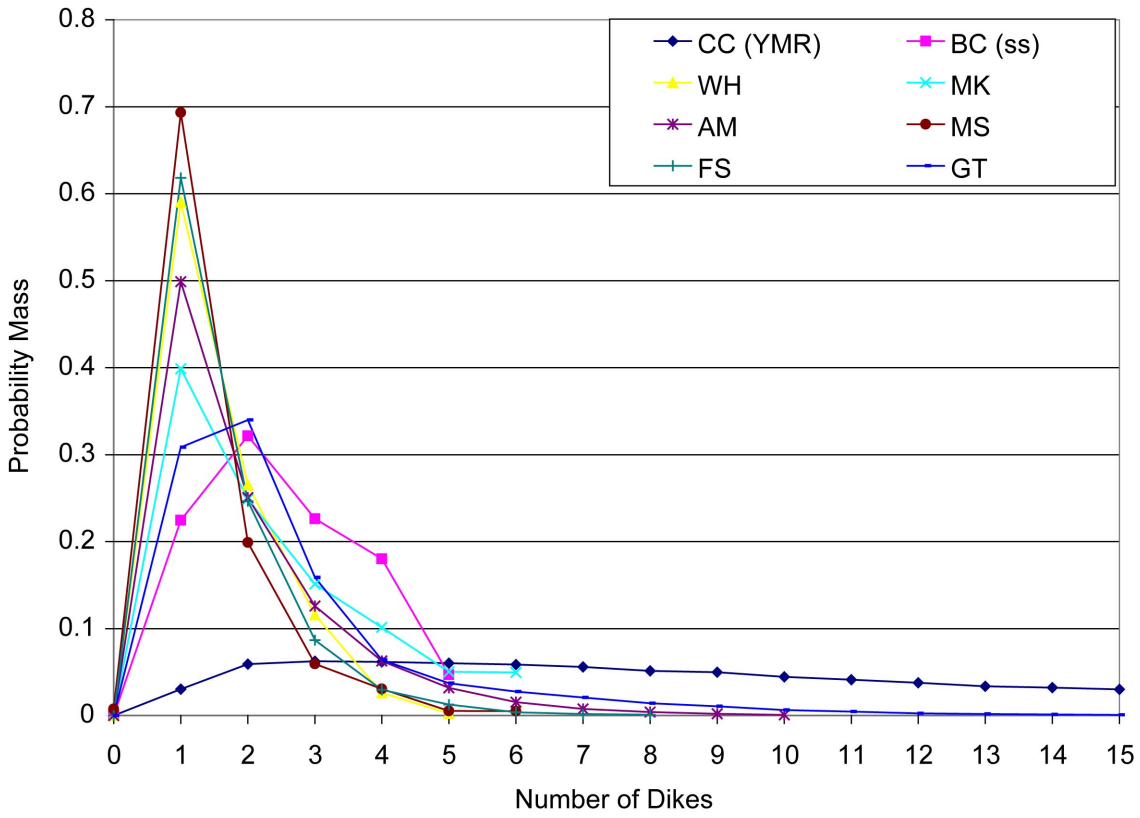

NOTES: Results from 100,000 iterations of the event simulator for each expert's event descriptions. Simulations with CC's event description generate up to 50 dikes (not shown), with very low probability. Simulations with GT's event description generate up to 23 dikes (not shown), with very low probability.

Lines connecting the points for each expert are provided only for ease of viewing; they should not be interpreted to imply that other-than-integer values are possible.

Figure 3.3-3. Distribution of the Number of Dikes in an Event Across Expert Models

The areal extent or "size" of an event is a function primarily of the number, length, and relative location of dikes. Defining the size of an event requires some interpretation of the various event descriptions. Five experts (GT, WH, MK, AM, and MS) specified that in events with more than one dike, those dikes would be arranged in en echelon geometry, with some uncertainty in the amount of overlap or underlap at the dike ends. For these experts, we assume an average overlap of zero at the ends of the dikes and use the total length of dikes in the event as the event length. Similarly, event width can be calculated based on the number of dikes in an event and the expert assessment of the perpendicular spacing between dikes.

Two experts (FS and BC) specified that dikes would be located randomly within some event area that they defined. For these experts, we define the length of the event as either (a) the length of the dike, for events including only one dike, or (b) the length of the defined event area, for events including multiple dikes. Similarly, event width is either the same as dike width (for single-dike events) or the width of the defined event area (for multiple-dike events).

One expert (CC) specified that events consist of one or more "centers," which could be spaced a fairly large distance apart, resulting in potentially large effective event size with clusters of low

igneous feature density and high igneous feature density across that event length. In this case, event length is either the length of the center (for one-center events) or the distance between the midpoints of the outermost centers, plus one center length (for multiple center events). The event width is defined as distance between center boundaries in the direction perpendicular to the alignment of centers.

Figure 3.3-4 illustrates the distribution on event lengths for all experts and Figure 3.3-5 illustrates the distribution on event widths for multiple-dike events, given these definitions of event dimensions. One of the alternative event definitions used by BC (that associated with his new cycle rate model) allows for very large event sizes. Although that model is defined as applying only for his 1-My assessment, it is displayed separately on all the plots that follow for comparison. CC's alternative event definitions have very little impact on these summary results, and so only the descriptions corresponding to the YMR data set are presented.

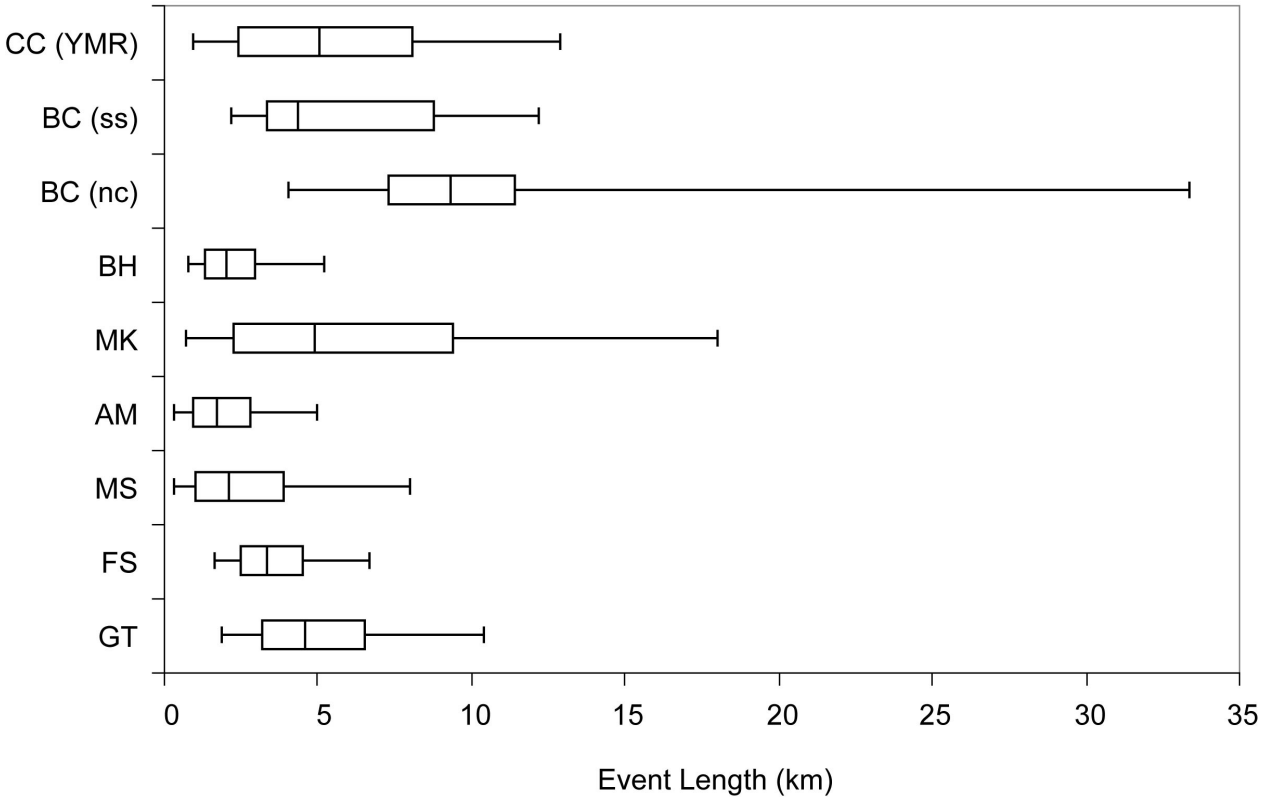

NOTES: Results from 100,000 iterations of the event simulator for each expert's event descriptions. The "box" for each expert shows the 25th to 75th percentiles of the event lengths; the vertical line within that box shows the median event length. The "error bars" show the 5th to 95th percentile range of event lengths.

CC (YMR) indicates the results for the event definition CC defined as associated with his YMR dataset; BC (ss) indicates results for the event definition BC defined as associated with his steady-state and increasing rate models; BC (nc) indicates results for the event definition BC defined as associated with his new cycle rate model.

Figure 3.3-4. Range of Event Lengths Based on Simulated Events Using the Event Descriptions of Each Expert

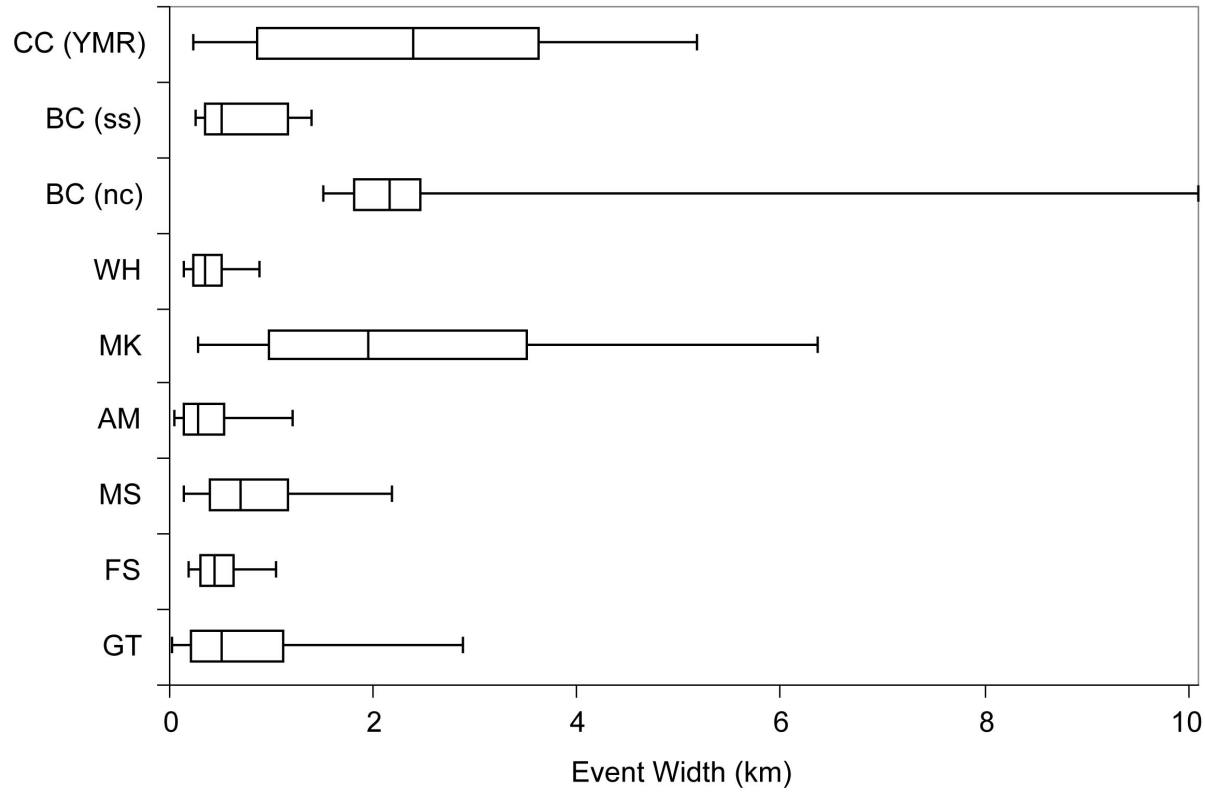

NOTES: Results from 100,000 iterations of the event simulator for each expert's event descriptions. The "box" for each expert shows the 25th to 75th percentiles of the event widths; the vertical line within that box shows the median event width. The "error bars" show the 5th to 95th percentile range of event widths.

CC (YMR) indicates the results for the event definition CC defined as associated with his YMR dataset; BC (ss) indicates results for the event definition BC defined as associated with his steady-state and increasing rate models; BC (nc) indicates results for the event definition BC defined as associated with his new cycle rate model.

Figure 3.3-5 Range of Event Widths Based on Simulated Events Using the Event Descriptions of Each Expert

All experts identified the most likely type of eruption in a future event would include a violent Strombolian phase; that is, to produce an eruption column that would carry an ash plume to an altitude of several kilometers. In the terminology used in this report, those eruptions are associated with "column-producing conduits." All experts also allow for the possibility of less explosive eruptions, but generally assigned lower probability to such eruptions. In the terminology used here, such eruptions are associated with "non-column producing vents." Two experts (CC and BC) defined vents and vent-like bodies as unique features in their event descriptions; other experts first defined "conduits," and then assigned a probability that each conduit would be eruption-column producing. For those experts, "conduits" that are not column-producing are referred to simply as vents. Although the potential for a hydromagmatic eruption was discussed at two of the workshops and in all of the elicitation interviews, it is discussed directly in only three of the elicitation summaries (CC, MK, and FS). All three of these experts assess the probability of a hydromagmatic eruption to be "low," and only one (MK) provided a (conditional) assessment on the likelihood that a future eruption would be hydromagmatic.

Figure 3.3-6 illustrates the distribution of the number of column-producing conduits in an event for each expert's event definition. For seven of the experts, the most likely number of conduits in an event is one; for the other (AM) the most likely number is two. For the events described by two experts (BC and GT), every event must include at least one column-producing conduit. Each expert provided an assessment of conduit diameter, and Figure 3.3-7 illustrates these distributions.

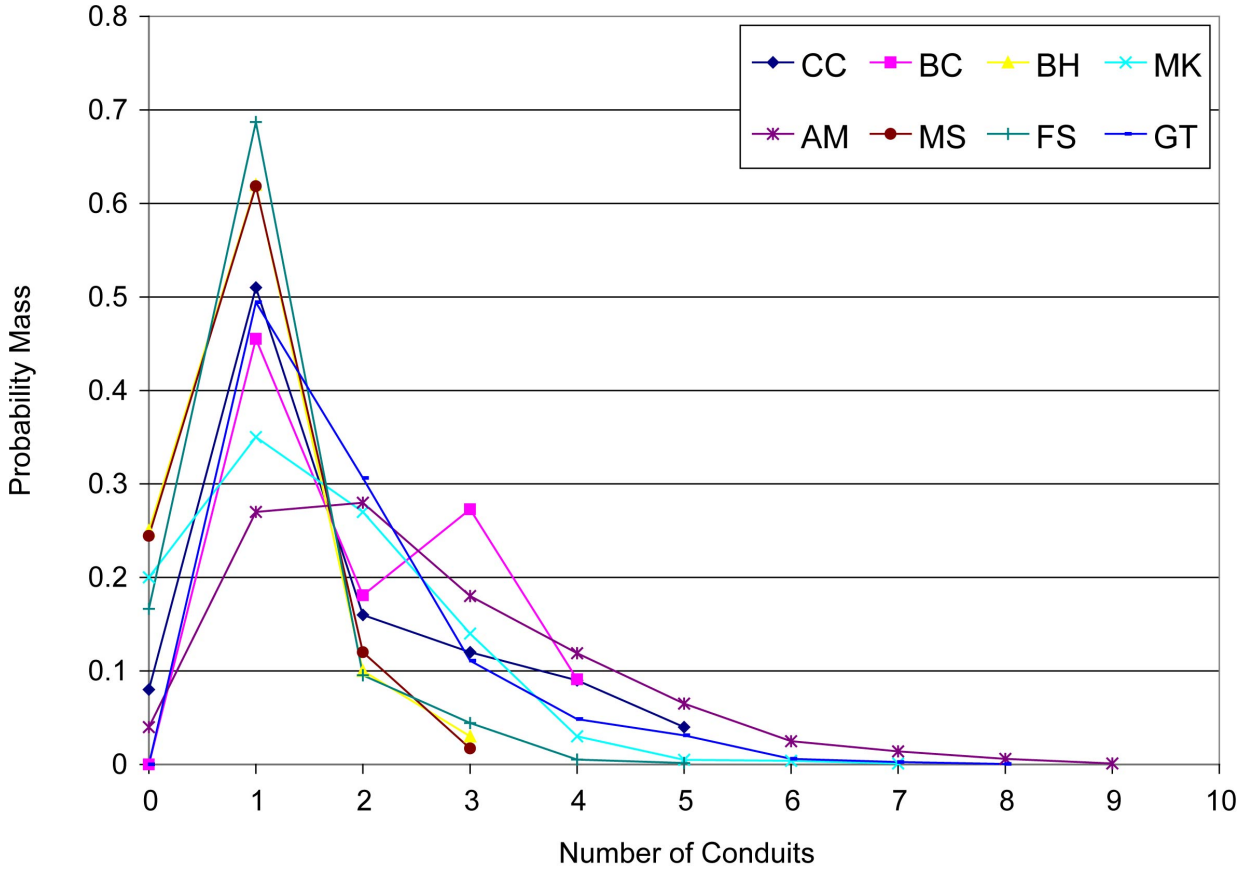

NOTE: Lines connecting the points for each expert are provided only for ease of viewing; they should not be interpreted to imply that other-than-integer values are possible.

Figure 3.3-6. Distribution of the Number of Column-Producing Conduits in an Event Based on Event Descriptions of Each Expert

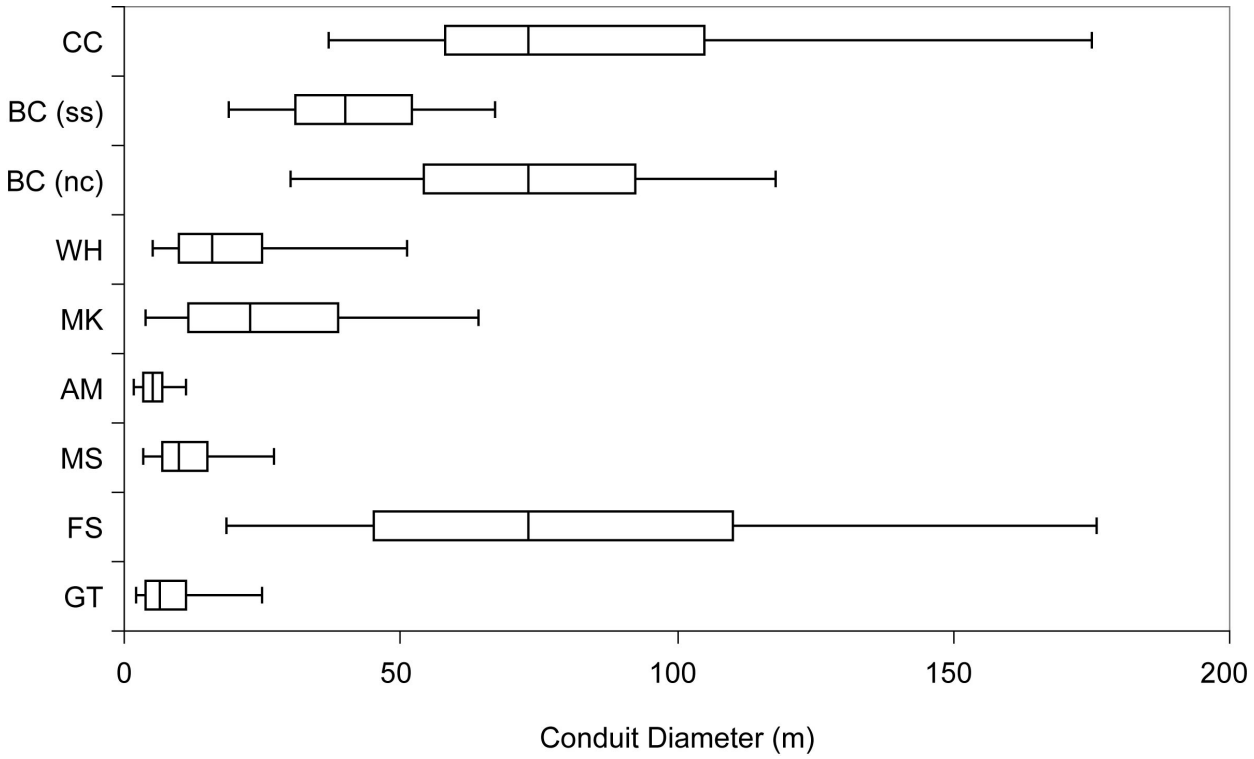

NOTES: The "box" for each expert shows the 25th to 75th percentiles of the conduit diameters; the vertical line within that box shows the median diameter. The "error bars" show the 5th to 95th percentile range of conduit diameters.

BC (ss) indicates results for events associated with BC's steady state and increasing rate models; BC (nc) indicates results for events associated with BC's new cycle rate model. CC provided a database of vent and vent-like bodies to be used directly in his model. The "diameter" represented here is estimated based on the area of the vent and an approximately circular shape.

Figure 3.3-7 Range of Conduit Diameters Based on Simulated Events Using the Event Descriptions of Each Expert

Figure 3.3-8 illustrates the distribution of the number of non-column-producing vents in an event for each expert's event definition. Two experts (CC and BC) defined vents as unique features in their event descriptions; the other experts defined "conduits," and then assigned a probability for each conduit that it would be column-producing. "Conduits" that are not column-producing are interpreted as non-column-producing vents. As shown, for those experts, the number of vents in an event is usually zero.

Finally, Figure 3.3-9 illustrates the distribution of the number of sills in an event based on each expert's event definition. In all cases, it is most likely that an event would not include a sill.

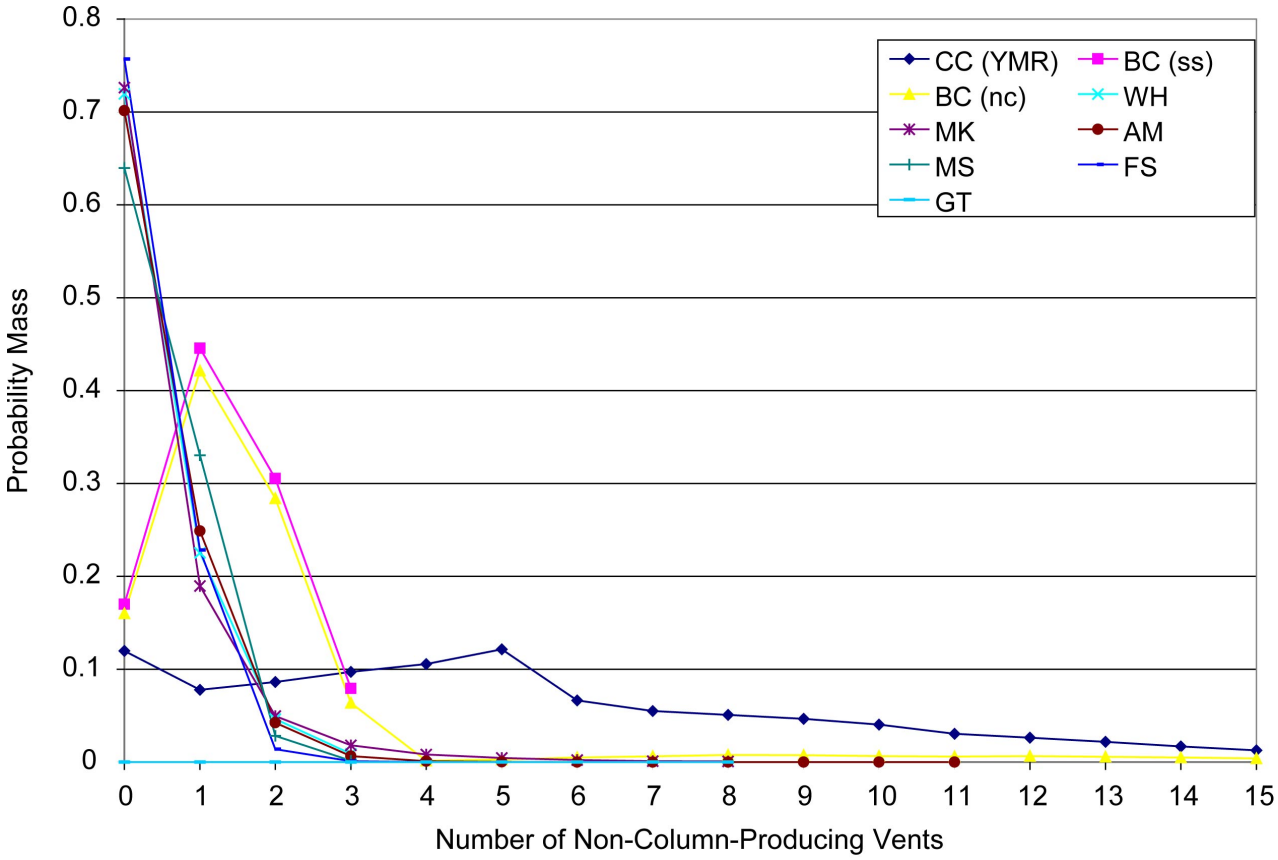

NOTE: Lines connecting the points for each expert are provided only for ease of viewing; they should not be interpreted to imply that other-than-integer values are possible. CC (YMR) indicates that the results are for simulated events associated with his YMR dataset; BC (ss) indicates results for events associated with BC's steady state and increasing rate models; BC (nc) indicates results for events associated with BC's new cycle rate model.

Figure 3.3-8. Distribution of the Number of Non-Column-Producing Vents in an Event Based on Event Descriptions of Each Expert

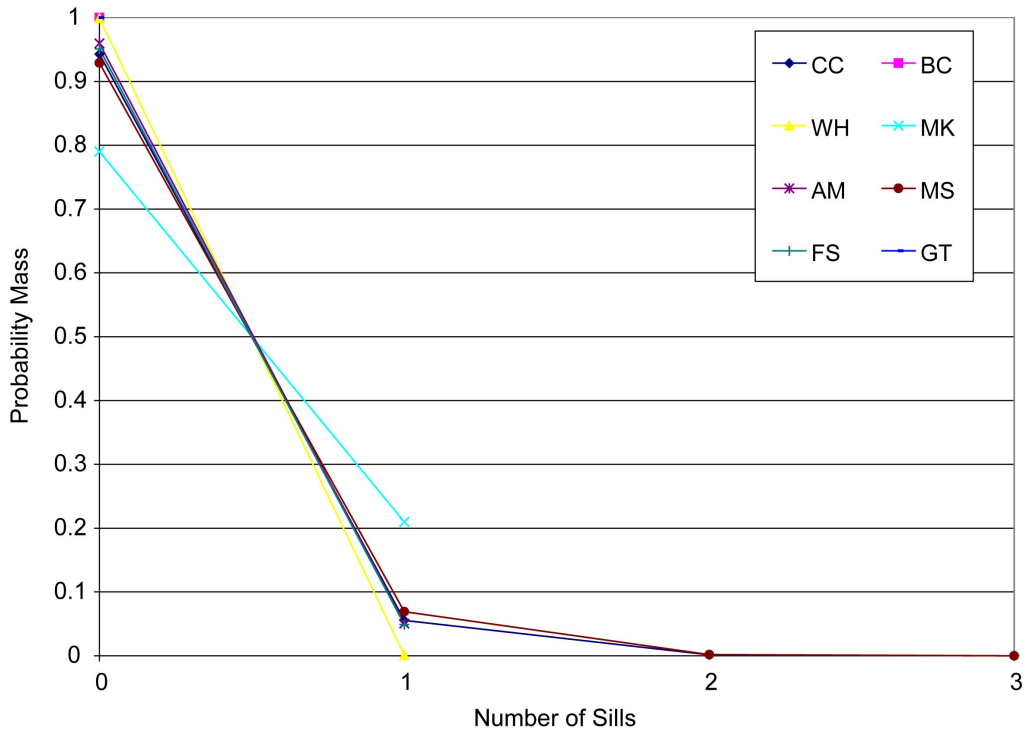

NOTE: Lines connecting the points for each expert are provided only for ease of viewing; they should not be interpreted to imply that other-than-integer values are possible.

Figure 3.3-9. Distribution of the Number of Sills in an Event Based on Event Descriptions of Each Expert

Conditional Probability of Intersection

A good summary measure of the impacts of the various event descriptions used by the different experts is the conditional probability of intersection map for each. Figure 3.3-10 shows the conditional probability of intersection of any feature with the repository footprint for all eight experts (note that larger versions of these maps are included in the individual model discussions in Section 3.2). There are two maps for CC, corresponding to his two alterative event descriptions, and three maps for BC, corresponding to his three alternative event descriptions. The most highly weighted event description for each of these is shown on the first page to facilitate direct comparison among experts; the additional event descriptions are shown on the subsequent pages.

There is a clear connection between the dimensions described above for event length and width and the relative size of the probability contours. MK's model includes the largest events (second to BC's new-cycle events), meaning that events centered relatively far from the repository footprint may intersect the footprint. This is seen in the large areal extent of his conditional probability of intersection contours. Those with smaller event dimensions have correspondingly smaller conditional probability of intersection contours.

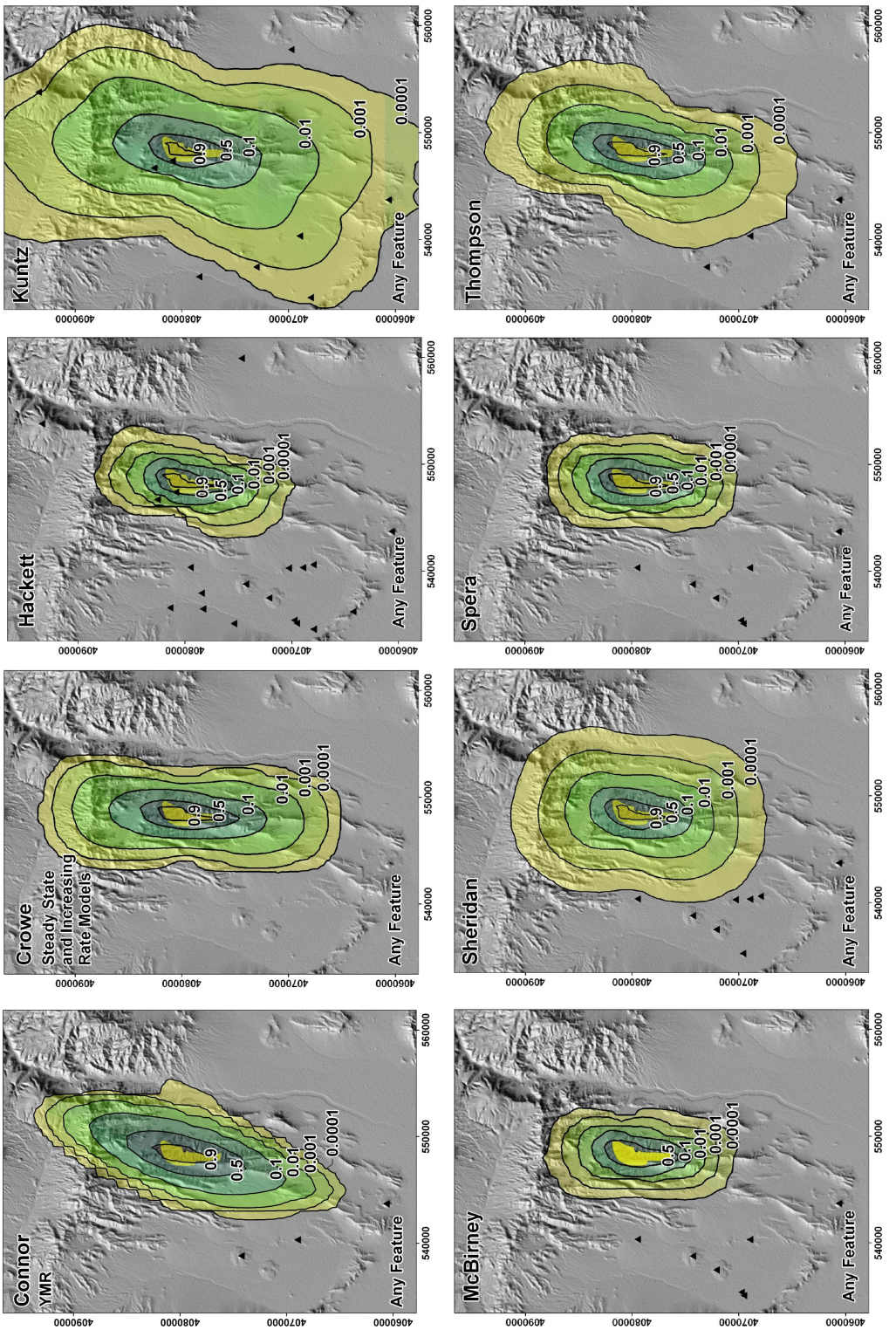

NOTE: Conditional probability of intersection is the probability of any feature interesting the repository footprint assuming an event at that location. Yellow polygon represents the repository footprint; black triangles represent past events judged relevant by each expert (their most likely event set is depicted). Map grid ticks are UTM meters; tick intervals are 10 km.

Figure 3.3-10. Conditional Probability of Intersection of Any Feature Based on the Event Descriptions of Each Expert.

NOTE: Conditional probability of intersection is the probability of any feature interesting the repository footprint assuming an event at that location. Yellow polygon represents the repository footprint; black triangles represent past events judged relevant by each expert (their most likely event set is depicted). Map grid ticks are UTM meters; tick intervals are 10 km. Note change in scale for the last map.

Figure 3.3-10. Conditional Probability of Intersection of Any Feature Based on the Event Descriptions of Each Expert (Continued)

INTENTIONALLY LEFT BLANK

4. PVHA-U RESULTS

This section of the report describes the hazard results for each individual expert's models and assessment (Section 4.1), as well as the aggregate results across all experts (Section 4.2). In addition, it compares the results of the update to the PVHA-96 results considering the limitations that result from differing event definitions between the respective elicitations (Section 4.3).

As described in Section 3.1, the quantitative result of this study is the annual probability (or annual frequency[1]) of an intersection of the repository footprint by an igneous event (also called the "hazard"). There are three main components in the hazard calculation: (a) the rate density (the frequency of events per unit time per unit area) for a specific set of models and parameters, (b) the conditional probability of intersection (the probability that an event will intersect the repository footprint, given that the event occurs) at every location in the expert's region of interest, and (c) the specification and quantification of alternative parameter sets (alternative models and input parameters) as summarized in a logic tree.

The rate density for a specific parameter set is calculated based on the specified spatial and temporal models. The conditional probability of intersection is calculated through Monte Carlo simulation based on specified event characteristics. Both of these results, the rate density and the conditional probability of intersection, are spatially varying, and are calculated on a 1-km by 1-km grid in the expert-defined region of interest. The frequency of intersection for each point in the region of interest is the product of the rate density and the conditional probability of intersection at that point. The overall frequency of intersection is then calculated by summing those values over the region of interest.

For each parameter set, or each path through the logic tree, a frequency of intersection is calculated. Those frequencies are combined with the probability of that parameter set to develop a probability distribution on the frequency of intersection for each expert's PVHA-U models and assessments.

The mean rate density, the conditional probability of intersection, and the logic tree describing the alternative parameter sets for each expert's models and assessments are described in the subsections of Section 3.2. Section 4.1 discusses the results of the hazard calculations corresponding to each expert's individual assessments.

4.1 INDIVIDUAL RESULTS

Several types of results are described below, and are shown for each expert's models and assessments in the subsections that follow.

Spatial Distribution of the Mean Frequency of Intersection

As described above, the mean rate density at each grid point is multiplied by the conditional probability of intersection at that grid point to yield a frequency of intersection at that location; this result represents the spatial distribution of the hazard, which can be displayed on a map.

[1] As described in Section 3.1, the annual probability is closely approximated by the annual frequency, and annual frequency is used in the text that follows

Figure 4.1-1 illustrates an example. Panel (a) shows a mean rate density map; panel (b) shows a conditional probability of intersection map, and panel (c) shows the resulting mean frequency of intersection. Panel (c) is calculated by multiplying the mean rate density at each point by the conditional probability of intersection for an event centered at that point, as specified in Equation 3-1, and the values at the points are mapped and contoured in the panel.

For all such maps in this section, the outermost contour represents the set of locations at which there is an annual probability of 1e-13 that an event would occur and result in a feature intersecting the repository footprint.[2] Outside that contour the probability is less, and inside the contour the probability is greater. Contours represent each order of magnitude change in value. On each map, only the outer and inner contours are labeled. While the outer contour is always at 1e-13, the probability associated with the inner contour varies across experts, based on their specific models.

[2] 1e-13 was chosen as the outer contour for consistency of display across experts. 1e-13 is the lowest probability contour that is produced consistently across all expert models.

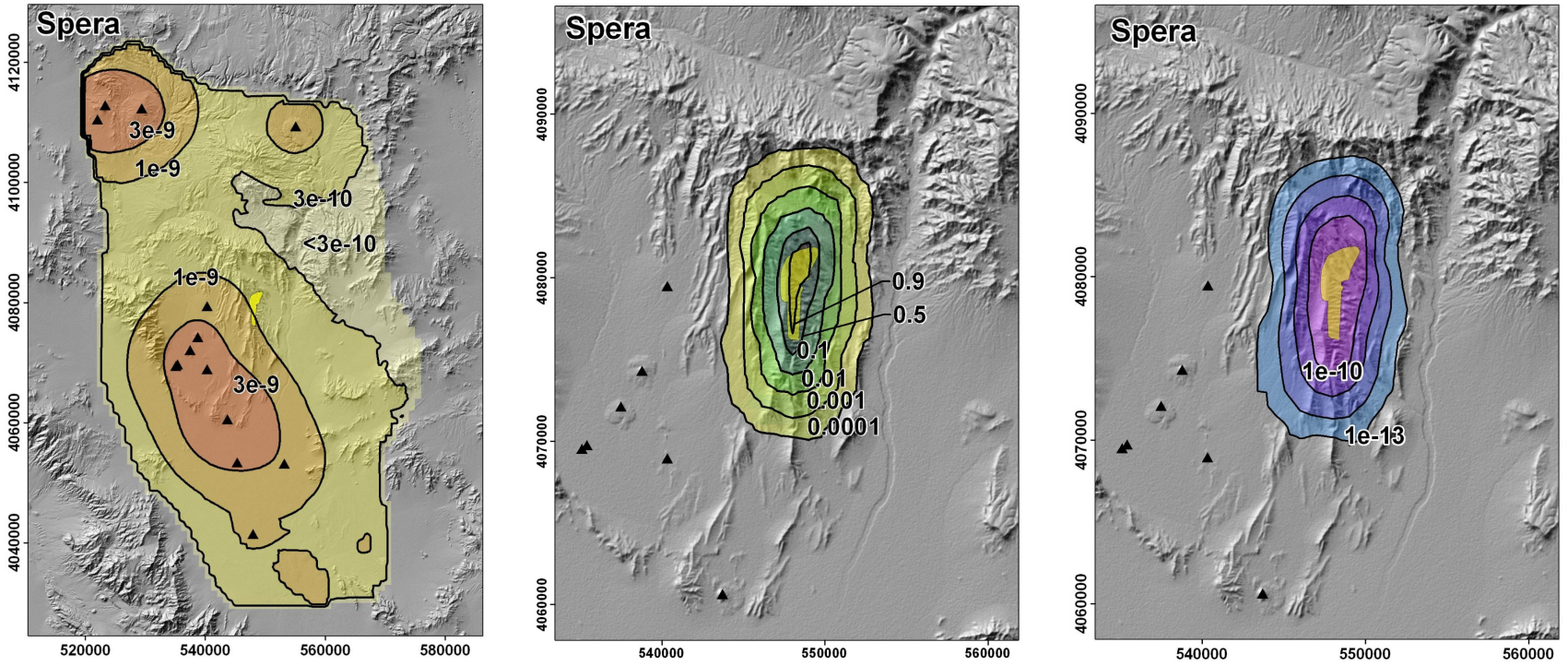

(a) Mean rate density. Contours represent the mean annual frequency of igneous events (events per year) per km^2.

(b) Conditional probability of intersection of any feature. Contours represent the probability that an event assumed to occur at each location would result in the intersection of any igneous feature with the repository footprint.

(c) Spatial distribution of the mean frequency of intersection. Contours represent the mean annual probability of an intersection of the repository footprint by an igneous feature.

NOTES: The repository footprint is shown as a yellow polygon. Map grid ticks are UTM meters; tick intervals for map (a) are 20 km; map (b) and (c) are 10 km. This example is shown for the models of Frank Spera, which are discussed in Section 4.1.7.

Figure 4.1-1. Example of the Components of the Hazard Calculation

Frequency of Intersection, Including Uncertainty

In addition to developing an estimate of the mean annual frequency of intersection, a goal of the PVHA-U effort was to capture and quantify the uncertainty in that estimate. As described above, each path through the logic tree specified by an expert (as described in the subsections of Section 3.2) has an associated probability and leads to a unique estimate of the frequency of intersection. Together, these values define a probability distribution on the annual frequency of intersection for that expert's models and assessments. An example of how these results are presented is shown in Figure 4.1-2. The top figure is a cumulative distribution function (CDF), and the bottom figure is a probability mass function (pmf). The values of the mean of the distribution (the probability-weighted average), the median (the 50th percentile), and the 5th and 95th percentiles are printed in the legend. In the figures, the mean value is shown with the dashed vertical line on both figures, the median is shown with an open square on the pmf, and the 5th to 95th percentile range is shown by the horizontal line and "error bars" associated with the median. For each expert, the frequency of intersection of any feature (dike, column-producing conduit, non-column producing vent, or sill) with the repository footprint is shown in the subsections below, and any differences that might be seen for the frequency of intersection of a specific type of feature are discussed in the text.

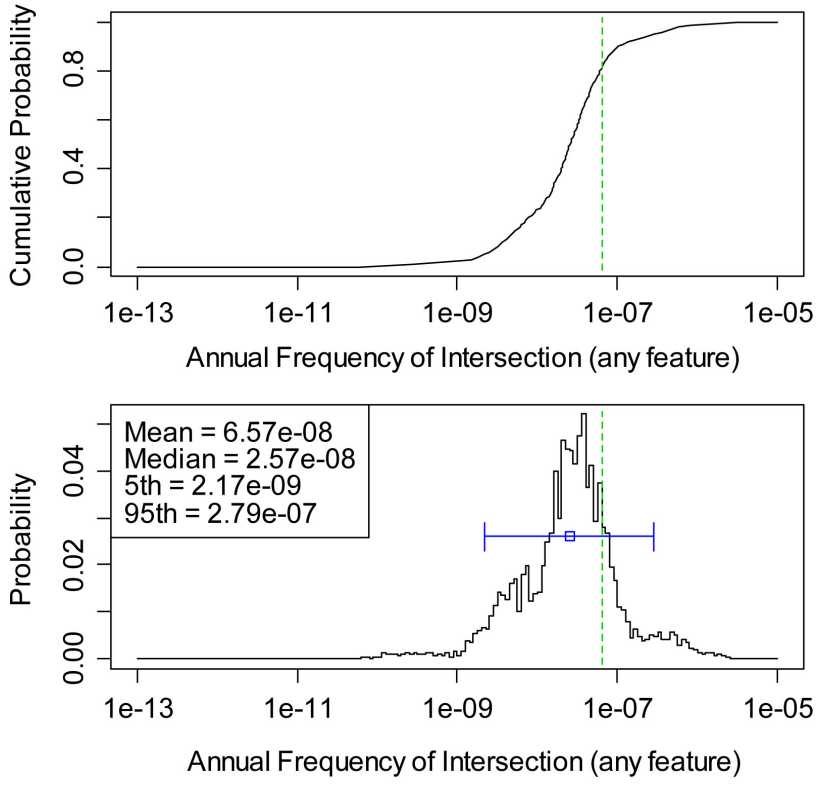

NOTE: Top figure is a cumulative distribution function, bottom figure is a probability mass function. The mean is shown by the dashed vertical line, the median with the open box, and the 5th to 95th percentiles with the horizontal line.

Figure 4.1-2. Example Presentation of Hazard Results: Distribution of the Frequency of Intersection

Contributions to Uncertainty

Two types of uncertainty are considered below: uncertainty in the *mean* hazard and *overall* uncertainty in the hazard estimate (e.g., the variance in the hazard estimate or the spread of the distribution).

A sensitivity analysis was conducted to explore both of these issues; each node in the logic tree for an expert's model was set or "controlled" to one of its branch values, and the hazard was recalculated with all other logic tree nodes implemented as specified. This protocol has the effect of "removing" that single uncertainty from the model, and allows one to see what effect that component has on the overall distribution. In the sensitivity analysis, the controlled node is set sequentially to each of its (n) branch values, and the frequency of intersection is calculated n times. The analysis is done for each node in the logic tree, and the results are shown in a sensitivity chart such as the example shown in Figure 4.1-3. On these sensitivity charts, the y-axis crosses the x-axis at the mean frequency of intersection for any feature for that expert's full model. The end of each bar represents the mean frequency of intersection calculated while holding the specified node of the logic tree constant at one value (one of the branches on that node) and letting all others vary as in the full analysis. The length of the bar represents the maximum change in the mean frequency that could be obtained by setting that node to any of its possible branches: that is, any of the alternative models or parameter values specified for that uncertainty. The longer the bar, the greater is the contribution of that uncertainty to the uncertainty in the mean hazard. For the example in Figure 4.1-3, uncertainty in the "Rate" parameter is the largest contributor to uncertainty in the mean hazard. Other parameters have lesser impacts, as shown by the decreasing change as one moves down the bars on the y-axis.

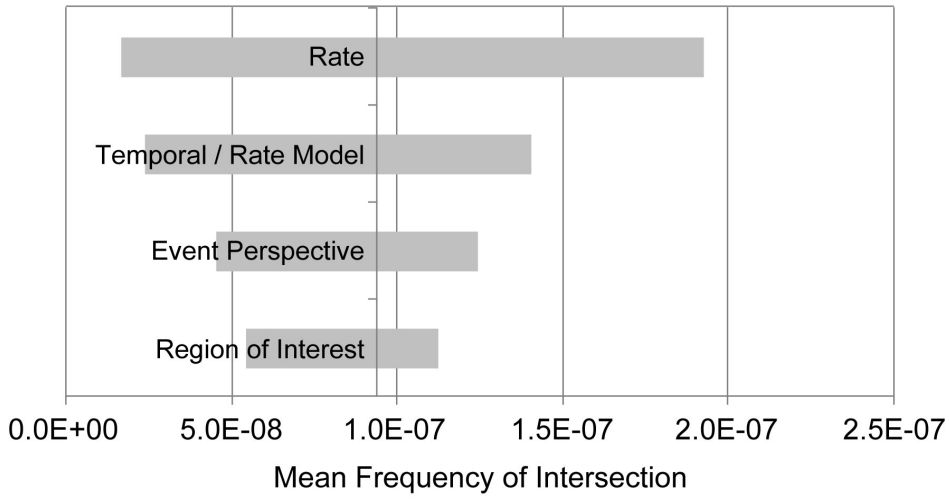

NOTE: Labels on each bar correspond to the nodes in the logic tree for that expert's model as described in Section 3.2. The length of each bar shows the range of the mean hazard values that result from fixing the value of the specified model component at one of its branch values. This range represents the degree to which the mean hazard is affected by uncertainty in the specified model component.

Figure 4.1-3. Example of Sensitivity Chart Illustrating the Contribution to Uncertainty in the Mean Hazard from Uncertainties in Individual Model Components and Assessments

In addition, sensitivity analysis allows one to consider the contribution of each individual uncertainty to the overall uncertainty in the hazard. This contribution is quantified by considering changes in the coefficient of variation (CoV)[3] for the distribution of intersection frequency as each node in the logic tree is held constant at one of its branch values. Figure 4.1-4 illustrates an example of the sensitivity chart used to summarize these results. The values shown in the figure are normalized relative to the CoV for the full distribution: the greater the difference in the relative CoV when a node is held constant, the more that uncertainty contributes to the overall uncertainty in the hazard. The model components are sorted so that the model components with the largest *average* contribution to uncertainty appear on the right. The average contribution to uncertainty is calculated as the mean value when each branch value for that model component is weighted by its probability (shown with the diamonds in the figure). The relative CoV that results when the model component is set to each branch is calculated, and the maximum and minimum change are plotted as the "error bars" associated with each model component. It is possible, then, for a model component to have a low average contribution to uncertainty, but for specific branches to result in large changes in the relative CoV; in such a case the model component would appear on the left, reflecting its small contribution on average, but the error bars would indicate large changes, reflecting the fact that the specific branch value matters. In the example figure, the differences in the impact on uncertainty for each model component are similar regardless of which branch is selected to represent the model component.

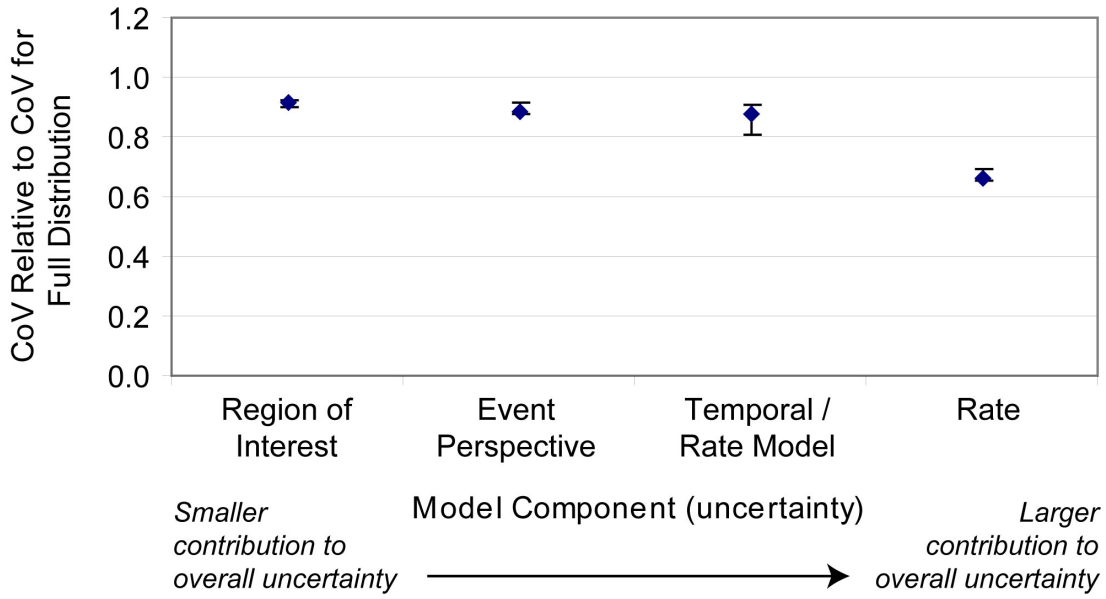

NOTE: Graph shows the CoV for the hazard distribution calculated with the specified model component fixed at each of its branch values, divided by the CoV for the full hazard distribution. Diamond shows the mean value with the relative CoV for each branch value weighted by its probability; "error bars" show the highest and lowest relative CoVs calculated across the branches for that model component.

Figure 4.1-4. Example of Sensitivity Chart Illustrating the Contribution to Overall Uncertainty in the Hazard from Uncertainties in Individual Model Components and Assessments

[3] The coefficient of variation for a distribution is defined as the ratio of the standard deviation to the mean, and is a measure of the spread of a distribution that is less sensitive to changes in the mean than the standard deviation alone.

The solid diamonds on this graph represent the probability-weighted average of the relative CoV for each model component/uncertainty, and the error bars represent the endpoints for the specific "branches" on that node.

Potential for Multiple Intersections

The PVHA-U experts all described events that could include multiple features, so it is possible that a single event might result in more than one intersecting feature. Figure 4.1-5 shows an example of how the potential for multiple intersections for each expert's models are presented. This figure shows a set of plots, each illustrating the distribution of the number of intersections of a specific feature (dikes, conduits, or vents) for an event centered at a specific point, conditional on at least one such intersection occurring. The example figure shows the approximate outline of the repository footprint in the center for reference, and plots representing locations within (or partially within) the repository are shown in green. At each point, the small plot shows the distribution of the number of intersections given least one intersection. Plots with no bars (e.g., in the upper left corner at 545 E, 4087 N) indicate that the probability of an intersection for an event at that location is zero. All other plots show the number of intersections *conditional* on at least one intersection occurring. The plot at 545 E, 4079 N, for example, indicates that there is at most one intersection for an event at that location. The plot at 548 E, 4078 N indicates that there can be multiple dike intersections given an event at that location (which is within the repository footprint). These plots are presented below for each expert for dikes, conduits, and vents.

Given that an intersection occurs, it is more likely to be from an event that is close to the footprint than from an event that is far from the footprint. Generally, events close to the footprint are also more likely to lead to multiple intersecting features. The example in Figure 4.1-6 shows how these results can be summarized: it shows the result of multiplying the distribution of number of intersecting features at each point by the relative frequency of events at those points.

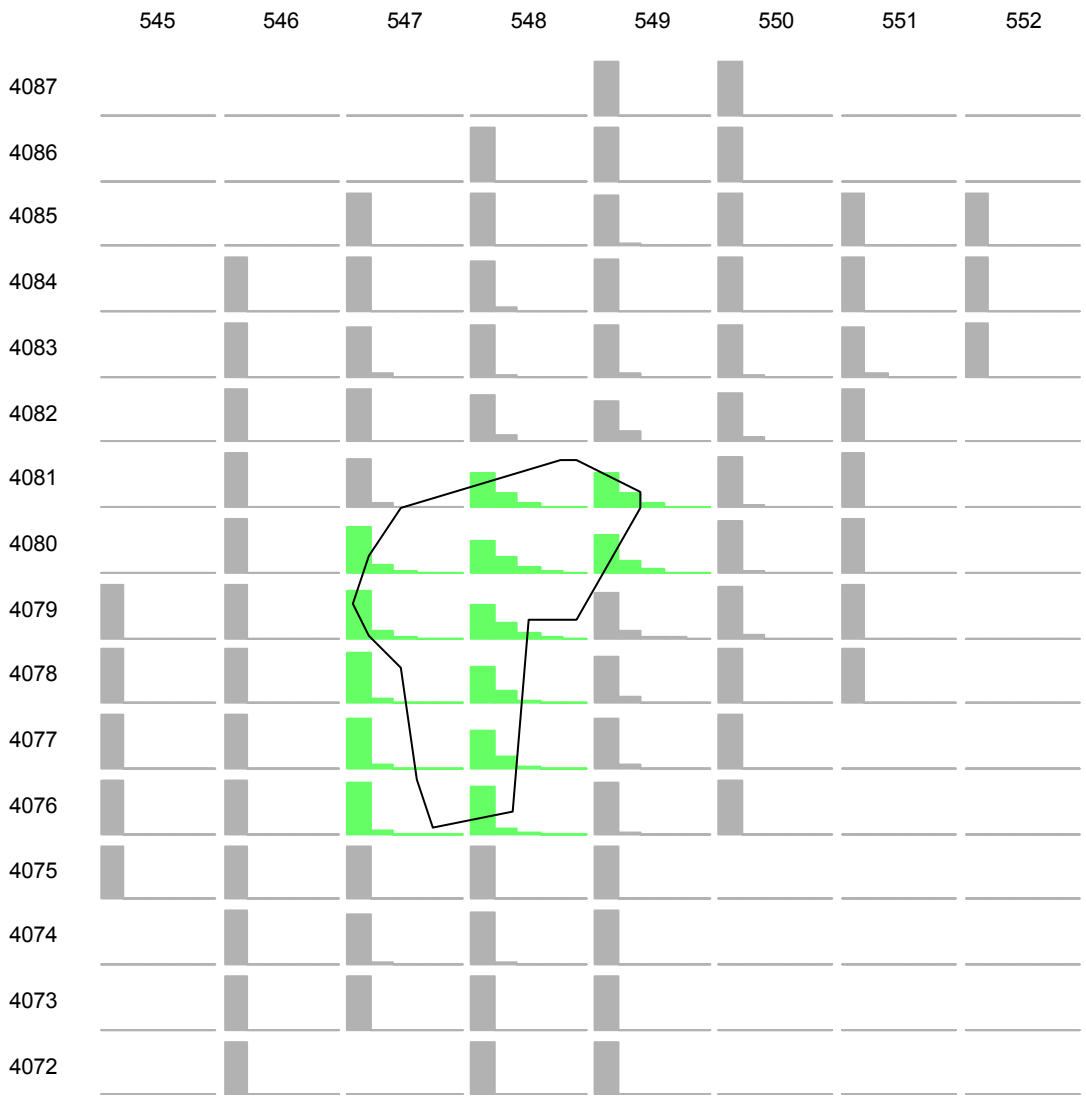

NOTE: Row and column labels represent grid points (UTM coordinates in km, NAD83) in the vicinity of the repository. Solid line represents the approximate boundary of the repository footprint for reference. Grid points representing locations that are within, or partially within, the repository footprint are plotted in green. Blank plots (e.g., in the upper left corner) indicate that the probability of an intersection for an event at that location is zero. All other plots show the number of intersections conditional on at least one. The plot at 545 E, 4079 N indicates that there is at most one intersection for events at that location. The plot at 548 E, 4077 N indicates that multiple intersections can occur given an event at that location.

Figure 4.1-5. Example of Schematic Showing the Distribution of the Number of Features That Intersect the Repository Footprint Given an Event at Each Grid Point, Conditional on at Least One Intersection

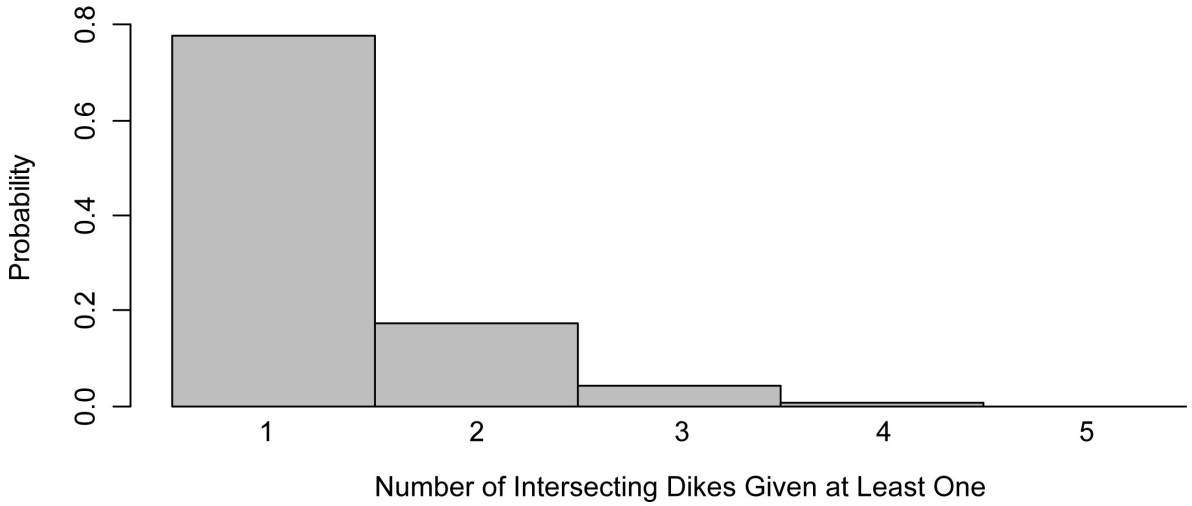

NOTE: Example figure corresponds to the conditional distribution of dike intersections, based on the example in Figure 4.1-5.

Figure 4.1-6. Example of Distribution of the Conditional Distribution of the Number of Dikes That Intersect the Repository Footprint, Given That at Least One Such Intersection Occurs

4.1.1 PVHA-U Results for Charles Connor

This section describes the results of the PVHA-U models specified by Charles Connor (CC). Those models and assessments are described in Section 3.2.1 and the elicitation summary in Appendix D. Section 4.1.1.1 discusses the results of the 10,000-year assessment for the frequency of intersection of any feature with the repository footprint. The frequency of intersection of specific features with the repository footprint is discussed in Section 4.1.1.2, and differences in the hazard calculated for the 10,000-year assessment and the 1-My assessment are discussed in Section 4.1.1.3.

4.1.1.1 Hazard Results for the 10,000-Year Assessment

Figure 4.1.1-1 summarizes the spatial distribution of hazard calculated using Charles Connor's PVHA-U models for the 10,000-year assessment. These contours extend slightly further to the SSW of the repository footprint than to the NNE (seen most clearly in the 1e-9 contour), reflecting the higher rate density in that direction.

Figure 4.1.1-2 illustrates the uncertainty in the frequency of intersection of any feature with the repository footprint. The mean frequency of intersection is marked on both graphs by a dashed vertical line, and the median, 5th, and 95th percentiles are shown on the pmf. The mean frequency of intersection of any feature with the repository footprint is 6.6e-08; the median frequency is 2.6e-8. The 5th and 95th percentiles are 2.2e-9 and 2.8e-07, respectively.

(a) Mean rate density. Contours represent the mean annual frequency of igneous events (events per year) per km^2.

(b) Conditional probability of intersection of any feature. Contours represent the probability that an event assumed to occur at each location would result in the intersection of any igneous feature with the repository footprint. Map shown is for events associated with the YMR data set only.

(c) Spatial distribution of the mean frequency of intersection. Contours represent the mean annual probability of an intersection of the repository footprint by an igneous feature.

NOTE: The repository footprint is shown as a yellow polygon. Past events are shown as black triangles. Map grid ticks are UTM meters; tick intervals for map (a) are 20 km; map (b) and (c) are 10 km.

Figure 4.1.1-1. Components of the Hazard Calculation for PVHA-U Models Specified by Charles Connor, for the 10,000-Year Assessment

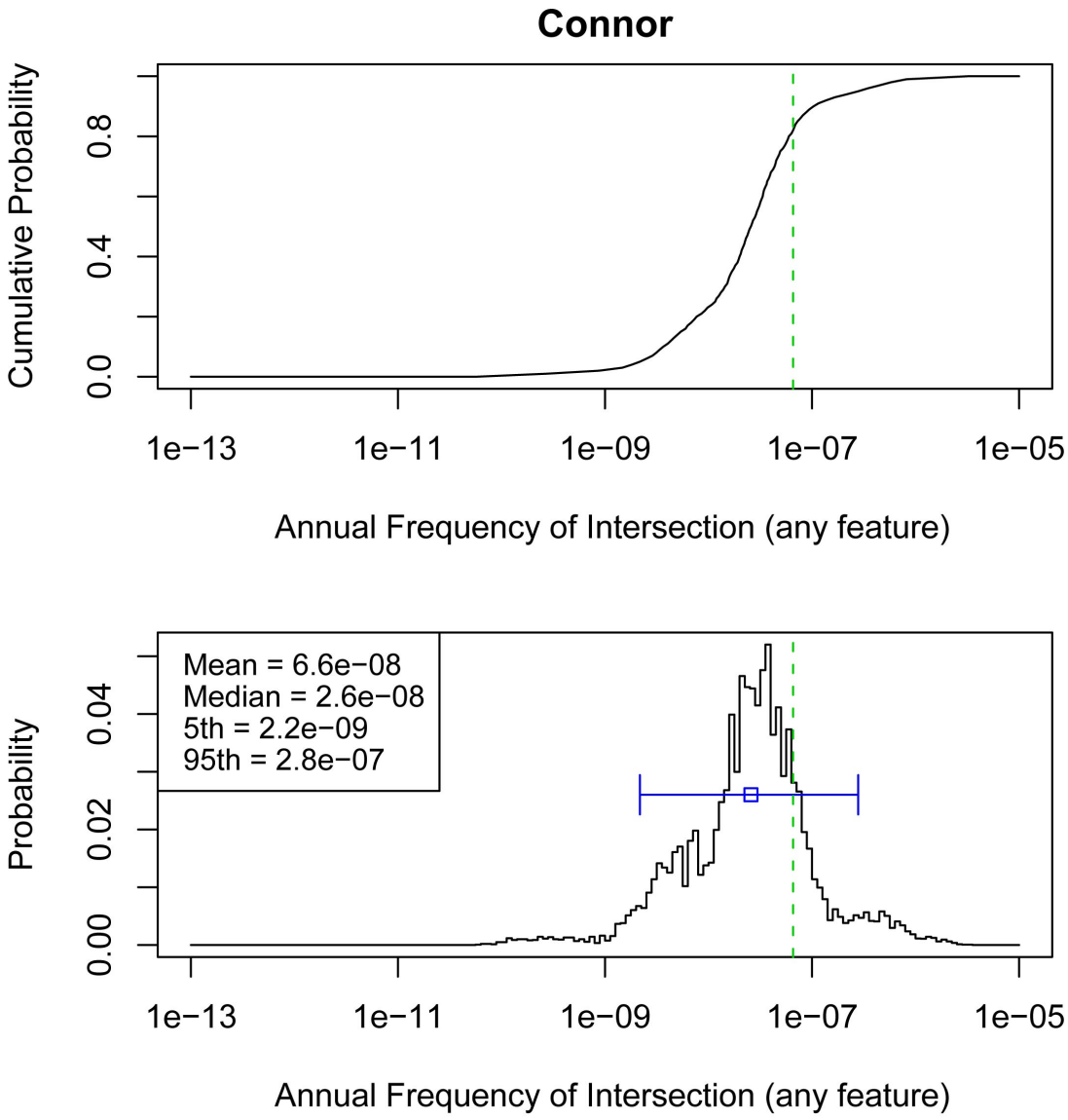

NOTE: Top figure is a cumulative distribution function, bottom figure is a probability mass function. The mean is shown by the dashed vertical line; median with the open box, and the 5th to 95th percentiles with the horizontal line.

Figure 4.1.1-2. Hazard Results for the 10,000-Year Assessment from PVHA-U Models Specified by Charles Connor

Contributions to Uncertainty

Contributions from various model components to uncertainty in the mean hazard in CC's models are illustrated in Figure 4.1.1-3. The largest contributor to uncertainty in the mean hazard in CC's models is the uncertainty in the temporal model. As described in Section 3.2.1, CC specified three alternative temporal models: a steady-state model based on the rate of past events in the YMR or the AVIP, an increased rate model based on rates in higher-density fields in the southern Great Basin, and a field extinction model with a rate derived from the longest time between events in the YMR. If the rate model were known with certainty to be the increased rate

model, the mean hazard would be 4e-07, as shown by the right end of the top bar (labeled "Temporal model") in the figure. Similarly, if the rate model were known with certainty to be the field extinction model, the mean hazard would be 5.8e-09, as shown by the left end of the "Temporal model" bar.

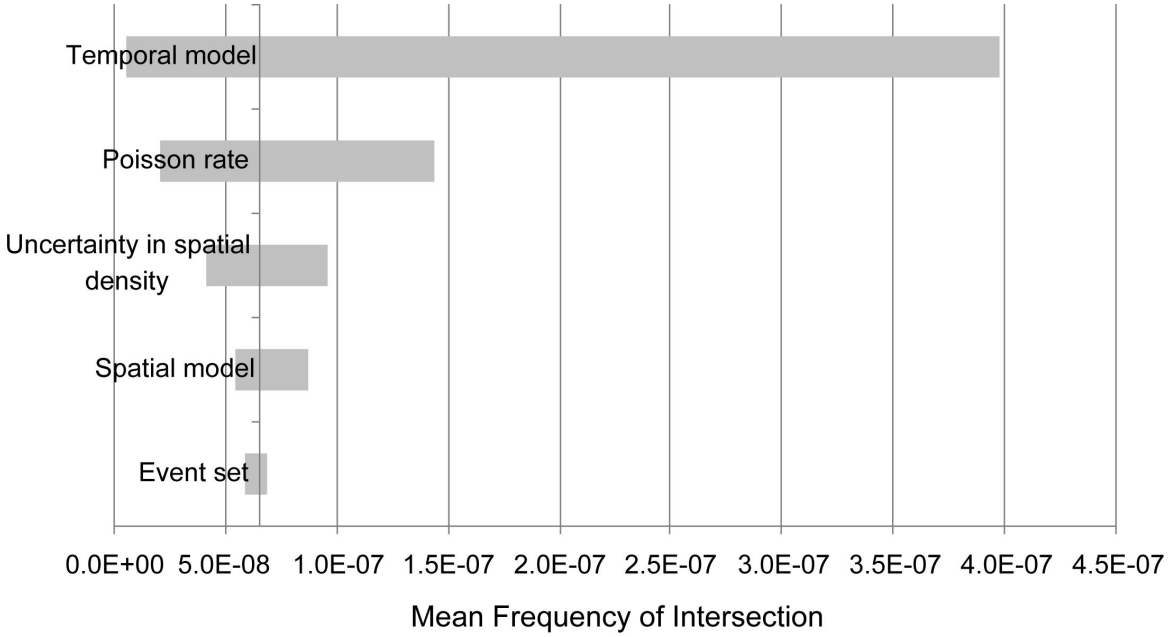

NOTE: Labels on each bar correspond to the nodes in the logic tree for CC's model as described in Section 3.2. The length of each bar shows the range of the mean hazard values that result from fixing the value of the specified model component sequentially at each of its branch values. This range represents the degree to which the mean hazard is affected by uncertainty in the specified model component.

Figure 4.1.1-3. Contribution of Uncertainty in PVHA-U Model Components to Uncertainty in the Mean Hazard, for Models for the 10,000-Year Assessment Specified by Charles Connor

Uncertainty in the rate itself (shown in the figure as the bar labeled "Poisson rate"), given a particular temporal model, also has a significant impact on the mean hazard. This bar represents a combination of several uncertainties: uncertainty in the rate for a Poisson model that is derived based on the past events identified as relevant by CC (for the steady-state and the field extinction temporal models), and uncertainty in the rate as specified by CC for the increased rate model.

Parameters related to the spatial model have less impact on the mean hazard than those related to the temporal model. Among the uncertainties related to the spatial distribution, mean hazard is most sensitive to the uncertainty in spatial density that results from fitting a kernel density estimate to the event set (the "Uncertainty in spatial density" bar).

Contribution of various model components to *overall uncertainty* in the hazard for CC's model is shown in Figure 4.1.1-4. Uncertainty in the frequency of intersection is most sensitive to the choice of temporal model. The small difference between the endpoints of the error bars indicates that the relative uncertainty in the hazard would be reduced by a similar amount regardless of which temporal model is selected. Uncertainty in the hazard is also sensitive to the uncertainty in the selection of the appropriate event set (YMR or AVIP). In contrast to the temporal model, the large difference shown by the error bars indicates that the relative uncertainty in hazard

would be reduced much more if one particular data set were selected as appropriate (in this case, uncertainty in the hazard is reduced more if the AVIP data set is used than if the YMR data set is used).

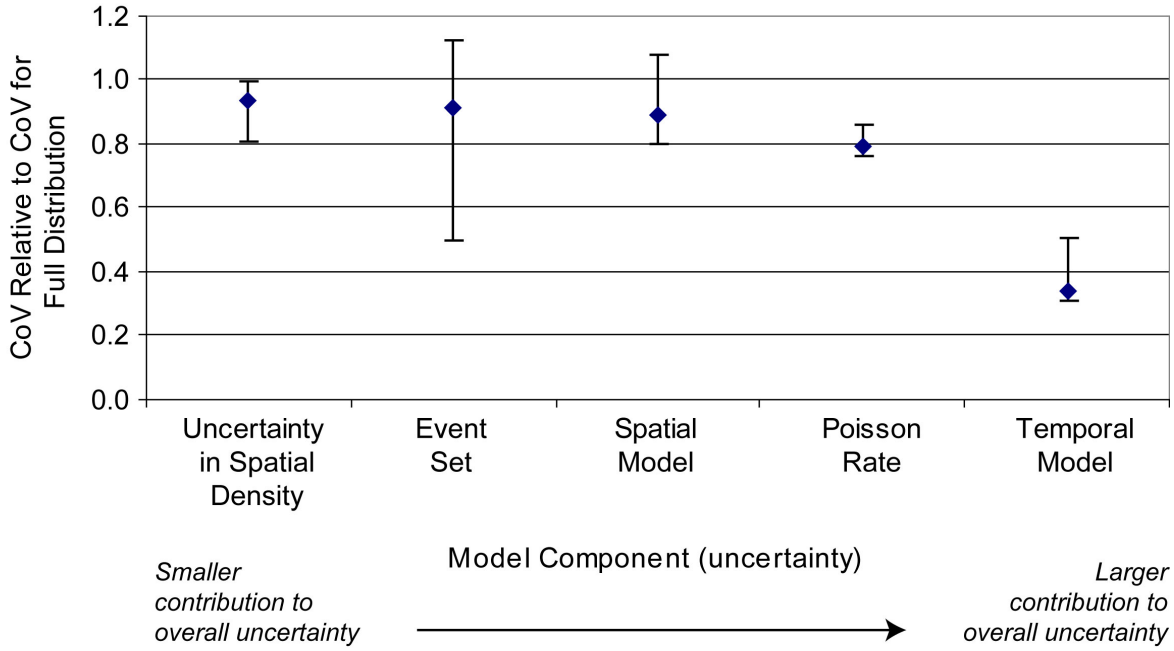

NOTE: Graph shows the CoV for the hazard distribution calculated with the specified model component fixed at each of its branch values, divided by the CoV for the full hazard distribution. Diamond shows the mean value with the relative CoV for each branch value weighted by its probability; "error bars" show the highest and lowest relative CoVs calculated across the branches for that model component.

Figure 4.1.1-4. Contribution of Uncertainty in PVHA-U Model Components to Overall Uncertainty in the Hazard Estimate, for Models for the 10,000-Year Assessment Specified by Charles Connor

4.1.1.2 Discussion of Individual Features

As described in Section 3.2.1, CC's events include dikes, column-producing conduits, and non-column producing vents. They may also include sills. The conditional probability of intersection of each type of feature with the repository footprint was illustrated in Section 3.2.1, and as discussed, the shape of the conditional probability of intersection maps for each individual feature is the same as for the conditional probability of intersection for any feature: no consistent clustering or grouping of individual features in an event occurs. Similarly, the full distribution of the frequency of intersection for any individual feature follows the same pattern as the distribution for any feature shown in Figure 4.1.1-2, simply shifted to the lower frequencies associated with the individual feature.

Table 4.1.1-1 shows the mean and median frequencies of intersection for each feature.

Table 4.1.1-1. Mean and Median Frequency of Intersection of Various Igneous Features with the Repository Footprint, for Charles Connor's 10,000-Year Assessment

Feature	Mean Frequency of Intersection	Median Frequency of Intersection
Any feature	6.6e-8	2.6e-8
Dikes	6.5e-8	2.5e-8
Column-producing conduits	2.0e-8	7.7e-9
Vents	3.0e-8	1.2e-8
Sills	1.9e-9	7.4e-10

Potential for Multiple Intersections

Because events could include multiple features, a single event might have more than one intersecting feature. Events that are "centered" closer to the repository footprint are more likely to have multiple features intersect the footprint than are events centered further away.

Figure 4.1.1-5 shows a set of plots illustrating the distribution of the number of dike intersections for an event centered at a specific point, conditional on at least one such intersection occurring. The maximum number of dike intersections that occurred over 100,000 simulations was 43, which occurred for an event centered in the southern portion of the repository footprint.

The graph in Figure 4.1.1-6 combines the conditional distribution of number of intersecting features at each point with the relative frequency of events at those points. As shown, assuming dike intersection occurs, it is most likely (about 32%) that only one dike intersects, but the potential exists for as many as 40 intersections. There is a 5% chance of more than 11 dike intersections.

Figures 4.1.1-7 and 4.1.1-8 show the same data for conduits: the distribution on number of conduit intersections given at least one conduit intersects the footprint. Given a conduit intersection, it is most likely that only one such intersection would occur, which results from the assessment that at most one vent per "center" would be a column-producing conduit and the relatively wide spacing of centers in an event. In CC's models, vents are more common than conduits, and so the probability of multiple vent intersections is higher than the probability of multiple conduit intersections. Figures 4.1.1-9 and 4.1.1-10 show the number of vent intersections, given at least one vent intersects the footprint.

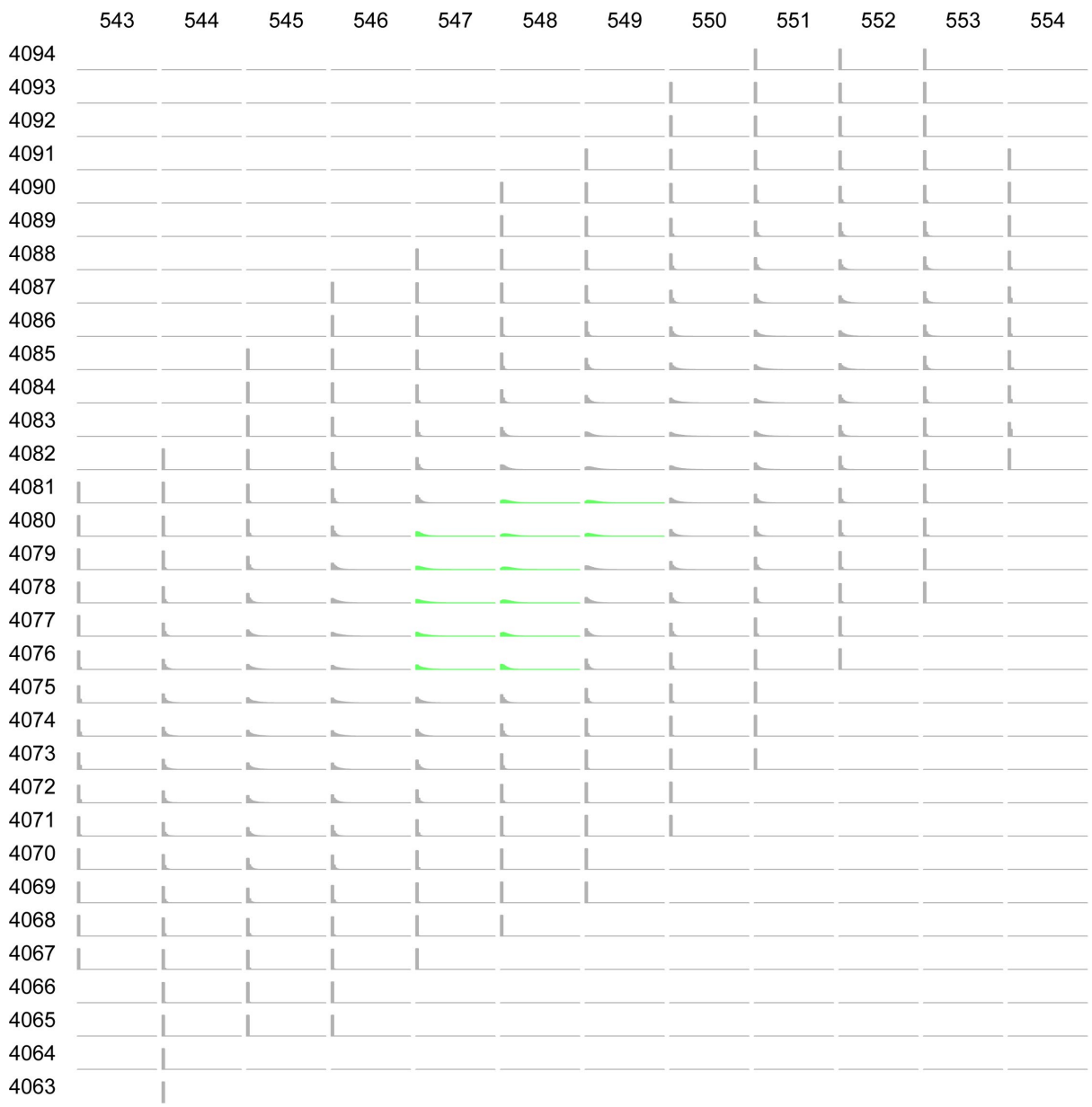

NOTE: Row and column labels represent grid points (UTM coordinates in km, NAD83) in the vicinity of the repository. Green plots show points inside or partially inside the repository footprint. Blank plots (e.g., in the upper left corner) indicate that the probability of intersection for an event at that location is zero. All other plots show the number of intersections conditional on at least one.

Figure 4.1.1-5. Schematic Showing the Distribution of the Number of Dikes That Intersect the Repository Footprint Given an Event at Each Grid Point, Given at Least One Dike Intersection Occurs (based on Charles Connor's event model associated with his YMR data set)

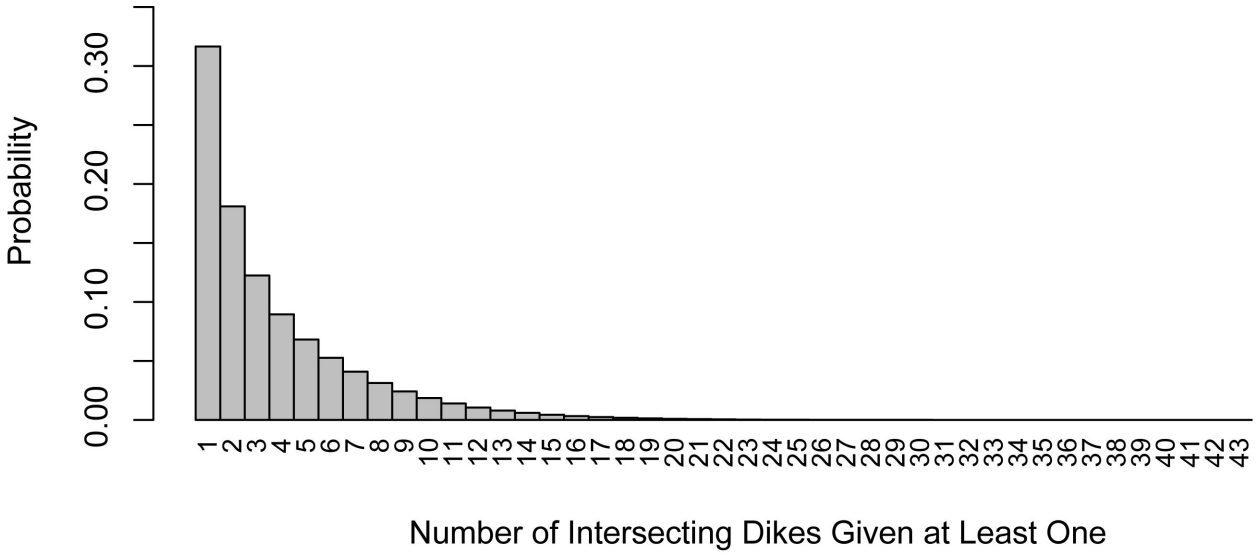

Figure 4.1.1-6. Conditional Distribution of the Number of Dikes That Intersect the Repository Footprint, Given That at Least One Dike Intersection Occurs (for Charles Conner's event model associated with the YMR data set)

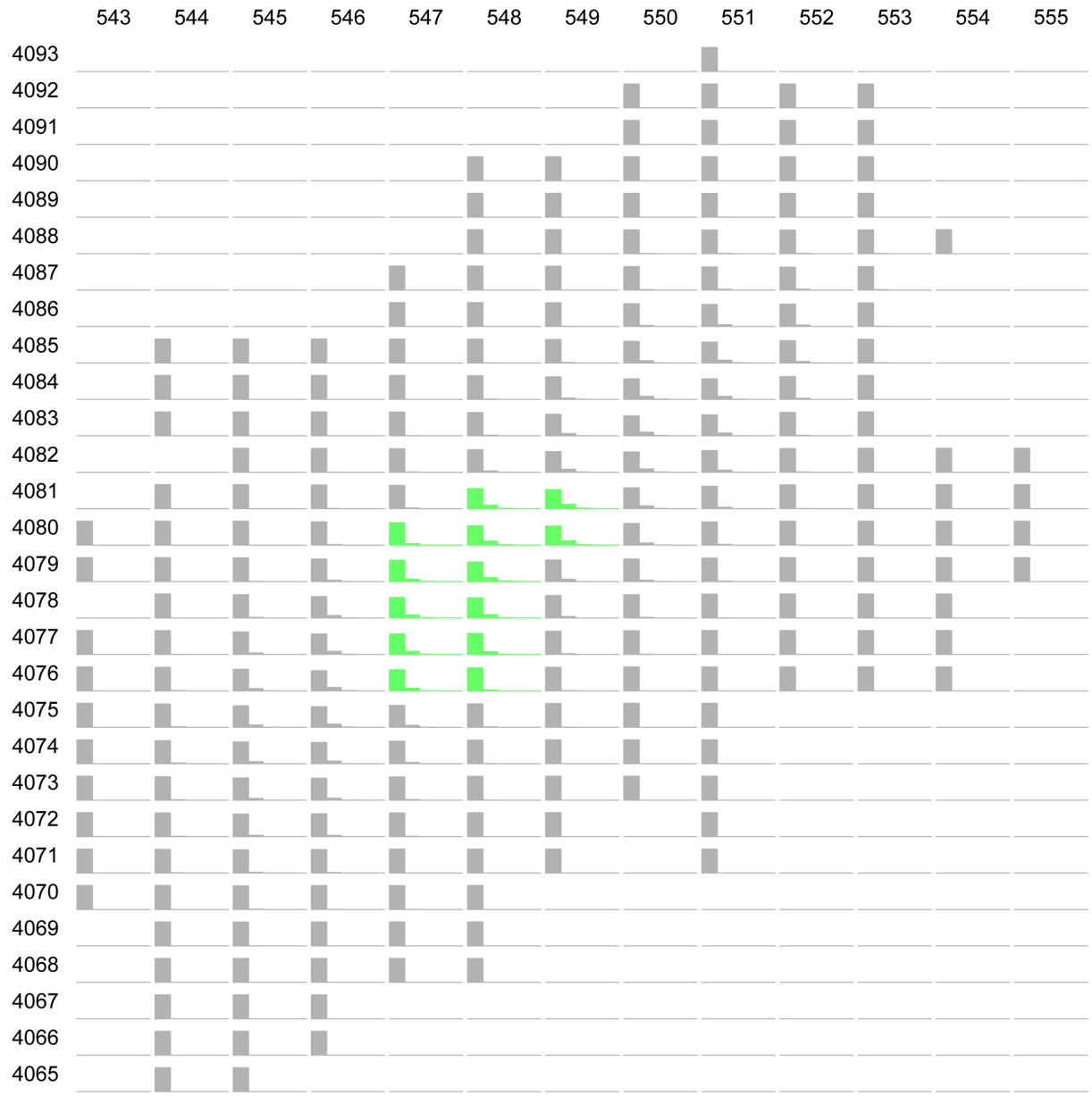

NOTE: Row and column labels represent grid points (UTM coordinates in km, NAD83) in the vicinity of the repository. Green plots show points inside or partially inside the repository footprint. Blank plots (e.g., in the upper left corner) indicate that the probability of intersection for an event at that location is zero. All other plots show the number of intersections conditional on at least one.

Figure 4.1.1-7. Schematic Showing the Distribution of the Number of Conduits That Intersect the Repository Footprint Given an Event at Each Grid Point, Given at Least One Conduit Intersection Occurs (for Charles Conner's event model associated with the YMR data set)

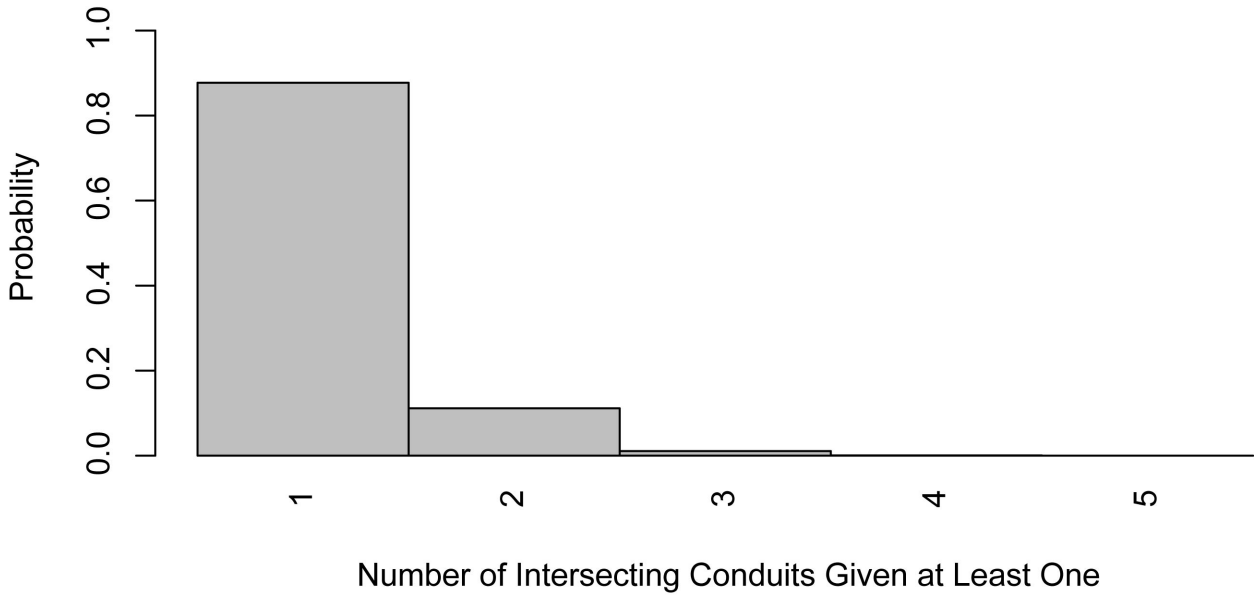

Figure 4.1.1-8. Conditional Distribution of the Number of Conduits That Intersect the Repository Footprint, Given That at Least One Conduit Intersection Occurs (for Charles Conner's event model associated with the YMR data set)

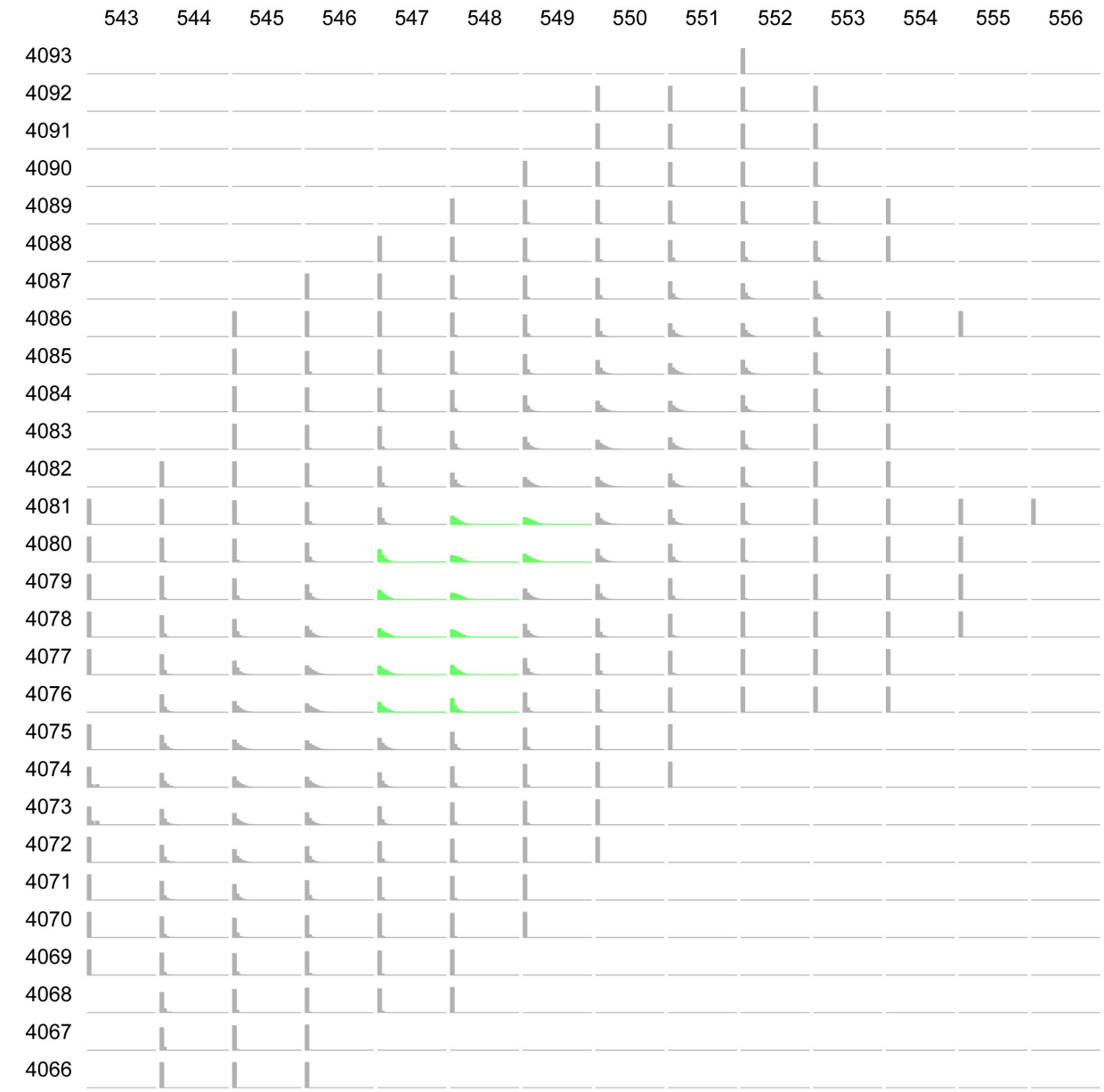

NOTE: Row and column labels represent grid points (UTM coordinates in km, NAD83) in the vicinity of the repository. Green plots show points inside or partially inside the repository footprint. Blank plots (e.g., in the upper left corner) indicate that the probability of intersection for an event at that location is zero. All other plots show the number of intersections conditional on at least one.

Figure 4.1.1-9. Schematic Showing the Distribution of the Number of Vents That Intersect the Repository Footprint Given an Event at Each Grid Point, Given at Least One Vent Intersection Occurs (for Charles Conner's event model associated with the YMR data set)

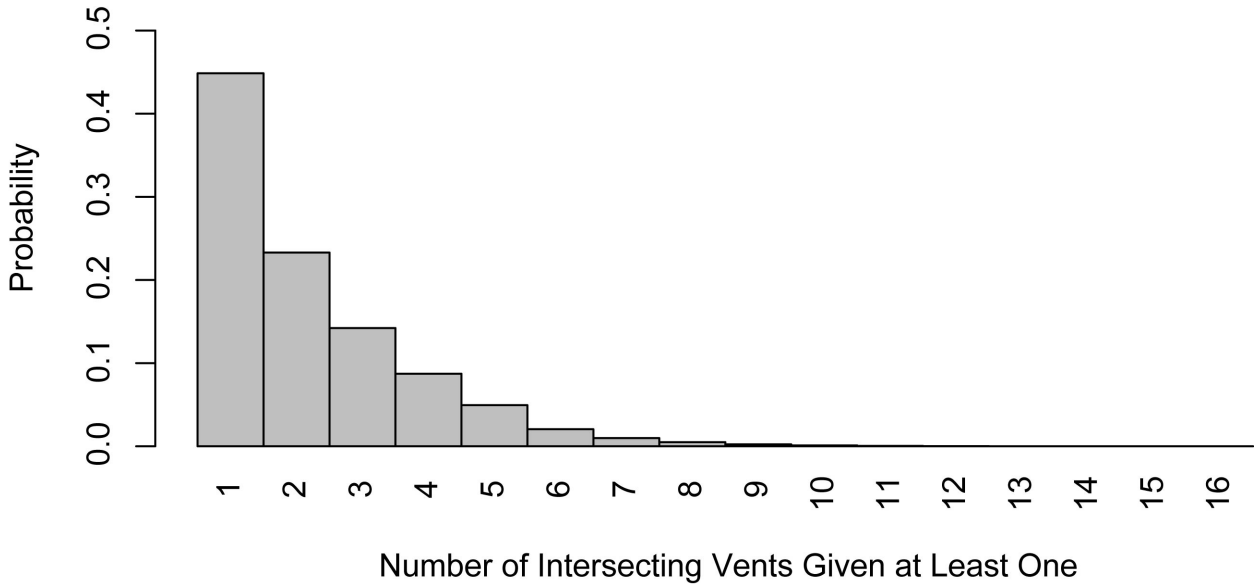

Figure 4.1.1-10. Conditional Distribution of the Number of Vents That Intersect the Repository Footprint, Given That at least One Vent Intersection Occurs (for Charles Conner's event model associated with the YMR data set)

4.1.1.3 Results at Different Future Times

The primary difference in CC's 10,000-year and 1-My assessments is that higher probabilities were assigned to the increased rate model and the field extinction rate model for the 1-My assessment. This results in greater uncertainty in the hazard estimate, as shown in Figure 4.1.1-11. As shown, the effect is not symmetric: the mean hazard increases for the 1-My assessment, even as the uncertainty in the hazard estimate also increases.

A sensitivity analysis similar to that described above was conducted using the models for CC's 1-My assessment. The relative impact of each of the model components on the mean hazard for the 1-My assessment is the same as for the 10,000-year assessment. Specifically, the mean hazard is most sensitive to the temporal model, second most sensitive to the Poisson rate for those temporal models, and so forth. The contribution of the various model components to overall uncertainty (shown in Figure 4.1.1-12) is slightly different for the 1-My assessment than for the 10,000-year assessment: all model components other than the temporal model have a slightly higher contribution to overall uncertainty than those same components have in the 10,000-year assessment. Note, for example, the "error bars" associated with the "Event set," which indicates that selecting one specific event set would not have as dramatic an effect on the CoV as it would for the 10,000-year assessment. This is a result of the increased uncertainty in the hazard estimate itself, which results from the higher probabilities assigned to alternative temporal models (the increased rate and field extinction models).

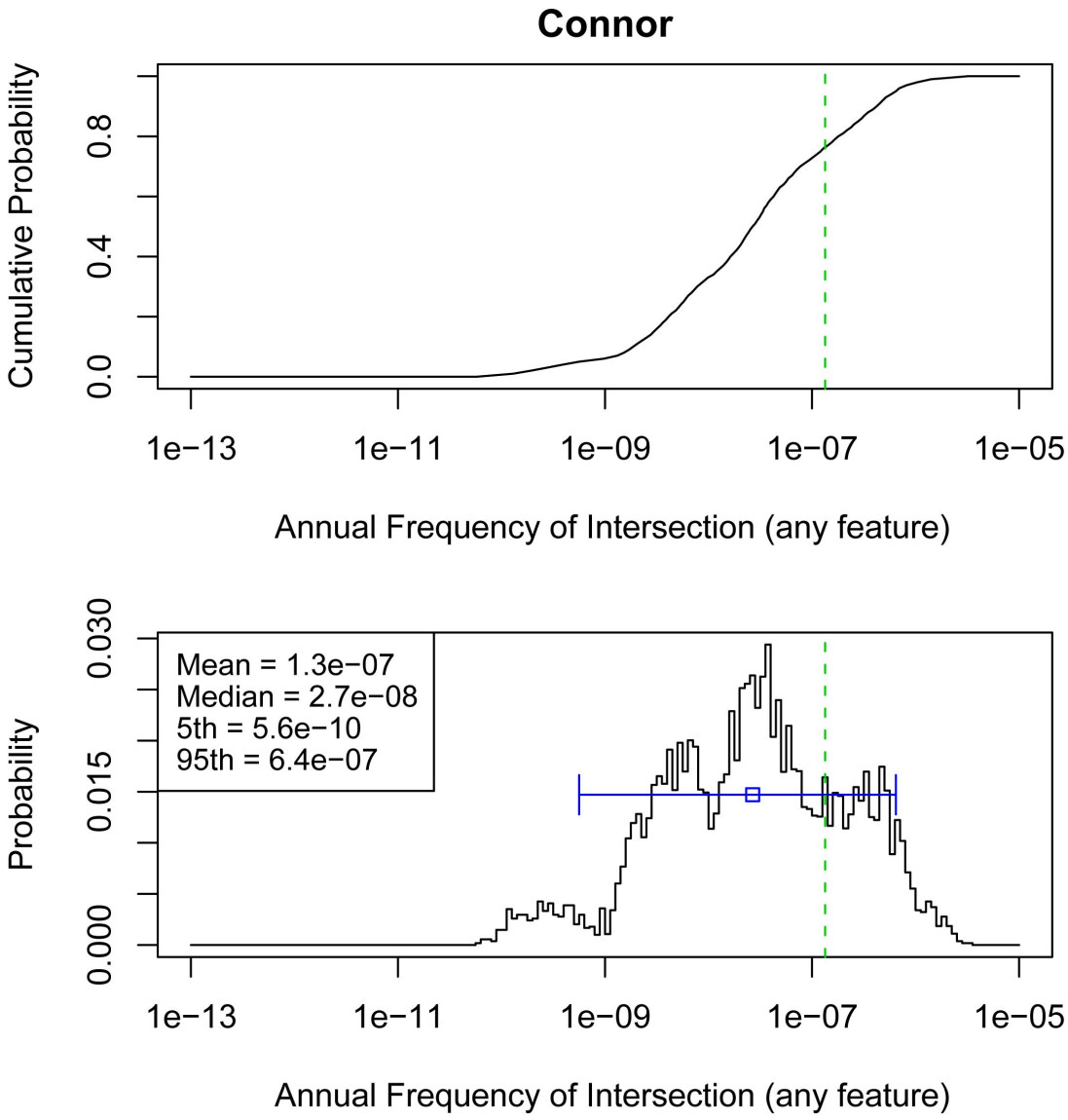

NOTE: Top figure is a cumulative distribution function, bottom figure is a probability mass function. The mean is shown by the dashed vertical line, the median with the open box, and the 5th to 95th percentiles with the horizontal line.

Figure 4.1.1-11. Hazard Results for the 1-My Assessment from PVHA-U Models Specified by Charles Connor

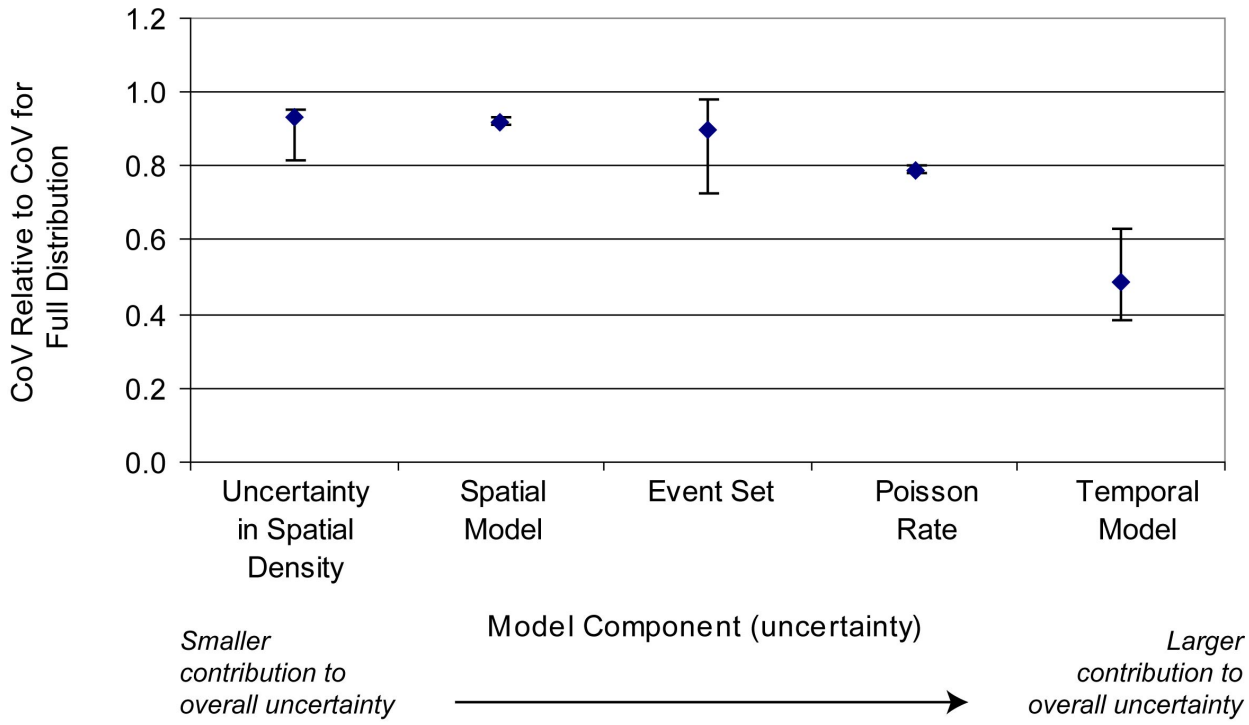

NOTE: Graph shows the CoV for the hazard distribution calculated with the specified model component fixed at each of its branch values, divided by the CoV for the full hazard distribution. Diamond shows the mean value with the relative CoV for each branch value weighted by its probability; "error bars" show the highest and lowest relative CoVs calculated across the branches for that model component.

Figure 4.1.1-12. Contribution of Uncertainty in Model Components to Overall Uncertainty in the Hazard Estimate, for PHVA-U Models for the 1-My Assessment Specified by Charles Connor

4.1.2 PVHA-U Results for Bruce Crowe

This section describes the results of the PVHA-U models specified by Bruce Crowe (BC). Those models and assessments are described in Section 3.2.2 and the elicitation summary in Appendix D. Section 4.1.2.1 discusses the results of the 10,000-year assessment for the frequency of intersection of any feature with the repository footprint. The frequency of intersection of specific features with the repository footprint is discussed in Section 4.1.2.2, and differences in the hazard calculated for the 10,000-year assessment and the 1-My assessment are discussed in Section 4.1.2.3.

4.1.2.1 Hazard Results for the 10,000-Year Assessment

Figure 4.1.2-1 summarizes the spatial distribution of hazard calculated using Bruce Crowe's PVHA-U models for the 10,000-year assessment. Panel (b) shows the conditional probability of intersection for events associated with the steady-state and increasing rate models only, which are weighted much higher than the decreased rate or the new cycle rate model for the 10,000-year assessment. Panel (c) shows the spatial distribution of mean hazard calculated using all rate models appropriately weighted. The "hole" in the mean frequency of intersection plot results directly from the small zone with zero rate density, defined by the area of high lithostatic pressure, located to the north of the repository footprint.

Figure 4.1.2-2 illustrates the uncertainty in the frequency of intersection of any feature with the repository footprint. The mean frequency of intersection is marked on both graphs by a dashed vertical line, and the median, 5th, and 95th percentiles are shown on the pmf. The mean frequency of intersection of any feature with the repository footprint is 9.4e-8; the median frequency is 8.1e-8. The 5th and 95th percentiles are 8.4e-9 and 2.4e-7, respectively.

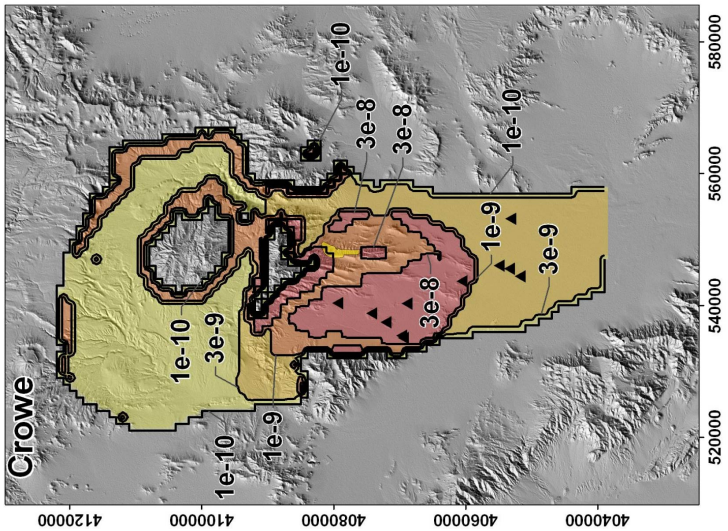

(a) Mean rate density. Contours represent the mean annual frequency of igneous events (events per year) per km^2.

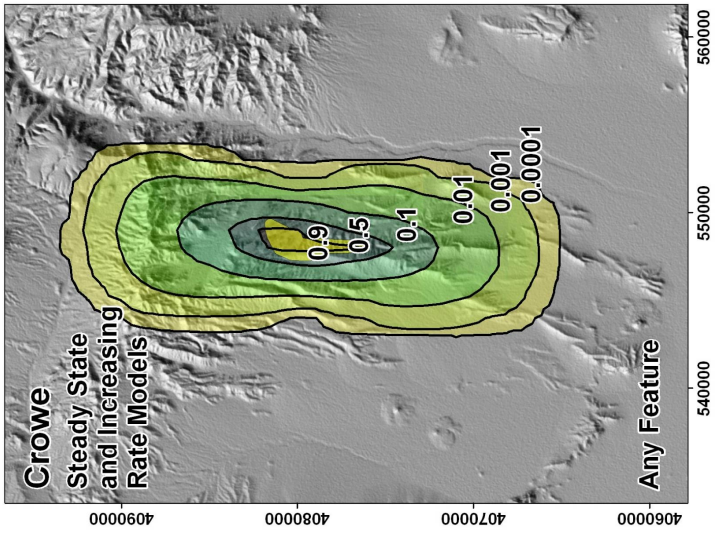

(b) Conditional probability of intersection of any feature. Contours represent the probability that an event assumed to occur at each location would result in the intersection of any igneous feature with the repository footprint. Map shown is for events associated with BC's steady-state and increasing rate models only.

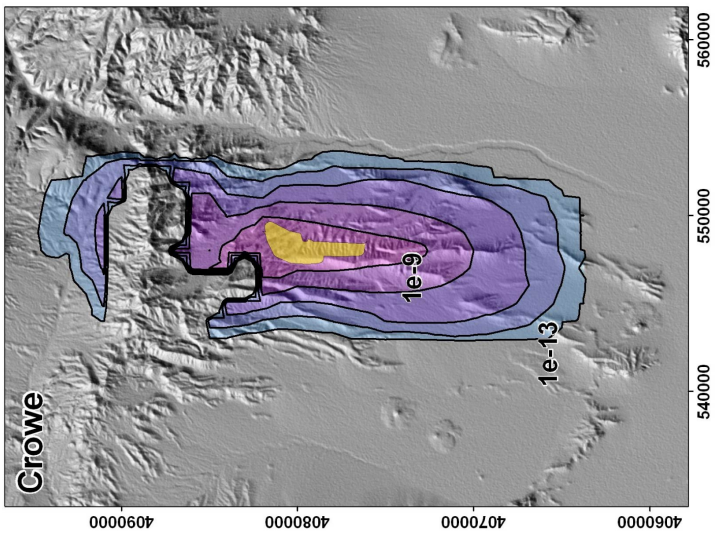

(c) Spatial distribution of the mean frequency of intersection. Contours represent the mean annual probability of an intersection of the repository footprint by an igneous feature.

NOTE: The repository footprint is shown as a yellow polygon. Map grid ticks are UTM meters; tick intervals for map (a) are 20 km; map (b) and (c) are 10 km.

Figure 4.1.2-1. Components of the Hazard Calculation for PVHA-U Models Specified by Bruce Crowe, for the 10,000-Year Assessment

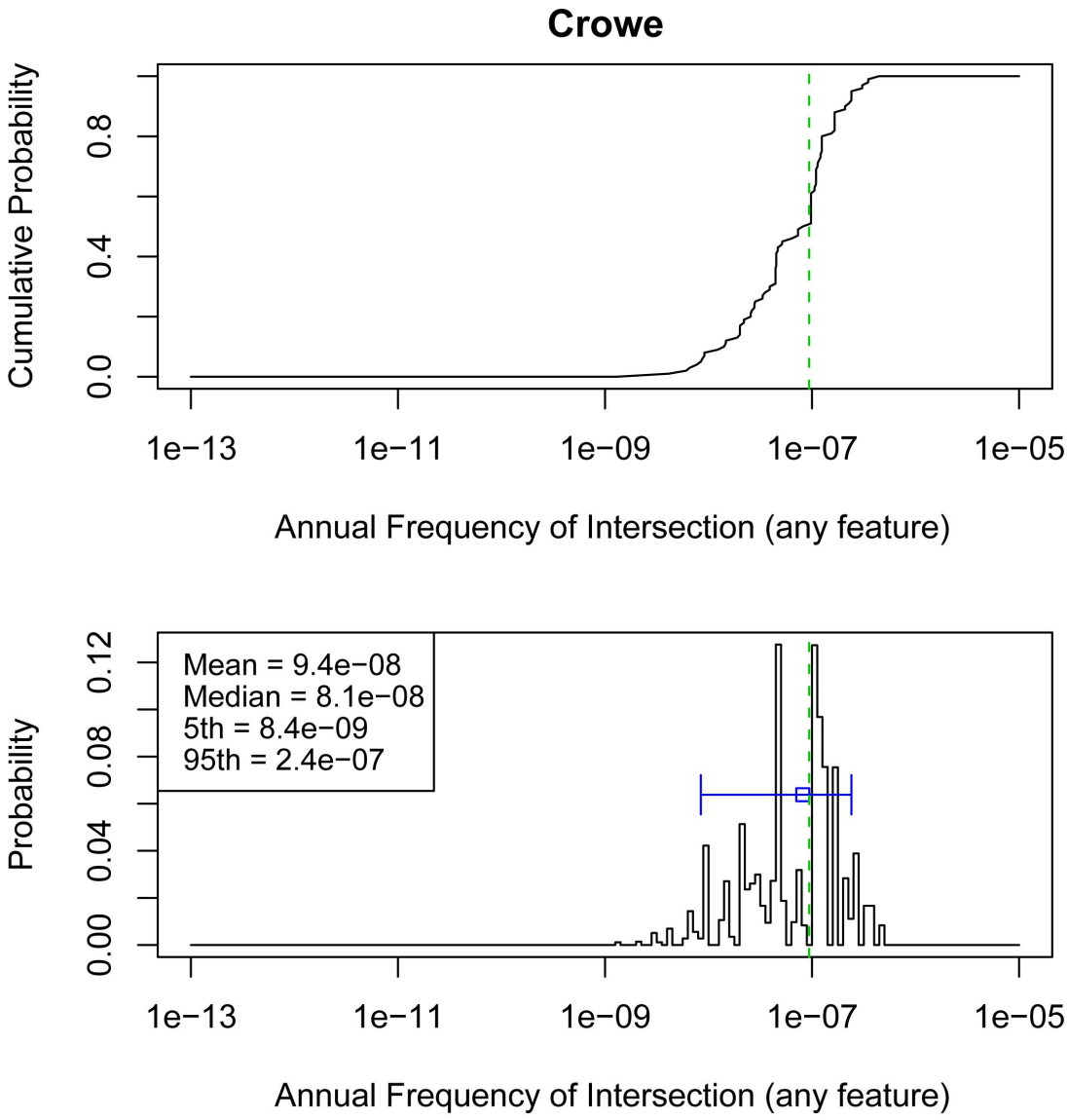

NOTE: Top figure is a cumulative distribution function, bottom figure is a probability mass function. The mean is shown by the dashed vertical line, the median with the open box, and the 5th to 95th percentiles with the horizontal line.

Figure 4.1.2-2. Hazard Results for the 10,000-Year Assessment from PVHA-U Models Specified by Bruce Crowe

Contributions to Uncertainty

Contributions from various model components to uncertainty in the mean hazard in BC's models are illustrated in Figure 4.1.2-3. The largest contributor to uncertainty in the mean hazard is the uncertainty in rate. The rate uncertainty also incorporates some uncertainty related to the selection of the appropriate temporal model. Because the logic tree structure uses a single node to represent uncertainty in the rate, when that node is set to one of its branches in the sensitivity analysis, it is set to that value for all the rate models simultaneously. The second largest contributor to uncertainty in the mean is the temporal model. As described in Section 3.2.2, BC

specified three alternative temporal models as relevant for the 10,000-year assessment: a steady-state model, an increased rate model, and a background rate model. If the rate model were known with certainty to be the increased rate model, the mean hazard would be 1.4e-7, as shown by the right end of the bar (labeled "Temporal model") in the sensitivity graph. Similarly, if the rate model were known with certainty to be the background rate model, the mean hazard would be 2.8e-08, as shown by the left end of the "Temporal model" bar.

Parameters related to the spatial model have less impact on the mean hazard than those related to the temporal model, but their impact is still large. The effect of alternative regions of interest, for example, can potentially change the mean hazard by half an order of magnitude, as shown by the length of the "Region of interest" bar at the bottom of the figure.

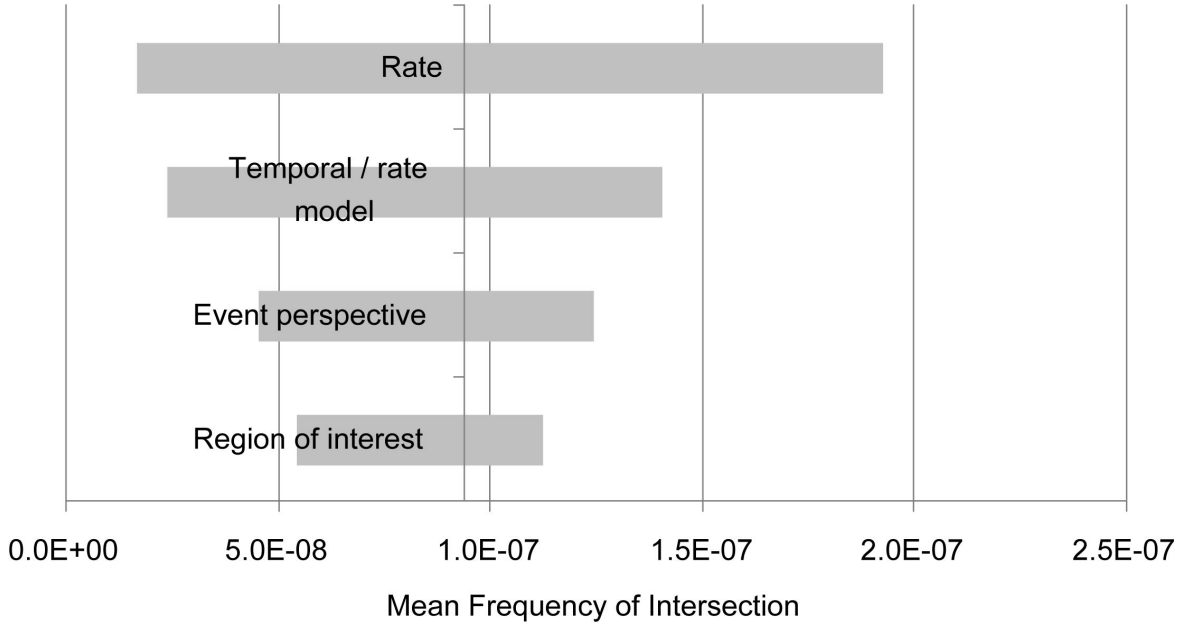

NOTE: Labels on each bar correspond to the nodes in the logic tree for BC's models as described in Section 3.2. The length of each bar shows the range of the mean hazard values that result from fixing the value of the specified model component at one of its branch values. This range represents the degree to which the mean hazard is affected by uncertainty in the specified model component.

Figure 4.1.2-3. Contribution of Uncertainty in PVHA-U Model Components to Uncertainty in the Mean Hazard, for Models for the 10,000-Year Assessment Specified by Bruce Crowe

Contribution of various model components to *overall uncertainty* in the hazard for BC's models is shown in Figure 4.1.2-4. For BC's models, the impacts of individual uncertainties in the models on the overall uncertainty are very similar to their impacts on uncertainty in the mean hazard.

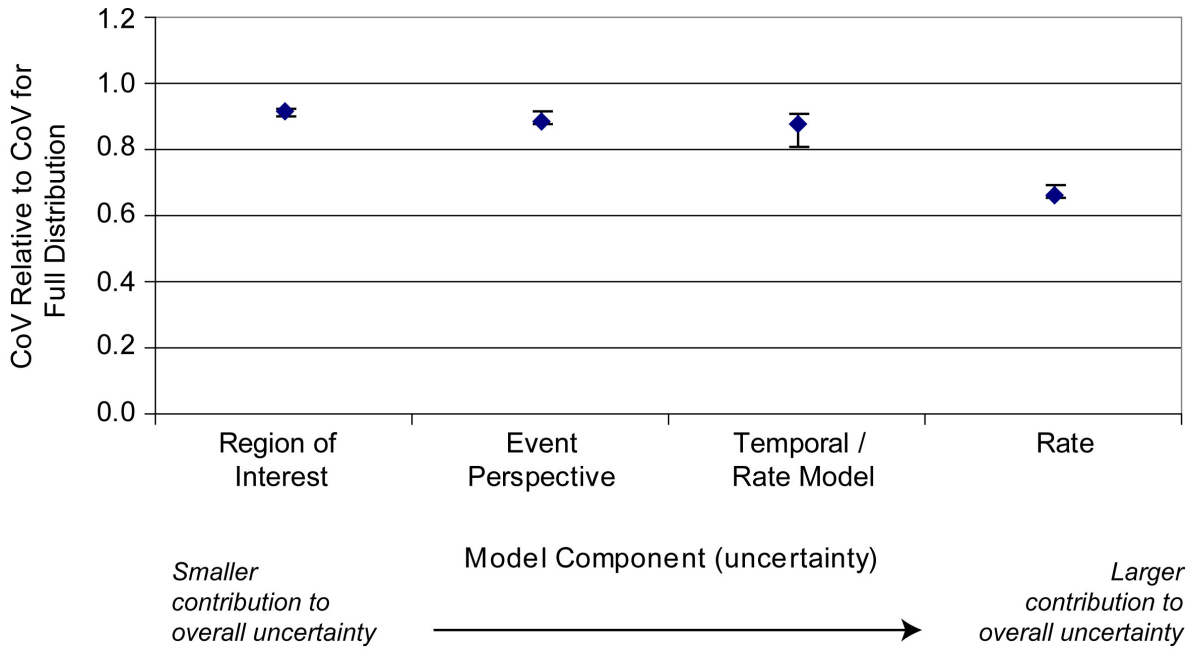

NOTE: Graph shows the CoV for the hazard distribution calculated with the specified model component fixed at each of its branch values, divided by the CoV for the full hazard distribution. Diamond shows the mean value with the relative CoV for each branch value weighted by its probability; "error bars" show the highest and lowest relative CoVs calculated across the branches for that model component.

Figure 4.1.2-4. Contribution of Uncertainty in Model Components to Overall Uncertainty in the Hazard Estimate, for PVHA-U Models for the 10,000-Year Assessment Specified by Bruce Crowe

4.1.2.2 Discussion of Individual Features

As described in Section 3.2.2, BC's events include dikes and column-producing conduits, and might also include non-column-producing vents. The conditional probability of intersection of each type of feature with the repository footprint was illustrated in Section 3.2.2. As discussed, the shape of the conditional probability of intersection maps for each individual feature is the same as for the conditional probability of intersection for any feature; no particular clustering or grouping of individual features in an event occurs. Similarly, the full distribution of the frequency of intersection for any individual feature follows the same pattern as the distribution for any feature shown in Figure 4.1.2-2, simply shifted to the lower frequencies associated with the individual feature.

Table 4.1.2-1 shows the mean and median frequencies of intersection for each feature.

Table 4.1.2-1. Mean and Median Frequency of Intersection of Various Igneous Features with the Repository Footprint, for Bruce Crowe's 10,000-Year Assessment

Feature	Mean Frequency of Intersection	Median Frequency of Intersection
Any feature	9.4e-8	8.1e-8
Dikes	9.4e-8	8.1e-8
Column-producing conduits	4.3e-8	3.8e-8
Vents	2.4e-8	2.0e-8

Potential for Multiple Intersections

Figure 4.1.2-5 shows a set of plots illustrating the distribution of the number of dike intersections for an event centered at a specific point, conditional on at least one such intersection occurring. The figure shows the number of dike intersections based only on the event descriptions corresponding to the steady-state and increased rate models, the most highly weighted models for the 10,000-year assessment. Events centered inside the repository footprint (e.g., at 548 E, 4079 N), are more likely to have two dikes intersect the footprint than to have one dike intersect.

The graph in Figure 4.1.2-6 combines the relative likelihood of a dike intersection at each point shown in Figure 4.1.2-5 with the conditional distribution of the number of dike intersections for an event at those points to yield a conditional distribution on the number of dike intersections, given that at least one such intersection occurs. As shown, assuming that a dike intersection occurs, it is most likely (probability of 0.66) that only one dike intersects, but the potential exists for as many as 5 intersections (with probability 0.005).

Figure 4.1.2-7 and 4.1.2-8 show the same data for conduits: the distribution on number of conduit intersections given that at least one conduit intersects the footprint. Given a conduit intersection, it is most likely that only one such intersection would occur, which results from the assessment that the distance between conduits for an event with multiple conduits is relatively large compared to the size of the repository. Figures 4.1.2-9 and 4.1.2-10 show the number of vent intersections, given that at least one vent intersects the footprint. In BC's models, non-column-producing vents are less likely than column-producing conduits.

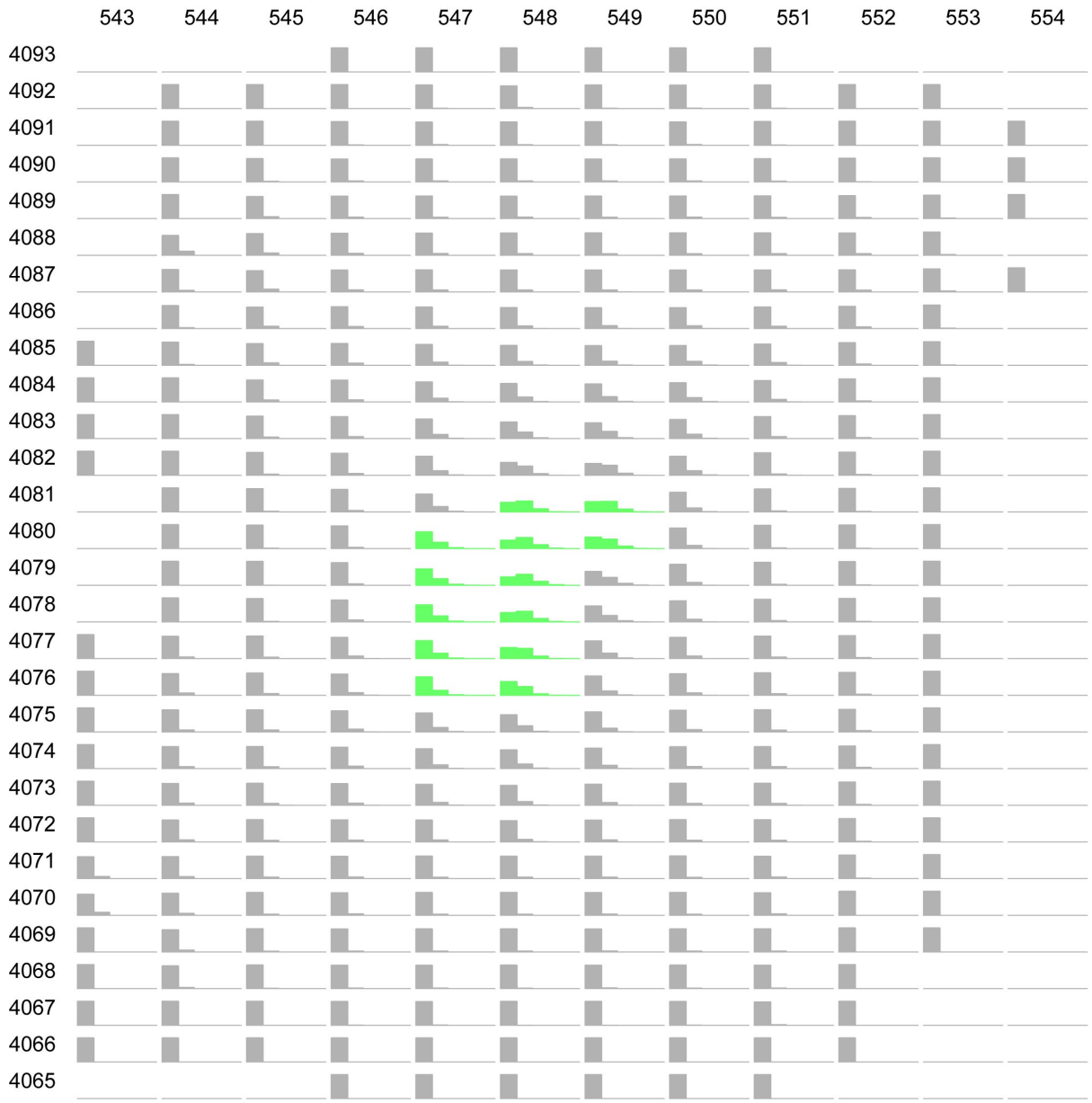

NOTE: Row and column labels represent grid points (UTM coordinates in km, NAD83) in the vicinity of the repository. Green plots show points inside or partially inside the repository footprint. Blank plots (e.g., in the upper left corner) indicate that the probability of intersection for an event at that location is zero. All other plots show the number of intersections conditional on at least one.

Figure 4.1.2-5. Schematic Showing the Distribution of the Number of Dikes That Intersect the Repository Footprint Given an Event at Each Grid Point, Given That at Least One Dike Intersection Occurs (based on Bruce Crowe's event model associated with his steady-state and increasing rate models)

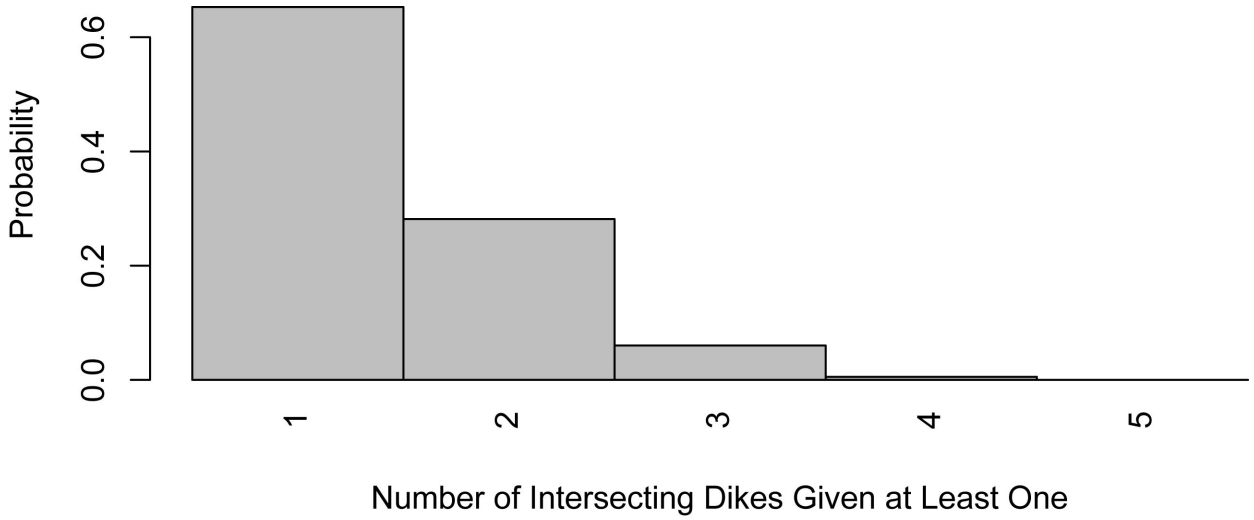

Figure 4.1.2-6. Conditional Distribution of the Number of Dikes That Intersect the Repository Footprint, Given That at Least One Dike Intersection Occurs (based on Bruce Crowe's event model associated with his steady-state and increasing rate models)

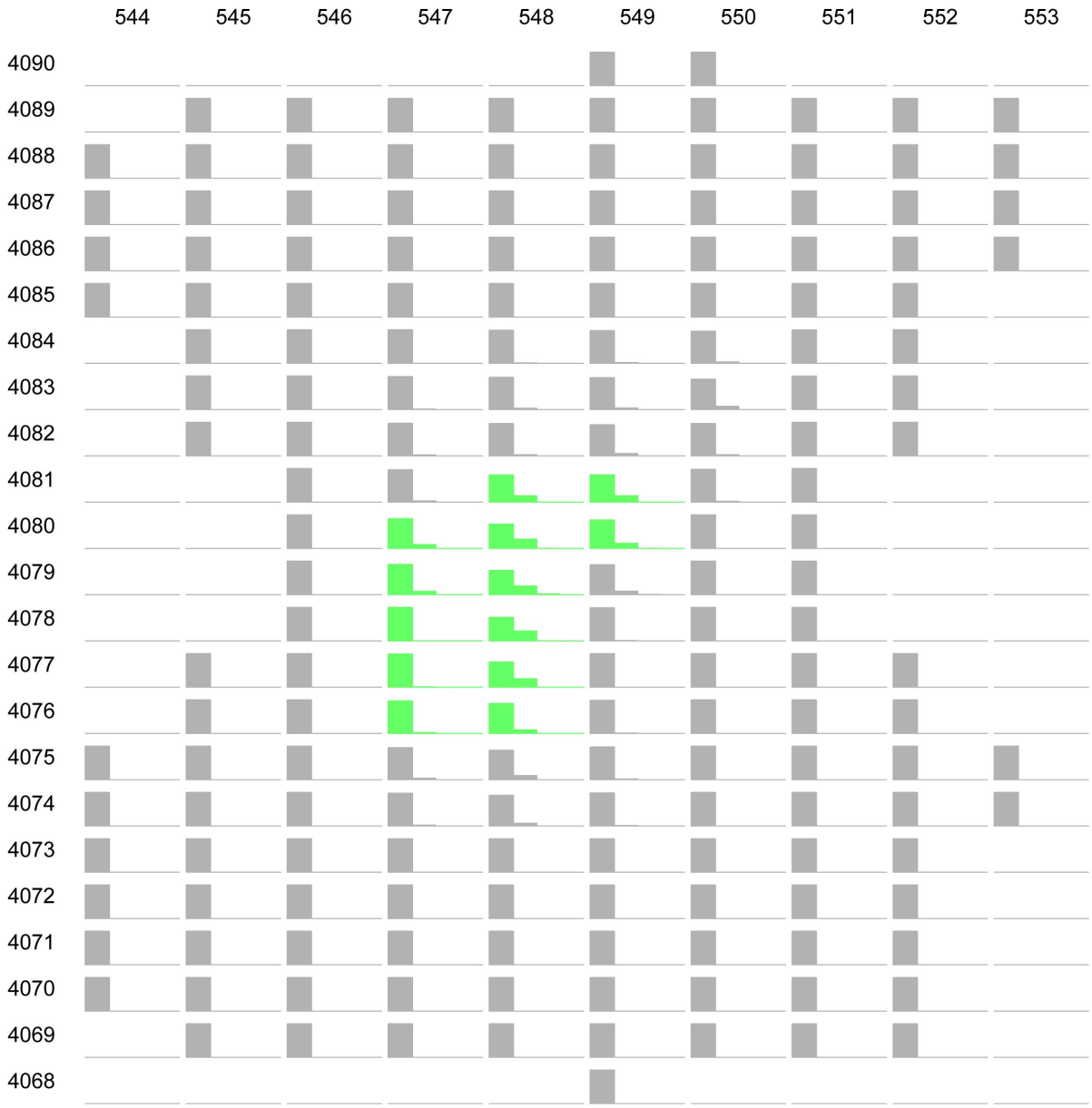

NOTE: Row and column labels represent grid points (UTM coordinates in km, NAD83) in the vicinity of the repository. Green plots show points inside or partially inside the repository footprint. Blank plots (e.g., in the upper left corner) indicate that the probability of intersection for an event at that location is zero. All other plots show the number of intersections conditional on at least one.

Figure 4.1.2-7. Schematic Showing the Distribution of the Number of Conduits That Intersect the Repository Footprint Given an Event at Each Grid Point, Given That at Least One Conduit Intersection Occurs (based on Bruce Crowe's event model associated with his steady-state and increasing rate models)

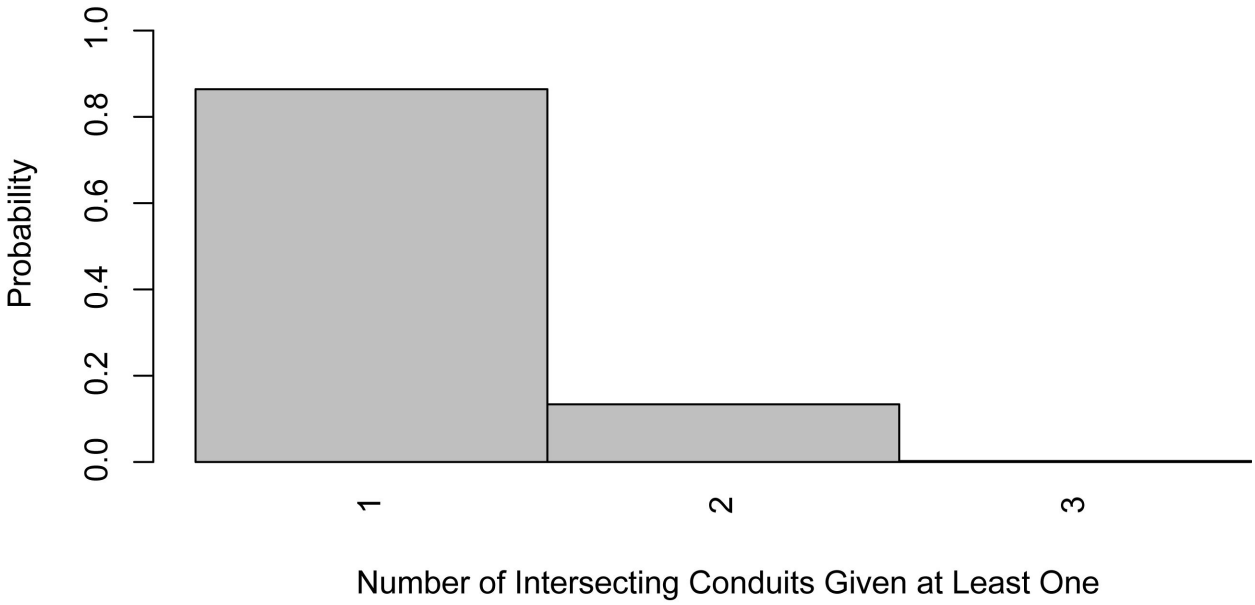

Figure 4.1.2-8. Conditional Distribution of the Number of Conduits That Intersect the Repository Footprint, Given That at Least One Conduit Intersection Occurs (based on Bruce Crowe's event model associated with his steady-state and increasing rate models)

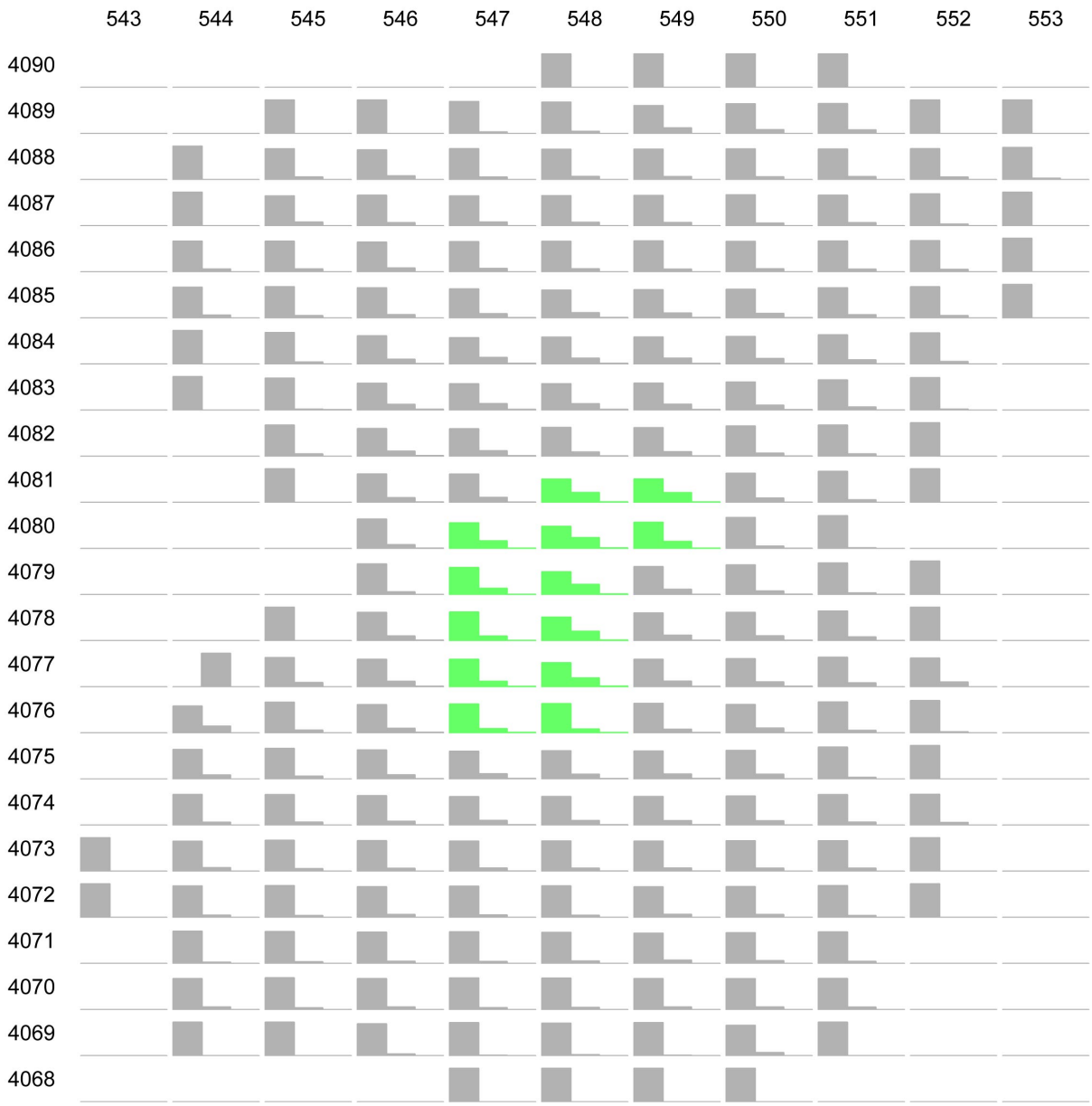

NOTE: Row and column labels represent grid points (UTM coordinates in km, NAD83) in the vicinity of the repository. Green plots show points inside or partially inside the repository footprint. Blank plots (e.g., in the upper left corner) indicate that the probability of intersection for an event at that location is zero. All other plots show the number of intersections conditional on at least one.

Figure 4.1.2-9. Schematic Showing the Distribution of the Number of Vents That Intersect the Repository Footprint Given an Event at Each Grid Point, Given That at Least One Vent Intersection Occurs (based on Bruce Crowe's event model associated with his steady-state and increasing rate models)

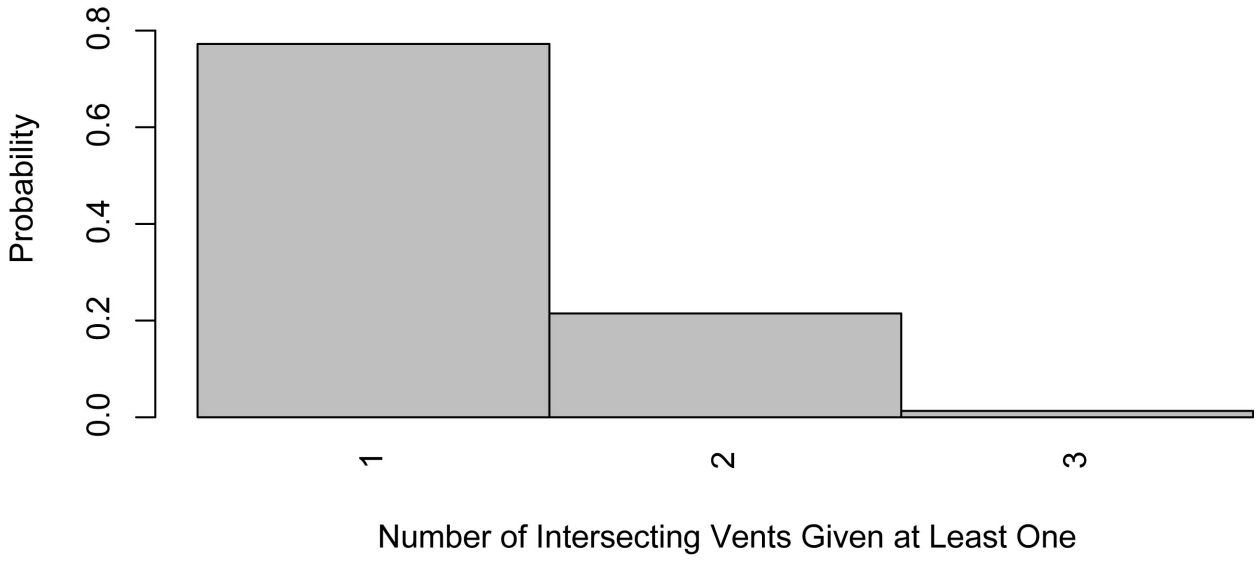

Figure 4.1.2-10. Conditional Distribution of the Number of Vents That Intersect the Repository Footprint, Given That at Least One Vent Intersection Occurs (based on Bruce Crowe's event model associated with his steady-state and increasing rate models)

4.1.2.3 Results at Different Future Times

The primary differences in BC's 10,000-year and 1-My assessments are that higher probabilities were assigned to the larger regions of interest, and higher probabilities were assigned to the new cycle and background rate models for the 1-My assessment. The inclusion of the new cycle rate model for the 1-My assessment also leads to the possibility of large-footprint events. The overall result of these differences is a slight increase in the overall uncertainty in the mean hazard estimate, as shown by the wider range of the 5th to 95th percentile in Figure 4.1.2-11. While the uncertainty in the hazard is greater for the 1My assessment than for the 10,000-year assessment, the mean and median hazard are both less, due to the higher probabilities assigned to the lower rate models and the larger regions of interest.

A sensitivity analysis parallel to that described above was conducted using the models for BC's 1-My assessment. The relative impact of each of the model components on the mean hazard for the 1-My assessment is the same as for the 10,000-year assessment. As a wider range of temporal models is used in the 1-My assessment, the contribution of the temporal model to overall uncertainty is greater for the 1-My assessment than for the 10,000-year assessment, as shown in Figure 4.1.2-12.

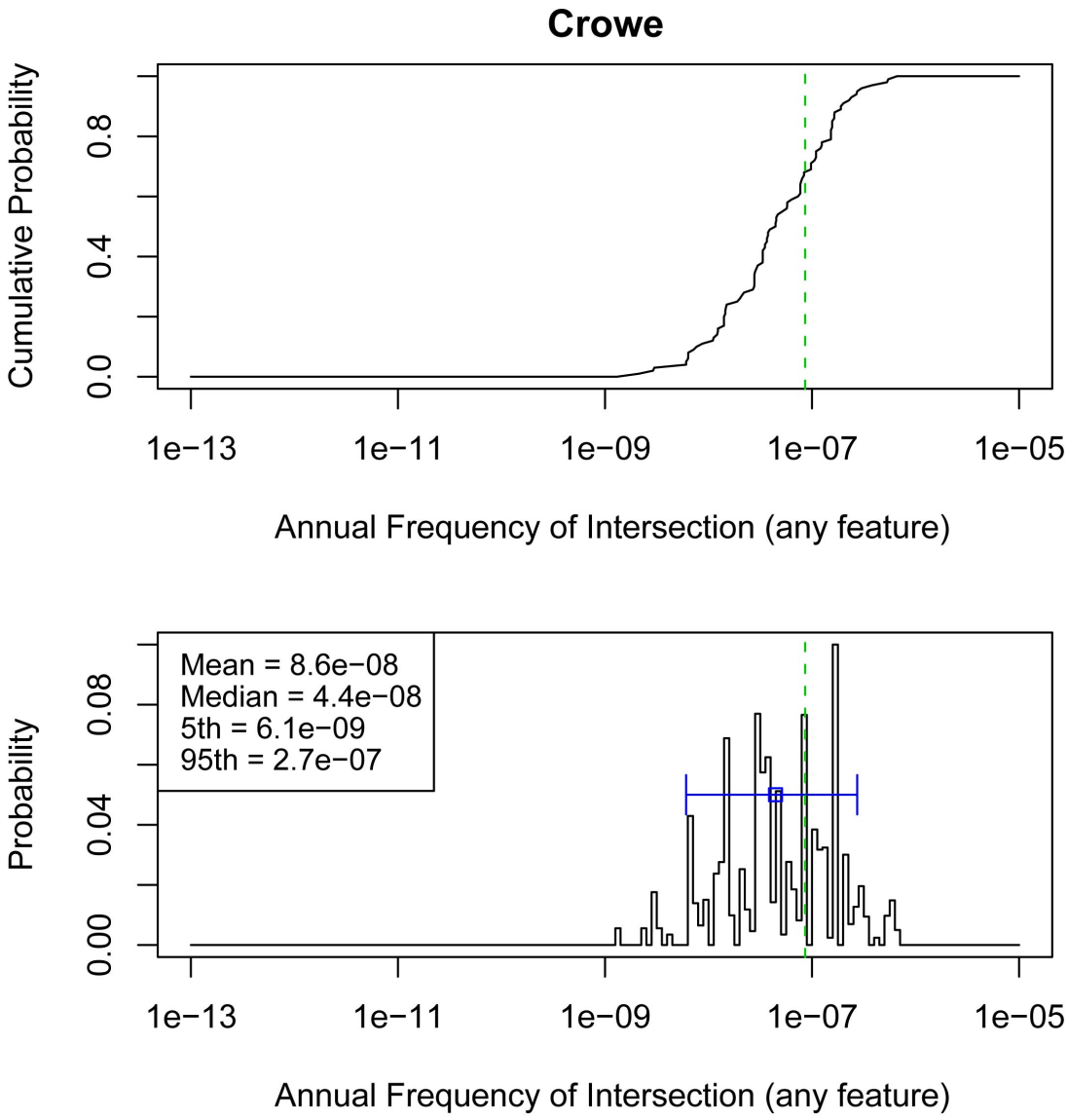

NOTE: Top figure is a cumulative distribution function, bottom figure is a probability mass function. The mean is shown by the dashed vertical line, the median with the open box, and the 5th to 95th percentiles with the horizontal line.

Figure 4.1.2-11. Hazard Results for the 1-My Assessment from PVHA-U Models Specified by Bruce Crowe

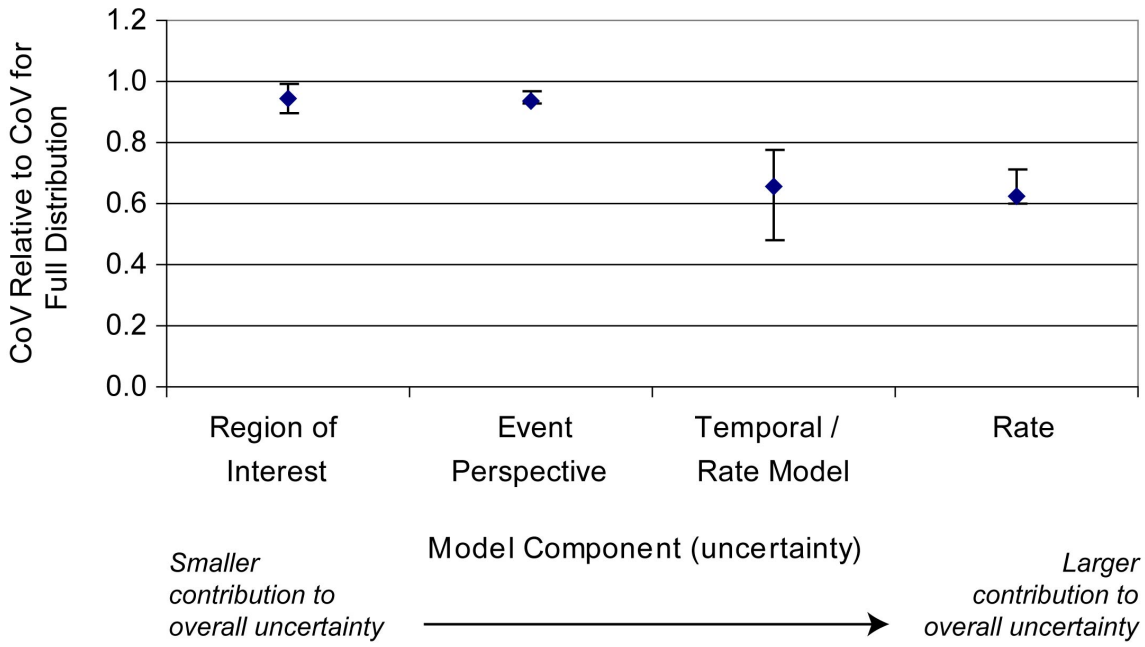

NOTE: Graph shows the CoV for the hazard distribution calculated with the specified model component fixed at each of its branch values, divided by the CoV for the full hazard distribution. Diamond shows the mean value with the relative CoV for each branch value weighted by its probability; "error bars" show the highest and lowest relative CoVs calculated across the branches for that model component.

Figure 4.1.2-12. Contribution of Uncertainty in Model Components to Overall Uncertainty in the Hazard Estimate, for PVHA-U Models for the 1-My Assessment Specified by Bruce Crowe

4.1.3 PVHA-U Results for William Hackett

This section describes the results of the PVHA-U models specified by William Hackett (WH). Those models and assessments are described in Section 3.2.3 and the elicitation summary in Appendix D. Section 4.1.3.1 discusses the results of the 10,000-year assessment for the frequency of intersection of any feature with the repository footprint. The frequency of intersection of specific features with the repository footprint is discussed in Section 4.1.3.2, and differences in the hazard calculated for the 10,000-year assessment and the 1-My assessment are discussed in Section 4.1.3.3.

4.1.3.1 Hazard Results for the 10,000-Year Assessment

Figure 4.1.3-1 summarizes the spatial distribution of hazard calculated using WH's PVHA-U models for the 10,000-year assessment. The spatial distribution of the mean frequency of intersection map in panel (c) looks like the conditional probability of intersection map in panel (b), as would be expected due to the small change in rate density across the area encompassed by a positive conditional probability of intersection. The effect of the region of interest boundary west of the repository footprint can be seen in the outer contours of the frequency of intersection map.

Figure 4.1.3-2 illustrates the uncertainty in the frequency of intersection of any feature with the repository footprint. The mean frequency of intersection is marked on both graphs by a dashed vertical line, and the median, 5th, and 95th percentiles are shown on the pmf. The mean frequency of intersection of any feature with the repository footprint is 4.7e-8; the median frequency is 3.1e-8. The 5th and 95th percentiles are 9.7e-9 and 1.6e-7, respectively.

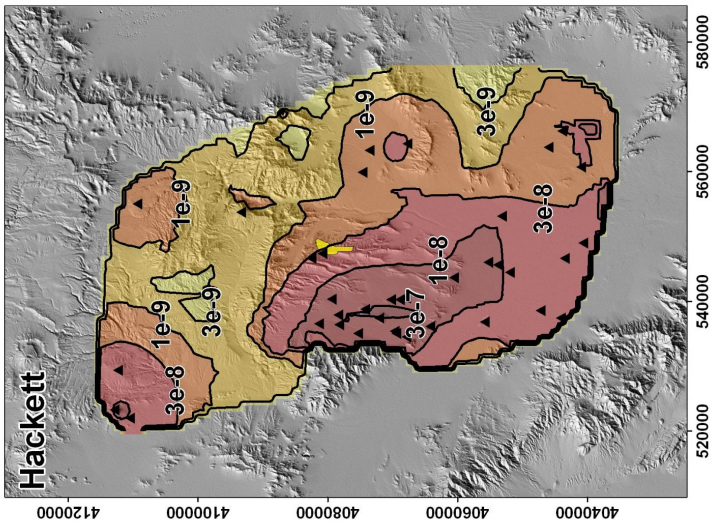

(a) Mean rate density. Contours represent the mean annual frequency of igneous events (events per year) per km^2.

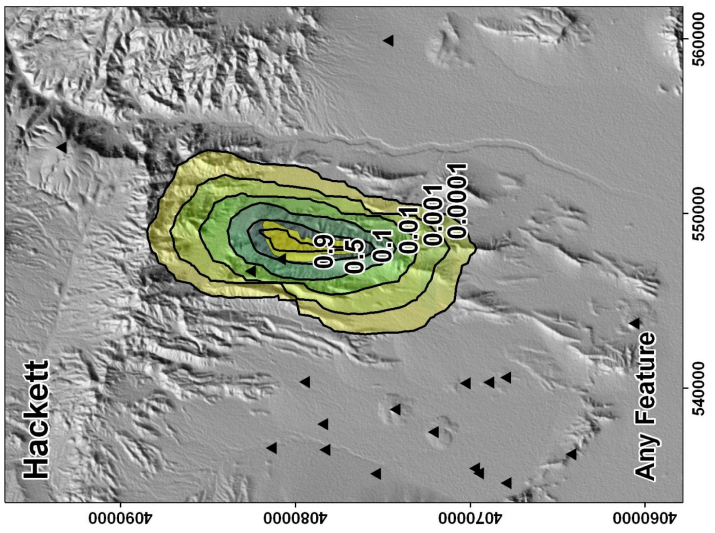

(b) Conditional probability of intersection of any feature. Contours represent the probability that an event assumed to occur at each location would result in the intersection of any igneous feature with the repository footprint.

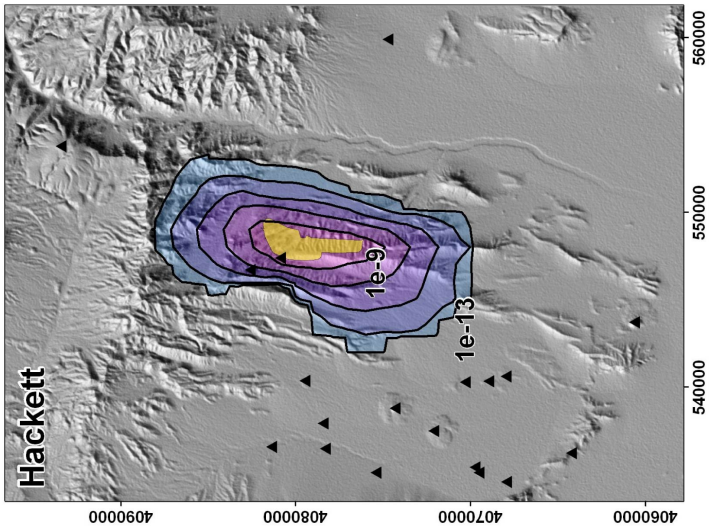

(c) Spatial distribution of the mean frequency of intersection. Contours represent the mean annual probability of an intersection of the repository footprint by an igneous feature.

NOTE: The repository footprint is shown as a yellow polygon. Past events are shown as black triangles. Map grid ticks are UTM meters; tick intervals for map (a) are 20 km; map (b) and (c) are 10 km.

Figure 4.1.3-1. Components of the Hazard Calculation for PVHA-U Models Specified by William Hackett, for the 10,000-Year Assessment

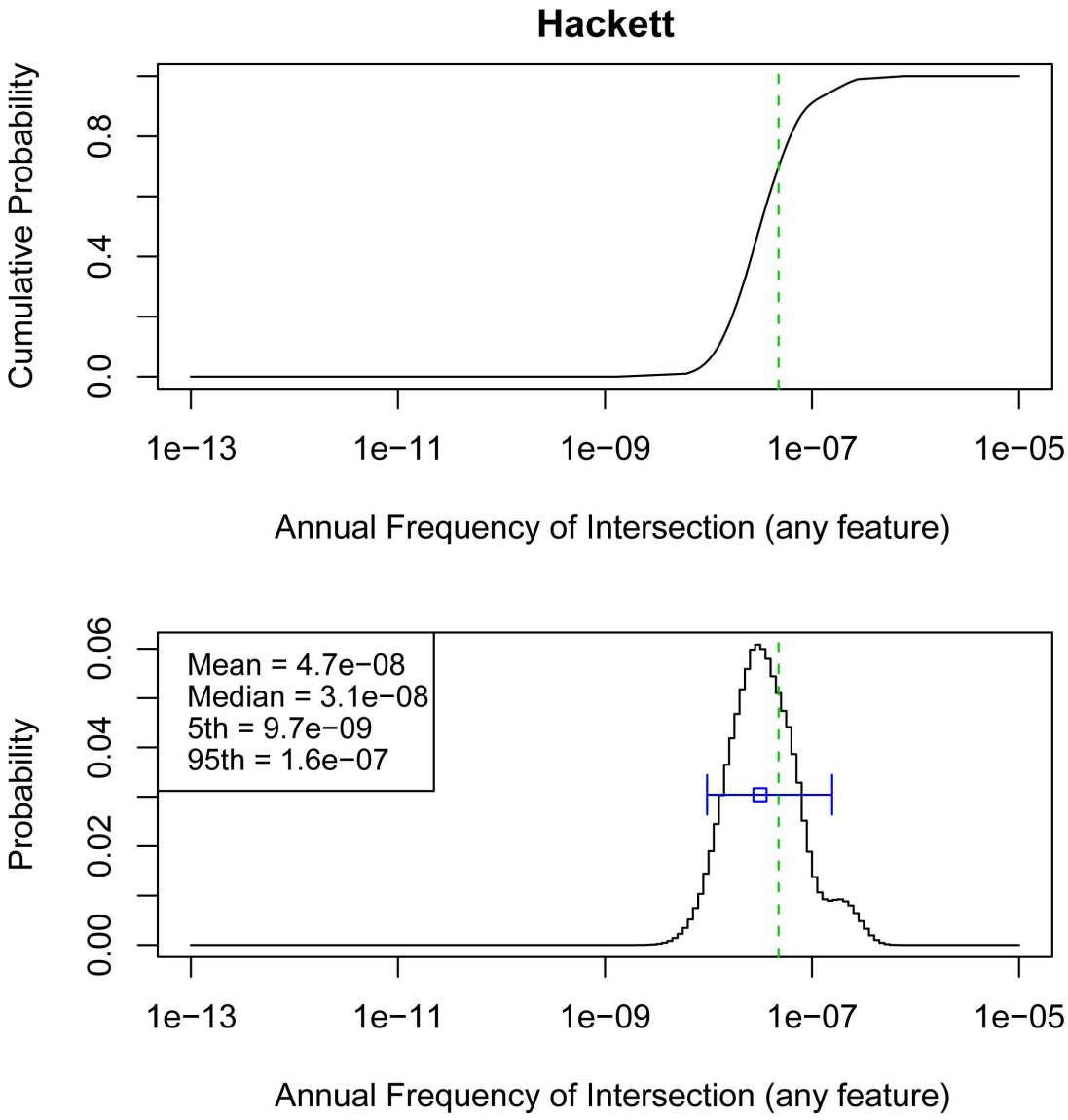

NOTE: Top figure is a cumulative distribution function, bottom figure is a probability mass function. The mean is shown by the dashed vertical line, the median with the open box, and the 5th to 95th percentiles with the horizontal line.

Figure 4.1.3-2. Hazard Results for the 10,000-Year Assessment from PVHA-U Models Specified by William Hackett

Contributions to Uncertainty

Contributions from various model components to uncertainty in the mean hazard in WH's models are illustrated in Figure 4.1.3-3. The four largest contributors to uncertainty in the mean hazard are all associated with the models used to estimate recurrence rate. Volume per event is the largest contributor, and the rate of change of cumulative volume (CV) over time is the third largest; together these parameters define the rate for the time-volume temporal approach. The uncertainty about the appropriate temporal modeling approach is the second largest contributor, and the uncertainty in the rate for the Poisson rate model is the fourth largest contributor to

uncertainty in the mean hazard. Note that in this figure, uncertainty related to the interpretation of past events is displayed for each event for which multiple interpretations were made. For example, the number of past events at Skull Mountain is interpreted to be either 3 or 6; the number of past events at Little Cones is interpreted to be either 1 or 2. The impacts of these alternative interpretations are explored one at a time, as those interpretations are independent. While the interpretation of each individual event has a small impact on the mean hazard, over the entire range of "past event sets,' the impact on mean hazard would be larger than displayed in Figure 4.1.3-3.

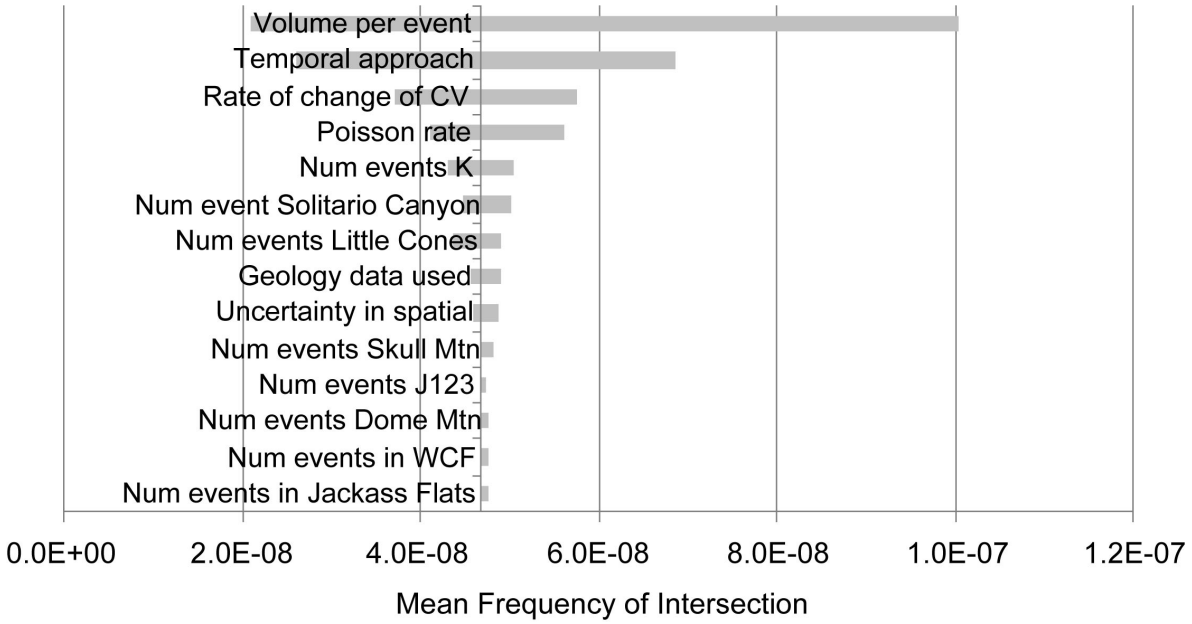

NOTE: Labels on each bar correspond to the nodes in the logic tree for WH's models as described in Section 3.2. The length of each bar shows the range of the mean hazard values that result from fixing the value of the specified model component at one of its branch values. This range represents the degree to which the mean hazard is affected by uncertainty in the specified model component. CV = cumulative volume; WCF = western Crater Flat; K, J, 1, 2, 3 are numbered/lettered anomalies.

Figure 4.1.3-3. Contribution of Uncertainty in Model Components to Uncertainty in the Mean Hazard, for PVHA-U Models for the 10,000-Year Assessment Specified by William Hackett

Contributions of various model components to *overall uncertainty* in the hazard for WH's models are shown in Figure 4.1.3-4. For WH's models, the impacts of the model components on the overall uncertainty are very similar to their impacts on uncertainty in the mean hazard: the uncertainty in hazard is most sensitive to uncertainties related to the temporal model, and significantly less sensitive to the uncertainties associated with the spatial model. Although the "average" impact of uncertainty in the Poisson rate on the relative CoV is small, note that the impact of a specific rate (the high or the low rate), if selected to represent that rate, may result in a greater change to the relative CoV, leading to an increase or decrease in CoV by about 20%.

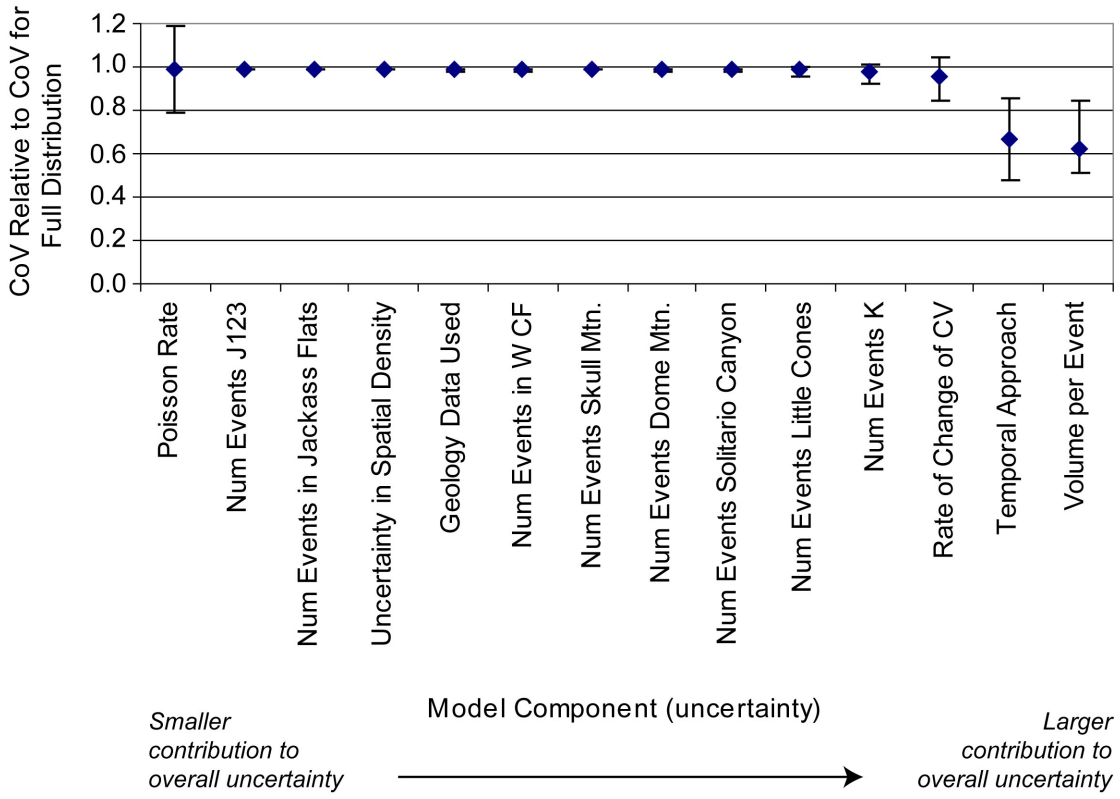

NOTE: Graph shows the CoV for the hazard distribution calculated with the specified model component fixed at each of its branch values, divided by the CoV for the full hazard distribution. Diamond shows the mean value with the relative CoV for each branch value weighted by its probability; "error bars" show the highest and lowest relative CoVs calculated across the branches for that model component. CV = cumulative volume; WCF = western Crater Flat; K, J, 1, 2, 3 are numbered/lettered anomalies.

Figure 4.1.3-4. Contribution of Uncertainty in Model Components to Overall Uncertainty in the Hazard Estimate, for PHVA-U Models for the 10,000-Year Assessment Specified by William Hackett

4.1.3.2 Discussion of Individual Features

As described in Section 3.2.3, WH's events all include dikes, and might also include column-producing conduits, non-column-producing vents, and sills. The conditional probability of intersection of each type of feature with the repository footprint was illustrated in Section 3.2.3, and, as discussed, the shape of the conditional probability of intersection maps for each individual feature is the same as for the conditional probability of intersection for any feature: no particular clustering or grouping of individual features in an event occurs. Similarly, the full distribution of the frequency of intersection for any individual feature follows the same pattern as the distribution for any feature shown in Figure 4.1.3-2, simply shifted to the lower frequencies associated with the individual feature.

Table 4.1.3-1 shows the mean and median frequencies of intersection for each feature.

Table 4.1.3-1. Mean and Median Frequency of Intersection of Various Igneous Features with the Repository Footprint, for William Hackett's 10,000-Year Assessment

Feature	Mean Frequency of Intersection	Median Frequency of Intersection
Any feature	4.7e-8	3.1e-8
Dikes	4.7e-8	3.1e-8
Column-producing conduits	1.7e-8	1.1e-8
Vents	7.0e-9	4.6e-9
Sills	5.9e-11	3.8e-11

Potential for Multiple Intersections

Figure 4.1.3-5 shows a set of plots illustrating the distribution of the number of dike intersections for an event centered at a specific point, conditional on at least one such intersection occurring. Because WH's events are much more likely to include one dike than to include multiple dikes, the most likely number of intersections across the region as shown in the figure is one, but multiple dike intersections are possible depending on the event location. Figure 4.1.3-6 combines the relative likelihood of a dike intersection at each point with the conditional distribution of the number of dike intersections for an event at those points to yield a conditional distribution on the number of dike intersections, given that at least one such intersection occurs. As shown, assuming that a dike intersection occurs, it is most likely (probability of 0.78) that only one dike intersects, but the potential exists for as many as 5 intersections. Four intersections have a probability of 0.005; five intersections have a probability of about 0.0001.

Figures 4.1.3-7 and 4.1.3-8 show the same data for conduits: the distribution on number of conduit intersections given at least one conduit intersects the footprint. Given a conduit intersection, it is most likely that only one such intersection would occur, as expected from the assessment that the most likely number of conduits in an event is one (as described in Section 3.2.3). While vents are less likely than conduits in WH's event descriptions, their relative locations and sizes are otherwise described by the same models, so the *conditional* frequency of vent intersection, as shown in Figures 4.1.3-9 and 4.1.3-10, follows that just described for conduits.

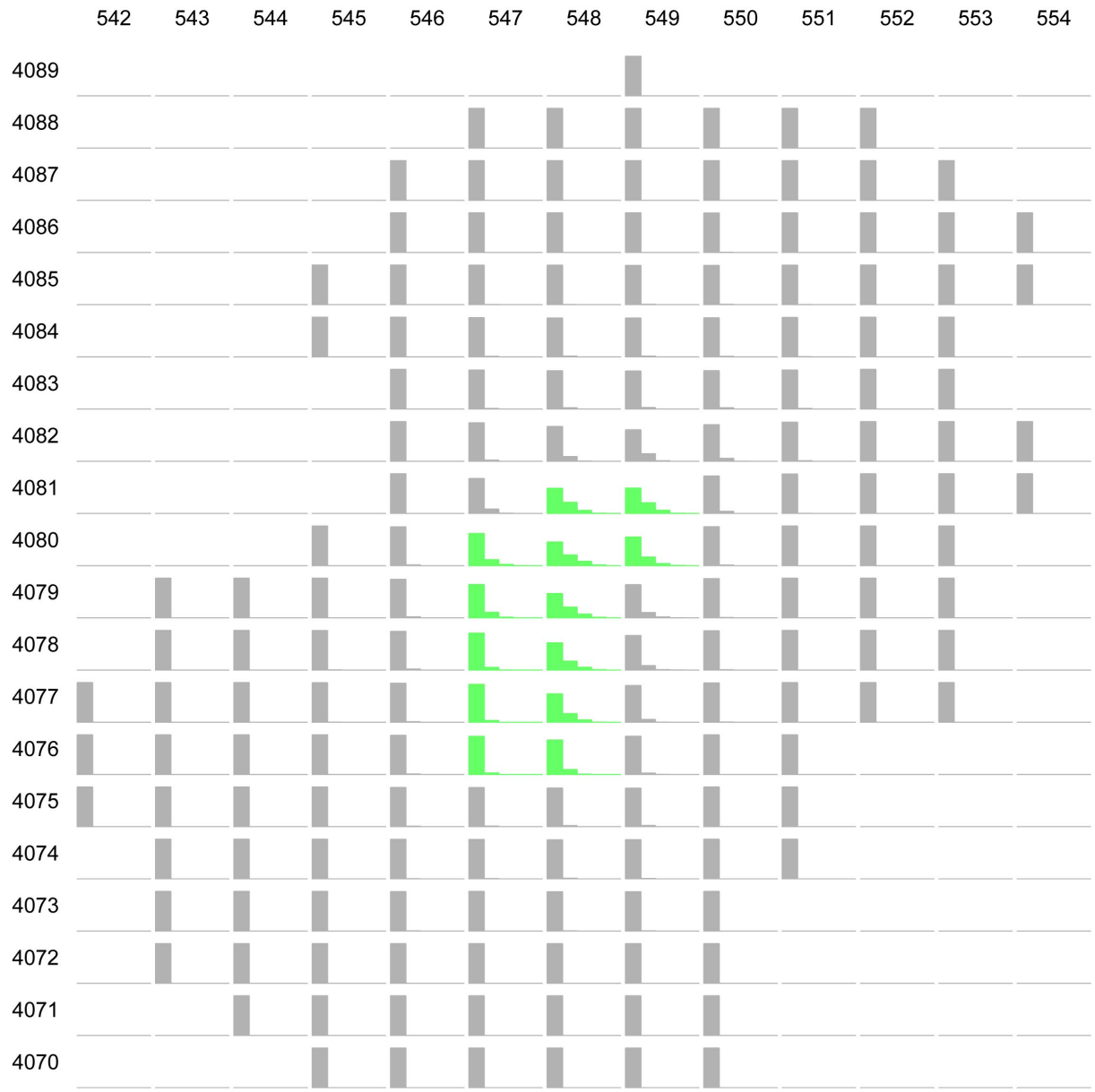

NOTE: Row and column labels represent grid points (UTM coordinates in km, NAD83) in the vicinity of the repository. Green plots show points inside or partially inside the repository footprint. Blank plots (e.g., in the upper left corner) indicate that the probability of intersection for an event at that location is zero. All other plots show the number of intersections conditional on at least one.

Figure 4.1.3-5. Schematic Showing the Distribution of the Number of Dikes That Intersect the Repository Footprint Given an Event at Each Grid Point, Given That at Least One Dike Intersection Occurs (for events defined by William Hackett)

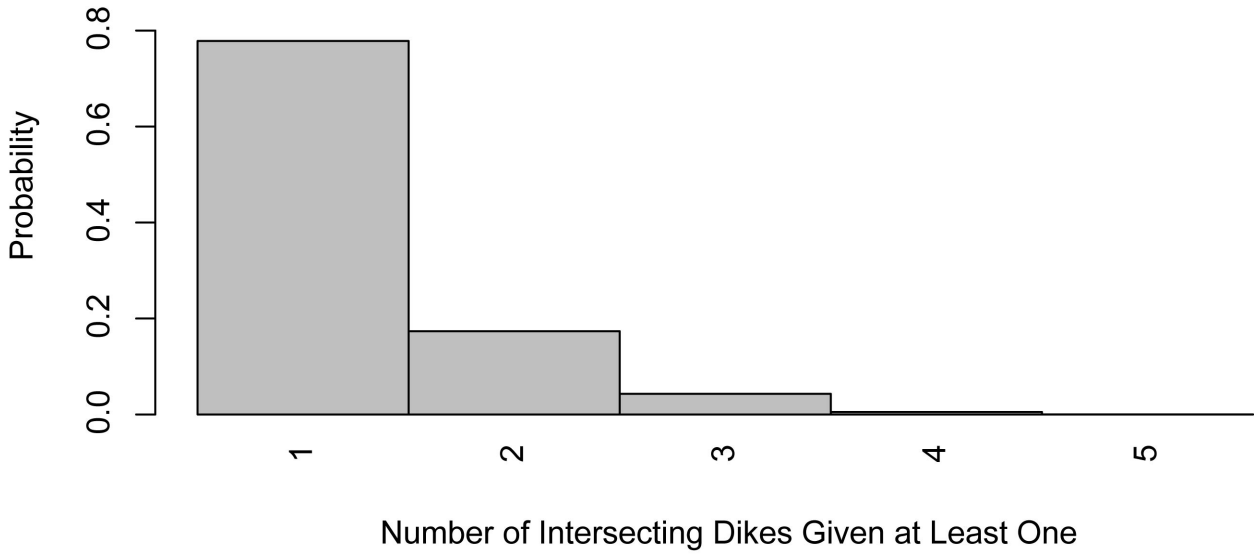

Figure 4.1.3-6. Conditional Distribution of the Number of Dikes That Intersect the Repository Footprint, Given That at Least One Dike Intersection Occurs (for events defined by William Hackett)

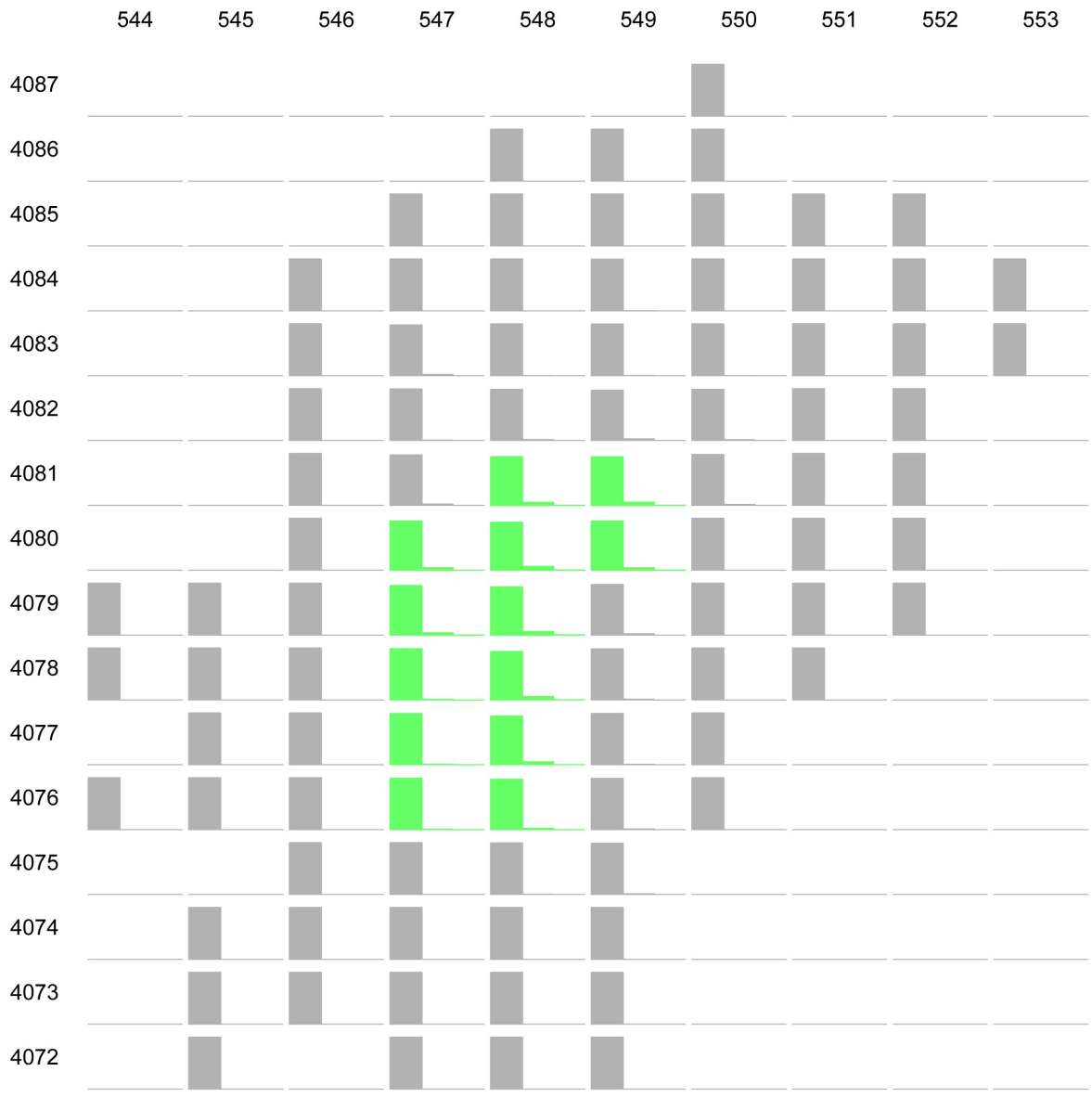

NOTE: Row and column labels represent grid points (UTM coordinates in km, NAD83) in the vicinity of the repository. Green plots show points inside or partially inside the repository footprint. Blank plots (e.g., in the upper left corner) indicate that the probability of intersection for an event at that location is zero. All other plots show the number of intersections conditional on at least one.

Figure 4.1.3-7. Schematic Showing the Distribution of the Number of Conduits That Intersect the Repository Footprint Given an Event at Each Grid Point, Given That at Least One Conduit Intersection Occurs (for events defined by William Hackett)

Figure 4.1.3-8. Conditional Distribution of the Number of Conduits That Intersect the Repository Footprint, Given That at Least One Conduit Intersection Occurs (for events defined by William Hackett)

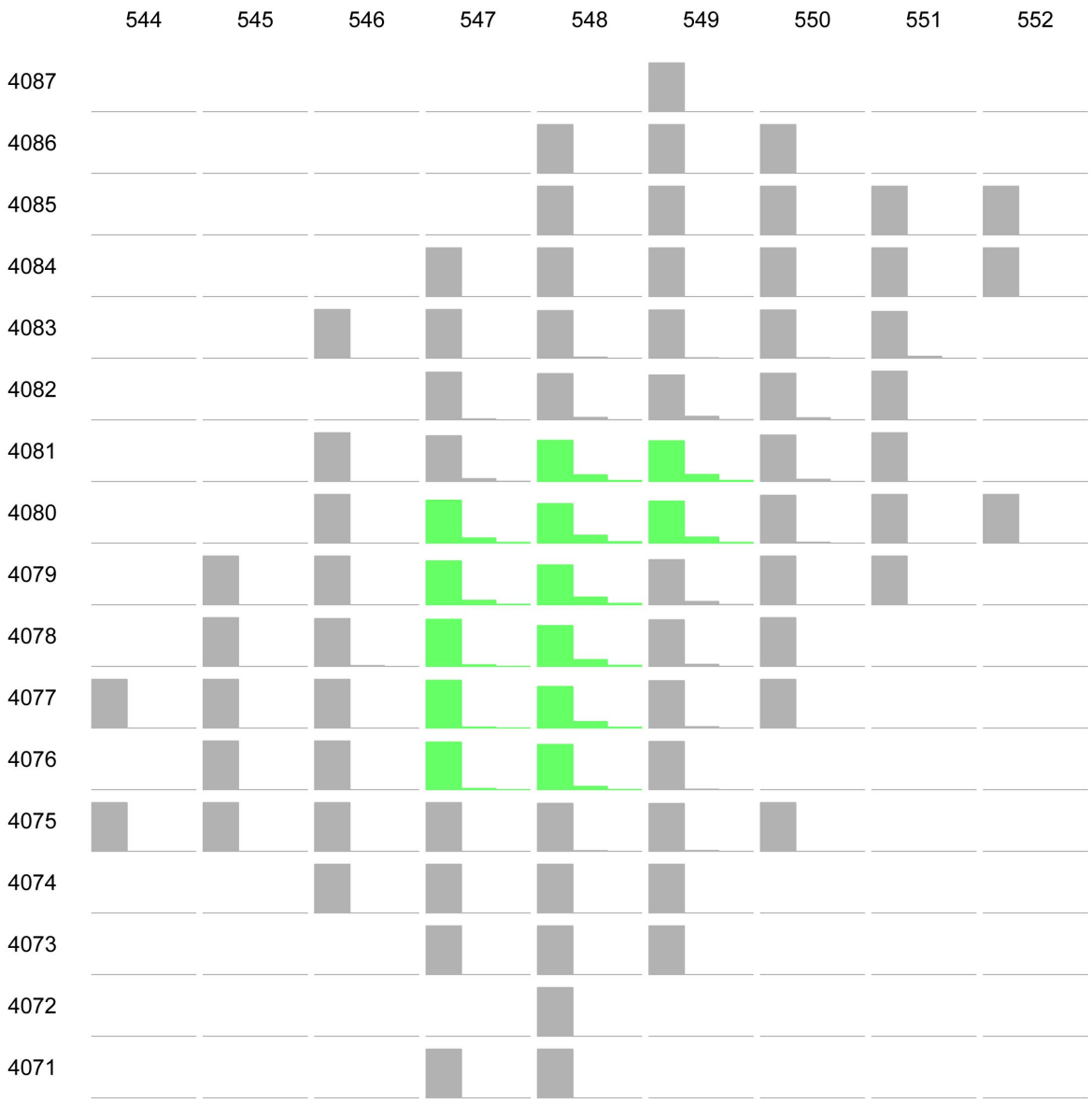

NOTE: Row and column labels represent grid points (UTM coordinates in km, NAD83) in the vicinity of the repository. Green plots show points inside or partially inside the repository footprint. Blank plots (e.g., in the upper left corner) indicate that the probability of intersection for an event at that location is zero. All other plots show the number of intersections conditional on at least one.

Figure 4.1.3-9. Schematic Showing the Distribution of the Number of Vents That Intersect the Repository Footprint Given an Event at Each Grid Point, Given That at Least One Vent Intersection Occurs (for events defined by William Hackett)

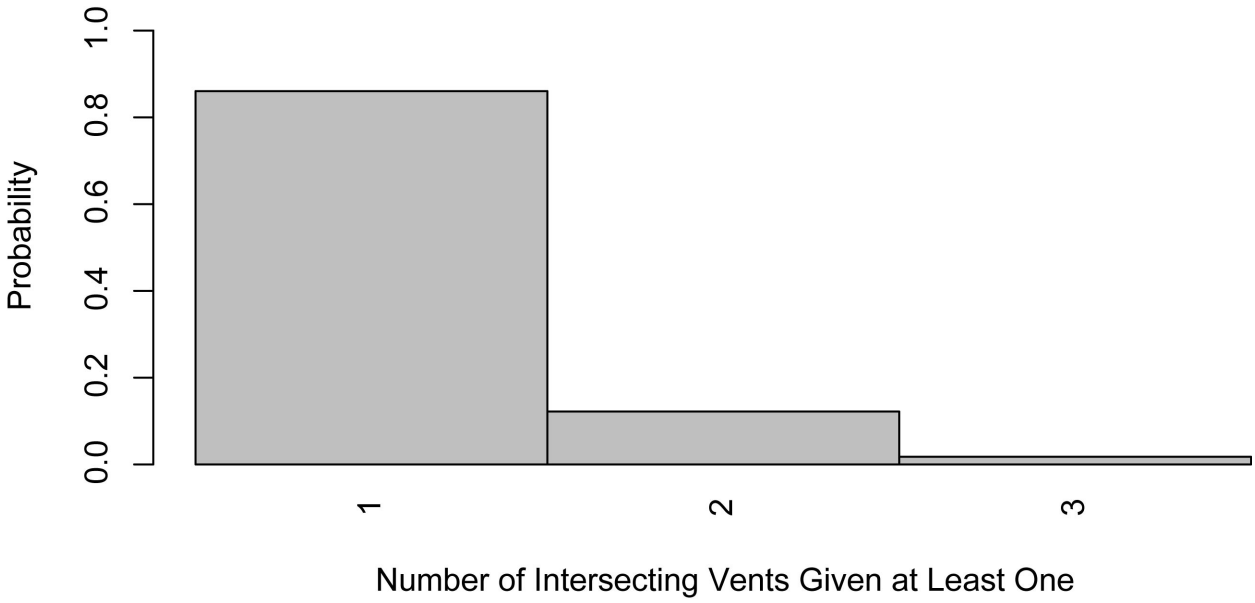

Figure 4.1.3-10. Conditional Distribution of the Number of Vents That Intersect the Repository Footprint, Given That at Least One Vent Intersection Occurs (for events defined by William Hackett)

4.1.3.3 Results at Different Future Times

WH defined one set of models as applying to both the 10,000-year and 1-My assessments. Those models include a time-volume model that leads to a time-dependent rate estimate. The mean frequency of intersection for the 1-My assessment for WH's models is 4.1e-8, slightly less than for the 10,000-year assessment. No meaningful differences were identified in the CDF and pmf graphs, nor in the contributions to uncertainty for the 1-My versus the 10,000-year assessments.

4.1.4 PVHA-U Results for Mel Kuntz

This section describes the results of the PVHA-U models specified by Mel Kuntz (MK). Those models and assessments are described in Section 3.2.4 and the elicitation summary in Appendix D. Section 4.1.4.1 discusses the results of the 10,000-year assessment for the frequency of intersection of any feature with the repository footprint. The frequency of intersection of specific features with the repository footprint is discussed in Section 4.1.4.2, and differences in the hazard calculated for the 10,000-year assessment and the 1-My assessment are discussed in Section 4.1.4.3.

4.1.4.1 Hazard Results for the 10,000-Year Assessment

Figure 4.1.4-1 summarizes the spatial distribution of hazard calculated using MK's PVHA-U models for the 10,000-year assessment. The contours extend further to the SSW of the repository footprint than to the NNE, reflecting both the greater rate density in the Crater Flat area and the large spatial extent of the conditional probability of intersection. Events located in the higher rate density Crater Flat zone have about a 0.001 or greater probability of intersection, as shown in panel (b).

Figure 4.1.4-2 illustrates the uncertainty in the frequency of intersection of any feature with the repository footprint. The mean frequency of intersection is marked on both graphs by a dashed vertical line, and the median, 5th, and 95th percentiles are shown on the pmf. The mean frequency of intersection of any feature with the repository footprint is 1.8e-8; the median frequency is 1.4e-8. The 5th and 95th percentiles are 4.8e-9 and 3.6e-8, respectively.

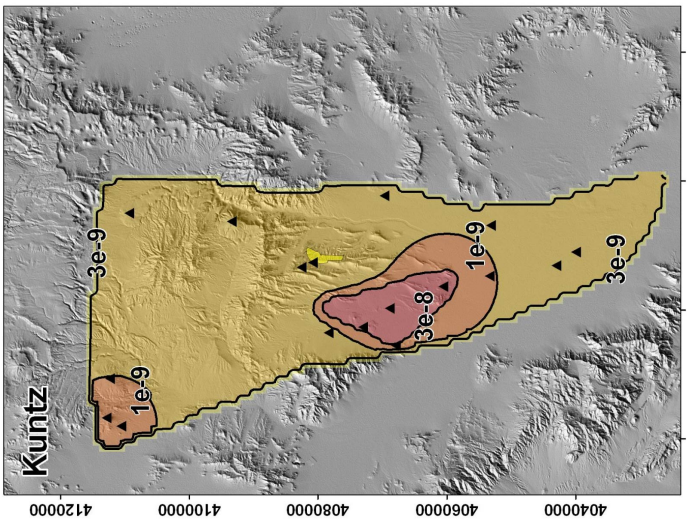

(a) Mean rate density. Contours represent the mean annual frequency of igneous events (events per year) per km^2.

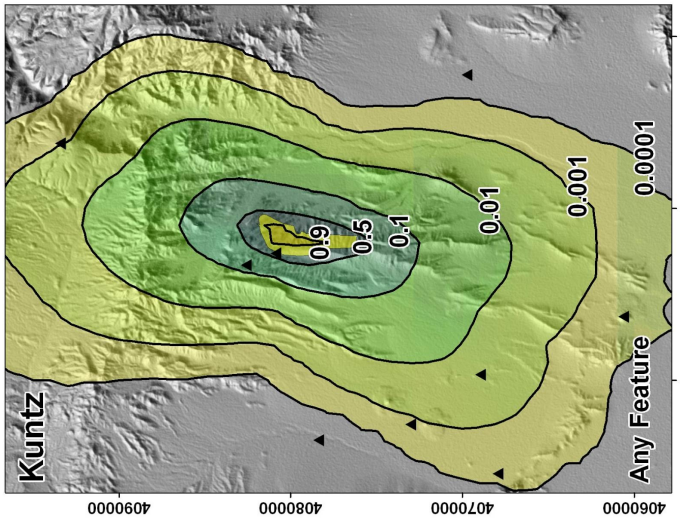

(b) Conditional probability of intersection of any feature. Contours represent the probability that an event assumed to occur at each location would result in the intersection of any igneous feature with the repository footprint.

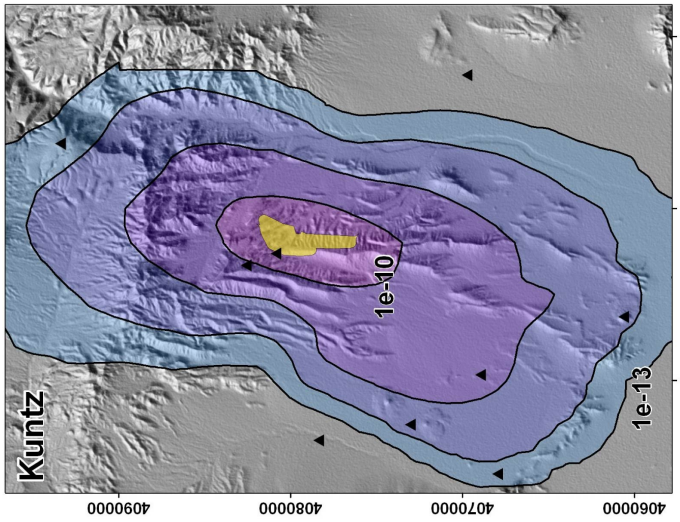

(c) Spatial distribution of the mean frequency of intersection. Contours represent the mean annual probability of an intersection of the repository footprint by an igneous feature.

NOTE: The repository footprint is shown as a yellow polygon. Past events are shown as black triangles. Map grid ticks are UTM meters; tick intervals for map (a) are 20 km; map (b) and (c) are 10 km.

Figure 4.1.4-1. Components of the Hazard Calculation for PVHA-U Models Specified by Mel Kuntz, for the 10,000-Year Assessment

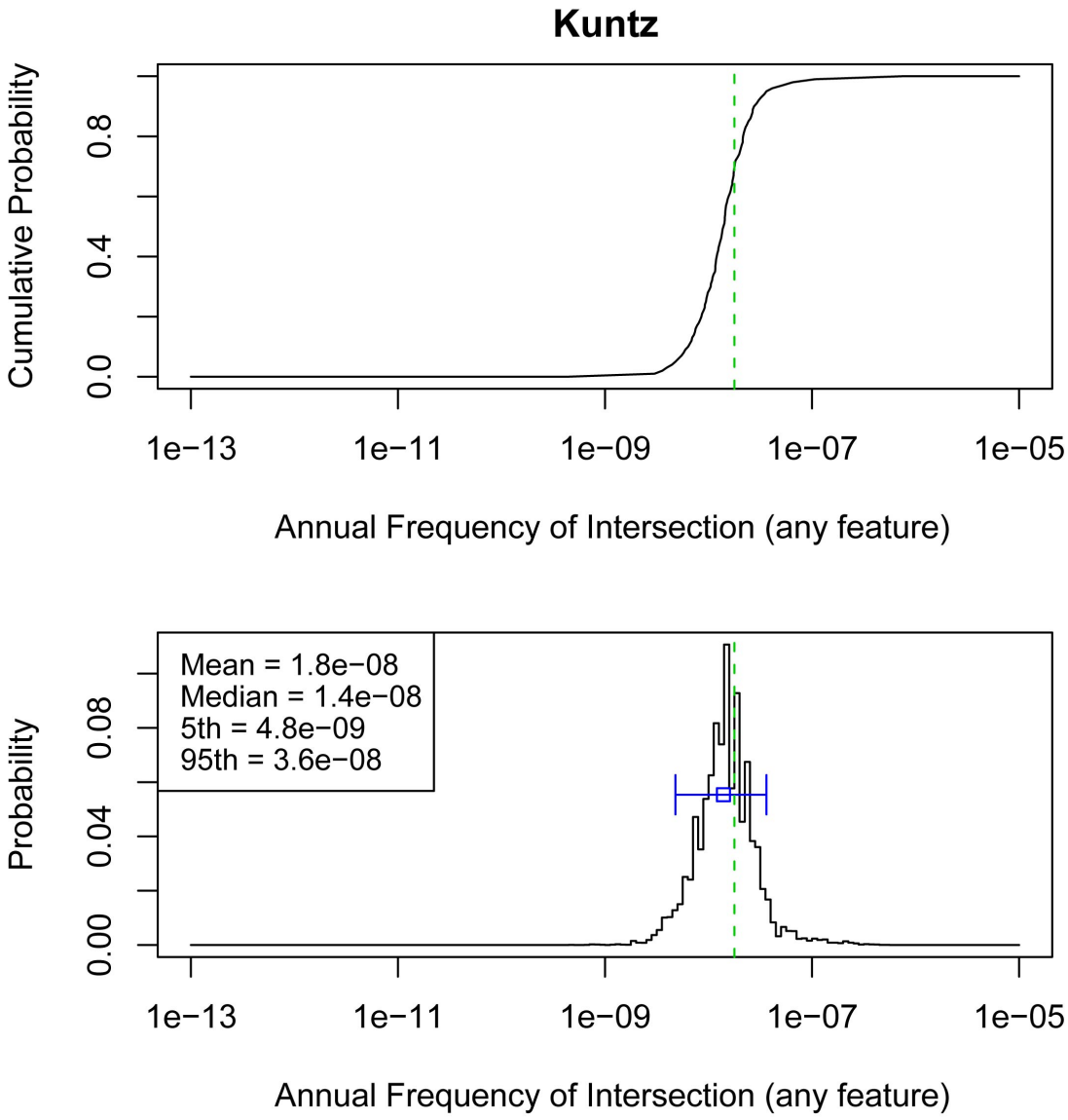

NOTE: Top figure is a cumulative distribution function, bottom figure is a probability mass function. The mean is shown by the dashed vertical line, the median with the open box, and the 5th to 95th percentiles with the horizontal line.

Figure 4.1.4-2. Hazard Results for the 10,000-Year Assessment from PVHA-U Models Specified by Mel Kuntz

Contributions to Uncertainty

Contributions from various model components to uncertainty in the mean hazard in MK's models are illustrated in Figure 4.1.4-3. The largest impact on the uncertainty in the mean hazard comes from the alternative temporal modeling approaches. The alternative temporal modeling approaches also incorporate modeling assumptions about the spatial distribution. As shown in the logic tree for MK's 10,000-year assessment in Section 3.2.4, the locally homogenous zones model is associated strictly with a homogenous Poisson rate model, with different rates in the Crater Flat zone and the background zone (the region of interest outside of

the Crater Flat zone). The geology-informed spatial smoothing model is associated with both a homogenous Poisson rate model (weighted 60%) and with a time-volume rate model. When only the homogenous Poisson model is used, the mean hazard is 1.4e-8, and when only the time-volume model is used (and thus only the geology-informed spatial smoothing approach), the mean hazard is 4.26e-8. These values represent the two ends of the "Temporal model" bar at the top of the figure. Because of the high probability assigned to the locally homogenous zone model, the uncertainty in the Poisson rate in the background zone also has a large impact on the mean hazard (as shown by the second bar in the figure). The mean hazard is somewhat sensitive to every model component, which is consistent with the high degree of interdependency within this model.

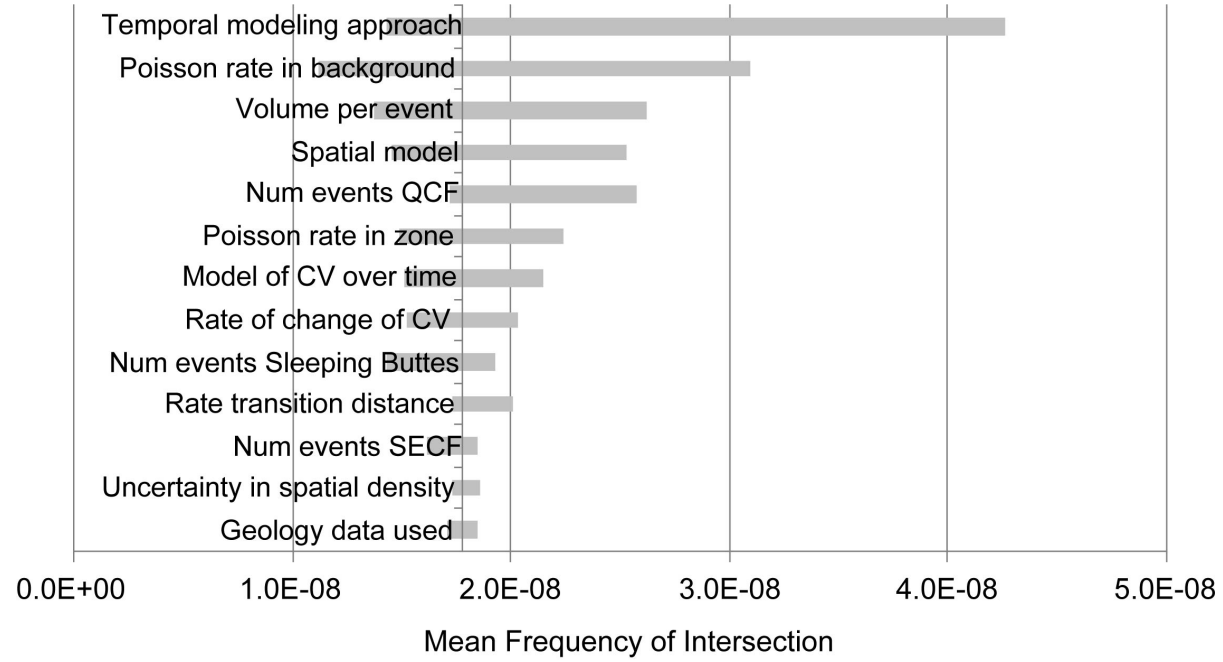

NOTE: Labels on each bar correspond to the nodes in the logic tree for MK's models as described in Section 3.2. The length of each bar shows the range of the mean hazard values that result from fixing the value of the specified model component at one of its branch values. This range represents the degree to which the mean hazard is affected by uncertainty in the specified model component. QCF = Quaternary Crater Flat; CV = cumulative volume; SECF = Southeast Crater Flat.

Figure 4.1.4-3. Contribution of Uncertainty in Model Components to Uncertainty in the Mean Hazard, for the PVHA-U Models for the 10,000-Year Assessment Specified by Mel Kuntz

Contributions of various model components to *overall uncertainty* in the hazard for MK's model are shown in Figure 4.1.4-4. On average, the uncertainty about the temporal modeling approach has the largest impact on the overall uncertainty in the hazard, shown by the location of the diamond on the far right side of the figure. Setting the temporal modeling approach to be the homogenous Poisson model reduces the relative CoV by a little over 50% while setting the temporal modeling approach to be the time-volume model has almost no effect on the relative CoV, as shown by the ends of the "error bars" associated with the "Temporal modeling approach" on the right side of the figure. Although the "average" impact of uncertainty in the Poisson rate in the background zone is very small (far left of the figure), note that the impact of a specific rate (the high or the low value), if selected to represent that rate, might result in a greater

change to the relative CoV, leading to either a large increase or a large decrease in the CoV. The large potential impact of this model component is partly a result of the fact that a 9-point approximation was used to represent this rate, which results in the inclusion of branches explicitly capturing the tails of the rate distribution, albeit with very low probabilities. The end-points on sensitivity figures such as these do not reflect or indicate that they could represent very low probability models.

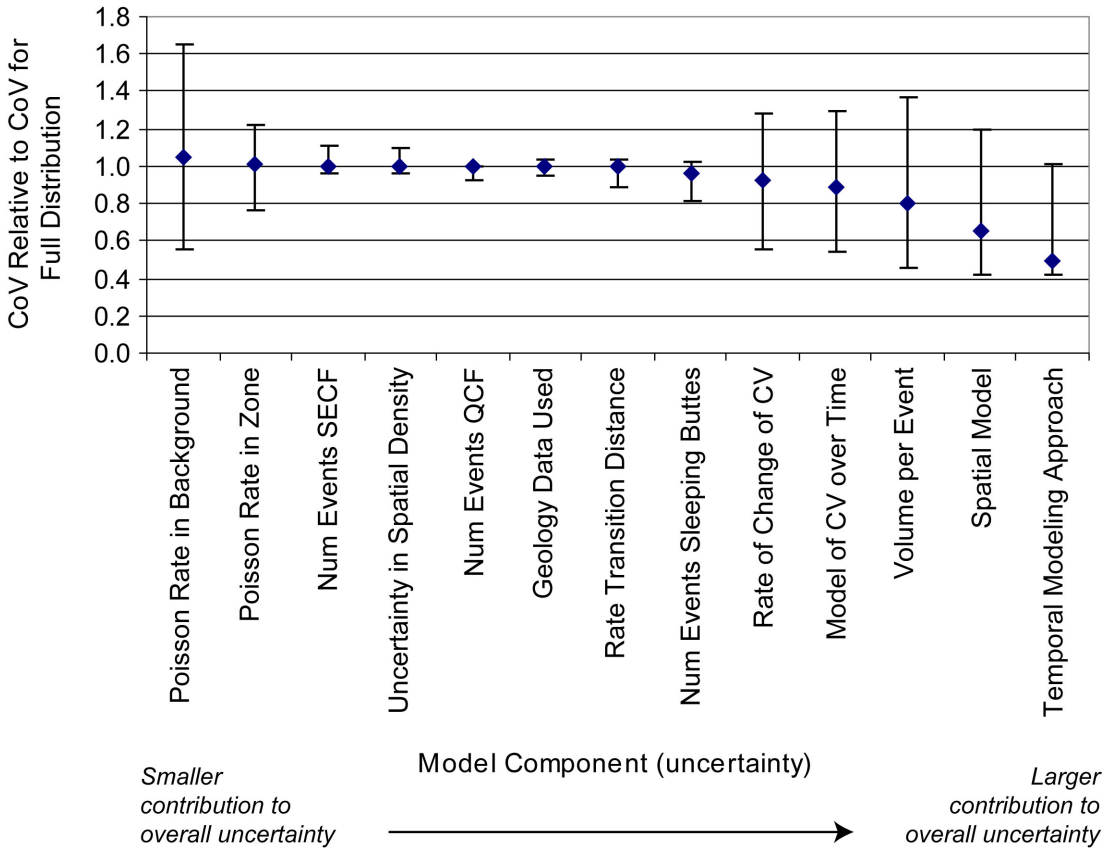

NOTE: Graph shows the CoV for the hazard distribution calculated with the specified model component fixed at each of its branch values, divided by the CoV for the full hazard distribution. Diamond shows the mean value with the relative CoV for each branch value weighted by its probability; "error bars" show the highest and lowest relative CoVs calculated across the branches for that model component. QCF = Quaternary Crater Flat; CV = cumulative volume; SECF = Southeast Crater Flat.

Figure 4.1.4-4. Contribution of Uncertainty in Model Components to Overall Uncertainty in the Hazard Estimate, for the PHVA-U Models for the 10,000-Year Assessment Specified by Mel Kuntz

4.1.4.2 Discussion of Individual Features

As described in Section 3.2.4, MK's events all include dikes, and might also include column-producing conduits, non-column producing vents, and sills. The conditional probability of intersection of each type of feature with the repository footprint was illustrated in Section 3.2.4, and, as discussed, the shape of the conditional probability of intersection maps for each individual feature is the same as for the conditional probability of intersection for any feature: no

particular clustering or grouping of individual features in an event occurs. Similarly, the full distribution of the frequency of intersection for any individual feature follows the same pattern as the distribution for any feature shown in Figure 4.1.4-2, simply shifted to the lower frequencies associated with the individual feature.

Table 4.1.4-1 shows the mean and median frequencies of intersection for each feature.

Table 4.1.4-1. Mean and Median Frequency of Intersection of Various Igneous Features with the Repository Footprint, for Mel Kuntz's 10,000-Year Assessment

Feature	Mean Frequency of Intersection	Median Frequency of Intersection
Any feature	1.8e-8	1.4e-8
Dikes	1.8e-8	1.4e-8
Column-producing conduits	4.3e-9	3.4e-9
Vents	1.2e-9	9.3e-10
Sills	2.7e-10	2.1e-11

Potential for Multiple Intersections

Figure 4.1.4-5 shows a set of plots illustrating the distribution of the number of dike intersections for an event centered at a specific point, conditional on at least one such intersection occurring. Because MK's events have the potential to be quite large (as shown by the conditional probability of intersection maps in Section 3.2.4 and in panel (b) of Figure 4.1.4-1), and the ability to read the plots on Figure 4.1.4-5 is limited by the page size, this figure was produced only for event locations with probabilities of dike intersection greater than 5% (similar graphs for other experts include any event location with a non-zero probability of dike intersection or, in some cases, event locations with a conditional probability of intersection greater than 1%). The most likely number of intersections across the region as shown in the figure is one, but multiple dike intersections are possible depending on the event location (e.g., event locations inside the repository footprint). Figure 4.1.4-6 combines the relative likelihood of a dike intersection at each point with the conditional distribution of the number of dike intersections for events at those points to yield a conditional distribution on the number of dike intersections, given that at least one such intersection occurs. As shown, assuming a dike intersection occurs, it is most likely (probability 0.83) that only one dike intersects, but the potential exists for as many as 6 intersections. Four intersections have a probability of 0.002; five intersections have a probability of about 0.00004.

Figures 4.1.4-7 and 4.1.4-8 show the same data for conduits: the distribution on the number of conduit intersections given at least one conduit intersects the footprint. Given a conduit intersection, it is most likely that only one such intersection would occur, but there is potential for as many as six conduit intersections (the probability of six intersections is 0.0004). The frequency of non-column producing vents is a function of the total dike length and the total number of features venting to the surface (conduits and vents). While the overall frequency of intersection for vents is less than for a column-producing conduit, the total possible number of intersecting vents is greater. Figures 4.1.4-9 and 4.1.4-10 show the conditional number of vent intersections.

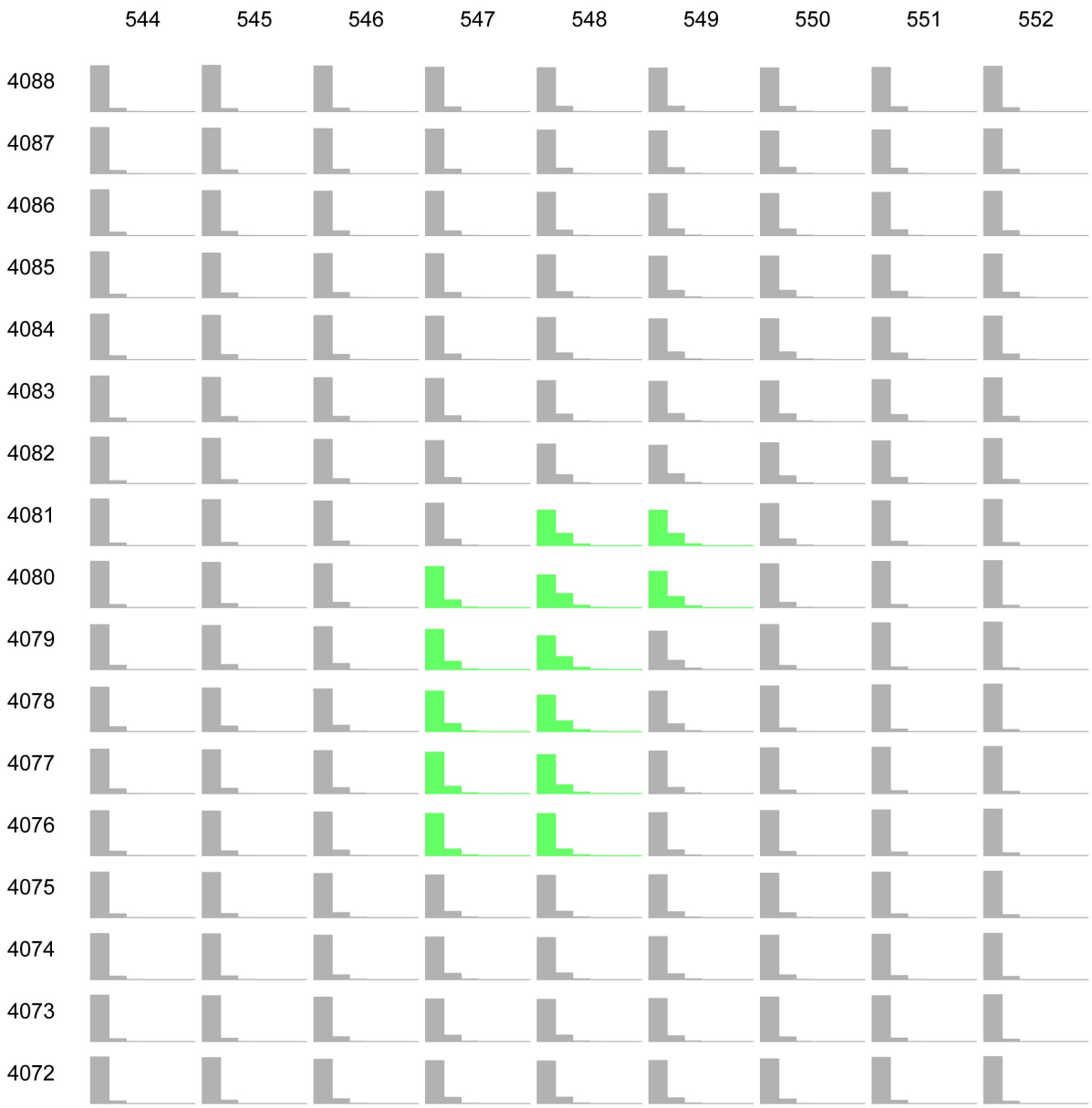

NOTE: Row and column labels represent grid points (UTM coordinates in km, NAD83) in the vicinity of the repository. Green plots show points inside or partially inside the repository footprint. Plots show the number of intersections conditional on at least one.

Figure 4.1.4-5. Schematic Showing the Distribution of the Number of Dikes That Intersect the Repository Footprint Given an Event at Each Grid Point, Given at Least a 95% Chance That One or More Dike Intersections Occur (based on events defined by Mel Kuntz)

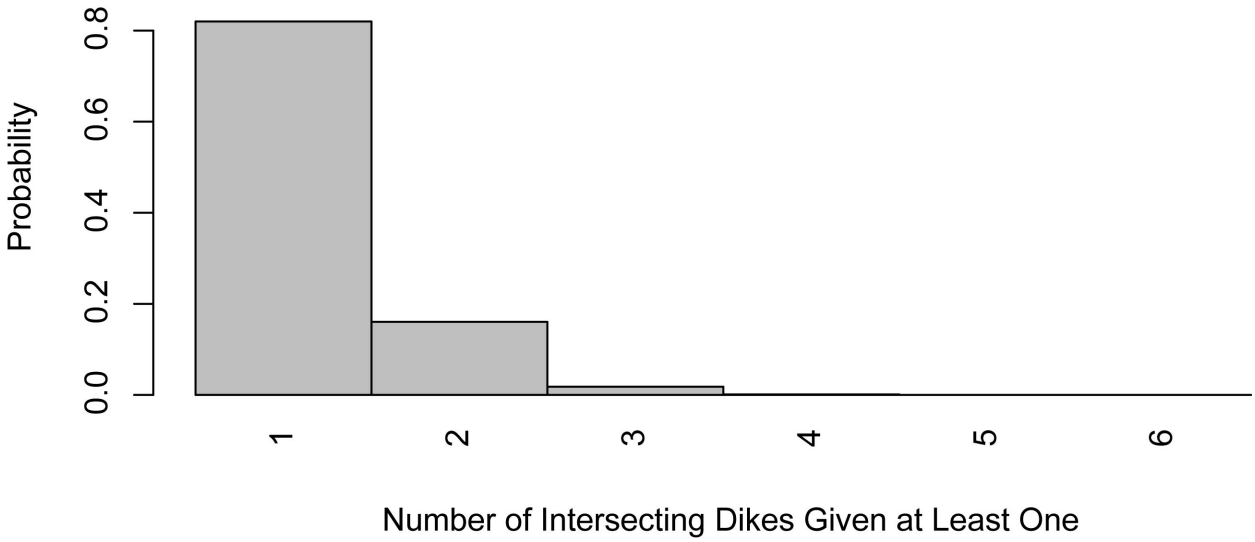

Figure 4.1.4-6. Conditional Distribution of the Number of Dikes That Intersect the Repository Footprint, Given That at Least One Dike Intersection Occurs (based on events defined by Mel Kuntz)

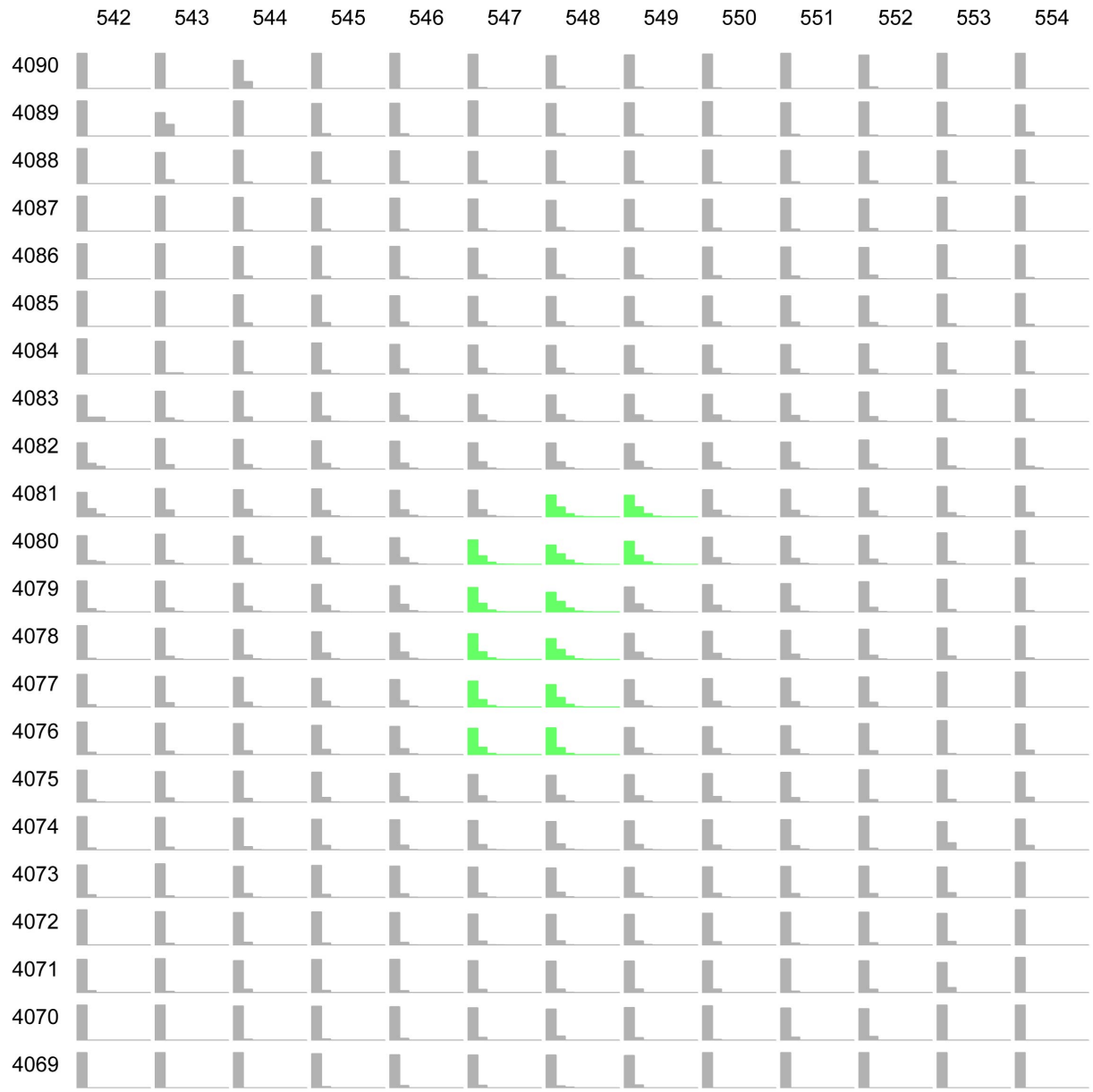

NOTE: Row and column labels represent grid points (UTM coordinates in km, NAD83) in the vicinity of the repository. Green plots show points inside or partially inside the repository footprint. Blank plots (e.g., in the upper left corner) indicate that the probability of intersection for an event at that location is zero. All other plots show the number of intersections conditional on at least one.

Figure 4.1.4-7. Schematic Showing the Distribution of the Number of Conduits that Intersect the Repository Footprint Given an Event at Each Grid Point, Given That at Least a 99% Chance of a Conduit Intersection Occurring (based on events defined by Mel Kuntz)

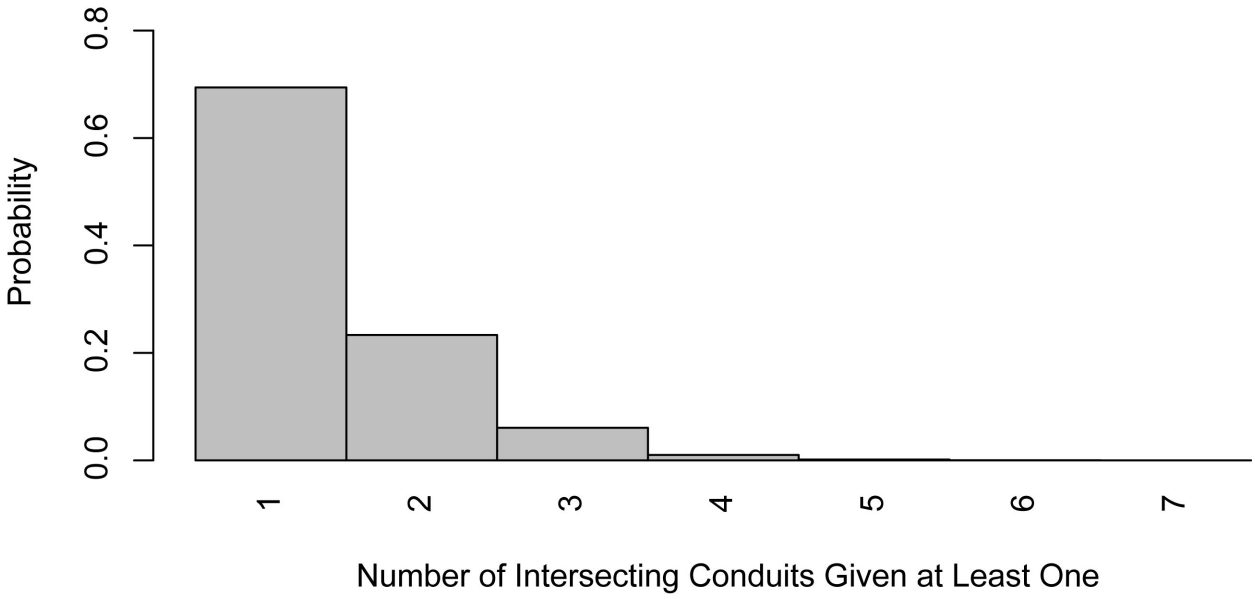

Figure 4.1.4-8. Conditional Distribution of the Number of Conduits That Intersect the Repository Footprint, Given That at Least One Conduit Intersection Occurs (based on events defined by Mel Kuntz)

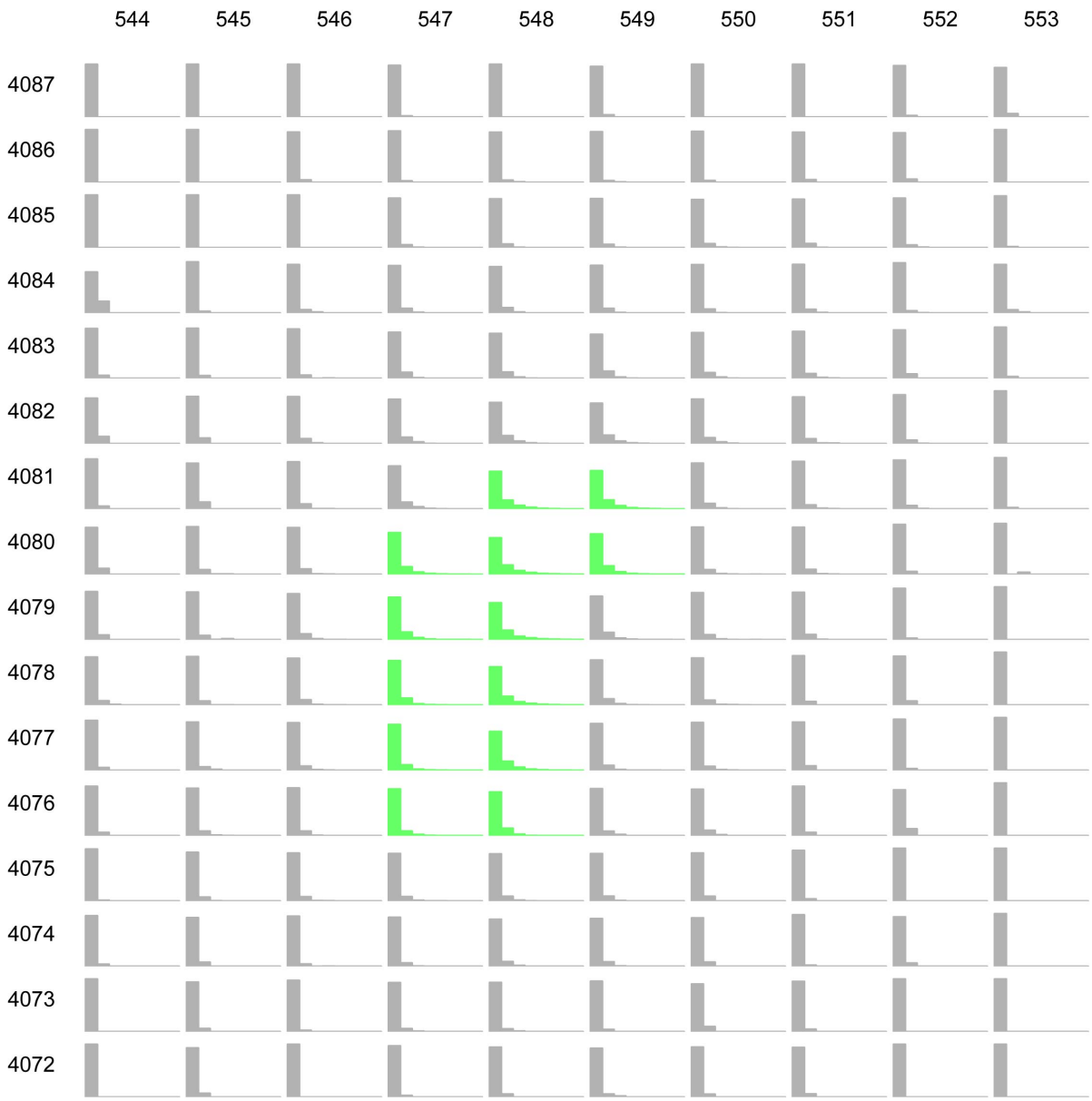

NOTE: Row and column labels represent grid points (UTM coordinates in km, NAD83) in the vicinity of the repository. Green plots show points inside or partially inside the repository footprint. Blank plots (e.g., in the upper left corner) indicate that the probability of intersection for an event at that location is zero. All other plots show the number of intersections conditional on at least one.

Figure 4.1.4-9. Schematic Showing the Distribution of the Number of Vents That Intersect the Repository Footprint Given an Event at Each Grid Point, Given That at Least a 99% Chance That a Vent Intersection Occurs (based on events defined by Mel Kuntz)

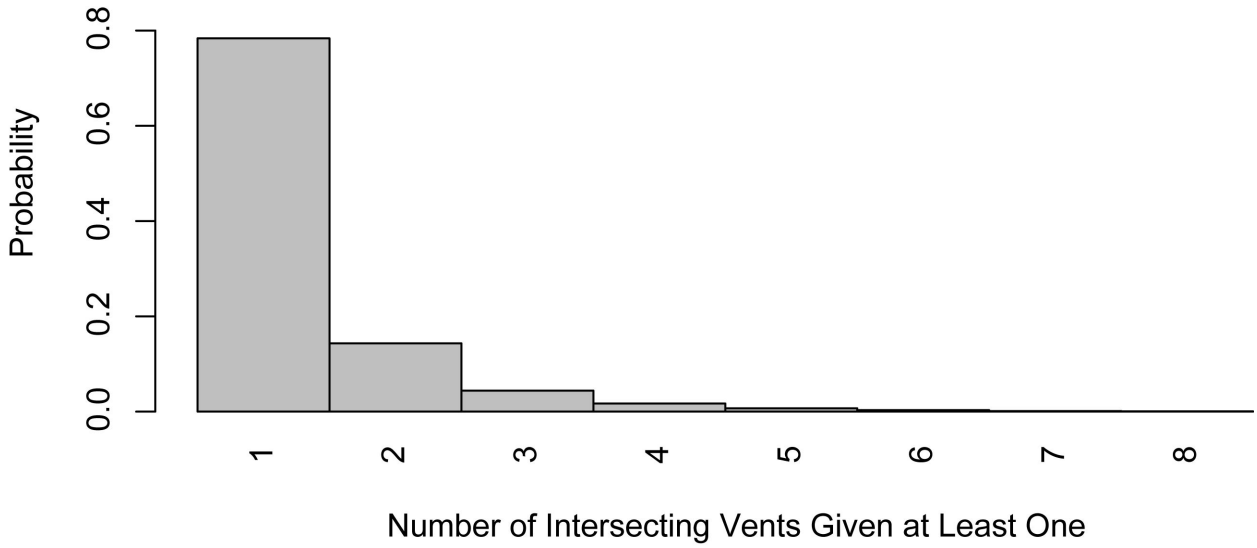

Figure 4.1.4-10. Conditional Distribution of the Number of Vents That Intersect the Repository Footprint, Given That at Least One Vent Intersection Occurs (based on events defined by Mel Kuntz)

4.1.4.3 Results at Different Future Times

The primary difference in MK's 10,000-year and 1-My assessments is the addition of models that include consideration of older events (alternative time periods of interest) in the 1-My assessment. This results in a slight shift of the entire hazard curve to higher frequencies, as shown in Figure 4.1.4-11.

A sensitivity analysis similar to that described above was conducted using the models for MK's 1-My assessment. The relative impact of each of the model components on the mean hazard for the 1-My assessment is the same as for the 10,000-year assessment, but several model components that are unique to the 1-My assessment are added. See, for example, the dark blue bar in Figure 4.1.4-12 labeled "Time period of interest." This represents the uncertainty about the relevant time period (post-4 Ma or post-11 Ma) introduced in the 1-My assessment. Similar differences are seen in the contribution to overall uncertainty: the time period of interest is an important contributor to overall uncertainty for the 1-My assessment, but the temporal modeling approach, the spatial modeling approach, and several factors related to the rate estimate remain the largest contributors to uncertainty.

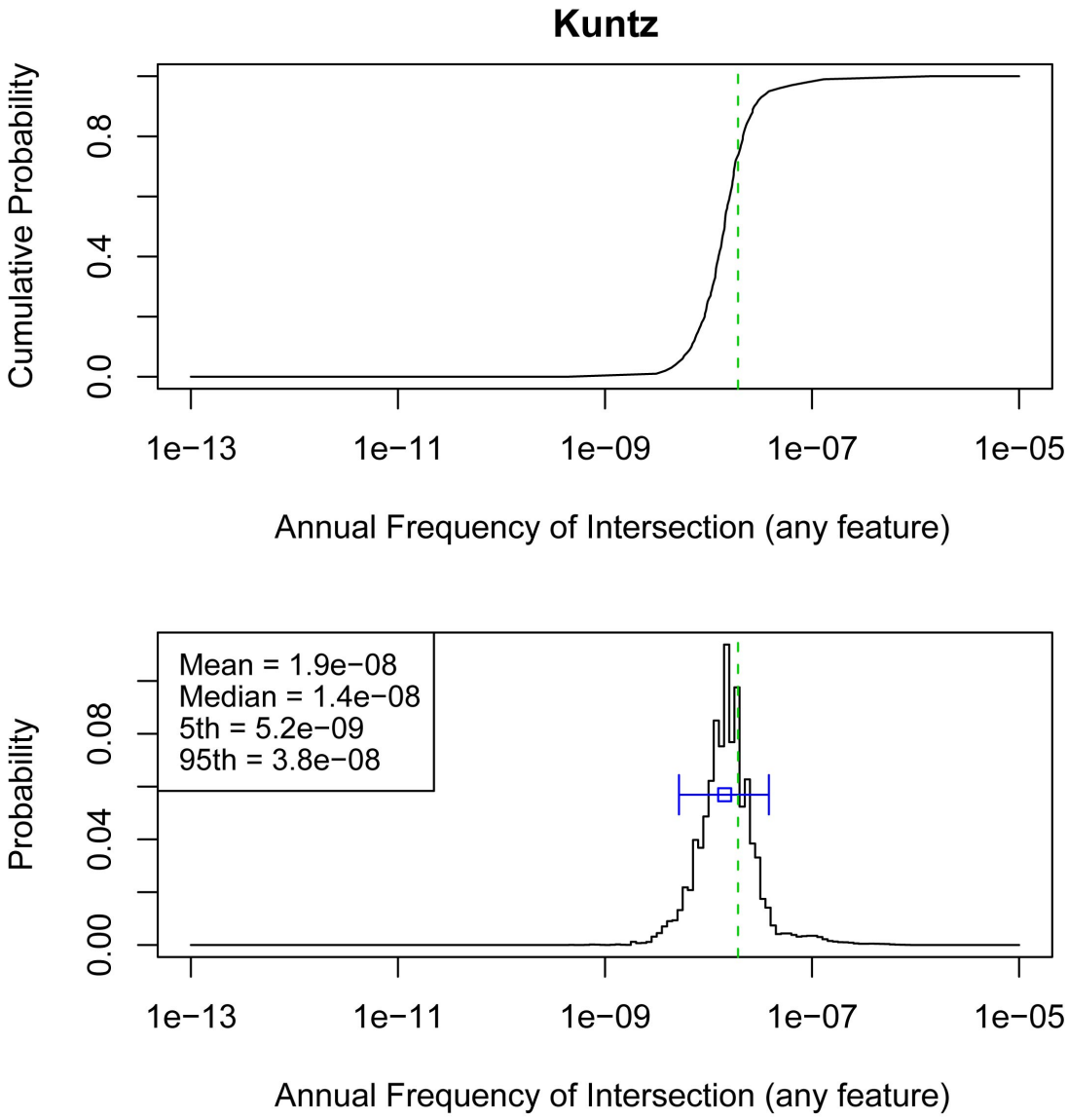

NOTE: Top figure is a cumulative distribution function, bottom figure is a probability mass function. The mean is shown by the dashed vertical line, the median with the open box, and the 5th to 95th percentiles with the horizontal line.

Figure 4.1.4-11. Hazard Results for the 1-My Assessment from PVHA-U Models Specified by Mel Kuntz

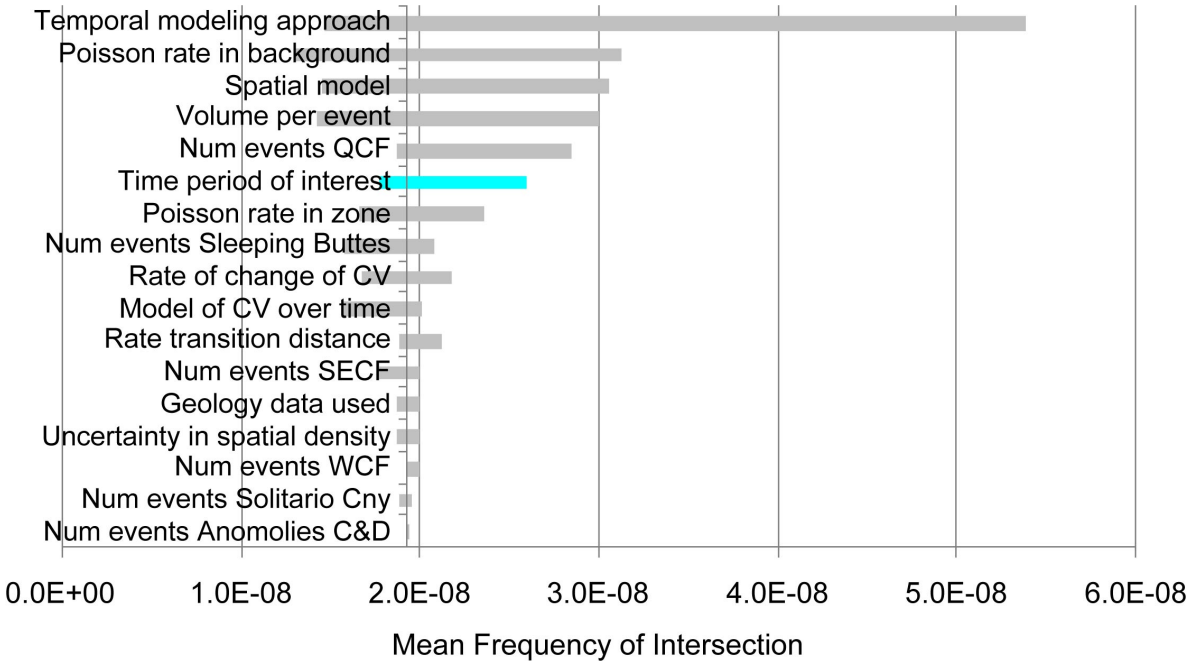

NOTES: Labels on each bar correspond to the nodes in the logic tree for MK's models as described in Section 3.2. The length of each bar shows the range of the mean hazard values that result from fixing the value of the specified model component at one of its branch values. This range represents the degree to which the mean hazard is affected by uncertainty in the specified model component. QCF = Quaternary Crater Flat; CV = cumulative volume; SECF = Southeast Crater Flat; WCF = Western Crater Flat.

Dark blue bar indicates a model component present in the 1-My assessment that is not used in the 10,000-year assessment

Figure 4.1.4-12. Contribution of Uncertainty in Model Components to Uncertainty in the Mean Hazard, for the PVHA-U Models for the 1-My Assessment Specified by Mel Kuntz

4.1.5 PVHA-U Results for Alexander McBirney

This section describes the results of the PVHA-U models specified by Alexander McBirney (AM). Those models and assessments are described in Section 3.2.5 and the elicitation summary in Appendix D. Section 4.1.5.1 discusses the results of the 10,000-year assessment for the frequency of intersection of any feature with the repository footprint. The frequency of intersection of specific features with the repository footprint is discussed in Section 4.1.5.2, and differences in the hazard calculated for the 10,000-year assessment and the 1-My assessment are discussed in Section 4.1.5.3.

4.1.5.1 Hazard Results for the 10,000-Year Assessment

Figure 4.1.5-1 summarizes the spatial distribution of hazard calculated using AM's PVHA-U models for the 10,000-year assessment. The lower-probability contours in this plot show the effect of the overlap of the conditional probability of intersection map with the mean rate density map: the extension of these contours to the SSW of the repository footprint shows the effect of the higher rate density of events within the Crater Flat zone. As events are more likely to occur in that zone, the mean frequency of intersection for events in that zone is greater than for events in the lower-rate density background zone to the east of the repository footprint.

Figure 4.1.5-2 illustrates the uncertainty in the frequency of intersection of any feature with the repository footprint. The mean frequency of intersection is marked on both graphs by a dashed vertical line, and the median, 5th, and 95th percentiles are shown on the pmf. The mean frequency of intersection of any feature with the repository footprint is 2.0e-9; the median frequency is 1.3e-9. The 5th and 95th percentiles are 2.6e-10 and 6e-9, respectively.

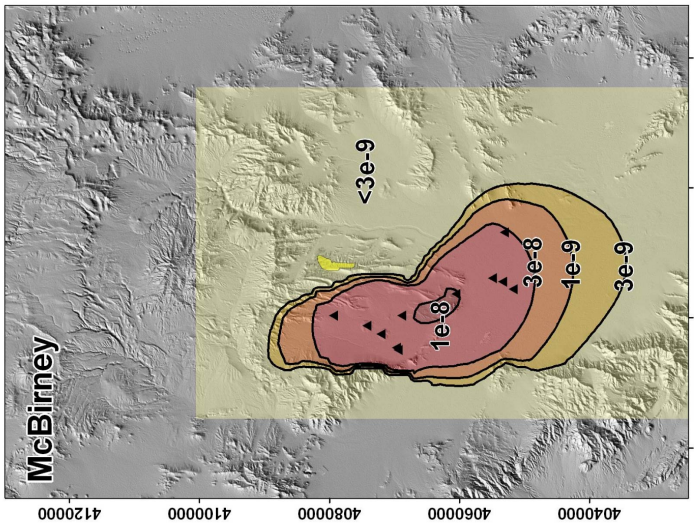

(a) Mean rate density. Contours represent the mean annual frequency of igneous events (events per year) per km^2.

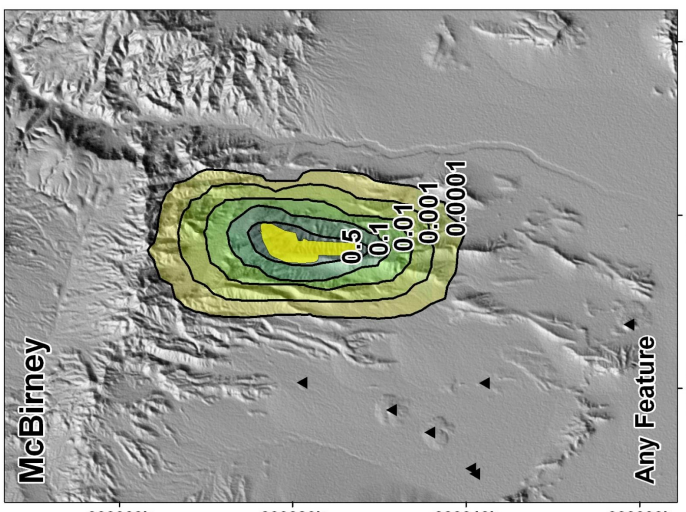

(b) Conditional probability of intersection of any feature. Contours represent the probability that an event assumed to occur at each location would result in the intersection of any igneous feature with the repository footprint.

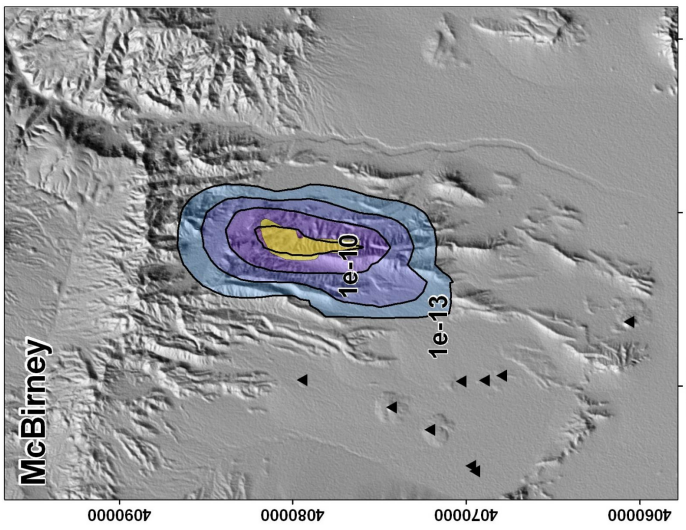

(c) Spatial distribution of the mean frequency of intersection. Contours represent the mean annual probability of an intersection of the repository footprint by an igneous feature.

NOTE: The repository footprint is shown as a yellow polygon. Past events are shown as black triangles. Map grid ticks are UTM meters; tick intervals for map (a) are 20 km; map (b) and (c) are 10 km.

Figure 4.1.5-1. Components of the Hazard Calculation for PVHA-U Models Specified by Alexander McBirney, for the 10,000-Year Assessment

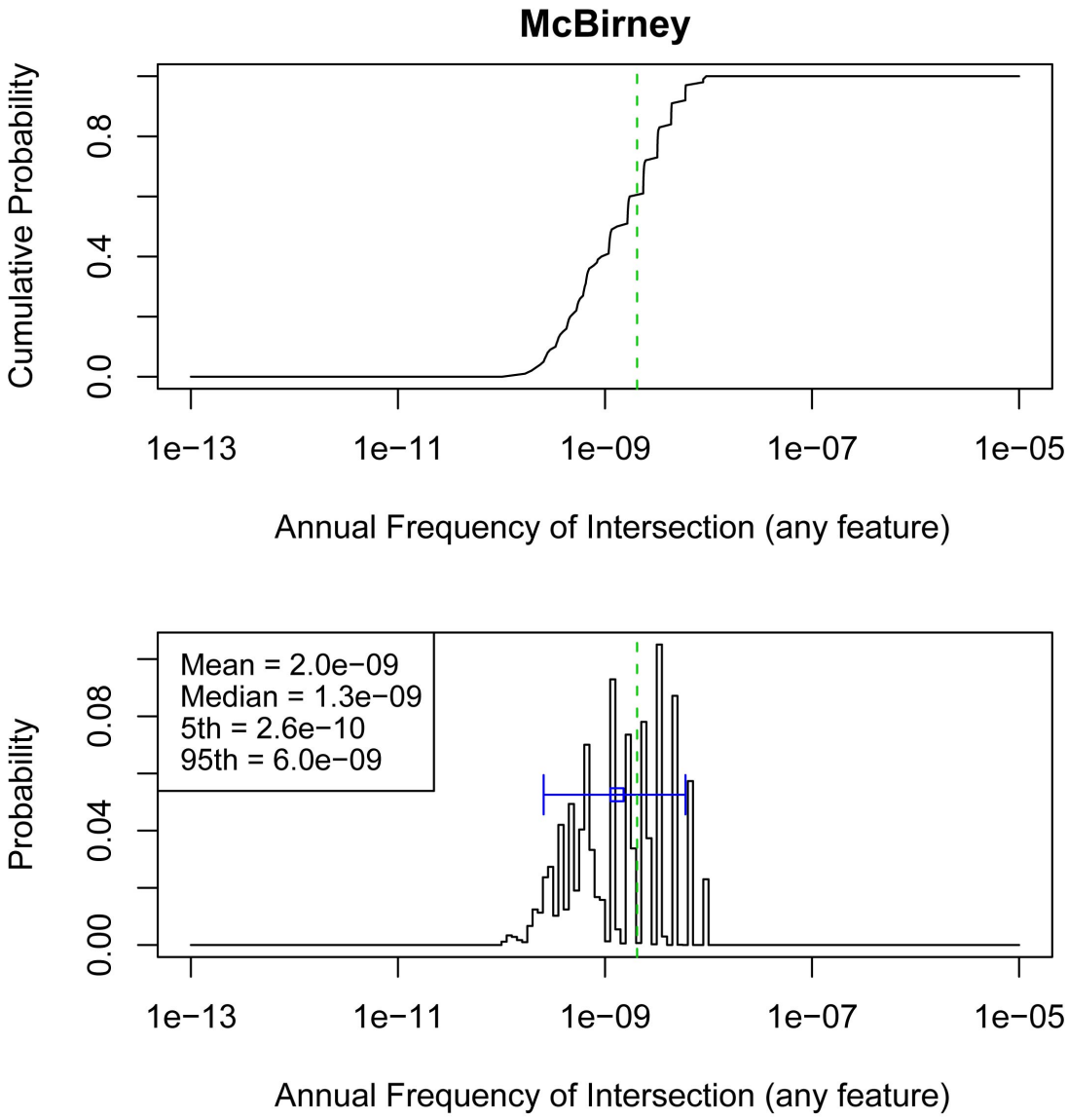

NOTE: Top figure is a cumulative distribution function, bottom figure is a probability mass function. The mean is shown by the dashed vertical line, the median with the open box, and the 5th to 95th percentiles with the horizontal line.

Figure 4.1.5-2. Hazard Results for the 10,000-Year Assessment from PVHA-U Models Specified by Alexander McBirney

Contributions to Uncertainty

Contributions from various model components to uncertainty in the mean hazard in AM's models are illustrated in Figure 4.1.5-3. Although Figure 4.1.5-1 does show the effect of the greater rate in the Crater Flat zone, and indicates that events located in that zone have the potential to intersect the repository footprint, the mean hazard estimate is most sensitive to uncertainty in the rate in the background zone, as shown by the top bar in the figure (labeled "Poisson rate in background"). The mean hazard is also sensitive to the time period of interest used to calculate that rate (the Quaternary or the Plio-Quaternary). All other uncertainties in the

model relate to the estimated rate density within the Crater Flat zone, and their contributions to uncertainty in the mean hazard are small.

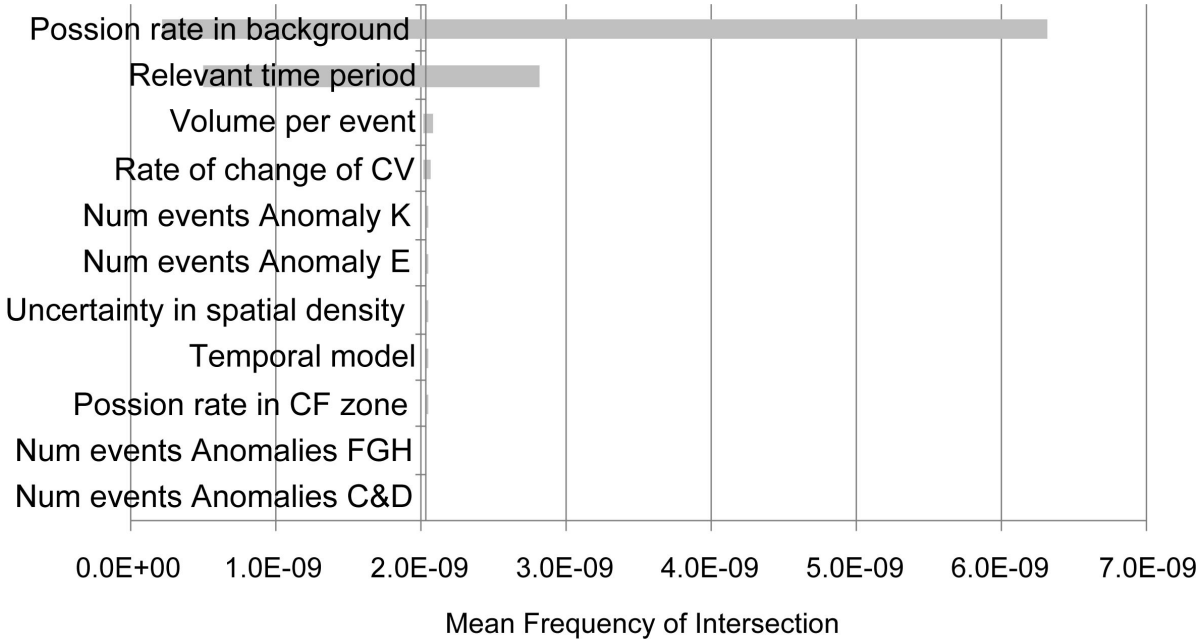

NOTE: Labels on each bar correspond to the nodes in the logic tree for AM's models as described in Section 3.2. The length of each bar shows the range of the mean hazard values that result from fixing the value of the specified model component at one of its branch values. This range represents the degree to which the mean hazard is affected by uncertainty in the specified model component. CV = cumulative volume; CF = Crater Flat.

Figure 4.1.5-3. Contribution of Uncertainty in Model Components to Uncertainty in the Mean Hazard, for the PVHA-U Models for the 10,000-Year Assessment Specified by Alexander McBirney

Contribution of various model components to *overall uncertainty* in the hazard for AM's model is shown in Figure 4.1.5-4. The impacts of individual uncertainties in the models on the overall uncertainty are very similar to their impacts on uncertainty in the mean hazard.

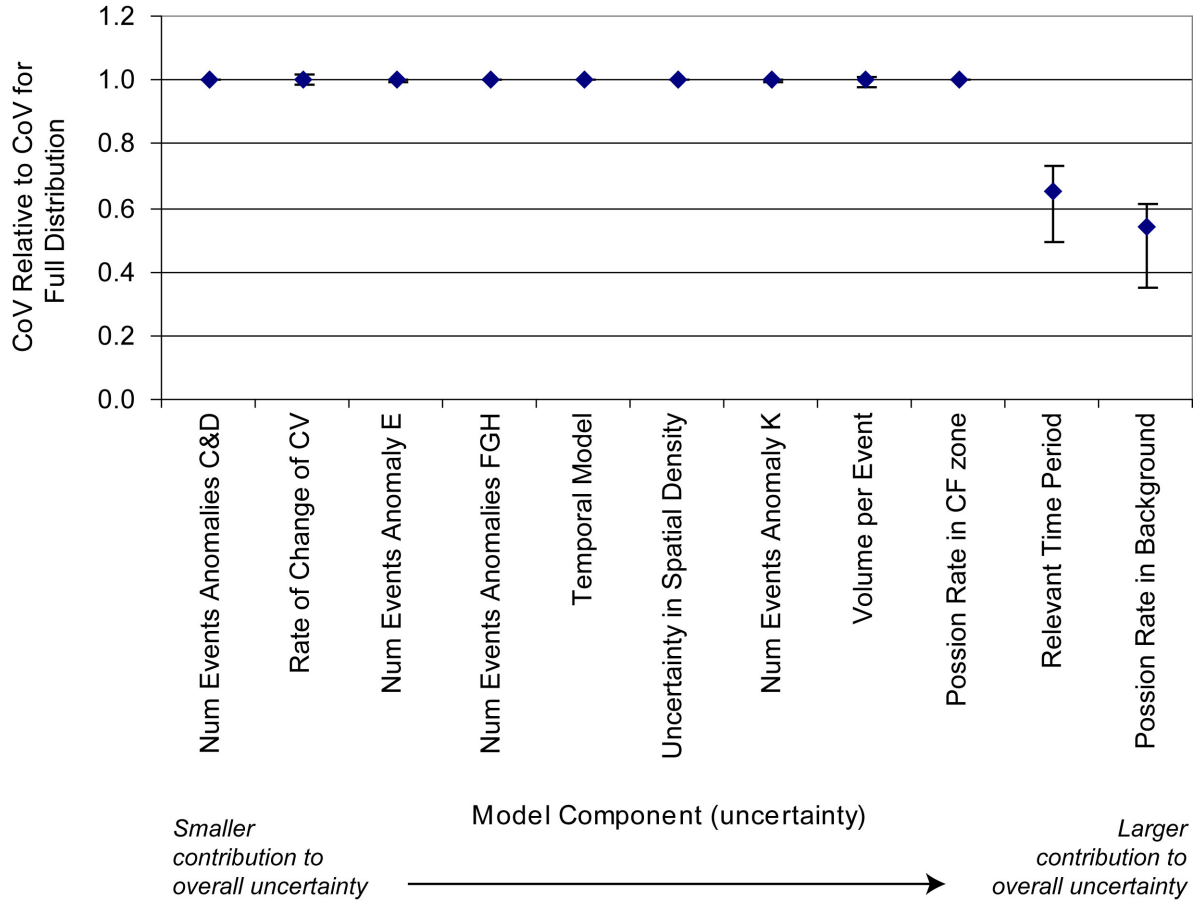

NOTE: Graph shows the CoV for the hazard distribution calculated with the specified model component fixed at each of its branch values, divided by the CoV for the full hazard distribution. Diamond shows the mean value with the relative CoV for each branch value weighted by its probability; "error bars" show the highest and lowest relative CoVs calculated across the branches for that model component. CV = cumulative volume; CF = Crater Flat.

Figure 4.1.5-4. Contribution of Uncertainty in Model Components to Overall Uncertainty in the Hazard Estimate, for the PVHA-U Model for the 10,000-Year Assessment Specified by Alexander McBirney

4.1.5.2 Discussion of Individual Features

As described in Section 3.2.5, AM's events all include dikes, at least one conduit or vent, and might also include sills. The conditional probability of intersection of each type of feature with the repository footprint was illustrated in Section 3.2.5, and, as discussed, the shape of the conditional probability of intersection maps for each individual feature is the same as for the conditional probability of intersection for any feature: no particular clustering or grouping of individual features in an event occurs. Similarly, the full distribution of the frequency of intersection for any individual feature follows the same pattern as the distribution for any feature shown in Figure 4.1.5-2, simply shifted to the lower frequencies associated with the individual feature.

Table 4.1.5-1 shows the mean and median frequencies of intersection for each feature.

Table 4.1.5-1. Mean and Median Frequency of Intersection of Various Igneous Features with the Repository Footprint, for Alexander McBirney's 10,000-Year Assessment

Feature	Mean Frequency of Intersection	Median Frequency of Intersection
Any feature	2.0e-9	1.3e-9
Dikes	2.0e-9	1.3e-9
Column-producing conduits	1.3e-9	7.4e-10
Vents	3.3e-10	1.9e-10
Sills	6.7e-12	5.0e-12

Potential for Multiple Intersections

Figure 4.1.5-5 shows a set of plots illustrating the distribution of the number of dike intersections for an event centered at a specific point, conditional on at least one such intersection occurring. The most likely number of intersections across the region as shown in the figure is one, but multiple dike intersections are possible depending on the event location (e.g., event locations inside the repository footprint). Figure 4.1.5-6 combines the relative likelihood of a dike intersection at each point with the conditional distribution of the number of dike intersections for an event at those points to yield a conditional distribution on the number of dike intersections, given that at least one such intersection occurs. As shown, assuming a dike intersection occurs, it is most likely (probability 0.7) that only one dike intersects, but the potential exists for as many as 10 intersections (with a probability of about 0.0004). The probability of four or more dike intersections, given at least one intersection, is less than 0.05.

Figures 4.1.5-7 and 4.1.5-8 show the same data for conduits: the distribution on number of conduit intersections given at least one conduit intersects the footprint. Given a conduit intersection, it is most likely that only one such intersection would occur, but there is potential for as many as 10 conduit intersections (with a probability of about 0.0006). While vents are less likely than conduits in AM's event descriptions, their relative location and size are otherwise described by the same models, so the *conditional* frequency of vent intersection, as shown in Figures 4.1.5-9 and 4.1.5-10, follows that just described for conduits.

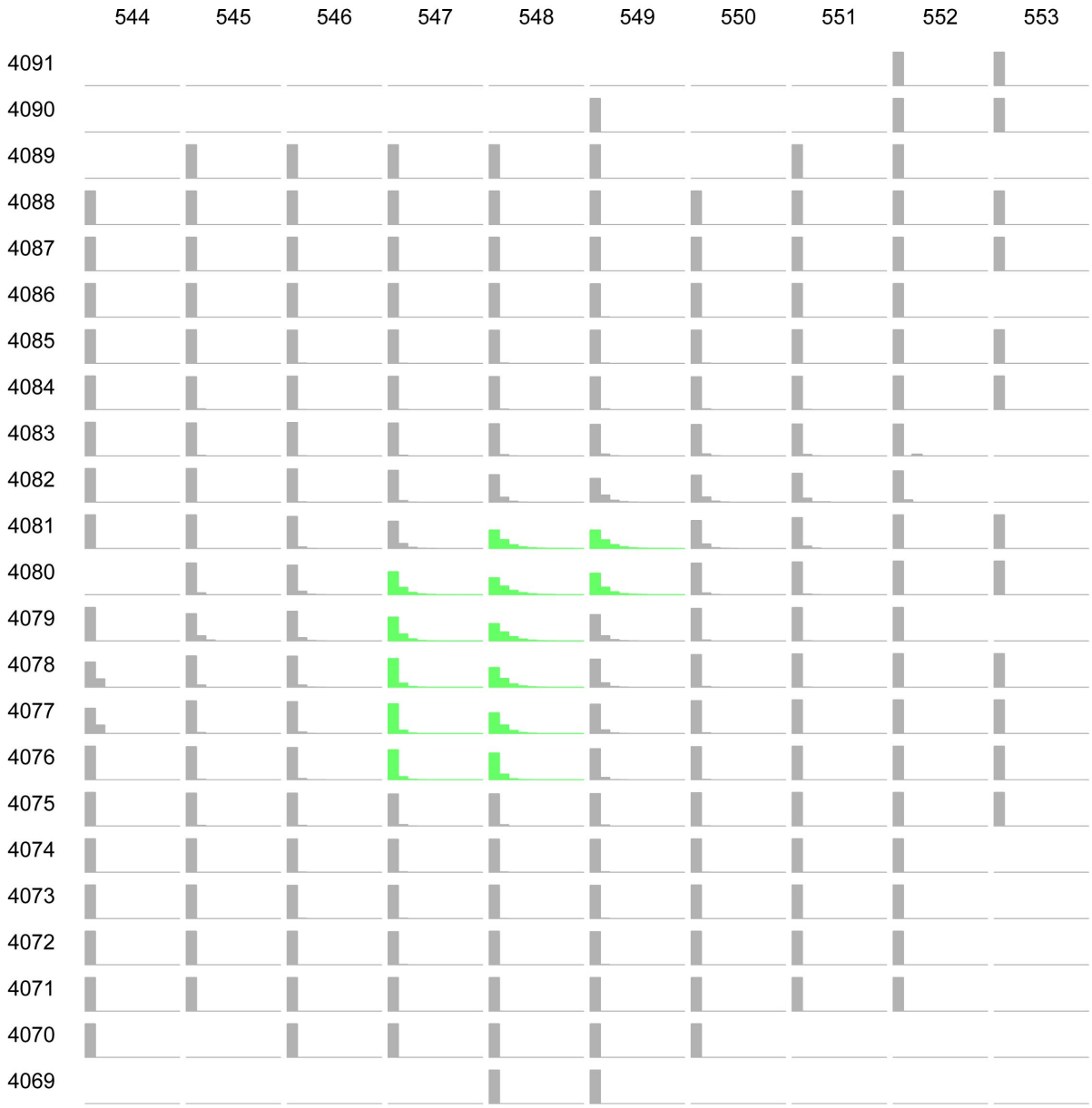

NOTE: Row and column labels represent grid points (UTM coordinates in km, NAD83) in the vicinity of the repository. Green plots show points inside or partially inside the repository footprint. Blank plots (e.g., in the upper left corner) indicate that the probability of intersection for an event at that location is zero. All other plots show the number of intersections conditional on at least one.

Figure 4.1.5-5. Schematic Showing the Distribution of the Number of Dikes That Intersect the Repository Footprint Given an Event at Each Grid Point, Given That at Least One Dike Intersection Occurs (based on the event descriptions of Alexander McBirney)

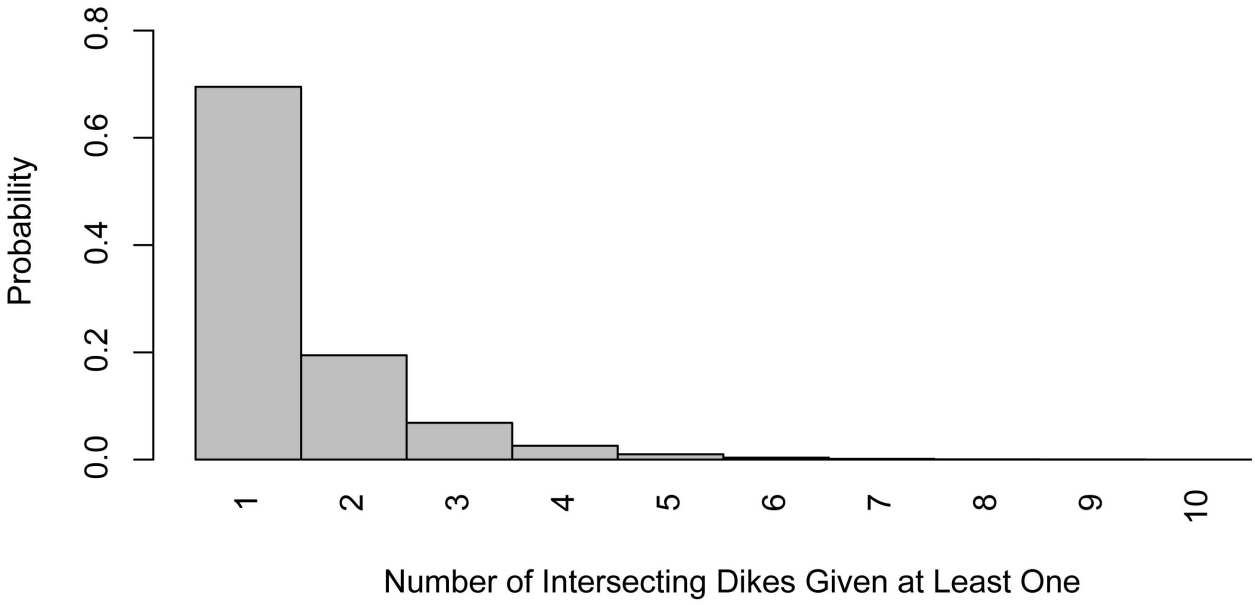

Figure 4.1.5-6. Conditional Distribution of the Number of Dikes That Intersect the Repository Footprint, Given That at Least One Dike Intersection Occurs (based on the event descriptions of Alexander McBirney)

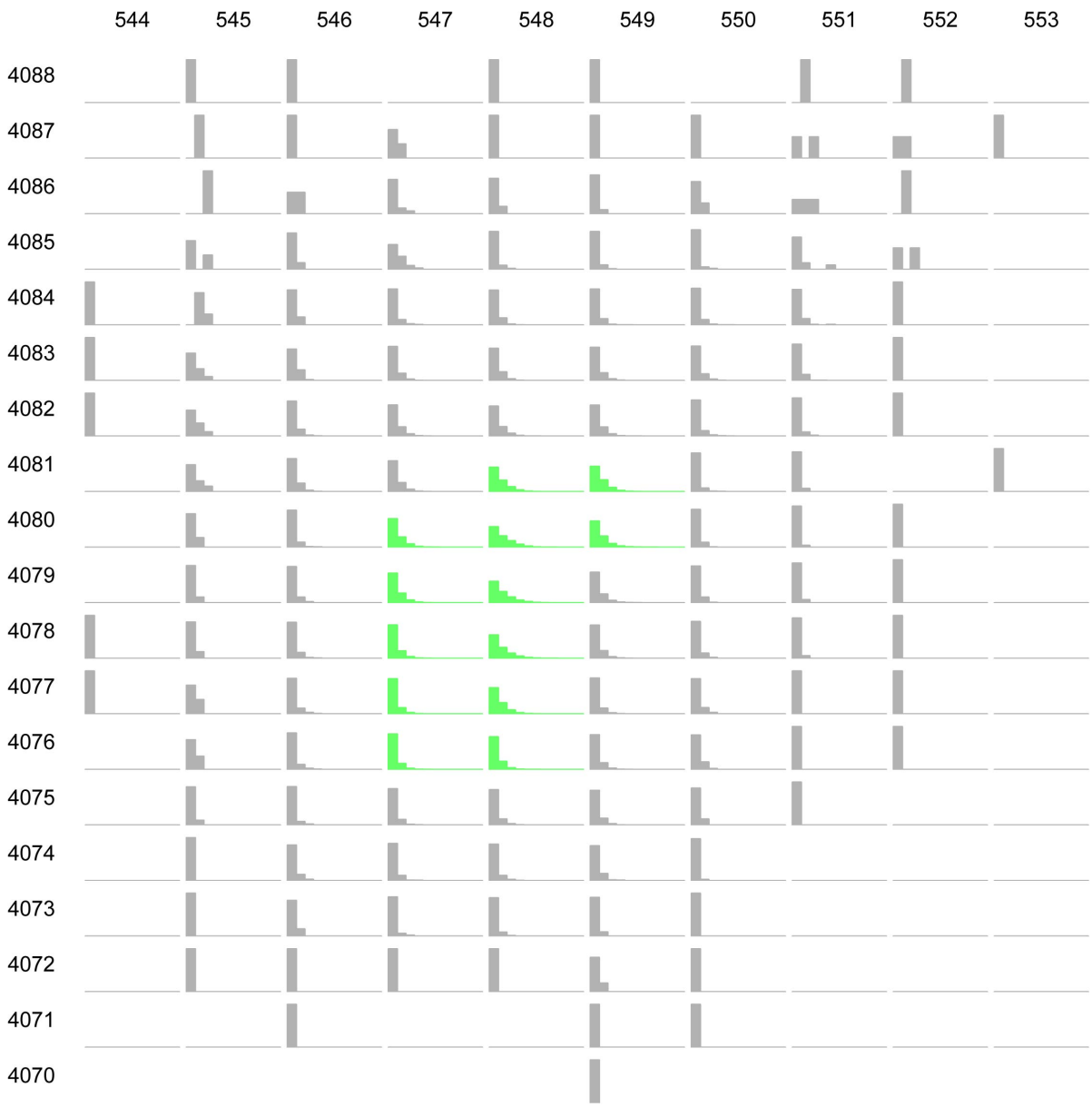

NOTE: Row and column labels represent grid points (UTM coordinates in km, NAD83) in the vicinity of the repository. Green plots show points inside or partially inside the repository footprint. Blank plots (e.g., in the upper left corner) indicate that the probability of intersection for an event at that location is zero. All other plots show the number of intersections conditional on at least one.

Figure 4.1.5-7. Schematic Showing the Distribution of the Number of Conduits That Intersect the Repository Footprint Given an Event at Each Grid Point, Given That at Least One Conduit Intersection Occurs (based on the event descriptions of Alexander McBirney)

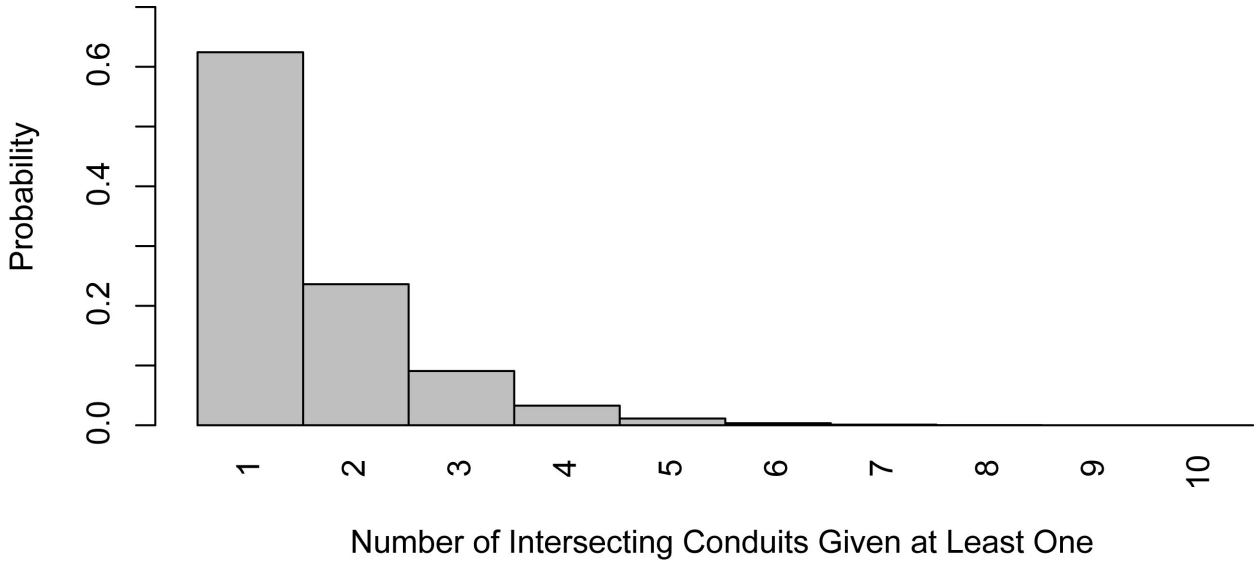

Figure 4.1.5-8. Conditional Distribution of the Number of Conduits That Intersect the Repository Footprint, Given That at Least One Conduit Intersection Occurs (based on the event descriptions of Alexander McBirney)

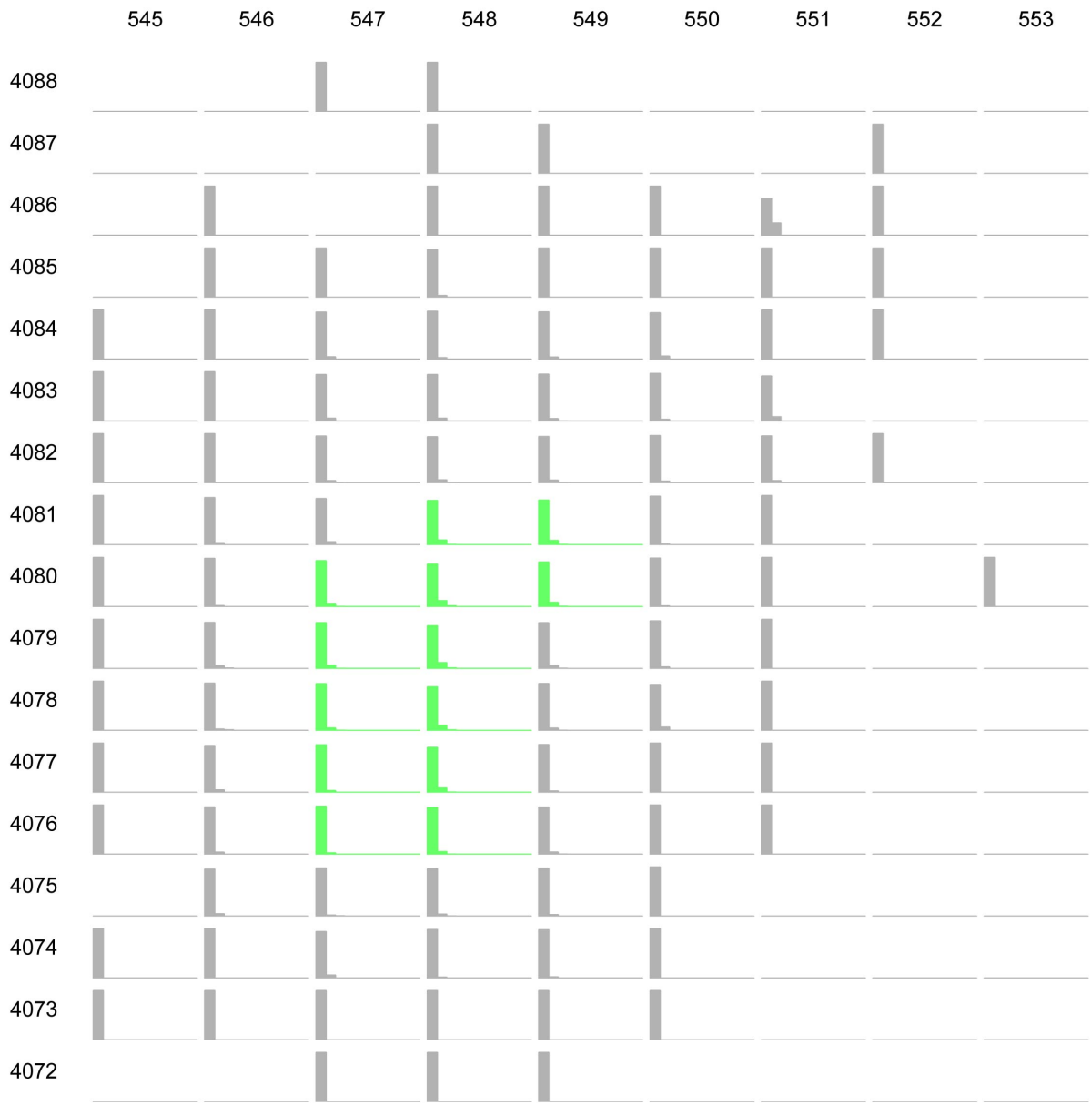

NOTE: Row and column labels represent grid points (UTM coordinates in km, NAD83) in the vicinity of the repository. Green plots show points inside or partially inside the repository footprint. Blank plots (e.g., in the upper left corner) indicate that the probability of intersection for an event at that location is zero. All other plots show the number of intersections conditional on at least one.

Figure 4.1.5-9. Schematic Showing the Distribution of the Number of Vents That Intersect the Repository Footprint Given an Event at Each Grid Point, Given That at Least One Vent Intersection Occurs (based on the event descriptions of Alexander McBirney)

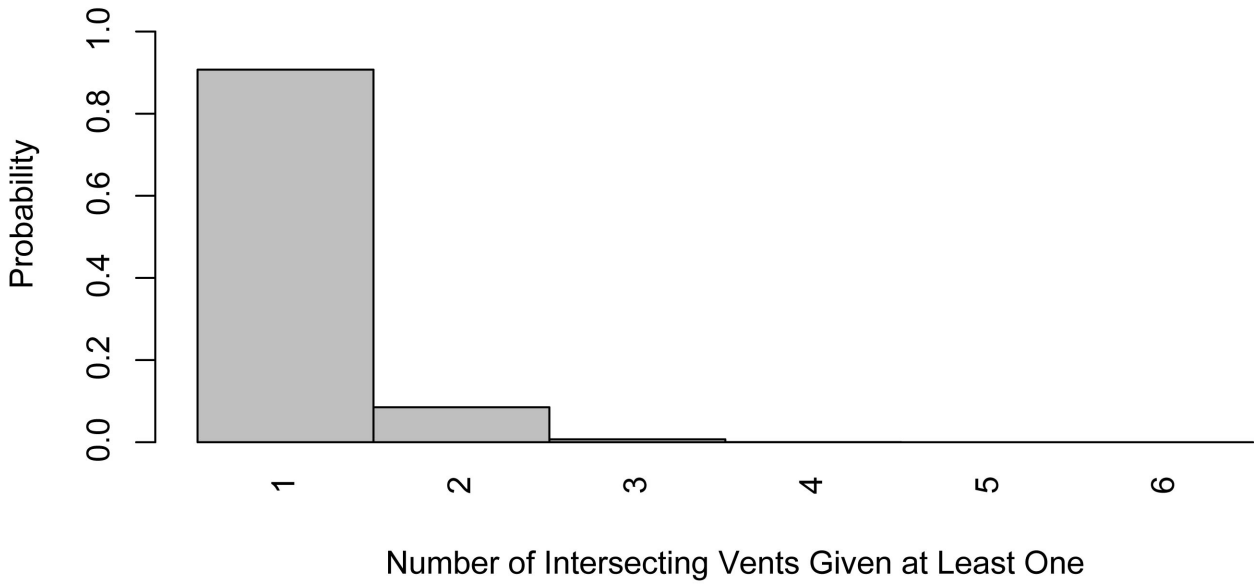

Figure 4.1.5-10. Conditional Distribution of the Number of Vents That Intersect the Repository Footprint, Given That at Least One Vent Intersection Occurs (based on the event descriptions of Alexander McBirney)

4.1.5.3 Results at Different Future Times

AM defined one set of models as applying to both the 10,000-year and 1-My assessments. Those models include a time-volume model that leads to a time-dependent rate estimate for the rate within the Crater Flat zone, but as discussed previously, the change in rate over a million years is small, and the frequency of intersection is most strongly a function of the rate in the background zone, which is not modeled with the time-volume rate model. The mean frequency of intersection for the 1-My assessment for AM's models is 2.0e-9, the same as for his 10,000-year assessment. There are no meaningful differences in the CDF and pmf graphs, nor in the contributions to uncertainty for the 1-My versus the 10,000-year assessments.

4.1.6 PVHA-U Results for Michael Sheridan

This section describes the results of the PVHA-U models specified by Michael Sheridan (MS). Those models and assessments are described in Section 3.2.6 and the elicitation summary in Appendix D. Section 4.1.6.1 discusses the results of the 10,000-year assessment for the frequency of intersection of any feature with the repository footprint. The frequency of intersection of specific features with the repository footprint is discussed in Section 4.1.6.2, and differences in the hazard calculated for the 10,000-year assessment and the 1-My assessment are discussed in Section 4.1.6.3.

4.1.6.1 Hazard Results for the 10,000-Year Assessment

Figure 4.1.6-1 summarizes the spatial distribution of hazard calculated using MS's PVHA-U models for the 10,000-year assessment. The contours in this plot show clearly the effect of the overlap of the conditional probability of intersection map with the mean rate density map: the extension of these contours to the SSW of the repository footprint show the effect of the greater rate density of events within the Crater Flat field. As events are more likely to occur SSW of the repository, the mean frequency of intersection for events located in that region is greater.

Figure 4.1.6-2 illustrates the uncertainty in the frequency of intersection of any feature with the repository footprint. The mean frequency of intersection is marked on both graphs by a dashed vertical line, and the median, 5th, and 95th percentiles are shown on the pmf. The mean frequency of intersection of any feature with the repository footprint is 3.4e-9; the median frequency is 1.4e-9. The 5th and 95th percentiles are 5.7e-10 and 1.5e-8, respectively.

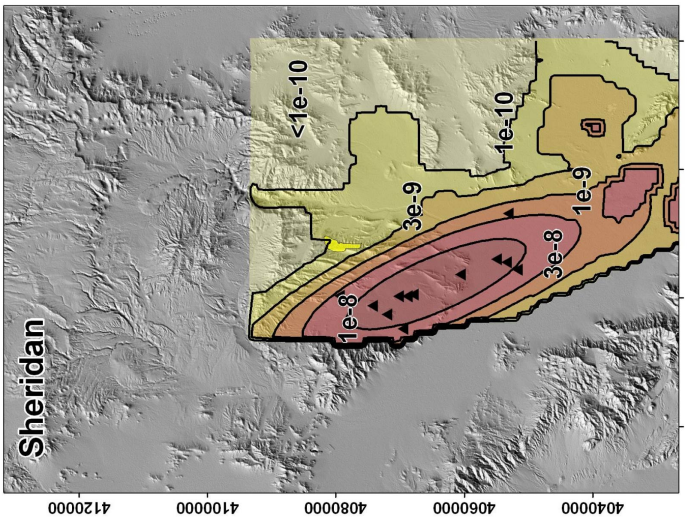

(a) Mean rate density. Contours represent the mean annual frequency of igneous events (events per year) per km^2.

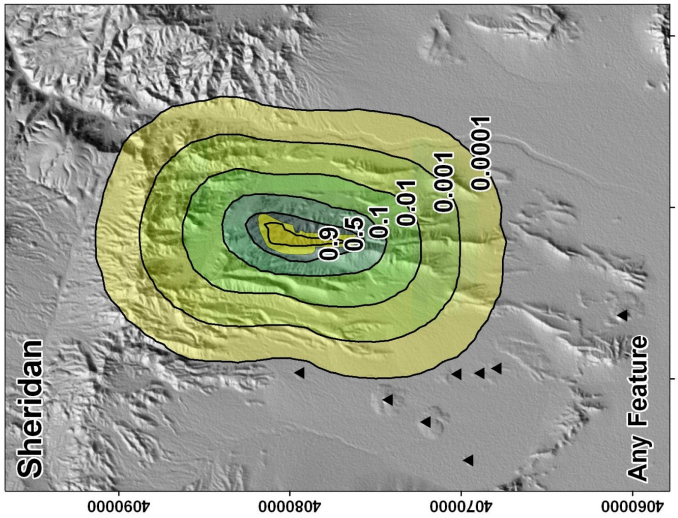

(b) Conditional probability of intersection of any feature. Contours represent the probability that an event assumed to occur at each location would result in the intersection of any igneous feature with the repository footprint.

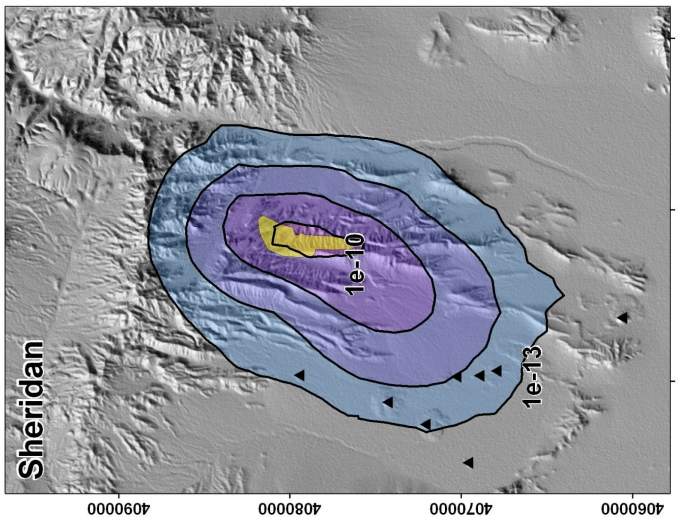

(c) Spatial distribution of the mean frequency of intersection. Contours represent the mean annual probability of an intersection of the repository footprint by an igneous feature.

NOTE: The repository footprint is shown as a yellow polygon. Past events are shown as black triangles. Map grid ticks are UTM meters; tick intervals for map (a) are 20 km; map (b) and (c) are 10 km.

Figure 4.1.6-1. Components of the Hazard Calculation for PVHA-U Models Specified by Michael Sheridan, for the 10,000-Year Assessment

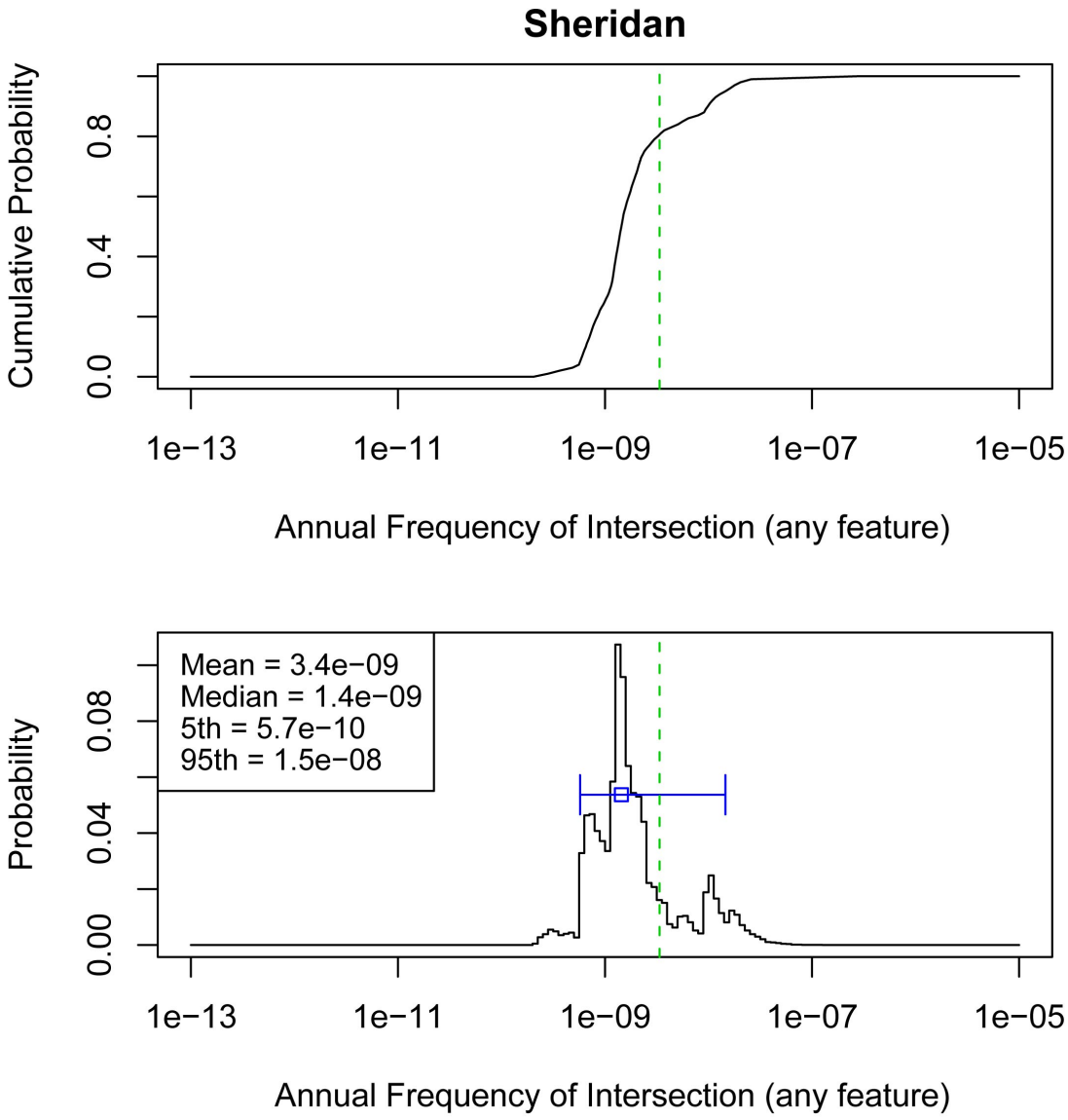

NOTE: Top figure is a cumulative distribution function, bottom figure is a probability mass function. The mean is shown by the dashed vertical line, the median with the open box, and the 5th to 95th percentiles with the horizontal line.

Figure 4.1.6-2. Hazard Results for the 10,000-Year Assessment from PVHA-U Models Specified by Michael Sheridan

Contributions to Uncertainty

Contributions from various model components to uncertainty in the mean hazard in MS's models are illustrated in Figure 4.1.6-3. As described in Section 3.2.6, MS specified two alternative temporal models for the rate in the CF field: a homogenous Poisson model and a temporal clustering model. The uncertainty about the appropriate temporal model for the Crater Flat (CF) volcanic field has the most significant effect on the mean hazard for MS's 10,000-year assessment, as shown by the top bar in the figure. The temporal clustering model produces a higher mean hazard estimate (8.2e-9) than the homogenous Poisson model (1.5e-9), as indicated

by the two ends of the "Temporal model for CF field" bar. Uncertainties specific to the temporal clustering model (whether the current time period is within a cluster or between clusters, and the Poisson arrival rate for clusters) are also important contributors to uncertainty in the mean hazard. The second largest contributor to uncertainty in the mean, however, is uncertainty in the fit of the bivariate Gaussian field shape model to the events specified by MS.

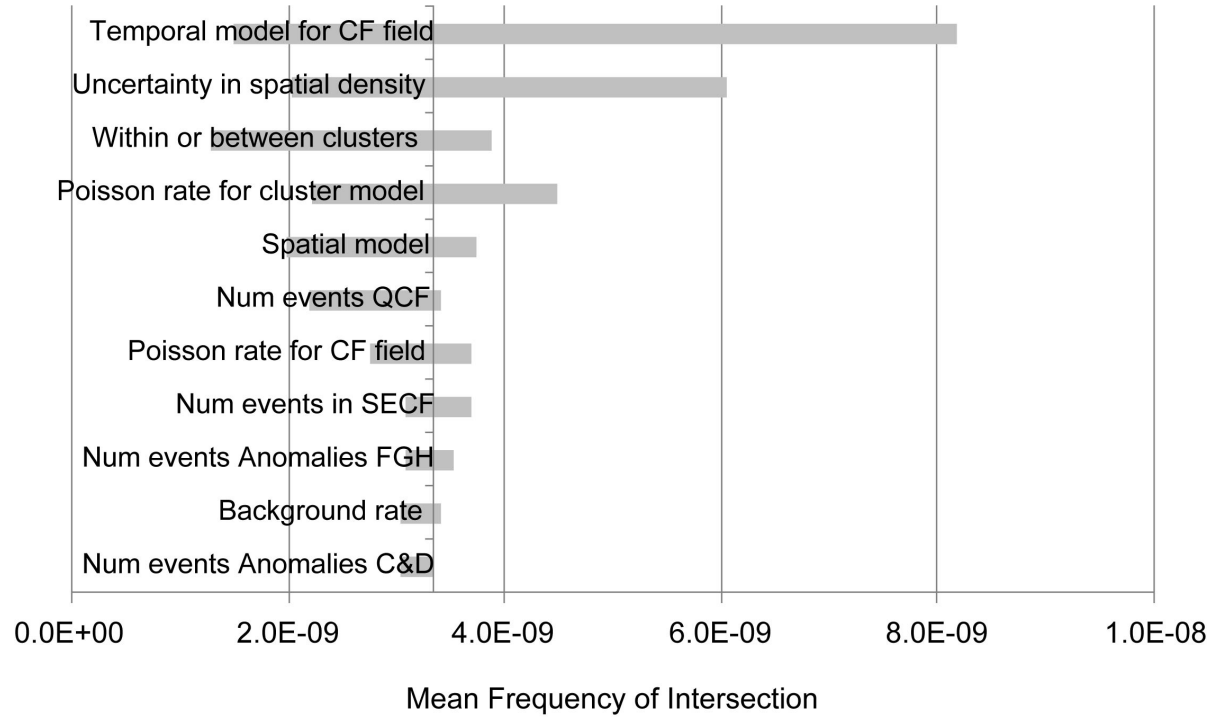

NOTE: Labels on each bar correspond to the nodes in the logic tree for MS's models as described in Section 3.2. The length of each bar shows the range of the mean hazard values that result from fixing the value of the specified model component at one of its branch values. This range represents the degree to which the mean hazard is affected by uncertainty in the specified model component. CF = Crater Flat; QCF = Quaternary Crater Flat; SECF = Southeastern Crater Flat

Figure 4.1.6-3. Contribution of Uncertainty in Model Components to Uncertainty in the Mean Hazard, for the PVHA-U Models for the 10,000-Year Assessment Specified by Michael Sheridan

Contribution of various model components to *overall uncertainty* in the hazard for MS's model is shown in Figure 4.1.6-4. The impacts of individual uncertainties in the models on the overall uncertainty are very similar to their impacts on uncertainty in the mean hazard, with uncertainties related to the temporal models, and the temporal clustering model in particular, being the largest contributors to overall uncertainty.

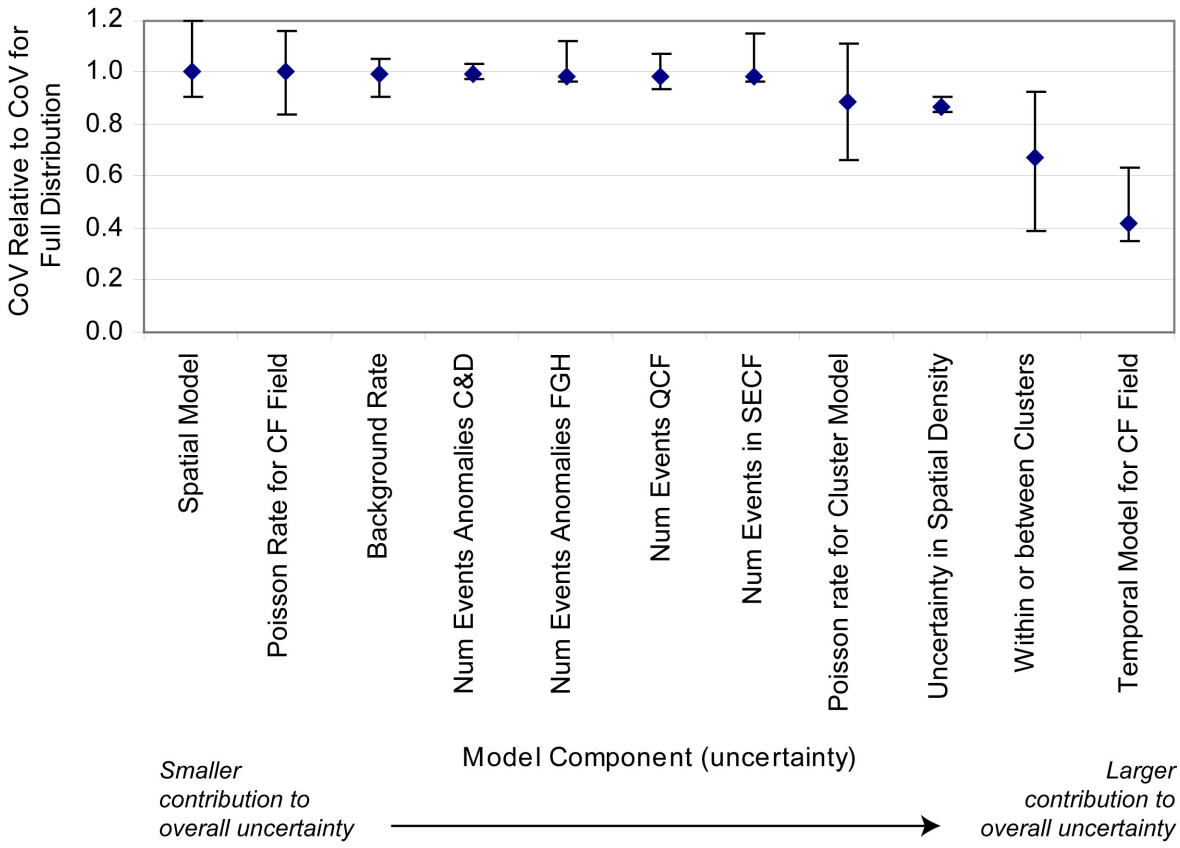

NOTE: Graph shows the CoV for the hazard distribution calculated with the specified model component fixed at each of its branch values, divided by the CoV for the full hazard distribution. Diamond shows the mean value with the relative CoV for each branch value weighted by its probability; "error bars" show the highest and lowest relative CoVs calculated across the branches for that model component. CF = Crater Flat; QCF = Quaternary Crater Flat; SECF = Southeastern Crater Flat

Figure 4.1.6-4. Contribution of Uncertainty in Model Components to Overall Uncertainty in the Hazard Estimate, for the PVHA-U Models for the 10,000-Year Assessment Specified by Michael Sheridan

4.1.6.2 Discussion of Individual Features

As described in Section 3.2.6, MS's events all include at least one conduit or vent, almost all include at least one dike, and any event might also include a sill. The conditional probability of intersection of each type of feature with the repository footprint was illustrated in Section 3.2.6. As discussed, the shape of the conditional probability of intersection maps for each individual feature is the same as for the conditional probability of intersection for any feature: no consistent clustering or grouping of individual features in an event occurs. Similarly, the full distribution of the frequency of intersection for any individual feature follows the same pattern as the distribution for any feature shown in Figure 4.1.6-2, simply shifted to the lower frequencies associated with the individual feature.

Table 4.1.6-1 shows the mean and median frequencies of intersection for each feature.

Table 4.1.6-1. Mean and Median Frequency of Intersection of Various Igneous Features with the Repository Footprint, for Michael Sheridan's 10,000-Year Assessment

Feature	Mean Frequency of Intersection	Median Frequency of Intersection
Any feature	3.4e-9	1.4e-9
Dikes	3.4e-9	1.4e-9
Column-producing conduits	8.8e-10	3.9e-10
Vents	3.9e-10	1.8e-10
Sills	9.1e-11	4.1e-11

Potential for Multiple Intersections

Figure 4.1.6-5 shows a set of plots illustrating the distribution of the number of dike intersections for an event centered at a specific point, conditional on there being at least a 1% chance of an intersection occurring. The most likely number of intersections across the region as shown in the figure is one, but multiple dike intersections are possible depending on the event location (e.g., event locations inside the repository footprint). Figure 4.1.6-6 combines the relative likelihood of a dike intersection at each point with the conditional distribution of the number of dike intersections for an event at those points to yield a conditional distribution on the number of dike intersections, given that at least one such intersection occurs. As shown, assuming a dike intersection occurs, it is most likely (probability 0.88) that only one dike intersects, but the potential exists for as many as 6 dikes to intersect the repository footprint. The conditional probability of 3 or more dikes intersecting the footprint is less than 0.02.

Figures 4.1.6-7 and 4.1.6-8 show the same data for conduits: the distribution on number of conduit intersections given that at least one conduit intersects the footprint. Given a conduit intersection, it is most likely that only one such intersection would occur, but the potential exists for as many as three conduit intersections. Figures 4.1.6-9 and 4.1.6-10 show the same data for vents.

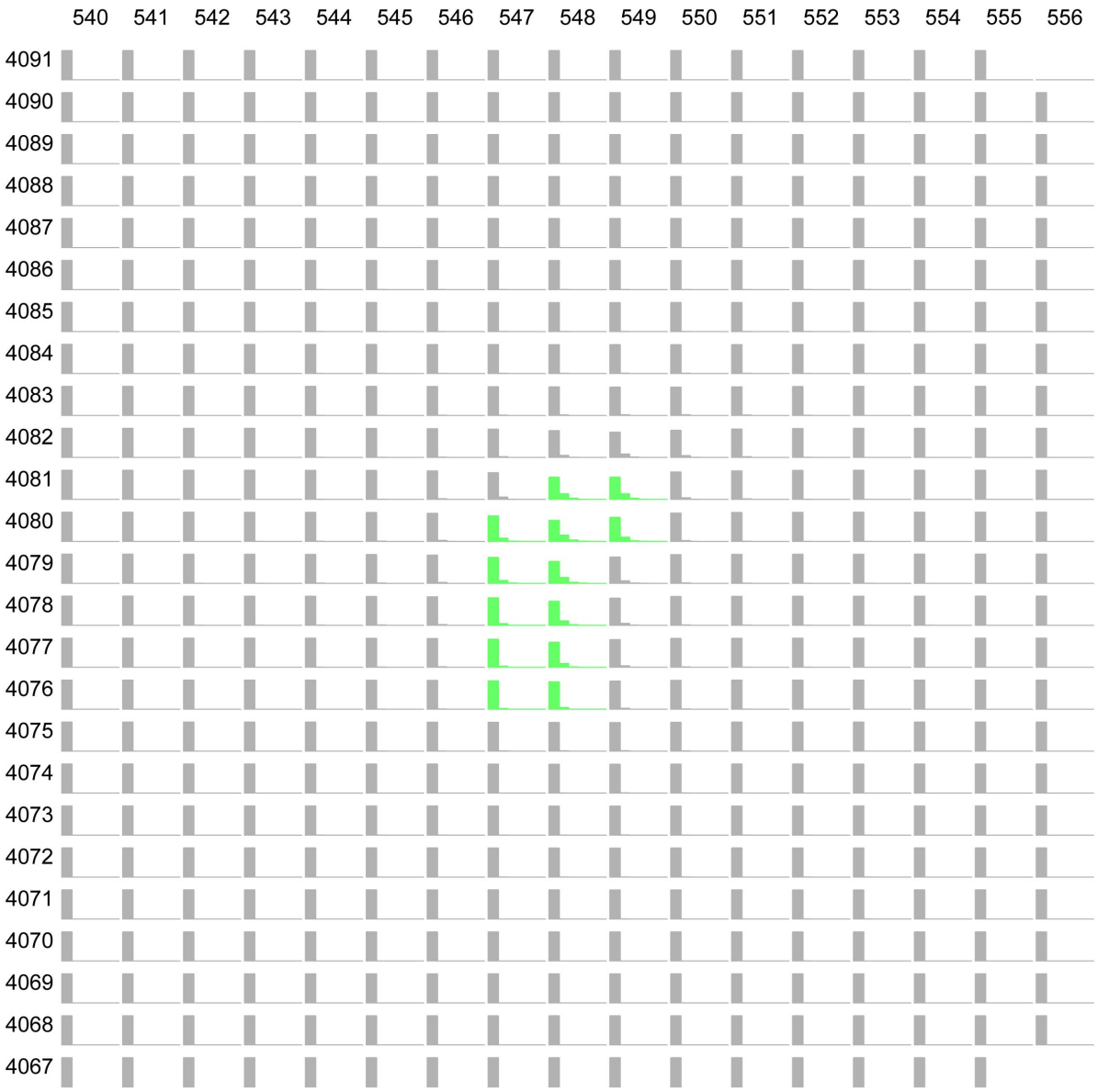

NOTE: Row and column labels represent grid points (UTM coordinates in km, NAD83) in the vicinity of the repository. Green plots show points inside or partially inside the repository footprint. Blank plots (e.g., in the upper left corner) indicate that the probability of intersection for an event at that location is zero. All other plots show the number of intersections conditional on at least one.

Figure 4.1.6-5. Schematic Showing the Distribution of the Number of Dikes That Intersect the Repository Footprint Given an Event at Each Grid Point, Given at Least a 99% Chance that a Dike Intersection Occurs (based on the event descriptions of Michael Sheridan)

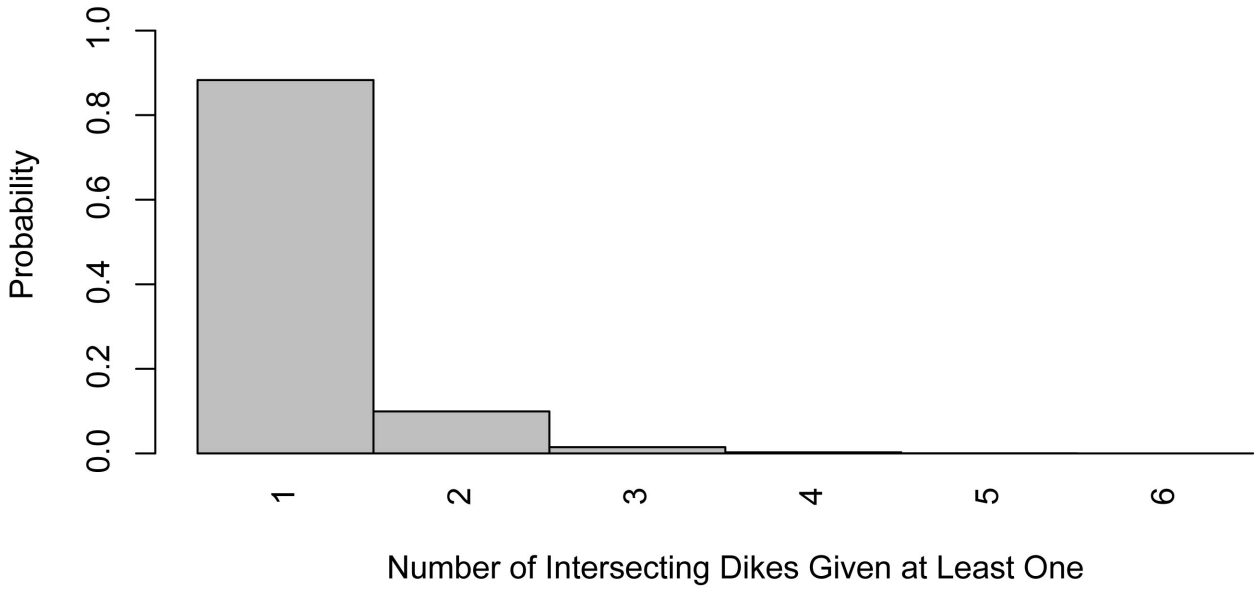

Figure 4.1.6-6. Conditional Distribution of the Number of Dikes That Intersect the Repository Footprint, Given That at Least One Dike Intersection Occurs (based on the event descriptions of Michael Sheridan)

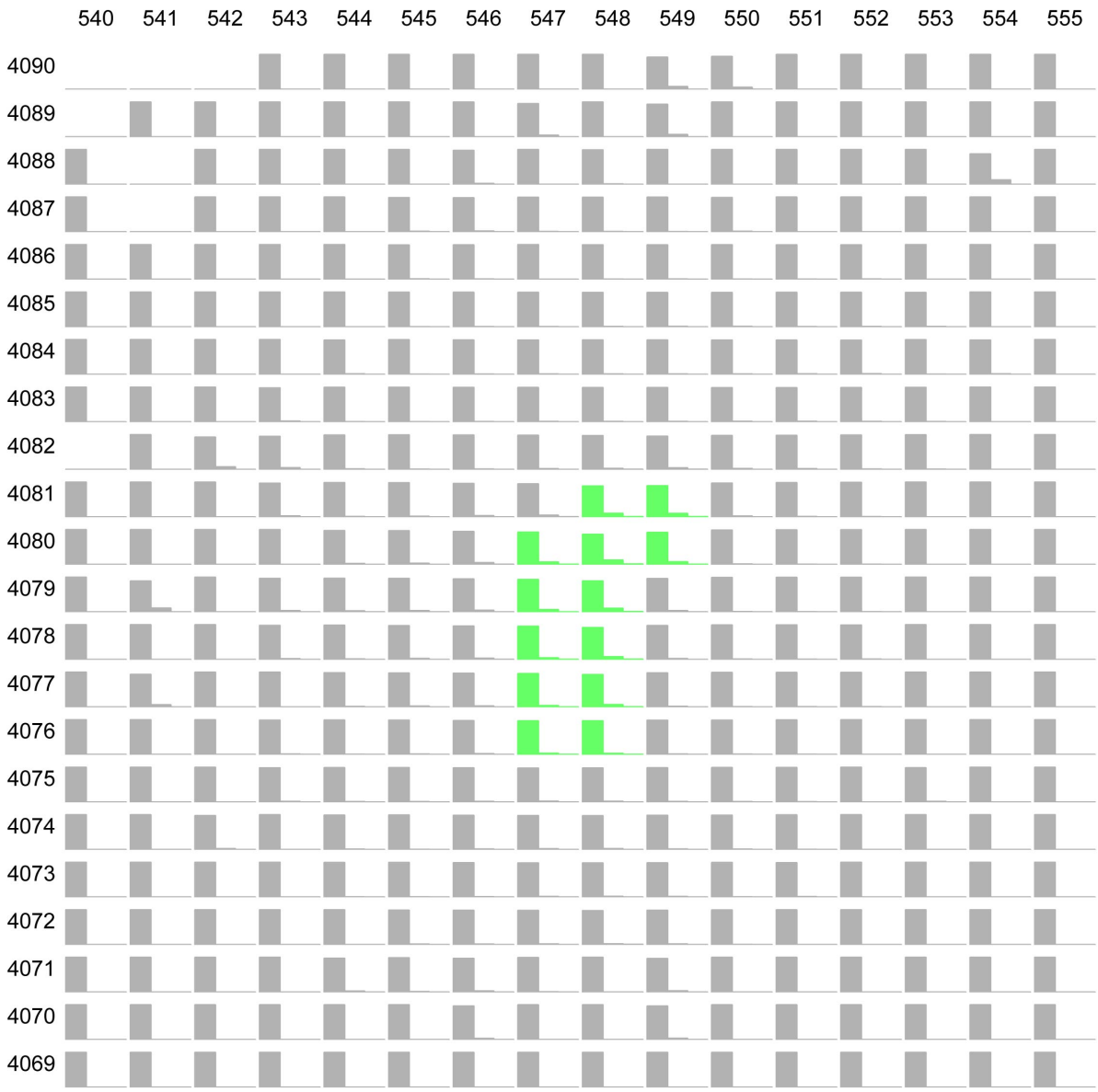

NOTE: Row and column labels represent grid points (UTM coordinates in km, NAD83) in the vicinity of the repository. Green plots show points inside or partially inside the repository footprint. Blank plots (e.g., in the upper left corner) indicate that the probability of intersection for an event at that location is zero. All other plots show the number of intersections conditional on at least one.

Figure 4.1.6-7. Schematic Showing the Distribution of the Number of Conduits That Intersect the Repository Footprint Given an Event at Each Grid Point, Given at Least a 99% Chance of a Conduit Intersection Occurs (based on the event descriptions of Michael Sheridan)

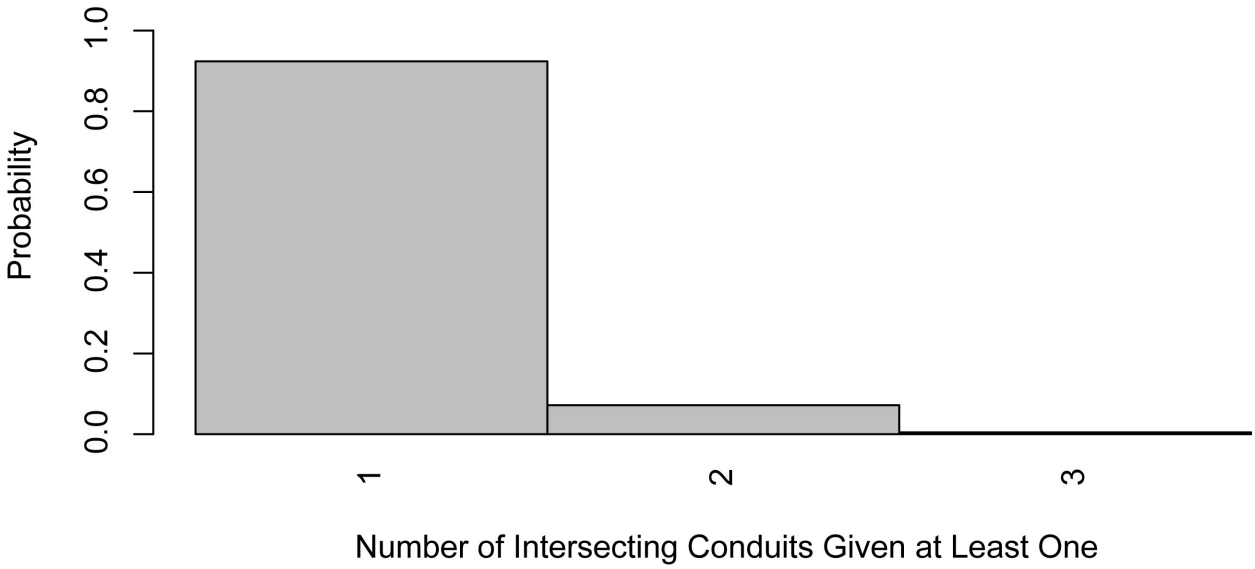

Figure 4.1.6-8. Conditional Distribution of the Number of Conduits That Intersect the Repository Footprint, Given That at Least One Conduit Intersection Occurs (based on the event descriptions of Michael Sheridan)

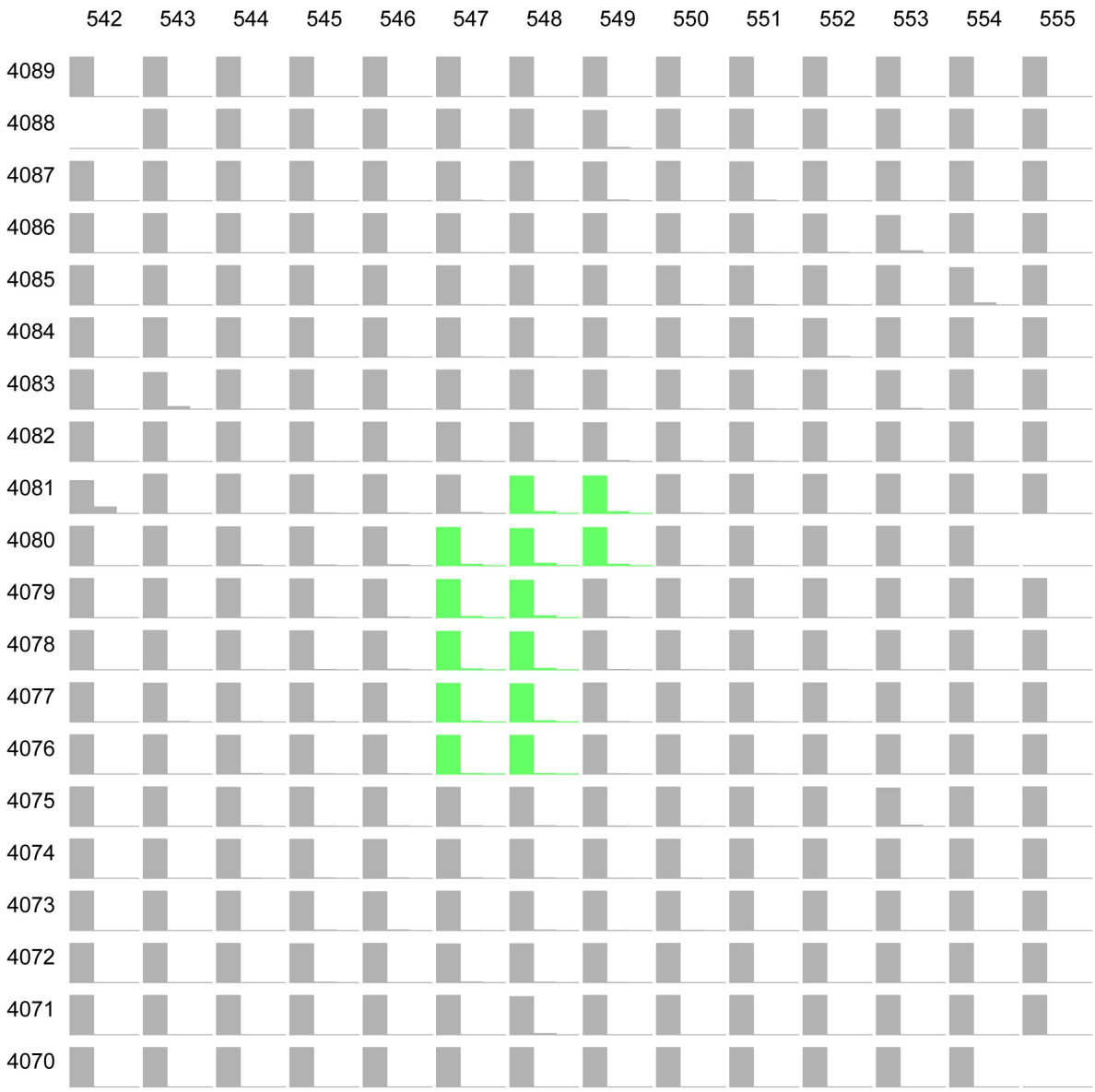

NOTE: Row and column labels represent grid points (UTM coordinates in km, NAD83) in the vicinity of the repository. Green plots show points inside or partially inside the repository footprint. Blank plots (e.g., in the upper left corner) indicate that the probability of intersection for an event at that location is zero. All other plots show the number of intersections conditional on at least one.

Figure 4.1.6-9. Schematic Showing the Distribution of the Number of Vents That Intersect the Repository Footprint Given an Event at Each Grid Point, Given That at Least a 99% Chance that a Vent Intersection Occurs (based on the event descriptions of Michael Sheridan)

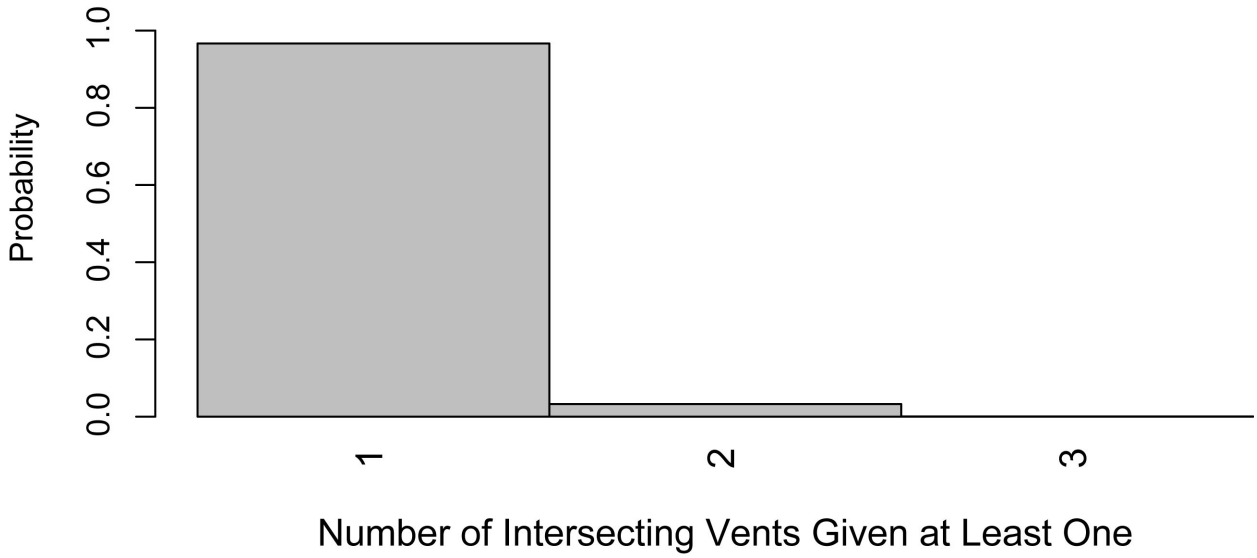

Figure 4.1.6-10. Conditional Distribution of the Number of Vents That Intersect the Repository Footprint, Given That at Least One Vent Intersection Occurs (based on the event descriptions of Michael Sheridan)

4.1.6.3 Results at Different Future Times

Although MS defined one set of models as applying to both the 10,000-year and 1-My assessments, the inclusion of the temporal clustering model leads to noticeable differences in the hazard as a function of time. As described in Section 3.1.6 and his elicitation summary in Appendix D, MS includes a temporal clustering model with clusters of an uncertain duration, and allows for the possibility that the "cluster" that began at Lathrop Wells is still active. The frequency of intersection under this conceptual model differs over time based on whether that time is "in a cluster" or "between clusters." A key factor in the hazard estimate over time is whether it is possible that the Lathrop Wells "cluster" is still active; the maximum duration of a cluster is defined as 300,000 years, so the hazard is strongly dependent on the time at which it is evaluated through about 220,000 years from the present. Beyond that time, the distribution on the frequency of intersection does not change. Figure 4.1.6-11 shows the hazard distribution (pmf) for evaluations at the present day (the 10,000-year assessment result), at 100,000 years in the future, and at 1 My in the future.

The most obvious change over time is the decrease and ultimately the elimination of the third "mode" in the pmf at about 1e-8. This portion of the rate distribution for the 10,000-year assessment was associated with the temporal clustering model: specifically with the probability that the Lathrop Wells cluster is still active at the time being evaluated. Based on MS's assessed cluster duration, there is zero probability at 1 My that the Lathrop Wells cluster is still active (note that this does not imply that there is zero probability of being in *a* cluster, just a zero probability of being in the Lathrop Wells cluster).

Figure 4.1.6-12 shows the sensitivity of the mean hazard evaluated at 1 My to the various model components. This sensitivity chart also shows the dramatic change that results from being beyond the time horizon where the Lathrop Well cluster can contribute to rate. Several bars are highlighted in blue to point out how the influence of those model components changes over time. For example, the temporal model for the Crater Flat field (the use of the homogenous Poisson versus the temporal clustering model) becomes dramatically less important to uncertainty in the mean hazard. This results from the similarity in the long-term mean rates of the two models (although as shown below the impact on overall uncertainty of the temporal model is still strong). Whether the current time is between or within clusters is, not surprisingly, the most important contributor to uncertainty in the mean hazard, and the relative impact of uncertainty in the field rate itself increased as the effect of the temporal model decreases.

Finally, Figure 4.1.6-13 shows the sensitivity of overall uncertainty to the various model components. As mentioned, the temporal model has a dramatic effect on the uncertainty in the hazard estimate: it is still the largest average contributor to overall uncertainty, and selection of one particular model (the temporal clustering model) would greatly increase the relative uncertainty in the hazard estimate.

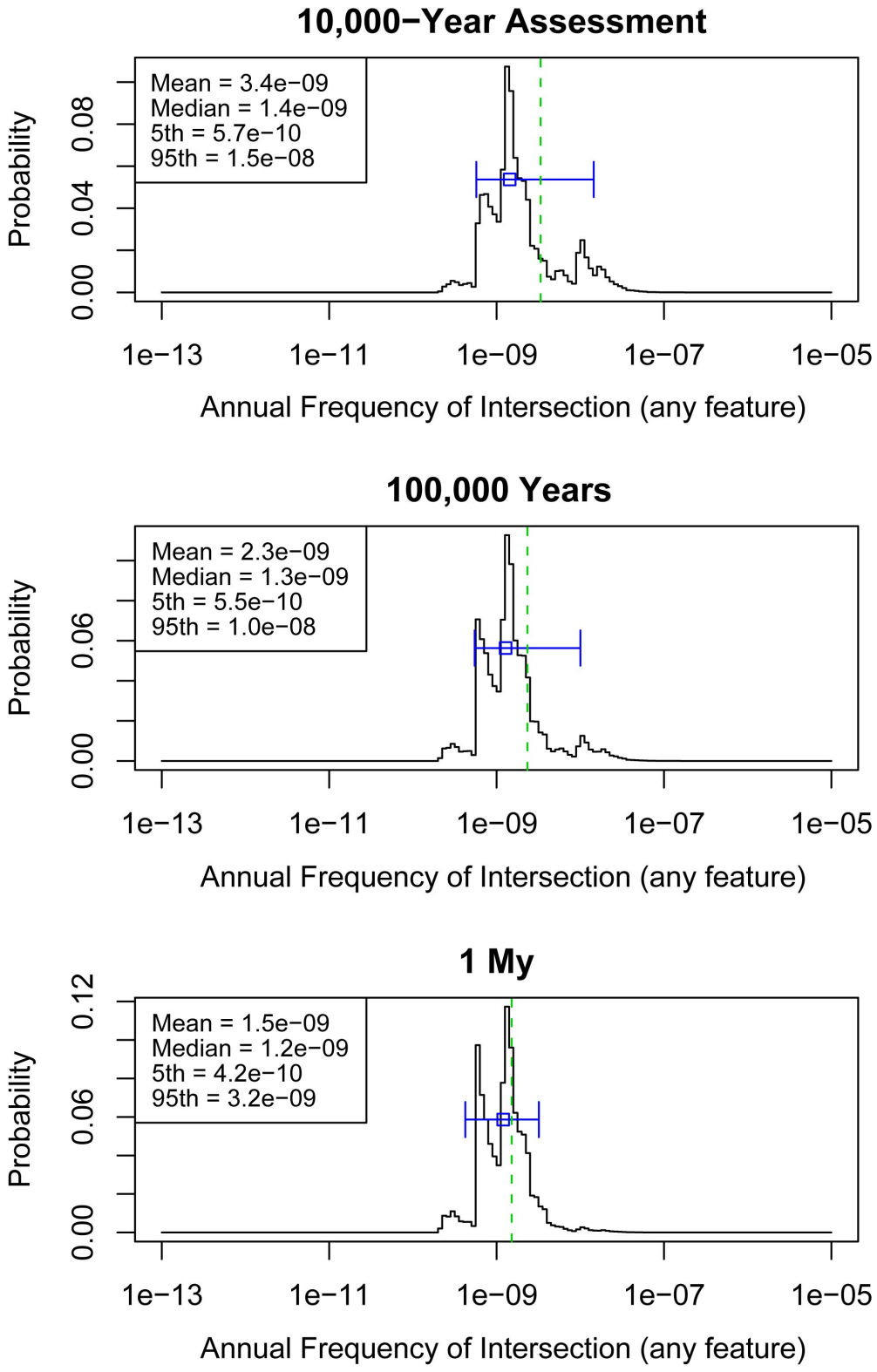

NOTE: The mean is shown by the dashed vertical line, the median with the open box, and the 5th to 95th percentiles with the horizontal line.

Figure 4.1.6-11. Hazard Results from PVHA-U Models Specified by Michael Sheridan Evaluated at Three Different Future Times

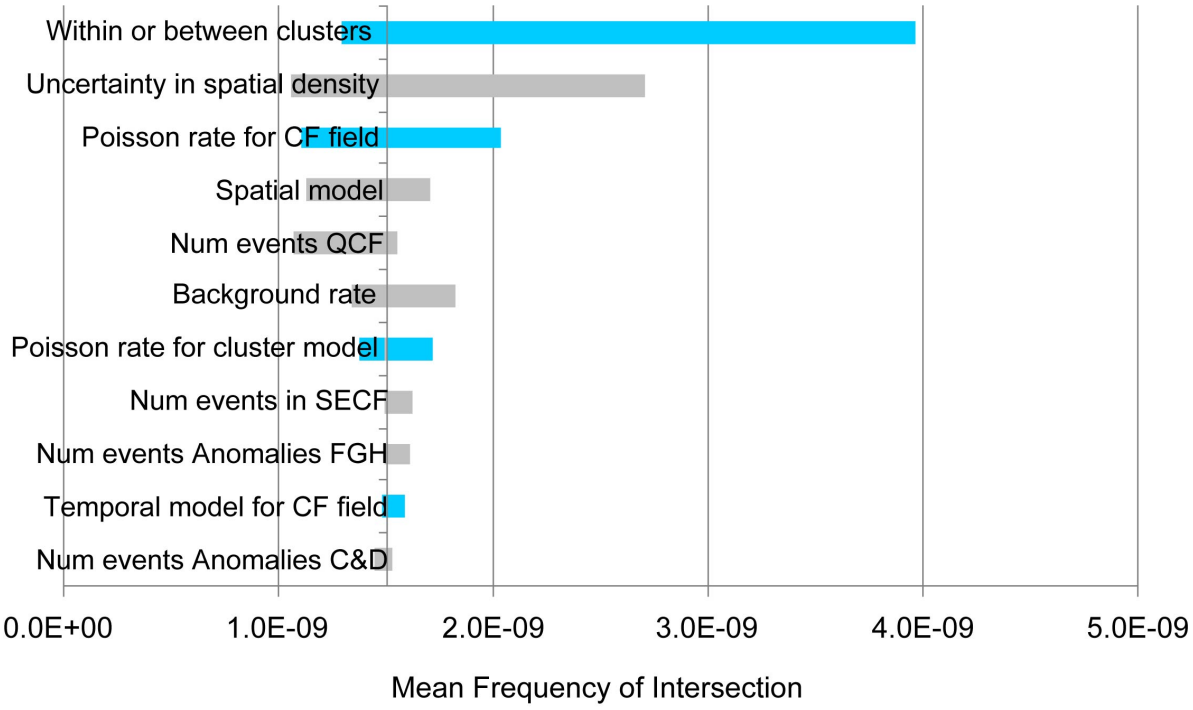

NOTE: Labels on each bar correspond to the nodes in the logic tree for MS's models as described in Section 3.2. The length of each bar shows the range of the mean hazard values that result from fixing the value of the specified model component at one of its branch values. This range represents the degree to which the mean hazard is affected by uncertainty in the specified model component. CF = Crater Flat; QCF = Quaternary Crater Flat; SECF = Southeastern Crater Flat

Figure 4.1.6-12. Contribution of Uncertainty in Model Components to Uncertainty in the Mean Hazard, for the PVHA-U Models Specified by Michael Sheridan, Evaluated at a Future Time of 1 My

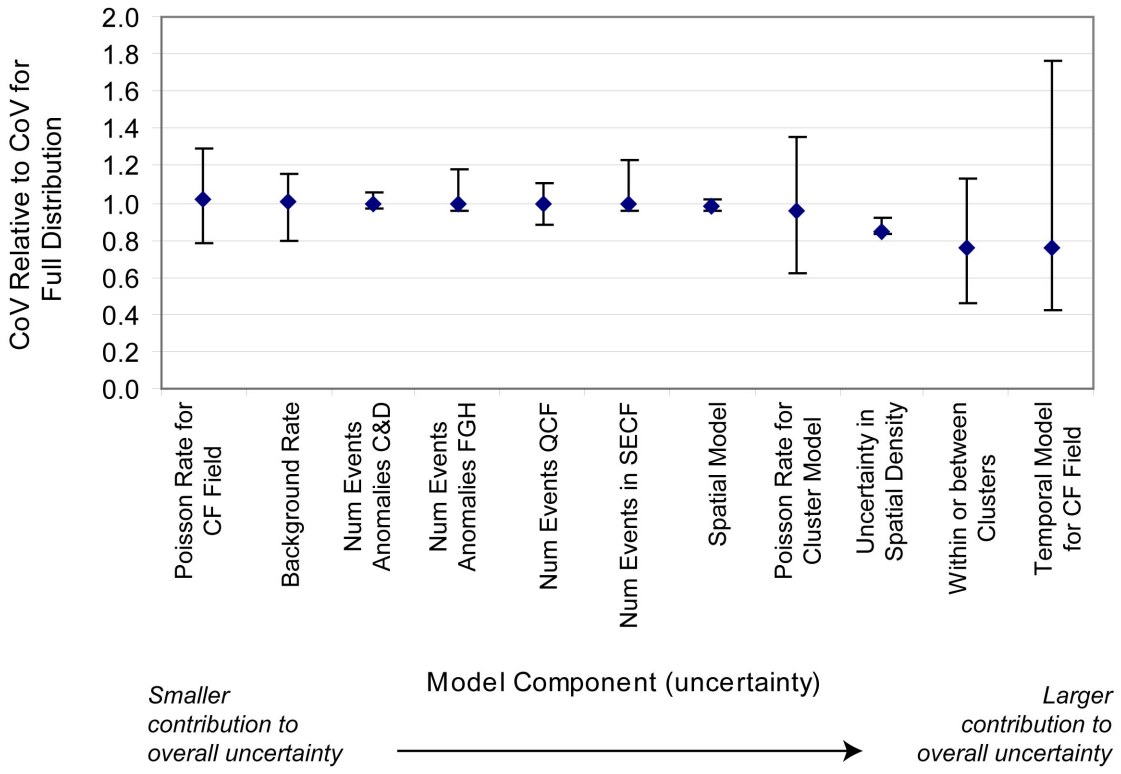

NOTE: Graph shows the CoV for the hazard distribution calculated with the specified model component fixed at each of its branch values, divided by the CoV for the full hazard distribution. Diamond shows the mean value with the relative CoV for each branch value weighted by its probability; "error bars" show the highest and lowest relative CoVs calculated across the branches for that model component. CF = Crater Flat; QCF = Quaternary Crater Flat; SECF = Southeastern Crater Flat

Figure 4.1.6-13. Contribution of Uncertainty in Model Components to Overall Uncertainty in the Hazard Estimate, for the PVHA-U Models Specified by Michael Sheridan, Evaluated at a Future Time of 1 My

4.1.7 PVHA-U Results for Frank Spera

This section describes the results of the PVHA-U models specified by Frank Spera (FS). Those models and assessments are described in Section 3.2.7 and the elicitation summary in Appendix D. Section 4.1.7.1 discusses the results of the 10,000-year assessment for the frequency of intersection of any feature with the repository footprint. The frequency of intersection of specific features with the repository footprint is discussed in Section 4.1.7.2, and differences in the hazard calculated for the 10,000-year assessment and the 1-My assessment are discussed in Section 4.1.7.3.

4.1.7.1 Hazard Results for the 10,000-Year Assessment

Figure 4.1.7-1 summarizes the spatial distribution of hazard calculated using FS's PVHA-U models for the 10,000-year assessment. The spatial distribution of the mean frequency of intersection map in panel (c) looks very similar in shape to the conditional probability of intersection map in panel (b), with a slight extension of the contours to the SSW of the repository footprint showing the effect of the greater rate density area in that portion of the YMR.

Figure 4.1.7-2 illustrates the uncertainty in the frequency of intersection of any feature with the repository footprint. The mean frequency of intersection is marked on both graphs by a dashed vertical line, and the median, 5th, and 95th percentiles are shown on the pmf. The mean frequency of intersection of any feature with the repository footprint is 1.5 e-8; the median frequency is 6.0e-9. The 5th and 95th percentiles are 5.7e-10 and 4.1e-8, respectively.

(a) Mean rate density. Contours represent the mean annual frequency of igneous events (events per year) per km^2.

(b) Conditional probability of intersection of any feature. Contours represent the probability that an event assumed to occur at each location would result in the intersection of any igneous feature with the repository footprint.

(c) Spatial distribution of the mean frequency of intersection. Contours represent the mean annual probability of an intersection of the repository footprint by an igneous feature.

NOTE: The repository footprint is shown as a yellow polygon; past events are represented as black triangles. Map grid ticks are UTM meters; tick intervals for map (a) are 20 km; map (b) and (c) are 10 km.

Figure 4.1.7-1. Components of the Hazard Calculation for PVHA-U Models Specified by Frank Spera, for the 10,000-Year Assessment

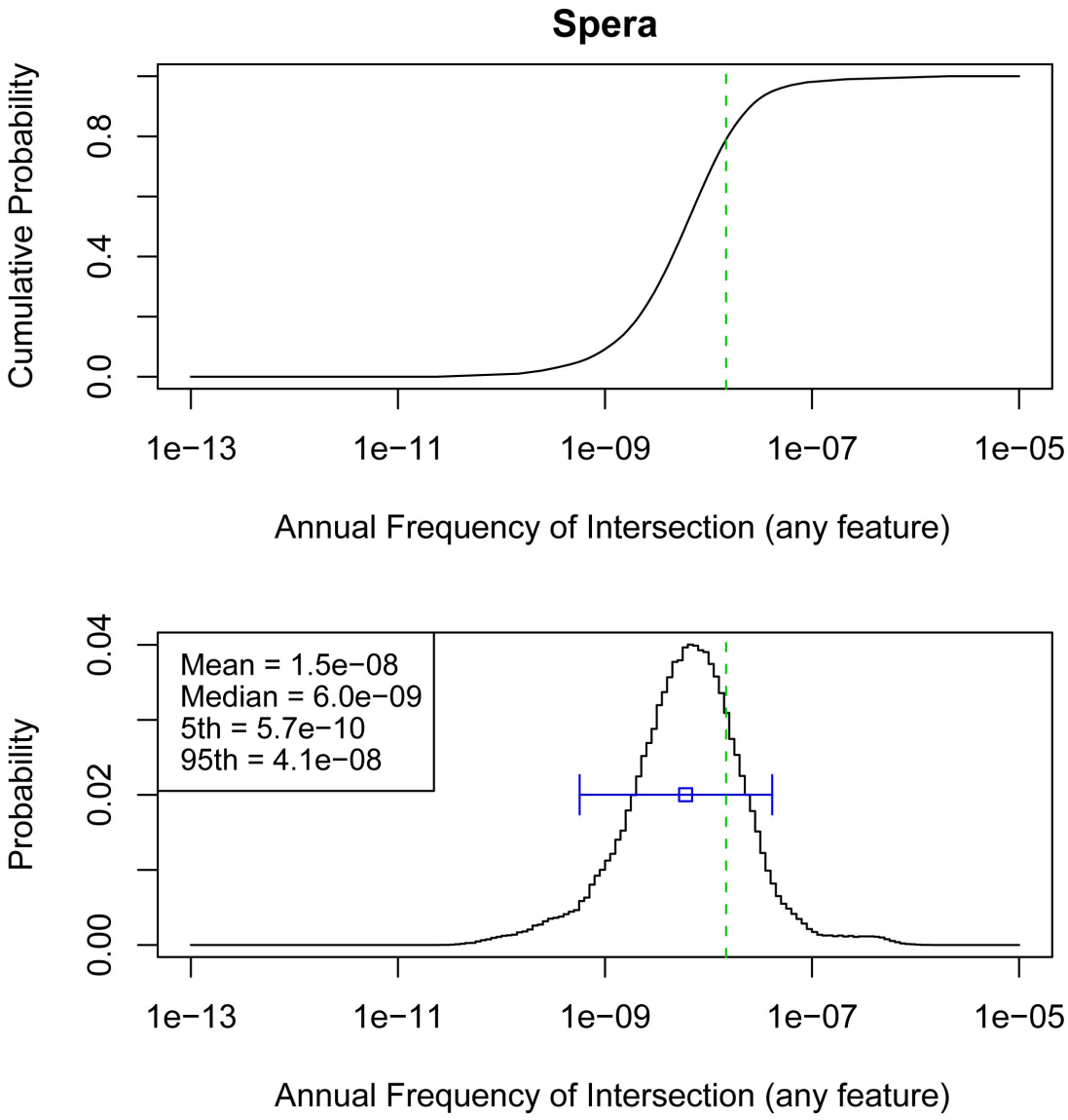

NOTE: Top figure is a cumulative distribution function, bottom figure is a probability mass function. The mean is shown by the dashed vertical line, the median with the open box, and the 5th to 95th percentiles with the horizontal line.

Figure 4.1.7-2. Hazard Results for the 10,000-Year Assessment from PVHA-U Models Specified by Frank Spera

Contributions to Uncertainty

Contributions from various model components to uncertainty in the mean hazard in FS's models are illustrated in Figure 4.1.7-3. The most significant contributor to uncertainty in the mean hazard is the volume per event, which is a key component of the rate calculation for the time-volume rate model FS used in his models. The width of this bar combines the effect of the alternative models used to estimate the volume per event and the uncertainty in the volume per event: because the uncertainty in the volume per event is represented by a single node in the logic tree (as shown in Section 3.2.7), setting that node to one of its branch values for sensitivity

analysis effectively sets it to the high value under both conceptual models of how volume per event should be estimated. Other model components are minor contributors to uncertainty in the mean hazard compared to the volume per event estimate.

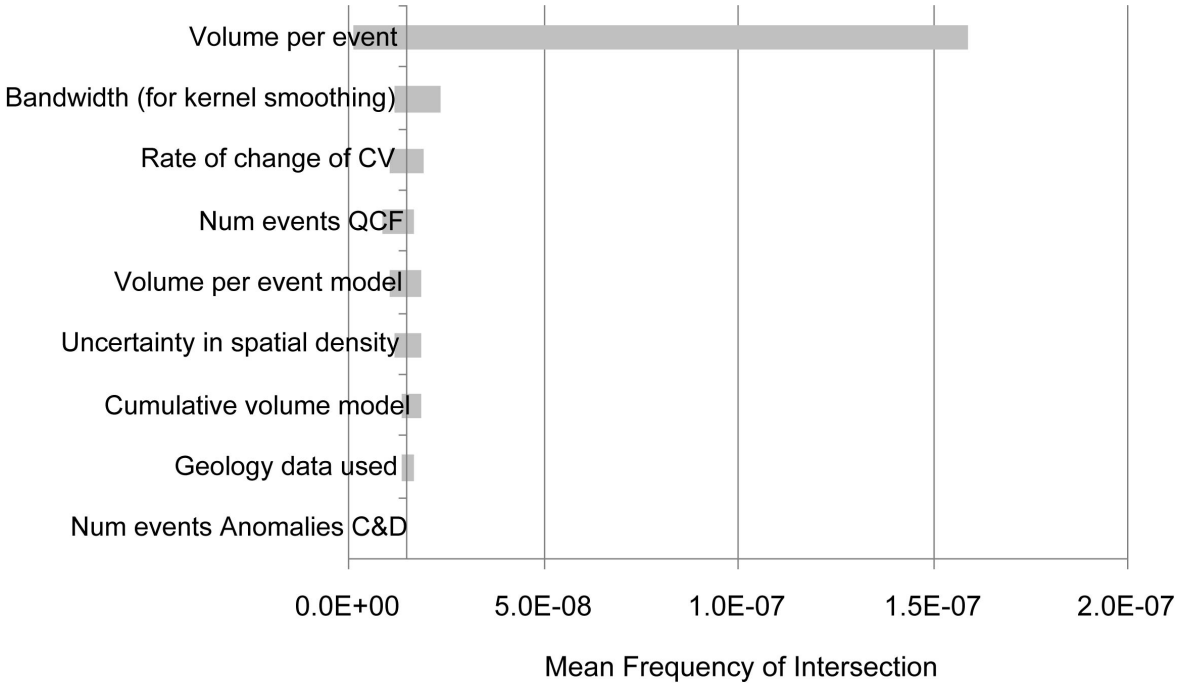

NOTE: Labels on each bar correspond to the nodes in the logic tree for FS's models as described in Section 3.2. The length of each bar shows the range of the mean hazard values that result from fixing the value of the specified model component at one of its branch values. This range represents the degree to which the mean hazard is affected by uncertainty in the specified model component. CV = cumulative volume; QCF = Quaternary Crater Flat.

Figure 4.1.7-3. Contribution of Uncertainty in Model Components to Uncertainty in the Mean Hazard, for the PVHA-U Models for the 10,000-Year Assessment Specified by Frank Spera

Contribution of various model components to *overall uncertainty* in the hazard for FS's model is shown in Figure 4.1.7-4. This figure shows more clearly the impact of the alternative volume per event models: if the volume per event model based on the volume of the Quaternary events only is used, the CoV for the hazard distribution would be much less than the CoV for the full distribution, as shown by the bottom of the "error bar" associated with the "Volume per event model" in the figure. If the volume per event is estimated directly from FS's assessment associated with his event model, the CoV increases slightly (the top of the "error bar" associated with the "Volume per event model" in the figure).

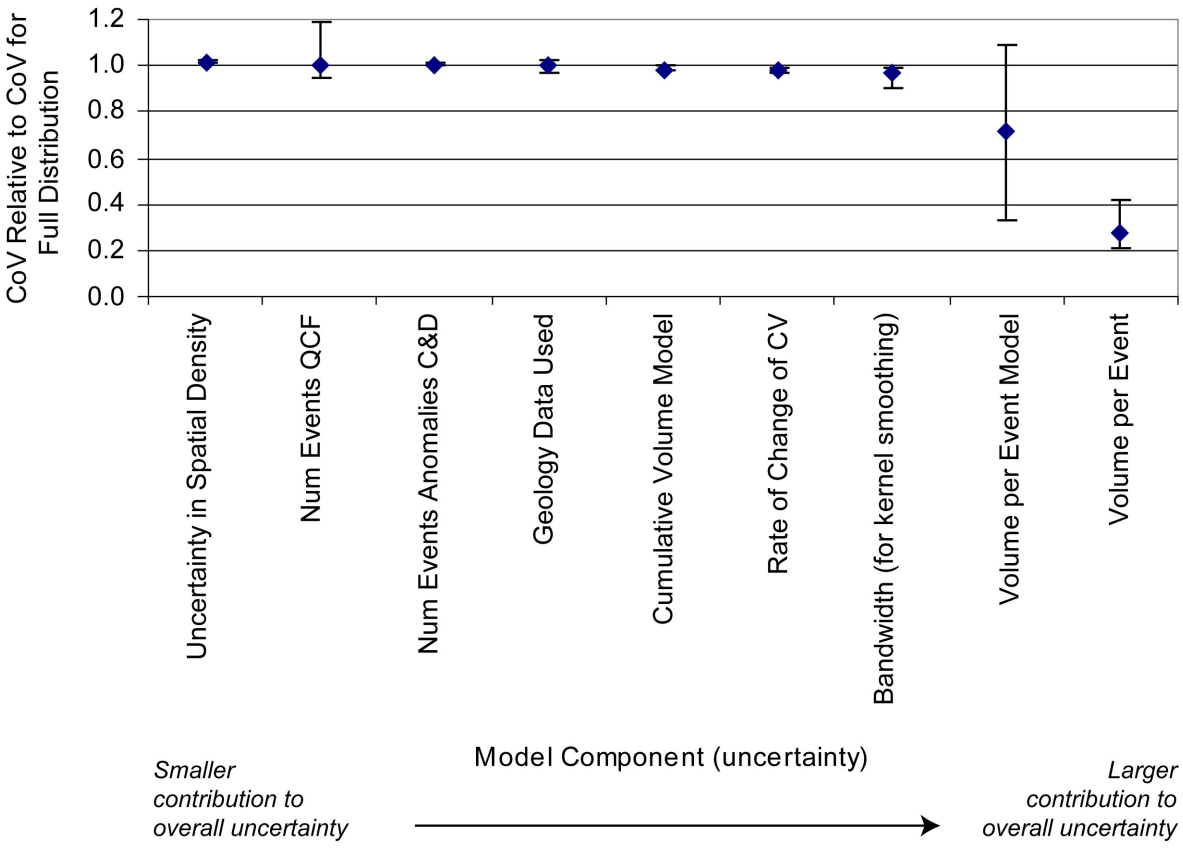

NOTES: Graph shows the CoV for the hazard distribution calculated with the specified model component fixed at each of its branch values, divided by the CoV for the full hazard distribution. Diamond shows the mean value with the relative CoV for each branch value weighted by its probability; "error bars" show the highest and lowest relative CoVs calculated across the branches for that model component. CV = cumulative volume; QCF = Quaternary Crater Flat.

Figure 4.1.7-4. Contribution of Uncertainty in Model Components to Overall Uncertainty in the Hazard Estimate, for the PVHA-U Models for the 10,000-Year Assessment Specified by Frank Spera

4.1.7.2 Discussion of Individual Features

As described in Section 3.2.7, FS's events all include dikes, at least one conduit or vent, and might also include sills. The conditional probability of intersection of each type of feature with the repository footprint was illustrated in Section 3.2.7, and, as discussed, the shape of the conditional probability of intersection maps for each individual feature is the same as for the conditional probability of intersection for any feature: no consistent clustering or grouping of individual features in an event occurs. Similarly, the full distribution of the frequency of intersection for any individual feature follows the same pattern as the distribution for any feature shown in Figure 4.1.7-2, simply shifted to the lower frequencies associated with the individual feature.

Table 4.1.7-1 shows the mean and median frequencies of intersection for each feature.

Table 4.1.7-1. Mean and Median Frequency of Intersection of Various Igneous Features with the Repository Footprint, for Frank Spera's 10,000-Year Assessment

Feature	Mean Frequency of Intersection	Median Frequency of Intersection
Any feature	1.5e-8	6.0e-9
Dikes	1.5e-8	6.0e-9
Column-producing conduits	6.1e-9	2.5e-9
Vents	1.6e-9	6.6e-10
Sills	5.3e-10	2.1e-10

Potential for Multiple Intersections

Figure 4.1.7-5 shows a set of plots illustrating the distribution of the number of dike intersections for an event centered at a specific point, conditional on at least one such intersection occurring. The most likely number of intersections across the region as shown in the figure is one, but multiple dike intersections are possible depending on the event location. Figure 4.1.7-6 combines the relative likelihood of a dike intersection at each point with the conditional distribution of the number of dike intersections for an event at those points to yield a conditional distribution on the number of dike intersections, given that at least one such intersection occurs. As shown, assuming a dike intersection occurs, it is most likely (probability 0.75) that only one dike intersects, but the potential exists for as many as 8 dikes to intersect the footprint. The probability of 4 or more dikes intersecting the repository footprint, given that at least one dike intersects, is about 0.01.

Figures 4.1.7-7 and 4.1.7-8 show the same data for conduits: the distribution on number of conduit intersections given that at least one conduit intersects the footprint. Given a conduit intersection, it is most likely that only one such intersection would occur (probability 0.88), but as many as 5 conduits intersecting the footprint is possible. While vents are less likely than conduits in FS's event descriptions, their relative location and size are otherwise described by the same models, so the *conditional* frequency of vent intersection, as shown in Figures 4.1.7-9 and 4.1.7-10, follows that just described for conduits.

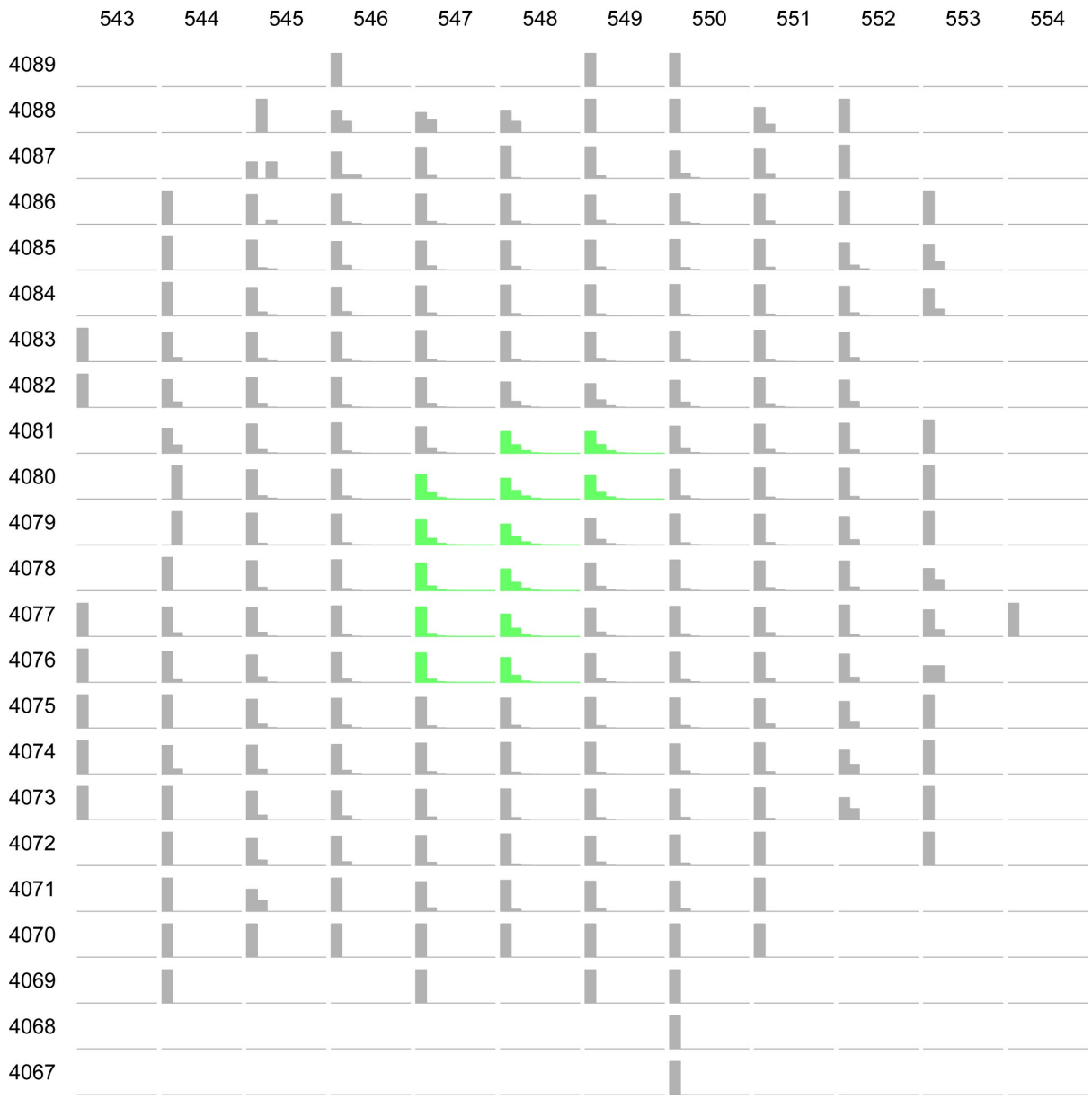

NOTE: Row and column labels represent grid points (UTM coordinates in km, NAD83) in the vicinity of the repository. Green plots show points inside or partially inside the repository footprint. Blank plots (e.g., in the upper left corner) indicate that the probability of intersection for an event at that location is zero. All other plots show the number of intersections conditional on at least one.

Figure 4.1.7-5. Schematic Showing the Distribution of the Number of Dikes That Intersect the Repository Footprint Given an Event at Each Grid Point, Given That at Least One Dike Intersection Occurs (based on the event descriptions of Frank Spera)

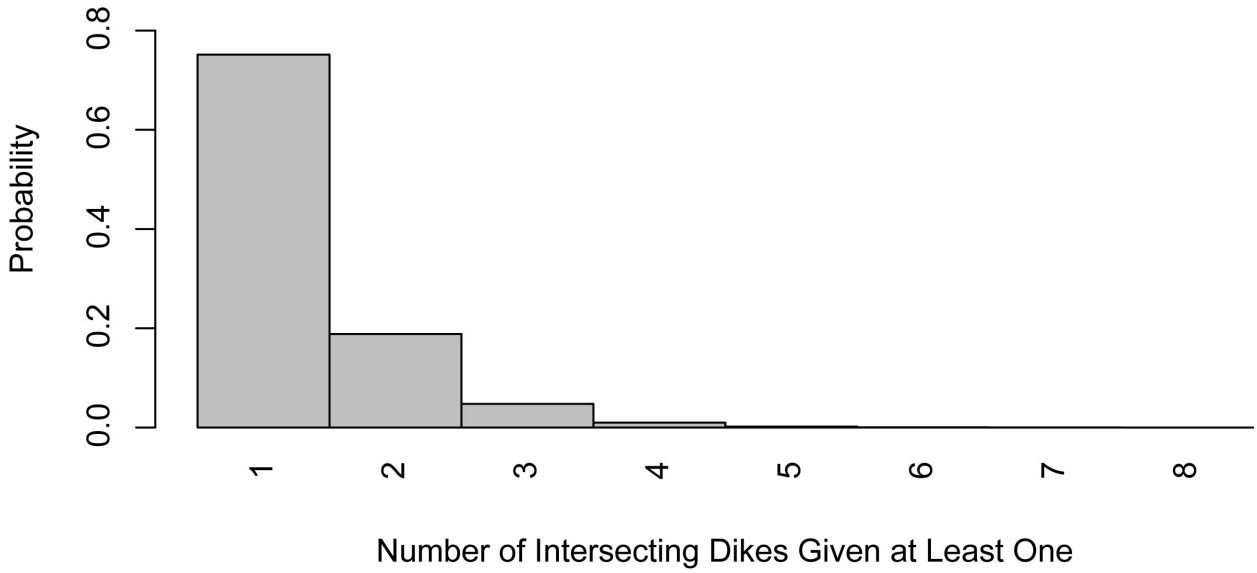

Figure 4.1.7-6. Conditional Distribution of the Number of Dikes That Intersect the Repository Footprint, Given That at Least One Dike Intersection Occurs (based on the event descriptions of Frank Spera)

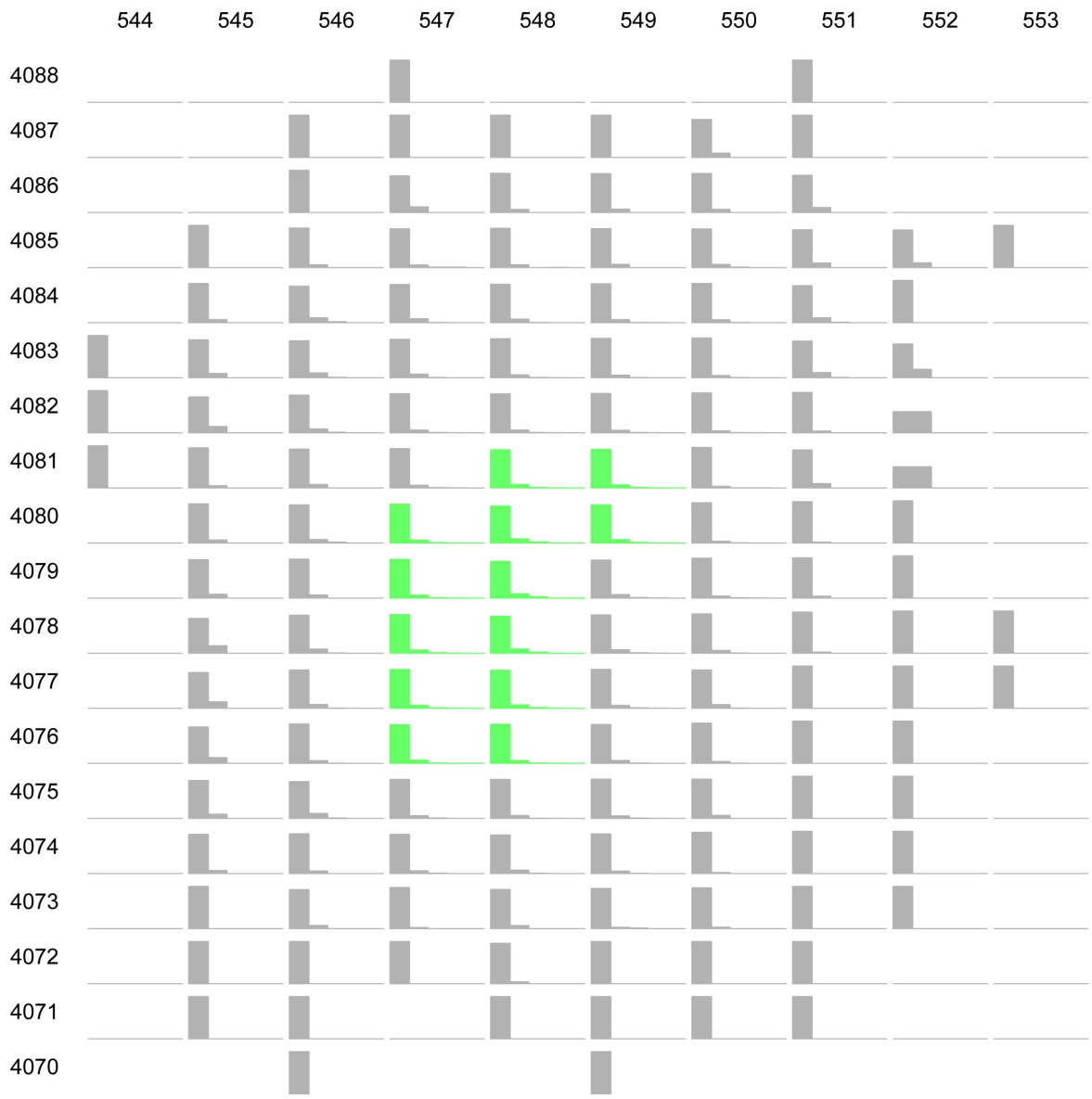

NOTE: Row and column labels represent grid points (UTM coordinates in km, NAD83) in the vicinity of the repository. Green plots show points inside or partially inside the repository footprint. Blank plots (e.g., in the upper left corner) indicate that the probability of intersection for an event at that location is zero. All other plots show the number of intersections conditional on at least one.

Figure 4.1.7-7. Schematic Showing the Distribution of the Number of Conduits That Intersect the Repository Footprint Given an Event at Each Grid Point, Given That at Least One Conduit Intersection Occurs (based on the event descriptions of Frank Spera)

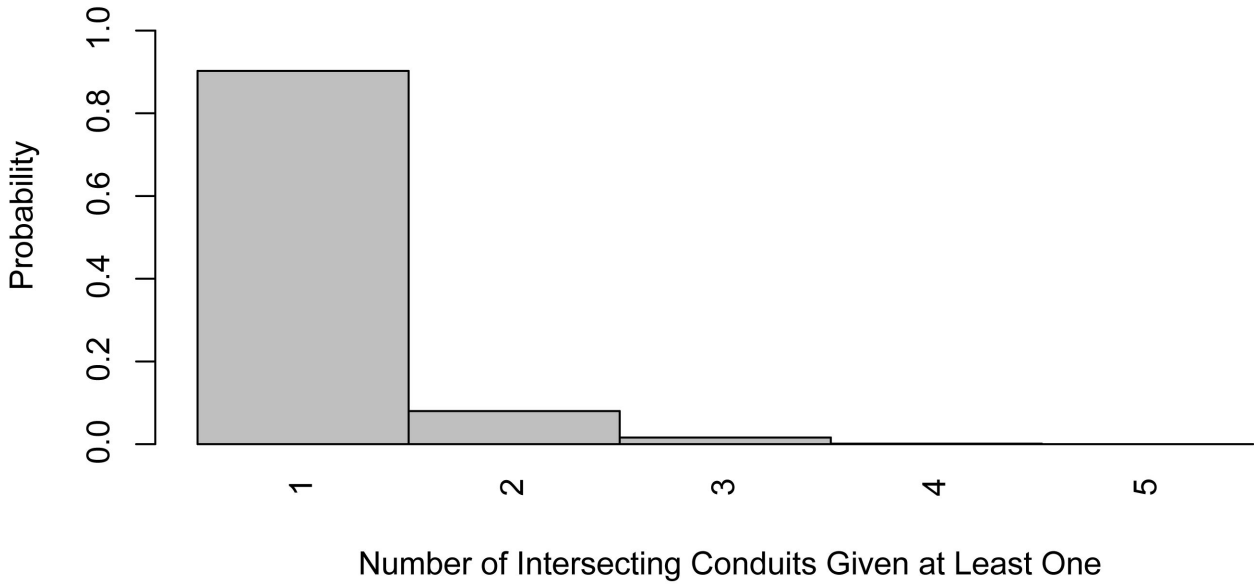

Figure 4.1.7-8. Conditional Distribution of the Number of Conduits That Intersect the Repository Footprint, Given That at Least One Conduit Intersection Occurs (based on the event descriptions of Frank Spera)

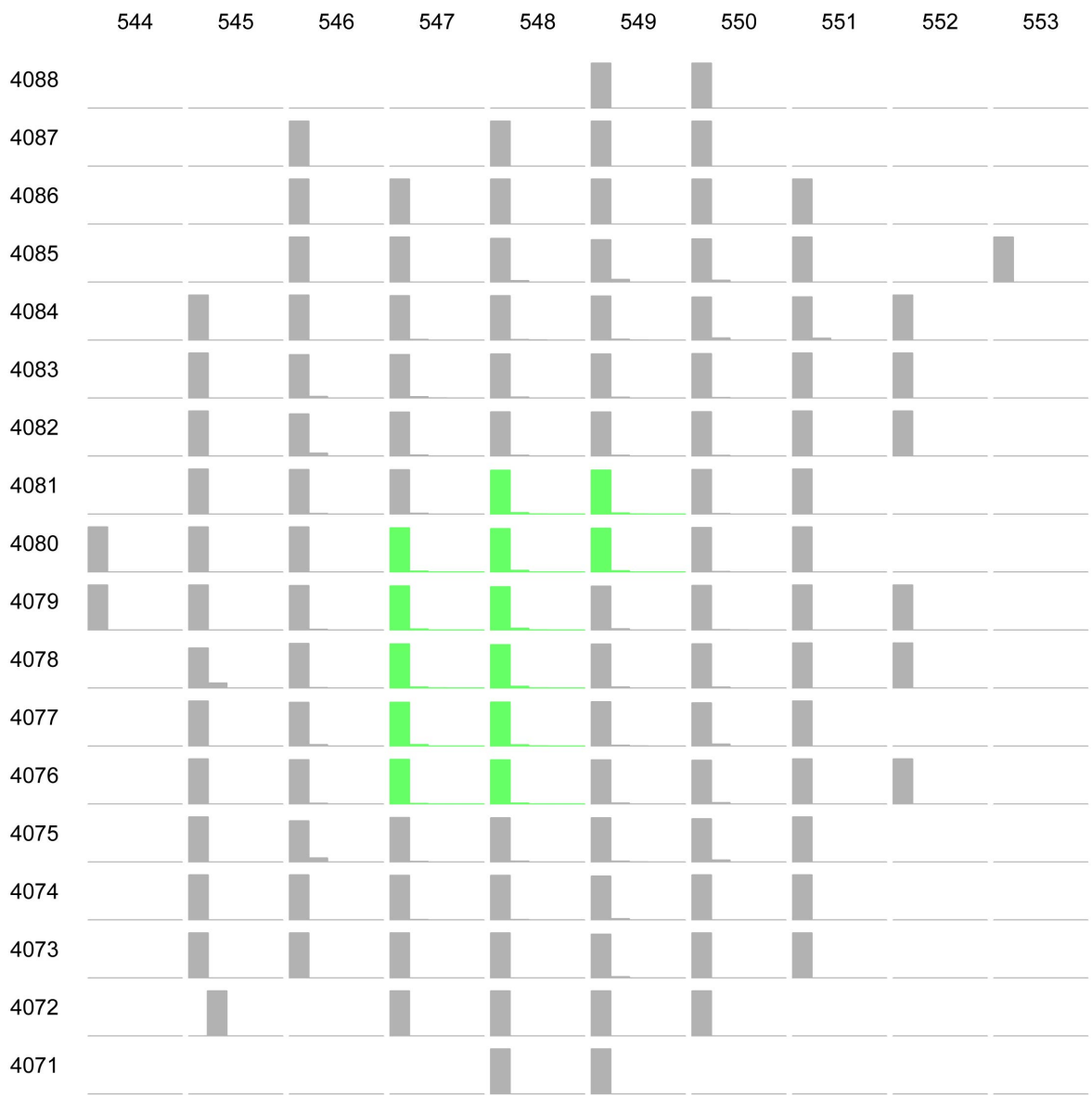

NOTE: Row and column labels represent grid points (UTM coordinates in km, NAD83) in the vicinity of the repository. Green plots show points inside or partially inside the repository footprint. Blank plots (e.g., in the upper left corner) indicate that the probability of intersection for an event at that location is zero. All other plots show the number of intersections conditional on at least one.

Figure 4.1.7-9. Schematic Showing the Distribution of the Number of Vents That Intersect the Repository Footprint Given an Event at Each Grid Point, Given That at Least One Vent Intersection Occurs (based on the event descriptions of Frank Spera)

Figure 4.1.7-10. Conditional Distribution of the Number of Vents That Intersect the Repository Footprint, Given That at Least One Vent Intersection Occurs (based on the event descriptions of Frank Spera)

4.1.7.3 Results at Different Future Times

FS defined one set of models as applying to both the 10,000-year and 1-My assessments, but as discussed in Section 3.2.7, the spatial model weights past events by the inverse of their estimated age. To calculate a hazard at a future time of 1 My, for the 1-My assessment, it is assumed that no new events occur between now and 1 My, the events in FS's relevant event sets are "aged" by 1 My, and the models are re-fit to the time-adjusted data. Although this has a noticeable effect on the mean rate density map, as discussed previously, it has little effect on the hazard estimate itself. The mean hazard for the 1-My assessment is 1.6e-8 compared to 1.5e-8 for the 10,000-year assessment. There are no noticeable differences in the hazard curves or the contributions to uncertainty plots between the 1-My results and the 10,000-year results.

4.1.8 PVHA-U Results for George Thompson

This section describes the results of the PVHA-U models specified by George Thompson (GT). Those models and assessments are described in Section 3.2.8 and the elicitation summary in Appendix D. Section 4.1.8.1 discusses the results of the 10,000-year assessment for the frequency of intersection of any feature with the repository footprint. The frequency of intersection of specific features with the repository footprint is discussed in Section 4.1.8.2, and differences in the hazard calculated for the 10,000-year assessment and the 1-My assessment are discussed in Section 4.1.8.3.

4.1.8.1 Hazard Results for the 10,000-Year Assessment

Figure 4.1.8-1 summarizes the spatial distribution of hazard calculated using GT's PVHA-U models for the 10,000-year assessment. The contours in panel (c) show clearly the effect of the overlap of the conditional probability of intersection map with the mean rate density map: the extension of these contours to the SSW of the repository footprint show the effect of the greater rate density of events within the Crater Flat zone. As events are more likely to occur in that zone, the mean frequency of intersection for events in that zone is greater than for events in the lower-rate density background zone to the east of the repository footprint.

Figure 4.1.8-2 illustrates the uncertainty in the frequency of intersection of any feature with the repository footprint. The mean frequency of intersection is marked on both graphs by a dashed vertical line, and the median, 5th, and 95th percentiles are shown on the pmf. The mean frequency of intersection of any feature with the repository footprint is 2.0e-9; the median frequency is 1.8e-9. The 5th and 95th percentiles are 6.5e-10 and 3.9e-9, respectively.

(a) Mean rate density. Contours represent the mean annual frequency of igneous events (events per year) per km^2.

(b) Conditional probability of intersection of any feature. Contours represent the probability that an event assumed to occur at each location would result in the intersection of any igneous feature with the repository footprint.

(c) Spatial distribution of the mean frequency of intersection. Contours represent the mean annual probability of an intersection of the repository footprint by an igneous feature.

NOTE: The repository footprint is shown as a yellow polygon; past events are shown as black triangles. Map grid ticks are UTM meters; tick intervals for map (a) are 20 km; map (b) and (c) are 10 km.

Figure 4.1.8-1. Components of the Hazard Calculation for PVHA-U Models Specified by George Thompson, for the 10,000-Year Assessment

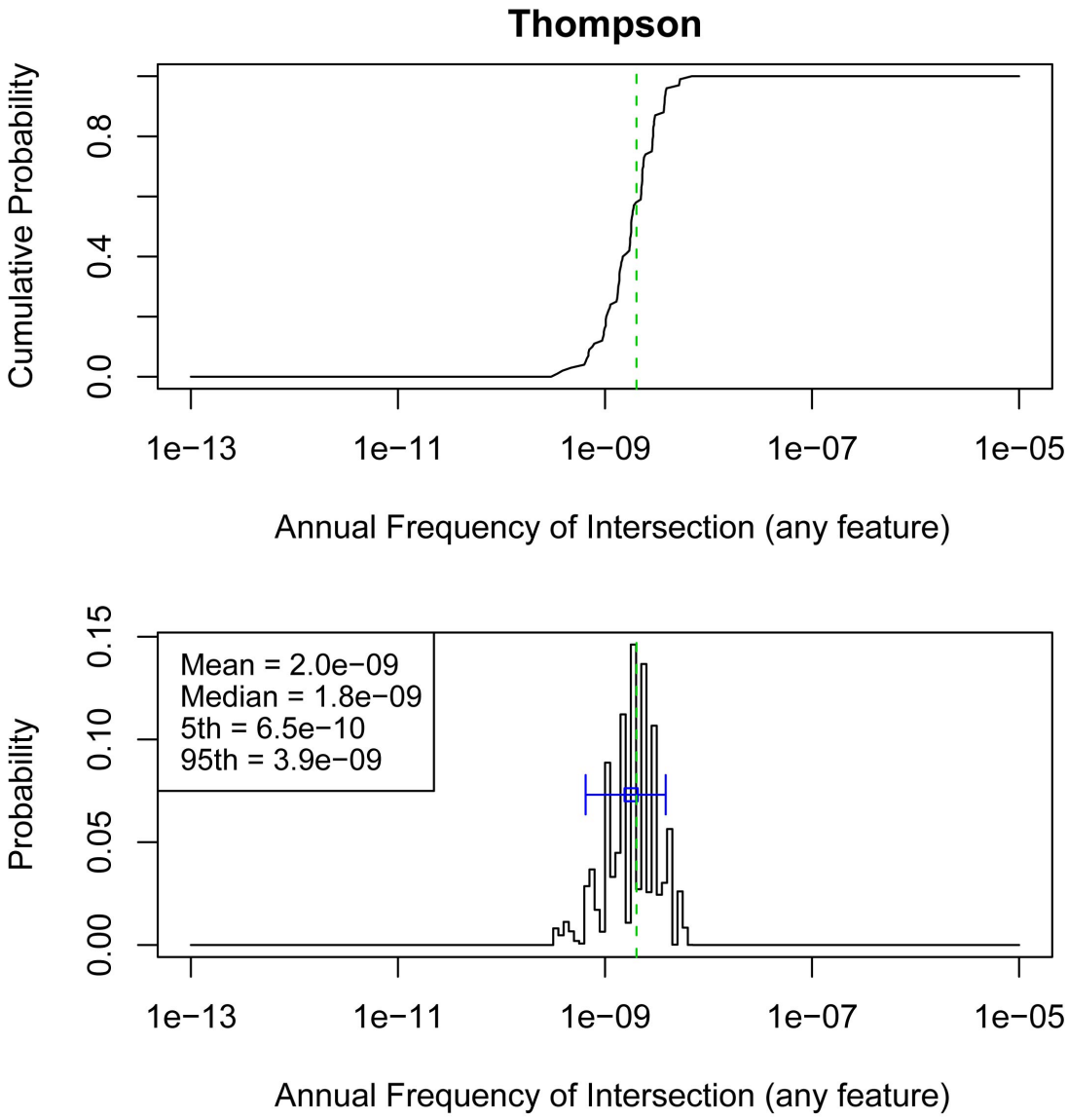

NOTES: Top figure is a cumulative distribution function, bottom figure is a probability mass function. The mean is shown by the dashed vertical line, the median with the open box, and the 5th to 95th percentiles with the horizontal line.

Figure 4.1.8-2. Hazard Results for the 10,000-Year Assessment from PVHA-U Models Specified by George Thompson

Contributions to Uncertainty

Contributions from various model components to uncertainty in the mean hazard in GT's models are illustrated in Figure 4.1.8-3. Although Figure 4.1.8-1 shows the effect of the higher rate in the Crater Flat zone, and indicates that events located in that zone have the potential to intersect the repository footprint, the mean hazard estimate is most sensitive to uncertainty in the rate in the background zone, as shown by the top bar (labeled "Poisson rate in background") in Figure 4.1.8-3. All other uncertainties in the model relate to the estimated rate density within the Crater Flat zone, and their contributions to uncertainty in the mean hazard are small.

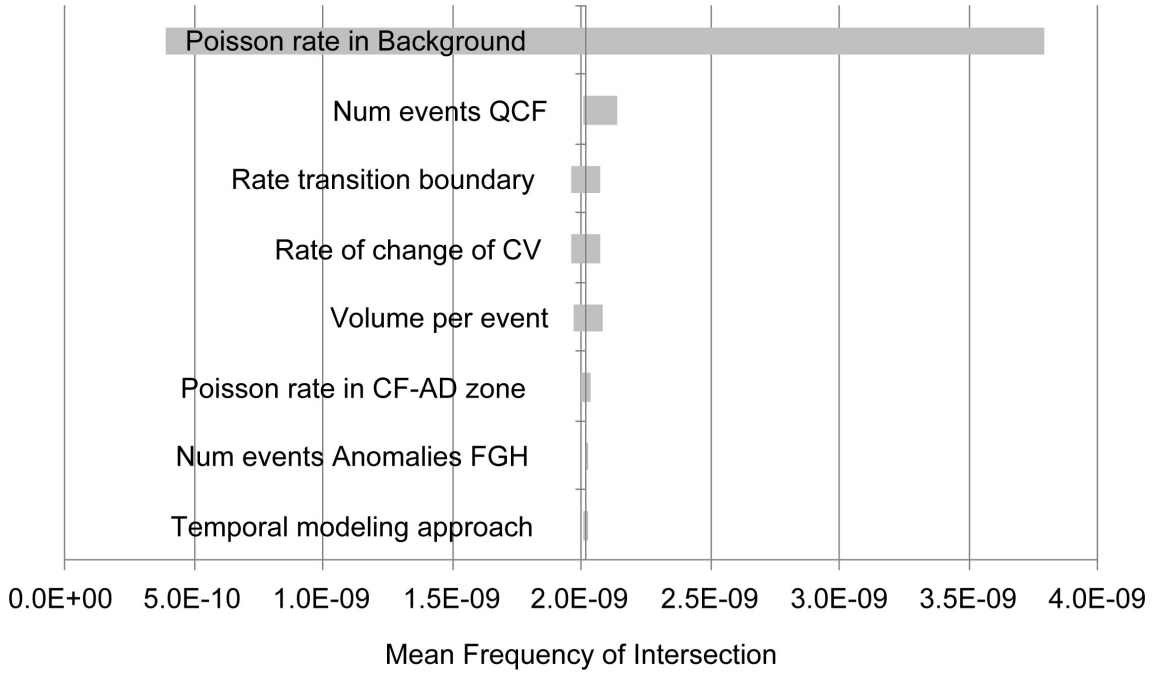

NOTE: Labels on each bar correspond to the nodes in the logic tree for GT's models as described in Section 3.2. The length of each bar shows the range of the mean hazard values that result from fixing the value of the specified model component at one of its branch values. This range represents the degree to which the mean hazard is affected by uncertainty in the specified model component. QCF = Quaternary Crater Flat; CV = cumulative volume; CF-AD = Crater Flat-Amargosa Desert.

Figure 4.1.8-3. Contribution of Uncertainty in Model Components to Uncertainty in the Mean Hazard, for the PVHA-U Models for the 10,000-Year Assessment Specified by George Thompson

Contribution of various model components to *overall uncertainty* in the hazard for GT's model is shown in Figure 4.1.8-4. This result is similar to the contributions to uncertainty in the mean hazard discussed above.

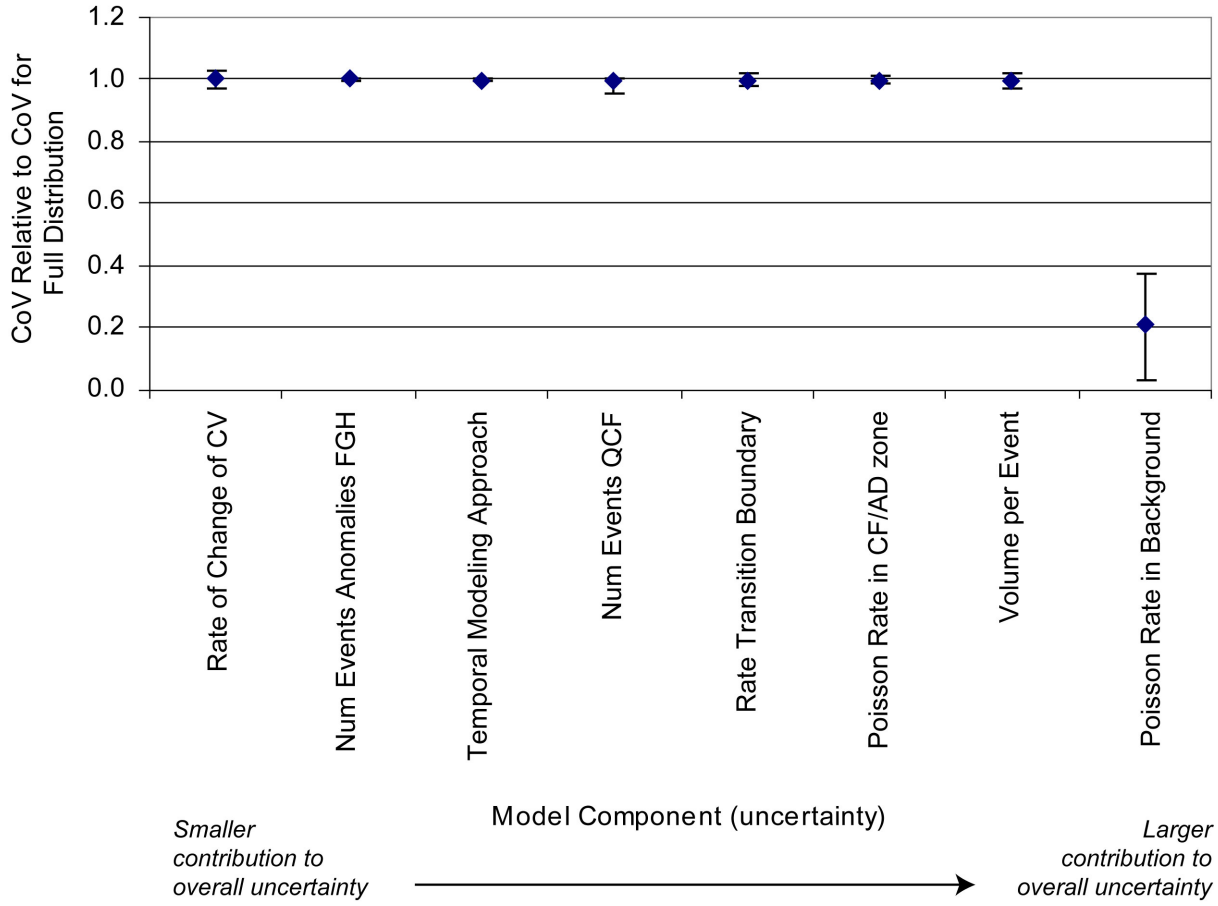

NOTE: Graph shows the CoV for the hazard distribution calculated with the specified model component fixed at each of its branch values, divided by the CoV for the full hazard distribution. Diamond shows the mean value with the relative CoV for each branch value weighted by its probability; "error bars" show the highest and lowest relative CoVs calculated across the branches for that model component. QCF = Quaternary Crater Flat; CV = cumulative volume; CF-AD = Crater Flat-Amargosa Desert.

Figure 4.1.8-4. Contribution of Uncertainty in Model Components to Overall Uncertainty in the Hazard Estimate, for the PVHA-U Models for the 10,000-Year Assessment Specified by George Thompson

4.1.8.2 Discussion of Individual Features

As described in Section 3.2.8, GT's events include dikes and conduits, and no other features. The conditional probability of intersection of each type of feature with the repository footprint was illustrated in Section 3.2.8, and, as discussed, the shape of the conditional probability of intersection maps for each individual feature is the same as for the conditional probability of intersection for any feature: no consistent clustering or grouping of individual features in an event occurs. Similarly, the full distribution of the frequency of intersection for any individual feature follows the same pattern as the distribution for any feature shown in Figure 4.1.8-2, simply shifted to the lower frequencies associated with the individual feature.

Table 4.1.8-1 shows the mean and median frequencies of intersection for each feature.

Table 4.1.8-1. Mean and Median Frequency of Intersection of Various Igneous Features with the Repository Footprint, for George Thompson's 10,000-Year Assessment

Feature	Mean Frequency of Intersection	Median Frequency of Intersection
Any feature	2.0e-9	1.8e-9
Dikes	2.0e-9	1.8e-9
Column-producing conduits	8.9e-10	7.9e-10
Vents	NA	NA
Sills	NA	NA

Potential for Multiple Intersections

Figure 4.1.8-5 shows a set of plots illustrating the distribution of the number of dike intersections for an event centered at a specific point, conditional on there being at least a 1% chance of an intersection occurring. The most likely number of intersections across the region as shown in the figure is one, but multiple dike intersections are possible depending on the event location. Figure 4.1.8-6 combines the relative likelihood of a dike intersection at each point with the conditional distribution of the number of dike intersections for an event at those points to yield a conditional distribution on the number of dike intersections, given that at least one such intersection occurs. As shown, assuming that a dike intersection occurs, it is most likely (probability 0.7) that only one dike intersects, but the potential exists for as many as 20 dikes to intersect the footprint. The probability of 4 or more dikes intersecting the repository footprint, given that at least one dike intersects, is about 0.03.

Figures 4.1.8-7 and 4.1.8-8 show the same data for conduits: the distribution on number of conduit intersections given that at least one conduit intersects the footprint. Given a conduit intersection, it is most likely that only one such intersection would occur (probability 0.87), but as many as 8 conduits intersecting the footprint are possible. The probability of 3 or more conduits intersecting the footprint, given that at least one conduit intersects, is about 0.02.

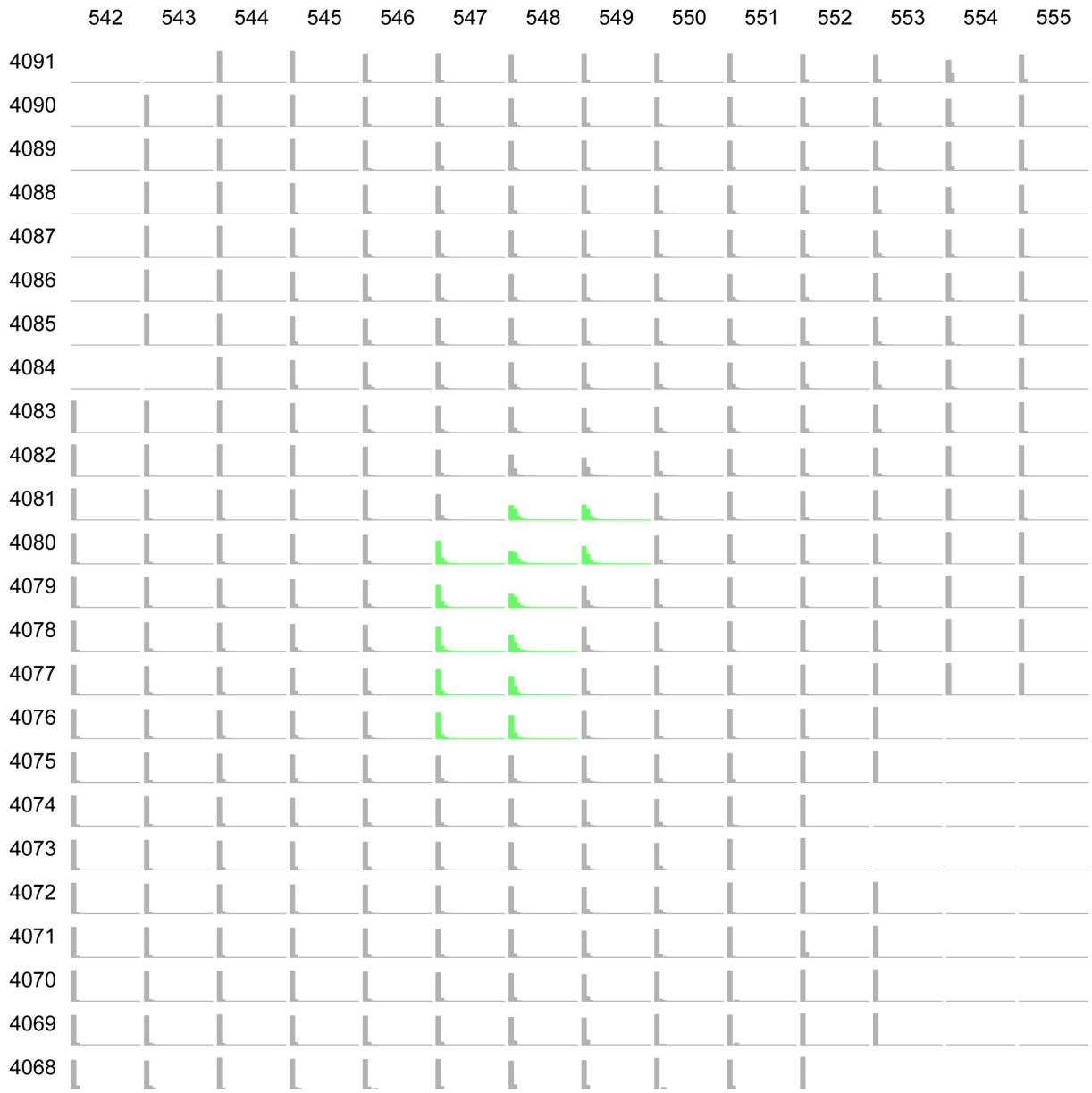

NOTE: Row and column labels represent grid points (UTM coordinates in km, NAD83) in the vicinity of the repository. Green plots show points inside or partially inside the repository footprint. Blank plots (e.g., in the upper left corner) indicate that the probability of intersection for an event at that location is zero. All other plots show the number of intersections conditional on at least one.

Figure 4.1.8-5. Schematic Showing the Distribution of the Number of Dikes That Intersect the Repository Footprint Given an Event at Each Grid Point, Given at Least a 99% Chance That a Dike Intersection Occurs (based on the event descriptions of George Thompson)

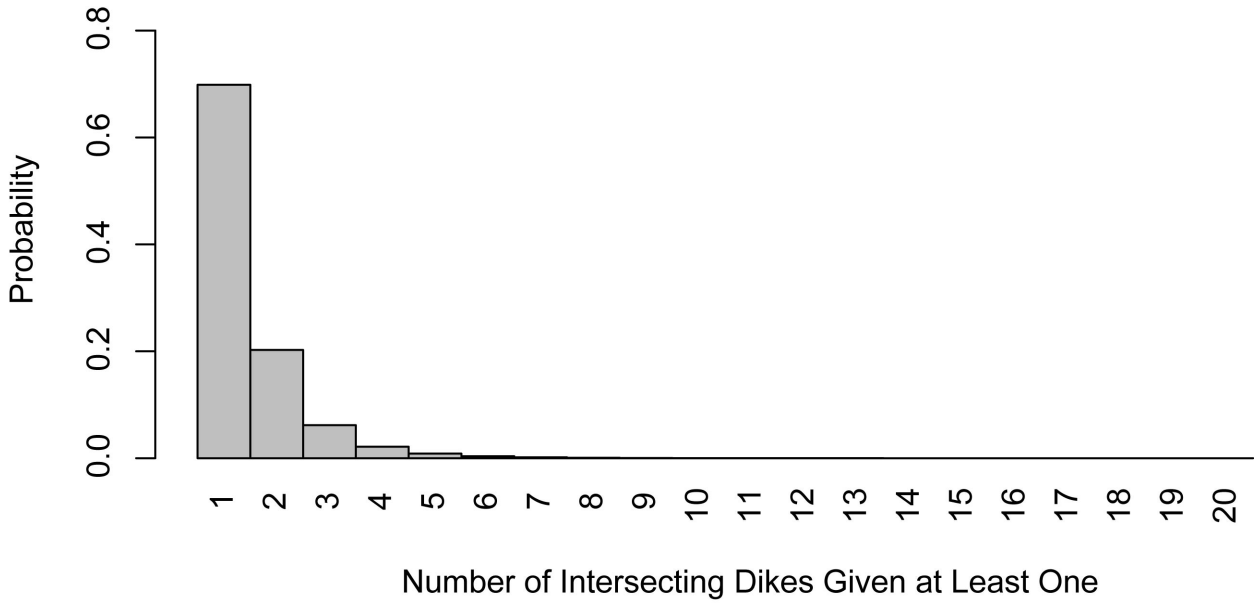

Figure 4.1.8-6. Conditional Distribution of the Number of Dikes That Intersect the Repository Footprint, Given That at Least One Dike Intersection Occurs (based on the event descriptions of George Thompson)

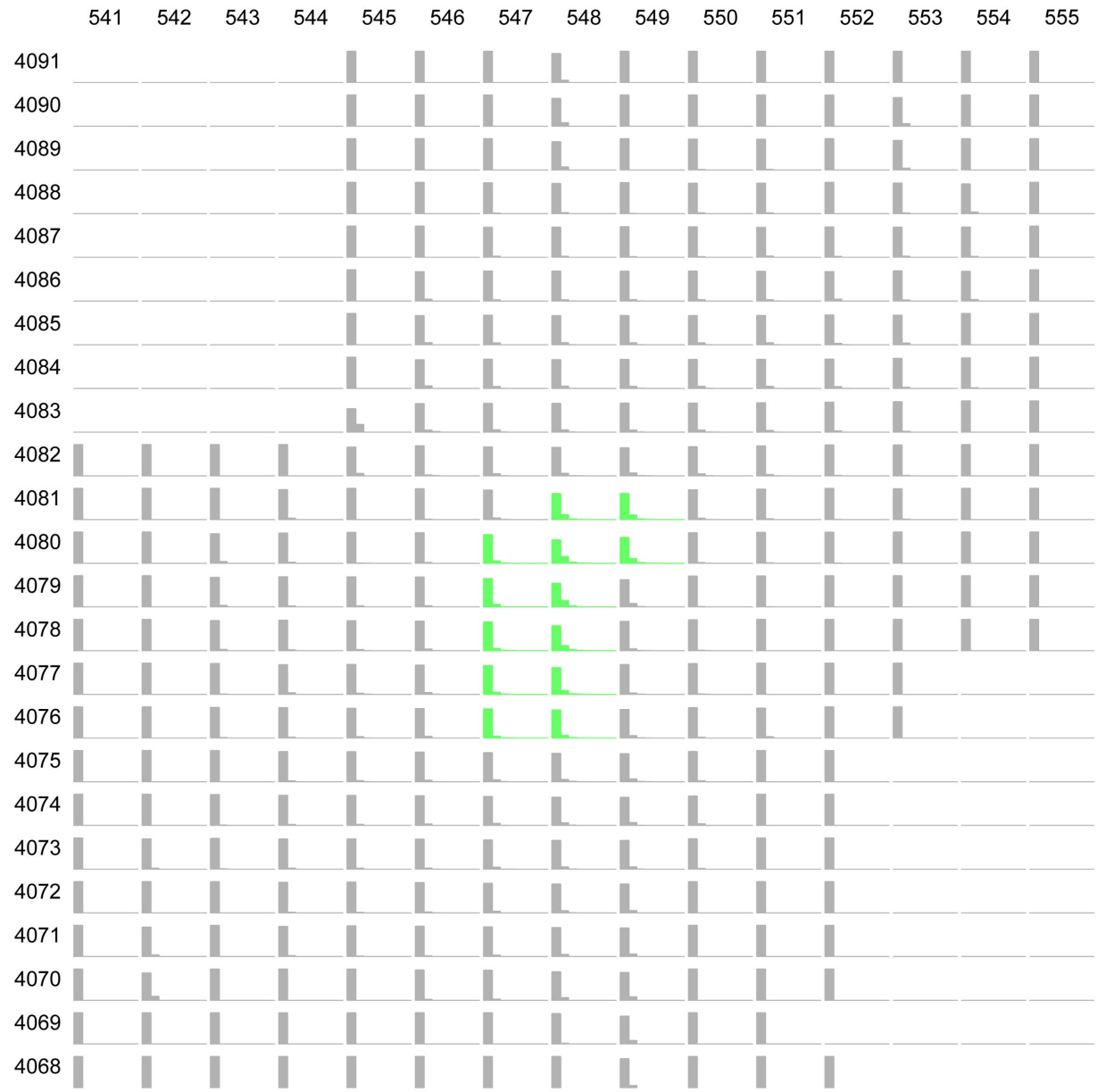

NOTE: Row and column labels represent grid points (UTM coordinates in km, NAD83) in the vicinity of the repository. Green plots show points inside or partially inside the repository footprint. Blank plots (e.g., in the upper left corner) indicate that the probability of intersection for an event at that location is zero. All other plots show the number of intersections given at least a 99% chance of at least one.

Figure 4.1.8-7. Schematic Showing the Distribution of the Number of Conduits That Intersect the Repository Footprint Given an Event at Each Grid Point, Given at Least a 99% Chance that a Conduit Intersection Occurs (based on the event descriptions of George Thompson)

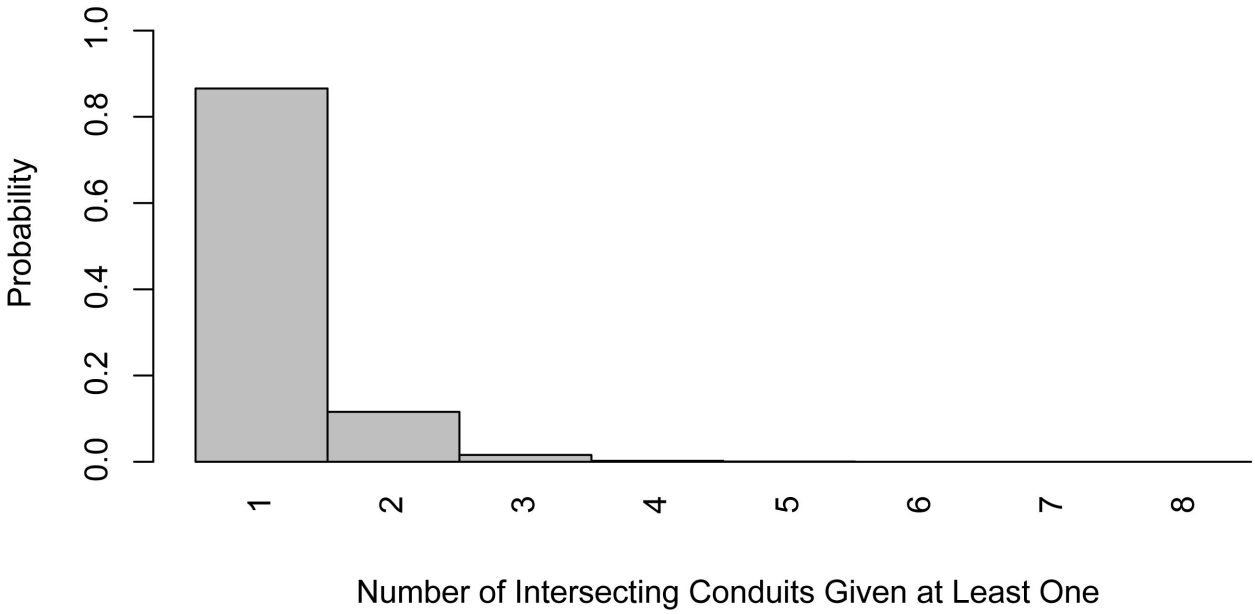

Figure 4.1.8-8. Conditional Distribution of the Number of Conduits That Intersect the Repository Footprint, Given That at Least One Conduit Intersection Occurs (based on the event descriptions of George Thompson)

4.1.8.3 Results at Different Future Times

GT defined one set of models as applying to both the 10,000-year and 1-My assessments. Those models include a time-volume model that leads to a time-dependent rate estimate for the rate within the Crater Flat zone, but as discussed previously, the change in rate over a million years is small, and the frequency of intersection is most strongly a function of the rate in the background zone, which is not modeled with the time-volume rate model. The mean frequency of intersection for both the 1-My assessment the 10,000-year assessment for GT's models is 2.0e-9. No meaningful differences were observed in the CDF and pmf graphs, nor in the contributions to uncertainty for the 1-My versus the 10,000-year assessments.

4.2 AGGREGATE RESULTS

This section presents the aggregate results of the PVHA-U analyses. Computing the aggregate frequency of intersection requires weighting and combining each expert's distributions. As discussed previously in Section 2.5, one of the goals of the PVHA-U process was to enable equal weighting of the experts' assessments, and for reasons described in Section 2.5, equal weights are appropriate for aggregating the assessments.

4.2.1 10,000-Year Assessment

Figure 4.2-1 shows the spatial distribution of the mean frequency of intersection for each of the experts' 10,000-year assessments. Each of these figures was presented and described in Section 4.1; they are presented together here as a visual summary of the differences in the spatial distribution of hazard. In all maps, the outer contour represents a mean frequency of intersection of 1e-13. The inner contour differs, based on the models of each expert. The value and size of this inner contour hints at the differences in the mean hazard estimate across experts: if the inner contour represents a relatively high value (e.g. 1e-9) and encloses a relatively large area (such as shown on the Connor and Crowe maps), the mean hazard would be higher than for other experts. Similarly, if the value is low (e.g., 1e-11) and encloses a relatively small area (such as shown on the Sheridan map), the mean hazard would tend to be lower than for other experts.

Figures 4.2-2 and 4.2-3 show the annual frequency of intersection distributions for each of the 8 PVHA-U experts and the aggregate distribution. Figure 4.2-2 shows the cumulative distribution functions (CDFs) for each expert's assessments, along with the aggregate CDF (the black line). Figure 4.2-3 shows the probability mass function (the pmf) for each expert's assessment as well as the aggregate distribution for all experts. Differences in the relative smoothness of the pmfs across experts are a result of differing levels of discretization in the logic trees: experts with more uncertainties and more branches representing those uncertainties have smoother-appearing pmfs.

The aggregate mean annual frequency of intersection shown in the figures is 3.1e-8. The median is 8.7e-9, and the 90% confidence interval (the 5th to 95th percentiles) is 5.7e-10 to 1.2e-7. The aggregate distribution has a long right tail (difficult to see in the figure due to the log scale), with the mean of the distribution about half an order of magnitude higher than the median of the distribution. The mean value lies at about the 76th percentile of the distribution. The shape of the aggregate distribution can be seen to be a function of the eight individual pmfs: three experts (McBirney, Sheridan, and Thompson) have significant mass just above 1e-9 in their models, leading to an apparent mode in the aggregate distribution at that value. Other experts have more mass centered between 1e-8 and 1e-7, leading to the second apparent mode in the aggregate distribution.

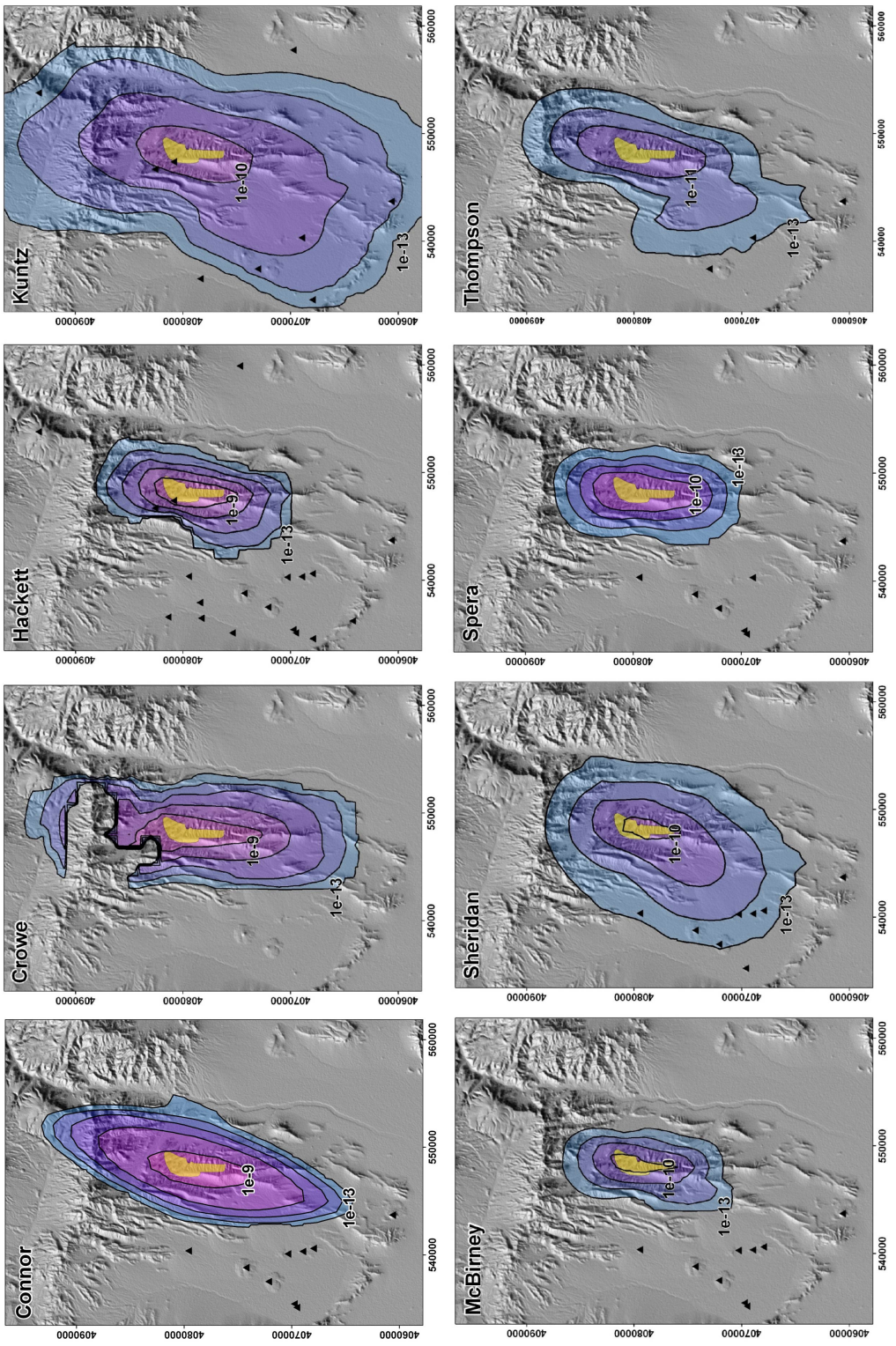

NOTE: The repository footprint is represented by the yellow polygon. Black triangles represent the past events identified as relevant by that expert (their most likely event set is plotted). Contours represent the mean frequency of intersection of any feature with the repository footprint for an event located at that point. Outer contour in all figures is 1e-13, inner contour is expert-specific. Map grid ticks are UTM meters; tick intervals are 10 km.

Figure 4.2-1. Spatial Distribution of the Mean Frequency of Intersection for Each Expert's 10,000-Year Assessment

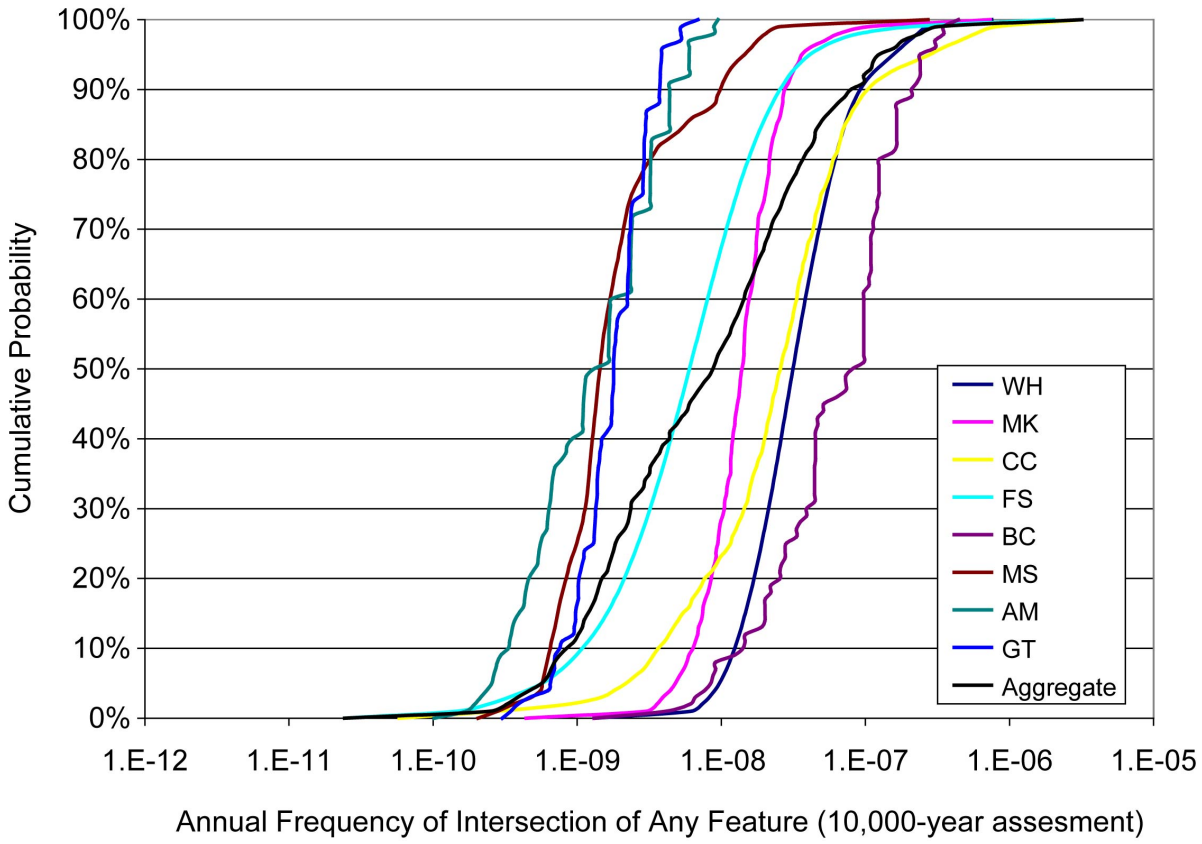

Figure 4.2-2. Annual Frequency of Intersection of Any Feature with the Repository Footprint: Aggregate and Individual Cumulative Probability Results for the 10,000-Year Assessment

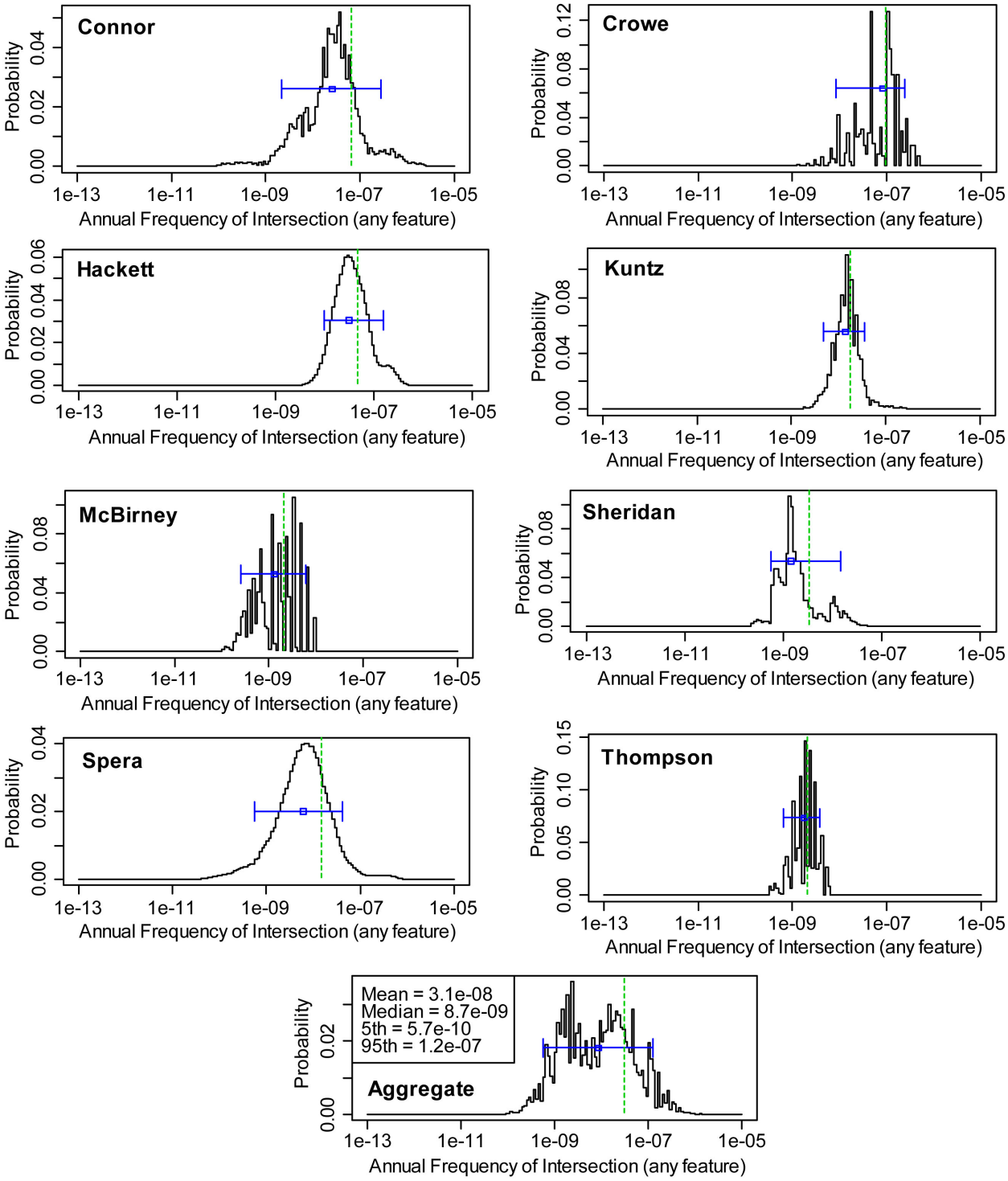

NOTE: Dashed vertical line indicates the mean, the open square the median, and "error bars" show the 5th to 95th percentile range.

Figure 4.2-3. Annual Frequency of Intersection of Any Feature with the Repository Footprint: Aggregate and Individual Probability Mass Results for the 10,000-Year Assessment

Figure 4.2-4 compares the 90% confidence intervals, as well as the means and medians for each expert's individual results and the aggregate results. Each bar represents the 5th to 95th percentile range for the expert listed. The mean is represented with a solid diamond, the median with an open diamond. The aggregate results are shown at the bottom of this figure. The individual means span about 1.8 orders of magnitude, and the medians span a similar range. All individual means and medians lie within the 90% confidence interval of the aggregate distribution.

The highest mean hazard estimate (mean annual frequency of intersection of 9.4e-8) results from Bruce Crowe's assessment, which places high weight on a model based on a relatively small region of interest, leading to higher rate density estimates than most other experts. The lowest mean hazard estimate (mean annual frequency of intersection of 2e-9) results from George Thompson's assessment, which is based on the definition of a zone of higher activity in Crater Flat, within a background zone of lower activity.

Most of the individual confidence intervals overlap. Exceptions are that George Thompson's confidence interval does not overlap with those of Bruce Crowe, William Hackett, or Mel Kuntz, and Alexander McBirney's confidence interval does not overlap with those of Bruce Crowe or William Hackett.[4] The narrowest confidence intervals are associated with George Thompson's and Mel Kuntz's models: each spans less than an order of magnitude. This results in both cases

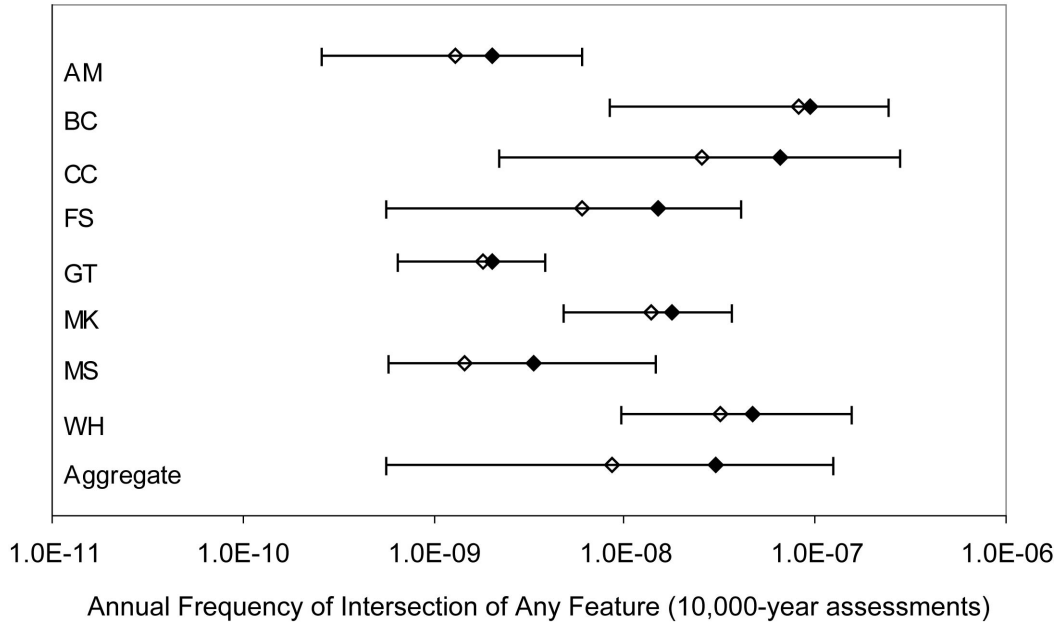

NOTE: Solid diamond represents the mean of the distribution, the open diamond represents the median, and the "error bars" represent the 5th to 95th percentile range.

Figure 4.2-4. Comparison of the 90% Confidence Intervals for the Frequency of Intersection: Individual and Aggregate Results for the 10,000-Year Assessment

[4] Although these 90% confidence intervals do not overlap, the CDFs in Figure 4.2-2 show that all distributions overlap across at least some portion of their full ranges.

from the influence of the spatial zones model and the importance of the background rate in determining the mean hazard. The widest confidence interval is associated with Charles Connor's model, which spans a little more than 2 orders of magnitude. CC's model includes several alternative temporal models that result in significantly different rate estimates, which is the major contributor to the overall uncertainty in his hazard estimate.

4.2.2 1-My Assessment

Figure 4.2-5 shows the aggregate distribution for the hazard results for the 1-My assessment, calculated based on the results of the individual models evaluated at a future time of 1 My. Note that for all experts except for Sheridan, the results calculated at 1 My in the future are representative of their results across the 1-My time period.[5] For the 1-My assessment, the aggregate mean annual frequency of intersection is 3.8e-8. The median is 6.8e-9, and the 90% confidence interval (the 5th to 95th percentiles) is 4.5e-10 to 1.6e-7. Comparing this figure to Figure 4.2-2 shows that the aggregate distribution for the 1-My assessment is both "wider" and "flatter" than that for the 10,000-year assessment, indicative of the increased uncertainty some experts associated with the 1-My assessment.

Figure 4.2-6 compares the 90% confidence intervals, as well as the means and medians for each expert's individual results and the aggregate results for both the 10,000-year and the 1-My assessments. As discussed in Section 4.1, those experts who included explicit model changes for the 1-My assessment (Connor, Crowe, and Kuntz) expanded their uncertainty about what might occur over the 1-My time horizon, generally resulting in wider uncertainty bands. This also leads to the increase in the size of the confidence interval on aggregate hazard for the 1-My assessment over the 10,000-year assessment.

[5] The hazard results for Michael Sheridan's model are strongly influenced by his temporal clustering model and the assessed probability at any point in time that "current cluster" is still active. After about 220,000 years from the present, the assessment is that the current cluster is over, and the hazard estimate is the same for each following year. The hazard assessed at 100,000 years, however, differs from that assessed at 1 My, as discussed in Section 4.1.6.

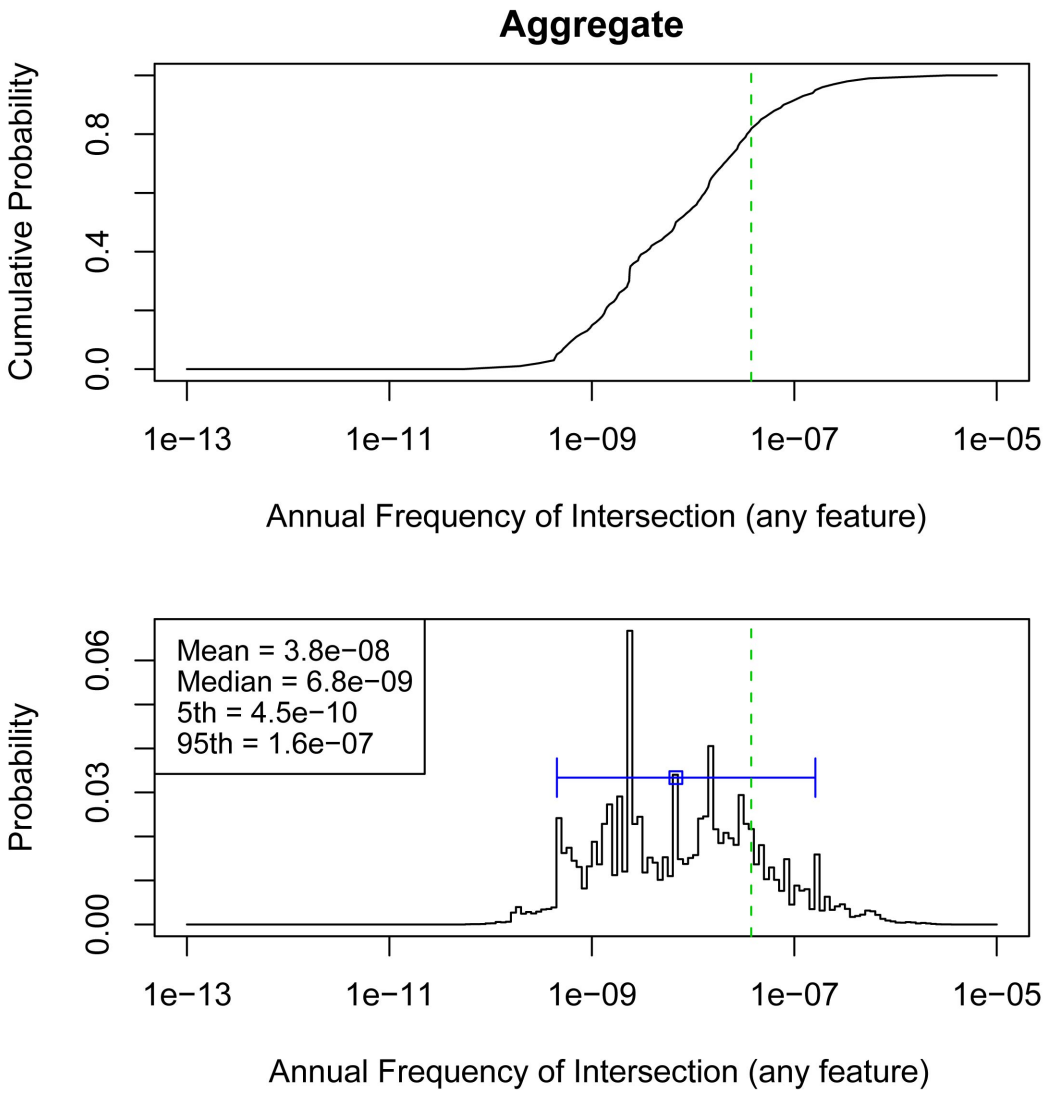

NOTE: Top figure is cumulative distribution function (CDF); bottom figure is a probability mass function (pmf). Dashed vertical line represents the mean value, the open square indicates the median, and "error bars" represent the 5th to 95th percentile range.

Figure 4.2-5. Annual Frequency of Intersection of Any Feature with the Repository Footprint: Aggregate Results for the 1-My Assessment

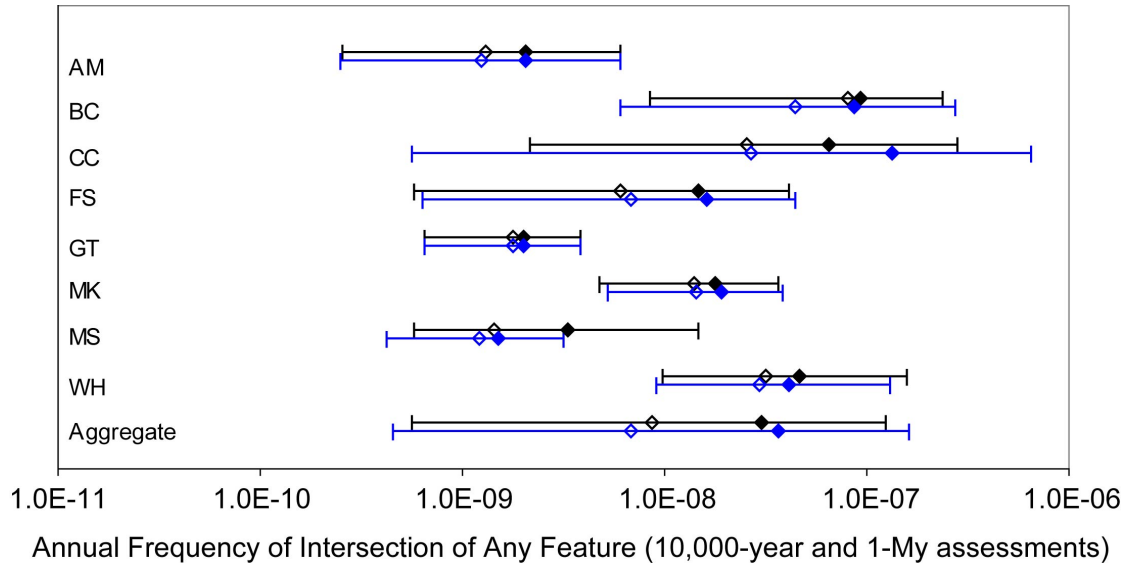

NOTE: For each expert the first line (black) shows the 10,000-year hazard results and the second (blue) shows the 1-My results. Solid diamond represents the mean of the distribution, open diamond represents the median, and "error bars" represent the 5th to 95th percentile range.

Figure 4.2-6. Comparison of the 90% Confidence Intervals for the Frequency of Intersection: Individual and Aggregate Results for both the 10,000-Year and 1-My Assessments

4.2.3 Contributions to Uncertainty

The uncertainty in the aggregate distribution is a function of both the differences between the experts' assessments (inter-expert differences) and the uncertainty within each of those assessments (intra-expert variability). The aggregate distribution is the equally weighted sum of the eight individual distributions. Let x represent the aggregate model, i represent the individual models, w_i represent the weight on each model, and μ and σ^2 represent the mean and variance. Then σ^2_x , the variance of the aggregate model, is:

$$\sigma^2{}_x = \sum_i w_i \sigma^2{}_i + \sum_i w_i \times (\mu_i - \mu_x)^2 \qquad \text{(Eq. 4-1)}$$

Interpreting the first term as the contribution to uncertainty from the individual variances (the intra-expert uncertainty), and the second term as the contribution to uncertainty from the differences in the mean estimates across experts (the inter-expert differences), we find that about 20% of the variance in the aggregate distribution is attributed to differences between experts, and that the majority of the uncertainty in the aggregate hazard is attributable to uncertainties within each of the expert models.

Equation 4-1 also suggests that one can examine the relative contribution to uncertainty in the aggregate hazard from each of the individual expert models. Figure 4.2-7 shows this result: the contribution to variance from each expert's component of Equation 4-1 was divided by the total variance to yield the percentage contribution to total variance for each. Not surprisingly, those experts with the largest variance in their individual models contribute the most to the variance in the aggregate hazard.

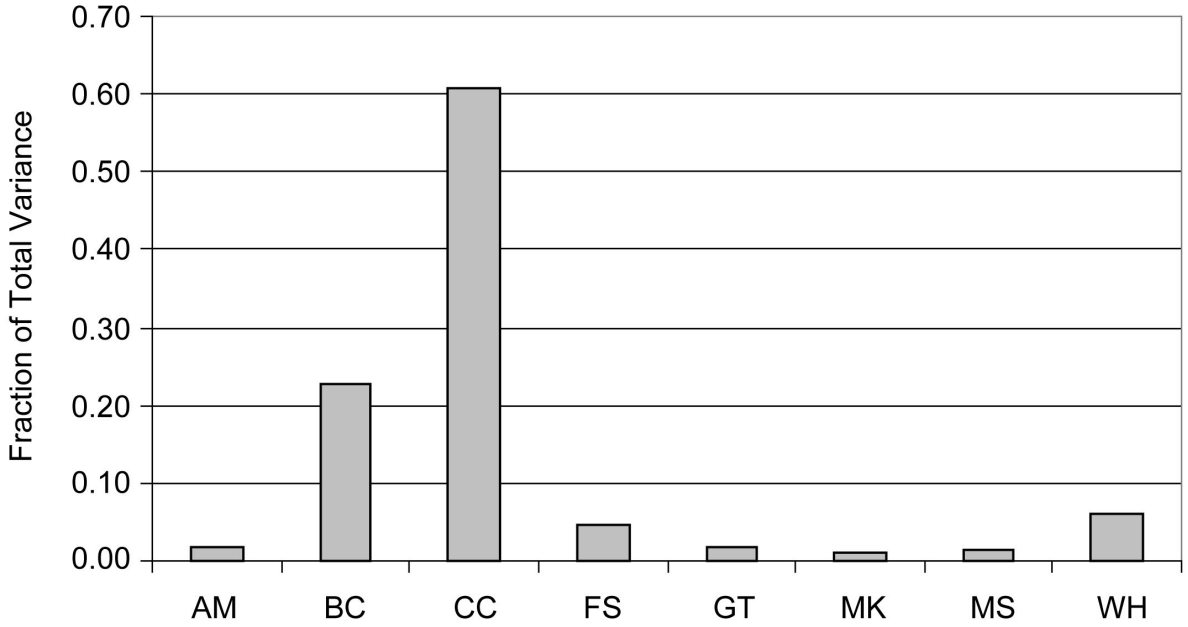

Figure 4.2-7. Relative Contribution of Each Expert's Individual Hazard Results to the Variance in the Aggregate Hazard Results

To further examine this impact, an additional sensitivity analysis was run: in that analysis, eight aggregate distributions were calculated, each including the results of seven of the eight experts. That is, each expert was sequentially "removed" from the aggregate hazard calculation. The impact of the removal on the mean hazard and on the coefficient of variation of the hazard distribution is shown in Figure 4.2-8. The figure shows, for example, that if Bruce Crowe's models are not included in the aggregate analysis, the mean hazard would decrease by a factor of almost 0.7, and that the uncertainty in the hazard (relative to the mean) would increase by a factor of just over 1.3. In other words, without the inclusion of Bruce Crowe's assessment, the aggregate mean hazard would be lower but more uncertain. In comparison, without the inclusion of Michael Sheridan's assessment, the aggregate mean hazard would be higher and less uncertain.

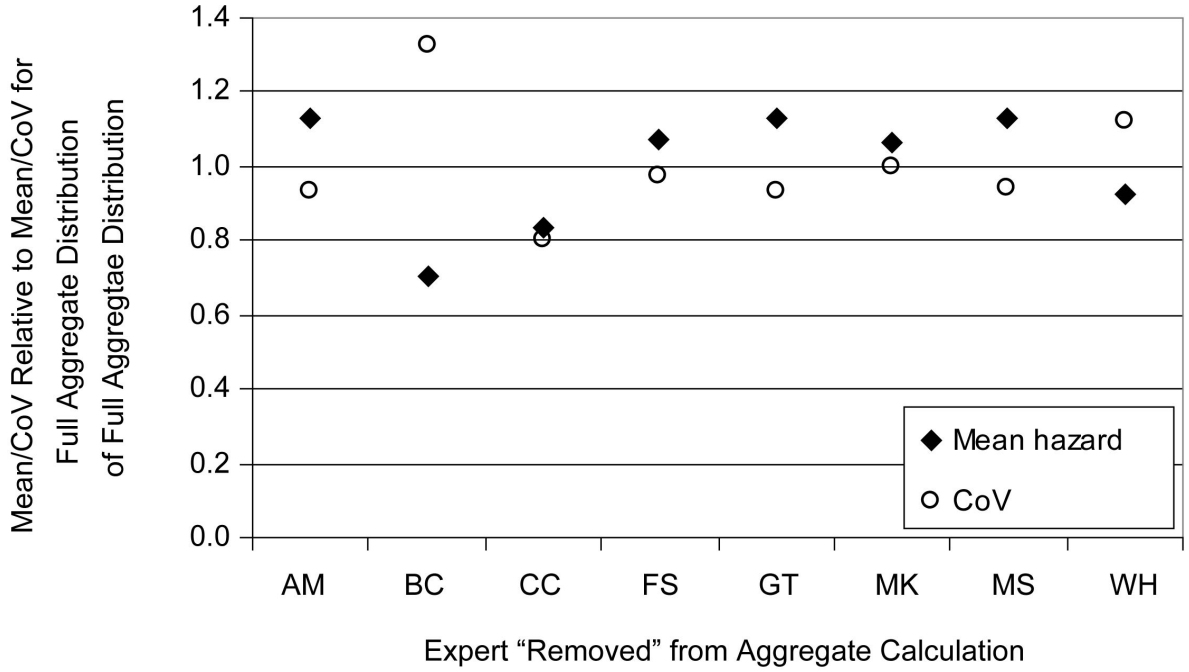

NOTE: Graph shows the mean hazard and the CoV calculated for an aggregate distribution calculated from seven experts, relative to those values for the full aggregate distribution. Labels on the x-axis indicate which expert's distribution was not included in the partial aggregate results.

Figure 4.2-8. Change in the Mean Hazard and the Overall Uncertainty in Hazard When an Individual Expert's Model Is Left Out of the Aggregate Calculation

Finally, to explore the stability of the hazard estimate to the number of experts included in the aggregate calculation, the range of mean frequency of intersection for every possible subset of expert (e.g., the 8 possible subsets of 7 experts, the 26 possible subsets of 6 experts, etc.) was calculated. Figure 4.2-9 shows the results of these calculations, done for the 10,000-year assessment. Each bar shows the minimum and maximum mean hazard calculated from the subsets with the stated number of experts. For 8 experts, of course, only one subset is possible, and the mean is equal to the aggregate hazard for the 10,000-year assessment. For 7 experts eight subsets are possible: the lowest mean frequency of intersection across these 8 groups was 2.2e-8, as indicated by the left end of the bar labeled "7 experts." The highest mean frequency of intersection across these eight groups was 3.47e-8 as indicated by the right side of the bar. With a combination of 6 of the expert models, it is possible that the aggregate hazard would be half of what it is for the full expert panel; with a combination of 5 of the expert models, it is possible the aggregate hazard would be 50% higher than what it is for the full panel.

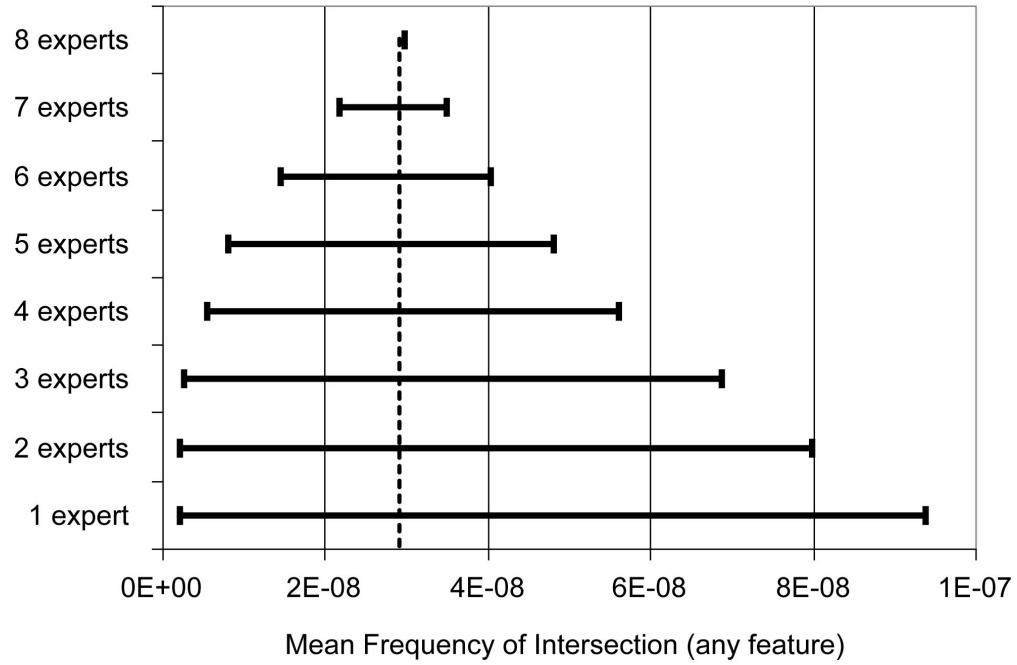

NOTE: Dashed vertical like indicates the mean frequency of intersection for the full panel. Each bar represents the range of mean frequencies that are obtained when all possible subsets of experts are aggregated. For example, the "7 experts" bar shows the range of mean values across the 8 possible subsets of 7 experts.

Figure 4.2-9. Range of Mean Frequency of Intersection for All Possible Subsets of Experts

4.3 COMPARISON WITH PVHA-96

As discussed in Section 1.1, this PVHA-U study was conceived as an update to the expert elicitation of volcanic hazard conducted more than a decade ago (CRWMS M&O 1996). While in many ways the PVHA-U study can be viewed as a completely new analysis, the primary goal of the two studies was essentially the same: to assess the probability of a volcanic event disrupting the repository at Yucca Mountain and to quantify the uncertainties associated with such an event. In this section of the report, we compare the results of the PVHA-U with the results from the original PVHA study (CRWMS M&O 1996, Section 5.3), hereafter referred to as "PVHA-96."

4.3.1 Event Definition

The most significant difference between the PVHA-96 study and the PVHA-U study described in this report is the more robust treatment of the definition and characteristics of an "igneous event" by the participating experts in the current study. In PVHA-96, considerably less focus was give to what an "event" would look like, and all experts were assumed to be defining their spatial and temporal models as they would relate to a relatively simple event: an igneous dike or dike set.

In this study, each expert's model included explicit identification and assessment of the characteristics of an igneous event: the type, number, size, shape, and spatial distribution of specific features within an event. In PVHA-U, all experts identified at least one type of igneous feature that could lead to an intrusion into the repository (dikes), and six of the eight also

included the potential for sills. All experts also identified the potential for one or more column-producing conduits as part of an igneous event, and all but one expert allow for the formation of a non-column producing vent that could first intersect the repository, then vent to the surface, but not produce an ash plume.

A comparison and discussion of the different event definitions developed by each expert was included in Section 3.3.

4.3.2 Aggregate Hazard

To compare the aggregate hazard from the two studies, it is first necessary to determine what aspect of the PVHA-U analysis is most comparable to the PVHA-96 aggregate hazard calculation. For the discussion that follows, we compare the aggregate hazard results from PVHA-96 with the aggregate annual frequency of intersection[6] of any feature with the repository footprint from PVHA-U for the 10,000-year assessment. The mean annual frequency of intersection resulting from PVHA-96 was 1.5e-8 (CRWMS M&O 1996). The PVHA-96 value was recalculated to reflect subsequent changes to the repository layout, and based on the latest recalculation the new mean annual frequency of intersection is 1.7e-8 (BSC 2004a). Because the repository footprint used in the 2004 recalculation is more similar to the repository footprint used for PVHA-U, the 2004 values are considered to be the most appropriate for comparison to the results of this PVHA-U. Although updated from the 1996 report, we will refer to the latest recalculation of the PVHA-96 results (mean value of 1.7e-8) as the PVHA-96 results.

The "hazard" in the PVHA-96 study represents the annual frequency of intersection by a dike or dike set, and was calculated using the total length of dikes as assessed by the experts. The annual frequency of intersection of "any feature" in the current results is directly related to the event size, which is most closely related to the total length of dikes as used in PVHA-96, so the comparison to the annual frequency of intersection of "any feature" is considered most relevant.

Figure 4.3-1 shows the aggregate hazard distributions for the two studies. The top figure shows the two cumulative distribution functions on a single plot, the middle figure shows the pmf for the PVHA-96 results, and the bottom figure shows the pmf for the PVHA-U results. The figures illustrate that the PVHA-U results span a wider range than the PVHA-96 results, and that there is more weight in the tails of the distribution: both more probability associated with lower estimates and more probability associated with higher estimates than in PVHA-96. The comparison of the pmfs shows that the PVHA-U results have more mass at lower values (e.g., at about 1.1e-9) than the PVHA-96 results, and more mass at higher values (e.g., at about 1.0e-7). The expansion of uncertainty and the increased weight in the upper tail leads to an increase in the mean annual frequency of intersection: from 1.7e-8 for PVHA-96 to 3.1e-8 for PVHA-U. The addition of probability mass in the lower end leads to a very slight decrease in the median annual frequency of intersection (from 9.8e-9 to 8.7e-9).

[6] As discussed in Section 3.1, the annual probability of intersection is closely approximated by the annual frequency of intersection and the terms are used interchangeably.

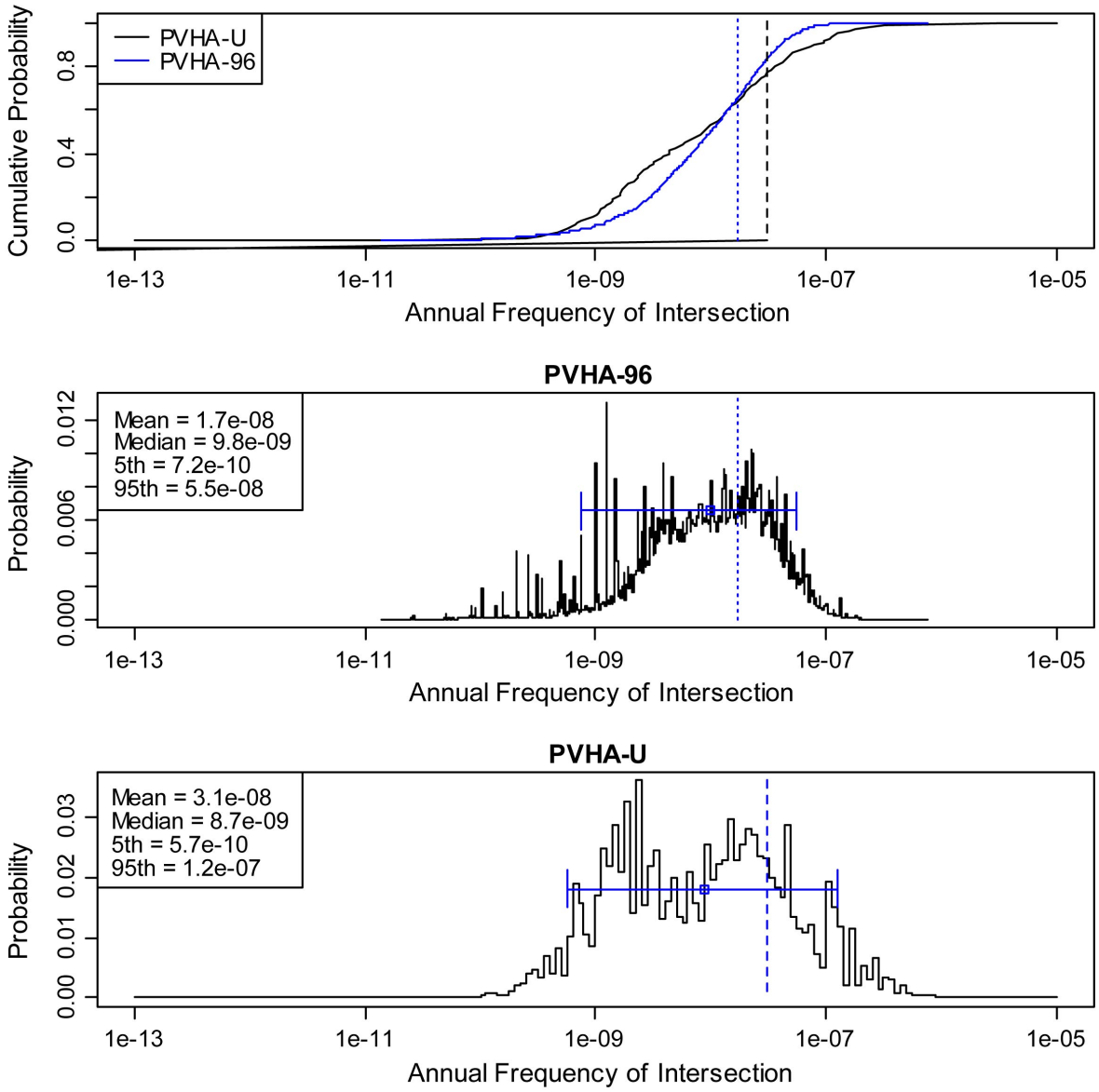

NOTE: Top figure shows two cumulative distribution functions, one for the PVHA-U and the other for PVHA-96. Middle figure shows the probability mass function (pmf) for the PVHA-96 results, and the bottom figure shows the pmf for the PVHA-U results. Dashed vertical line marks the mean for each distribution and plot, open square indicates the median, and "error bars" show the 5th to 95th percentiles.

Figure 4.3-1. Comparison of the Aggregate Hazard Distributions for PVHA-U 10,000-Year Assessment and PVHA-96

Figure 4.3-2 adds the 90% confidence interval (and mean and median estimates) from the PVHA-96 results to the comparison across experts for the 10,000-year and 1-My assessments shown in Figure 4.2-6. For six of the eight experts, the mean hazard for their 10,000-year assessment lies within the 90% confidence interval of the PVHA-96 results. For two experts (Connor and Crowe), the mean estimate is higher than the 90% confidence interval from PVHA-96. For all experts except Crowe, the median estimates lie within the 90% confidence interval for the PVHA-96 results.

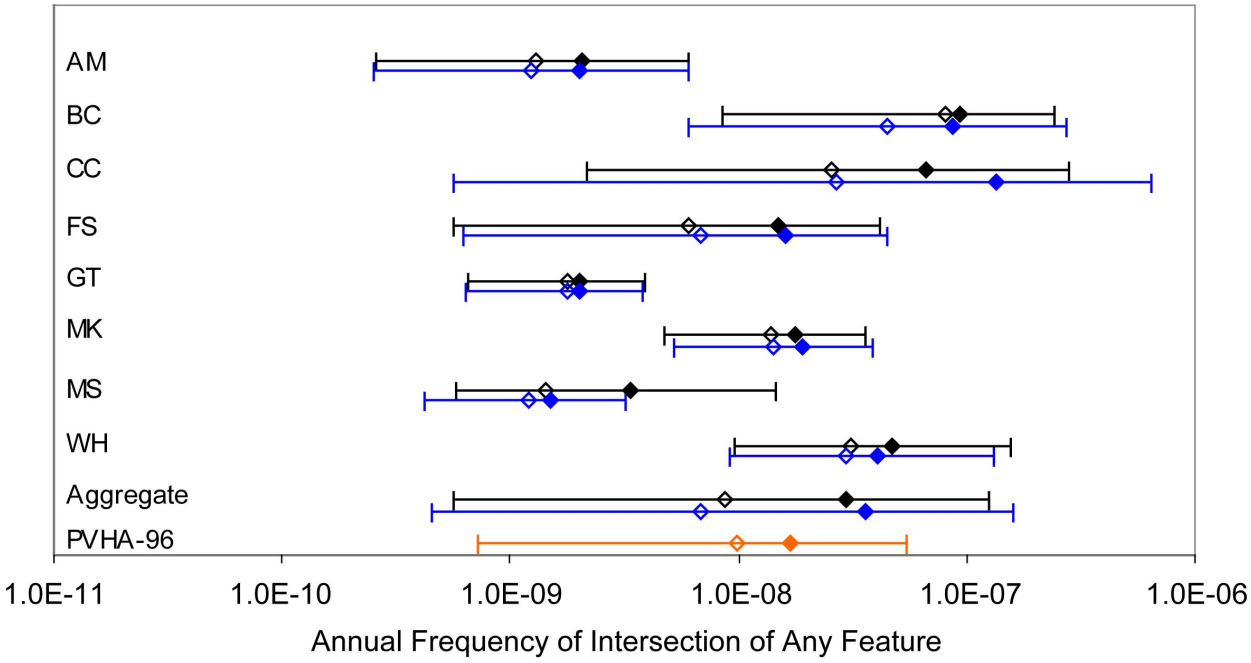

1-My and 10,000-Year Assessments for PVHA-U, Aggregate Assessment for PVHA-96

NOTE: For each expert the first line (black) shows the 10,000-year hazard results and the second (blue) shows the 1-My results. The bottom line (orange) shows the PVHA-96 results. Solid diamond represents the mean of the distribution, open diamond represents the median, and "error bars" represent the 5th to 95th percentile range.

Figure 4.3-2. Comparison of the 90% Confidence Intervals for the Frequency of Intersection: Individual and Aggregate Results for both the 1-My and the 10,000-Year Assessment for PVHA-U and Aggregate Results for PVHA-96

There are several importance differences between the PVHA-U and the original PVHA-96 studies that may contribute to the differences in the results. Fundamentally, the central estimates between the two studies, as represented by the median hazard values, are essentially the same. The key difference between the results is the broadening of the range of hazard results (as represented in the 5th to 95th percentile spread) in the PVHA-U, which also contributes to the increase in the mean hazard. A reasonable explanation for the broadening of the uncertainty in the hazard results relates to the evolution of the state of the science for probabilistic volcanic hazard analyses, and for probabilistic hazard analyses in general. At the time of the PVHA-96 the basic structure and framework for a probabilistic volcanic hazard analysis was fairly new and the manner of addressing the spatial and temporal components was still being developed and explored. The experts in the PVHA-96 study focused their time and efforts on understanding those approaches and developing the necessary parameter estimates. By the time of the

PVHA-U, the basic components were better understood, and more sophisticated modeling approaches were in common use. As the experts were now more familiar with the basic modeling approaches, they devoted considerable effort to considering a broader range of conceptual models, to capturing more complex models and approaches to defining the spatial and temporal behavior, and to characterizing the events more thoroughly. It is likely that inclusion of these additional models and approaches was the primary contributor to the broader range of hazard results.

INTENTIONALLY LEFT BLANK

5. REFERENCES

10 CFR 63. 2007. Energy: Disposal of High-Level Radioactive Wastes in a Geologic Repository at Yucca Mountain, Nevada. Internet Accessible.

40 CFR 191. Protection of Environment: Environmental Radiation Protection Standards for Management and Disposal of Spent Nuclear Fuel, High-Level and Transuranic Radioactive Wastes. Internet Accessible.

40 CFR 197. Protection of Environment: Public Health and Environmental Radiation Protection Standards for Yucca Mountain, Nevada. Internet Accessible.

70 FR 49014. Public Health and Environmental Radiation Protection Standards for Yucca Mountain, NV. Internet Accessible.

Energy Policy Act of 1992. Public Law No. 102-486, 106 Stat. 2776.

Abrahamson, N.A. & J.J. Bommer 2005. "Probability and uncertainty in seismic hazard analysis." *Earthquake Spectra* 21(2), 603-607.

ACNW&M 2007. "Igneous Activity at Yucca Mountain: Technical Basis for Decisionmaking," A Report Prepared by the Advisory Committee on Nuclear Waste and Materials, U.S. Nuclear Regulatory Commission, June 2007.

Blakely, R.J.; Langenheim, V.E.; Ponce, D.A.; and Dixon, G.L. 2000. *Aeromagnetic Survey of the Amargosa Desert, Nevada and California: A Tool for Understanding Near-Surface Geology and Hydrology.* Open-File Report 00-188. Denver, Colorado: U.S. Geological Survey.

Benjamin, J.R. and Cornell, C.A. 1970. *Probability, Statistics, and Decision for Civil Engineers.* New York, New York: McGraw-Hill.

Bommer, J.J., F. Scherbaum, H. Bungum, F. Cotton, F. Sabetta & N.A. Abrahamson 2005. "On the use of logic trees for ground-motion prediction equations in seismic hazard assessment." *Bulletin of the Seismological Society of America* 95(2), 377-389.

Brillinger, D. R. 1982. "Some bounds for seismic risk." *Bulletin of the Seismological Society of America*, v. 72, p. 1403-1410.

Brocoum, S.J. 1997. "Evaluation of Data Provided at U.S. Department of Energy (DOE) and U.S. Nuclear Regulatory Commission (NRC) Igneous Activity Technical Exchange, February 25-26, 1997." Letter from S.J. Brocoum (DOE/YMSCO) to J.T. Greeves (NRC), June 4, 1997, with enclosure.

BSC (Bechtel SAIC Company) 2004a. *Characterize Framework for Igneous Activity at Yucca Mountain, Nevada.* ANL-MGR-GS-000001 REV 02. Las Vegas, Nevada: Bechtel SAIC Company.

BSC 2004b. *Expert Elicitation, LP-AC.1Q-BSC,* Rev. 0, ICN 1. Washington, D.C.: U.S. Department of Energy, Office of Civilian Radioactive Waste Management.

BSC 2005. *Plan for the Expert Elicitation to Update the Probabilistic Volcanic Hazard Analysis (PVHA) for Yucca Mountain, Nevada.* PLN-MGR-GS-000001 REV 01. Las Vegas, Nevada: Bechtel SAIC Company.

Budnitz, R.J.; Apostolakis, G.; Boore, D.M.; Cluff, L.S.; Coppersmith, K.J.; Cornell, C.A.; and Morris, P.A. 1997. *Recommendations for Probabilistic Seismic Hazard Analysis: Guidance on the Uncertainty and Use of Experts.* NUREG/CR-6372. Two volumes. Washington, D.C.: U.S. Nuclear Regulatory Commission.

Connor, C.B. and L.J. Connor (in press). "Estimating spatial density with kernel methods." In: C.B. Connor, N.A. Chapman, and L.J. Connor (eds). *Volcanic and Tectonic Hazard Assessment for Sites of Nuclear Facilities*. Cambridge University Press.

Coppersmith, K.J., and Youngs, R.R. 1986. "Capturing uncertainty in probabilistic seismic hazard assessments with intraplate tectonic environments." in *Proceedings, 3rd U.S. National Conference on Earthquake Engineering,* vol. 1, Charleston, S.S., pp. 301-312.

Cornell, C. A. 1968. "Engineering seismic risk analysis." *Bulletin of the Seismological Society of America,* v. 58, p. 1583-1606.

Cornell, C., A. 1971. "Probabilistic analysis of damages to structures under seismic loads." In Howells, D.A.., Haigh, I.P., and Taylor, C. eds. *Dynamic Waves in Civil Engineering*. John Wiley, London.

Crowe, B.M., Perry, F.V., Geissman, J., McFadden, L., Wells, S., Murrell, M. Poths, J., Valentine, G.A., Bowker, L., and Finnegan, K., 1995. *Status of Volcanism Studies for the Yucca Mountain Site Characterization Projects*. Los Alamos National Laboratory Report LA-12908-MS, issued March, 1995.

CRWMS (Civilian Radioactive Waste Management System) M&O (Management and Operating Contractor) 1996. *Probabilistic Volcanic Hazard Analysis for Yucca Mountain, Nevada.* BA0000000-01717-2200-00082 REV 0. Las Vegas, Nevada: CRWMS M&O.

CRWMS M&O 1998a. *Probabilistic Seismic Hazard Analyses for Fault Displacement and Vibratory Ground Motion at Yucca Mountain, Nevada*. Milestone SP32IM3, September 23, 1998. Three volumes. Las Vegas, Nevada: CRWMS M&O. ACC: MOL.19981207.0393.

CRWMS M&O 1998b. *Total System Performance Assessment - Viability Assessment Base Case.* B00000000-01717-0210-00011 REV 01. Las Vegas, Nevada: CRWMS M&O. ACC: MOL.19981202.0279.

CRWMS M&O 2000. Total *System Performance Assessment for the Site Recommendation*. TDR-WIS-PA-000001 REV 00. Las Vegas, Nevada: CRWMS M&O. ACC: MOL.20001005.0282.

Dickinson, W.R. 2006. "Geotectonic evolution of the Great Basin." *Geosphere* volume 2. Boulder, Colorado, December 2006, Geological Society of America, pp. 353-368.

DOE (U.S. Department of Energy) 2008a. Design Document for: EventSim Version 1.0. Document ID: 11247-DD-1.0-00. Las Vegas, Nevada: U.S. Department of Energy, Office of Repository Development.

DOE 2008b. Design Document for: RateDens Version 1.0. Document ID: 11246-DD-1.0-01. Las Vegas, Nevada: U.S. Department of Energy, Office of Repository Development.

DOE 2008c. Design Document for: LTree Version 1.0. Document ID: 11245-DD-1.0-00. Las Vegas, Nevada: U.S. Department of Energy, Office of Repository Development.

Efron, B. 1981. "Nonparametric estimates of standard error: The jackknife, the bootstrap and other methods." *Biometrika* 68: 589–599.

Efron B., and R. Tibshirani 1993. "An Introduction to the Bootstrap." CRC Press. ISBN:0412042312.

Fridrich, C.J., Whitney, J.W., Hudson, M.R., Crowe, B.M., 1999. "Space-time patterns of Late-Cenozoic extension, vertical axis rotation, and volcanism in the Crater Flat basin, southwest Nevada." *Special Paper Geological Society of America* 333, 197–212.

Gelman, S, J.B. Carlin, H.S. Stern, and D.B. Rubin, 1995. *Bayesian Data Analysis*. Chapman & Hall/CRC Press, Boca Raton, FL. ISBN: 0-412-03991-5.

Heizler, M.T., Perry, F.V., Crowe, B.M., Peters, L., Appelt, R. 1999. "The age of the Lathrop Wells volcanic center: an $^{40}Ar/^{39}Ar$ dating investigation." *Journal of Geophysical Research*. 104, 767–804.

Johnson, R.A., and Wichern, D.W. 1992. *Applied Multivariate Statistical Analysis*. 3rd Edition, Prentice Hall, New Jersey.

Kahneman, D. , Slovic, P., and Tversky, A. 1982. *Judgment Under Uncertainty: Heuristics and Biases*. Cambridge University Press, Cambridge.

Keefer, D.L. and Bodily, S.E. 1983. "Three-point approximations for continuous random variables." *Management Science* v. 29, No. 5, pp. 595-609.

Keeney, R.L., and von Winterfeldt, D. 1991. "Eliciting Probabilities from Experts in Complex Technical Problems." *Engineering Management, IEEE Transactions*, v. 38, issue 3, p. 191-201.

Kotra, J.P.; Lee, M.P.; Eisenberg, N.A.; and DeWispelare, A.R. 1996. *Branch Technical Position on the Use of Expert Elicitation in the High-Level Radioactive Waste Program.* NUREG-1563. Washington, D.C.: U.S. Nuclear Regulatory Commission.

Kulkarni, R.B., R.R. Youngs & K.J. Coppersmith 1984. "Assessment of confidence intervals for results of seismic hazard analysis." *Proceedings of the Eighth World Conference on Earthquake Engineering*, San Francisco, vol. 1, 263-270.

Meyer, M.A. and J.M. Booker 2001. *Eliciting and Analyzing Expert Judgment: A Practical Guide*, ASA-SIAM Series on Statistics and Applied Probability. 7, Philadelphia, PA: SIAM, ISBN: 0-89871-474-5.

Miller, A.C, and T. R. Rice 1930. "Discrete Approximations of Probability Distributions." *Management Science* v. 29, no. 3, March 1930, pp. 352-362.

National Research Council 1995. *Technical Bases for Yucca Mountain Standards*. Washington, D.C.: National Academy Press. TIC: 217588.

O'Leary, D.W.; Mankinen, E.A.; Blakely, R.J.; Langenheim, V.E.; and Ponce, D.A. 2002. *Aeromagnetic Expression of Buried Basaltic Volcanoes Near Yucca Mountain, Nevada.* Open-File Report 02-020. Denver, Colorado: U.S. Geological Survey.

Perry, F.V., Crowe, B.M., Valentine, G.A., Bowker, L.M. 1998. *Volcanism Studies: Final Report for the Yucca Mountain Project*. Los Alamos National Laboratory Report LA-13478-MS. 554 pp.

Perry, F.V., Cogbill, A.H., Kelley, R.E. 2005. "Uncovering buried volcanoes at Yucca Mountain: new data for volcanic hazard assessment." *Eos, Trans. Am. Geophys. Union* 86, 485-488.

Reamer, C.W. 2004. "Pre-Licensing Evaluation of Igneous Activity Key Technical Issue Agreement 1.02." Letter from C.W. Reamer (NRC) to J. Ziegler (DOE/ORD), November 5, 2004, 1110043890, with enclosures.

Reiter, L. (1990). *Earthquake Hazard Analysis: Issues and Insights*. Columbia University Press.

Robert, C.P, and G. Casella 2005. *Monte Carlo Statistical Methods*, Springer, ISBN: 978-0-387-21239-5.

Sawyer, D.A., Fleck, R.J., Lanphere, M.A., Warren, R.G., Broxton, D.E., Hudson, M.R. 1994. "Episodic caldera volcanism in the Miocene southwestern Nevada volcanic field: Revised stratigraphic framework, $^{40}Ar/^{39}Ar$ geochronology, and implications for magmatism and extension." *Geological Society of America Bulletin* 106, 1304–1318.

Schlueter, J.R. 2002. "Request for Additional Information – Igneous Activity Agreement 1.02." Letter from J.R. Schlueter (NRC) to J.D. Ziegler (DOE), December 19, 2002, with enclosure, "NRC Review of DOE Documents Pertaining to Igneous Activity Key Technical Issue Agreement Item 1.02."

Sheridan, M. F. 1992. "A Monte Carlo technique to estimate the probability of volcanic dikes." *Proceedings, High Level Radioactive Waste Management*, v. 2, p. 2033-2038.

Silverman, B.W. 1986. "Density Estimation for Statistics and Data Analysis." Monographs on Statistics and Applied Probability, 26. Chapman and Hall, New York.

Smith, J.E. 1993. "Moment methods for decision analysis." *Management Science*, Vol. 39, No. 3, pp. 340-358.

SNL (Sandia National Laboratories) 2007. *Plan for the Expert Elicitation to Update the Probabilistic Volcanic Hazard Analysis (PVHA) for Yucca Mountain, Nevada.* PLN-MGR-GS-000001 REV 02. Las Vegas, Nevada: Sandia National Laboratories.

Solow, A.R. 2001. "An Empirical Bayes Analysis of Volcanic Eruptions." *Mathematical Geology*, v. 233, no.1.

Sonder, L.J., Jones, C.H. 1999. "Western United States extension: how the west was widened." *Annu. Rev. Earth Planet. Sci.* 27, 417–462.

Strang, G. 1980. *Linear Algebra and Its Applications*. Academic Press.

Ziegler, J.D. 2002. "Transmittal of Report Addressing Key Technical Issue (KTI) Agreement Item Igneous Activity (IA) 1.02." Letter from, J.D. Ziegler (DOE) to J.R. Schlueter (NRC), September 26, 2002, Las Vegas, Nevada, U.S. Department of Energy.

Ziegler, J.D. 2003. "Igneous Activity Agreement (IA) 1.02 Additional Information Needed (AIN 1): U.S. Department of Energy (DOE) Position on Volcanic Hazard at Yucca Mountain, Nevada, and Plans for Confirmatory Studies." Letter from, J.D. Ziegler (DOE) to J.R. Schlueter (NRC), November 11, 2003, Las Vegas, Nevada, U.S. Department of Energy.

INTENTIONALLY LEFT BLANK

APPENDIX A

BIOGRAPHIES OF EXPERT PANEL MEMBERS

The eight individuals whose qualifications and experience are summarized below comprised the final expert panel for the Probabilistic Volcanic Hazard Analysis Update (PVHA-U). Brief biographies of the eight panel members are presented below in alphabetical order.

Dr. Charles B. Connor is Chairman of the Geology Department at the University of South Florida, where he also serves as a Full Professor of volcanology and geophysics. He began studying basaltic volcanic fields in the early 1980s, at which time he focused on the structural setting of small-volume basaltic volcanism and the tectonic controls on the distribution of volcanoes. While a faculty member at Florida International University (1987 to 1992), Dr. Connor developed methods to assess both the rates of volcanic activity and the development of volcanic clusters. While working under contract to the Nuclear Regulatory Commission at the Southwest Research Institute (1992 to 2001), Dr. Connor developed methods for incorporating nonparametric density estimates and Bayesian inference into probabilistic volcanic hazard assessment in order to connect geologic models of volcanism more strongly with quantitative hazard assessments. He applied those methods to assess volcanic hazards first at Yucca Mountain, then at nuclear facilities in Japan, Armenia, and Indonesia. In addition, Dr. Connor has developed methods for forecasting eruptions from lava domes, for probabilistically forecasting the dispersion of volcanic ash, and for improving geophysical data inversion. He currently focuses on utilizing networks of sensors to monitor the processes that affect heat and mass transfer at active volcanoes. Dr. Connor has served on National Science Foundation panels pertaining to volcanology and to reviewing proposals to the Science and Technology Center. He also served on a National Research Council panel to review the U.S. Geologic Survey Volcanic Hazard Program; chaired an International Atomic Energy Agency panel charged with developing guidelines for volcanic hazard assessments for nuclear power plants; and was a Leverhulme Fellow at the Institute for Advanced Studies at the University of Bristol, UK. Dr. Connor obtained his B.S. in Geology and B.A. in Anthropology from the University of Illinois at Champaign-Urbana in 1982, and M.S. (1984) and Ph.D. (1988) degrees in Geology from Dartmouth College.

Dr. Bruce M. Crowe is a Senior Research Leader with the Battelle Memorial Institute, Columbus, Ohio. Before accepting his current post, he worked for 29 years at Los Alamos National Laboratory (LANL). In 1979 he initiated volcanic hazard studies of basaltic volcanism in the Yucca Mountain region through a joint project between LANL and the U.S. Geological Survey. Dr. Crowe developed and applied the approach used in the early 1980s for probabilistic volcanic hazard assessment of the Yucca Mountain region. From the early 1980s until 1994 he was Principal Investigator on the Yucca Mountain volcanism project for the U. S. Department of Energy. Dr. Crowe has conducted research on the volcanic geology of the southern Basin and Range province, the California borderland, the central Cascade Range, the Jemez volcanic field, and the southwest Nevada volcanic field. He participated in and directed teams monitoring volcanic activity in the Caribbean, Mount St. Helens, and Hawaii and worked on joint volcanologic and atmospheric studies of the trace-element compositions of volcanic gases emitted by Kilauea Volcano throughout the mid-1980s. Dr. Crowe has been Group Leader of both the Applied Geosciences and Isotope Geochemistry groups at LANL and served as Deputy Technical Project Officer, Technical Project Officer, and Geochemistry Coordinator for LANL programs conducted for the Yucca Mountain Project. Dr. Crowe serves as the science advisor for environmental management programs at the Nevada Site Office of the National Nuclear Security Administration. He currently is involved in probabilistic modeling studies for disposing

of low-level and transuranic radioactive waste and transport of radioactive material from underground testing of nuclear weapons at the Nevada Test Site. He was a member of the expert panel for the 1996 Probabilistic Volcanic Hazard Analysis for Yucca Mountain. Dr. Crowe earned his B.A. in Geology from Fresno State University (1969) and M.A. (1972) and Ph.D. (1974) degrees in Geology from the University of California at Santa Barbara.

Dr. William R. Hackett has more than 25 years of experience as a geoscientist involved in studying igneous processes, physical volcanology, volcanic petrology, volcanic-hosted ore deposits, the probabilistic assessment of volcanic and seismic hazards, and environmental geology. He remains on the Affiliate Graduate Faculty at Idaho State University, where he was a tenured faculty member from 1982 to 1990. From 1990 to 1994, as a Staff Scientist with the Idaho National Laboratory (INL), he focused on regional tectonics, environmental geosciences, the potential impacts of volcanism on the energy infrastructure of the Western United States, the performance assessment of waste-storage facilities, and the development of comprehensive geologic and geophysical data for the safety analysis of critical INL nuclear facilities. Dr. Hackett has been an independent consulting geologist for more than 15 years; has authored or co-authored numerous journal articles, encyclopedia articles, and book chapters; and is the editor of two geoscience books. He was a member of the expert panel for the 1996 Probabilistic Volcanic Hazard Analysis for Yucca Mountain. In 2003, Dr. Hackett joined the Yucca Mountain Project (YMP) as a Principal Scientist employed with Integrated Science Solutions Inc. He co-authored Technical Basis Document 13, *The Probability and Consequences of Volcanism at Yucca Mountain*. In 2004, Dr. Hackett was a member of the YMP's Regulatory Integration Team, charged with updating and revising documentation related to igneous processes for the YMP in support of the project's license application to the U.S. Nuclear Regulatory Commission. Dr. Hackett earned his B.A. in Geology from Franklin & Marshall College (1974), his M.S. in Earth Science from Case Western Reserve University (1977), and his Ph.D. in Geology from the Research School of Earth Science, Victoria University of Wellington, New Zealand (1985).

Dr. Mel A. Kuntz is a Research Geologist Emeritus with the U.S. Geological Survey (USGS), Denver. His specialties are volcanology, volcanic hazards, the petrology of volcanic and plutonic igneous rocks, and field geology. Dr. Kuntz spent most of his 30-year career studying the basaltic volcanic rocks of the eastern Snake River Plain, Idaho. His studies included field mapping, petrographic and petrochemical studies, radiometric studies, evaluation of volcanic hazards at the Idaho National Laboratory (INL), which is located in the plain, and theoretical analysis of the generation of basaltic magma and eruption mechanisms. With other USGS hydrologists, geologists, and isotope geochemists, he studied the three-dimensional subsurface stratigraphy of basaltic lava flows beneath INL. Dr. Kuntz is the author or co-author of approximately 60 publications relating to the geology of the eastern Snake River Plain and INL, including the geologic maps of INL and of the Craters of the Moon, Kings Bowl, and Wapi lava fields. After participating in field studies of pyroclastic flow and related deposits of the 1980 eruptions of Mount St. Helens, Dr. Kuntz and two USGS colleagues published geologic maps and journal papers relating to those deposits. In addition to his 30 years of volcanologic studies, he also has studied the plutonic rocks of the western margin of the Idaho batholith near McCall, Idaho. He was a member of the expert panel for the 1996 Probabilistic Volcanic Hazard Analysis for Yucca Mountain. Dr. Kuntz has a B.A. in Geology and American History from Carleton

College (1961), an M.S. in Geology from Northwestern University (1964), and a Ph.D. in Geology and Geochemistry from Stanford University (1968).

Dr. Alexander R. McBirney, now Professor Emeritus at the University of Oregon in Eugene, founded the university's Center for Volcanology in 1965 and was Chairman of the Department of Geology from 1968 to 1971. He also was a visiting professor at the California Institute of Technology in 1978 and at the University of Paris, Orsay, from 1985 to 1986. During his 40 years of research in volcanology and igneous rocks, Dr. McBirney has worked extensively in the volcanic provinces of Central America, the Cascades, the Galapagos Islands, and East Greenland. He was founding editor of the *Journal of Volcanology and Geothermal Research,* where he served as editor-in-chief from 1976 to 1989. His publications include the widely used book, *Volcanology*, which he co-authored with the late Howel Williams, and another text with the same name written jointly with J.-M. Bardintzeff. Dr. McBirney has written numerous papers on volcanic hazards and has provided consultation to private corporations and the United Nations regarding volcanic hazards at Mount St. Helens, the Philippines, and Indonesia. For many years, he was a permanent member of the International Atomic Energy Agency panel charged with evaluating volcanic hazards that could affect nuclear facilities. In 1990, he received the N.L. Bowen Award from the American Geophysical Union. He was a member of the expert panel for the 1996 Probabilistic Volcanic Hazard Analysis for Yucca Mountain. Dr. McBirney received his bachelor's degree from the United States Military Academy at West Point (1946) and his Ph.D. in Geology from the University of California at Berkeley (1961).

Dr. Michael F. Sheridan is Director of the Center for Geohazards Studies at the University at Buffalo, New York. Between 1990 and 1999 he was Chairman of the university's Geology Department and has been Emeritus Distinguished Professor of Geology since May 2006, when he retired from the teaching faculty. Before joining the University at Buffalo, Dr. Sheridan was Professor of Geology at Arizona State University. His early research incorporated field work, laboratory experiments, and computer models focused on the processes and products of explosive volcanism. That work utilized data on the size and shape of fragments, textures of deposits, and geometry of the major dispersed units to better understand the generation and dispersal of volcanic materials. A large part of that work was devoted to studying hydro-volcanism, which involves the explosive interaction of magma with external water. Dr. Sheridan has studied the products of some of the major explosive eruptions of historical time and has published volcanic risk evaluations and/or volcanic hazard maps of Vesuvius, Popocatépetl, Pico de Orizaba, and Colima volcanoes. He organized international workshops on explosive volcanism in Italy in 1982 and on Mount St. Helens in 1984. His current academic interests focus on using computer simulations of volcanic flows to evaluate volcanic hazards and developing methods for mitigating risks. In January 1995, the Mexican government invited Dr. Sheridan to apply his three-dimensional computer flow simulations to help prepare a volcanic hazard map of Popocatépetl Volcano. He was a Fulbright Scholar in Iceland and a visiting scientist at universities in Italy, France, New Zealand, and Mexico, where he taught courses on volcanology. Dr. Sheridan was a member of the expert panel for the 1996 Probabilistic Volcanic Hazard Analysis for Yucca Mountain. He earned his A.B. in Geology from Amherst College (1962) and his M.S. (1964) and Ph.D. (1965) degrees in Geology from Stanford University.

Dr. Frank J. Spera has been Professor of Earth and Planetary Sciences at the University of California at Santa Barbara since 1986. From 1977 to 1986, he was Professor of Geological Sciences at Princeton University. Dr. Spera studies the fluid dynamics and thermodynamics of magmas based on field data, laboratory results (experimental rheology of molten rocks), and computer simulation of petrogenesis, including the generation, segregation, ascent, storage, differentiation, and eruption of magma. Currently he applies the molecular dynamics method to study the connection between (1) the atomic-scale structure and properties of silicate liquids and (2) the geochemical evolution of magma bodies affected by simultaneous assimilation, recharge, eruption, and fractional crystallization. Dr. Spera has been a visiting professor in earth sciences at the University of Rome and the University of Naples, where he taught courses on volcanology and did field studies at Mt. Vesuvius and Mt. Etna. He was elected Fellow of the Mineralogical Society of America in 1997. Dr. Spera was a member of the Igneous Consequences Peer Review Panel that the U.S. Department of Energy formed in 2002 to review the technical basis for analyzing the consequences of igneous events that might affect the proposed Yucca Mountain repository. Dr. Spera earned his A.B. in Geology from Franklin & Marshall College in 1972 and his M.S. (1974) and Ph.D. (1977) degrees in Geology and Geophysics from the University of California at Berkeley.

Dr. George A. Thompson has been recalled to active duty at Stanford University, where he serves as Professor Emeritus of Geophysics. He helped establish the university's Geophysics Department more than 40 years ago, then served as Chair of the Geophysics Department (1967 to 1986), Chair of the Geology Department (1979 to 1982), and Dean of the School of Earth Sciences (1987 to 1989). Before joining the Stanford faculty, he was a geologist and geophysicist with the U.S. Geological Survey (USGS), where he studied mineral deposits and Basin and Range/Sierra Nevada tectonics. While at Stanford, Dr. Thompson helped design and interpret the lunar gravity experiment on Apollo 17. In recent years, his research with students has focused on deep seismic exploration of the crust and on the interplay between magmatism and earthquakes. His numerous professional roles have included consultant to the Advisory Committee on Nuclear Waste of the U.S. Nuclear Regulatory Commission; member of the Senior External Events Review Group, Lawrence Livermore National Laboratory; vice-chairman of the National Research Council Panel on Coupled Processes at Yucca Mountain; and chairman of the National Research Council committee on the proposed low-level nuclear waste site at Ward Valley, California. He is a member of the National Academy of Sciences (Chair, Geology Section, 2000 to 2003) and a Fellow of the Geological Society of America (President, 1996; George P. Woollard award, 1983), the American Geophysical Union, and the American Association for the Advancement of Science. Dr. Thompson was a Guggenheim Foundation Fellow from 1963 to 1964 and in 1999 received the John Wesley Powell Award from the USGS. He was a member of the expert panel for the 1996 Probabilistic Volcanic Hazard Analysis for Yucca Mountain. Dr. Thompson has a B.S. in Geology from Pennsylvania State (1941), an M.S. in Geology from M.I.T. (1942), and a Ph.D. in Geology from Stanford University (1949).

APPENDIX B

REFERENCES AND REQUESTED MATERIALS PROVIDED TO THE EXPERT PANEL

Section 2.3.2 of the main report summarizes the process of assembling and disseminating technical information to the members of the expert panel, and describes the key aspects of the data collection efforts that were part of this overall study. This Appendix provides a comprehensive list of all the references identified (by the MDT and the expert panel members themselves) for consideration by the panelists, in Section B.1. A large portion of this list was assembled prior to the first workshop, but the reference list was expanded upon when additional references and data sources were identified throughout the entire PVHA-U process. Section B.2 describes various types of technical information that was developed by the MDT in response to specific request from the expert panel. As described in Section 2.3.2, this information was provided to the individual members of the panel in whatever form they requested, and responses to request made by any one individual were made available to all experts.

B.1 REFERENCES IDENTIFIED FOR THE EXPERT PANEL

Ackermann, H.D.; Mooney, W.D.; Snyder, D.B.; and Sutton, V.D. 1988. Preliminary Interpretation of Seismic-Refraction and Gravity Studies West of Yucca Mountain, Nevada and California. Chapter 3 in Carr, M.D.; and Yount, J.C., eds., Geologic and Hydrologic Investigations of a Potential Nuclear Waste Disposal Site at Yucca Mountain, Southern Nevada. Denver, Colorado: U.S. Geological Survey Bulletin 1790.

Alaniz-Alvarez, S.A.; Nieto-Samaniego, A. F.; and Ferrari, L. 1998. Effect of Strain Rate in the Distribution of Monogenetic and Polygenetic Volcanism in the TransMexican Volcanic Belt. Geology, vol. 26, p. 591-594.

Aranda-Gomez, J.J.; Luhr, J.F.; Housh, T.B.; Connor, C.B.; Becker, T.; and Henry, C.D. 2003. Synextensional Pliocene-Pleistocene Eruptive Activity in the Camargo Volcanic Field. Geological Society of America Bulletin, vol. 115, no. 3, p. 298-313.

Armstrong, R.L. 1968. Sevier Orogenic Belt in Nevada and Utah. Geological Society of America Bulletin, vol. 79, p. 429-458.

Axen, G.J.; Taylor, W.J.; and Bartley, J.M. 1993. Space-Time Patterns and Tectonic Controls of Tertiary Extension and Magmatism in the Great Basin of the Western United States. Geological Society of America Bulletin, vol. 105, no. 1, p. 56-76.

Baldwin, J.M.; and Jahren, C.E. 1982. Magnetic Properties of Drill Core and Surface Samples from the Calico Hills Area, Nye County, Nevada. U.S. Geological Survey Open-File Report 82-536, p. 27.

Bechtel SAIC Company (BSC). 2005. Peak Ground Velocities for Seismic Events at Yucca Mountain, Nevada. Las Vegas, Nevada: Bechtel SAIC Company. ANL-MGR-GS-000004, REV 00.

BSC. 2004a. Yucca Mountain Site Description. Las Vegas, Nevada: Bechtel SAIC Company. TDR-CRW-GS-000001, REV 02, ICN 01. ACC: DOC.20040504.0008, two volumes.

BSC. 2004b. Characterize Eruptive Processes at Yucca Mountain, Nevada. Las Vegas, Nevada: Bechtel SAIC Company. ANL-MGR-GS-000002, REV 02.

BSC. 2004c. Characterize Framework for Igneous Activity at Yucca Mountain, Nevada. ANL-MGR-GS-000001, REV 02. Las Vegas, Nevada: Bechtel SAIC Company.

BSC. 2004d. Future Climate Analysis. Las Vegas, Nevada: Bechtel SAIC Company. ANL-NBS-GS-000008, REV 01.

BSC. 2004e. Drift Degradation Analysis. Las Vegas, Nevada: Bechtel SAIC Company. ANL-EBS-MD-000027, REV 03.

BSC. 2004f. Dike/Drift Interactions. Las Vegas, Nevada: Bechtel SAIC Company. MDL-MGR-GS-00005, REV 01.

BSC. 2002. Geologic Framework Model (GFM2000). Las Vegas, Nevada: Bechtel SAIC Company. MDL-NBS-GS-000002, REV 01.

Bennett, R.A.; Wernicke, B.P.; Niemi, N.A.; Friedrich, A.M.; and Davis, J.L. 2003. Contemporary Strain Rates in the Northern Basin and Range Province from GPS Data. Tectonics, vol. 22, no. 2, p.1008.

Biasi, G. 2005. Tomographic Imaging of the Crust and Upper Mantle in the Southern Great Basin—Interpretation. Presented at PVHA-U Workshop 2, University of Nevada, Reno, February.

Blakely, R.J.; Langenheim, V.E.; and Ponce, D.A. 2000a. Summary of Geophysical Investigations of the Death Valley Regional Water-Flow Modeling Project, Nevada and California. Denver, Colorado: U.S. Geological Survey Open-File Report 00-189.

Blakely, R.J.; Langenheim, V.E.; Ponce, D.A.; and Dixon, G.L. 2000b. Aeromagnetic Survey of the Amargosa Desert, Nevada and California—a Tool for Understanding Near-Surface Geology and Hydrology. Denver, Colorado: U.S. Geological Survey Open-File Report 00-188.

Blakely, R.J.; Jachens, R.C.; Calzia, J.P.; and Langenheim, V.E. 1999. Cenozoic Basins of the Death Valley Extended Terrane as Reflected in Regional-Scale Gravity Anomalies. In Wright, L.A.; and Troxel, B.W., eds., Cenozoic Basins of the Death Valley Region. Boulder, Colorado: Geological Society of America Special Paper 333, p.1-16.

Blakely, R.J.; Morin, R.L.; McKee, E.H.; Schmidt, K.M.; Langenheim, V.E.; and Dixon, G.L. 1998. Three-Dimensional Model of Paleozoic Basement beneath Amargosa Desert and Pahrump Valley, California and Nevada—Implications for Tectonic Evolution and Water Resources. U.S. Geological Survey Open-File Report 98-496, p. 29.

Brocher, T.M.; Hunter, W.C.; and Langenheim, V.E. 1998. Implications of Seismic Reflection and Potential Field Geophysical Data on the Structural Framework of the Yucca Mountain-Crater Flat Region, Nevada. Geological Society of America Bulletin, vol. 110, no. 8, p. 947-971.

Byers, F.M., Jr.; Carr, W.J.; Orkild, P.P.; Quinlivan, W.D.; and Sargent, K.A. 1976a. Volcanic Suites and Related Cauldrons of Timber Mountain-Oasis Valley Caldera Complex, Southern Nevada. Washington, D.C.: U.S. Geological Survey Professional Paper 919.

Byers, F.M., Jr.; Carr, W.J.; Christiansen, R.L.; Lipman, P.W.; Orkild, P.P.; and Quinlivan, W.D. 1976b. Geologic Map of the Timber Mountain Caldera Area, Nye County, Nevada. Denver, Colorado: U.S. Geological Survey Miscellaneous Investigations Series Map I-891.

Byth, K.; and Ripley, B.D. 1980. On Sampling Spatial Patterns by Distance Methods. Biometrics, vol. 36, p. 279-284.

Carl, B.S.; and Glazner, A.F. 2002. Extent and Significance of the Independence Dike Swarm, Eastern California. In Glazner, A.F.; Walker, J.D.; and Bartley, J.M., eds., Geologic Evolution of the Mojave Desert and Southwestern Basin and Range. Geological Society of America Memoir 195, p. 117-130.

Carr, M.D.; Waddell, S.J.; Vick, G.S.; Stock, J.M.; Monsen, S.A.; Harris, A.G.; Cork, B.W.; and Byers, F.M., Jr. 1986. Geology of Drill Hole UE25p#1, a Test Hole into Pre-Tertiary Rocks near Yucca Mountain, Southern Nevada. Menlo Park: U.S. Geological Survey Open-File Report 86-175, 87 p.

Carr, W.J. 1990. Styles of Extension in the Nevada Test Site Region, Southern Walker Lane Belt—an Integration of Volcano-Tectonic and Detachment Fault Models. Chapter 13 in Wernicke, B.P., ed., Basin and Range Extensional Tectonics near the Latitude of Las Vegas, Nevada. Boulder, Colorado: Geological Society of America Memoir 176.

Carr, W.J. 1984. Regional Structural Setting of Yucca Mountain, Southwestern Nevada, and Late Cenozoic Rates of Tectonic Activity in Part of the Southwestern Great Basin, Nevada and California. Denver, Colorado: U.S. Geological Survey Open-File Report 84-854.

Carr, W.J. 1982. Volcano-Tectonic History of Crater Flat, Southwestern Nevada, as Suggested by New Evidence from Drill Hole USW-VH-1 and Vicinity. Denver, Colorado: U.S. Geological Survey Open-File Report 82-457.

Carr, W.J.; and Parrish, L.D. 1985. Geology of Drill Hole USW-VH-2 and Structure of Crater Flat, Southwestern Nevada. Denver, Colorado: U.S. Geological Survey Open-File Report 85-475.

Carrigan, C. 2000. Plumbing Systems. In Sigurdsson, H., ed., Encyclopedia of Volcanoes. Academic Press, p. 219-235.

Champion, D.E. 1995. Volcanic Episodes near Yucca Mountain as Determined by Paleomagnetic Studies at Lathrop Wells, Crater Flat, and Sleeping Butte, Nevada. Reston, Virginia: U.S. Geological Survey Open-File Report 95-563.

Christiansen, R.L.; and Lipman, P.W. 1965. Geologic Map of the Topopah Spring NW Quadrangle, Nye County, Nevada. Washington, D.C.: U.S. Geological Survey Geologic Quadrangle Map GQ-444.

Christiansen, R.L.; Lipman, P.W.; Carr, W.J.; Byers, F.M., Jr.; Orkild, P.P.; and Sargent, K.A. 1977. The Timber Mountain-Oasis Valley Caldera Complex of Southern Nevada. Geological Society of America Bulletin, vol. 88, no. 7, p. 943-959.

Cogbill, A.H. 2006a. Detectability of Basaltic Dikes using the 2004 Yucca Mountain Aeromagnetic Survey. Los Alamos National Laboratory, Technical Report for PHVA-U, 11 p.

Cogbill, A. 2006b. Crustal Density Variations from Isostatic Gravity Anomalies. Los Alamos National Laboratory, Technical Report for PVHA-U. July.

Cogbill, A.H. 2005a. High-Resolution Aeromagnetic Survey near Yucca Mountain, Nevada. Los Alamos National Laboratory, Technical Report for PHVA-U, 13 p.

Cogbill, A.H. 2005b. Interpretation of Magnetic Anomalies at Yucca Wash, Nevada. Los Alamos National Laboratory, Technical Report for PHVA-U, 7 p.

Cogbill, A.H. 2005c. Quick Estimation of Pressure Variations from Free-Air Anomalies. Los Alamos National Laboratory, Technical Report for PHVA-U, 2 p.

Cogbill, A.H. 2005d. Topography and Free-Air Anomaly Plot—Profile across Crater Flat and Yucca Mountain. Los Alamos National Laboratory, Technical Report for PHVA-U.

Coleman, N.M.; and Abramson, L.R. 2004. Testing Claim about Volcanic Disruption of a Potential Geologic Repository at Yucca Mountain, Nevada. Geophysical Research Letters, vol. 31, p. L24601.

Condit, C.D.; and Connor, C.B. 1996. Recurrence Rates of Volcanism in Basaltic Volcanic Fields—an Example from the Springerville Volcanic Field, Arizona. Geological Society of America Bulletin, vol. 108, no. 10, p. 1225-1241.

Connor, C.B. 1994. Crater Flat Magnetic Survey. Notes from Scientific Notebook Archived at the Center for Nuclear Waste Regulatory Analyses (CNWRA) Quality Assurance Vault.

Connor, C.B. 1990. Cinder Cone Clustering in the TransMexican Volcanic Belt—Implications for Structural and Petrologic Models. Journal of Geophysical Research, vol. 95, no. B12, p. 19,395-19,405.

Connor, C.B.; and Hill, B.E. 1995. Three Nonhomogeneous Poisson Models for the Probability of Basaltic Volcanism—Application to the Yucca Mountain Region, Nevada. Journal of Geophysical Research, vol.100, no. B6, p. 10,107-10,125.

Connor, C.B.; and Hill, B.E. 1993. Estimating the Probability of Volcanic Disruption at the Yucca Mountain Site using Nonhomogeneous Poisson Models. Proceedings of the Topical Meeting on Site Characterization and Model Validation, FOCUS '93, September 26-29, 1993, Las Vegas, Nevada, p.174-181. La Grange Park, Illinois: American Nuclear Society.

Connor, C.B.; and Sanders, C.O. 1994. Geophysics Topical Report—Application of Seismic Tomographic and Magnetic Methods to Issues in Basaltic Volcanism. San Antonio, Texas: Center for Nuclear Waste Regulatory Analyses, CNWRA 94-013.

Connor, C.B.; Sparks, R.S.J.; Mason, R.M.; Bonadonna, C.; and Young, S.R. 2003. Exploring Links between Physical and Probabilistic Models of Volcanic Eruptions—the Soufriere Hills Volcano, Montserrat. Geophysical Research Letters, vol. 30, no. 13, p. 1701.

Connor, C.B.; Stamatakos, J.; Ferrill, D.; Hill, B.E.; Ofoegbu, G.; and Conway, F.M. 2000a. Volcanic Hazards at the Proposed Yucca Mountain, Nevada, High-Level Radioactive Waste Repository. Journal of Geophysical Research, vol. 105, p. 417-432.

Connor, C.B.; Stamatakos, J.A.; Ferrill, D.A.; Hill, B.E.; Ofoegbu, G.I.; Conway, F.M.; Sagar, B.; and Trapp, J. 2000b. Geologic Factors Controlling Patterns of Small-Volume Basaltic Volcanism—Application to a Volcanic Hazards Assessment at Yucca Mountain, Nevada. Journal of Geophysical Research, vol. 105, no. B1, p. 417-432.

Connor, C.B.; Stamatakos, J.A.; Ferrill, D.A.; and Hill, B.E. 1999. Comment on Detecting Strain in the Yucca Mountain Area, Nevada. Science, vol. 282, p. 1007b.

Connor, C.B.; Lane-Magsino, S.; Stamatakos, J.A.; Martin, R.H.; La Femina, P.C.; Hill, B.E.; and Lieber, S. 1997. Magnetic Surveys Help Reassess Volcanic Hazards at Yucca Mountain, Nevada. Eos, Transactions of the American Geophysical Union, vol. 78, no. 7, p. 73, 77, 78.

Connor, C.B.; Condit, C.D.; Crumpler, L.S.; and Aubele, J.C. 1992. Evidence of Regional Structural Controls on Vent Distribution, Springerville Volcanic Field, Arizona. Journal of Geophysical Research, vol. 97, p. 349-359.

Conway, M.; Connor, C.B.; Hill, B.E.; Condit, C.D.; Mullaney, K.; and Hall, C.M. 1998. Recurrence Rates of Basaltic Volcanism in the SP Cluster, San Francisco Volcanic Field, Arizona. Geology, vol. 26, no. 7, p. 655-658.

Conway, M.F.; Ferrill, D.A.; Hall, C.M.; Morris, A.P.; Stamatakos, J.A.; Connor, C.B.; Halliday, A.N.; and Condit, C. 1997. Timing of Basaltic Volcanism along the Mesa Butte Fault Zone in the San Francisco Volcanic Field, Arizona, from $^{40}Ar/^{39}Ar$ Ages—Implications for Longevity of Cinder Cone Alignments. Journal of Geophysical Research, vol. 102, no. B1, p. 815-824.

Cressie, N. 1991. Statistics for Spatial Data. New York: John Wiley and Sons, Inc., 922 p.

Crowe, B.M. 1986. Volcanic Hazard Assessment for Disposal of High-Level Radioactive Waste. Chapter 16 in Active Tectonics—Impact on Society. Commission on Physical Sciences, Mathematics, and Applications. Washington, D.C.: National Academy Press.

Crowe, B.; Wohletz, K., Vaniman, D., Gladney, E., and Bower, N. 1986. Status of Volcanic Hazard Studies for the Nevada Nuclear Waste Storage Investigations. Los Alamos National Laboratory Report LA-8325-MS, vol. II.

Crowe, B.; Perry, F.; Geissman, J.; McFadden, L.; Wells, S.; Murrell, M.; Poths, J.; Valentine, G.A.; Bowker, L.; and Finnegan, K. 1995. Status of Volcanism Studies for the Yucca Mountain Site Characterization Project. Los Alamos National Laboratory Report LA-12908-MS.

Crowe, B.M.; Vaniman, D.T.; and Carr, W.J. 1983. Status of Volcanic Hazard Studies for the Nevada Nuclear Waste Storage Investigations. Los Alamos National Laboratory Report LA-9325-MS.

Crowe, B.M.; Johnson, M.E.; and Beckman, R.J. 1982. Calculation of the Probability of Volcanic Disruption of a High-Level Radioactive Waste Repository within Southern Nevada, USA. Radioactive Waste Management and the Nuclear Fuel Cycle, vol. 3, no. 2, p. 167-190.

Crump, T. 2005. Summary of References Pertaining to Stress in the Yucca Mountain Region. Las Vegas, Nevada: Bechtel-SAIC Company.

CRWMS M&O.1999. Geologic Framework Model (GFM3.1). Analysis Model Report. Las Vegas, Nevada: CRWMS M&O. MDL-NBS-GS-000002, REV 00C.

CRWMS M&O 1998. *Probabilistic Seismic Hazard Analyses for Fault Displacement and Vibratory Ground Motion at Yucca Mountain, Nevada.* Milestone SP32IM3, September 23, 1998. Three volumes. Las Vegas, Nevada: CRWMS M&O.

Damjanac, B.; and Carranza-Torres, C. 2005. Topographical Effects on the Propagation and Localization of a Dike. Minneapolis, Minnesota: Itasca Consulting Group, 11 p.

Damjanac, B.; and Radakovic-Guzina, Z. 2006. Dike/Fault Interaction below Yucca Mountain, Revised. Minneapolis, Minnesota: Itasca Consulting Group, 20 p.

Davis, J.L.; Bennett, R.A.; and Wernicke, B.P. 2003. Assessment of GPS Velocity Accuracy for the Basin and Range Geodetic Network (BARGEN). Geophysical Research Letters, vol. 30, no. 7, p. 1411.

Davis, J.L.; Wernicke, B. P.; and Bennet, R.A. 1998. Response—Detecting Strain in the Yucca Mountain Area, Nevada. Science, vol. 282, p.1007b.

Day, W.C.; Potter, C.J.; Sweetkind, D.S.; Dickerson, R.P.; and San Juan, C.A. 1998a. Bedrock Geologic Map of the Central Block Area, Yucca Mountain, Nye County, Nevada. Washington, D.C.: U.S. Geological Survey Miscellaneous Investigations Series Map I-2601.

Day, W.C.; Dickerson, R.P.; Potter, C.J.; Sweetkind, D.S.; San Juan, C.A.; Drake, R.M., II; and Fridrich, C.J. 1998b. Bedrock Geologic Map of the Yucca Mountain Area, Nye County, Nevada. Denver, Colorado: U.S. Geological Survey Geologic Investigations Series Map I-2627.

Detournay, E.; Mastin, L.G.; Pearson, J.R.A.; Rubin, A.M.; and Spera, F.J. 2003. Final Report of the Igneous Consequences Peer Review Panel, with Appendices. Las Vegas, Nevada: Bechtel SAIC Company.

Dickson, L.D. 1998. Volcanology and Geochemistry of Pliocene and Quaternary Basalts on Citadel Mountain, Lunar Crater volcanic Field, Pancake Range, Nevada. Master's Thesis, University of Nevada, Las Vegas. (Map only).

Diggle, P.J. 1985. A Kernel Method for Smoothing Point Process Data. Applied Statistics, vol. 34, p. 138-147.

Eichelberger, J.C. 1997. Drilling Volcanoes. Science, vol. 278 (5340), p. 1084-1085.

Eichelberger, J.C. 1986. Research Hole to Intersect Inyo Dike. Eos, Transactions of the American Geophysical Union, vol. 67, no. 40, p. 768.

Eichelberger, J.C.; Vogel, T.A.; Younker, L.W.; Miller, C.D.; Heiken, G.H.; and Wolhletz, K.H. 1988. Structure and Stratigraphy beneath a Young Phreatic Vent—South Inyo Crater, Long Valley Caldera, California. Journal of Geophysical Research, vol. 93, no. B11, p. 13,208-13,220.

Ekren, E.B.; Anderson, R.E.; Rogers, C.L.; and Noble, D.C. 1971. Geology of the Northern Nellis Air Force Base Bombing and Gunnery Range, Nye County, Nevada. Washington, D.C.: U.S. Geological Survey Professional Paper 651.

Elosegui, P.; Davis, J.L.; Mitrovica, J.X.; Bennett, R.A.; and Wernicke, B.P. 2003. Crustal Loading near Great Salt Lake, Utah. Geophysical Research Letters, vol. 30, no. 3, p. 1111.

Faulds, J.E.; Bell, J.W.; Feuerbach, D.L.; and Ramelli, A.R. 1994. Geologic Map of the Crater Flat Area, Nevada. University of Nevada, Reno: Geophysical Investigations Map 101.

Feditov, S.A.1978. Ascent of Basic Magmas in the Crust and the Mechanism of Basaltic Fissure Eruptions. International Geology Review, v. 20, p. 33-48.

Ferrill, D.A.; and Morris, A.P. 1997. Geometric Considerations of Deformation above Curved Normal Faults and Salt Evacuation Surfaces. The Leading Edge, vol. 16, p. 112-1133.

Ferrill, D.A.; Stamatakos, J.A.; and Sims, D. 1999a. Normal Fault Corrugation— Implications for Growth and Seismicity of Active Normal Faults. Journal of Structural Geology, vol. 21, no. 8-9, p. 1027-1038.

Ferrill, D.A.; Winterle, J.; Wittmeyer, G.; Sims, D.; Colton, S.; Armstrong, A.; and Morris, A.P. 1999b. Stressed Rock Strains Groundwater at Yucca Mountain, Nevada. GSA Today, vol. 9, no. 5, p. 1-8. Boulder, Colorado: Geological Society of America.

Ferrill, D.A.; Morris, A.P.; Jones, S.M.; and Stamatakos, J.A. 1998. Extensional Layer-Parallel Shear and Normal Faulting. Journal of Structural Geology, vol. 20, p. 355-362.

Ferrill, D.A.; Stamatakos, J.A.; and McKague, H.L. 1997. Reply—Quaternary Slip History of the Bare Mountain Fault (Nevada) from the Morphology and Distribution of Alluvial Fan Deposits. Geology, vol. 25, p.190.

Ferrill, D.A.; Stirewalt, G.L.; Henderson, D.B.; Stamatakos, J.A.; Morris, A.P.; Spivey, K.H.; and Wernicke, B.P. 1996a. Faulting in the Yucca Mountain Region—Critical Review and Analyses of Tectonic Data from the Central Basin and Range. Washington, D.C.: U.S. Nuclear Regulatory Commission NUREG/CR-6401.

Ferrill, D.A.; Stamatakos, J.A.; Jones, S.M.; Rahe, B.; McKague, H.L.; Martin, R.H.; and Morris, A.P. 1996b. Quaternary Slip History of the Bare Mountain Fault (Nevada) from the Morphology and Distribution of Alluvial Fan Deposits. Geology, vol. 24, no. 6, p. 559-562.

Fink, J.H. 1985. Geometry of Silicic Dikes beneath the Inyo Domes, California. Journal of Geophysical Research, vol. 90, no. B13, p. 11,127-11,133.

Fleck, R.J.; Turrin, B.D.; Sawyer, D.A.; Warren, R.G.; Champion, D.E.; Hudson, M.R.; and Minor, S.A. 1996. Age and Character of Basaltic Rocks of the Yucca Mountain Region, Southern Nevada. Journal of Geophysical Research, vol. 101, no. B4, p. 8205-8227.

Fridrich, C.J. 1999. Tectonic Evolution of the Crater Flat Basin, Yucca Mountain Region, Nevada. Chapter 7 in Wright, L.A.; and Troxel, B.W., eds., Cenozoic Basins of the Death Valley Region. Boulder, Colorado: Geological Society of America Special Paper 333.

Fridrich, C.J.; Whitney, J.W.; Hudson, M.R.; and Crowe, B.M. 1999. Space-Time Patterns of Late Cenozoic Extension, Vertical Axis Rotation, and Volcanism in the Crater Flat Basin, Southwest Nevada. Chapter 8 in Wright, L.A.; and Troxel, B.W., eds., Cenozoic Basins of the Death Valley Region. Boulder, Colorado: Geological Society of America Special Paper 333.

Friedrich, A.M.; Wernicke, B.P.; and Niemi, N.A. 2003. Comparison of Geodetic and Geologic Data from the Wasatch Region, Utah, and Implications for the Spectral Character of Earth Deformation at Periods of 10 to 10 Million Years. Journal of Geophysical Research, vol. 108, no. B4, p. 2199.

Frizzell, V.A., Jr.; and Shulters, J. 1990. Geologic Map of the Nevada Test Site, Southern Nevada. Denver, Colorado: U.S. Geological Survey Miscellaneous Investigations Series Map I-2046.

Gaffney, E.S; and Damjanac, B. 2006. Localization of volcanic activity: Topographic effects on dike propagation, eruption and conduit formation. Geophysical Research Letters, vol. 33, L14313, doi:10.1029/2006GL026852.

Gaffney, E.S.; Damjanac, B.; and Valentine, G.A. 2007. Localization of volcanic activity: 2. Effects of pre-existing structure. Earth and Planetary Science Letters, vol. 263, p. 323-338.

Gillett, S.L.; and Van Alstine, D.R. 1982. Remagnetization and Tectonic Rotation of Upper Precambrian and Lower Paleozoic Strata from the Desert Range, Southern Nevada. Journal of Geophysical Research, vol. 87, p. 10,929-10,953.

Hamilton, W.B. 1988. Detachment Faulting in the Death Valley Region, California and Nevada. Chapter 5 in Carr, M.D.; and Yount, J.C., eds., Geologic and Hydrologic Investigations of a Potential Nuclear Waste Disposal Site at Yucca Mountain, Southern Nevada. Denver, Colorado: U.S. Geological Survey Bulletin 1790.

Haneberg, W. 2000. Deterministic and Probabilistic Approaches to Geologic Hazard Assessment. Environmental and Engineering Geoscience, vol. 6, no. 3, p. 209-226.

Hardyman, R.F.; and Oldow, J.S.1991. Tertiary Tectonic Framework and Cenozoic History of the Central Walker Lane, Nevada. In Raines, G.L.; Lisle, R.E.; Schafer, R.W.; and Wilkinson, W.H., eds., Proceedings of the Symposium on Geology and Ore Deposits of the Great Basin. Reno/Sparks, Nevada, April 1-5, 1990. Geological Society of Nevada. p.1, 279-301.

Harrington, P. 2005. Yucca Mountain Design Status. Presented to Institute of Nuclear Materials Management—Spent Fuel Management Seminar XXII. Washington, D.C.: U.S. Department of Energy, Office of Repository Development.

Heizler, M.T.; Perry, F.V.; Crowe, B.M.; Peters, L.; and Appelt, R. 1999. The Age of Lathrop Wells Volcanic Center—an $^{40}Ar/^{39}Ar$ Dating Investigation. Journal of Geophysical Research, vol. 104, no. B1, p. 767-804.

Hill, B.E.; and Stamatakos, J.A. 2002. Evaluation of Geophysical Information Used to Detect and Characterize Buried Volcanic Features in the Yucca Mountain Region. San Antonio, Texas: Center for Nuclear Waste Regulatory Analyses (CNWRA).

Ho, C.-H. 1992. Risk Assessment for the Yucca Mountain High-Level Nuclear Waste Repository Site—Estimation of Volcanic Disruption. Carson City, Nevada: Nevada State Agency for Nuclear Projects/Nuclear Waste Project Office.

Ho, C.-H. 1991. Time Trend Analysis of Basaltic Volcanism for the Yucca Mountain Site. Journal of Volcanology and Geothermal Research, vol. 46, p. 61-72.

Ho, C.-H.; and Smith, E.I. 2006. Hazard Area and Probability of Volcanic Disruption of the High-Level Radioactive Waste Repository at Yucca Mountain, Nevada, USA. Bulletin of Volcanology, vol. 69, p. 117-123.

Ho, C.-H.; and Smith, E.I. 1998. A Spatial-Temporal/3-D Model for Volcanic Hazard Assessment—Application to the Yucca Mountain Region, Nevada. Mathematical Geology, vol. 30, no. 5, p. 497-510.

Ho, C.-H.; and Smith, E.I. 1997. Volcanic Hazard Assessment Incorporating Expert Knowledge—Application to the Yucca Mountain Region, Nevada, U.S.A. Mathematical Geology, vol. 29. p. 615-627.

Ho, C.-H.; Smith, E.I.; Feuerback, D.L.; and Naumann, T.R. 1991. Eruptive Probability Calculation for the Yucca Mountain Site, U.S.A.—Statistical Estimation of Recurrence Rates. Bulletin of Volcanology, vol. 54, p. 50-56.

Hoisch, T.D.; Heizler, M.T.; and Zartman, R.E. 1997. Timing of Detachment Faulting in the Bullfrog Hills and Bare Mountain Area, Southwest Nevada—Inferences from $^{40}Ar/^{39}Ar$, K-Ar, U-Pb, and Fission Track Thermochronology. Journal of Geophysical Research, vol. 102, no. B2, p. 2815-2833.

Holm, D.K.; Geissman, J.W.; and Wernicke, B. 1993. Tilt and Rotation of the Footwall of a Major Normal Fault System—Paleomagnetism of the Black Mountains, Death Valley Extended Terrain, California. Geological Society of America Bulletin, vol. 105, p. 1373-1387.

Hudson, M.R. 1992. Paleomagnetic Data Bearing on the Origin of Arcuate Structures in the French Peak-Massachusetts Mountains Area of Southern Nevada. Geological Society of America Bulletin, vol. 104, p. 581-594.

Hudson, M.R.; Minor, S.A.; and Fridrich, C.J. 1996. The Distribution, Timing, and Character of Steep-Axis Rotations in a Broad Zone of Dextral Shear in Southwestern Nevada. Geological Society of America Abstracts with Programs, vol. 28, no. 7, p. A-451.

Hudson, M.R.; Sawyer, D.A.; and Warren, R.G. 1994. Paleomagnetism and Rotation Constraints for the Middle Miocene Southwestern Nevada Volcanic Field. Tectonics, vol. 13, no. 2, p. 258-277.

Humphreys, E. 2006. Assessment of Glenn Biasi's P-wave Tomography of the Upper Mantle beneath the NTS Region. University of Oregon, Technical Report for PHVA-U, 12 p.

Humphreys, E.D.; Dueker, K.G.; Schutt, D.L.; and Smith, R.B. 2002. Beneath Yellowstone—Evaluating Plume and Nonplume Models Using Teleseismic Images of the Upper Mantle. GSA Today, vol. 10, no. 12, p. 1-7.

International Atomic Energy Agency Volcanology Working Group (Aramaki, S.; Connor, C.; McBirney, A.; and Pasquare, G.). 1995. Volcanoes and Associated Topics in Relation to Nuclear Power Plant Siting. Vienna, Austria: International Atomic Energy Agency Safety Series No. 50-SG-(S2).

Janssen, B.; and King, G. 2000. Tectonic Modeling of Yucca Mountain. In Whitney, J.W.; and Keefer, W.R., eds., Geologic and Geophysical Characterization Studies of Yucca Mountain, Nevada, a Potential High-Level Nuclear Waste Repository. U.S. Geological Survey Digital Data Series DDS-0058, Version 1.

Jaquet, O.; and Carniel, R. 2001. Stochastic Modeling at Stromboli Volcano—a Volcano with a Remarkable Memory. Journal of Volcanology and Geothermal Research, vol. 105, p. 249-262.

Jaquet, O.; Low, S.; Martinelli, B.; Dietrich, V.; and Gilby, D. 2000. Estimation of Volcanic Hazards Based on Cox Stochastic Processes. Physics and Chemistry of the Earth, Part A, Solid Earth Geodesy, vol. 25, p. 571-579.

Jaupart, C. 2000. Magma Ascent at Shallow Levels. In Sigurdsson, H., ed., Encyclopedia of Volcanoes. Academic Press, p. 237-245.

Kane, M.F.; and Bracken, R.E. 1983. Aeromagnetic Map of Yucca Mountain and Surrounding Regions, Southwest Nevada. Denver, Colorado: U.S. Geological Survey Open-File Report 83-616.

Karakhanian, A.; Djrbashian, R.; Trifonov, V.; Philip, H.; Arakelian, S.; Avagian, A.; Baghdassaryan, H.; Davtian, V.; and Ghoukassyan, Y. 2003. Volcanic Hazards in the Region of the Armenian Nuclear Power Plant. Journal of Volcanology and Geothermal Research, vol. 126, p. 31-62.

Keating, G.N.; Valentine, G.A.; Krier, D.J.; and Perry, F.V. 2008, Shallow Plumbing Systems for Small-Volume Basaltic Volcanoes. Bulletin of Volcanology, vol. 70, p. 563-582 (provided to PVHA-U expert panel as an in-press preprint).

Klinger, R.E.; and Anderson, L.W. 1994. Topographic Profiles and their Implications for Late Quaternary Activity on the Bare Mountain Fault, Nye County, Nevada. Geological Society of America Abstracts with Programs, vol. 26, no. 2, p. 63-64.

Kondo, H.; Kaneko, K.; and Tanaka, K. 1998. Characterization of Spatial and Temporal Distribution of Volcanoes since 14 Ma in the Northeast Japan Volcanic Arc. Bulletin of the Volcanological Society of Japan, Series 2 , 43 ,p. 173-180.

Kotra, J.P.; Lee, M.P.; Eisenberg, N.A.; and DeWispelare, A.R. 1996. Branch Technical Position on the Use of Expert Elicitation in the High-Level Radioactive Waste Program. Washington, D.C.: U.S. Nuclear Regulatory Commission NUREG-1563.

La Femina, P.C.; Connor, C.B.; Stamatakos, J.A.; and Farrell, D.A. 2002. Normal Fault in Alluvium by High-Resolution Magnetic and Electromagnetic Surveys. Environmental and Engineering Geoscience, vol. 8, no. 3, p. 193-207.

Langenheim, V.E. 2000. Constraints on the Structure of Crater Flat, Southwest Nevada, Derived from Gravity and Magnetic Data. In Whitney, J.W.; and Keefer, W.R., eds., Geologic and Geophysical Characterization Studies of Yucca Mountain, Nevada, a Potential High-Level Nuclear Waste Repository. U.S. Geological Survey Digital Data Series DDS-0058.

Langenheim, V.E. 1995. Magnetic and Gravity Studies of Buried Volcanic Centers in the Amargosa Desert and Crater Flat, Southwest Nevada. Menlo Park, California: U.S. Geological Survey Open-File Report 95-564.

Langenheim, V.E.; and Ponce, D.A. 1995. Ground Magnetic Studies along a Regional Seismic-Reflection Profile across Bare Mountain, Crater Flat, and Yucca Mountain, Nevada. Menlo Park, California: U.S. Geological Survey Open-File Report 95-834.

Langenheim, V.E.; and Ponce, D.A. 1994. Gravity and Magnetics Investigations of Yucca Wash, Southwest Nevada. Proceedings of the Fifth Annual International Conference on High-Level Radioactive Waste Management. Las Vegas, Nevada, May 22-26. American Nuclear Society; American Society of Civil Engineers, vol. 4.

Lutz, T.M.; and Gutmann, J.T. 1994. An Improved Method of Determining Alignments of Point-like Features and its Implications for the Pinacate Volcanic Field, Mexico. Journal of Geophysical Research, vol. 100, p. 17, 659-17,670.

Magill, C.R.; McAneney, K.J.; and Smith, I.E.M. 2005. Probabilistic Assessment of Vent Locations for the New Auckland Volcanic Field Event. Mathematical Geology, vol. 37, p. 227-242.

Magill, C.; Blong, R.; and McAnency, J. 2004. Volcanic Loss for the Auckland Region (abstract): Workshop on Statistics in Volcanology, Bristol, England, March 23.

Magsino, S.L.; Connor, C.B.; Hill, B.E.; Stamatakos, J.A.; La Femina, P.C.; Sims, D.A.; and Martin, R.H. 1998. CNWRA Ground Magnetic Surveys in the Yucca Mountain Region, Nevada (1996-1997). San Antonio, Texas: Center for Nuclear Waste Regulatory Analyses (CNWRA) Report 98-001.

Maldonado, F. 1990. Structural Geology of the Upper Plate of the Bullfrog Hills Detachment Fault System, Southern Nevada. Geological Society of America Bulletin, vol. 102, p. 992-1006.

Maldonado, F.; and Koether, S.L. 1983. Stratigraphy, Structure, and Some Petrographic Features of Tertiary Volcanic Rocks at the USW G-2 Drill Hole, Yucca Mountain, Nye County, Nevada. Denver, Colorado: U.S. Geological Survey Open-File Report 83-732.

Margulies, T.; Lancaster, L.; Eisenberg, N.; and Abramson, L. 1992. Probabilistic Analysis of Magma Scenarios for Assessing Geologic Waste Repository Performance. New York, New York: American Society of Mechanical Engineers Report 92-WA/SAF-11.

Martin, A.J.; Umeda, K.; Connor, C.B.; Weller, J.N.; Zhao, D.; and Takahashi, M. 2004. Modeling Long-Term Volcanic Hazards through Bayesian Inference—Example from the Tohoku Volcanic Arc, Japan. Journal of Geophysical Research, vol. 109, no. B10, p. 208.

Martin, A.J.; Umeda, K.; and Yusa, Y. 2003. Probabilistic Approaches for Predicting the Long-Term Spatial and Temporal Characteristics of Monogenetic Volcanoes in Japan. Acta Geophysica Polonica, vol. 51, no. 3, p. 271-291.

Martinez, L.; Meertens, C.M.; and Smith, R.B. 1998. Anomalous Intraplate Deformation of the Basin and Range-Rocky Mountain Transition from Initial GPS Measurements. Geophysical Research Letters, vol. 24, p. 2741-2744.

McBirney, A.; and Godoy, A. 2003. Notes on the IAEA Guidelines for Assessing Volcanic Hazards at Nuclear Facilities. Journal of Volcanology and Geothermal Research, vol. 126, p. 1-9.

McBirney, R.; Serva, L.; Guerra, M.; and Connor, C.B. 2003. Volcanic and Seismic Hazards at a Proposed Nuclear Power Site in Central Java. Journal of Volcanology and Geothermal Research, vol. 126, p. 11-30.

McCafferty, A.E.; and Grauch, V.J.S. 1997. Aeromagnetic and Gravity Anomaly Maps of the Southwestern Nevada Volcanic Field, Nevada and California. Denver, Colorado: U.S. Geological Survey Geophysical Investigations Map GP-1015.

McCaffrey, R.; Long, M.D.; Goldfinger, C.; Zwick, P.C.; Nabelek, J.L.; Johnson, C.K.; and Smith, C. 2000. Rotation and Plate Locking at the Southern Cascadia Subduction Zone. Geophysical Research Letters, vol. 27, no. 19, p. 3117-3120.

McKay, E.J.; and Sargent, K.A. 1970. Geologic Map of the Lathrop Wells Quadrangle, Nye County, Nevada. Washington, D.C.: U.S. Geological Survey Map GQ-883.

Miller, M.M.; Melbourne, T.; Johnson, D.J.; and Sumner, W.Q. 2002. Periodic Slow Earthquakes from the Cascadia Subduction Zone. Science, vol. 295, no. 5564, p. 2423.

Miller, M.M; Endo, E.; Freymueller, J.T.; Goldfinger, C.; Kelsey, H.M.; Humphreys, E.D.; Johnson, D.J.; McCaffrey, R.; Oldow, J.S.; Qamar, A.; and Rubin, C.M. 1998. Precise Measurements Help Gauge Pacific Northwest's Earthquake Potential. Eos, Transactions of the American Geophysical Union, vol. 79, no. 23, p. 269-275.

Minor, S.A.; Hudson, M.R.; and Fridrich, C.J. 1997. Fault-Slip Data, Paleomagnetic Data, and Paleostress Analyses Bearing on the Neogene Tectonic Evolution of Northern Crater Flat Basin, Nevada. Denver, Colorado: U.S. Geological Survey Open-File Report 97-285.

Monsen, S.A.; Carr, M.D.; Reheis, M.C.; and Orkild, P.P. 1992. Geologic Map of Bare Mountain, Nye County, Nevada. Reston, Virginia: U.S. Geological Survey Miscellaneous Investigations Series Map I-2201.

Moore, J.G.; and Hopson, C.A. 1961. The Independence Dike Swarm in Eastern California. American Journal of Science, vol. 259, p. 241-259.

Morris, A.P.; and Ferrill, D.A. 1999. Constant Thickness Deformation above Curved Normal Faults. Journal of Structural Geology, vol. 21, p. 67-83.

Morris, A.P.; Ferrill, D.A.; Sims, D.W.; Franklin, N.; and Waiting, D.J. 2004. Patterns of Fault Displacement and Strain at Yucca Mountain, Nevada. Journal of Structural Geology, vol. 26, no.9, p.1707-1725.

Morris, A.; Ferrill, D.A.; and Henderson, D.B. 1996. Slip-Tendency Analysis and Fault Reactivation. Geology, vol. 24, no. 3, p. 275-278.

Nicholis, M.G.; and Rutherford, M.J. 2004. Experimental Constraints on Magma Ascent Rate for the Crater Flat Volcanic Zone Hawaiite. Geology, vol. 32; no. 6; p. 489-492.

Nielson, J.E.; and Nakata, J.K. 1994. Mantle Origin and Flow Sorting of Megacryst-Xenolith Inclusions in Mafic Dikes of Black Canyon, Arizona. U.S. Geological Survey Professional Paper 1541, 41 p.

Niemi, N.A.; Wernicke, B.P.; Friedrich, A.M.; Simons, M.; Bennett, R.A.; and Davis, J.L. 2004. BARGEN continuous GPS Data across the Eastern Basin and Range Province, and Implications for Fault System Dynamics. Geophysical Journal International, vol. 159, no. 3, p. 842-862.

Oldow, J.S.; Kohler, G.; and Donelick, R.A. 1994. Late Cenozoic Extensional Transfer in the Walker Lane Strike-Slip Belt, Nevada. Geology, vol. 22, p. 637-640.

O'Leary, D.W. 2000. Tectonic Significance of the Rock Valley Fault Zone, Nevada Test Site. In Whitney, J.W.; and Keefer, W.R., eds., Geologic and Geophysical Characterization Studies of Yucca Mountain, Nevada, a Potential High-Level Nuclear Waste Repository. U.S. Geological Survey Digital Data Series DDS-0058.

O'Leary, D.W. 1996. Synthesis of Tectonic Models for the Yucca Mountain Area. Chapter 8 in Whitney, J.W., ed., Seismotectonic Framework and Characterization of Faulting at Yucca Mountain, Nevada. Denver, Colorado: U.S. Geological Survey. Milestone 3GSH100M.

O'Leary, D.W.; Mankinen, E.A.; Blakely, R.J.; Langenheim, V.E.; and Ponce, D.A. 2002. Aeromagnetic Expression of Buried Basaltic Volcanoes near Yucca Mountain, Nevada. Denver, Colorado: U.S. Geological Survey Open-File Report 02-020.

Oliver, H.W.; and Fox, K.F. 1993. Structure of Crater Flat and Yucca Mountain, Southeastern Nevada, as Inferred from Gravity Data. Proceedings of the Fourth Annual International Conference on High-Level Radioactive Waste Management. Las Vegas, Nevada, April 26-30. Vol. 2, p. 1812-1817. La Grange Park, Illinois: American Nuclear Society.

Oliver, H.W., Ponce, D.A.; and Blank, H.R. 1995. Magnetic Investigations. Chapter 3 in Oliver, H.W.; Ponce, D.A.; and Hunter, W.C., eds., Major Results of Geophysical Investigations at Yucca Mountain and Vicinity, Southern Nevada. U.S. Geological Survey Open-File Report 95-74, p. 55-72.

Perman, R.C., 2005. Stress/strain Data for the Yucca Mountain Region. Oakland, California: Geomatrix Consultants, Inc., Technical Report for PHVA-U, 3 p.

Perry, F.V. 2007. Preliminary Summary of Isotopic and Rare-Earth-Element Data for Miocene to Pleistocene Basalts of the Yucca Mountain Region—Comparison with Other Volcanic Fields and Evidence for Decreased Partial Melting Accompanying Volume Decrease through Time. Los Alamos National Laboratory. Technical Report for PHVA-U, 9 p.

Perry, F.V. 2005. Geochronology, Geochemical, and Paleomagnetic Data Bearing on Interpretation of the Number of Quaternary Volcanic Events in Crater Flat. Los Alamos National Laboratory, Technical Report for PHVA-U, 15 p.

Perry, F.V.; and Straub, K.T. 1996. Geochemistry of the Lathrop Wells Volcanic Center. Los Alamos National Laboratory Report LA-13113-MS.

Perry, F.V.; Cogbill, A.H.; Kelley, R.E.; Lewis, C.; Cline, M.; Fleck, R.; and Peterman, Z. 2006. Preliminary Results and Interpretations of a High-Resolution Aeromagnetic Survey and Drilling Program to Investigate Buried Volcanic Features near Yucca Mountain, Nevada. Los Alamos National Laboratory, Rev. 05, 22 p.

Perry, F.V.; Cogbill, A.H.; and Kelley, R.E. 2005. Uncovering Buried Volcanoes at Yucca Mountain. Eos, Transactions of the American Geophysical Union, vol. 86, no. 47, p. 485-488.

Perry, F.; Valentine, G.; Desmarais, E.; and WoldeGrabriel, G. 2001. Probabilistic Assessment of Volcanic Hazard to Radioactive Waste Repositories in Japan—Intersection by a Dike from a nearby Composite Volcano. Geology, vol. 29, p. 255-258.

Perry, F.V.; Crowe, B.M.; Valentine, G.A.; and Bowker, L.M., eds. 1998. Volcanism Studies—Final Report for the Yucca Mountain Project. Los Alamos National Laboratory Report LA-13478-MS.

Peterson, F.F.; Bell, J.W.; Dorn, R.I.; Ramelli, A.R.; and Ku, T.L. 1995. Late Quaternary Geomorphology and Soils in Crater Flat, Yucca Mountain Area, Southern Nevada. Geological Society of America Bulletin, vol. 107 no. 4, p. 379-395.

Ponce, D.A. 1997. Gravity Data of Nevada. Denver Colorado: U.S. Geological Survey Digital Data Series DDS-42.

Ponce, D. A.; and Langenheim, V. E. 1994. Preliminary Gravity and Magnetic Models across Midway Valley and Yucca Wash, Nevada. U. S. Geological Survey Open-File Report 94-572, 25 p.

Ponce, D.A.; and Oliver, H.W. 1995. Gravity Investigations. Chapter 2 in Oliver, H.W.; Ponce, D.A.; and Hunter, W.C., eds., Major Results of Geophysical Investigations at Yucca Mountain and Vicinity, Southern Nevada. Menlo Park, California: U.S. Geological Survey Open-File Report 95-74. p. 33-54.

Ponce, D.A.; Mankinen, E.A.; Davidson, J.G.; Morin, R.L.; and Blakely, R.J. 1999. Digital Isostatic Gravity Map of the Nevada Test Site and Vicinity, Nye, Lincoln, and Clark Counties, Nevada, and Inyo County, California. Denver, Colorado: U.S. Geological Survey Open-File Report 99-554-C.

Potter, C.J.; Day, W.C.; Sweetkind, D.S.; and Dickerson, R.P. 2004. Structural Geology of the Proposed Site Area for a High-Level Radioactive Waste Repository, Yucca Mountain, Nevada. Geological Society of America Bulletin, vol. 116, no. 7/8, p. 858-879.

Potter, C.J.; Dickerson, R.P.; Sweetkind, D.S.; Drake, R.M., II; Taylor, E.M.; Fridrich, C.J.; San Juan, C.A.; and Day, W.C. 2002. Geologic Map of the Yucca Mountain Region, Nye County, Nevada. Denver, Colorado: U.S. Geological Survey Geologic Investigations Series Map I-2755.

Quade, J.; Mifflin, M.D.; Pratt, W.L.; McCoy, W.; and Burckle, L. 1995. Fossil Spring Deposits in the Southern Great Basin and their Implications for Changes in Water-Table Levels near Yucca Mountain, Nevada, during Quaternary Time. Geological Society of America Bulletin, vol. 107, no. 2, p. 213-230.

Rechard, R.P.; and Tierney, M.S. 2005. Improbability of an Igneous Intrusion Promoting a Critical Event in Spent Nuclear Fuel Disposed in Unsaturated Tuff. Risk Analysis, vol. 25, no. 4, p. 997-1028.

Reches, Z.; and Fink, J. 1988. The Mechanism of Intrusion of the Inyo Dike, Long Valley Caldera, California. Journal of Geophysical Research, vol. 93, no. 5, p. 4321-4334.

Reheis, M.C. 1988. Preliminary Study of Quaternary Faulting on the East Side of Bare Mountain, Nye County, Nevada. Chapter 8 in Carr, M.D.; and Yount, J.C., eds., Geologic and Hydrologic Investigations of a Potential Nuclear Waste Disposal Site at Yucca Mountain, Southern Nevada. Denver, Colorado: U.S. Geological Survey Bulletin 1790.

Rogers, G.; and Dragert, H. 2003. Episodic Tremor and Slip on the Cascadia Subduction Zone—the Chatter of Silent Slip. Science, vol. 300, p. 1942.

Rosenbaum, J.G. 1986. Paleomagnetic Directional Dispersion Produced by Plastic Deformation in a Thick Miocene Welded Tuff, Southern Nevada—Implications for Welding Temperatures. Journal of Geophysical Research, vol. 91, no. B12, p. 12,817-12,834.

Rosenbaum, J.G.; Hudson, M.R.; and Scott, R.B. 1991. Paleomagnetic Constraints on the Geometry and Timing of Deformation at Yucca Mountain, Nevada. Journal of Geophysical Research, vol. 96, no. B2, p. 1963-1979.

Rubin, A.M. 1995. Propagation of Magma-Filled Cracks. Annual Review of Earth and Planetary Sciences, vol. 23, p. 287-336.

Sandia National Laboratories. 1997. Hydraulic Fracturing Stress Measurements in Test Hole ESF-AOD-HDFR#1, Thermal Test Facility, Exploratory Studies Facility at Yucca Mountain. Albuquerque, New Mexico: Sandia National Laboratories Report WA-0065.

Sargent, K.A.; McKay, E.J.; and Burchfiel, B.C. 1970. Geologic Map of the Striped Hills Quadrangle, Nye County, Nevada. Washington, D.C.: U.S. Geological Survey Map GQ-882.

Savage, J.C. 1998. Comment on Detecting Strain in the Yucca Mountain Area, Nevada. Science, vol. 282, 1007a.

Savage, J.C.; Svarc, J.L.; and Prescott, W.H. 2001. Strain Accumulation at Yucca Mountain, Nevada, 1993-1998. Journal of Geophysical Research, vol. 106, no. B8, p. 16,483-16,488.

Savage, J.C.; Connor, C.B.; Stamatakos, J.A.; Ferrill, D.A.; Hill, B.E.; Davis, J.L.; Wernicke, B.P.; and Bennett, R.A. 1998. Detecting Strain in the Yucca Mountain Area, Nevada. Science, vol. 282 (5391), p. 1007b.

Savage, J.C.; Lisowski, M.; Gross, W.K.; King, N.E.; and Svarc, J.L. 1994. Strain Accumulation near Yucca Mountain, Nevada, 1983-1993. Journal of Geophysical Research, vol. 99, no. B9, p. 18,103-18,107.

Sawyer, D.A.; Fleck, R.J.; Lanphere, M.A.; Warren, R.G.; Broxton, D.E.; and Hudson, M.R. 1994. Episodic Caldera Volcanism in the Miocene Southwestern Nevada Volcanic Field—Revised Stratigraphic Framework, $^{40}Ar/^{39}Ar$ Geochronology, and Implications for Magmatism and Extension. Geological Society of America Bulletin, vol. 106, no. 10, p. 1304-1318.

Schweickert, R.A.; and Lahren, M.M. 1997. Strike-Slip Fault System in Amargosa Valley and Yucca Mountain, Nevada. Tectonophysics, vol. 272, p. 25-41.

Sharpe, S. 2003. Future Climate Analysis—10,000 to 1,000,000 Years after Present. Reno, Nevada: Desert Research Institute. MOD-01-001, REV 01.

Shelton, J.W. 1984. Listric Normal Faults. America Association of Petroleum Geologists Bulletin, vol. 68, 7, p. 801-815.

Silverman, B.W. 1986. Density Estimation for Statistics and Data Analysis. Monographs on Statistics and Applied Probability 26. New York, New York: Chapman & Hall.

Simonds, F.W.; Whitney, J.W.; Fox, K.F.; Ramelli, A.R.; Yount, J.C.; Carr, M.D.; Menges, C.M.; Dickerson, R.P.; and Scott, R.B. 1995. Map Showing Fault Activity in the Yucca Mountain Area, Nye County, Nevada. Denver, Colorado: U.S. Geological Survey Miscellaneous Investigations Series Map I-2520.

Singer, D.A. 1996. An Analysis of Nevada's Metal-Bearing Mineral Resources. Reno, Nevada: Nevada Bureau of Mines and Geology Open-File Report 96-2.

Slate, J.L., et al. 1999. Digital Geologic Map of the Nevada Test Site and Vicinity, Nye, Lincoln, and Clark Counties, Nevada, and Inyo County, California, Revision 4. U.S. Geological Survey Open-File Report 99-554-A.

Smith, E.I; Keenan, D.L.; and Plank, T. 2002. Episodic Volcanism and Hot Mantle—Implications for Volcanic Hazard Studies at the Proposed Nuclear Waste Repository at Yucca Mountain, Nevada. GSA Today, vol. 4. p. 4-10.

Smith, E.I.; Morikawa, S.A.; and Sanchez, A. 1997. Volcanism Studies Related to Probabilistic Volcanic Hazard Assessment—Summary of the Activities of the Center for Volcanic and Tectonic Studies, University of Nevada, Las Vegas. Final Report to the State of Nevada, Nuclear Waste Project Office for the period 1986 to 1996, 26 p.

Smith, E.I.; Feuerbach, D.L.; Naumann, T.R.; and Faulds, J.E. 1990. The Area of Most Recent Volcanism near Yucca Mountain, Nevada—Implications for Volcanic Risk Assessment. Proceedings of the International Topical Meeting on High-Level Radioactive Waste Management. Las Vegas, Nevada, April 8-12. American Nuclear Society and American Society of Civil Engineers, vol. 1, p. 81-90.

Smith, K.D.; von Seggern, D.; Blewitt, G.; Preston, L.; Anderson, J.G.; Wernicke, B.P.; and Davis, J.L. 2004. Evidence for Deep Magma Injection beneath Lake Tahoe, Nevada-California. Science, vol. 305, no. 5688, p. 1277-1280. August.

Smith, K.D.; Li Li, Brune, J.N.; Anooshehpoor, R.; and Savage, M.K. 2000. Preliminary Results from the NPE-Ryan Reversed Refraction Profile. Chapter D in Whitney, J.W.; and Keefer, W.R., eds., Geologic and Geophysical Characterization Studies of Yucca Mountain, Nevada, a Potential High-Level Nuclear Waste Repository. U.S. Geological Survey Digital Data Series DDS-0058, Version 1.0.

Snow, J.K. 1992. Large-Magnitude Permian Shortening and Continental-Margin Tectonics in the Southern Cordillera. Geological Society of America Bulletin, vol. 104, p. 80-105.

Snyder, D.B.; and Carr, W.J. 1984. Interpretation of Gravity Data in a Complex Volcano-Tectonic Setting, Southwestern Nevada. Journal of Geophysical Research, vol. 89, no. B12, p. 10,193-10,206.

Snyder, D.B.; and Carr, W.J. 1982. Preliminary Results of Gravity Investigations at Yucca Mountain and Vicinity, Southern Nye County, Nevada. Menlo Park, California: U.S. Geological Survey Open-File Report 82-701.

Sonder, L.J.; Jones, C.H.; Salyards, S.L.; and Murphy, K.M. 1994. Vertical Axis Rotations in the Las Vegas Valley Shear Zone, Southern Nevada—Paleomagnetic Constraints on Kinematics and Dynamics of Block Rotations. Tectonics, vol. 13, no. 4, p. 769-788.

Stamatakos, J.A.; and Ferrill, D.A. 1998. Strike-Slip Fault System in Amargosa Valley and Yucca Mountain, Nevada—Comment. Tectonophysics, vol. 294, p. 151-160.

Stamatakos, J.A.; Ferrill, D.A.; and Spivey, K.H. 1998. Paleomagnetic Constraints on the Tectonic Evolution of Bare Mountain, Nevada. Geological Society of America Bulletin, vol. 110, no. 12, p. 1530-1546.

Stamatakos, J.A.; Kodama, K.P.; and Pavlis, T.P. 1988b. Paleomagnetism of Eocene Plutonic Rocks, Matanuska Valley, Alaska. Geology, vol. 16, p. 618-622.

Stamatakos, J.A.; Connor, C.B.; and Martin, R.H. 1997. Quaternary Basin Evolution and Basaltic Volcanism of Crater Flat, Nevada, from Detailed Ground Magnetic Surveys of the Little Cones. University of Chicago, Illinois: Journal of Geology, vol. 105, p. 319-330.

Stewart, J.H. 1988. Tectonics of the Walker Lane Belt, Western Great Basin—Mesozoic and Cenozoic Deformation in a Zone of Shear. In Ernst, W.G., ed., Metamorphism and Crustal Evolution of the Western United States. Rubey Vol. 7, p. 683-713. Englewood Cliffs, New Jersey: Prentice-Hall.

Stickney, E.K. 2004. Quaternary Basaltic Volcanism in the Northern Part of the Lunar Crater Volcanic Field, Nevada. Master's Thesis, University of Nevada, Las Vegas.

Stock, J.M.; and Healy, J.H. 1988. Stress Field at Yucca Mountain, Nevada. Chapter 6 in Carr, M.D.; and Yount, J.C., eds., Geologic and Hydrologic Investigations of a Potential Nuclear Waste Disposal Site at Yucca Mountain, Southern Nevada. Denver, Colorado: U.S. Geological Survey Bulletin 1790.

Swadley, W C; and Carr, W.J. 1987. Geologic Map of the Quaternary and Tertiary Deposits of the Big Dune Quadrangle, Nye County, Nevada, and Inyo County, California. Denver, Colorado: U.S. Geological Survey Miscellaneous Investigations Series Map I-1767.

Swadley, W C; and Parrish, L.D. 1988. Surficial Geologic Map of the Bare Mountain Quadrangle, Nye County, Nevada. Denver, Colorado: U.S. Geological Survey Miscellaneous Investigations Series Map I-1826.

Tamura, Y.; Tatsumi, Y.; Zhao, D.; Kido, Y.; and Shukuno, H. 2002. Hot Fingers in the Mantle Wedge—New Insights into Magma Genesis in Subduction Zones. Earth and Planetary Science Letters, vol. 197, p. 105-116.

Thompson, G.A. 2000. Perspectives on Basin and Range Structure and Basaltic Volcanism, Bare Mountain-Crater Flat Area, Nye County, Nevada, in Whitney, J.W.; and Keefer, W.R., eds., Geologic and Geophysical Characterization Studies of Yucca Mountain, Nevada, a Potential High-Level Nuclear Waste Repository. U.S. Geological Survey Digital Data Series DDS-0058, Version 1.0.

Thordarson, W. 1983. Geohydrologic Data and Test Results from Well J-13, Nevada Test Site, Nye County, Nevada. Denver, Colorado: U.S. Geological Survey Water-Resources Investigations Report 83-4171.

Turrin, B.D.; Champion, D.; and Fleck, R.J. 1991. $^{40}Ar/^{39}Ar$ Age of the Lathrop Wells Volcanic Center, Yucca Mountain, Nevada. Science, vol. 253 (5020), p. 654-657.

Tynan, M.C.; Savino, J.M.; and Vogt, T. 2006. An Alternative Conceptual Model for Re-assessing Spatial and Temporal Distribution of Basaltic Volcanism near Yucca Mountain, Nevada—Interpreted Mega-rings, Banded Basalt Distribution, and Geophysical Anomalies Encompassing the Timber Mountain Nested Calderas. U.S. Department of Energy, Office of Civilian Radioactive Waste Management, 286 p.

U.S. Geological Survey (USGS). 2000. Geologic and Geophysical Characterization Studies of Yucca Mountain, Nevada, a Potential High-Level Radioactive-Waste Repository. Whitney, J.W.; and Keefer, W.R., eds. Denver, Colorado: U.S. Geological Survey DDS-058, Version 1.0.

Valentine, G.A.; and Keating, G.N. 2007. Eruptive Styles and Inferences about Plumbing Systems at Hidden Cone and Little Black Peak Scoria Cone Volcanoes (Nevada, U.S.A.). Bulletin of Volcanology, vol. 70, no. 1, p. 105-113. DOI 10.1007/s00445-007-0123-8.

Valentine, G.A.; and Krogh, K.E.C. 2006. Emplacement of Shallow Dikes and Sills beneath a Small Basaltic Volcanic Center—the Role of Pre-existing Structure (Paiute Ridge, Southern Nevada, USA). Earth and Planetary Science Letters, vol. 246, Issue 3-4, p. 217-230.

Valentine, G.A.; and Perry, F.V. 2007. Tectonically Controlled, Time-Predictable Basaltic Volcanism from a Lithospheric Mantle Source (Central Basin and Range Province, USA). Earth and Planetary Science Letters, vol. 261, p. 201-216.

Valentine, G.A.; and Perry, F.V. 2006. Decreasing Magmatic Footprints of Individual Volcanoes in a Waning Basaltic Field. Geophysical Research Letters, vol. 33, L14305. p. 1-5.

Valentine, G.A.; Krier, D.J.; Perry, F.V.; and Heiken, G. 2007. Eruptive and Geomorphic Processes at the Lathrop Wells Scoria Cone Volcano. Journal of Volcanology and Geothermal Research, vol. 161, p. 57-80.

Valentine, G.A.; Perry, F.V.; Krier, D.; Keating, G.N.; Kelley, R.E.; and Cogbill, A.H. 2006. Small-Volume Basaltic Volcanoes—Eruptive Products and Processes, and Post-eruptive Geomorphic Evolution in Crater Flat (Pleistocene), Southern Nevada. Geological Society of America Bulletin, vol. 118, no. 11/12, p.1313-1330.

Valentine, G.; Krier, D.; Perry, F.; and Heiken, G. 2005. Scoria Cone Construction Mechanisms, Lathrop Wells Volcano, Southern Nevada, USA. Geology, vol. 33, no. 8, p. 529-632.

Vaniman, D.T.; Crowe, B.M.; and Gladney, E.S. 1982. Petrology and Geochemistry of Hawaiite Lavas from Crater Flat, Nevada. Contributions to Mineralogy and Petrology, vol. 80, p. 341-357.

Vogel, T.A.; Eichelberger, J.C.; Younker, L.W.; Schuraytz, B.C.; Horkowitz, J.P.; Stockman, H.W.; and Westrich, H.R. 1989. Petrology and Emplacement Dynamics of Intrusive and Extrusive Rhyolites of Obsidian Dome, Inyo Craters Volcanic Chain, Eastern California. Journal of Geophysical Research B, Solid Earth and Planets, vol. 94, no. 12, p. 17,937-17,956.

Von Mises, R. 1957. Probability, Statistics, and Truth. New York: Dover Publications, Inc.

Weller, J.N.; Martin, A.J.; Connor, C.B.; Connor, L.J.; and Karakhanian, A. 2006. Modelling the Spatial Distribution of Volcanoes—an Example from Armenia. In Mader, H.M.; Coles, S.G.; Connor, C.B.; and Connor, L.J., eds., Statistics in Volcanology. Special Publication Number 1 of the International Association of Volcanology and Chemistry of the Earth's Interior. Bath, UK: The Geological Society Publishing House, p. 77-88.

Wells, D.L.; and Coppersmith, K.J. 1994. New Empirical Relationships among Magnitude, Rupture Length, Rupture Width, Rupture Area, and Surface Displacement. Bulletin of the Seismological Society of America, vol. 84, no. 4, p. 974-1002.

Wernicke, B.P.; Davis, J.L.; Bennett, R.A.; Normandeau, J.E.; Friedrich, A.M.; and Niemi, N.A. 2004. Tectonic Implications of a Dense Continuous GPS Velocity Field at Yucca Mountain, Nevada. Journal of Geophysical Research, vol. 109, no. B12, p. 404, December.

Wernicke, B.; Davis, J.L.; Bennett, R.A.; Elosegui, P.; Abolins, M.J.; Brady, R.J.; House, M.A.; Niemi, N.A.; and Snow, J.K. 1998. Anomalous Strain Accumulation in the Yucca Mountain Area, Nevada. Science, vol. 279, p. 2096-2100.

Wernicke, B.; Axen, G.J.; and Snow, J.K. 1988. Basin and Range Extensional Tectonics at the Latitude of Las Vegas, Nevada. Geological Society of America Bulletin, vol. 100, no. 11, p. 1738-1757.

Whitney, J.W.; and Berger, D.L. 2000. A 3.7-Million-year Offset Rate on the Windy Wash Fault at the South End of Yucca Mountain, Nevada. In Whitney, J.W.; and Keefer, W.R., eds., Geologic and Geophysical Characterization Studies of Yucca Mountain, Nevada, a Potential High-Level Radioactive-Waste Repository. Denver, Colorado: U.S. Geological Survey Digital Data Series DDS-058, Version 1.0.

Wilson, D.; and Aster, R. 2003. Imaging Crust and Upper Mantle Seismic Structure in the Southwestern United States Using Teleseismic Receiver Functions. The Leading Edge, vol. 22, no. 232, p. 234-237.

B.2 REQUESTED MATERIALS THAT WERE PROVIDED TO THE EXPERT PANEL

Description	Source(s)
Geologic, Geochemical, and Volcanologic Data	
Data for Miocene-Quaternary basalts and fault locations in GIS map format. (Basalt and fault data were included as GIS layers on all GIS maps provided to the expert panel.)	Slate et al. 1999
High-resolution shaded-relief map of Crater Flat and Yucca Mountain, extending south to the Lathrop Wells volcano.	Map# m201461, REV 00, LANL GIS
Multiple topographic profiles through volcanoes in the Crater Flat-Yucca Mountain and Sleeping Butte areas. Crater Flat profiles show the elevation of the repository relative to Crater Flat/Lathrop Wells volcanoes.	Map# m201517, REV 00, LANL GIS; Map# m2015126, REV 00, LANL GIS
Data file and GIS map showing locations and ages of basaltic vents in south-central Nevada and part of eastern California, including vents in the Lunar Crater, southwestern Nevada, Death Valley, and Cima areas. GIS map shows the locations of 274 Miocene, Pliocene, and Quaternary vents in relation to regional topography. Data file also lists percentage of Quaternary vents located in basins versus ranges.	DTN: LA0709DK150308.001; Map# m201473, REV 01, LANL GIS
Data compiled on a table and map. Table lists volcanic features of the Yucca Mountain region, including the volume, age, and location of Miocene, Pliocene, and Quaternary volcanic features and buried basalt bodies. The associated GIS map shows the locations of 32 vents, dikes, or magnetic anomalies in relation to regional topography.	DTN: LA0710DK150308.001; Map# m201787, REV 01, LANL GIS
Table presenting analogue data compiled regarding event (dike and conduit) geometry derived from eroded volcanic centers in the Yucca Mountain region. Table contains data on volume, dike length, dike azimuth, number and spacing of dikes in a swarm, fissure length, number of vents, vent spacing, vent location, and conduit diameter. Data for Pliocene and Miocene centers published subsequently by Keating et al. (2008).	Keating et al. 2008; DTN: LA0710DK150308.002
Report describing data that may constrain the number of Quaternary volcanic events in Crater Flat.	Perry 2005
Report describing variations in basalt geochemistry (derived from isotopic and other data) through time in the Yucca Mountain region. Report includes an assessment of whether the decreasing volumes observed through time are accompanied by decreased partial melting of the mantle source.	Perry 2007
Table presenting geochemical (whole-rock major and trace-element) data for all post-Miocene volcanic centers in the Yucca Mountain region. Information is provided in a data file that presents geochemical analyses sorted by volcanic center.	Perry and Straub 1996; Perry et al. (eds.) 1998
Report describing a conceptual model for the distribution of basalt in the Yucca Mountain region.	Tynan et al. 2006
GIS map plus data file containing extension data compiled for Crater Flat. Data include contours of cumulative crustal extension, contour digitization, and gridding for Crater Flat. Map shows contours of percent cumulative extension in relation to surface basaltic volcanism and topography. Contours taken from Fridrich et al. (1999, Figure 5A).	Fridrich et al. 1999; DTN: LA0712DK150308.001; Map# m201753, REV 0, LANL GIS
Geologic cross sections and block diagrams representing the structural characteristics of the area between Yucca Mountain and Crater Flat.	Day et al. 1998b; BSC 2002
Figure showing data compiled regarding depths of maar volcanoes.	Crowe et al. 1986
Detailed maps showing data compiled regarding eruptive centers in the Lunar Crater volcanic field.	Maps from Dickson 1998 (ref list says 1997) and Stickney 2004

Description	Source(s)
Web site presenting data compiled on earthquake hypocenters in the Yucca Mountain region.	Web site for the Nevada Seismological Lab Earthquake Center: http://www.seismo.unr.edu/Catalog/search.html
Seismic data compiled regarding a potential intrusive event in 2003 in the Lake Tahoe region.	Smith et al. (2004); Web site for the Nevada Seismological Lab Earthquake Center: http://www.seismo.unr.edu/Catalog/search.html
Animation of data on temporal and spatial patterns of silicic and basaltic volcanism in the Western United States.	Web site for the North American Volcanic and Intrusive Rock Database (NAVDAT): http://navdat.kgs.ku.edu/
Description of stress/strain data for the Yucca Mountain region along with references for those data.	Perman 2005; Crump 2005
Data from Aeromagnetic Survey/Drilling/Data Collection Program	
Data file containing aeromagnetic data and GIS map showing aeromagnetic data in relation to surface volcanism and topography. Data were derived from 2004 aeromagnetic survey and parts of a survey performed by the USGS in 1999 (Blakely et al. 2000b).	DTN: LA0411AC831142.001; Map# m201425, REV 01, LANL GIS; Perry et al. 2005
Table showing characteristics of aeromagnetic anomalies in the Yucca Mountain region, including drilling priority; location; estimates of depth and volume; and confidence of basalt (high, medium, or low) as assigned by the USGS and CNWRA.	DTN: LA0711DK150308.001
Technical report providing detailed description and analysis of aeromagnetic data from 2004 aeromagnetic survey.	Cogbill 2005a
Table presenting and evaluating data compiled regarding age estimates for Anomalies C and D. Estimates are based on regional rates of sedimentation.	DTN: LA0709DK150308.002
Report evaluating magnetic anomalies in Yucca Wash as described by Ponce and Langenheim (1994).	Cogbill 2005b
Technical report assessing the usefulness of aeromagnetic data for detecting dikes.	Cogbill 2006a
Data file of tables containing information regarding ages of basalts. Data include K-Ar and $^{40}Ar/^{39}Ar$ dates for buried and surface basalts.	DTN: GS070508318512.003
Table of geochemical data for basalts. Data include major-element, trace-element, and Sr and Nd isotopic data for buried basalts encountered in drill holes and in surface samples used for correlation.	DTN: GS070308318512.001; DTN: GS070408318512.002
Technical report presenting preliminary results of the aeromagnetic survey and drilling program performed for the PVHA-U.	Perry et al. 2006
Other Geophysical Data	
Data files and GIS maps presenting compiled gravity data (isostatic, Bouguer, and free-air). Maps show gravity variations in relation to surface volcanism and regional topography at both a regional and local scale.	Ponce 1997; DTN: LA0709DK150308.003
Compilation of variations in lithostatic pressure calculated from free-air gravity data for the Yucca Mountain region and the Lunar Crater/Reveille volcanic field. Information provided in a report, in data files, and on GIS maps that show pressure variations in relation to surface basaltic volcanism and topography.	Cogbill 2005c; DTN: LA0709DK150308.004; Map# m201748, REV 00, LANL GIS; Map# m201786, REV 01, LANL GIS
Figure (and topographic profile) presenting data compiled on a free-air gravity anomaly along the same line as the seismic reflection line given by Brocher et al. (1998).	Cogbill 2005d

Description	Source(s)
Technical report presenting variations in mean upper crustal density as calculated from isostatic gravity data. Information also provided in a data file and on a map.	Cogbilll 2006b; DTN: LA0805SLCDNYMR.000
Data file and GIS map showing variations in seismic velocity, including seismic tomography, for the upper mantle beneath the Yucca Mountain region. Biasi also presented the data to the expert panel in Workshop 2.	Biasi 2005; DTN: LA0807MTLTMGYM.000
Technical report reviewing seismic tomography data of Biasi (2005). Humphreys created an inversion of seismic data, which is presented in his report.	Humphreys 2006
Information on Dike Propagation	
Technical memo on localization of volcanic activity. Topics include the effects of topography on dike propagation, eruption, and conduit formation. (Later published as Gaffney and Damjanac 2006)	Damjanac and Carranza-Torres 2005
Technical memo on the effects of pre-existing geologic structures on the localization of volcanic activity. [Later published as Gaffney et al. (2007 not in ref list).]	Damjanac and Radakovic-Guzina 2006
Report describing contemporary two- and three-dimensional models of dike propagation.	BSC 2004f; Detournay et al. 2003
Miscellaneous Data	
Figure presenting data compiled on depth to groundwater in the Crater Flat/Yucca Mountain area.	BSC 2004a, Figure 8-15
Report providing information on future climatic conditions (10,000 to 1,000,000 years after present).	Sharpe 2003

NOTE: CNWRA = Center for Nuclear Waste Regulatory Analyses; GIS = Geographic Information System; LANL = Los Alamos National Laboratory; PVHA-U = Probabilistic Volcanic Hazard Analysis-Update; USGS = U.S. Geological Survey.

APPENDIX C

WORKSHOPS AND FIELD TRIP SUMMARIES

This appendix contains detailed summaries of the five workshops and one field trip conducted as part of the PVHA-U project. These summaries were prepared immediately after each workshop (and immediately after the field trip), and were distributed along with all presentation materials from the relevant workshop to the expert panel members and to all participants and observers at the workshop (or field trip) who signed an attendance list.

PROBABILISTIC VOLCANIC HAZARD ANALYSIS UPDATE
YUCCA MOUNTAIN PROJECT

WORKSHOP 1
KEY ISSUES AND AVAILABLE DATA

October 12-14, 2004
Las Vegas, Nevada

SUMMARY

The Workshop on Key Issues and Available Data was the first in a series of workshops conducted by the U.S. Department of Energy (DOE) in support of the Probabilistic Volcanic Hazard Analysis Update (PVHA-U) for the Yucca Mountain Project (YMP). The PVHA-U relates to the technical bases that will be provided in the project's license application to the U.S. Nuclear Regulatory Commission (NRC). The PVHA-U relies on formal elicitation of the assessments of a panel of expert volcanologists to estimate the probability that the Yucca Mountain repository could be disrupted by a future igneous event (i.e., the volcanic hazard at the site). The goals of this workshop were to (1) introduce members of the expert panel to the PVHA-U project goals, their roles, and the expert elicitation process; (2) describe how the results of the original PVHA completed in 1996 (PVHA-96) were used to support the performance assessment of the repository and identify the key issues the experts will address during the update; (3) review the new data acquired since completion of the PVHA-96; (4) identify data sets that the experts need to perform their evaluations; and (5) train the experts in methods for quantifying uncertainty, avoiding bias, and using probabilities to express uncertainties.

DAY 1 – TUESDAY, OCTOBER 12

Greetings and introductory presentations were offered by four members of the PVHA-U project team: Mr. Eric Smistad, technical lead for volcanism at DOE; Dr. Jerry King and Mr. Michael Cline, PVHA-U project managers for Bechtel SAIC Company (BSC); and Dr. Kevin Coppersmith, PVHA-U technical facilitator/integrator (Coppersmith Consulting).

Dr. Coppersmith welcomed the meeting participants and asked them to introduce themselves. Dr. Coppersmith identified the members of the expert panel, including eight from the PVHA-96 expert panel and two new members. The expert panel members introduced themselves and spoke briefly about the volcanology research they had performed since PVHA-96.

Then Mr. Smistad (DOE) thanked members of the expert panel for participating, noting his own role as technical lead for volcanism at DOE, and mentioning that Mr. Tim Sullivan had been the

DOE's technical lead for PVHA-96. Mr. Smistad described reasons for requesting an update of the PVHA-96, specifically that (1) new information has been gathered since 1996 that is relevant to estimating volcanic probability at the repository site, and (2) the NRC staff expressed concerns about the sensitivity studies conducted by the YMP utilizing aeromagnetic data obtained in 1999. Mr. Smistad described the relevance of estimating volcanic probabilities to NRC regulations and the calculation of doses. He stated that the DOE had committed to the NRC (Ziegler 2003) to: (1) gather new aeromagnetic data, (2) drill significant aeromagnetic anomalies and analyze the samples, and (3) update the PVHA in light of these new data. He noted that the results would be provided to the NRC during the review period for the YMP license application.

Dr. King, Disruptive Events Manager for BSC, welcomed the workshop participants. Dr. King noted that the PVHA-U is being conducted based on the acquisition of additional relevant data. He briefly described analyses performed by the YMP regarding the sensitivity of hazard results to data that became available after completion of the PVHA-96, as well as the DOE's commitment to collect additional data in support of updating the PVHA-96. Dr. King then identified members of the PVHA-U Methodology Development Team, the expert panel members, and the technical presenters scheduled to address the workshop regarding data collected since 1996. Mr. Cline (BSC) continued the introductory comments, reviewing the planned schedule of studies of igneous-related activities for the YMP in Fiscal Year 2005, which will examine both probabilities (including via the PVHA-U) and consequences of igneous events. Mr. Cline reviewed the PVHA-U schedule, noting key dates for workshops and elicitation interviews. Dr. Coppersmith noted that the hazard calculations would be redone completely for the PVHA-U.

Dr. Coppersmith gave the third introductory presentation, in which he described some of the expert elicitations completed since the PVHA-96 (including several for the YMP). Noting that much had been learned about expert elicitation processes in the past nine or ten years, he described relevant procedures and guidance in the BSC quality assurance procedure, *Expert Elicitation* (LP-AC.1Q-BSC; BSC 2004); the NRC's *Yucca Mountain Review Plan, Final Report* (NUREG-1804; NRC 2003) and *Branch Technical Position on the Use of Expert Elicitation in the High-Level Radioactive Waste Program* (NUREG-1563; Kotra et al. 1996); and the Senior Seismic Hazard Analysis Committee's *Recommendations for Probabilistic Seismic Hazard Analysis: Guidance on Uncertainty and Use of Experts* (NUREG/CR-6372; Budnitz et al. 1997). Dr. Coppersmith described the types of participation in the PVHA-U, including the role of the experts; reviewed ground rules for the workshops; and discussed the criteria for selecting experts, including the availability for continued participation on the expert panel. He discussed the integration of expert evaluations and the goal of developing a defensible basis for assigning equal weights when combining the experts' assessments. The steps being taken to achieve this goal were discussed, as were the roles/responsibilities of project participants in achieving integration. A major goal of expert elicitation is to have the composite representation across the expert panel members reflect the larger informed technical community.

Workshop participants discussed the use of expert judgment and the extent to which the PVHA-96 results had been accepted by the community of volcanologists. Participants noted differences in opinions in the technical communities of Europe versus the United States. Participants also discussed how to identify appropriate analogues and relevant data sets,

particularly regarding fault control of volcanism. Potentially publishing the final results of the PVHA-U also was discussed.

After a short break, Mr. Cline gave a talk on "Igneous Consequences and Igneous Scenario Class for the TSPA Model." He listed the consequence analysis and modeling reports prepared by the YMP, noting the regulatory and technical bases for addressing volcanic consequences. He discussed the key points of the DOE's Igneous Consequence Peer Review and reviewed the model cases used in the total system performance assessment (TSPA) for igneous events (both intrusive and extrusive volcanic events). He mentioned that the Lathrop Wells volcano may serve as a useful analogue for assessing the characteristics of potential future volcanism in the repository area. Mr. Cline described both the ASHPLUME code, which implements a mathematical ash dispersion model, and the probability-weighted estimates of doses from igneous disruption, including the uncertainty in those estimates.

After a break for lunch, Dr. Robert Youngs (Geomatrix Consultants) presented a talk titled "Overview of 1996 PVHA, Application of Results, and Required Outputs of Update." He reviewed the process and results of the PVHA-96, summarized how those results were applied to develop inputs to the TSPA, and described the additional outputs required from the PVHA-U, particularly as related to defining an igneous event. Dr. Youngs described the analyses needed to assess volcanic consequences in the TSPA for both intrusive and extrusive disruption effects. He described the parameters needed, which include conditional distributions for both (1) the lengths and azimuths of intersecting dikes and (2) the number of eruptive centers within the repository footprint. He concluded by describing the geometries of intrusive and extrusive events to be assessed for the PVHA-U. Workshop participants discussed definitions of volcanic events. Dr. Coppersmith asked experts to inform him promptly if they did not feel capable of providing the assessments required for the PVHA-U.

After a short break, Dr. Frank Perry of Los Alamos National Laboratory (LANL) gave a talk titled "Review of Yucca Mountain Region Basaltic Volcanism and Data Gathered Since 1996." He summarized the volcanic framework of the Great Basin region in which Yucca Mountain is located, including the spatial and temporal distribution of basalts, the geochronology of the area, and associated geochemical data. Then, he briefly described significant information published since 1995 in the categories of geophysical data, geodetic strain data, geologic mapping, structural data, geochronology, and petrology/geochemistry. These data are available in journals, organization reports (e.g., by LANL), and YMP reports.

Dr. Don Krier (LANL) gave the next talk, co-authored with Dr. Greg Valentine (LANL), on the characteristics of past volcanic events in the Yucca Mountain region. He described the parameters of dikes and conduits that directly affect the probability of an intersection between an igneous event and the repository footprint. Also discussed were field observations of volcanic features, including dike lengths, orientations, and widths, along with the occurrence of multiple dikes at Paiute Ridge and Crater Flat in southwest Nevada and at the San Rafael swell in Utah. Conduit diameters were discussed, using data from various locations, including Grants Ridge, New Mexico.

The scheduled talks for the day having concluded, Dr. Coppersmith opened the meeting to comments from participants. Topics included the forward time frame for which the experts must

make their evaluations (e.g., for the next 10,000 or one million years); potentially publishing the results of the project in a peer-reviewed journal; and available data sets. Then Dr. Coppersmith adjourned the meeting for the day.

DAY 2 – WEDNESDAY, OCTOBER 13

Day 2 of the workshop began with a discussion of the 1999 U.S. Geological Survey (USGS) aeromagnetic survey of the Amargosa Desert, Nevada, described by Dr. Rick Blakely (USGS). Dr. Blakely provided a list of the USGS publications that describe this study, which focused on the tectonics and hydrology of the Amargosa Desert located in the Yucca Mountain region. He showed a series of regional maps, briefly describing the basin boundaries and the role of features such as Stateline fault in the formation of the basins near Yucca Mountain. Dr. Blakely described how the aeromagnetic data were processed to emphasize shallow features and identify magnetic lineaments. Dr. Blakely concluded that although the survey highlights structures in the volcanic terrain, including evidence of exposed and concealed vents, it probably is inadequate for identifying typical volcanic dikes.

Dr. Allen Cogbill (LANL) presented the next talk, which described the recently completed 2004 DOE aeromagnetic survey in the region surrounding Yucca Mountain. He described the survey objectives: to reliably map possible basaltic rocks within the upper 400 m of the subsurface, to distinguish between magnetic tuffs and basalts, and to provide uniform coverage of the area of interest. He described the data acquisition process and showed maps displaying the survey results. Dr. Perry then discussed preliminary interpretations of the 2004 aeromagnetic data. He stated that the survey data will be combined with information obtained from other studies in the area, including borehole and ground magnetic investigations. Participants discussed interpretations of various features, including possible locations of faults that are identified on geologic maps based primarily on surface data. Workshop participants discussed the characteristics and importance of faults.

After a short break, Dr. Chuck Connor (University of South Florida) presented "Ground Magnetic Studies by the CNWRA" (Center for Nuclear Waste Regulatory Analyses). In introducing this talk, Dr. Coppersmith noted that Dr. Connor previously was employed by the CNWRA, where he contributed to some of the work he was going to describe, but that he was no longer associated with the CNWRA. Dr. Connor provided a list of CNWRA publications on magnetic studies. He described the basic goal of the studies: to identify, map, and interpret magnetic anomalies that may represent basaltic volcanic rocks buried in the shallow subsurface. He showed maps of anomalies and described some of the modeling work and interpretations CNWRA investigators had developed. He showed analytical results regarding the relative confidence that various anomalies are basaltic volcanoes (as described in Hill and Stamatakos 2002). Dr. Connor provided his conclusions (noting that they were his personal opinions and not necessarily those of the CNWRA), stating that buried volcanoes underlie many areas of the Yucca Mountain region. Workshop participants discussed the rate of sedimentation in Crater Flat and the importance of obtaining age dates for anomalies (deeper anomalies correlating roughly with greater age).

Dr. Glenn Biasi (University of Nevada at Reno) then presented a talk titled "Tomographic Imaging of the Crust and Upper Mantle in the Southern Great Basin." He outlined teleseismic

tomographic findings for both the region and the local Yucca Mountain area. He described the method and source data, showed mapped data that indicate a vertical, high-velocity structure at increasingly greater depths, and then showed cross sections along lines at various azimuths. After providing the regional summary, Dr. Biasi presented a local model, again providing images from layers at various depths and displaying a series of cross sections. He discussed a possible low-velocity zone at depths of approximately 80 to 100 km in the Yucca Mountain region.

Following a lunch break, Dr. Tom Brocher (USGS) gave a talk on seismic reflection and gravity surveys. He described a survey conducted in 1988 to obtain tectonic information along an east-west line in the Amargosa Desert. He showed several seismic reflection lines, both with and without interpretation lines, and pointed out the Gravity fault, lava flows, and other structural features that could be interpreted from the images. Dr. Brocher then described a second survey, conducted in 1994, along a reflection line that crossed both Crater Flat and Yucca Mountain, extending into Jackass Flats. Utilizing cross sections, he noted interpretations of the seismic reflection data, then showed the seismic lines containing the features that formed the basis for the interpretations. He described the gravity and ground magnetic data collected along the seismic lines and the models developed to be consistent with the data sets.

Dr. Christopher Potter (USGS) gave the next talk on geologic mapping in the Yucca Mountain vicinity from 1996 to the present. He showed maps at various scales, noting the complexity of the regional geology, before focusing on Yucca Mountain and the adjacent basins and calderas to the north. He showed maps of selected areas at various scales, describing features such as a dike along part of the Solitario Canyon fault (dated at 10 million years old (My) or older) and the Sundance fault. On a cross section, he indicated the moderately to steeply dipping block-bonding faults (e.g., the Solitario Canyon and Bow Ridge faults) and intra-block faults that commonly are sub-vertical. He described the most recently published geologic map of the Yucca Mountain region (Potter et al. 2002; 1:50,000 scale). He then provided a list of the geologic maps and publications available for the Yucca Mountain area.

After a short break, Dr. Connor gave his second talk of the day, “Nature of Volcano-Tectonic Interaction and Application to PVHA at Yucca Mountain,” which focused on the structural geology identified and tectonic models developed by CNWRA staff. He stated that volcano-tectonic interaction has a strong effect on the spatial distribution of volcanoes and the timing and recurrence rate of volcanism. He described data sets that provide the bases for tectonic models. He showed maps and photographs of volcanic features from various field locations and discussed relationships between (1) the rate of regional extension and the rate of volcanism and (2) rates of seismic activity and volcanism.

The final talk of the day, presented by Dr. James Davis (Smithsonian Astrophysical Observatory, Harvard-Smithsonian Center for Astrophysics), concerned the acquisition and analysis of geodetic data for the YMP. The goal of this effort is to make highly accurate determinations of present-day crustal deformation near Yucca Mountain. Dr. Davis described the two observational techniques his group uses: (1) temporally continuous surveying/geodetic monitoring that utilizes the Global Positioning System (GPS), a technique that provides high temporal resolution, and (2) measuring spatially continuous deformation utilizing interferometric synthetic aperture radar (InSAR), a technique that provides high spatial resolution. He then described acquisition of the GPS data and the factors that affect the accuracy of the analysis.

The GPS data products regarding horizontal site velocities can be reported relative to stable North America or relative to a frame of selected instrument locations. Next, Dr. Davis discussed the assessment of accuracy and analytical validation for the GPS data performed by independent analyses. These analyses identified only small errors in the surveys. He then briefly described InSAR data, the potential applications of which currently are being examined.

DAY 3 – THURSDAY, OCTOBER 14

Dr. Coppersmith began by reviewing the objectives for this morning's session: (1) to develop a list of additional data sets that the experts need to conduct their evaluations, and (2) to review the data collection activities LANL researchers plan to undertake. Dr. Coppersmith showed a list of the issues the PVHA-U will address, organized into three primary areas: spatial evaluation, temporal evaluation, and event definition (Table 1 of this summary). In the discussion that followed, members of the expert panel expressed the concern that the list of issues might limit the flexibility of the experts to develop new approaches or conceptual models. Dr. Coppersmith agreed that as long as they address spatial, temporal, and event definition issues, the experts may use whatever approaches or conceptual models they wish. Given the technical issues that the PVHA-U must address, the panel discussed a number of data sets they would like to obtain and identified issues for which additional information is needed. Those items are listed in Table 2 of this workshop summary.

Following a short break, Dr. Perry gave a talk titled "Planned Activities: Drilling of Aeromagnetic Anomalies, Geochronology, and Geochemistry." The goals of this data collection effort are to better constrain the number and ages of volcanic events, to reduce uncertainty, and to facilitate consideration of alternative conceptual models for the PVHA-U. Dr. Perry explained the criteria for selecting anomalies to be drilled. He showed the drilling targets in the Crater Flat/Amargosa Desert area and in Jackass Flats, discussing the rationales for selecting or not selecting specific anomalies. Because of the long lead time required to obtain drilling permits, permits already are being pursued for a number of sites. Additional information on the processed aeromagnetic data will be provided to the members of the expert panel in approximately six weeks. It is uncertain when the drilling program will begin, although Mr. Smistad indicated that December 2004 or January 2005 were likely starting times.

Workshop participants discussed how the aeromagnetic data should be interpreted and the rationale for selecting various candidate drilling sites. Participants made recommendations for additional processing of the aeromagnetic data, including developing cross sections and subduing features that are not of interest to the expert panel (for example, features located at great depths, which are of little interest because they are not suspected of containing young basalt). Also discussed were the relative importance of drilling in Crater Flat versus Jackass Flats and the importance of characterizing features such as possible alignments of volcanic cones. Dr. Youngs discussed the results of sensitivity studies, performed after PVHA-96 was completed, that assessed the effect of increased event counts on hazard results. He stated that increasing the number of young basaltic events in Jackass Flats could greatly affect the probability that an igneous event would intersect the repository footprint. His analysis, however, did not change any of the models used in the PVHA-96.

After a lunch break, Dr. Coppersmith distributed the BSC procedure, *Expert Elicitation* (LP-AC.1Q-BSC; BSC 2004) for the experts to review. He noted that he had collected conflict-of-interest forms from all the experts, and reminded them to provide their biographies for inclusion in the final project report. Dr. Coppersmith then introduced Dr. Karen Jenni (Geomatrix Consultants), a decision analyst who will serve as the PVHA-U's normative expert (defined as having a theoretical and conceptual knowledge of probability and practical experience in the elicitation of judgments from individuals). Dr. Jenni gave a talk, "Introduction to Probability Assessment and Elicitation." She began by reviewing the objectives of the project; the roles of the expert panel members and other project team members; and the general PVHA-U process, including the series of workshops and individual meetings. Beginning with a short history of uncertainty and the evolution of the concepts of probability and risk assessment, she discussed the use of probability to quantify uncertainty. She then discussed the representation of uncertainty, covering terminology, probability trees, probability distributions, and expected values. Dr. Jenni distributed some exercises for the experts, asking them to answer questions about various expressions of uncertainty used to estimate specific (but unknown) quantities.

Following a short break, Dr. Jenni discussed using probabilities to communicate about uncertainty, then summarized the process of probability assessment. She described cognitive and motivational biases that complicate the process of assessing and expressing subjective judgments, including anchoring (the tendency to focus on an initial estimate without adjusting sufficiently for uncertainty or new data). The completed exercises and questions answered before the break served to illustrate some cognitive biases, prompting discussion among the panel members about potential cognitive and motivational biases that might affect their judgments in this project. Some experts discussed the potential to anchor on their assessments made in PVHA-96, or to overweight data sets with which they have extensive personal experience. Dr. Jenni described the six-step process that will be followed in developing probability assessments: motivate the elicitation, structure the assessment and the uncertain quantities to be elicited, condition each expert to counter cognitive biases, encode the probability judgments, verify that the assessments accurately capture each expert's judgment, and, when necessary, convert continuous probability distributions into an appropriate discrete approximation for use in probability trees. While discussing the overall process, Dr. Jenni highlighted the structuring step as the point at which each expert will describe and define the sub-issues he believes he can best use to characterize spatial evolution, temporal evolution, and event characteristics. Although different experts may develop different structures, each structure will ultimately address those three primary issues. Dr. Jenni described how these steps fit into the PVHA-U (e.g., motivating occurs in the group meetings and workshops, and encoding full probability distributions occurs during the individual elicitation interviews). Aggregation of expert assessments was discussed.

Dr. Coppersmith thanked all the meeting participants and adjourned the workshop. The second workshop for the PVHA-U is scheduled tentatively for February 15 through 17, 2005.

TABLE 1
ISSUES AND POTENTIAL SUB-ISSUES TO BE ADDRESSED IN PVHA-U
PVHA-U Workshop 1: Key Issues and Available Data

Spatial Evaluation
- Region of interest
- Spatial model
  - Source zones
    - Alternative zonations
    - Nature of zone boundaries
  - Spatial smoothing
    - Smoothing operator
    - Smoothing distance
  - Other conceptual models?

Temporal Evaluation
- Homogeneous
- Nonhomogeneous
- Other conceptual models?
- Period of interest
- Event rates (for various magnitudes [see event definition below])
- Undetected events

Event Definition
- "Magnitude" of events (e.g., violent Strombolian or Strombolian)
- Geometry of intrusive events
  - Length, azimuth, and location of dike system relative to event; dike width (similar to PVHA-96 assessment)
  - Description of dike swarm (e.g., number and spacing of parallel dikes in a dike system)
  - Influence of repository opening on dike intersection
- Geometry of extrusive events
  - Number and locations of eruptive centers (conduits) associated with a volcanic event
  - Conduit diameter at repository level
  - Influence of repository openings on location of eruptive conduit

TABLE 2
INFORMATION REQUESTED BY THE EXPERT PANEL
PVHA-U Workshop 1: Key Issues and Available Data

Note: During Workshop 1 the expert panel members noted their need for the following data and information in order to address the PVHA-U issues.

1. List of references that address probabilistic volcanic hazard assessments around the world
2. Information on limits of detection for dikes in the shallow subsurface
3. Data on dike swarms
4. Modeling and processing information for the 2004 aeromagnetic survey in order to develop recommendations on locations and priorities for drilling, including modeling of specific anomalies for source depth and profiles of data
5. Reference pertaining to an area containing lava tubes having possible implications to dikes that subsequently were evacuated and now are open features
6. Information on dike propagation
7. Information on boundaries between zones in the Yucca Mountain region, particularly between Crater Flat and the Yucca Mountain block
8. Teleseismic tomographic data from analogue areas
9. GPS data from analogue areas having high data density
10. GPS information using PANGA data set
11. GPS data processed to indicate magnitude of strain in Crater Flat
12. Geodetic information for the Basin and Range area (based on extensional tectonics near Yucca Mountain combined with strike-slip faulting typical of Walker Lane)
13. Reference on results of directional drilling at Inyo Craters
14. Results of CNWRA magnetic survey between Red Cone and Black Cone
15. Compilation of data pertaining to volcanism in Crater Flat derived from activities such as drilling and age-dating
16. Information on characteristics of the repository (e.g., geometry of drifts, configuration of waste packages, projected thermal effects of repository)
17. Additional information on USGS magnetic data (including for Anomaly A)

PROBABILISTIC VOLCANIC HAZARD ANALYSIS UPDATE
YUCCA MOUNTAIN PROJECT

WORKSHOP 2
ALTERNATIVE MODELS

February 15-18, 2005
Las Vegas, Nevada

SUMMARY

The Workshop on Alternative Models was the second in a series of workshops conducted by the U.S. Department of Energy (DOE) in support of the Probabilistic Volcanic Hazard Analysis Update (PVHA-U) for the Yucca Mountain Project (YMP). The PVHA-U relates to the technical bases that will be provided in the project's license application to the U.S. Nuclear Regulatory Commission (NRC). The PVHA-U relies on formal elicitation of the assessments of a panel of expert volcanologists to estimate the probability that the Yucca Mountain repository could be disrupted by a future igneous event (i.e., the volcanic hazard at the site). The objectives of this workshop were to (1) review the PVHA-U project goals, the roles of the project participants, the process of expert elicitation, and the project schedule; (2) review the technical issues the expert panel must address; (3) discuss alternative interpretations of the tectonics of the Yucca Mountain region; (4) discuss alternative models for assessing the spatial and temporal distribution of potential future volcanism; (5) discuss characteristics of volcanic events; and (6) discuss alternative approaches to performing probabilistic volcanic hazard analysis, including international studies.

DAY 1 – TUESDAY, FEBRUARY 15

The workshop was opened by Dr. Kevin J. Coppersmith (Coppersmith Consulting, Inc.), who welcomed the group and asked members of the project team and observers to introduce themselves. He mentioned that the panel includes the eight out of ten experts from PVHA-96 who were able to serve, along with two new members.

Mr. Eric Smistad (DOE) welcomed the group, noting that the DOE greatly appreciates the willingness of the expert panel members to participate in this analysis. Mr. Smistad provided background information on the PVHA-U. A major reason for conducting the project is that new information relevant to estimating volcanic probability has become available since the original PVHA was completed in 1996 (the PVHA-96). Although the results of this study will not be available for the initial submittal of the YMP license application, they will be available during the NRC's review of the application.

Mr. Michael Cline of Bechtel SAIC Company (BSC) also welcomed the workshop participants, then gave an overview of the PVHA-U. He described the project organization and participants, including the Methodology Development Team (MDT), the expert panel members, and the process peer reviewers. Mr. Cline summarized the activities of Workshop 1, naming speakers who had described information and data that have become available since 1996 concerning igneous activity in the Yucca Mountain region. In describing the purpose of Workshop 2, Mr. Cline reviewed the schedule for the drilling, sampling, and analysis of aeromagnetic anomalies,

noting that the post-Workshop 2 schedule will be driven by the time needed to acquire the data. Finally, he described the overall schedule for the PVHA-U.

Then Dr. Coppersmith also described the goals and approach of Workshop 2. For those who had not attended Workshop 1, he noted that the PVHA-U results will supplement the analyses obtained during PVHA-96. He described the applicable procedures and regulatory guidance for the process of expert elicitation, reviewed the schedule of workshops and the key milestones, and highlighted the objective of performing a probabilistic hazard analysis. Next, Dr. Coppersmith reviewed the roles of the various participants in the project and the ground rules for the workshops. He described the integration of expert evaluations, for which the goal is to have a defensible basis for assigning equal weights to the assessments of all ten members of the expert panel, as those assessments are combined for developing the final probabilistic analysis. Finally, Dr. Coppersmith reviewed the technical issues to be addressed in PVHA-U and the goals and approach for Workshop 2.

The project team discussed the analyses that will be needed for PVHA-U. The assessments will be more extensive than those developed for PVHA-96, particularly as regards the definition of volcanic events that may intersect the repository. Mr. Cline described the boundary between the hazard or probability assessment, which is the focus of the PVHA-U, and the separate assessment of igneous consequences.

In the fourth introductory talk, Dr. Allen Cogbill of Los Alamos National Laboratory (LANL) described the aeromagnetic survey of the Yucca Mountain area performed by helicopter in 2004. He first noted how the survey generally was conducted and showed maps indicating radar altimeter, magnetic field, and analytic signal results. Dr. Cogbill then displayed maps and profiles of survey results that reveal specific basaltic features and anomalies. He described the characteristics of the features and the bases for estimating their source depths. Dr. Cogbill concluded that the aeromagnetic survey has greatly enhanced details of the subsurface geology for some locations. He also noted that no new magnetic anomalies have been discovered that likely represent shallow (less than 200 m in depth) basaltic sources in the vicinity of Yucca Mountain.

The various anomalies indicated by the aeromagnetic data and alternative ways of analyzing and interpreting the features were discussed. It was noted that information on many of the anomalies is provided by O'Leary et al. (2002).

Dr. Dennis O'Leary of the U.S. Geological Survey (USGS) then gave a talk titled "Basaltic Intrusion near Yucca Mountain and Relationship to Tectonic Models." His talk was aimed at discerning whether tectonic models provide insights for evaluating future volcanism at Yucca Mountain. He began by summarizing the history of volcanism and the structural elements in the region. He showed the roughly NW-SE trend of volcanism in Crater Flat and the orientations of faults that trend roughly N-S. He posed the question: How likely is it that there are fault-controlled dikes in the Crater Flat basin? In the second part of his presentation, Dr. O'Leary gave his definition of an igneous event, noting that causal mechanisms can produce one or more coeval volcanic eruptions within a characteristic tectonic setting. He described aspects of tectonic models that have been proposed for the Yucca Mountain region during the past couple of decades. He presented an illustration of the Solitario Canyon fault, which is

interpreted to intersect the Bare Mountain fault at a depth of about 8 to 10 km, based on structure contour maps developed by Dr. Fridrich (the next presenter on the workshop agenda). Dr. O'Leary suggested that the tectonic models be combined to obtain a model that addresses elements of importance from all models. In conclusion, he provided a table listing the tectonic models that were considered and weighted in logic trees developed by the six teams who characterized seismic sources for the probabilistic seismic hazard analysis for Yucca Mountain (CRWMS M&O 1998).

The project team discussed the applicability of a planar fault model to the Yucca Mountain region. Dr. O'Leary noted that although the planar fault model does not fit well for all features (e.g., Lathrop Wells), it appears overall to be a good model for the region. The petrology of the cones in the area was discussed, as were studies of reservoirs of molten material underlying the region and structures that might focus the ascent of a shallow eruption.

After a short break, Dr. Christopher Fridrich (USGS) gave a talk titled "Volcanic and Tectonic Evolution of the Crater Flat Basin and of the Death Valley Region as a Whole." He showed slides of structural features and described the Cenozoic stratigraphy of the region. He described tectonic elements expressed during various time intervals of the Cenozoic, focusing on the stress regimes. Dr. Fridrich illustrated the pattern of volcanism during each time interval, noting that Quaternary volcanism in the eastern Walker Lane belt was associated with fields that had formed during the Pliocene and late Miocene. He noted that the current rate of extension is too low to generate melt and is occurring only in areas that previously experienced volcanism. He stated his belief that the rate of tectonic activity in the system is declining. In focusing on the Crater Flat structural basin, Dr. Fridrich next described the feature (hinge line) he has defined to separate a more deformed area to the west from a less deformed area to the east (the western area where Crater Flat volcanism has occurred is also the area of greatest extension). He noted the amounts of extension that have occurred in the basin through time. Following Dr. Fridrich's presentation, the group discussed the nature of the hypothetical hinge line in Crater Flat and the possibility that shallow structures correlate with the hinge line at depth.

In introducing the next talk, Dr. Coppersmith explained that the NRC's contractor for information pertaining to volcanism is the Center for Nuclear Waste Regulatory Analyses (CNWRA), but because information developed by the CNWRA might be used in reviewing the license application for Yucca Mountain, the NRC concluded that CNWRA scientists should not make presentations at the workshop. Therefore, Dr. Charles Connor (University of South Florida) addressed "Quaternary Evolution of Crater Flat Basin," based on work performed by the CNWRA. He described the characteristics of Crater Flat, showing a stratigraphic section and indicating major structural features such as faults. He showed a profile of the basin—a half-graben in which the Bare Mountain fault is an east-dipping master fault that forms a detachment about 10 km below the basin and west-dipping antithetic faults lie in the vicinity of Yucca Mountain. Using gravity data and a density model, he summarized the features of Crater Flat, noting that the CNWRA interpretations share many similarities with the information provided by Dr. Fridrich. Dr. Connor next noted constraints on the timing of extension in the basin. He described the character of the rock sequence from the basement through the Quaternary, reviewing various interpretations of the sequence of causative events based on the geophysical information available for the basin. He showed the volcanic features of Pliocene and Quaternary Crater Flat and conceptual models of fault controls on volcanism. Dr. Connor

stated that some faults are more ready for dike injection than others because they experience a greater dilation tendency due to regional stress. He presented paleomagnetic data on rotation of the vertical axis, which indicates that deformation occurred primarily 11 to 12 million years ago (Ma), with little since that time. He presented models for how vertical-axis rotation manifests in normal fault systems. Dr. Connor then described CNWRA's conceptual model of the development of the Crater Flat basin, noting the low rates of extension and fault slip distributed across the basin, along with low rates of sedimentation and basaltic volcanism throughout it. The group then discussed the relationship between faults and propagating dikes, as well as controlling factors such as regional stress and rock quality. Dr. Connor concluded by noting the complexity of dike propagation.

After a lunch break, Dr. Glenn Biasi of the University of Nevada, Reno (UNR), gave a talk titled "Interpretation of Tomographic Imaging of the Crust and Upper Mantle in the Southern Great Basin." He described the method and source data used for the imaging and the station coverage. He summarized the velocity-scaling relationships and the influence of various factors on velocity, including temperature and composition (degree of volatile depletion) of the melt fraction. He showed maps of the tomographic data at various depths and profiles from various locations. Next, Dr. Biasi described the synthetic tests he used to evaluate resolution of the data; he concluded that resolution overall is excellent, although lateral resolution is better than vertical. After describing his general interpretations of the regional tomography, he presented a more detailed, local model based on maps showing layers of data from various depths and the structural features and characteristics those data indicate. Showing profiles of Crater Flat, he interpreted a possible magma source area at a depth of about 50 to 60 km for the Quaternary volcanoes. Dr. Biasi stated that P-wave tomography provides a third dimension that provides useful resolution for the region. He then summarized several interpretations about the root structure of the region and the spatial association of basaltic centers with subsurface features. Finally, he discussed melting depth and mantle heterogeneity. Following Dr. Biasi's talk, the group discussed the relationship between his study area and the larger Basin and Range region. Participants discussed the locations of low-velocity zones in those areas.

The next talk, "Tectonic Implications of a Dense, Continuous GPS Velocity Field at Yucca Mountain, Nevada," was presented by Dr. Brian Wernicke (California Institute of Technology), who acknowledged his co-author Dr. James Davis (presenter at Workshop 1). Dr. Wernicke described the geometry of the Basin and Range geodetic network. He showed field velocity data and the variations in data that define the geodetic provinces across the Southwest. Based on velocity data, sites east of Yucca Mountain show little motion, whereas the Yucca Mountain vicinity shows a relatively greater strain gradient that involves motion toward the northeast. Dr. Wernicke then compared relative motion between stations in the area. In general, the data fit a model of fairly homogeneous NNW right-lateral shear. Dr. Wernicke then presented points to consider: active right-lateral shear of about 1 mm per year has been confirmed; however, he does not believe this rate will continue for a long time (using a scale of a few thousand years). Showing transects of velocity with longitude at two latitudes, he noted that the transects indicate alternating contraction and extension across the Basin and Range. Dr. Wernicke then described a sequence of earthquakes on the northern edge of Lake Tahoe that may indicate movement of magma. The small earthquakes derived from depths of about 32 to 27 km for about five months in 2003. He showed time-series results for various stations, indicating the velocity changes during the 1997-to-2004 period of record. Strain rates differ at various stations, although overall

there is similar movement throughout the Basin and Range. Noting that geodetic velocity fields appear to be highly transient, he emphasized that past performance is not a good indicator of future conditions. In conclusion, he stated that crustal motions should continue to be monitored geodetically in the Yucca Mountain region.

Following Dr. Wernicke's presentation, the group discussed the amount of extension in the Yucca Mountain region. Dr. Wernicke noted that the measurable residual contains a small amount of extension, of which the principal axis of extension is about N65°W and the principal axis of contraction about N25°E. These axes are consistent with other types of data from the area. Also discussed were the earthquakes near the northern end of Lake Tahoe, interpreted as indicators of rising magma.

Dr. Leiph Preston, of the Nevada Seismological Laboratory at UNR, gave the next talk: "3-D P-Wave Velocity Structure of the Yucca Mountain Region." After acknowledging his co-authors Ken Smith and David von Seggern (also UNR), Dr. Preston described a velocity model constructed for the upper 10 km of crust based on sources both natural (earthquakes) and controlled (nuclear explosions). He showed the locations of seismographic stations in the Yucca Mountain vicinity that were used to develop the model and described the data set collected for earthquakes from 1981 to 2003. Showing maps of the P-wave velocity data from various depths, Dr. Preston described some of the velocity features and their associations with geologic structures. He noted that connections with features observed on the surface largely disappear by a depth of 4 km. He showed a profile of velocity with depth that indicated the structure of the Crater Flat basin, clearly defined on the west by the Bare Mountain fault and on the east by the Mine Mountain fault. In conclusion, he stated that northern Yucca Mountain is underlain to a depth of about 8 km by competent material that possibly is a plutonic body.

Dr. Frank Perry (LANL) gave the final presentation of the day (postponed from the morning session) on "Status of Modeling of Aeromagnetic Data and Sample Analysis Program." He described the effort underway to re-date Miocene basalts using samples recovered from drilling to improve the confidence in age correlations. Quaternary volcanoes also will be re-dated to help distinguish the timing of eruptions. Samples for age-dating recently were collected and will be analyzed by the USGS. Dr. Perry then showed maps of aeromagnetic data in the vicinity of the Lathrop Wells cone and indicated locations of faults, including NNW-trending faults both north and south of Lathrop Wells. Next he described an agglutinated body in Lathrop Wells that could be part of a fissure system and that is coincident with a fault interpreted to trend NNW. He noted that the Lathrop Wells cone is elongated to the NNW, consistent with the interpreted fault and fissure system.

Dr. Coppersmith opened the workshop to comments and questions from observers. Participants first discussed the expert elicitation process for the PVHA-U. One observer noted that it is vital that this process be transparent and well documented. Given the new data available since completion of PVHA-96, the same observer asked how the hazard results might change in the PVHA-U. Dr. Coppersmith stated that the PVHA-U encompasses a complete reassessment, because all aspects of the original analysis could be affected by new data. Next, observers asked for clarifications pertaining to some of the presentations. Discussed were features in Crater Flat observed from the aeromagnetic data, along with the degree of resolution that can be obtained from the data.

Dr. Coppersmith ended the day by thanking the workshop participants and noting that the meeting would re-convene at 8:30 A.M. the following day.

DAY 2 – WEDNESDAY, FEBRUARY 16

Mr. Cline welcomed everyone to the second day of the workshop. In response to a request from panelists for information on the design of the repository, he had available a handout called "Yucca Mountain Design Status" from a January 2005 talk Mr. Paul Harrington (DOE) gave on repository characteristics. The handout includes figures showing the repository footprint, the area for which the PVHA-U will calculate the annual frequency of intersection of a volcanic event. Dr. Coppersmith reviewed a slide, "Issues to Address in PVHA-U," from his talk the previous day, and described how the second day of the workshop would help address those issues.

Dr. Connor gave the first talk in the session on *Models for Characterizing the Spatial Distribution of Future Volcanism*: "Bayesian Approach to Forecasts of Volcano Spatial Intensity." He said that he uses a Bayesian approach because the observed pattern of volcanism is too limited to provide reliable estimates of the spatial density of volcanism in the Yucca Mountain region, and the approach enables integration of geologic models with the observed data. First he described the central elements of the approach as applied to estimating the spatial intensity of igneous activity. In this approach, he suggests using the past distribution of volcanic events to establish an initial estimate of the spatial distribution (known formally as a "prior" distribution), which is augmented or updated using an expert-specified probability density function relating other geologic/geophysical data to the spatial distribution of igneous activity. Dr. Connor showed a flow chart for the approach, indicating the various steps leading to the evaluation of hazard, and illustrated the mathematical formulation of Bayes' theorem. He described advantages and potential disadvantages of the Bayesian approach, then showed a constructed example (model) used to calculate the spatial intensity around three volcanoes. He illustrated the difference between a spatial intensity function derived from a bivariate normal distribution fit to the existing data and one derived by combining that model with one based on geologic interpretation of gravity data. He explained his use of a finite-element model for the Crater Flat region to conclude that changes in lithostatic pressure across the Bare Mountain fault might induce partial melting, flow, or both. He described other models, giving an example from Japan. He concluded that Bayes' formula could be utilized to combine a range of data and models, including gravity, percent extension, fault density, and seismic tomographic information, with a data-derived distribution.

Following Dr. Connor's presentation, members of the expert panel discussed how various types of data could be transformed into a form useable for a Bayesian model (utilizing probability density functions). The importance and potential difficulty in validating the analyses also were discussed. Dr. Coppersmith noted that members of the MDT would be available to make sample calculations for the experts.

Mr. Mark Tynan (DOE) gave the next talk, "Mega-rings Surrounding Timber Mountain Nested Calderas, Geophysical Anomalies: Rethinking Structure and Volcanism near Yucca Mountain, Nevada." He acknowledged his co-authors, John Savino (Golder Associates) and Tim Vogt (BSC), who assisted with data collection and analysis. He began by stating his belief that the

distribution of basaltic volcanism may be linked closely to elements of a mega-ring rift system (indicated by the arcuate patterns of large structural features that are defined at scales of tens of kilometers in the Yucca Mountain region.) He stated that if his theory has merit, the next volcanic event in the region likely would occur in the outer ring (arcuate feature) interpreted to surround Crater Flat, not within the basin or the repository footprint. Mr. Tynan described the geologic setting of the area and showed the arcuate-trending mega-rings that can be identified on geologic maps. He illustrated how various data sets, including topographic, distribution of basalts, tomographic, aeromagnetic, gravity, and seismicity, might be consistent with the interpretation of mega-rings. He described analogue evidence from the laboratory and from geographic areas, including caldera systems worldwide and on the planet Venus. He presented his integrated model for volcanism in the Yucca Mountain area and the sequence of regional geologic events since the Miocene.

After a short break, Dr. Michael Sheridan (State University of New York at Buffalo) presented a talk, "Bivariate Normal Probability Distribution for Monogenetic Scoria Cone Fields." His rationale for using a bivariate normal distribution is that approximately normal distributions occur in many situations because of the central-limit theorem. He described a conceptual model for magma rise, assuming a source zone about 60 to 80 km below the surface. Dr. Sheridan described the shapes and sizes of scoria cone fields (a small field comprises 1 to 10 cones) and the relationship of field size to rate of magma production. He noted that because the PVHA-U will focus on a small field, it is important to consider how to move from concepts pertinent to large fields to those applicable to small fields. Possible analogues to the Crater Flat area are the Cima field, which comprises more than 30 cones, the Taos field comprising about 40 cones, and the Reveille field containing about 50 cones, all of which have volcanoes younger than about 5 million years (My). He described the orientation of cones and general orientation of these fields, stating that clustering may reflect patchy melting (as opposed to a huge, uniformly melted area). Dr. Sheridan showed the mathematical construct for bivariate normal distributions, describing parameters and how to determine eigenvectors. Next he applied bivariate normal distributions to scoria cone fields. In the Yucca Mountain region, the Crater Flat volcanic zone (from Sleeping Butte to the Amargosa Valley anomalies) is an obvious choice for the model, but he believes outliers such as Buckboard Mesa also should be included if they fit the conceptual model. To explore the consequences of some of the models proposed during the PVHA-96, he used Monte Carlo simulations for three cases that reflect different distributions of cones. He showed mapped simulation results and their intersections with the repository footprint. Dr. Sheridan cautioned that estimated (subjective) parameters can greatly affect probabilities and that choosing which volcanoes to include in the model is critical (i.e., it is important to include those that create the volcanic field and are likely to erupt in the future). He concluded that the bivariate normal probability is a good choice for modeling distributions of scoria cones. The expert panel then discussed the use of this model combined with the Bayesian approach that Dr. Connor had described.

The next talk, "Transport and Storage of Magma," was presented by Dr. Claude Jaupart (Institut de Physique du Globe de Paris). Dr. Jaupart began by showing three different "plumbing" systems for volcanoes, stating that magma transport is driven by differences in buoyancy. He illustrated how an edifice (e.g., a shield volcano or stratovolcano such as Mt. Adams in the Washington Cascades) acts to focus magma transport toward a central area. Vertical dike propagation depends on initial driving pressure, magma density, and ambient stress field. Dr.

Jaupart showed a graph of magma density versus edifice height, indicating which magmas would be eruptible and which would be trapped. Next he discussed horizontal dike propagation both with and without an edifice, noting where an eruption would occur. He addressed the question: what will happen if magma is too dense to be erupted through the focal area? He showed a plot indicating when an eruption could occur in a focal area and when magma would be trapped and stored as a function of magma density and edifice height. High viscosity impedes lateral motion and hence enhances vertical dike propagation. Next Dr. Jaupart described lateral magma transport and the effects of an edifice. Finally, he described magma transport viewed from above, showing a map of Spanish Peaks, Colorado, where dike trajectories curve in response to changes in the ambient stress field. His major conclusion was that, by definition, magma overpressure is the same as regional stress. He stated that controls on magma transport and eruption sites are related to buoyancy, local stress field (as affected by topography and edifice), and regional stress field.

Following Dr. Jaupart's presentation, the project team discussed possible edifice effects that could occur in the vicinity of the repository. Dr. Jaupart said he believes any future volcanic eruption would occur in the Crater Flat basin rather than within Yucca Mountain, because the topography of Yucca Mountain creates a confining pressure. As an analogue, he described the Reunion area in the Indian Ocean, where volcanoes occur in a graben but never in adjoining blocks, because confining pressures cannot be overcome in the blocks. The influence of least-principal tectonic stress on the formation of dikes also was discussed. Dr. Jaupart noted that one must consider integrated density throughout the vertical column of magma, as many factors influence the column.

After a lunch break, Dr. Edward Gaffney (Gaffney Associates, Inc.) gave a talk on "Topographic Factors that Influence Dike Propagation at Yucca Mountain." He stated that he would discuss the effect of topographic stresses in two dimensions, then show a three-dimensional dike rising into uneven terrain. Dr. Gaffney described the effect of elevation on the conditional probability that a dike or dike system associated with a volcanic event would intersect the repository footprint. He showed samples of the various perspectives modeled using the computer program FLAC3D. Initial results indicate that the point of emergence of magma is 1 km offset from the center of a dike. Thus, any magma beneath the repository would lag by 300 m from the peak of the intrusion, perhaps as a result of the edifice effect described in Dr. Jaupart's earlier talk. Dr. Gaffney showed a film of a dike propagating upward and being diverted from the higher topography of Yucca Mountain. He concluded that magma flow would be diverted from high ground to break out first in lowlands. Under high ground, dikes would be very narrow (5 to10 cm), and magma velocity would be low (only millimeters per second). Expert panel members discussed the dike properties used in the model and the effects of varying parameters (e.g., fractured or faulted rock) on dike behavior. Also discussed was the occurrence of volcanoes within both basin and upland areas in the Western United States.

In a concluding short presentation on spatial models, Dr. George Thompson (Stanford University) commented on the evidence for the Yucca Mountain region's stress regime. He described a hydrofracture experiment conducted in the area that indicated a least-horizontal principal stress of N60° to 65°W, noting that this measurement was consistent with the data Dr. Wernicke reported on the first day of the workshop. Dr. Thompson noted that dikes inflate against (perpendicular to) the least-principal stress in a region. He showed alignments of

volcanoes in Crater Flat, the Reveille Range, and near Battle Mountain that indicate the stress vector has been consistent over time, noting that this is a fundamental piece of evidence. Dr. Jaupart noted that oil companies have found, through extensive experience, that hyrofractures are deflected by high topography.

Dr. Coppersmith opened the workshop to general discussion of models for the spatial distribution of volcanic activity. Participants discussed the selection of prior and likelihood functions in the Bayesian approach, especially how and when to include geologic data, as well as the value of using analogues as confirmation. It was noted that limited data are available for the Yucca Mountain area simply because the level of volcanic activity is very low. Additional discussion concerned accessing the databases available to the experts and the process to be followed for the expert elicitations. Dr. Coppersmith noted that a broad range of data is available and that each expert will need to identify the methods and approaches he considers most appropriate.

After a break, Dr. Perry described the aeromagnetic anomalies in the Yucca Mountain region that have been assigned the highest priority for drilling and laboratory analyses. Five anomalies in the Amargosa Valley have been selected and permits for drilling obtained. Dr. Perry showed a map of potential drilling locations in Jackass Flats, reviewing the bases for selecting locations for drilling. Dr. Perry asked the experts to consider the priority for drilling in the mapped locations or near other anomalies, because the topic would be discussed later in the workshop.

The next session of the workshop, *Models for Characterizing the Temporal Distribution of Future Volcanism* began with a talk by Dr. Connor: "General Methods for Estimating Temporal Recurrence Rate." He began by explaining that the word *event* is both a noun and a verb (e.g., the volcano erupts). The geologic record is interpreted in terms of events and their characteristics (how large, how many, how often). To estimate the recurrence rate of events for which data are limited, he used an example to describe how to define a confidence interval around an estimated recurrence rate. Given more data, various models can be used to estimate a repose interval. Dr. Connor examined the consistency of various models with eruption data from the Soufriere Hills volcano in Montserrat, West Indies. Neither a homogeneous Poisson (exponential) model nor a Weibull model fit the Monserrat data well. The best fit is provided by a log-logistic model. There is a link between the physics of a system and the model used. Dr. Connor showed a plot of various hazard functions and identified the systems they represent. The log-logistic model also provides a good fit to the repose interval distribution based on a catalog of larger-volume eruptions (VEI 4). He stated that the extremely limited data make it difficult to determine a survivor function for Yucca Mountain; he suspects that the temporal recurrence rate may be nonhomogeneous. Dr. Connor concluded by describing the advantages and disadvantages of homogeneous and nonhomogeneous Poisson methods.

The next talk, given by Dr. Richard Carlson (Carnegie Institute of Washington), was titled "An Alternative to Counting Volcanoes for Estimating Eruption Frequency." Dr. Carlson began by noting that using event counts for models of the Yucca Mountain region is problematic because the number of events is so limited. To develop a potential alternative, he plotted number of volcanic centers versus age in an attempt to identify a geologic basis for estimating frequency. He presented an animation of volcanism in the Western United States showing that volcanism in the region is related not only to extension, but probably to plate interaction as well (specifically, removal of the shallow-dipping Farallon plate and demise of the subduction system during the

past 50 million years (My)). Next Dr. Carlson showed the changing location of volcanism in the Basin and Range throughout the past 11 My. Most volcanic centers, except for those in the Yucca Mountain region, have moved outward toward the edges of the province. Next Dr. Carlson showed plots reflecting conductive adjustment to a new basal temperature in the lithosphere, mimicking loss of the subducting slab. The model indicates that eruption volume in the Yucca Mountain region is decreasing with time and volume per eruption is decreasing exponentially, implying that eruption frequency is increasing. These effects may reflect the fact that the melting rate is determined by the cooling lithosphere; alternatively, eruption volume may be controlled by volatile saturation, and smaller-volume melts have higher volatile contents.

The group discussed various aspects of Dr. Carlson's modeling. When asked to explain the decreasing repose times indicated by the model, Dr. Carlson stated that frequent and smaller eruptions may reflect decreasing production of melt. It was noted that changes in the geochemistry of basalts emplaced after about 5 million years ago (Ma) are consistent with the model results.

Dr. Coppersmith opened the meeting to comments from observers. Discussions focused on the thermal environment the repository will produce shortly after closure, as well as the period covered by the PVHA-U assessments (10,000 and one million years). Mr. Smistad noted that the period to be used in the license application to the NRC is 10,000 years; the PVHA-U is considering a longer time in anticipation of potential changes to the regulations. The ability to use GIS for the project was discussed. Much of the data for the PVHA-U are new and/or unpublished. Data sets will include some that are not specific to the Yucca Mountain area (i.e., from analogue areas). Dr. Coppersmith stated that providing the experts with access to data sets and GIS support are essential components of the PVHA-U process.

DAY 3 – THURSDAY, FEBRUARY 17

Dr. Coppersmith again reviewed the slide titled "Issues to Address in PVHA-U," focusing on the aspects of event definition to be covered in the first session of the third day of the workshop.

Dr. Frank Spera (University of California, Santa Barbara) began the session titled, *Characteristics of Possible Future Volcanic Events in the Yucca Mountain Area (Event Definition)*. He described his talk, "Magma Properties and Likely Eruptive Style in the Yucca Mountain Region," as primarily a review. He listed the types of information needed to define characteristics of the "most probable" eruption at the repository site, including volcanologic and geochemical history of the region, magmatic properties, and eruption dynamics for an "expected" eruption. Dr. Spera then reviewed each of these characteristics, beginning with patterns of eruptive volume/time for the Pliocene-Quaternary basaltic volcanism in Crater Flat. He stated that geochronologic data currently are insufficient to distinguish the ages of features of Quaternary Crater Flat volcanism, but suggested possible ways to remedy this situation. Next he briefly described the spatial distribution of basaltic centers near Yucca Mountain. Dr. Spera then discussed the petrologic and geochemical evolution of those rocks and their spatial geochemistry to assess how many distinct magma batches were erupted in the post-Miocene. He described work in progress on the origin of the Lathrop Wells basalt, specifically efforts to deduce the depth and water content of the source. He showed results of analyzing a peridotite and assessing its initial conditions regarding both percent of water and pressure effects. He then briefly

described magma properties and eruption dynamics, including depths of magma fragmentation. Dr. Spera concluded by describing the chronology of an eruption, addressing the propagation of a magma-filled crack, intensity of eruption, and duration of eruption. He presented an illustrative eruption scenario.

Dr. Sheridan gave the next talk, "Dike System near Hoover Dam: A Natural Analog for Igneous Intrusion at Yucca Mountain." Dr. Sheridan said that he believes analogue dike systems can provide useful information for estimating probabilities as well as analyzing consequences. He described field data from the Boulder dike system in Nevada near Hoover Dam, including distribution of bubble and crystal sizes in the dike and characteristics of the chill margin. Dr. Sheridan described the locations of the dikes and their stratigraphy and characteristics, including their chemical composition. He discussed large-scale aspects of overall length, segment lengths, and spacing between parallel dike sets, as well as small-scale features such as dike widths and dips. He also pointed out internal characteristics that provide information on flow and cooling history. Field relationships indicate that the dikes were emplaced less than 200 m below ground surface. Dr. Sheridan then described several processes that should be quantified, including degassing and crystallization. He described the field geometry of the dikes, such as conduit diameter. He showed a series of overlays of the Boulder dike system on the volcanoes of the Crater Flat region. He concluded that the Boulder dike/Hoover Dam swarm is a good analogue for Crater Flat events and could be useful in assessing both probabilities and consequences.

After a short break, Dr. Mel Kuntz (USGS, Emeritus) continued the session on event definition by discussing "Field Evidence for Dike Lengths in the Snake River Plain, Idaho, and Implications for Event Definition." After noting that no dikes are visible in the lava fields of the Snake River Plain (SRP), he described SRP features: the Craters of the Moon (about 60 flows during a 15,000-year interval; last eruption about 2,000 years ago); Kings Bowl; and Wapi lava fields. Series of tension cracks and eruptive fissures are found near the Kings Bowl and Wapi lava fields. Dr. Kuntz showed a conceptual model of dike propagation and development of an associated crack system. He illustrated dimensions of the systems using cross sections along the length of an eruptive fissure or tension crack system and a profile of the dikes developed below them. Next he discussed similarities and differences between the SRP and the Yucca Mountain region, such as slightly different eruption types, lava types, and areas and volumes of lava fields. Dike lengths in the SRP typically are 15 to 40 km, much longer than the lengths the PVHA-96 estimated for the Yucca Mountain region. Dr. Kuntz described the numbers and spacing of eruptive centers (conduits) and dike swarms (there is no evidence of multiple dikes in the SRP). Volcano-tectonic interactions and structures associated with dikes also were discussed.

Dr. Connor presented the next topic, "CNWRA Approach to Hazard Assessment." He noted that CNWRA scientists have produced a large volume of literature and that his presentation was based on talks by Dr. Britt Hill to the Advisory Committee on Nuclear Waste (ACNW). Dr. Connor began by describing the CNWRA approach to PVHA, including use of field data, definitions of igneous events, and investigations of the temporal and spatial clustering of volcanism. He then described four approaches to a PVHA developed for Japan's high-level waste program: deterministic, empirical, probabilistic, and Bayesian. Using flow charts, Dr. Connor summarized how each of these models produces an evaluation of hazard at a site. He showed maps of the volcanoes in the Yucca Mountain vicinity, noting that aeromagnetic anomalies create some uncertainty about the number of igneous events. He showed a profile of

the timing of volcanism after 11.4 Ma, describing different interpretations of recurrence intervals based in part on different assumptions about the ages of anomalies. Dr. Connor described the Bayesian spatial intensity approach that CNWRA uses, noting key points in the CNWRA analyses concerning the characteristics of volcanism in the Crater Flat/Yucca Mountain area.

Next, Dr. Connor presented information to deepen participants' understanding of the consequences of igneous events. In describing geochemical constraints on eruption dynamics, he provided examples from observed volcanic events, including a Cerro Negro eruption in 1992, and a laboratory experiment intended to mimic dike-intersection of volatile-free magma with the repository. He described numerical simulations of volatile-rich magmas that suggest the possibility of magma flows in repository drifts. Among his conclusions dealing with uncertainties and probable magma behavior was the possibility that undetected events represent an irreducible uncertainty, depending on the event definition used.

Following a break for lunch, Dr. Greg Valentine (LANL) presented "Expected Conduit Diameters and Other Eruptive Event Characteristics in the YM Region," first acknowledging his contributors at LANL. He first described the assumptions used to assess consequences for repository waste packages given both a dike intersection (intrusion scenario) and a conduit intersection (eruption scenario). Next, he reviewed the findings of recent field work conducted at the Lathrop Wells volcano. He showed photographs of the cone, in which active cinderblock quarrying is revealing progressively more deeply buried parts of the cone, and pointed out various features indicating eruptive facies. Based on these findings, Dr. Valentine presented an eruptive model for Lathrop Wells that consists of an early phase of Strombolian bursts followed by a later phase of violent Strombolian eruption. Next, Dr. Valentine summarized the field review of other cones in Crater Flat, describing characteristics of Red Cone, Black Cone, Little Cones, and North Cone. These features reflect a range of explosive processes. Next he discussed field evidence that supports the interpretation of one primary dike and one possible fissure alignment at Lathrop Wells. He described the characteristics of the 3.7-Ma basalts and 8.6-Ma rocks at Paiute Ridge. He then discussed conduit dimensions, describing mechanisms that widen conduits/dikes. Dr. Valentine then described theoretical approaches to modeling conduit flow, field evidence from eruptive products at Lathrop Wells and analogue volcanoes, and field evidence from eroded centers at various locations. He concluded by summarizing the issues surrounding conduits, noting that it is important to integrate conduit width so that it reflects the full duration of the event. Following the presentation, the project team discussed event definitions, shallow intrusions, depths of fragmentation, vertical and horizontal propagation of dikes, and dike dimensions.

Following a break, Dr. Neil Coleman (ACNW) gave a talk titled "Testing Claims about Volcanic Disruption of a Potential Repository at Yucca Mountain." He thanked his co-authors, Lee Abramson (NRC) and Bruce Marsh (Johns Hopkins University), then noted that his talk represents the views of the authors and not those of the ACNW/NRC. He first noted that regional studies suggest that the probability of future volcanism in the Yucca Mountain area is sufficiently high for the NRC to require the DOE to evaluate the consequences of a dike possibly intersecting the repository. He described the volcanic features in the region and characteristics of the volcanism, including the volume of magma erupted over time. He showed estimates made since 1982 of the potential volcanic disruption of a repository at Yucca Mountain. Describing the conjectured volcanic activity within the footprint of the repository, Dr. Coleman noted that

because no penetrating dikes have been observed in the 13-Ma rocks, the calculated hazards are inconsistent with the evidence derived from exploration. He described the intrusion-frequency bounds based on non-detection of dikes in the repository footprint. Next, Dr. Coleman described his analysis of data sets to obtain the calculated volcanic events per each million years in the Yucca Mountain region needed to produce rates of repository intersection of 10^{-8} to 10^{-10} per year. He said that he believes the large numbers of calculated events are inconsistent with observations.

Dr. Coleman recommended using the recurrence rate of Quaternary volcanism to estimate the frequency of potential future repository intersection. He noted several advantages to this approach, including reducing concerns about any older events that may not have been detected. Based on the eight known Quaternary events, and using the CNWRA code for PVHA, he estimates a frequency of repository intersection of 5.4×10^{-8}. Dr. Coleman discussed event clustering in natural processes, giving the example of major hurricane landfalls in the United States during the past 100 years. He concluded that his analysis raises doubts that the repository could be penetrated by a dike once every million years (i.e., 10^{-6}). Following Dr. Coleman's presentation, the group discussed the occurrence of volcanic features in the Yucca Mountain region and the uncertainty in estimating recurrence rates and repose intervals.

Dr. Coppersmith stated that Dr. Eugene Smith (University of Nevada, Las Vegas) had developed an alternative model for assessing future volcanism in the Yucca Mountain region. Although asked to present his model at the workshop, Dr. Smith declined because of policy considerations, so Dr. Coppersmith briefly summarized the key aspects of the model. In this model, volcanoes in Crater Flat are considered to be part of a larger zone of basaltic volcanism that stretches from Death Valley to the Lunar Crater field in the northeast. Volcanism within this zone is characterized by coeval and episodic periods of activity. An area of deep, hot mantle may underlie the entire zone. If this hypothesis is correct, then the higher recurrence rates for volcanism observed in Lunar Crater and the Reveille Range may apply to the Yucca Mountain area. Following Dr. Coppersmith's summary, the project team discussed the spatial distribution of volcanic centers and the evidence for shallow versus deep melting in the defined zone.

Dr. Coppersmith asked the workshop observers for any comments or questions. When no comments were offered, talk returned to the topic of drilling anomalies identified in the aeromagnetic data. The various drilling targets and their characteristics were discussed. The possibility of drilling all the identified anomalies was explored. Mr. Cline described the level of funding currently allocated for the task, which he estimated would allow for drilling approximately 10 holes. He stated that additional funding possibly could be obtained for drilling additional holes, but that the expert panel needed to provide input into prioritizing the drilling effort. Ms. April Gil (DOE) also confirmed the need to prioritize drilling efforts. It was decided that Dr. Perry would develop a table showing his prioritization of 18 anomalies, which would be discussed at an early start to the workshop the following morning. Dr. Coppersmith thanked the participants and adjourned the workshop for the day.

DAY 4 – FRIDAY, FEBRUARY 18

Dr. Coppersmith began the fourth and final day of the workshop by asking panel members about alternative dates for holding Workshop 2A (in late August or early September 2005). There was

tentative agreement on holding it August 30 and 31, 2005. Then, Dr. Perry re-opened the discussion of selecting anomalies for drilling. He showed his table listing relative priorities for drilling 18 anomalies and described the rationale for his ranking. Members of the expert panel again expressed their interest in drilling as many anomalies as possible. At the end of the discussion, Dr. Coppersmith assured the panel members that they would be kept informed of the progress and results of the drilling and lab analyses.

Dr. Coppersmith then re-opened the session on approaches to assessing hazard. He introduced Dr. Olivier Jacquet (Colenco, Switzerland), who talked about "Estimation of Volcanic Hazards Using Geostatistical Models with Applications from Germany and Japan." His stated objective was to present a methodology for using geostatistical models to estimate long-term volcanic hazards, which he would illustrate with examples. Given the complexity and uncertainty in assessing future volcanism, he considers probabilistic models to be most appropriate. Dr. Jacquet described the use of random functions to model the distribution and occurrence of volcanic events. He discussed the formalisms of interpolation versus simulation. Once the formalization is decided, a model can be selected. He described available models: Poisson process (constant potential), nonhomogeneous Poisson process (deterministic potential), and Cox process (random potential). He showed simulations of the potential for volcanic events and of clustering in space and time based on each model, then compared the results of using the Poisson and Cox processes. Illustrating how the Monte Carlo method can be used as a next step in developing a hazard map, Dr. Jacquet showed a flow chart of the steps in the methodology for probabilistic hazard assessment. Next, he illustrated the approach used to assess Quaternary volcanoes in the Tohoku volcanic arc in Japan and a Quaternary volcanic field in Osteifel, Germany. He described the characteristics of each area and showed a flow chart of the analysis that led to a probabilistic hazard map. He demonstrated the results of alternative Cox simulations of the spatial variability of volcanism in the regions and showed final hazard maps developed after Monte Carlo simulations. Dr. Jacquet stressed the importance of integrating geophysical data into the assessment of the potential for future volcanism.

Following the presentation, members of the expert panel expressed interest in using the Cox simulation and having Dr. Jaquet apply his approach to assessing volcanic hazard at the repository.

As the final presentation in the session, Dr. Andrew Martin (Quintessa, Japan) gave a talk titled "Volcanic Hazard Assessment for High-Level Waste Facilities in Japan." He began by showing the tectonic setting of Japan and the distribution of Quaternary volcanism in the region. After noting the organizations responsible for nuclear waste disposal in Japan, he described his research. Dr. Martin showed maps and photos of both monogenetic volcanoes (which erupt at the surface and form a cone) and polygenetic volcanoes, describing clusters of volcanoes in Japan. Then he discussed probabilistic models based on location and age data, describing the smoothing coefficients of Gaussian and Cauchy kernels. He displayed profiles showing the results of using different smoothing coefficients and presented the corresponding maps of probability plots. Next, Dr. Martin described recasting geophysical data into a probability density function suitable for use in the Bayesian approach. He demonstrated using Bayes' rule to incorporate velocity information from seismic tomographic data into the probability analysis. Next, he discussed extreme-value statistics, which provide a powerful tool for modeling rare events that have significant consequences. An example was assessing the upper-bound

probability of volcanism in Japan. Dr. Martin showed cumulative plots made using the annual maxima, or Gumbel method. Next, he described a method termed evidence support logic, which utilizes a three-value logic to assess the evidence both for and against a process, with residual uncertainty also defined. Dr. Martin concluded by briefly describing a code titled The Evidence Support Logic Application (TESLA), showing the formulation, an example of the process, and a resulting plot of ratios.

After a short break, Dr. Coppersmith commented on the overall process and path forward for the PVHA-U. He reviewed the procedures and guidance for the expert elicitation process. He noted that plans for the PVHA-U call for documenting expert assessments in a final report, with no formal documentation of interim assessments. Dr. Coppersmith then reviewed the schedule of activities for the rest of the project.

Next Dr. Karen Jenni (Geomatrix Consultants) described plans for developing influence diagrams in the upcoming individual expert interviews. She showed a flow chart of the six-step probability assessment she had described in Workshop 1 (the six steps being motivate, structure, condition, encode, verify, and discretize). After noting the "structure" part of the process, in which models, variables, and assumptions are defined, Dr. Jenni showed an example influence diagram for structuring an assessment of potential financial profits. Finally, she showed an example of how volcanic hazard at the repository could be portrayed on an influence diagram, based on the information discussed at the workshop.

Finally, the project team discussed the importance of developing clear event definitions. They also reviewed the assessments that will be elicited from the experts in PVHA-U. The process for making assessments was discussed. If they choose to, experts may perform their own intermediate calculations; ultimately, however, the experts' models will be reproduced in the hazard calculation code that will be qualified for use by the Yucca Mountain Project. (Codes used by experts in intermediate steps do not have to be qualified.) Dr. Coppersmith stressed the importance of experts informing the MDT of the data sets or supporting calculations they require in order to develop their assessments.

Observers offered no comments or questions, so Dr. Coppersmith thanked the expert panel members, presenters, and support staff and adjourned the workshop.

PROBABILISTIC VOLCANIC HAZARD ANALYSIS UPDATE
YUCCA MOUNTAIN PROJECT

WORKSHOP 2A
APPROACHES TO VOLCANIC HAZARD MODELING

August 30-31, 2005
Las Vegas, Nevada

SUMMARY

The Workshop on Approaches to Volcanic Hazard Modeling was the third in a series of workshops conducted by the U.S. Department of Energy (DOE) in support of the Probabilistic Volcanic Hazard Analysis Update (PVHA-U) for the Yucca Mountain Project (YMP). The PVHA-U relates to the technical bases that will be provided in the project's license application to the U.S. Nuclear Regulatory Commission (NRC). The PVHA-U relies on formal elicitation of the assessments of a panel of expert volcanologists to estimate the probability that the Yucca Mountain repository could be disrupted by a future igneous event (i.e., the volcanic hazard at the site). Workshop 2A was added to the four workshops originally planned for the PVHA-U in response to requests from expert panel members to provide additional time for experts to discuss their approaches as a group. The objectives of this workshop were to (1) review the goals and schedule of the PVHA-U; (2) summarize the status of the PVHA-U database and the results of ongoing data collection; (3) provide a forum for the expert panel members to discuss their initial approaches to modeling volcanic hazard at Yucca Mountain, including their approaches to defining igneous events, modeling temporal processes, and modeling spatial processes; and (4) identify additional data and information that the experts need in order to apply their modeling approaches.

DAY 1 – TUESDAY, AUGUST 30

After Dr. Kevin J. Coppersmith (Coppersmith Consulting) opened the workshop, Mr. Eric Smistad (DOE) welcomed the group and thanked panel members for their participation, then briefly described the current drilling program. Mr. Michael Cline of Bechtel SAIC Company (BSC) also welcomed the group, commented briefly on the drilling program, and thanked the expert panel members for their patience with the contractual arrangements required to secure their participation.

Dr. Coppersmith summarized the schedule, goals, and approach of the PVHA-U. He described the goal of a probabilistic hazard analysis, the role of the experts, ground rules for the workshops, and the issues to be addressed in the PVHA-U (e.g., spatial evaluation, temporal evaluation, and event definition). He reiterated that the product of the PVHA-U is the probability (expressed as a probability distribution) of a future igneous event that could disrupt the repository. He briefly described the initial individual interviews held with each expert in May and June of 2005, which included discussing alternative approaches to modeling hazards, identifying data needed for each model, and developing influence diagrams showing the logic of the assessments required to implement those models. Dr. Coppersmith discussed the goals of Workshop 2A: to summarize the data and information compiled in the current PVHA-U

database, to describe the field work being performed to obtain additional information to support the experts' evaluations, and to provide a forum for the experts to discuss their potential approaches to modeling volcanic hazards at Yucca Mountain.

The two-day workshop comprised four sessions. Dr. Frank Perry of Los Alamos National Laboratory (LANL) opened the first session, *Summary of PVHA-U Database and Data Collection Activities*, with a talk titled "Status of Drilling Program, PVHA-U Database, and Expert Requests." He noted that results, obtained from the recent drilling at Anomaly Q after today's talk was printed, changed some of his previous conclusions. Dr. Perry discussed those new results and his updated conclusions, agreeing to update the presentation to reflect those changes. Drilling began at Anomaly Q on August 1, 2005. It was not expected that basalt would be found to be the source of the anomaly, but basalt was found at a depth of 140 m below a mega-breccia layer, which is interpreted to have been produced by slide blocks off Bare Mountain. A review of local stratigraphic information revealed a stratigraphic sequence in drill hole USW VH-2, approximately 5 km south of Anomaly Q, that was nearly identical to the sequence observed at the anomaly. The basalt layer in VH-2 was dated at 11.3 million years ago (Ma). Surface exposures at the southern end of Crater Flat also show a relationship between slide blocks and basalts dated at 11.3 Ma. The similarities between the sequences, plus the similar olivine-phyric composition of basalts drilled at Anomaly Q and VH-2, indicate that the basalt at Anomaly Q probably also has an age of 11.3 Ma. A sample of the basalt from the Anomaly Q drill hole will be submitted to a lab for age-dating. Depending on the age of the basalt, target anomalies may be re-assessed in order to guide the drilling effort, reprioritizing drilling targets as appropriate.

Next, Dr. Perry described the database established to ensure that all experts have access to the same technical references, data, and white papers. This database will be updated throughout the project, both in response to requests from experts and to include new information as it becomes available from YMP drilling and analogue studies. Dr. Perry showed a map created by LANL's GIS laboratory that incorporates multiple data sets to display volcanic features, topography, isostatic gravity contours, and aeromagnetic anomalies. He described a YMP study of the relationship between topography and locations of volcanic vents. Results of this study indicate that of the 12 Quaternary vents in the Southern Great Basin/Death Valley/Eastern Mojave region, 10 (83%) occur in basins or other topographic lows, although only about 50% of the region could be characterized as topographic lows. The group discussed some of the available data sets and the use of potassium-argon age-dating as an alternative to the argon-argon method. Age data derived from potassium-argon dating are less precise but can be obtained more quickly.

Next, Dr. Gordon Keating (LANL) presented "Analog Studies to Support Event Definition for PVHA-U." Data on the characteristics of dikes and dike swarms, numbers of vents (conduits) and their locations along a dike system, and characteristics of the conduits at repository depth are being studied at potential analogue sites in the Western United States. Researchers will select analogue sites that have an extensional tectonic setting and magma volumes and compositions similar to those of volcanoes in the Yucca Mountain region. Dr. Keating described observations and interpretations from field mapping in Nevada's Paiute Ridge, Basalt Ridge, and the 3.7-Ma basalt in Crater Flat. Grants Ridge in New Mexico, located on the edge of the Colorado Plateau, also was described. Dr. Keating displayed geologic cross sections and photographs of each area, along with interpretations of the geologic features. Next he described the ancient Madinah

Fissure eruption, a 52-day eruption that occurred in Saudi Arabia in 1256 A.D. Alkali basalt was erupted from seven vents along a single 2.25-km-long dike on the east flank of the Red Sea rift. Dr. Keating summarized characteristics of and conclusions regarding the observed volcanic features at the Madinah Fissure. He ended by describing additional field work, planned for autumn of 2005, to quantify dike and conduit characteristics at several other potential analogue sites. This information will be provided to expert panel members in a white paper, spreadsheet, and/or YMP reports. Much of the information is included in a recently completed report, *Magma Dynamics at Yucca Mountain, Nevada* (BSC 2005), which also will be made available to panel members. Workshop participants discussed mechanisms for the formation of conduits, interpretations of eruptive history, the influence of local and regional stress regimes on dike propagation, and which sites in the Great Basin might serve as appropriate analogues to Yucca Mountain.

"Approaches for Combining Multiple Datasets in Spatial Models" was the next talk, given by Mr. Timothy Nieman (Geomatrix Consultants) and based on work that he performed with Dr. Karen Jenni (also Geomatrix Consultants). The talk was developed because expert panel members had expressed interest in incorporating and/or combining available data sets into their spatial models and wanted to understand better how to implement some of the approaches to spatial modeling described in Workshop 2. Mr. Nieman described the spatial models used in the PVHA-96 and their positions along a spectrum of models that ranged from those that rely solely on the location of past events to those that rely solely on geologic interpretation. He described the conceptual model, modeling approach, and expert judgments required for various models along the spectrum. Mr. Nieman then listed example data sets and potential ways to use them in the analyses. Approaches ranged from using multiple data sets to support the expert judgments required for any of the models used in the PVHA-96, to using the Bayesian approach introduced by Dr. Charles Connor and Dr. Andrew Martin at Workshop 2 to modify a spatial distribution based on the locations of past events. Mr. Neiman described how to implement the Bayesian approach, focusing on the specific expert judgments required, which include: the form and parameters of the spatial model based on locations of past events; the likelihood of future events depending on which values in the data set(s) are considered; and the degree of independence between the location of past events and the estimated likelihood of future events based on the data.

Referring to a prototype model, Mr. Neiman illustrated the application of a Bayesian approach using a Gaussian kernel model updated with elevation data for the Yucca Mountain region. He illustrated various interpretations of how elevation data might be assumed to predict the locations of future events, and showed how each different interpretation of the data ultimately results in a different spatial distribution. Mr. Neiman noted the importance of considering the underlying geophysical processes and described using multiple data sets to perform sequential updating. Mr. Nieman invited the expert panel members to experiment during the workshop with the prototype model code installed on both his and Dr. Jenni's laptop computers.

Following a lunch break, the second session of the workshop began. In this session, called *Defining Possible Future Events in the Yucca Mountain Area*, the experts described which approaches to modeling volcanic hazard they are considering for use in their models. Dr. William Hackett (Integrated Science Solutions, Inc.) began the session by considering a small batch of magma, first describing its source and composition, then tracing its ascent until it

produced dikes above the brittle/ductile transition in the crust and near-surface. He described the vesiculation that begins at a depth of about 1 km and the possible formation of a graben at the surface as the ascending dike reaches the near-surface. After defining a dike as a magma-filled crack, Dr. Hackett described the characteristics of dikes, such as length, width, and azimuth, above the brittle/ductile transition. He showed a schematic of a dike system and associated tensile features that form at the ground surface. Next, he described three scenarios involving a dike system intersecting the Yucca Mountain repository, with results that ranged from tensile fractures and small-displacement normal faults to magma erupting at the surface after intruding the repository. For the scenario in which magma erupts after intruding the repository, Dr. Hackett described possible volcanic styles/magnitudes and the preliminary relative weights he has assigned to them. He discussed the effects that the repository and Yucca Mountain might have on the propagation of dikes, based in part on YMP information he reviewed. In conclusion, he described a duration (time frame) of a few hours to several years for a dike event that might occur in the Yucca Mountain region. The group discussed the various parameters Dr. Hackett had addressed, as well as types of eruptions, including maar eruptions.

Dr. Michael Sheridan (State University of New York at Buffalo) gave the next talk, noting that it is critical to define *event*. He began by stating that two types of igneous events could disrupt the repository: an igneous intrusion into the repository, or an eruption (conduit) through it. The size and geometry of the potential event are important, and the length and width of a dike are related by an aspect ratio. Dr. Sheridan posited that in the future only small volumes of magma will be available in the Yucca Mountain region, and dike dimensions correlate with those small volumes. Curvature on the surface of a dike and dike intersection with topography control locations of magma breakout. He noted that he considers the existing cones (conduits) near Yucca Mountain to represent events, and considers these the best available data for understanding the nature of potential future events in the area. Dr. Sheridan will develop probabilities for two igneous events: a conduit (new cone) that intersects the footprint of the repository, and a dike that extends beyond a cone to intersect the repository footprint as an intrusive event. Dr. Sheridan then discussed the definition of an intrusive event, models that can be used to define an intrusion, and analogue sites. He described the likely characteristics of an eruption through the repository, including conduit geometry. He discussed dike geometry and the factors that influence it, as well as the magma source for the Quaternary cones in Crater Flat. Dr. Sheridan estimated that among events he had observed, only about 1 in 10 to 1 in 20 are hydrovolcanic events. Such events typically occur in areas of low topography; he knew of no maar eruption occurring on a topographic high not covered by water. The group discussed the characteristics of the Crater Flat cones.

After a short break, Dr. Charles Connor (University of South Florida) presented his views on defining an igneous event. First he noted the importance of using one definition consistently throughout an individual's analysis (i.e., the event definition must be consistent with the spatial and temporal models). Dr. Connor proposed that rather than defining the characteristics of events by conduit and dike dimensions, one might characterize "igneous event scenarios" based on mapped analogue sites. Using this approach, spatial and temporal models would be developed to identify the locations of so-called event centers, and then uncertainty about event characteristics would be characterized by sampling from a set of mapped analogues. The analogues would be superimposed on maps showing event centers to predict whether the event scenarios might intersect the repository. Dr. Connor stated that dike systems associated with

event scenarios would be affected by the rate of magma supply, faulting, and regional stresses specific to the Yucca Mountain area. Next, he showed analogues from the San Rafael volcanic field in Utah, highlighting an area at Willow Springs where a dike swarm, including conduits and breccia zones, has been mapped in detail. A second example, from the Carmel area in the San Rafael field, consists of a large, circular conduit and nearby smaller conduits within a breccia zone. He noted that the complexity of the mapped features makes it difficult for him to define and select specific parameters that define an event, which is what motivated his idea of using mapped event scenarios. Dr. Connor concluded his talk by discussing the advantages and disadvantages of using the scenario approach. Expert panel members discussed the application of event scenarios to the Yucca Mountain region, including the characteristics and associated uncertainties of a potential intersection with the repository at a depth of 300 m. Dr. Coppersmith noted that using a suite of scenarios, rather than probability distributions for specific parameters such as dike length and width, still would require an explicit quantification of uncertainties. The alternative scenarios might have to be weighted in order to express the uncertainties appropriately.

Dr. Mel Kuntz (U.S. Geological Survey, Emeritus) gave the final talk of the session and the day. He defined an igneous event as one that results in the formation of a recognizable individual volcano within a space characterized by a specific affected area and within a time frame defined as the lifetime of an active volcano system. He stated that it is possible to predict with some confidence the kind of event that could occur in the vicinity of the repository, along with its magnitude, development, and location. In describing various potential events, Dr. Kuntz noted analogue areas within the Great Basin. He stated that an eruption in Crater Flat, whereby dikes could propagate toward the repository, would be more likely than an eruption beneath Yucca Mountain, but whether such an event would intersect the repository is a key question. Dr. Kuntz emphasized the distinction between eruptive and non-eruptive events, based on evidence from non-eruptive events in the Snake River Plain. He said he plans to use processes observed in the Snake River Plain to assess the number of non-eruptive events in the Yucca Mountain vicinity. He described the dike dimensions and the characteristics of conduits and sills that he might use in his elicitation. While stating that hydrovolcanic eruptions are unlikely at Yucca Mountain, Dr. Kuntz noted that eruption type can change during the lifetime of a volcano, as indicated by the Lathrop Wells cone. Showing a sequence of eruption types, he noted that the eruption process may stop at any time, a concept he plans to factor into his elicitation. He stressed the importance of the data that will be obtained from drilling and age-dating the aeromagnetic anomalies.

Miscellaneous topics were discussed following the final talk of the day. Dr. Perry described a newly developed plan to expedite obtaining age dates from drill samples. Dr. Connor proposed that expert panel members consider two opportunities: (1) participating in a session on volcanic hazard and risk analyses being organized for an American Geophysical Union conference in December of 2005, and (2) contributing to a book on volcanic and tectonic hazards for high-level waste facilities that he and others plan to compile. The group discussed the application of Dr. Connor's scenario approach and the use of Monte Carlo sampling; the need for expert judgment to evaluate the appropriateness of analogues; and the relationships among magma volume, dike length, and other volcanic features.

Dr. Coppersmith then opened the workshop to comments from observers. Topics included field observations of magma eruptions that propagated to higher topographic surfaces and the response of magma to local stress regimes. The workshop was adjourned for the day.

DAY 2 – WEDNESDAY, AUGUST 31

Dr. Coppersmith welcomed participants to the third session of the Workshop 2A, titled *Models for Characterizing the Temporal Distribution of Future Volcanism*. Dr. Bruce Crowe (Apogen Technologies) gave the first talk, which concerned various ways in which he has examined alternative temporal models. He discussed three alternatives to the temporal modeling he used in the PVHA-96: (1) reassessing the estimated recurrence rate based on a modified event definition; (2) forecasting future recurrence rate based on estimated past recurrence rate and uncertainty about the temporal trend (waxing, waning, or steady state); and (3) examining time slices of past recurrence intervals. Dr. Crowe explained his new approach to estimating recurrence rate based on his revised definition of *event*. He now defines events as magma pulses or ascent events rather than individual centers. His new approach emphasizes uncertainty in the characteristics of an event, rather than uncertainty in event counts. Dr. Crowe illustrated his concept that an event may consist of single cones, coalesced cones, and/or dispersed cones. He showed influence diagrams indicating how available information is used to obtain integrated event recurrence rates. Next he described the uncertainty in using the estimated past recurrence rate to forecast recurrence rates out to 10,000 years: specifically, uncertainty about whether the current volcanic system is waxing, waning, or steady state. Using data about past events, Dr. Crowe is considering how to assign probabilities to each of these states in order to assess an integrated rate for Quaternary and Plio-Quaternary periods. His third approach is to search for recurrence patterns in past time slices, each of which encompasses 2 million years (My). Based on volcanism observed during one 2-My period, he predicted the location of volcanic activity during the next period. He found that his predictions were consistently mediocre and/or contained unexpected events, up until the Quaternary, for which predictions were reasonably accurate. Dr. Crowe then illustrated the unique uncertainties associated with predicting recurrence behavior out to one million years. Decision branches were included for continued activity in Crater Flat and for cessation of volcanism. Dr. Crowe noted that the probability of a changed tectonic regime must be considered also. The group proposed possible reasons for the differences in Dr. Crowe's predicted results and discussed aspects of the regional tectonic setting, both in the past and as it may or may not change in the future.

The second talk of the session was given by Dr. Wendell Duffield (USGS, retired), who stated that he considers the Quaternary record to be the most important for predicting the future. He began by tracing the path of a magma source rising through the crust. He then defined a 40-km-diameter circular area of interest around the repository. Within this area, he plotted the cones of Quaternary age, considering ages of both 0.9 Ma and 1.1 Ma for the four Crater Flat cones. Dr. Duffield emphasized the importance of eruptive volume through time, based on information on waning systems presented by Drs. Richard Carlson and Christopher Fridrich in Workshop 2; information on dike orientation provided by Dr. George Thompson (also in Workshop 2); and the observation that no eruption has occurred within the repository footprint since emplacement of the tuff that comprises Yucca Mountain. Dr. Duffield ended by noting that he is considering the possibility of a completely different type of eruption occurring within the one-million-year future period. Specifically, a large magma reservoir could accumulate,

producing a siliceous eruption or caldera. Members of the project team discussed the Solitario Canyon dike (intruded at about 10 or 11 Ma) and the possibility of a future episode of siliceous volcanism, which several experts considered extremely unlikely.

Dr. Frank Spera (University of California, Santa Barbara) gave the next talk on temporal models. He examined simple approaches, such as counting cones and examining the relationship between magma volume and number of cones. He termed his approach "actualistic," because it is based on geologic observables. After defining what he considers to be the region of interest, Dr. Spera discussed the possibility of enlarging it, but noted that doing so would roughly double not only the eruptive volumes to be considered but also the time frame. After defining a 4.88-Ma period of interest, he described aspects of geochemistry, petrology, and magma transport relevant to temporal evaluation. Showing a plot of fragmentation pressure versus volatile content of a magma, Dr. Spera translated pressures to depths beneath Yucca Mountain. These data indicate that fragmentation depth would be below the level of the repository. Dikes therefore could be assumed to vent (erupt) to the surface, so that the number of cones provides a crude estimate of the number of events that could disrupt the repository. Scaling relationships can be developed among eruptive volume, cumulative length of fissures, and number of cones (conduits) along fissures. After showing the data set for volcanic features within his region of interest, Dr. Spera described several parameters derived from these data: total eruptive volume, volume per event, event count, and frequency of eruption events. Based on these parameters and four alternative approaches to counting eruption events, Dr. Spera calculated a range of frequencies for such events. Next, he derived a new set of parameters and a new estimated frequency of eruption events based on scaling relations from a global database. The five approaches he described produce estimated eruptive frequencies that differ by about a factor of 100. Applying all five approaches to estimate the number of potential dike intersections with the repository footprint, the calculated result is 1 chance in 6,000 in the next 10,000 years (similar to the annual probability of 10^{-8} assessed in previous studies). Dr. Spera noted that the estimate is based on an assumption of temporal homogeneity, which is known not to apply, so uncertainty in this parameter must be incorporated. He also described incorporating other information that would inform the process, including spatial inhomogeneity.

After a short break, Dr. Alexander McBirney (University of Oregon, Emeritus) spent a few minutes examining the volcanism of the Yucca Mountain area within the framework of a larger region. Giving examples from the Cascade Range in Oregon and from Central America, he described the roughly correlated timing in the two areas of a pattern of mid-Miocene and younger volcanism. He also showed patterns of synchronous volcanism in the Cascades, Columbia River Plateau, and Snake River Plain, as well as throughout the Western United States. These patterns show a peak in volcanism about 15 Ma and another peak within the past 3 to 4 Ma. Dr. McBirney noted the difficulty in assessing whether volcanic events in the Yucca Mountain region indicate a waxing or a waning cycle.

Dr. Coppersmith asked the entire expert panel to continue the discussion of temporal models as applied to the Yucca Mountain region. Topics included volcanic cycles and assessments of the temporal position of a specific field within that cycle (e.g., waxing or waning system); consideration of a longer period to reduce the effects of low numbers of events; relationships between episodes of faulting and volcanism and between the Quaternary pulse of volcanism and Pliocene volcanism; the persistence of volcanism in specific areas (e.g., the Sleeping

Butte/Thirsty Mesa region); analogue areas where eruptive volume is correlated with recurrence rate/repose time; the applicability of a Poisson process/model versus a clustering model for volcanoes in the Great Basin; and weighting of alternative models (e.g., whether the present period is within or outside a cluster of volcanism).

Following a lunch break, participants began the fourth and final workshop session, *Models for Characterizing the Spatial Distribution of Future Volcanism*. Dr. Richard Carlson (Carnegie Institute of Washington) gave the first talk, describing what he referred to as the big picture of magma source history and the control that the mantle source (whether asthenospheric or lithospheric depending on isotopic composition) has over melting. He described the melting conditions specific to the Yucca Mountain region, where old continental lithospheric mantle is the magma source, unlike in other areas of the Basin and Range where the source is the asthenosphere. Dr. Carlson presented a map showing the distribution of Miocene and post-Miocene basalts around the siliceous Timber Mountain Caldera complex, a circular volcanic field around which small centers are distributed more or less randomly, with some possible clustering. Quaternary basalt centers in this region have a northwest alignment and unclear geologic control. Dr. Carlson proposed two spatial models, which differ primarily in assessments of the degree of structural control over spatial evolution. He said that choosing between the options requires understanding the causes of the aeromagnetic anomalies, because information from selected anomalies can be used to test the structural control of the Bare Mountain fault and the length of the Crater Flat alignment. He noted that melt input from the mantle may be a stronger control over the location of volcanism than are near-surface geologic features, and that structural features in the upper crust may assume greater control over magma ascent in a waning volcanic system. The group discussed the appropriateness and physical bases of the models Dr. Carlson described.

The group also discussed the appropriateness of spatial models based on field shape (parametric models) compared with nonparametric models. One panel member stated his strong belief that the bivariate Gaussian spatial model is inappropriate because it incorporates an assumption about the shape of volcanic fields that he believes is not supported by data. He held that because nonparametric estimation of spatial density of volcanic activity requires fewer assumptions, it should be used instead. The group discussed the differences between parametric and nonparametric spatial models and the role that expert judgment plays in applying each type of model.

The next talk, given by Dr. George Thompson (Stanford University), dealt with basalt dikes, stress, and free-air gravity information. Dr. Thompson began by reviewing the interplay between strain and stress and their apparent influence on the emplacement of basalt dikes. Next, he discussed the observed preferential location of dikes and vents along zones of greatest tectonic extension (i.e., valleys) and why this localization may be enhanced by the higher lithostatic pressure beneath mountains. He showed maps and figures of the Yucca Mountain region that illustrate the NNE direction of greatest extension, along which it would be expected that most dikes would be emplaced. There is reasonably close agreement regarding direction of maximum principal stress derived from earthquake focal mechanisms, fault slip lines, vent alignments, and measurements of hydraulic fractures. Dr. Thompson then discussed what geodetic data indicated about horizontal velocities in the Yucca Mountain region relative to a stable North America. He showed diagrams of elastic extension that can be relieved in rebound by faulting or dike

intrusion. For the next part of his talk, Dr. Thompson displayed a free-air gravity profile along a seismic reflection line across Bare Mountain, Crater Flat, and Yucca Mountain. He said that the low free-air anomaly beneath Crater Flat helps explain why past eruptions have been confined to that area. Vents are correlated with areas of low lithostatic stress; magma pressure from a low-volume area is insufficient to intrude into Yucca Mountain. The group discussed the tectonic history of the region.

In the final talk of the workshop, Dr. McBirney relayed observations about the Eldjia fissure in Iceland. He described exposures of a dike throughout approximately 25 km and the apparent role of low-elevation topography in influencing where the dike reached the surface. Next, he discussed the hazards of phreato-magmatic eruptions. He described the conditions under which such eruptions usually occur and the components of the eruptions. Dr. McBirney concluded that although conditions for a phreato-magmatic eruption once existed at Crater Flat and could recur in the future, they currently do not exist on Yucca Mountain.

Discussion ensued regarding the manner in which uncertainties should be expressed in the PVHA-U, including the need to make statistical arguments for the viability of one conceptual model over another. Dr. Coppersmith reiterated that there is no requirement for the experts to "prove" their assessments statistically; nor do they need to be adept at statistical modeling, because the Methodology Development Team (MDT) will assist them in those areas. Rather, the experts are to focus on their conceptual models of volcanism in the Yucca Mountain region and the physics upon which those models are based. The full range of each expert's uncertainty, as reflected in both alternative conceptual models and differing values for parameters, must be captured in the PVHA-U. The MDT will assist the experts in utilizing tools for quantifying uncertainties (e.g., logic trees). Dr. Coppersmith also reviewed the schedule of future project activities, including a field trip to review analogue locations for volcanic events.

Dr. Coppersmith then opened the session to comments from observers. Topics included the long quiescent interval since the Lathrop Wells eruption (approximately 80,000 years), and eruption cycles that begin with a maar eruption and end with the formation of cinder cones.

In closing, Dr. Coppersmith thanked all the participants, particularly those who contributed to the logistical operation of the workshop.

PROBABILISTIC VOLCANIC HAZARD ANALYSIS UPDATE
YUCCA MOUNTAIN PROJECT

FIELD TRIP
VOLCANIC EVENT DEFINITION AND HISTORY OF VOLCANISM
IN THE YUCCA MOUNTAIN REGION

May 1-4, 2006
Southern Nevada

SUMMARY

The Field Trip on Volcanic Event Definition and History of Volcanism in the Yucca Mountain Region was the fourth in a series of meetings (following Workshops 1, 2, and 2A) conducted by the U.S. Department of Energy (DOE) in support of the Probabilistic Volcanic Hazard Analysis Update (PVHA-U) for the Yucca Mountain Project (YMP). The PVHA-U relates to the technical bases that will be provided in the project's license application to the NRC. The PVHA-U relies on formal elicitation of the assessments of a panel of expert volcanologists to estimate the probability that the Yucca Mountain repository could be disrupted by a future igneous event (i.e., the volcanic hazard at the site). The goal of the field trip was to enable expert panel members to observe directly the characteristics of volcanic and intrusive features in the Yucca Mountain region so they could refine and finalize their definitions of igneous events. Both before and during field trip stops, Los Alamos National Laboratory (LANL) geologists provided information about their research on volcanic centers in the region. The field trip enabled experts to examine issues such as (1) the ways in which eruptive style and the characteristics of magma feeder systems change through geologic time; (2) the relationships between faults and dikes/fissures in the region; and (3) the role of topography, as opposed to other factors such as mantle source or crustal structure, in determining the locations of volcanoes.

DAY 1 – MONDAY, MAY 1

Members of the expert panel were briefed on the purpose of the field trip Monday evening. After welcoming the group, Mr. Michael Cline of Bechtel SAIC Company (BSC) discussed logistics for the trip. Dr. Kevin J. Coppersmith (Coppersmith Consulting, Inc.) described the field trip as an opportunity for expert panel members to observe field evidence that may assist in further developing their definitions of an igneous event. He reviewed the role of the experts in the forthcoming elicitations and the issues to be addressed in the PVHA-U (spatial evaluation, temporal evaluation, and event definition). Dr. Coppersmith presented an updated schedule of project activities, which indicated that elicitation interviews will begin in mid-summer of 2006.

Dr. Frank Perry (LANL) then gave an overview of the field trip, discussing the purpose of the field stops, the major conclusions derived from research on eroded analogue volcanic centers, and a short overview of results from the aeromagnetic survey and drilling program in Crater Flat, the Amargosa Desert, and Jackass Flats. He mentioned that studies of volcanic analogues highlight important differences between volcanic centers in the region that are Miocene-Pliocene

in age and those that are Quaternary in age. Dr. Perry's talk provided an introduction to a series of presentations planned for Day 2 before the field excursions began.

DAY 2 – TUESDAY, MAY 2

Dr. Perry gave the first of several talks describing studies conducted by LANL investigators. He reviewed results and interpretations of the 2004 aeromagnetic survey of the region and of the drilling program designed to investigate aeromagnetic anomalies that might represent buried volcanic features. Seven drill holes were completed in Crater Flat, Jackass Flats, and the Amargosa Desert. Dr. Perry detailed information obtained from the drill holes and discussed possible correlations between basalts encountered in the new drill holes and basalts identified in outcrops and from previous drill holes. Both the drilling and the aeromagnetic survey clarify episodes of Miocene volcanism in Crater Flat and Jackass Flats. After age-dating and laboratory analyses are completed, those interpretations will be reevaluated. Dr. Perry concluded that available data, which enable a comprehensive interpretation of the volcanic history of Crater Flat and Jackass Flats, indicate that no post-Miocene volcanic activity has occurred in Jackass Flats.

Dr. Greg Valentine (LANL) gave the next two talks. The first described erosion and eruption characteristics of volcanoes in the Yucca Mountain region. After reviewing information on the characteristics of each volcano in Crater Flat, he concluded that, for Quaternary volcanoes, all eruptive products came from the area of the primary cone. Thus, all these eruptions are interpreted to be monogenetic. Dr. Valentine also compared and emphasized the major differences in volume, lava effusion rate, and fissure length for Pliocene versus Quaternary eruptions. He noted that all basaltic dikes observed in the region appear to be located preferentially along pre-existing normal faults.

Next, Dr. Valentine described the characteristics of shallow dikes and sills emplaced beneath a small basaltic volcano at Paiute Ridge, a site to be visited on Day 4 of the field trip. He indicted that inelastic, or irrecoverable, deformation and erosion of dike walls contributed to observed dike widths of 1.2 to 9 m. Dr. Valentine also described the apparently strong influence of pre-existing structures on the emplacement of sills.

Drs. Gordon Keating and Don Krier (both of LANL) together described the parameters to be included in an event definition. They discussed field observations of volcanic features, including the association of dikes with pre-existing faults, based on recently completed field work at Lathrop Wells cone, Little Cones, Red Cone, Black Cone, Paiute Ridge, Basalt Ridge, and Basalt Ridge East. The talk focused on the event geometry (number, size, shape, and vertical extent of conduits and feeder dikes) represented by those analogues and on how appropriate the analogue information may be for modeling a basaltic volcanic system at repository depths.

The final talk of the morning was given by Dr. Ed Gaffney (Gaffney Associates), who presented the results of two modeling projects. He first described modeling the effects of topography on dike propagation. His model indicates that a dike propagating upward in an area of transition from low topography (e.g., Crater Flat) to higher topography (e.g., Yucca Mountain) would be deflected away from the area of higher topography. Eruptions on topographic highs are not precluded if the strike of the dike is nearly parallel to that of a ridge or if the dike has a limited strike length. Dr. Gaffney then discussed a two-dimensional analysis of deep structures,

addressing the conditions under which a dike could be captured by a fault. An analytic solution indicated that a fault could capture a dike only if the dip of the fault was high or the depth of the dike was shallow (hundreds of meters or less). Capture is more likely in rocks that exhibit high fracture toughness.

Following these technical presentations, the group traveled to the Nevada Test Site to begin the field trip. After obtaining security badges at the Mercury entrance, the group gathered on the crest of Yucca Mountain to observe the Solitario Canyon dike. This dike has two short, narrow segments, both of which lie within fault planes of the Solitario Canyon fault, indicating the fault captured this dike in the shallow crust. Dr. Perry summarized the geologic setting of the Solitario Canyon dike. He described the dike's length and width, chemistry, and age of between about 10 and 12 million years ago (Ma). Dr. Dennis O'Leary (U.S. Geological Survey, Denver), who has studied the Solitario Canyon area in detail, described the stratigraphic and lithologic features of the dike and their distributions. Field trip participants examined several outcrops of the dike.

DAY 3 – WEDNESDAY, MAY 3

The first stop of the day was on the north side of Highway 95, at the south end of Crater Flat near Bare Mountain. Field trip participants observed three basalt flows, dated at about 11.3 Ma. These basalts are overlain by dolomite and limestone slide deposits that originated from Bare Mountain. A similar stratigraphic sequence has been observed in both drill hole VH-2 and the recently drilled hole at Anomaly Q.

The next stop was on Nellis Air Force Base at Thirsty Mountain. Drs. Perry and Valentine described the geologic parameters and chemistry of volcanic events in the area. Thirsty Mountain is composed of 4.8-Ma flows that originated from Black Mountain, the Pliocene volcano to the north that produced the highest volumes of flows in the region. Drs. Perry and Valentine discussed the Quaternary Sleeping Butte complex, consisting of Hidden Cone and Little Black Peak, both of which are dated at about 300 Ka. Although the two cones form a northeast-trending alignment (as do other volcanic centers in the region), mapped faults do not support the conclusion that a northeast-trending structure connects the two cones. The differing trace-element compositions of the two Quaternary cones suggest that they originated from separate magmas and therefore separate feeder dikes.

The second stop of the day was at the Pliocene volcanic outcrops in southeast Crater Flat. Drs. Keating, Perry, and Valentine described the geometry of the system, pointing out various volcanic facies. The outcrops are associated with a 3.5-km-long fissure system, the basalts of which are dated at 3.7 Ma. The outcrops represent multiple volcanic vents localized along prominent dikes. The fissure segments, which are en echelon and overlapping, have consistent north-south trends. Drs. Keating, Perry, and Valentine described the eruptions occurring on each fissure segment as continuous "curtains of fire" that rapidly coalesced into three to five loci of eruption and finally focused in a single enlarged conduit.

The third and final stop of the day was the Quaternary Lathrop Wells cone, where a quarrying operation has been underway for more than a decade. The LANL investigators recently collected field data in this area that have enabled delineation of early and later cone facies. The

early eruptions are interpreted to be classical Strombolian eruptions accompanied by abundant material rafted away from the cone. Later pyroclastic eruptions were of the violent Strombolian type, perhaps including hydrovolcanic eruptions. These later eruptions, which produced the cone facies, bedded cinder deposits, and tephra sheet deposits of the Lathrop Wells cone, were accompanied by less rafting. All eruption products apparently vented from the primary cone; no evidence has been observed for additional fissures or vents.

DAY 4 – THURSDAY, MAY 4

The final day of the field trip began with a visit to the Paiute Ridge area near the middle of the eastern boundary of the Nevada Test Site. This area contains evidence of a single late Miocene magmatic event that occurred in a small, north-trending graben. This event comprised multiple dikes and sills emplaced beneath a small-volume, alkali basaltic volcanic center. Dr. Perry described processes that occurred within the largest sill whereby alkali basalt differentiated to form small bodies of monzonite and syenite. He suggested that an analogous mechanism occurred within the basanite encountered in the drill hole at Anomaly A, which exhibits similar differentiated zones. Drs. Valentine and Keating described how the major dikes are all coplanar with normal faults. Sills found in the hanging-wall blocks of faults are connected to the dikes by narrow stems. In each case, dikes continue to rise above the level of the sill. The complex coalescence of a zone of eight mapped dikes formed the central conduit for the eruption. The conduit is surrounded by a zone of brecciation, melting, and remobilization of country rock. The convergence of dikes appears to be controlled at least partly by local structures.

The group then visited the Sample Management Facility at the Nevada Test Site to observe cores and cuttings of basalt and basanite recovered from the most recent drill holes. Before the group observed the core, Dr. Perry briefly described evidence for a north-northwest-striking fissure beneath the Lathrop Wells cone. After observing the drill core and discussing their observations, expert panel members requested additional data, including earthquake hypocenters, tomographic data, reports summarizing Dr. Gaffney's modeling and Dr. Valentine's interpretations of a so-called magma footprint, and various other reports or publications. Also discussed was the fact that current plans call for the PVHA-U to consider the potential hazard for the next 10,000 and one million years. For the one-million-year assessment, the proposed rule (70 FR 53313) specifies retaining the concept of geologic stability. Experts therefore will not consider models that include, for example, potential for changes in tectonic patterns.

The first elicitation interviews of expert panel members are planned for July and August of 2006, and Workshop 3 is scheduled for September 26 and 27, 2006. Dr. Coppersmith thanked all the field trip participants and adjourned the meeting.

PROBABILISTIC VOLCANIC HAZARD ANALYSIS UPDATE
YUCCA MOUNTAIN PROJECT

WORKSHOP 3
PRELIMINARY ASSESSMENTS

September 26-27, 2006
Las Vegas, Nevada

SUMMARY

Workshop 3 on Preliminary Assessments was the fourth workshop (following Workshops 1, 2, and 2A) conducted by the U.S. Department of Energy (DOE) in support of the Probabilistic Volcanic Hazard Analysis Update (PVHA-U) for the Yucca Mountain Project (YMP). The PVHA-U relates to the technical bases that will be provided in the project's license application to the U.S. Nuclear Regulatory Commission (NRC). The PVHA-U relies on formal elicitation of the assessments of a panel of expert volcanologists to estimate the probability that the Yucca Mountain repository could be disrupted by a future igneous event (i.e., the volcanic hazard at the site). The objectives of this workshop were to (1) review the goals and schedule for the PVHA-U; (2) provide an update on the status of the PVHA-U database and the results of ongoing data collection and interpretation; (3) provide a forum for expert panel members to present and discuss their preliminary assessments of the technical issues, as formulated during their initial elicitation interviews in July and August of 2006; and (4) focus discussion on the uncertainties in models and parameters to prepare the experts for the second round of elicitation interviews planned for November and December of 2006. Workshop presentations and discussions were organized into three sessions according to the experts' preliminary assessments in three subjects: event definition, spatial models, and temporal models.

DAY 1 – TUESDAY, SEPTEMBER 26

The workshop was opened by Mr. Michael Cline, Disruptive Events Manager at Bechtel SAIC Company (BSC), who welcomed everyone and thanked those who had helped organize the workshop. Mr. Eric Smistad (DOE) also welcomed the group, expressing his appreciation to the expert panel members. Mr. Cline then stated that organizational changes in the YMP have resulted in Sandia National Laboratory assuming the role of Lead Laboratory for scientific work conducted by the YMP. Mr. Cline stated that his official involvement with the PVHA-U will end, although he will continue to work with BSC on other aspects of the YMP. He introduced Mr. Thomas Pfeifle from Sandia, the new Disruptive Events Manager, who will assume responsibility for the PVHA-U effective October 1, 2006.

Dr. Kevin Coppersmith (Coppersmith Consulting, Inc.) then welcomed the group and reviewed the goals and approach of the workshop. He summarized the expert elicitation process being followed and noted that Workshop 3 provides a forum for the expert panel members to present and discuss their preliminary assessments of the technical issues. He reviewed the ground rules for workshops, the different expert roles of proponents and evaluators, and the schedule of future activities and key milestones. Next, Dr. Coppersmith noted that schedule conflicts had required two of the experts—Drs. Richard Carlson and Wendell Duffield—to cease further participation

on the panel. He reviewed the original criteria used for selection of the experts and indicated that these criteria are also the bases by which the experts are evaluated for their continued participation on the panel. In this case, Drs. Carlson and Duffield were unable to fulfill their commitment to devote the necessary time and effort to the project. He also indicated that the Methodology Development Team (MDT) considered the need to replace the panel members and concluded that the remaining eight-member panel provides adequate breadth, depth, and expertise for the PVHA update.

Dr. Coppersmith reviewed the issues that the PVHA-U must address and described the individual elicitation interviews that took place in July and August of 2006, which considered those issues. He emphasized that the elicitation, which began with this first round of individual interviews will not end until completion of each expert's elicitation summary, the fundamental documentation of each expert's assessments that will be included in the PVHA-U final report. Dr. Coppersmith said he expected that during the elicitation period the experts' judgments may change as they are exposed to interactions with other panel members and to feedback. The experts should feel free to modify and refine their judgments along the way and should not feel anchored by their preliminary assessments. He showed an example of a preliminary assessment of parameters and a preliminary model structure for assessing potential future dike intersection with the repository footprint. Dr. Coppersmith then discussed the one-million-year period proposed in the draft revision to the dose standard (40 CFR 197) and its implications for the PVHA-U hazard assessments. For the PVHA-U, the experts are to begin with an assessment for the 10,000-year period and then consider how that assessment might differ for a one-million-year period.

Dr. Frank Perry of Los Alamos National Laboratory (LANL) gave the first presentation on the status of the PVHA-U database and responses to the experts' requests for information. The database is intended to give all experts common access to technical references, data, data visualizations (e.g., GIS-produced maps), and other work products needed to develop their hazard assessments. Experts began requesting data during Workshop 1 and may continue to do so until the end of the elicitation period. Dr. Perry provided examples of database information recently developed, including models of local tomographic inversions and results from age-dating and chemical analysis of drill holes. He discussed preliminary results of argon-argon age-dating at Black Cone, revised estimates of volumes of volcanic episodes based on buried volcanoes recently encountered by drilling, and estimates of the ages of anomalies based on burial depth and burial rate. Also described were development of a numerical three-dimensional grid for contour maps that represent the estimated cumulative percent of extension in Crater Flat (initially proposed in Fridrich et al. 1999); event geometry based on the example of East Basalt Ridge (a Miocene-age analogue); and depth to groundwater beneath Yucca Mountain.

Next, members of the expert panel made presentations for the first session of the workshop, titled *Preliminary Assessments—Event Definition*. Dr. William Hackett (Integrated Science Solutions, Inc.) gave the first presentation, on the topic of "Dike Geometries." In his assessments, he plans to emphasize the Quaternary igneous record in the Yucca Mountain region. He also plans to use the "magmatic footprint" approach published by Valentine and Perry (2006), according to which intrusive features (such as dikes) scale to the size of the eruptive products and the mantle source region. Dr. Hackett then described constraints on dike geometry, noting that little or no surface geologic evidence indicates that Quaternary dikes extend far beyond the footprint of the

associated eruptive products. He also described his assessments of dike length, width, azimuth, number, and spacing.

The second talk on "Dike Geometries" was given by Dr. Mel Kuntz (U.S. Geological Survey, Emeritus), who discussed his assessment of dike length. He stated that a "popsicle stick" analogy for dike shape produces an aspect ratio that is applicable to dikes in the Yucca Mountain region. He noted that tectonic environment, magma volume, and magma flux may influence dike injection and shape. Dr. Kuntz then described his assessments of dike length and width, based on analogues both within the Yucca Mountain region and worldwide. Next, he discussed his assessments of dike orientation, which are based on known or inferred dike orientations and regional stress conditions. He emphasized the importance of dike capture by pre-existing faults and described his assessment of the number and spacing of dikes per event (e.g., dike swarms).

Dr. Frank Spera (University of California Santa Barbara) gave the final talk on "Dike Geometries." He has chosen to develop scaled assessments of geometry based on estimated magma volumes. Noting that the Quaternary-Pliocene is his period of interest, he said that Quaternary events in the Yucca Mountain region demonstrate only one-tenth the eruptive volumes of Pliocene events. He described his assessment of dike length, which is dependent on eruptive volume, and noted that at the depth of the proposed repository, dike length is equal to fissure length. Dr. Spera has developed two distributions for fissure length, one based on magma volumes from the Pliocene and the other on magma volumes from Quaternary events. He will weight or combine these distributions in his final assessment. His estimates of dike width are informed by heat transfer arguments as well as observations from analogue regions. Dr. Spera indicated that when assessing dike azimuth he would weight most heavily local stress indicators. His assessments of future magma volume will be based on Quaternary eruptive volumes.

During the subsequent panel discussion of dike geometries, experts asked some speakers to further clarify their assessments and added information from their own observations. Among the topics discussed were the relationships between dike length and volume and between dike width and length, as well as lateral propagation of magma and eruption of basaltic magma above the fractionation depth.

Following a short break, presentations began on the second topic of the first session: "Eruptive Conduits and Sills," with the first talk given by Dr. George Thompson (Stanford University). Dr. Thompson emphasized two observations pertaining to the Yucca Mountain region: (1) eruption volumes have decreased steadily during the past 15 million years (My), indicating a cooling mantle and waning volcanic system; and (2) the immediate domain of Yucca Mountain has been intrusion-free for the past 10 My. In his discussion of eruptive conduits, Dr. Thompson showed a representation of the relationship among magmatism, faulting, and the stress field, then discussed the requirements for the occurrence of normal faulting, dike formation, and sill formation. He stated his belief that the sills at Paiute Ridge (visited during the PVHA-U field trip May 1 through 4, 2006) formed in a volcanic system having a higher magma flux than do the systems near Yucca Mountain. He stated that the waning volcanism in the Yucca Mountain region causes him to expect that future events there will not have the volume, vigor, or potential for sill formation found at Paiute Ridge.

Next, Dr. Spera described his assessment of sills. A key basis for his assessment is Paiute Ridge, where sills are associated with lithologic changes that affect elastic-thermal (rheological) properties. He has examined the abundant YMP information on the thermal-physical properties of the tuffs beneath Yucca Mountain. His close examination of those properties revealed variations in the rocks that could affect sill formation, although the magnitude of that influence is unknown. Dr. Spera also mentioned that a possible rotation in the principal stress tensor resulting from transient heating in the repository could affect sill development. Next, he discussed his assessments of conduit geometry, which are based primarily on analogue studies.

Dr. Hackett gave the final talk on "Eruptive Conduits and Sills," first describing eruptive conduits. He stated his belief that conduit formation and location depend on the formation and location of the eruptive center, based on a one-to-one relationship (one eruptive center is associated with one conduit). Conduit geometry for future eruptions can be inferred from analogue information, specifically the xenolith content of eruptive products, the diameter of craters, and the exposed conduits of Mio-Pliocene analogues in the Yucca Mountain region. Sill formation requires special circumstances that he believes are unlikely to occur beneath Yucca Mountain. The large magma volume that is correlated with sill formation also is unlikely. Based on these observations, Dr. Hackett concluded that sills pose an insignificant hazard to the repository. Finally, he commented on the effects of the repository on the geometry and dynamics of intrusions. Given the form of the repository and properties of the surrounding rock, he expects that any future intrusive or eruptive phenomena within the drifts would not differ significantly from the Quaternary basaltic volcanism that has occurred elsewhere in the Yucca Mountain region.

Following a lunch break, presenters addressed the third topic in the first session: "Scenarios of Event Characteristics." Dr. Charles Connor (University of South Florida) gave the first talk, describing how he has defined scenarios based on analogue igneous events shown on geologic maps. He said he plans to use mapped systems directly as event scenarios. Dr. Connor began by defining four scenarios he plans to use, each of which comprises a complete definition of an event. Dr. Connor said that if a sufficient number of scenarios can be defined and/or the relative credibility of scenarios can be weighted, the result can be used in assessing the frequency with which defined igneous features potentially could intersect the repository. He described scenarios defined from the San Rafael volcanic field and Willow Springs area in Utah and from Paiute Ridge in Nevada. Dr. Connor has selected one geologic event from each area to be superimposed on the Yucca Mountain vicinity. He then enumerated the advantages and disadvantages of using mapped analogue events as event scenarios. Following this talk, expert panel members discussed Dr. Connor's approach.

Next, Dr. Bruce Crowe (Apogen Technologies) described how he has defined event characteristics. He said he defines events as "magma pulses or ascent events" (not individual centers), using the geologic record to identify pulses of volcanic activity and to assess the variability in the expression of pulses. He described an event as a discrete distribution that reflects the variability in the record of events within volcanic cycles. Dr. Crowe showed an event table in which he had divided eruptions in the Yucca Mountain area into clusters that ranged from a single cone (e.g., Lathrop Wells) to four-cone temporal clusters (e.g., the Crater Flat events that have ages of about 1.1 My). Next, he described the specific volcanic cycles in the region and the event patterns within those cycles, commenting on cycle duration, number of

events, recurrence rate, and uncertainty in event characteristics. Dr. Crowe presented event patterns for Yucca Flat/Frenchman Flat and both Pliocene and Quaternary events in the Amargosa Trough.

Expert panel members then discussed the two approaches presenters had described for characterizing the uncertainty about future event characteristics—one approach based on scenarios, the other based on defining parameters (which involves direct assessment of dike length, width, and other characteristics).

The last workshop topic in the first session was: "Types of Future Eruptions." Dr. Crowe introduced the topic by describing the volcanic events of the past 1 My in the Yucca Mountain region and how information about those events could be used to make predictions about potential future events (including the most likely future event) in the area. He used the 10,000-year recurrence rate for volcanic events to examine three potential future conditions: steady state, waning volcanic activity, and waxing volcanic activity. Dr. Crowe also defined three scenarios for the proposed one-million-year period: continued activity in Crater Flat; cessation of volcanic activity; or a change in tectonic regime, resulting in formation of a new volcanic cycle at a random location in the Amargosa Trough.

Furthering the topic of "Types of Future Eruptions," Dr. Kuntz referred to analogue volcanoes in the region to define the characteristics of events involving large, intermediate, or small volumes. He listed representative analogues in the region, noting the magma composition and geologic/structural controls, including faults. Dr. Kuntz then described the characteristics of what he considers the most likely scenario for a future eruption: a low-volume, perhaps Strombolian and/or violent Strombolian, eruption in Crater Flat similar to the Lathrop Wells eruption.

After a break the expert panel discussed the topics presented in the first session, *Summary of Preliminary Assessments—Event Definition.* Dr. Coppersmith noted that the results of the PVHA-U could not be predicted accurately relative to the PVHA-96 results, because of the complex relationships among event parameters and the spatial and temporal models used. He therefore discouraged panel members from speculating on whether the hazard estimates would "go up" or "go down" relative to the 1996 assessment. Participants discussed differences between likely characteristics of potential eruptions within the next 10,000 versus one million years. Future climates and their potential effects on groundwater levels were considered in the context of eruption dynamics. Panel members summarized and continued an e-mail discussion that had begun between two expert panel members the previous week. That discussion focused on the Solitario Canyon dike (emplaced about 10.5 million years ago (Ma)) and the likelihood of a similar event occurring in the future near Yucca Mountain, based on whether geologic conditions in the area currently are similar to conditions 10 Ma. Participants discussed geologic conditions and their potential relevance to future volcanism.

Dr. Coppersmith then opened the workshop to comments from observers. Topics of discussion included volcanic cycles and varying levels of activity within them, geochemical information, the interface between hazard and consequence analyses, the presence of Lathrop Wells ash in fault zones, and the characteristics of the magma that potentially could impact the repository. Following the discussion, Dr. Coppersmith adjourned the meeting for the day.

DAY 2 – WEDNESDAY, SEPTEMBER 27

Dr. Coppersmith welcomed everyone to the second day of the workshop and introduced the topic of "Spatial Zones," the first of three topics within the session titled, *Summary of Preliminary Assessments—Spatial Models*. Dr. Michael Sheridan (State University of New York at Buffalo) began by describing his region of interest, the Pliocene and Quaternary volcanic centers within the Amargosa Trough. Dr. Sheridan said he is pursuing two spatial approaches: (1) bivariate Gaussian parameters to create the basic field shape for potential future volcanoes, and (2) a Gaussian field shape modified by geophysical and geologic data maps (including a lithostatic pressure map and the extension contours of Fridrich et al. 1999). He described the number of events represented by igneous features in the Yucca Mountain vicinity. Dr. Sheridan said he might modify his spatial models based on information regarding both lithostatic pressure and extension. In calibrating his model of the relationship between lithostatic pressure and extension and the spatial distribution of potential future events, he plans to consider data from a pressure map of the Reveille and Lunar fields.

The next talk on "Spatial Zones" was given by Dr. Alexander McBirney (University of Oregon, Emeritus), who began by listing three factors that govern the spatial distribution of potential igneous activity: seismic tomography (in which high velocities reflect little or no melt and low water content); prior Quaternary activity; and a favorable structural setting. Each of these factors can be quantified and manipulated by methods such as contouring. Dr. McBirney proposed applying the factors so as to divide the Yucca Mountain region into three sub-areas ranked in terms of their potential for future volcanic activity. Based on the factors, Crater Flat had the highest potential, followed by Jackass Flats and Sleeping Butte, and finally the south end of Yucca Mountain.

Dr. Thompson gave the final talk on "Spatial Zones." He began by describing the usefulness of free-air gravity anomaly data, which indicate the rock pressure that must be overcome for magma intrusion to occur. He described his subdivision of the region into the Yucca Mountain domain of normal faulting and the Crater Flat-Amargosa Desert domain of volcanism and subdued faulting. Dr. Thompson showed a cross section of the Bare Mountain-Crater Flat-Yucca Mountain region, highlighting the fault convergence and associated locus of greatest extension beneath the center of Crater Flat. Although he has calculated 8 km of extension in the center of Crater Flat, only a small amount of that extension occurred in the Quaternary, when it was associated with multiple displacements along the Solitario Canyon fault. This information suggests that the probability of volcanic activity in the structural trough beneath Crater Flat is higher than in adjacent areas. Dr. Thompson's general conclusion was that Yucca Mountain lies within a domain where extension occurs by normal faulting and where magma intrusion could be inhibited by higher rock pressure as well as by a longer path to the surface. In contrast, the adjacent volcanic domain that includes Crater Flat is a locus of greater extension and lower rock pressure, both conditions that allow intrusion.

Members of the expert panel commented on the effects of lithostatic pressure, the possible relationship between magma volume and pressure, processes in the shallow crust versus at mantle depths, geochemical information on partial melting and incompatible elements, and regional and local patterns of volcanism.

After a break, expert panel members addressed the second topic in the second session: "Events within Regions of Interest." Because both Drs. Spera and Kuntz were scheduled to give talks, they both had prepared handouts that were distributed to the experts and observers and are available on the CD of information from Workshop 3. In response to requests from panel members, however, the agenda was revised so that Dr. Spera could use the available time to describe factors that could affect variations in velocities observed in seismic tomographic data. He discussed measuring the speed of compressional waves, given that velocity is a material property (i.e., the velocity of a compressional wave will change when a rock is squeezed isotropically). Dr. Spera noted that the assessment is complex, because of variables such as rock mineralogy, water content, temperature, and the presence of melt. He described each of these variables and how they are interconnected (i.e., the distribution of hydrous phases controls the distribution of water, which influences the distribution of melt). Melt, which is generated at grain boundaries, must segregate; compaction can drive the liquid to accumulate and move upward into fractures, potentially producing flow at the surface. Next, Dr. Spera described the role of melting in the formation of magma. Primary mechanisms involve the influx of heat (conductive and radiogenic heat) and of water (which lowers the solidus curve, resulting in melt at lower temperatures). Dr. Spera described isentropic decompression (sometimes called adiabatic decompression) and the role of pressure. The expert panel then discussed issues related to those factors and the tomographic data available for the Yucca Mountain region.

The third topic in the second session was: "Geologic Data Sets Relevant for Estimating Spatial Intensity." In giving the first talk on this topic ("Data and Spatial Intensity"), Dr. Connor began by showing location data for 282 volcanoes of Miocene to Quaternary age within his defined region of interest. He said that for one of his spatial models, he intends to use a kernel density estimation approach fit to the locations of past events. Dr. Connor described a Monte Carlo simulation approach he has used to characterize the uncertainty in the resulting spatial distribution (for both a single kernel and a bandwidth estimate). He presented an example using several data sets: 33 Miocene-Quaternary events in the Yucca Mountain region; 20 Pliocene-Quaternary events; 11 "major" Pliocene-Quaternary events; and three Quaternary events (Black Cone, Hidden Cone, and Lathrop Wells). He noted that the quantified uncertainty in spatial intensity increases as the data set becomes smaller. Showing a series of maps that displayed mean crustal density, lithospheric pressure, and cumulative percent extension, Dr. Connor discussed quantifying extension based on potential field data and data sets for faults.

Dr. Sheridan gave the next talk on the topic of "Geologic Data Sets Relevant for Estimating Spatial Intensity," first describing his general conceptual model of volcanism: Tectonic extension in the Basin and Range caused thinning of the crust, which allowed the mantle to rise, resulting in the wave of volcanism that occurred across the Great Basin during the past 11 Ma. As discussed above, Dr. Sheridan is pursuing two spatial approaches: (1) bivariate Gaussian parameters to create the basic field shape for new volcanoes, and (2) a Gaussian field shape altered by geophysical and geologic data maps (including a lithostatic pressure map and the extension contours of Fridrich et al. 1999). He described several factors that are important to consider when developing spatial models. In addition to defining events, identifying the region of interest, and identifying the locations and sizes of events, it is necessary to evaluate geologic and tectonic factors that could influence magma rise. Dr. Sheridan noted the obvious decrease in magma volumes through time. He plans to use Pliocene (<3.8 Ma) and younger events in the Yucca Mountain region as a data set, informed by maps of local pressure variation and calibrated

against comparable maps of the Reveille Range. The expert panel discussed these and other available data, such as GPS data.

A workshop observer, Dr. Eugene Smith (University of Nevada Las Vegas), commented on the information available for events in the Reveille and Lunar Crater volcanic fields. He noted the need to examine the volcanism in those fields in time slices. For instance, the Reveille field has experienced three episodes of volcanism, the most recent of which began about 3.4 Ma. Dr. Smith asserted that this youngest episode is the best analogue for the Yucca Mountain region. He noted some observations of those fields, including the percentage of events in topographically high areas and relative amounts of area uplift. He also offered to provide unpublished Master's theses that contain information on volcanic events in the Reveille Range.

Following a lunch break, Dr. Karen Jenni (Insight Decisions) gave the first talk of the afternoon and the final talk in the session titled *Summary of Preliminary Assessments—Spatial Models*. Dr. Jenni developed this talk in response to questions that arose during elicitation interviews, wherein some experts expressed interest in combining multiple data sets into their spatial models but were uncertain about how that information could be used. In her introduction, Dr. Jenni summarized spatial models used in the PVHA-96 and potential ways to use the geologic data sets available for the current study. Dr. Jenni then discussed the judgments required for the Bayesian approach, describing an example data set and the associated expert judgments required to use that data to support a spatial model. One could formulate the judgments necessary to support the assessment by: (1) using analogues to develop relationships between the relevant data and the locations of potential future events, or (2) using the relationship between the data and past events in the region. Dr. Jenni then showed example functions derived using the second approach, noting the judgments necessary to convert the derived relationships into functions that can be used in spatial models. She discussed combining spatial models or data sets, for which one must assess the relative weights of the approaches or models. Following Dr. Jenni's talk, the expert panel discussed the independence of various data sets and the possibility of double-counting events when using Bayesian updating.

Following the discussion of spatial models, the third session began on *Summary of Preliminary Assessments—Temporal Models*. Dr. Sheridan began by describing his plan to use two temporal approaches—a homogeneous model for average recurrence, and a cluster/episodic model for grouped events. The first approach, which considers 13 events during the past 3.8 million years, leads to a recurrence interval of about 300,000 years. The second approach considers clusters that occur at 0.08, 1.08, 3.8, and 4.8 Ma; the duration of each episode is estimated to be about 200,000 years. Dr. Sheridan described the frequency of events within clusters, noting that the rate of volcanism within a cluster is about five times higher than the overall recurrence rate estimated using the first approach. Finally, Dr. Sheridan discussed whether the Lathrop Wells event represents the beginning of a new cluster. The long period of quiescence since this event (80,000 years) indicates a significant probability that cluster activity is not underway.

Next, Dr. McBirney described temporal trends of igneous activity in the Yucca Mountain region. He first noted that the low magnesium content of magmas in the area indicates that they are not primary, mantle-derived melts, but rather have evolved to differing degrees by crystal fractionation. Secondly, the degree of silica saturation has become increasingly diverse through time (i.e., the basalts show no apparent temporal trend and have a wide range of silica

saturation). Thirdly, the volumes of erupted magma have declined with time. Fourth, their trace-element compositions indicate that the magmas represent spatially isolated melts of a depleted mantle source. Dr. McBirney's conclusion was that temporal trends indicate overall decreasing igneous activity in the region, independent of the episodic activity of small groups of eruptions.

Dr. Connor gave the final talk in the session *Summary of Preliminary Assessments—Temporal Models*. In his talk, "Episodic Recurrence Rates," he categorized event clusters differently than did Dr. Sheridan, postulating that temporal clusters are related to spatial location. He described an analysis he conducted in the early 1990s showing that the clusters are significant and that volcanism has returned periodically to clusters (i.e., that clusters have been re-activated). Dr. Connor asked whether it is reasonable to treat the Quaternary Crater Flat volcanoes as a single event. He examined the ages of vents that formed in the alignment of volcanoes in the Black Rock Desert of Utah throughout about 10,000 years. The Black Rock Desert has a high density of faults, some of which cut volcanoes, thereby indicating coeval faulting and volcanism. Dr. Connor concluded that to develop models of recurrence rate, one must seek to understand several issues, including the recurrence rate of temporal clusters, whether the Lathrop Wells alignment may still be forming, and how those issues affect spatial models.

The expert panel then discussed temporal clustering, noting the limitations of using only two episodes of volcanism (Quaternary and Pliocene) to define a trend. Dr. Eugene Smith noted that he was struck by the fact that volcanism had returned to the same areas time after time. He suggested that perhaps melting is very deep (in the asthenosphere) beneath Crater Flat, Lunar Crater, and similar areas in southern Nevada.

Dr. Coppersmith then described the path forward and the schedule for the PVHA-U. According to this schedule, the second set of elicitation interviews will be held in November and December of 2006. After these interviews are completed, preliminary hazard calculations and sensitivity analyses will be performed and then discussed in Workshop 4, currently scheduled for April of 2007.

Dr. Coppersmith opened the workshop to comments from observers. Dr. Brittain Hill (NRC) thanked the panel for the enlightening conversations during the past few days. He noted the importance of developing a clear event definition, considering alternative models, and conforming to quality assurance (QA) requirements. Dr. Coppersmith noted that PVHA-U activities are following the QA directives defined in the BSC quality assurance procedure, *Expert Elicitation* (LP-AC.1Q-BSC; BSC 2004), which is consistent with the regulatory guidance given in *Branch Technical Position on the Use of Expert Elicitation in the High-Level Radioactive Waste Program* (NUREG-1563; Kotra et al. 1996). Dr. Coppersmith thanked all the workshop participants and adjourned the meeting.

PROBABILISTIC VOLCANIC HAZARD ANALYSIS UPDATE
YUCCA MOUNTAIN PROJECT

WORKSHOP 4
FEEDBACK

May 10-11, 2007
Las Vegas, Nevada

SUMMARY

Workshop 4 on Feedback was the sixth and last in a series of meetings (including Workshops 1, 2, 2A, 3, 4, and the field trip) conducted by the U.S. Department of Energy (DOE) in support of the Probabilistic Volcanic Hazard Analysis Update (PVHA-U) for the Yucca Mountain Project (YMP). The PVHA-U relates to the technical bases that will be provided in the project's license application to the NRC. The PVHA-U relies on formal elicitation of the assessments of a panel of expert volcanologists to estimate the probability that the Yucca Mountain repository could be disrupted by a future igneous event (i.e., the volcanic hazard at the site). The objectives of this workshop were to (1) provide the expert panel members with feedback on their models and assessments, including the methods and approaches they used; (2) use sensitivity calculations to examine the uncertainties in various parameters and demonstrate their effect on the analyses, thereby furthering expert panel members' understanding of the relative importance of major technical issues; and (3) discuss the event definitions each expert used and other potential sources of variations in interpretation (different assumptions or models).

The workshop presentations were organized around three topics: (1) the experts' definitions of an igneous event, (2) the experts' various approaches to modeling the spatial and temporal distribution of potential future events, and (3) hazard sensitivities and the technical issues that are most important to each expert's estimates of volcanic hazard.

DAY 1 – THURSDAY, MAY 10

Mr. Eric Smistad (the DOE lead for volcanism) opened the workshop by welcoming participants to the workshop and thanked the expert panel members for their work. Mr. Thomas Pfeifle (Sandia National Laboratories, Disruptive Events Manager) then welcomed the group and explained that in October 2006 postclosure scientific work for the YMP was transferred to Sandia, now the Lead Laboratory for the YMP. He then turned the meeting over to Dr. Kevin Coppersmith (Coppersmith Consulting), who reviewed the goals and approach of the workshop and described the project schedule. He noted that the workshop would examine results based on the assessments each expert developed during the individual elicitation interviews held in November and December of 2006 and subsequent follow-on work. Dr. Coppersmith emphasized that expert panel members will have an opportunity to review, revise, and finalize their assessments after the workshop and after the subsequent individual feedback interviews. Elicitation summaries documenting the experts' final assessments are scheduled to be completed in July of 2007. The final report on the PVHA-U project will be completed by July 2008. Dr. Coppersmith emphasized and cautioned that calculations shown during the workshop are for purposes of feedback only, may well be revised, and are not considered final.

Dr. Coppersmith also described the changes in PVHA-U management related to Sandia assuming the role of Lead Laboratory for the YMP. Work for the PVHA-U continues to be controlled by a formal expert elicitation procedure (Lead Laboratory Procedure SO-PRO-002, *Expert Elicitation*) that is consistent with guidance developed by the NRC. Dr. Coppersmith reviewed the ground rules for workshops, the experts' different roles as proponents and evaluators, and the issues the expert panel members must address (listed in Table 1 of the Workshop 1 Summary). He then reviewed project events that have occurred since Workshop 3, which was held in September of 2006. Those events included individual elicitation interviews and follow-up with each expert as the Methodology Development Team (MDT) implemented their models to develop the results to be examined in Workshop 4. Dr. Coppersmith described the structure of Workshop 4, which will involve the MDT making presentations, and encouraged panel members to participate fully. During the workshop the basic elements of the PVHA-U will be summarized, with a focus on sensitivities calculated across the panel rather than on individual assessments. Specific individual sensitivity analyses will be addressed during each expert's forthcoming individual feedback interview.

Dr. Frank Perry of Los Alamos National Laboratory (LANL) gave the final talk in the opening session, describing the experts' requests for information, the new database products provided to the experts, and examples of the geologic data the experts had incorporated into their hazard models. After outlining the responses to experts' requests for data, he summarized results of the program that collected aeromagnetic data and the associated drilling and laboratory testing program. The youngest basaltic anomaly identified in the drilling program is dated at 3.9 million years ago (Ma); others are older than 9 Ma. Dr. Perry also reviewed age-dating information for the Crater Flat Quaternary cones, in particular the argon-argon dates for Little Cones, which may indicate they are younger than the other Quaternary Crater Flat cones. There is significant uncertainty about the age of the Little Cones. Dr. Perry described the results of chemical analyses, which indicate that the eight Quaternary cones in the Yucca Mountain region contain a greater proportion of light, rare-earth elements than do older basalts in the region. He stated that trends in eruptive volume and composition suggest decreasing partial melting through time, consistent with a decrease in the regional extension rate or cooling of the mantle source. Next, Dr. Perry outlined a few examples of geophysical and geologic data incorporated into spatial models. The panel discussed the capture of dikes by faults, the chemistry of basalts, and alternative interpretations of the origins of some anomalies (e.g., the possibility that Anomaly A is a sill).

Dr. Karen Jenni (Insight Decisions) opened the detailed discussion of the experts' assessments by describing how the experts defined igneous events. She described the importance of the event definition, emphasizing the need for internal consistency within each expert's assessments and models. It is not necessary for all the experts to share a uniform definition of an event, because all events ultimately include some collection of igneous features (e.g., dikes, conduits, and/or sills), with the result of the overall assessment being the annual probability that each specific feature might intersect the repository footprint. This result is comparable among all experts regardless of how they group specific features into events. Dr. Jenni described two alternative conceptual models experts used to characterize events, one based on igneous features, the other on groups of features in the volcanic record. She noted that experts who defined events by the second approach generally expected future events to have a larger footprint than did those who used the first approach. In a group discussion, some experts described and clarified their event

definitions, noting differences among expert interpretations. Participants discussed variations in the temporal extent defined for an event and the number of dikes and conduits associated with an event. Experts received a list of the characteristics of igneous features common to all experts' event definitions. Dr. Jenni then showed slides comparing all experts' assessments of each event characteristic. She also described how the MDT modeled each expert's events by using a Monte Carlo simulation to calculate the conditional probability that various features might intersect the repository footprint. Workshop participants then took a break, during which they could view maps on the meeting room walls that showed examples of each expert's typical events and his conditional probability of a potential future dike intersecting the repository.

Following the break, Dr. Jenni discussed the range of event characteristics that help determine the probability that a dike would intersect the repository if an event were to occur. Topics included dike azimuths, the association of conduits with dikes, the characteristics of conduits, and occurrences of dikes without a conduit. Also discussed were changes in eruptive characteristics through time (e.g., fissure eruptions may occur first, progressing to conduit formation) and the associations among dikes, conduits, and eruptive features such as cones. Experts discussed their alternative interpretations of conduits and vents, and Dr. Perry noted that expert panel members will be asked to assess the likelihood and dimensions of a conduit that intersects the repository footprint producing an eruptive column, because this information will be used in modeling volcanic consequences. The group also discussed the effects the repository openings might have on the formation of conduits.

Following a lunch break, Dr. Jenni made a presentation titled "Introduction to Sensitivity Analyses: Effect of Uncertainties on the Probability of Dike Intersection." She began by noting that the annual probability of an igneous feature intersecting the repository footprint is a function of the characteristics of the event and the location-specific annual probability of an event. The annual probability of such an intersection is one input to the analysis of igneous consequences, which, in turn, is an input to the total system performance assessment. After showing each expert's current calculated uncertainty surrounding the probability of dike intersection with the repository footprint, Dr. Jenni described two sensitivity analyses that would be used throughout the rest of the workshop: the uncertainty in the probability of a dike intersection associated with uncertainty in the assessment of each aspect of event geometry, and a graph comparing the conditional spatial intensity of events along a transect crossing the repository footprint based on applying different conceptual models.

Next, Dr. Jenni spoke on "Spatial Distribution of Future Events." First she showed each expert's interpretation of the number of relevant past events in the Yucca Mountain region and the four conceptual models the experts used to estimate the spatial distribution of potential future events. The four conceptual models defined the conditional spatial intensity of potential future events using different basic approaches: (1) identifying zones, each of which has a different recurrence rate for volcanism; (2) identifying relevant past events and using spatial smoothing/estimates of kernel density to calculate conditional intensity based on proximity to those events; (3) identifying past volcanic field(s) and their characteristic shape(s), then estimating conditional spatial intensity based on the field shape; and (4) modifying one of the basic models (1 through 3) by quantitative use of geologic data.

For each of the first three conceptual models, Dr. Jenni used one expert's model to illustrate the sources of uncertainty/expert judgments each model requires. For the zone model, she showed a sample map of rate density, a plot showing the uncertainty in rate density as a function of uncertainty in zone boundary, and the sensitivity of the probability of dike intersection with the repository to uncertainties in the spatial model. For the smoothing model, Dr. Jenni illustrated the effects of varying the smoothing distance and of weighting past events by their estimated volumes and the inverse of their estimated ages. Dr. Jenni discussed the sensitivity of the probability of dike intersection to those uncertainties in the smoothing model. She concluded the talk by describing alternative means of estimating the spatial distribution of future events, such as an elliptical kernel estimator or a parametric field shape, as proposed by some members of the expert panel. She illustrated the effects of the uncertainties in each of these spatial models. Expert panel members discussed uncertainty related to their chosen sets of events and spatial models.

Following a break, Dr. Jenni described how experts used geologic data in their models of the spatial distribution of future events. Some experts used such data qualitatively; others used them quantitatively in combination with other spatial models. Experts' spatial models incorporated various geologic data sets: lithostatic pressure, tomographic, and/or cumulative extension data. Dr. Jenni showed how experts used the data in spatial models and model combinations. The weights experts assigned to the geologic data sets ranged from 0% to 50%. She described general findings from combining an expert's interpretation of geology with his basic spatial model. Expert panel members discussed the weights they assigned to various models and the uncertainties in the models. Dr. Coppersmith addressed the difficulty and necessity of weighting alternative conceptual models, noting that there are epistemic uncertainties that must be captured.

Expert panel members discussed the number of aligned Crater Flat Quaternary events/cones, which ranges from one to five depending on the event definition used. Experts noted the difficulty in developing models based on a low number of events and the resulting uncertainties in assessments. They also discussed the possibility of a heterogeneous magma source in the Yucca Mountain region.

Dr. Coppersmith then opened the workshop to comments from observers. Topics included event definitions and the need to have a clear link between results of the volcanic hazard analyses (e.g., annual probability of dike intersection) and the modeling of consequences due to those hazards; assessments of the potential effects of the repository openings on ascending magma; low-probability volcanic events relative to future assessments for 10,000 and one million years; local sources of heat and related melting of magma and our ability to use geophysical techniques to image those sources; the active volcanic field in the Death Valley region; and whether the panel is charged with recommending alternative repository sites in light of difference in volcanic hazards. Dr. Coppersmith indicated that the Nuclear Waste Policy Act calls for the characterization and evaluation of only the Yucca Mountain site, and that therefore the PVHA-U panel is charged with considering only the Yucca Mountain site.

DAY 2 – FRIDAY, MAY 11

The first talk of the day, given by Dr. Jenni, focused on temporal models. Dr. Jenni described the three basic conceptual models experts used to estimate a recurrence rate for potential future

igneous events: a homogeneous Poisson process, a time-volume model, and temporal clustering. She first described using a homogenous Poisson model to estimate a recurrence rate. She then illustrated the sensitivity of the homogeneous Poisson estimate to assessed number of events, and showed how alternative characterizations of past events affected each expert's estimated Poisson recurrence rate. The number of events, time period, and region of interest affected rates and the associated uncertainty.

Next, Dr. Jenni described the time-volume model of recurrence rate, considered an attractive conceptual model because it explicitly addresses the decline in erupted volumes over time noted in the region. She described different ways to estimate cumulative eruption volume as a function of time and the volume per event over time. The choice of a model's functional form relies on an expert assessment that typically is based on geologic information. In most cases, the experts chose to model the volume per potential future event based on the volumes of Quaternary events. Dr. Jenni then described the temporal clustering model. She noted that estimates of recurrence rate derived from both the time-volume and temporal clustering models are time-dependent.

Dr. Jenni described the differences among the three models (homogeneous Poisson, time-volume, and temporal clustering), explaining that the experts must choose a model(s) to represent their individual belief about what is occurring in the Yucca Mountain region. She showed each expert's initial distributions on recurrence rate, which incorporate alternative event sets, alternative conceptual models, and uncertainty in model fit(s) to the data. Panel members discussed the range in uncertainty in possible rates of future volcanism, and discussed a conceptual model that could predict future rates that differ significantly from the rates estimated using a steady-state conceptual model. At one extreme, the Crater Flat area could begin to resemble an active volcanic field such as the Cima field; at the other extreme, all volcanic activity could cease. Dr. Jenni described an approach that could include these alternative conceptual models explicitly in the analysis. Using this approach, experts would define and weight three alternative models for future rates of volcanism in the area: (1) a new process initiates, increasing the future rate compared to the rate observed in the recent past; (2) the future rate is similar to the rate in the recent past; and (3) the future rate is much lower than in the past.

Dr. Jenni then gave the final presentation of the workshop, titled "Feedback: Rate Density, Hazard Calculations, and Sensitivity Analyses." She presented maps of rate density that combined each expert's spatial and temporal evaluations. Rate density is calculated by multiplying the conditional spatial intensity by the annual probability of an igneous event. Rate density maps for each expert were displayed on the walls of the meeting room, where experts could review them during a break.

After the break, panel members discussed the assessment of mean rate density, including variations in background rate and the shapes (e.g., smooth versus stepped) of rate/density curves along a transect.

Dr. Jenni next discussed the hazard calculations that indicate the annual probability that each type of igneous feature would intersect the repository footprint. Referring to each expert's uncertainty in the probability of dike intersection with the repository, as discussed on Day 1, she noted that the factors that contribute to this uncertainty had been discussed throughout the workshop. The expert panel members discussed the range of uncertainty across the panel and the

reasons that experts' assessments differed. Dr. Jenni also illustrated the uncertainty in the probability of a conduit intersecting the repository footprint, and in the number of conduits intersecting the repository if a dike intersection were to occur.

Finally, Dr. Jenni discussed sensitivity analyses for each expert's assessment. She showed a map of mean rate density and uncertainty in rate density, then described the sensitivity of the probability of dike intersection to uncertainties in each expert's model. The purpose of providing this information was to enable experts to confirm that their modeled uncertainty correctly reflected their beliefs. If it did not, they may modify their assessments. The expert panel discussed rates of volcanism in background zones and delineating zone boundaries to reflect an appropriate uncertainty.

The objective of the workshop, Dr. Jenni reiterated, was to give the experts feedback about their models. Each expert will receive more detailed information during the forthcoming individual feedback interviews. Dr. Jenni then examined specific aspects of some of the experts' models based on using different numbers of aligned Quaternary Crater Flat events.

Following a lunch break, Dr. Jenni showed and described each expert's current spatial distribution of the frequency of future dike intersection with the repository footprint. The frequency of intersection is calculated by multiplying the rate density times the conditional probability of a dike intersection given an event.

After the formal talks concluded, Dr. Coppersmith addressed a matter discussed repeatedly throughout the workshop: whether all the experts should use a common event definition. Experts' observations in the Yucca Mountain region and elsewhere have caused them to develop differing opinions about how best to define events. After listing some of the PVHA-U results that will be taken forward into consequence analyses, Dr. Coppersmith reiterated that experts do not need to use identical processes for obtaining those results, although each individual expert must use one event definition consistently throughout his assessments. Dr. Coppersmith asked the expert panel members to give their opinions about adopting a common event definition. The experts expressed their strong preference not to be constrained by a uniform event definition, noting that the range of event definitions reflects natural variability and that using different event definitions provides for more uncertainty in the analyses. After discussing their event definitions, expert panel members talked about changes in the geologic setting of the region that could occur between the 10,000- and one-million-year future periods of interest.

Dr. Coppersmith then described the path forward for the PVHA-U project. The next planned activity is conducting individual feedback interviews, in which each expert will review his models and make any final changes. After that interview each expert will complete his elicitation summary, which will document the final models he is using and the technical bases for all his assessments.

The last item on the agenda was an opportunity for workshop observers to make comments. Issues included ranges of uncertainty in models, the value of fully incorporating geologic information into assessments, and functional forms of the assessed distributions. Also discussed was the stability of the PVHA-U results—specifically, what might cause the current hazard results to differ from those developed in 1996 and what might happen in the next 15 to 20 years

to change the hazard models and results even further. Members of the expert panel mentioned the information that became available after 1996, such as more detailed mapping and chemical analyses of volcanic features in the region, information about buried anomalies provided by the aeromagnetic mapping and drilling programs, and the improved computational tools available for conducting assessments. Some experts stated that more detailed tomographic data would be valuable, whereas others opined that those data cannot be resolved to a level of detail adequate for this hazard study.

After thanking those who assisted with workshop logistics, the MDT, peer reviewers, and members of the expert panel, Dr. Coppersmith adjourned the workshop.

REFERENCES CITED IN WORKSHOP SUMMARIES

BSC (Bechtel SAIC Company) 2004. *Expert Elicitation* LP-AC.1Q-BSC, Rev. 0, ICN 1. Washington, D.C.: U.S. Department of Energy, Office of Civilian Radioactive Waste Management.

BSC 2005. *Magma Dynamics at Yucca Mountain, Nevada.* ANL-MGR-GS-000005 REV 00. Las Vegas, Nevada: Bechtel SAIC Company.

Budnitz, R.J.; Apostolakis, G.; Boore, D.M.; Cluff, L.S.; Coppersmith, K.J.; Cornell, C.A.; and Morris, P.A. 1997. *Recommendations for Probabilistic Seismic Hazard Analysis: Guidance on the Uncertainty and Use of Experts.* NUREG/CR-6372. Two volumes. Washington, D.C.: U.S. Nuclear Regulatory Commission.

CRWMS M&O 1998. *Probabilistic Seismic Hazard Analyses for Fault Displacement and Vibratory Ground Motion at Yucca Mountain, Nevada.* Milestone SP32IM3, September 23, 1998. Three volumes. Las Vegas, Nevada: CRWMS M&O.

Fridrich, C.J.; Whitney, J.W.; Hudson, M.R.; and Crowe, B.M. 1999. "Space-Time Patterns of Late Cenozoic Extension, Vertical Axis Rotation, and Volcanism in the Crater Flat Basin, Southwest Nevada." Chapter 8 of *Cenozoic Basins of the Death Valley Region.* Wright, L.A. and Troxel, B.W., eds. Special Paper 333. Boulder, Colorado: Geological Society of America.

Hill, B.E. and Stamatakos, J.A. 2002. *Evaluation Of Geophysical Information Used to Detect and Characterize Buried Volcanic Features in the Yucca Mountain Region.* San Antonio, Texas: Center for Nuclear Waste Regulatory Analyses.

Kotra, J.P.; Lee, M.P.; Eisenberg, N.A.; and DeWispelare, A.R. 1996. *Branch Technical Position on the Use of Expert Elicitation in the High-Level Radioactive Waste Program.* NUREG-1563. Washington, D.C.: U.S. Nuclear Regulatory Commission.

NRC (U.S. Nuclear Regulatory Commission) 2003. *Yucca Mountain Review Plan, Final Report.* NUREG-1804, Rev. 2. Washington, D.C.: U.S. Nuclear Regulatory Commission, Office of Nuclear Material Safety and Safeguards.

O'Leary, D.W.; Mankinen, E.A.; Blakely, R.J.; Langenheim, V.E.; and Ponce, D.A. 2002. *Aeromagnetic Expression of Buried Basaltic Volcanoes Near Yucca Mountain, Nevada.* Open-File Report 02-020. Denver, Colorado: U.S. Geological Survey.

Potter, C.J.; Dickerson, R.P.; Sweetkind, D.S.; Drake, R.M., II; Taylor, E.M.; Fridrich, C.J.; San Juan, C.A.; and Day, W.C. 2002. *Geologic Map of the Yucca Mountain Region, Nye County, Nevada.* Geologic Investigations Series I-2755. Denver, Colorado: U.S. Geological Survey.

Valentine, G.A., and Perry, F.V. 2006. "Decreasing Magmatic Footprints of Individual Volcanoes in a Waning Basaltic Field." *Geophysical Research Letters*, *33*, (14), p. L14305.

Ziegler, J.D. 2003. "Igneous Activity Agreement (IA) 1.02 Additional Information Needed (AIN-1): U.S. Department of Energy (DOE) Position on Volcanic Hazard at Yucca Mountain, Nevada, and Plans for Confirmatory Studies." Letter from, J.D. Ziegler (DOE) to J.R. Schlueter (NRC), November 11, 2003, Las Vegas, Nevada, U.S. Department of Energy.

APPENDIX D

ELICITATION SUMMARIES

This appendix consists of the Elicitation Summaries developed by the eight PVHA-U experts. They have been written to describe their expert evaluations in detail, including the technical bases for their assessments. For purposes of consistency in format in this report, the Elicitation Summaries have been slightly reformatted from the final versions prepared by each expert. Any changes made for purposes of formatting are entirely editorial in nature and no changes have been made to the technical content.

D.1 CHARLES CONNOR'S ELICITATION SUMMARY FOR PVHA-U PROJECT

D.1.1 INTRODUCTION

This summary presents the background for and results of my expert elicitation regarding volcanic hazards at Yucca Mountain. The following section provides perspectives on volcanic hazard assessment generally and Yucca Mountain in particular. Here I emphasize the need for careful and comprehensive assessment, which I hope this expert elicitation process demonstrates. The section also discusses the general goals of volcanic hazard assessment, especially for comparing alternative sites, and the usefulness of state-of-the-art geophysical techniques. The perspectives presented are my own and do not necessarily reflect those of other panel members involved in this probabilistic volcanic hazard assessment update (PVHA-U) or of the Methodology Development Team. Subsequent sections describe my assessment of volcanic events, their spatial density, and temporal recurrence rate.

D.1.2 PERSPECTIVES ON VOLCANIC HAZARD ASSESSMENT

On July 16, 2007, a Mw-6.8 earthquake occurred on Japan's west coast, rocking the nearby Kashiwazaki Kariwa nuclear power plant (KK NPP), the Earth's largest nuclear power station. Ground accelerations at the plant were approximately 680 cm s^{-2}, exceeding by a factor of more than two the plant's seismic design specification of 273 cm s^{-2}, which had been developed during the site's seismic hazard assessment in the 1980s (Akira Chigama, International Atomic Energy Agency, written personal communication, 2007). The potential seismic hazard at the site was underestimated because the deterministic hazard assessment failed to account for the possibility of seismic events greater than Mw 6.0 and closer to the site than 40 km. Although reports indicate that KK NPP reactors shut down automatically and without mishap, water containing radioactive material was spilled from an on-site storage area and released into the Japan Sea. Currently, the power plant is shut down, reportedly for at least one year, while new geophysical investigations are made of the site vicinity and measures are taken to increase the resilience of the KK NPP. Total cost of the shutdown reached US $5 billion by March, 2008.

The goal of probabilistic hazard assessment is to avoid scenarios such as occurred at the KK NPP by providing accurate information for use in risk analyses that inform decisions regarding public safety. If all other considerations are equal, clearly the best strategy is to locate a facility where the probability of hazardous natural events is minimal. Every probability assessment for the Yucca Mountain region, for example, has shown that the probability of future volcanism decreases by orders of magnitude east of Yucca Mountain in areas such as eastern Jackass Flats, Yucca Flat, and Kiwi Mesa (e.g., Crowe et al., 1983; Connor and Hill, 1995; Smith et al., 1990; Connor et al., 2000). From the perspective of minimizing volcanic hazards, those areas are better suited for siting a long-term high-level waste (HLW) repository than is Yucca Mountain (YM).

Of course, issues other than volcanic hazard also must be considered in evaluating the suitability of alternative sites.

Once the Nuclear Waste Policy Act (NWPA) identified the YM site as the only one to be considered as a potential repository, the goal of hazards assessments became that of providing inputs to the total system performance assessment to determine whether the site is considered safe enough according to the regulations in 10 CFR 63. From a scientific perspective, this means that volcanic hazards must be quantified, and uncertainties associated with those assessments estimated. Ultimately, the Nuclear Regulatory Commission (NRC) will utilize those estimates in deciding whether the proposed YM site meets safety regulations. If the site is deemed not to comply with the regulations, the NWPA provides for the consideration of alternative sites.

Worldwide, this approach is relatively common in siting nuclear facilities, and has occasionally contributed to political problems with these facilities after construction. One example is the closed nuclear power plant at the Bataan site in the Philippines. This power plant, constructed on the flanks of Natib volcano and which received tephra (volcanic ash) fallout from the 1991 eruption of Pinatubo volcano, was cited by the Union of Concerned Scientists as being at particular risk from volcanic activity (D'Amato and Engel, 1988). Although it is certainly arguable that state of the art methods were used by consultants at the time of siting this facility (including one member of this PVHA panel) these methods were not sufficient to fully characterize the site in terms of volcanic hazards (C. Newhall, written communication to James O'Shea, NRC, 1979). Another example is the Metsamor nuclear power plant, Armenia, which was constructed within a region of many small basaltic volcanoes that will inevitably experience future eruptions. Post-construction hazard assessments have found that the NPP site is located adjacent to one of the most active clusters of monogenetic volcanoes in Armenia (Kharakanian et al., 2003; Weller et al., 2006). In Taiwan, new seismic investigations have demonstrated that volcanoes located close to two NPP sites are more active than previously thought, with 'tornillo' –style earthquakes occurring, indicating the rapid movement of fluids in the subsurface (Lin et al., 2005) and elevated $^{3}He/^{4}He$ in hot springs, indicating a mantle component in these fluids.

Do these problems mean that nuclear facilities at these sites create extraordinary risk? Of course not. But it is inevitable that these sites will continue to be reassessed and evaluated because they were constructed in volcanically active regions. Commonality among these sites and others (Connor et al., 2008) exists in that techniques developed and applied after construction caused a reinterpretation of the volcanic hazard. For example, at the Bataan site, Philippines, improved mapping and radiometric dating of pyroclastic flow deposits clarified rates for volcanic activity in the region long after construction of the facility (C. Newhall, written personal communication). At the Metsamor NPP, new methods of assessing spatial density of volcanism using Gaussian kernel functions resulted in a clarification of the hazard – the probability of lava flow inundation of the site. In Taiwan, application of relatively new techniques in volcano seismology and isotope geochemistry led to reevaluation of volcanic activity near the site.

These observations are important and relevant because volcanology is a rapidly developing science. Volcanic hazards at YM will likely be reassessed in the future using improved information, and this information may change the hazard assessment. Furthermore, there are techniques currently extant in the scientific community that have not been used at YM to assess volcanic hazards. For example, seismic tomography and magnetotellurics are two techniques that

are used in Japan to assess long term volcanic hazards for potential HLW geologic repositories (Martin et al., 2004; Umeda et al., 2006). Seismic tomography has revealed that along-arc variations in mantle P- and S-wave velocity correlates well with rates of volcanic activity. These data have been integrated into improved probabilistic volcanic hazard assessments. Magnetotellurics has been used to identify mid- to lower-crust magma bodies in the back-arc of Japan, in a region where no volcanism has occurred since the Mesozoic. Umeda et al. (2006) consider this to be evidence of potential future volcanic unrest, which should be factored into probabilistic assessments. These state-of-the-art geophysical surveys have not been done at Yucca Mountain. Some seismic tomography analysis has been performed and presented to the PVHA panel (Biasi, PVHA presentation, Humphries, written communication), but not with a sufficiently dense network of sensors or in a dedicated experiment.

Reassessment has already been necessary for the Yucca Mountain site, in the sense that the PVHA panel was reconvened after 10 yr due to the development of new information (e.g. aeromagnetic surveys and drilling results, improved radiometric age determinations) and ultimately new techniques (e.g., improved methods in spatial density estimation). Although the consideration of alternative sites is not part of my evaluation for the PVHA-U, nor is it provided for in the NWPA, it is important to realize that it is extremely doubtful that such reassessment would be necessary for a site located just 20 km to the east of Yucca Mountain, where volcanism has not occurred since the Miocene. It is short-sighted, especially considering the nearly inconceivable performance period of the repository, not to use the results of hazards assessments as motivation to seriously assess alternative sites on and adjacent to the NTS.

D.1.3 BACKGROUND OF THE YUCCA MOUNTAIN REGION

Volcanic hazards exist at the site of the proposed Yucca Mountain high-level nuclear waste repository because the site is located at the edge of an active basaltic volcanic field. Potential volcanic hazards include basaltic eruptions within the repository, which could transport radionuclides into the biosphere either through direct eruption or through destruction of geologic and engineered barriers and subsequent transport of radionuclides in groundwater. The immediate site area has not experienced volcanic activity since about 11 Ma, when a basaltic dike intruded faults on the west side of Yucca Mountain (Smith et al., 1997). This dike intrusion occurred about 500 m from the boundary of the repository as currently designed. Monogenetic volcanism has persisted primarily west and south of Yucca Mountain, where approximately 34 volcanic vents, mostly scoria cones, have formed in the past 5 Ma (Figure D.1-1). The most recent of these events created (1) the ~200-m-high Lathrop Wells cinder cone, which lies approximately 20 km from the repository site and was formed at approximately 0.08 Ma (Valentine and Perry, 2007), and (2) Ubehebe maar, Death Valley, which erupted during the Holocene approximately 6,000 years ago (Figure D.1-1). The volcanic hazard assessment is designed to estimate the magnitude, spatial density, and recurrence rate of potential future volcanism at the Yucca Mountain site based on this distribution of events.

Several types of igneous features are identified as having the potential to disrupt the repository: an igneous intrusion into the repository (a dike or sill) and intersection of the repository by a vent or vent-like body that could reach the surface, or development of magma flows within drifts resulting from magma intrusion into the repository. Igneous intrusions, such as sills, at shallow depths beneath the repository may also result in disruption of the waste package inventory. The

probability that any of these igneous features would disrupt the repository is a function of the physical geometry of igneous features and the spatial and temporal distribution of volcanism in the Yucca Mountain region (YMR, defined as the region with a radius of about 50 km centered on Yucca Mountain). These factors, and the relationships among them, are illustrated in Figure D.1-2. Models and assessments of the geometry of dikes, dike systems, conduits, and sills are summarized in the Event Definition below and in Figure D.1-3. Models and assessments of the spatial and temporal distributions follow.

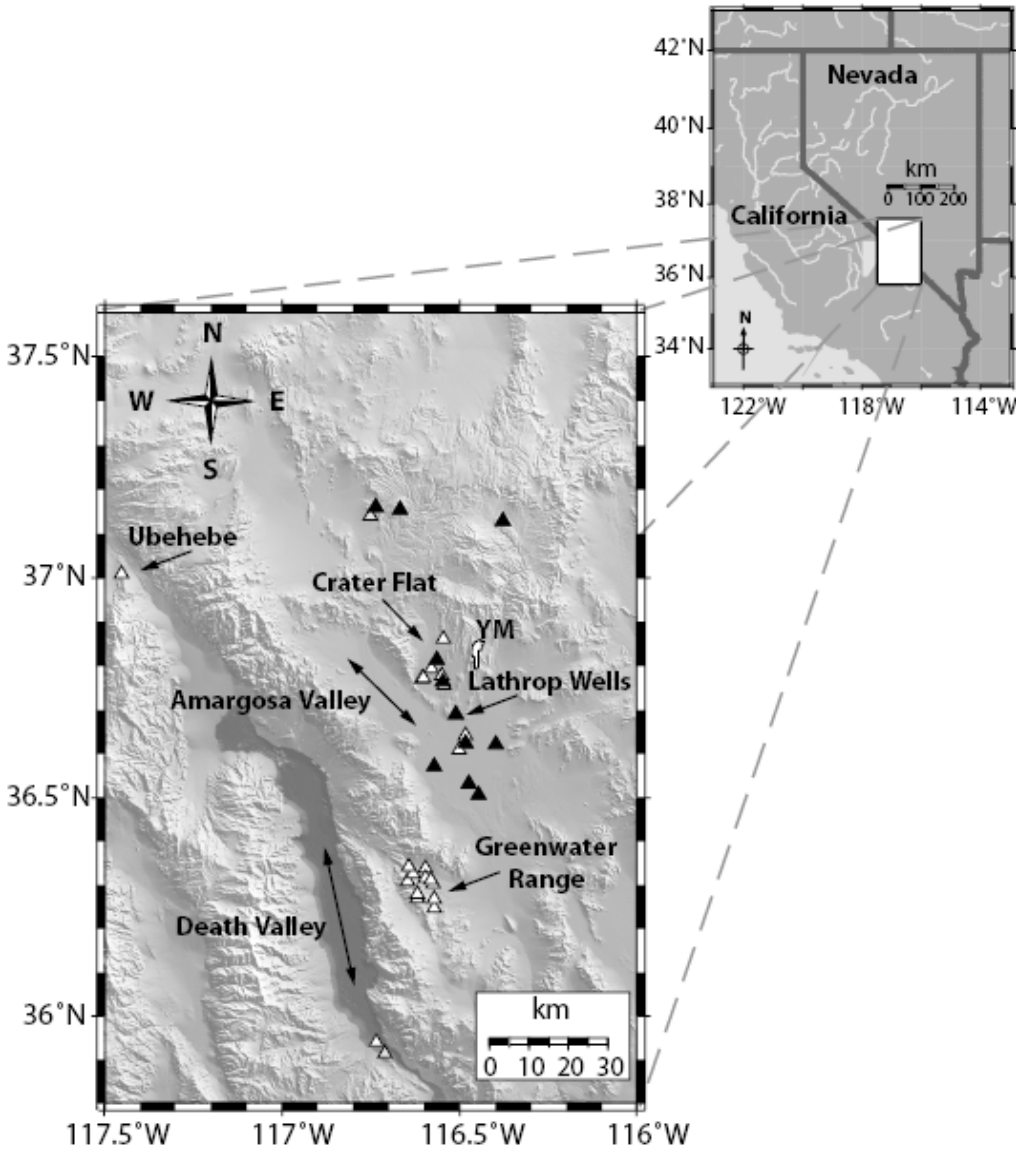

NOTE: Volcanic events included in the YMR data set are shown as solid black triangles; vents included in the AVIP data set are shown as white triangles. The two data sets serve as the basis for estimating spatial intensity in this volcanic hazard assessment. The shaded-relief digital elevation model is based on Shuttle Radar Topography Mission data (Jarvis et al., 2006). The map datum is WGS84.

Figure D.1-1. Locations of Plio-Quaternary Volcanoes near the Proposed Yucca Mountain (YM) High-Level Radioactive Waste Repository

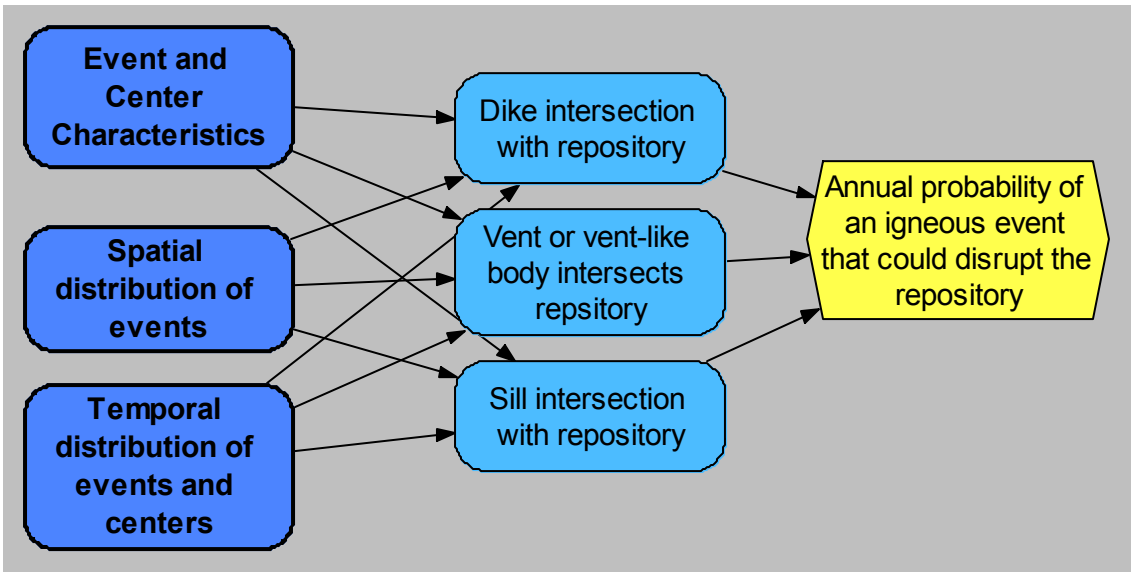

NOTE: The yellow hexagon represents the final result of the assessment. Dark blue nodes represent sub-models; light blue nodes represent values calculated from other inputs; and arrows indicate influences of one variable on one or more others.

Figure D.1-2. Overall Structure of Model

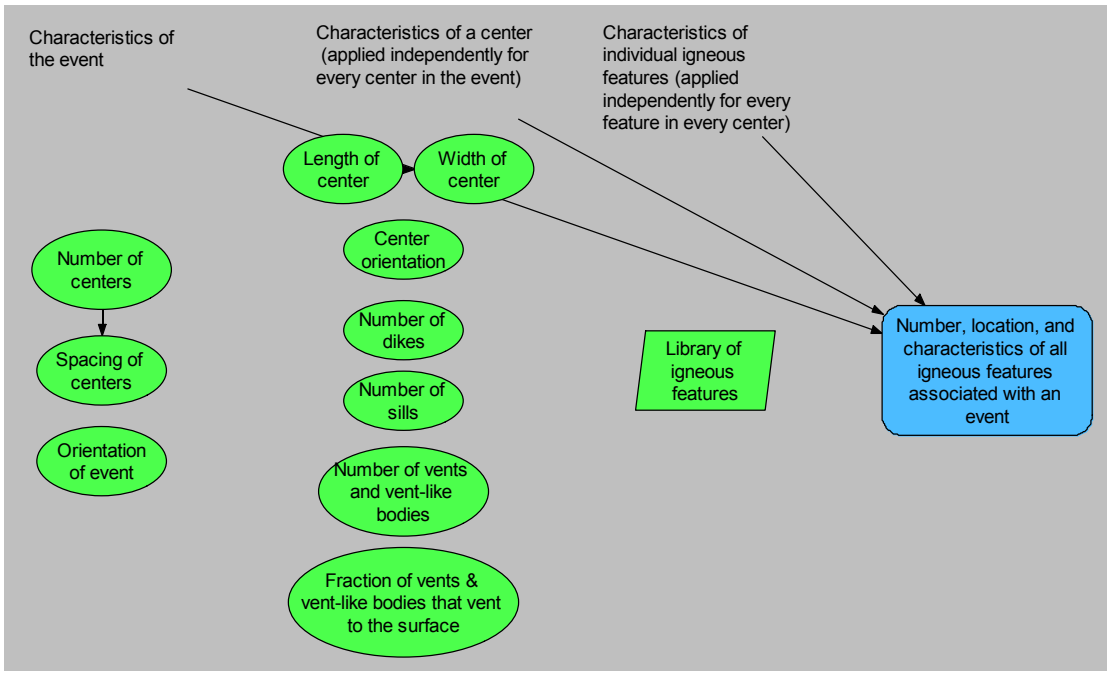

NOTE: Events are characterized by the number, spacing, and orientation of centers, as shown in the first column of green ovals. Centers are characterized by the variables in the second column of green ovals. The characteristics of each igneous feature are drawn from a library of features derived from actual events in the San Rafael volcanic field, Utah. All variables are combined to generate the event description in the final blue rounded rectangle. Some variables are dependent on others (as indicated by the arrows), but most are independent.

Figure D.1-3. Sub-model of Characteristics of Events and Centers

D.1.4 EVENT DEFINITION

The term *igneous event* includes all features and processes associated with intrusion of magma into the shallowest part of the crust (a depth <1 km). In this analysis an event may include emplacement of igneous dikes (reaching at least repository level), development of volcanic vents, development of vent-like bodies (reaching at least repository level), and intrusion of sills (including sills emplaced below the level of the repository that might affect repository performance through degassing and deformation).

D.1.4.1 Definitions of Terms

The following volcanologic terms are used to describe igneous features and events throughout this analysis.

Dike

A dike is a sheet-like igneous intrusion that cuts across older geologic strata and is most often vertical or sub-vertical (having a dip >80 degrees). Dikes transport magma, which in the YMR has a basaltic composition, toward the surface or laterally in fracture-like conduits. Magma cools within the fracture-like conduits, becoming igneous rock.

Dikes often occur in complex systems, sometimes called dike swarms. Individual dikes often appear as dike segments that form discontinuous features in outcrop. Occasionally, individual segments are not collinear, because dikes can follow locally complex structures as they ascend along low-energy flow paths, or rotate in response to changing stress. Individual dikes are on the order of one meter thick (commonly 10 cm to 5 m thick) and range in length from approximately 100 m to approximately 10 km. Where dikes and vent-like bodies are exposed together in outcrop, tens of dikes often are associated with a single vent or cluster of vents.

Vent or Vent-Like Body

A *vent* is a crater formed at the Earth's surface when material is emitted during explosive or effusive eruption or material collapses into the volcanic conduit. Vents often are circular, but may be highly elongate, reflecting the geometry of the underlying shallow conduit. Material that may be emitted from and/or collapse into a vent include pyroclasts, lava, and host rock.

Because by definition vents are found at the surface, the term does not capture the subsurface character of conduits beneath vents. The term *vent-like bodies* is used to refer to the subsurface equivalent of vents. Some vent-like bodies do not form vents at the surface, as observed in the San Rafael volcanic field, Utah. Although such structures have vent-like planimetric outlines, there is no evidence of sustained flow within a conduit. Vent-like bodies include textural features, such as small fragments of country rock, which are unaltered in a matrix of basalt. These are the "breccia bodies" of Delaney and Gartner (1997), but unlike true breccias, many of them consist of more than 50 percent basalt by volume. Areas intruded by such bodies are disrupted completely and replaced by either basaltic magma or brecciated wall rock. Ignimbrite blocks in the Lathrop Wells cinder cone (Doubik and Hill, 1999) are evidence that similar conduit processes operate during volcanic eruptions in the YMR.

Sill

Sills are tabular igneous intrusions that form parallel to bedding planes in the host rock. Sills are common in eroded basaltic volcanic fields, such as the San Rafael field and Miocene centers in the YMR. Because local stress fields change during episodes of volcanic activity, conditions may develop that favor the injection of sills rather than dikes. Subtle changes in rock properties may also result in sill development. Sills often cover tens of square kilometers in planimetric area and commonly are meters thick (generally <10 m thick). In the field, sills and dikes often are observed to have complex relationships. Dikes feed sills, and sills feed dikes and vent-like bodies, forming a network of igneous intrusions in the subsurface.

Volcano

A *volcano* is a naturally occurring vent or fissure at the Earth's surface, through which molten, gaseous, and solid materials erupt. Among the many types of volcanoes are the monogenetic volcanoes of the YMR. Monogenic volcanoes are formed during relatively brief (e.g., <100-year) eruptive episodes that build relatively small-volume (e.g., <0.1 km^3) volcanoes and lava flow fields. When eruptive activities cease at a monogenetic volcano, it is thought not to reactivate. Rather, future volcanic activity occurs at a new monogenetic volcano.

Center

The term *center* describes spatially associated dikes, sills, vents, and vent-like bodies that occur along an alignment (described below). An igneous event comprises one or more centers.

D.1.4.2 Characteristics of Igneous Events

The igneous features described above together make up an igneous event. For our purposes, an igneous event begins with the ascent of magma through the lithosphere. Magmas ascend in response to buoyancy forces that result from the density contrast between the comparatively cold and rigid rock of the crust and the hot ascending magma. The viscosity of magma and the rheology of the host rock dictate the mechanisms that govern the ascent of magma.

Basaltic magmas most often ascend through the crust inside vertical planar fractures (dikes). Studies of the seismic swarms and deformations that preceded eruptions of the Kilauea volcano, Hawaii, and the Krafla and Hekla volcanoes, Iceland, reveal dike ascent velocities of 0.5 to 3 m s^{-1} in the shallow crust (Aki et al., 1977; Einarsson and Brandsdóttir, 1980; Linde et al., 1993). Studies of xenoliths in alkaline lavas (e.g., Spera, 1984) indicate that minimum ascent velocities for mantle-derived dikes range from 0.001 to 10 m s^{-1}.

Igneous events may involve the ascent of more than one dike through the lithosphere. Because subsequent dikes encounter different stresses, their paths of ascent may differ from that of the original dike. This effect further distributes volcanic features and centers associated with individual igneous events as those events develop over time.

In the lower ductile crust, basaltic dikes ascend parallel to the maximum horizontal compressional stress. Several factors affect their ascent through the brittle crust. First, stress orientation may rotate. If so, the dike also rotates, thereby breaking into segments. Individual

bladed segments then continue to rise toward the surface. Bladed segments that reach the surface can erupt and form an alignment of vents. In the YMR, this process is reflected in the formation of NE-trending alignments of cinder cones (Quaternary Crater Flat and Sleeping Butte) and magnetic anomalies interpreted to be vent alignments (the three northeast-trending magnetic anomalies south of Lathrop Wells. The longest such alignment in the YMR reaches a length of approximately 11 km. Even longer alignments occur in other volcanic fields. As defined above, the term *center* is used to describe spatially associated dikes, sills, and vent-like bodies that occur along such alignments. An igneous event comprises one or more centers.

As dikes rise into the brittle crust, they encounter faults. If the stress required to dilate the fault is less than the minimum horizontal compressional stress, the dike's path of ascent may change to follow the fault. In the YMR, dikes at repository depth are assumed to trend predominantly roughly N-S, parallel to geologic structures in the area. Evidence for a predominant N-S trend includes the orientation of mapped Pliocene dikes in Crater Flat; the orientation of the Solitario Canyon fault and dike segments along and near this fault; the orientation of closely spaced vent alignments at Thirsty Mesa; the close association of Northern Cone with N-S-trending faults and magnetic anomalies (interpreted to represent faults cross-cutting this cone); and the elongate NNW nature of the Lathrop Wells cinder cone and the oxidized zone within this cone. Thus, although events in the YMR are aligned N30°E overall, igneous features that are part of the events have predominantly N-S trends.

D.1.4.3 Characteristics of Igneous Events Past Events in the Region

It is critical to ascertain which geologic features represent independent events. Great earthquakes, for example, are followed by aftershocks. An earthquake aftershock, however, is not the same type of event as a great earthquake. Thus the distribution of aftershocks may not give the best sense of the spatial intensity of great earthquakes, although the two are correlated.

Similarly, volcanoes are complex geologic structures. In monogenetic volcanic fields such as the YMR, alignments of volcanic cones often reflect single igneous events. As each individual igneous dike ascends, it might form segments that rotate within the shallow crust, each segment potentially feeding a separate vent and potentially building a volcanic cone. If the goal of analysis is to forecast the distribution of future igneous events, each of which might produce more than one monogenetic volcano, geologic data must be gathered that can group volcanoes formed by the same igneous event.

It is difficult to determine the independence of events in the YMR. Rather than simply counting volcanoes on a geologic map, one must assess the independence of the data, generally through detailed analyses of radiometric ages, stratigraphic correlations, and related geologic data. Even detailed analyses often do not resolve whether specific features should be grouped as a single event or treated as separate, independent events. Uncertainties inherent in radiometric age determinations, for example, make it difficult to resolve whether the Little Cones of Crater Flat represent an independent event that produced two volcanoes, or are part of the greater Crater Flat alignment that includes Red Cone, Black Cone, and Northern Cone.

Extensive radiometric age-dating indicates that some volcanoes (e.g., Quaternary Crater Flat, Quaternary Sleeping Butte, and Pliocene Crater Flat) should be grouped into single events that

include numerous eruptions over a comparatively short period. I follow this logic to group such volcanoes into independent (single) events for this analysis. Grouping igneous features into independent events is more problematic in the Amargosa Desert, where most volcanic features are interpreted from undrilled aeromagnetic anomalies. Because three closely spaced, NE-trending aeromagnetic anomalies south of Lathrop Wells form an alignment, they are grouped as a single event comprising at least three volcanoes. Other magnetic anomalies in the Amargosa Desert, including the drilled Anomaly B and undrilled Anomalies C, D, and E, are each considered independent events. In total, 11 independent Plio-Quaternary events are identified in this area (Figure D.1-1, Table D.1-1). I refer to these events as the YMR data set.

Table D.1-1. Relevant Events in the YMR

Event	Number of Centers	Age (Ma)
Lathrop Wells	1	0.08
Sleeping Butte	2	0.35
Quaternary Crater Flat	4 or 5	1.1
Buckboard Mesa	1	2.9
3 anomalies in a NE-trending alignment south of Lathrop Wells	3	3.8
Pliocene Crater Flat	1	3.8
Anomaly B	1	3.9
Anomaly C	1 to 2 (see note)	3.8 to 5.8
Anomaly D	1 to 2 (see note)	
Anomaly E	1 to 2 (see note)	
Thirsty Mesa	1	4.7

NOTE: More work could be done to determine the total number of associated vents and centers for each of these three magnetic anomalies. Uncertainty increases for older events because (1) some of them are buried, and (2) uncertainties in radiometric age determinations are greater, primarily because fewer age determinations have been gathered with the goal of differentiating centers. Each anomaly could represent a single center, or could indicate a multi-center event. It is unlikely any of them represent a three-center or larger event.

Table D.1-1 shows how I group volcanoes in the YMR into independent igneous events. Each past event is characterized by the number of centers and by its age. There are multiple interpretations of the number of centers for some past events, as shown in the table. For example, Quaternary Crater Flat can be considered to comprise either (1) four centers, with Red Cone, Black Cone, and Northern Cone each representing a center and the Little Cones interpreted to be a single center having two vents, or (2) five centers, with each of the two Little Cones interpreted as representing a separate center.

Smith et al. (1997) and others have argued reasonably that, based on the isotope geochemistry of basalts, the area of YMR volcanism should encompass a wider region, including Death Valley and the Greenwater Range. This larger area, termed the Amargosa Valley Isotopic Province (AVIP), displays volcanism that appears to be dominated by lithospheric melts, as opposed to the asthenoshperic melts that predominate in volcanic fields to the north and south (Yogodzinski et al., 1996; Smith et al., 1997; Valentine and Perry, 2007). Consequently, I use a second data set derived from past events in the AVIP: it includes all mapped vents in the YMR plus all known Plio-Quaternary events in Death Valley and the Greenwater Range (I refer to this as the AVIP

data set). Because radiometric age determinations are few in the Greenwater Range, it is impossible to group vents in that area into events as was done for the YMR data set. Consequently, the AVIP data set consists of the location of all Pliocene-Quaternary vents (Figure D.1-1).

Table D.1-2 shows the estimated age and number of centers for each of the three Quaternary events in the AVIP. The vents in the Greenwater Range, which are older and less well characterized than events in the YMR, are not shown in the table.

Table D.1-2. Quaternary Events in the AVIP Region of Interest

Event	Number of Centers	Age (Ma)
Ubehebe	1	0.006
Split Cone	1	0.3
Shoreline Butte	1	0.7

D.1.4.4 A Simulator for Future Events

Investigations of the subsurface structures associated with eroded vents in basaltic volcanic fields reveal complex igneous features. Basaltic conduits are revealed in awesome detail in the San Rafael volcanic field (Figures D.1-4 through D.1-6). In this Pliocene volcanic field, more than 60 conduits occur in outcrops near more than 1,700 dike segments (Delaney and Gartner, 1997). Rapid erosion of the sedimentary host rocks has placed the sub-volcanic intrusive structures in stark relief. Based on detailed stratigraphic analysis, the depth of exposure of these conduits is estimated to range from 500 to 2,000 m (Delaney and Gartner, 1997). Magma compositions reflect a typical intraplate alkaline basalt. High water contents are suggested by magmatic biotite and related geochemical and physical features. Those characteristics indicate that the conduit outcrops in the San Rafael field probably represent the bubbly flow region of a volcano conduit. In some areas conduits are close to the fragmentation level (or fragmentation zone), as indicated by vesicle content and vesicle size. In other words, the conduits are reasonably representative of what would be found at volcanic vents at repository depths in the YMR.

Field work in the San Rafael field demonstrates that those volcano conduits bear little resemblance to the “circular tubes” invoked in some models. Outcrops reveal complex zones or boundary layers within conduits (Figures D.1-4 through D.1-6). The various zones are characterized by variations in: (1) abundance of xenoliths derived from the local sedimentary section, (2) bubble density and size, (3) bubble elongation, and possibly (4) distribution of crystal sizes. In other words, in horizontal section each conduit is characterized by dramatically variable rheology. In addition, preliminary mapping reveals that development of conduits is coupled with deformation in the surrounding wall rock. Some conduits are surrounded by wall rock that is fractured on concentric planes tangential to the conduit wall. Elsewhere, for instance at the margins of a conduit, we can observe “micro-dikes” that may be several millimeters wide injected into individual sedimentary xenoliths. This diverse set of features results from changes in conduit pressure relative to lithostatic pressure, with low conduit pressure indicated by tangential fractures, and high conduit pressure indicated by radial magma-filled fractures. Most conduit walls are characterized by abrupt contacts, indicating that erosion of the surrounding

rock during conduit formation is brittle rather than associated with ductile flow or widespread melting.

Some, but not all, conduits occur along relatively long dikes, most commonly at the offset between individual dike segments (Figure D.1-6). Rarely is dike width observed to change close to a conduit. Rather, the conduit grows over the dike. Some conduits appear to be transitional from bulges (buds, in the terminology of Delaney and colleagues) along dikes; others have diameters that reach hundreds of meters. In the San Rafael volcanic field, vent areas range from about 1,000 to about 40,000 m^2.

NOTE: Based on stratigraphy and topographic reconstruction, the vents have been eroded to a depth of approximately 800 m. This alignment consists of six vents (dark rocks, sometimes obscured by sandstone screens), each >50 m in diameter. These features serve as analogs for the characteristics of igneous events in the YMR.

Figure D.1-4. Basaltic Vents in the San Rafael Volcanic Field, Utah

NOTE: Note the transition from basalt containing rare xenoliths (right), to xenolith-rich conduit fill (left). Such complex breccia zones are common in conduits beneath vents.

Figure D.1-5. Close-up of the Margins of a Conduit

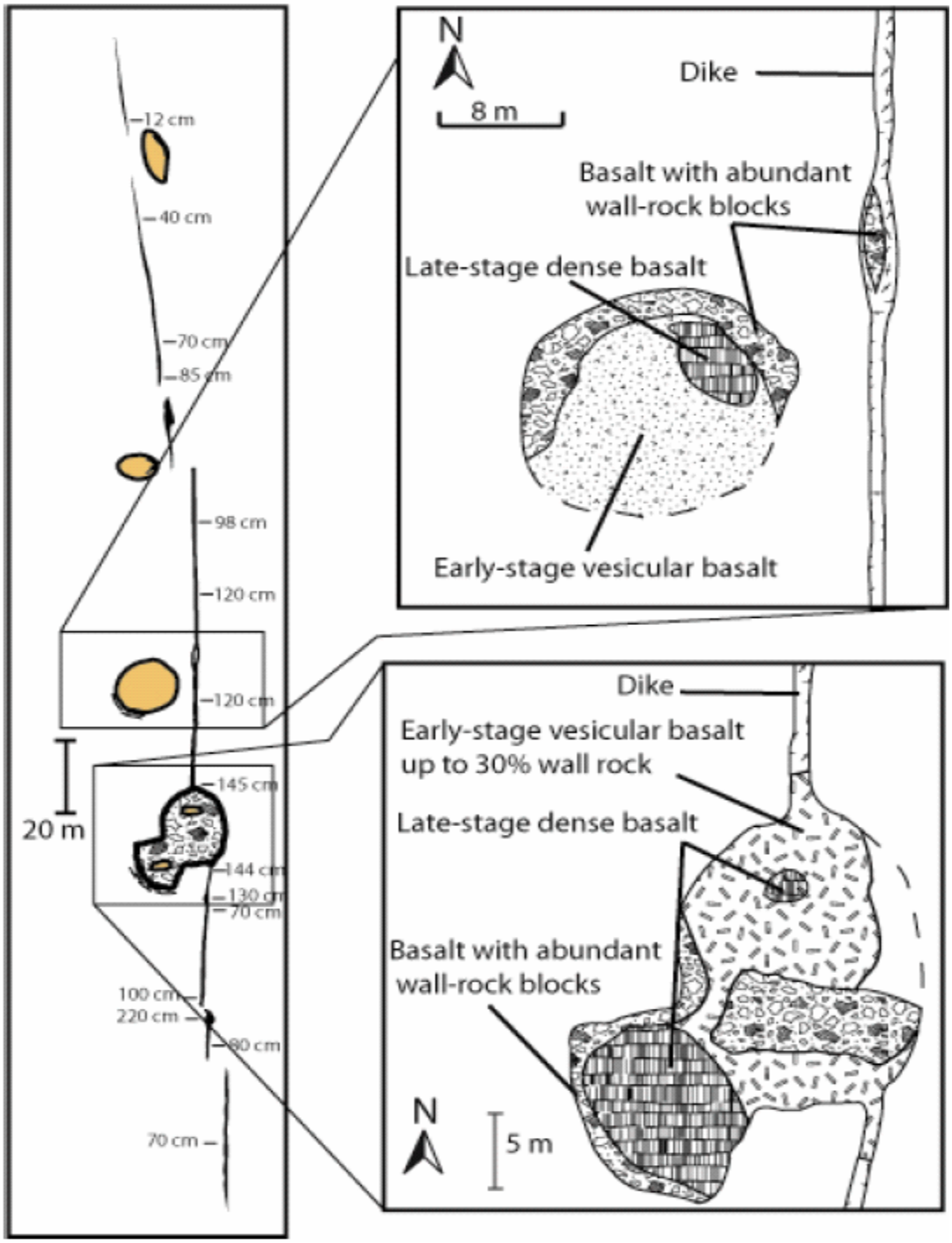

NOTE: These and other data reveal the geometric complexity of volcanic structures.

Figure D.1-6. Map of a Vent and Dike System in the San Rafael Volcanic Field, Utah

Given the above descriptions, igneous events cannot be modeled using simple circular zones and single, long rectangles of fixed width. To capture the complexity of real igneous events, I developed an event simulator based on a library of mapped igneous features. This library of dike, vent, and sill geometries is derived from geologic maps and new mapping in the well-exposed San Rafael volcanic field. The library comprises geologic data derived from 93 mapped dikes, 38 mapped vents, and 3 mapped sills. After comparing this library with the sparse dike and sill data collected in the YMR and published data on dike and sill dimensions, I consider the library to be representative of monogenetic fields generally, and volcanism in the YMR in particular.

The event simulator generates a random event, defined by the number and location of igneous features and based on the assessments described below. These assessments are intended to reflect major characteristics of basaltic volcanism in the YMR. Supplement A provides details of the event simulator process.

The event simulator incorporates the following assessments and general characteristics of what future igneous events in the YMR might look like.

- Igneous events may comprise one or more centers.
- Centers associated with individual events are distributed along N30E-trending alignments, parallel to the regional maximum horizontal compressional stress.
- Dikes segment and rotate as they rise in the shallow crust. Dike trends in the shallow crust, which may be oblique to regional maximum horizontal compressional stress, will tend to be oriented approximately N-S.
- Dikes may extend far from vent areas (as far as 10 km has been mapped in the San Rafael field).
- Dike orientations are roughly consistent with regional structural patterns (that is, they follow joints and faults), but occasionally are oblique to those patterns.
- Most igneous events include multiple dikes.
- Most igneous events include multiple vent-like bodies, which usually are distributed along one or more dikes and found most commonly at dike offsets.
- Not all vent-like bodies sustain flow or build scoria cones at the surface.
- Vent-like bodies develop complex zones of interaction with adjacent wall rock, often involving areas >100 m in diameter.
- Although sills may occur in an igneous event, they are much less likely.

Parameters Used in the Event Simulator

Estimates of specific parameters used in the event simulator are described below and summarized in Tables D.1-3 and D.1-4.

Number of Centers per Event. The number of centers in each past event, as described above and summarized in Tables D.1-1 and D.1-2, provides the basis for developing a probability distribution for the number of centers in a potential future event. An event comprises between one and five centers. Table D.1-3 shows my assessment of the number of centers per event to be used with each of the two data sets.

Table D.1-3. Distribution of Number of Centers per Event

Number of Centers	YMR Data Set	AVIP Data Set
1	0.375	0.733
2	0.25	0.067
3	0.125	0.067
4	0.125	0.067
5	0.125	0.066

For the YMR data set, the distribution is based on the assumption that 3 of the 8 YMR events (Buckboard Mesa, Lathrop Wells, and Pliocene Crater Flat) consist of a single center, and that having two centers per event is more likely than having three or more centers. This assumption is made because the buried and undrilled aeromagnetic anomalies (C, D, and E) likely comprise fewer than three centers each. Because the AVIP data set is based on vent locations rather than more aggregated events, the distributions for the number of centers per event for models based on that data set is more heavily weighted towards one center per event, but allows for the possibility of multiple-center events.

Spacing of Centers. The spacing between centers in an event is evaluated based on the spacing of volcanoes in the YMR. If the number of centers in an event is two, the linear distance between the two centers is given by a uniform distribution [1,000 m; 5,000 m]. If the number of centers in an event is three, the distance between the two end-point centers is given by a uniform distribution [3,000 m; 7,000 m], and the third center is located randomly between the two end points. If the number of centers in the event is four, the distance between the two end-point centers is given by a uniform distribution [4,000 m; 11,000 m], and the third and fourth centers are located randomly between the two end points. If the number of centers in the event is five or six, the distance between the two end-point centers is given by a uniform distribution [6,000 m; 13,000 m], and the third, fourth, and fifth centers are located randomly between the two end points. In any multiple-center events, all centers are aligned N30°E. These distributions are based on the geometries of mapped features in the YMR and similar basaltic volcanic fields.

Dimensions of a Center. Each center is modeled as having a rectangular area in which lie the midpoints of all of the center's igneous features. Centers are assigned dimensions according to the following distributions.

- Length: half-normal distribution [600 m; 2,000 m] (a normal distribution truncated to the left of the mean)

- Width: half-normal distribution [100 m; 1,000 m] (width must be less than length)

- Orientation: north-south.

Individual dikes and vents may extend outside the area of the center, but the midpoint or center of mass of each igneous feature is inside the area. Features are placed in the center as described below. These dimensions enable us to distribute volcanic features within a center in a manner consistent with the distribution of those features in the San Rafael volcanic field. This distribution is thought to be analogous with subsurface features in the YMR.

Features within Centers

The event simulator assigns the following characteristics to features in igneous centers.

Number of Vents and Vent-like Bodies. There are between zero and six vents and vent-like bodies per center, with equal likelihoods. The maximum observed in the YMR is approximately five (Pliocene Crater Flat and Thirsty Mesa), fewer than for some centers in the San Rafael basin. Although the volcanic record makes it difficult to distinguish between vents (which may be observed at the surface) and vent-like bodies (which lie underground), probably only 25 to 30 percent of the features in the YMR vented to the surface.

Number of Dikes. This distribution is half-normal [1; 5], rounded to the nearest integer value. There is at least one dike per center.

Number of Sills. The frequency of sill formation in the YMR is unknown, but sills are present at the Miocene Pauite Ridge. Drilling indicates that magnetic Anomaly A likely is a sill. Other sills may be present, for example at magnetic Anomalies C or D. I judge sills in future events to be possible but much less likely than igneous events without sills. The number of sills in an event is modeled as exponential [0; 0.167], rounded to the nearest integer. This means that 95% of centers will have no sills; 4.98% will have one sill; and 0.02% will have two sills.

Observations in many volcanic fields indicate that vents are not associated randomly with dike swarms, but tend to cluster on specific dikes or closely spaced dike sets. To model this phenomenon in the simulator, vents are placed preferentially at dike nodes along one or more dikes in the event. Vents are placed at dike nodes, because vents often occur at the tips of individual dike segments, such as at offsets in en echelon sets of closely spaced dikes. Sills are similarly located at dike nodes. At the spatial scale of the event library, dike nodes represent these features (tips of individual segments and offsets in en echelon sets of closely spaced dikes).

Based on these assessments, the minimum center consists of one dike, no vents, no vent-like bodies, and no sills. A center could consist of 10 dikes (95th percentile of the distribution of number of dikes); 6 vents and vent-like bodies, of which 2 can be assumed to vent to the surface; and 1 sill (95th percentile of the distribution of number of sills).

Table D.1-4. Summary of Event Characteristics

Geologic Feature	Statistical Distribution	Estimated Parameters	Notes
Dimensions of a center	Half-normal	(1) N-S dimension: mean = 600 m, standard deviation = 2,000 m (2) E-W dimension: mean =100 m, Standard deviation = 1,000 m N-S dimension must exceed E-W dimension	Igneous features may extend beyond a center, but their origins lie within the area of each center defined by a rectangle.
Separation between outermost centers	Uniform	If two centers: minimum = 1 km, maximum = 5 km If three centers: minimum = 3 km, maximum = 7 km If four centers: minimum = 4 km, maximum = 11 km If five centers: minimum = 6 km, maximum = 13 km	All centers are aligned N30°E. If more than two centers, outermost centers are assumed to be placed at a distance given by the distribution in the previous columns; any remaining centers are placed randomly between the outermost centers.
Number of dikes per center	Half-normal, rounded to nearest integer	Mean = 1 Standard deviation = 5	At least one dike must occur in each center.
Number of vents or vent-like bodies per center	Uniform	Minimum = 0 Maximum = 6	Geologic mapping indicates not all vent-like bodies sustain eruptions at the surface (e.g., build cinder cones). Vents are distributed along dikes.
Number of sills per center	Exponential distribution, rounded to nearest integer	Rate parameter = 0.167	Approximately 1 in 30 centers will have a sill.

Vent, Dike, and Sill Geometry

Rather than define the geometry of specific igneous features, I developed a library of dike, vent, and sill geometries derived from geologic maps and new mapping in the well-exposed San Rafael volcanic field in Utah. This library, which comprises 93 mapped dikes, 38 mapped vents, and 3 mapped sills, defines my assessment of the characteristics of the individual dikes, vents, vent-like bodies, and sills in any modeled center. The library is used directly in modeling, and the data defining dikes, vents and vent-like bodies, and sills is included as Supplement D. For example, to model any dike in an event, one is selected randomly from the library of 93 dikes, thereby determining its length, segmentation, and orientation. When multiple dikes are selected, each dike is selected randomly from the event library and drawn on the map. The same procedure is followed for vents and sills. The simulator can create millions of different events, each within a specified range of features that is geologically realistic and strongly linked to the characteristics of mapped igneous intrusions. In the libraries of dike, vent and sill geometries, dikes and elongated vent bodies were rotated from the primarily NNW trends in the San Rafael volcanic field to primarily N-S trends, consistent with mapped dikes and fault orientations in the YMR.

In this analysis, sill dimensions are consistent with small mapped sills in the San Rafael region and at Paiute Ridge and with inferred dimensions of a sill at Anomaly A. All the sills used in the simulations were emplaced at depths of less than one kilometer. It is assumed that a sill

emplaced in the upper one kilometer of crust near the proposed repository would impact its performance adversely. Assuming that sills are randomly distributed vertically, approximately one-third of sills would reach repository depth. In many volcanic fields where sills are exposed by erosion, however, stacked sills are observed. Thus, I assumed that 50% of sills would reach repository depth and result in magmatic intrusion, and 50% of sills would not intersect the repository directly, but would result in indirect effects.

Intensity of Eruptions and Column-Producing Conduits

During explosive volcanism, such as the violent Strombolian activity often observed to accompany the construction of cinder cones, muzzle velocities at the vent often range from 70 to 120 m s^{-1}. During such eruptions, continuous flows of magma through the vent can occur in a quasi-steady state and persist for hours, such as observed during the 1943 to 1952 eruption of Parícutin cinder cone (Mexico); the 1975 eruption of Tolbachik cinder cone (Russia); and the 1968, 1971, and 1992 eruptions of Cerro Negro cinder cone, Nicaragua (Figure D.1-7). Eruptive activity often pulsates, whereby individual explosions, spaced a few seconds apart, achieve high muzzle velocities for a few seconds (Figure D.1-8). Such pulsating behavior at cinder cones has been observed to last for weeks.

NOTE: The cinder cone is visible at the base of the ~5-km-high eruption column. During this activity, blocks as large as 1 m in diameter (mass on the order of 1,000 kg) were ejected from the vent at velocities of approximately 100 m s^{-1}. (Photo C. Connor.)

Figure D.1-7. Explosive, Violent Strombolian Activity at Cerro Negro Volcano in 1992

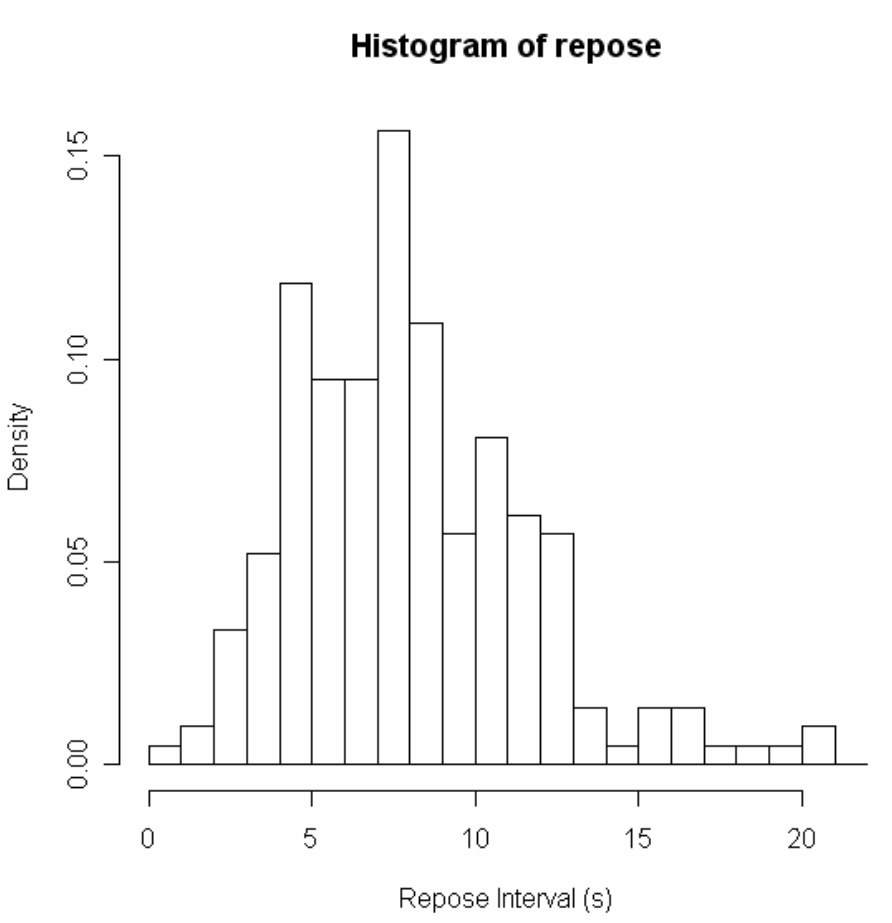

NOTE: Mean repose interval between explosions was about 8 seconds.

Figure D.1-8. Repose Intervals between Explosive Eruptions at a Vent on Cerro Negro Volcano during the 1992 Eruption

Cumulatively, explosive and effusive activity at individual vents may last for months to centuries. For example, a single vent was active for nine years during the eruption of Parícutin, and a single vent has been active intermittently at Cerro Negro volcano for more than 150 years. During the formation of a single cinder cone, multiple vents often are active, sometimes for short periods (e.g., <1 day). Multiple vents formed along a north-south trend at Cerro Negro, for example. In a 1999 eruption, two vents formed by emission of pyroclasts and lavas, while another vent formed by the collapse of material into the conduit. Those vents buried a similar vent formed in 1968. At Cerro Negro, other vents formed on other flanks of the volcano during eruptions in 1929, 1947, and other years. Similarly, at Parícutin and Jorullo volcanoes, Mexico, vents formed about the volcano intermittently throughout decade-long eruptions. Distributed vents associated with a single cinder cone can occur throughout several square kilometers.

The volcanologic literature is beginning to describe models that link surface observations of eruptions from basaltic vents with subsurface conditions (Figure D.1-9). The models provide a sense of the magnitude of disruption of the subsurface during explosive basaltic eruptions. For magmas that have 4% by weight volatiles and basaltic rheology, for example, ascent velocities at

repository depths are on the order of 80 m s^{-1}. Although such models give a sense of mass flow and velocity, they are simplifications.

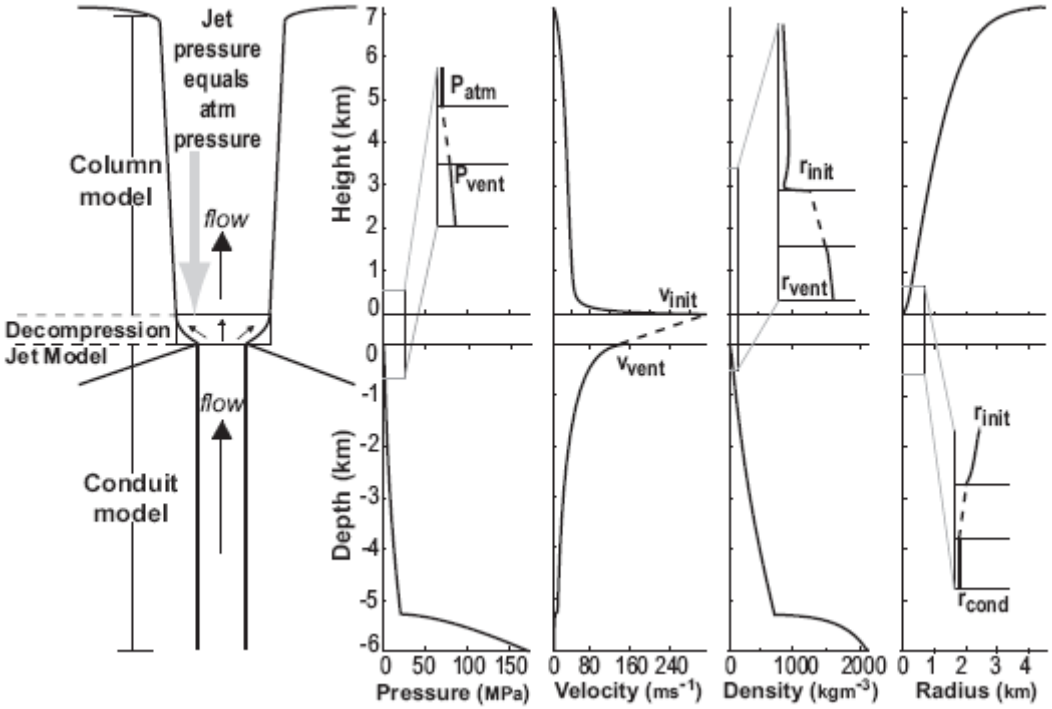

NOTE: Magma rheology and water content (initial volatile fraction of 4 wt %) is based on the 1992 eruption of Cerro Negro, which is believed to be similar to the 80 ka Lathrop Wells eruption.

Figure D.1-9. Association between Surface and Subsurface Processes at an Erupting Vent (based on Díez, 2006)

Quaternary volcanic events in the area surrounding Yucca Mountain reflect a range of Strombolian to violent Strombolian eruptions. My assessment is that potential future eruptions would be Strombolian, in that 6 in 7 vents would produce a violent Strombolian eruption (having columns on the order of 7 to 12 km high). This ratio is consistent with observations in the YMR and other Basin and Range volcanic fields. In any center, one vent is primary and is likely to be a column-producing conduit. For modeling purposes, the largest vent is assumed to be a column-producing conduit, although there is a small chance (about 1 in 7) that the eruption would not be of the violent Strombolian type. Hydromagmatic volcanoes, which are associated with shallow water tables, are unlikely in the repository area given the mountain block setting. If the repository were to become flooded with water, for example in response to climate change, dike injection could result in a hydromagmatic eruption.

D.1.3 SPATIAL MODELS

The following sections describe my consideration and development of a spatial model to describe potential future volcanism in the Yucca Mountain region (YMR).

D.1.3.1 Spatial Density

The goal of estimating spatial density in the context of volcanic hazard assessments is to estimate the likely locations of potential future igneous events, or the probability of an igneous event at a specific location, *given that such events occur* within a region of interest. The mathematical definitions of spatial density and spatial intensity are described further in Supplement B.

Assumptions behind Estimates

Developing a best estimate of spatial density is problematic because we have only one realization of the underlying statistical process—that is, the distribution of past volcanic events—and we cannot repeat geologic experiments in a natural system. Ideally, we would have a complete geophysical model for events. If we knew the distribution of melt in the asthenosphere and lithosphere, and knew the state of the lithosphere through which magma would rise, we could better predict where volcanoes likely will form next. We lack such a complete geophysical perspective, however. Some data, for example seismic tomographic models of "slowness" in the lithosphere and asthenosphere, give an idea of where partial melting of the mantle might occur (e.g., Zhao, 2001; Humphries, personal communication). Other data, such as variations in gravity (Connor et al., 2000; Parsons et al., 2006), show some correlation with the distribution of existing volcanoes in some circumstances, but we do not understand fully the mechanisms that relate gravity anomalies to the origin of magmas. As a result, although these types of data have been used to support estimates of spatial density (e.g., Connor et al., 2000; Martin et al., 2004), all proposed models rely principally on the spatial distribution of past events. Similarly, seismologists have attempted to create blended hazard maps based on a variety of geophysical criteria, but they generally rely on the earthquake catalog (e.g., Ward, 1994).

Relying on the distribution of past events implies that these realizations are representations of the underlying random variable, **X,** which will govern the distribution of potential future events. This assumption raises a fundamental question: which past events should we use to estimate the spatial intensity? In determining the appropriate event data sets to use for estimating the spatial density of future events, it is important to be consistent with several characteristics of geologic processes, as described below.

Changes over Time

On time scales of tens of millions of years, plate boundaries change, volcanic systems wax or wane, and the mantle is depleted. These factors must be considered when weighing the validity of using specific data to develop spatial intensity models for probabilistic hazard assessments, which may have to be applied to a period as long as one million years. We must consider which events best represent the distribution of potential future events. For processes such as volcanism, geologic records usually persist for tens of millions of years. The distribution of Miocene events in the YMR, however, might be much less relevant than the distribution of Pliocene and Quaternary volcanoes. Thus, estimating spatial intensity requires a model of the geologic evolution of the system. This geologic model is used to justify including some geologic features in the event data set, while excluding others.

In the YMR, clusters of igneous events appear to persist throughout many millions of years. Geophysical mapping and drilling by the U.S. Department of Energy (DOE) and others (e.g., Connor et al., 1997) has shown that the Crater Flat cluster has been the locus of volcanism since the Miocene. The 11.2-Ma (?) Solitario Canyon dike, for example, is part of the Crater Flat cluster (Connor and Hill, 1995), as are Miocene basalts in the Will Carr Hills of southern Crater Flat and igneous structures (sills?) that the DOE encountered when drilling in Crater Flat (magnetic Anomaly A). Volcanism in this cluster has persisted during the Pliocene and Quaternary. Similarly, in the Sleeping Butte area volcanism has occurred in the Miocene (Rocket Wash basalts), the Pliocene (Thirsty Mesa basalts), and the Quaternary (Hidden Cone and Little Black Peak cinder cone). In the Amargosa Desert, volcanism has occurred in the Quaternary (Lathrop Wells); the Pliocene (aeromagnetic Anomalies B, G, H, and I); and the Miocene (e.g., outcrops east of the "gravity fault"). In contrast, in parts of the YMR Miocene volcanism occurred without subsequent Plio-Quaternary activity (e.g., Paiute Mesa and Nye Canyon). Looking at the greater region, several areas have undergone extensive Pliocene volcanism without obvious correlation with the Miocene (e.g., the Greenwater Range). Based on this information, it makes sense to forecast the future distribution of igneous events based on the distribution of Pliocene and Quaternary volcanoes, as shown in Table D.1-1, but not on the distribution of Miocene volcanoes.

Completeness of Record

The geologic record of igneous events in the YMR might give an inaccurate estimate of the distribution of potential igneous events. Geologic investigations might not discover volcanic vents buried in sediment or otherwise obscured (e.g., Connor et al., 1997). Furthermore, we know that we are unlikely to detect igneous events that lack volcanic features but that intruded to the stratigraphic level of the proposed repository. The magnetic signature of a dike in ignimbrite, for example, is such that the dike will go undetected (Connor and Sanders, 1994).

In the YMR the possibility of undetected events has been evaluated using geophysical methods and a limited drilling program. Aeromagnetic surveys, sparked by earlier geophysical investigations (Langenheim et al., 1993; Connor et al., 1997), mapped the region of the northern Amargosa Desert, Crater Flat, Yucca Mountain, and Jackass Flats. Cumulatively, these surveys suggested many targets for further investigation (potential igneous features that lack outcrops). Several of those anomalies were drilled. Basalt was found in several of them, including aeromagnetic Anomaly A (Figure D.1-10), which appears to be a thick (>90 m), sill-like body. Several prominent magnetic anomalies in the Amargosa Desert were not drilled to evaluate their nature or age. For the purposes of estimating spatial density, I assume that the undrilled aeromagnetic anomalies are Pliocene basaltic volcanoes and that the aeromagnetic survey identified all Pliocene-Quaternary volcanic features in the survey area.

A major assumption underlying my estimate of spatial density is that the distribution of intrusive igneous features is described by the distribution of known volcanic features. This assumption is important because, as described below, the low number of volcanic events creates uncertainty in the estimate. One unidentified Pliocene igneous intrusion, for example in Jackass Flats, would change the spatial density estimate. Beyond the area of the aeromagnetic map, the distribution of igneous features is known only from surface outcrops (in the areas of the Greenwater Range,

southern Amargosa Desert, Sleeping Butte, and Death Valley). I assumed, therefore, that the distributions of igneous events in those areas are captured by the distributions of surface features.

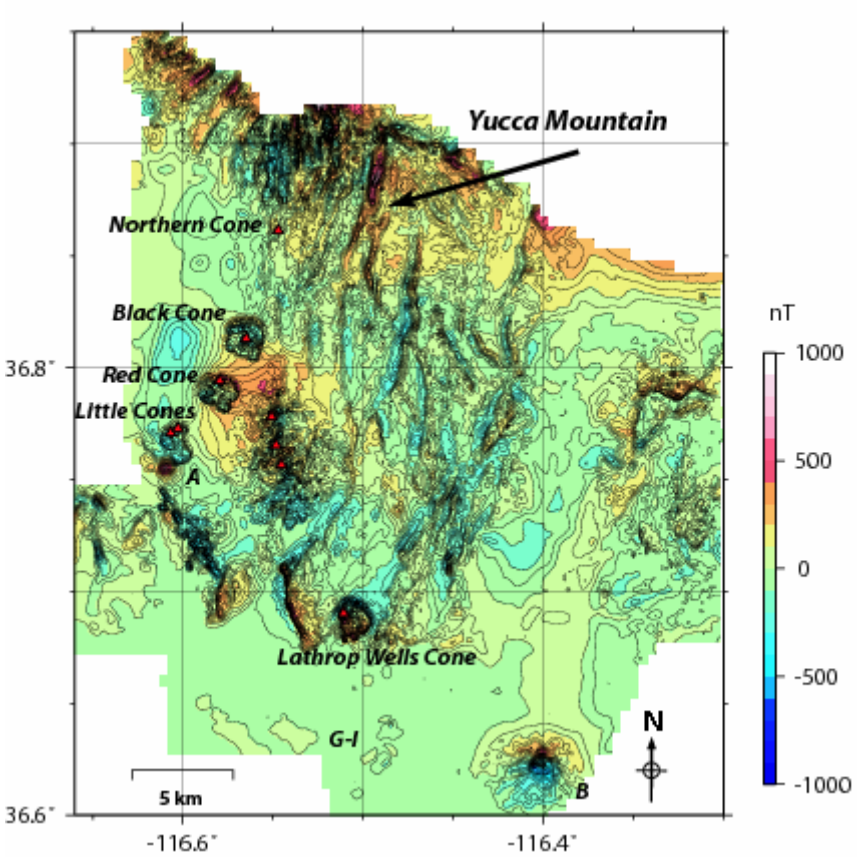

NOTE: Magnetic gradients on Yucca Mountain are too large to enable detection of dikes or related igneous features. Because the aeromagnetic survey was not flown over Anomalies C, D, E, or others in the Amargosa Desert, those anomalies could not be characterized fully.

Figure D.1-10. Volcanoes and Some Prominent Aeromagnetic Anomalies (A and B) Mapped in the YMR

Number of Events

Even when all igneous events are identified, they may be so few as to give an incomplete picture of the underlying geophysical processes that gave rise to them. Consider a single igneous event as X_n, a realization of a random variable, **X**. If **X** has a uniform random spatial distribution, the observed set of realizations likely will be distributed randomly throughout region R. The underlying density often has additional statistical structure, causing independent realizations to cluster. Volcano clustering in monogenetic volcanic fields is well documented in every tectonic setting on Earth (e.g., Connor, 1990; Connor and Conway, 2000; Weller et al., 2006, Jaquet and Carneil, 2006), presumably because such clusters form above zones of partial melting in the mantle. For random variables that have a great deal of statistical structure, such as many modes in spatial intensity, a great number of events might be required to identify the statistical structure of the random variable.

Volcanism in the YMR is relatively rare, even in comparison with other active monogenetic volcanic fields in the Western United States (Connor and Conway, 2000). Given the few known igneous events, one might miss statistical structure in the spatial intensity of volcanism. This uncertainty can be assessed, as done below, but cannot be eliminated from the analysis. In practical terms, because few events are used to construct the estimate, the spatial density is a smoothed representation of reality. Some areas of the YMR might have higher spatial intensity, and others lower, than estimated.

D.1.3.2 Alternative Models of Spatial Density

Spatial intensity models based on the distribution of past volcanic events might be either parametric or nonparametric, as described below.

Parametric Models

Parametric models involve fitting a distribution, usually one of a common set of distributions (e.g., uniform, random, or bivariate Gaussian), to the distribution of volcanoes throughout a region or within zones (subsets) of the region. This estimate yields a set of parameters, such as mean location of the volcanic field in northing and easting coordinates, variance in northing and easting coordinates, and rotation. Uncertainty in the fit of the distribution and in estimates of the spatial intensity parameters can be calculated using estimates of maximum likelihood. A significant drawback of the parametric method is that it assumes a priori that the distribution of volcanoes is explained by the parametric distribution, for example that volcano distribution is described reasonably as a bivariate Gaussian density. Such a distribution may not reflect reality. Parametric models may smooth completely the documented clustering of volcanoes within volcanic fields, for instance.

Nonparametric Models

A nonparametric approach to estimating spatial intensity involves estimating kernel density (Silverman, 1978, 1986; Diggle, 1985; Wand and Jones, 1995). This technique utilizes a kernel function and observed event locations to estimate the spatial intensity at any point in a region.

Implementing this approach requires two key judgments: what kernel function should be used, and what bandwidth, or smoothing distance, should be used. Nearly all kernel estimators used in geologic hazard assessment have relied on a symmetric Gaussian kernel function (e.g., Woo, 1996; Stock and Smith, 2002; Connor and Hill, 1995; Condit and Connor, 1996). The bandwidth used to calculate the spatial intensity function is selected based on some criterion, often visual smoothness of the resulting spatial intensity plots. Alternatively, in an adaptive kernel function, spatial intensity varies as a function of event spatial intensity (e.g., Stock and Smith, 2002; Weller et al., 2006). These adaptive kernel functions are radially symmetric.

I use a more general approach here, applying a bivariate Gaussian kernel and a bandwidth matrix fit to past events, which eliminates the requirement for radial symmetry. This kernel is described in Supplement C.

Estimating Bandwidth Matrix. A difficulty with elliptical kernel functions is the need to estimate all three unique elements of the bandwidth matrix (the bandwidth in the east direction,

the bandwidth in the north direction, and the rotation of the kernel). Several methods have been developed for estimating the optimal bandwidth matrix (e.g., Wand and Jones, 1995), most recently summarized in the statistics literature by Duong (2007). My analysis utilizes a modified asymptotic mean-integrated squared error (AMISE) bandwidth estimator developed by Duong and Hazelton (2003) and called the SAMSE pilot bandwidth selector. In addition, I utilize the smoothed cross-validation (SCV) scheme of Hall et al. (1992). These bandwidth estimators appear in the freely available R Project for Statistical Computing [found online in Hornik (2007) and described by Duong (2007)].

Four versions of this model were developed based on the two alternative data sets [data set for the YMR and data set for the Amargosa Valley Isotopic Province (AVIP)] and two alternative bandwidth estimators.

For the YMR data set (N = 11), the SAMSE bandwidth selector yields:

$$\mathbf{H} = \begin{bmatrix} 57.4 & -105.4 \\ -105.4 & 440.8 \end{bmatrix} \quad \text{(Eq. D.1-1)}$$

For comparison, the SCV bandwidth selector yields:

$$\mathbf{H} = \begin{bmatrix} 29.2 & -45.1 \\ -45.1 & 213.1 \end{bmatrix} \quad \text{(Eq. D.1-2)}$$

For the AVIP data set (N = 34), the SAMSE bandwidth selector yields:

$$\mathbf{H} = \begin{bmatrix} 27.4 & -10.89 \\ -10.9 & 165.1 \end{bmatrix} \quad \text{(Eq. D.1-3)}$$

And the SCV bandwidth selector for the AVIP data set yields:

$$\mathbf{H} = \begin{bmatrix} 36.9 & 15.6 \\ 15.6 & 432.8 \end{bmatrix} \quad \text{(Eq. D.1-4)}$$

Maps of these four different spatial density estimates are shown in Figure D.1-11. When only events identified in the YMR are considered, the SCV (Figure D.1-11(a)) and SAMSE (Figure D.1-11(b)) bandwidth selectors both produce maps showing predominant NNW trends, roughly parallel to the topographic expression of the Death Valley fault system and adjacent regional tectonic structures. This feature corresponds well with the Crater Flat volcanic zone defined by Crowe et al. (1983). The most prominent difference between Figure D.1-11(a) and (b) is that the mapped SAMSE results tend to create clusters, whereas the SCV map shows a smoother result. Given that clustering is a predominant feature of cinder cone volcanism, and of the YMR in particular (Connor and Hill, 1995), the map based on the SAMSE technique appears to better represent spatial density in the YMR.

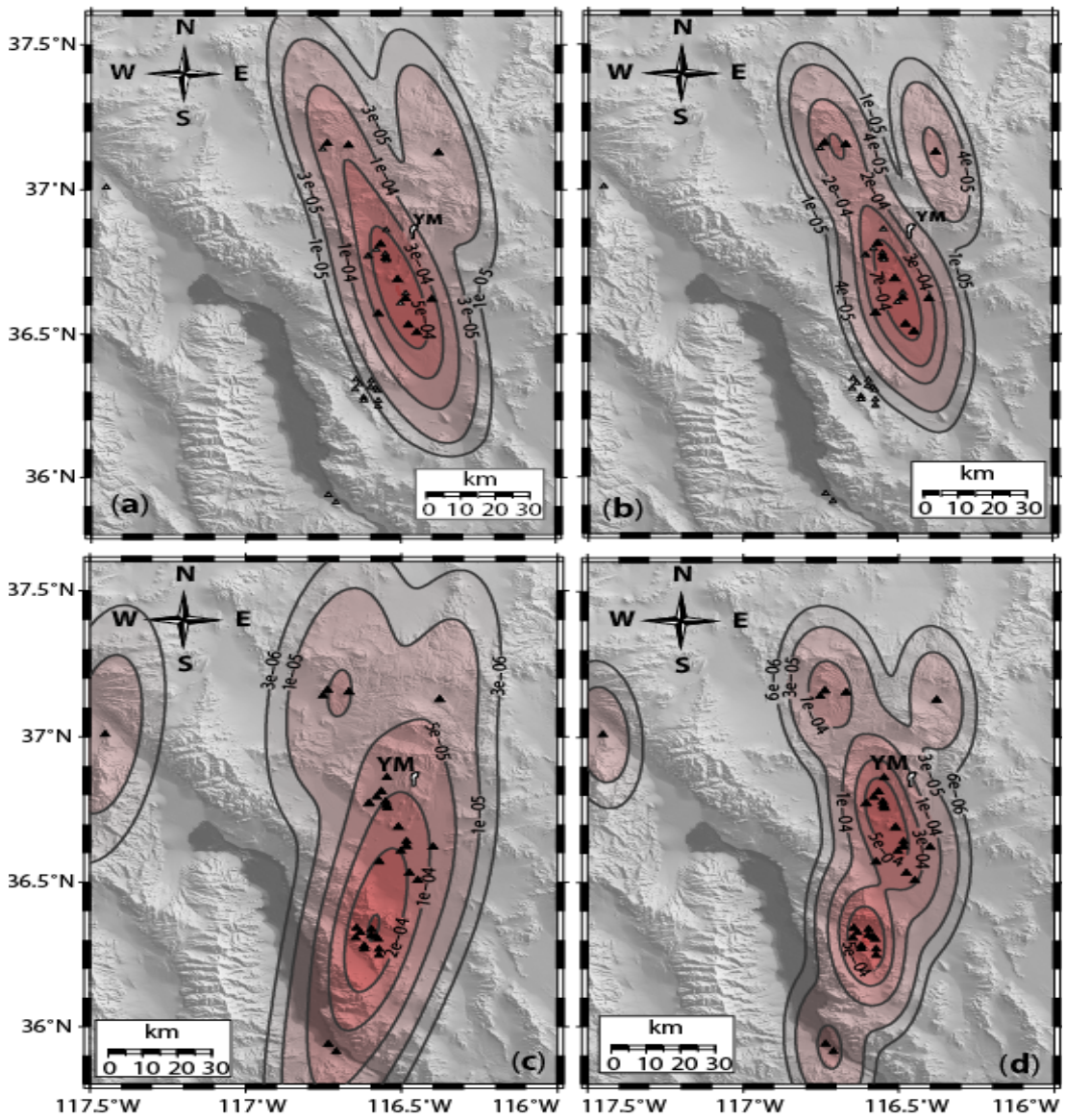

NOTE: Four estimates are shown, based on two data sets and two bandwidth estimators: (a) YMR data set and SCV bandwidth estimator, (b) YMR data set and SAMSE bandwidth estimator, (c) AVIP data set with SCV bandwidth estimator, and (d) AVIP data set with SAMSE bandwidth estimator. Contours are drawn at the 25th, 50th, 75th, 95th, and 99th percentile boundaries. For example, on map (a), locations within the 1e-04 contour line (75th quartile) have a conditional spatial density greater than 1×10^{-4} km^{-2}. Given a volcanic event in the region, there is a 75% chance it will occur within this quartile contour, based on this estimate of spatial density.

Figure D.1-11. Conditional Spatial Density Estimates of Potential Volcanism in the Region of the Proposed Yucca Mountain Repository

The kernel functions, and the resulting pattern of spatial density, change when the AVIP data set is used (Figure D.1-11(c) and (d)). Now the trend of the map changes to NNE, reflecting the regional distribution of volcanism described by Yogodzinski et al. (1996) and colleagues. The Ubehebe crater, the westernmost vent shown in Figure D.1-1, is a spatial outlier, the occurrence of which is not well predicted by these spatial density models. As before, the SAMSE model

appears to reflect the clustering of events better than does the SCV kernel, which appears to over-smooth the spatial density.

Incorporating Geologic Data Sets. A potential disadvantage of kernel functions is that they are not sensitive to geologic boundaries. One might hope that a complete understanding of the regional geology would enable one to modify the density estimate derived from a mathematical function. In fact, Connor et al. (2000) and Martin et al. (2004) discuss various methods of weighting density estimates in light of geologic or geophysical information. Such weighting unfortunately relies on a subjective definition of the relationship between geologic observations and the locations of future events. Furthermore, geologic insight may not be consistent with event distributions. Musson (1997), for example, noted that epicenter distribution in the United Kingdom does not correlate well with known major geologic structures that would be expected to produce earthquakes. Thus, even if a zonation model is used in hazard assessment, kernel-based density estimates should be calculated and any discrepancies in the models considered.

For the YMR, Connor et al. (2000) proposed using gravity data to weight the spatial density estimates made using kernel functions. This analysis uses the same approach. Briefly, regional gravity data reveal that Pliocene-Quaternary volcanoes in the YMR generally are confined to the Amargosa Trough (Figure D.1-12). The Lathrop Wells cinder cone lies outside the Crater Flat topographic basin but, on the basis of gravity data, is located within the larger north-trending structural basin and at the margin of the prominent basement low in southernmost Crater Flat. Aeromagnetic anomalies in the Amargosa Valley (Langenheim, 1995; Langenheim et al., 1993), produced by buried Pliocene (?) basalts, also lie within or at the margins of the southern extension of this basin. The most voluminous of these buried basalts lies close to a north-trending gravity anomaly that marks the eastern edge of the Amargosa Valley alluvial basin in this area. In the YMR, only Miocene basalt is mapped outside of the trough.

An explanation for the occurrence of Pliocene-Quaternary basalt in the Amargosa Trough is that the Bare Mountain fault and related structures on the west side of the trough have created a contrast in crustal density sufficient to initiate small-volume decompression melting. Decompression melting is favored in zones of enriched mantle lithosphere (Farmer et al., 1989; Leeman and Fitton, 1989; Lachenbruch and Morgan, 1990; Pedersen and Ro, 1992; Bergantz and Dawes, 1994; Hawkesworth et al., 1995), such as the YMR, that previously were enriched in incompatible elements, enabling melt to form at lower temperatures than is possible in normal or depleted mantle (McKenzie and Bickle, 1988; Yogodzinski and Smith, 1995). Based on mineralogical phase relationships and geochemical studies, decompression-induced partial melting of enriched lithospheric mantle likely occurs at depths between 40 and 80 km in the western Great Basin (Takahashi and Kushiro, 1983; Rogers et al., 1995). In stark contrast to the depth at which decompression generates melt, crustal extension most strongly influences the upper brittle crust (depth of <15 km) by producing large-density variations across faults. The direct link between crustal extension and magmatism relies on the possibility that extension produces density variations in the crust that are sufficient to initiate decompression melting much deeper within the mantle. Connor et al. (2000) used finite-element models to illustrate this mechanism and to propose that such density contrasts produce very small changes in pressure. Parsons et al. (2006) expanded on those ideas to suggest that one should use free-air gravity anomalies, rather than Bouguer gravity anomalies as used by Connor et al. (2000).

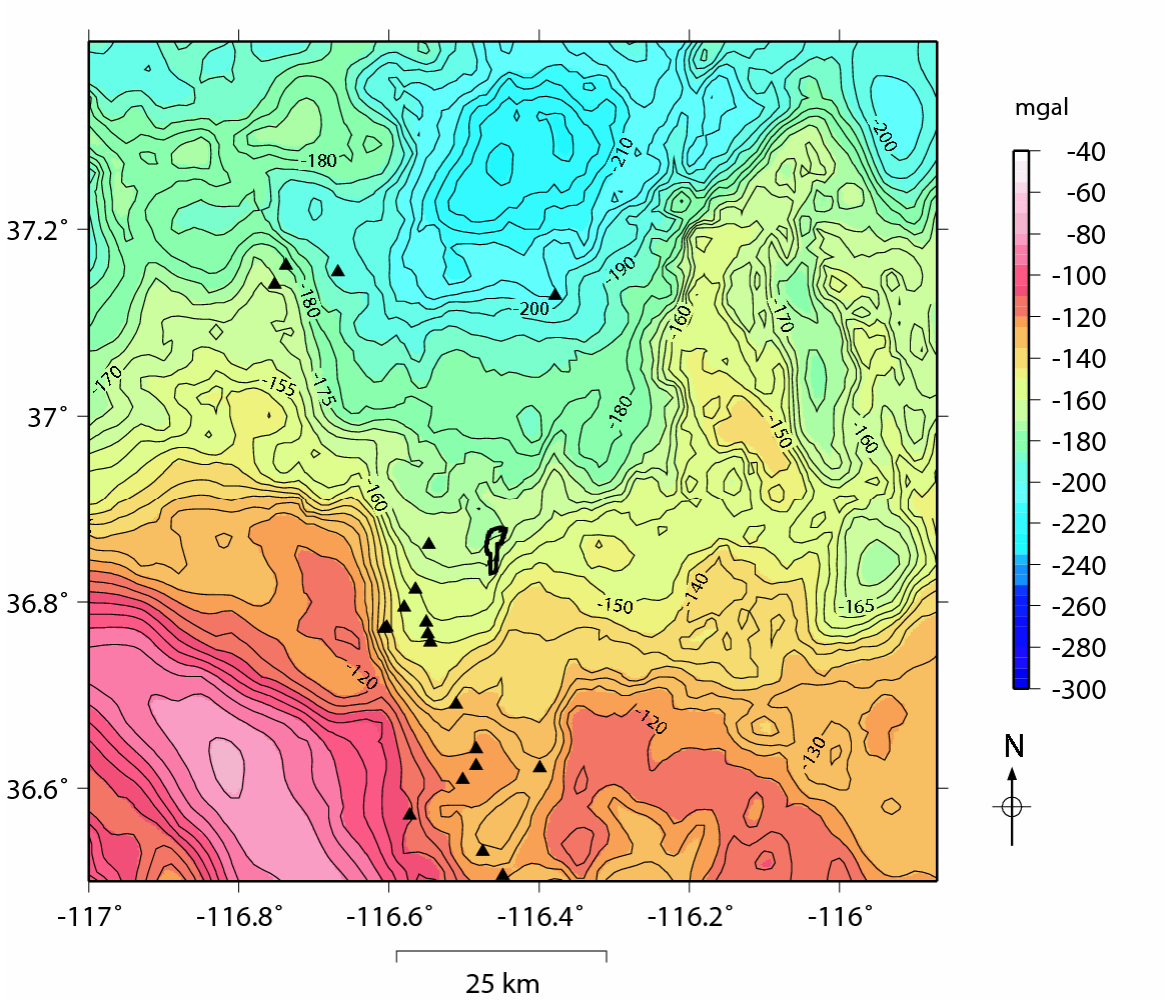

NOTE: Volcanoes generally occur in the Amargosa Trough, a north-trending region of low gravity values. Volcanism appears to be bounded on the west by the Bare Mountain fault (shown by the steep gravity gradient) and its extension south into the Amargosa Desert and north through the Sleeping Butte. Contour interval is 5 milligals. (Mercator projection, WGS84.)

Figure D.1-12. Bouguer Gravity Anomalies near Yucca Mountain (solid black outline) and Their Relationship to Pliocene and Quaternary Volcanoes (black triangles)

Using either Bouguer or free-air gravity data (which are linearly related), the question is how to transform gravity data into a probability density function that might be used to weight the spatial density map. This transformation is subjective. In this analysis the probability density function based on gravity data was constructed so that there is an abrupt transition in probability across the Bare Mountain fault.

My assessment of the weighting function for gravity data is based on consideration of the gravity values at locations across the YMR, where past events both have and have not occurred. The data are given in Table D.1-5, and my assessment shown in Table D.1-6.

Table D.1-5. Gravity Data: Number of Locations with and without Events

Mean Crustal Density (g/cm^3)		Locations with Events*	Locations without Events*
Low Value	High Value		
2.38	2.41	0	129
2.41	2.44	0	200
2.44	2.47	1	276
2.47	2.5	0	580
2.5	2.53	1	1,152
2.53	2.56	2	1,452
2.56	2.59	1	1,705
2.59	2.62	3	2,213
2.62	2.65	2	1,804
2.65	2.68	1	2,667
2.68	2.71	0	1,896
2.71	2.74	0	539
2.74	2.77	0	238
2.77	2.8	0	309
2.8	2.83	0	80
2.83	2.86	0	0
2.86	2.89	0	0
2.89	2.92	0	0
2.92	2.95	0	0
2.95	2.98	0	0

* Binned data on 1-km grid spacing. Crustal density values calculated from isostatic gravity data.

Table D.1-6. Weighting Function for Gravity Data

Cumulative Weight	Mean Crustal Density (g/cm^3)
0	>2.71
10%	<2.68
30%	<2.65
50%	<2.62
60%	<2.59
80%	<2.56
90%	<2.53
100%	<2.5

D.1.3.3 Uncertainty in Spatial Models

Uncertainty in estimates of spatial density stems from (1) the ambiguity in event data sets used to develop kernel estimates, (2) application of the kernel density function, (3) uncertainty in the bandwidth used to estimate the kernel density function, and (4) few event data. Uncertainty in event data sets was discussed previously; points (2) through (4) are considered below, in particular the uncertainty arising from sparse data.

Application of Kernel Functions

Estimates of spatial density made using kernel functions, as opposed to hazard zonation models (e.g., Crowe et al., 1983; Musson, 1997) or parametric models, are explicitly data driven. An advantage of using kernel functions is that spatial density estimates will be consistent with the known data. The model I selected above uses a bivariate Gaussian kernel. Numerous authors have shown that using a different kernel, such as Epanechnikov (Connor and Hill, 1995) or Cauchy (Martin et al., 2004), has little effect on the final density estimate (e.g., Silverman, 1986; Wand and Jones, 1995). Kernel functions that have infinite tails (e.g., Gaussian) are preferred in hazard assessments, because the probability is positive everywhere, albeit very small far from past events.

Uncertainty in Bandwidth

Selecting the bandwidth is key to estimating kernel density in general, and is particularly important in both seismic and volcanic hazard studies (e.g., Stock and Smith, 2002; Connor et al., 2000; Abrahamson, 2006; Jaquet et al., in press 2008). Narrow bandwidths focus density near past events. A large bandwidth, on the other hand, may over-smooth the density estimate, resulting in unreasonably low estimates near clusters of past events, and overestimated density far from past events. Selecting bandwidths arbitrarily can create ambiguity in the interpretation of spatial density (e.g., Abrahamson, 2006).

Bivariate bandwidth selectors such as the SCV and SAMSE appear promising. Although they are mathematically complex, these selectors rely on the data to select optimal bandwidth estimates, thereby reducing subjectivity. The bandwidth selectors used in this analysis provide global estimates of density, in the sense that one bandwidth or bandwidth matrix is used to describe variation across the entire region. An alternative method is to use adaptive kernel estimates, in which bandwidth changes along with event density (Stock and Smith, 2002; Weller et al., 2006). Adaptive bandwidths are calculated assuming radially symmetric kernel functions.

Paucity of Data

Volcanic hazard assessment for the Yucca Mountain repository faces the "problem" of having few data from which to forecast future events. That is, the repository site is not located where volcanic events are frequent enough to make the geologic hazards obvious. A spatial density estimated using hundreds of volcanoes can be assumed to represent well the true density. Uncertainty in hazard assessment for the YMR, on the other hand, is comparatively high, because the spatial density estimate is based on few volcanic events. The discovery of a single additional volcano buried in sediment, for example, might alter the shape of the estimated spatial density for the YMR.

To assess the uncertainty in spatial density related to sparse data, Connor and Connor (in press) modified a smoothed bootstrap method proposed by Press et al. (1992) based on the bootstrap methods of Efron and Tibishrani (1991). Conceptually, a given set of N past events can be considered one sample from an underlying "true spatial density" distribution, and a kernel density estimate can be seen as one estimate ($\hat{\lambda}_1(\mathbf{s})$) of that underlying spatial density. In the smoothed bootstrapping approach, a sample of size N is taken from the calculated spatial density,

$\hat{\lambda}_1(\mathbf{s})$, and a new kernel density estimate (using the same kernel function and bandwidth operator as before) is fit to those sampled points, resulting in a second estimate ($\hat{\lambda}_2(\mathbf{s})$) of the underlying "true" spatial density. If N is large, there will be little difference between the first and second estimates of spatial density. If N is small, however, the new spatial density may differ significantly from the original estimate. Although the model has not changed, the locations of event data will have changed. The differences between the first and second spatial density estimates give a sense of the uncertainty resulting from the size N of the event data set.

The re-sampling of estimated density suggests a Monte Carlo procedure. The original estimate is re-sampled multiple times, creating a family of spatial density estimates, from which we can derive confidence intervals for spatial density.

D.1.3.4 Uncertainty Related to Yucca Mountain

Applying the smoothed bootstrap approach to estimating the uncertainty in spatial density at the Yucca Mountain site, we find that the estimate of spatial density does not vary greatly with bandwidth selector or event data set (Figure D.1-13). All the analyses yield spatial densities of about 1×10^{-4} km^{-2}. The smoothed bootstrap procedure yields slightly higher median values of spatial density, about 2×10^{-4} km^{-2}, because the Yucca Mountain site is relatively close to a small cluster of vents in Crater Flat. Because the kernel bandwidths are comparatively large and each simulation is based on few events, re-sampling tends to increase the spatial density at the site compared to the original estimate. The uncertainty in spatial density at the site determined using the smoothed bootstrap method is consistently less when applied to the event data set for the Amargosa Valley Isotopic Province (AVIP) than to the YMR event data set, because the AVIP data set includes more events that are located farther from the site. Uncertainty does not differ markedly between the SAMSE and SCV bandwidth selectors. In this case the data set of events has more effect on uncertainty than does the choice of bandwidth selector.

If spatial density is estimated on a set of grid points across the map region, then the Monte Carlo procedure can be run on the entire grid. Although this process provides a sense of uncertainty in density or spatial intensity estimates across the entire map region, it requires a great deal of computation.

Uncertainty across the entire map region can be represented by plotting the median spatial densities derived from the smoothed bootstrap analysis. Such maps no longer illustrate probability density functions, because the integral of the median values across the map region may no longer be unity. One can either normalize the map or simply plot values that are not normalized. For the YMR, contours of the median values from 1,200 simulations at each grid point (not normalized) show that clusters tend to smooth (Figure D.1-14). That is, we can be reasonably confident in some features of the spatial density, such as the clustering of volcanoes west of Yucca Mountain and in the Greenwater Range, but less confident in the clustering of the fewer volcanoes in southeast Death Valley or the northern part of the map area.

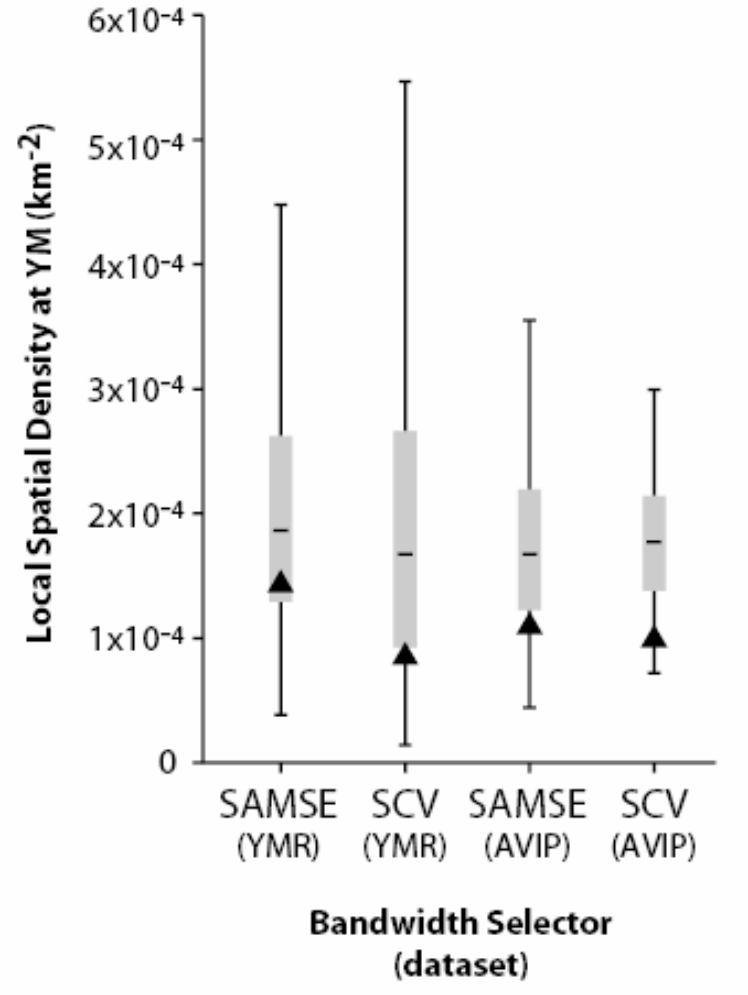

NOTE: The four estimates are based on two bandwidth estimators (SAMSE and SCV) and two data sets (YMR and AVIP). The quartile boundaries are enclosed in gray; the median (50%) value is indicated by a black horizontal bar. The bars extending beyond the quartile boundaries represent the 5th and 95th percentiles. Black triangles represent a point estimate of spatial density using the original data sets.

Figure D.1-13. Box Plots Illustrating Uncertainty in Estimates of the Conditional Spatial Density of Volcanism at Yucca Mountain Obtained from a Smoothed Bootstrap Re-sampling (with 1,200 samples) of Each of Four Conditional Estimates

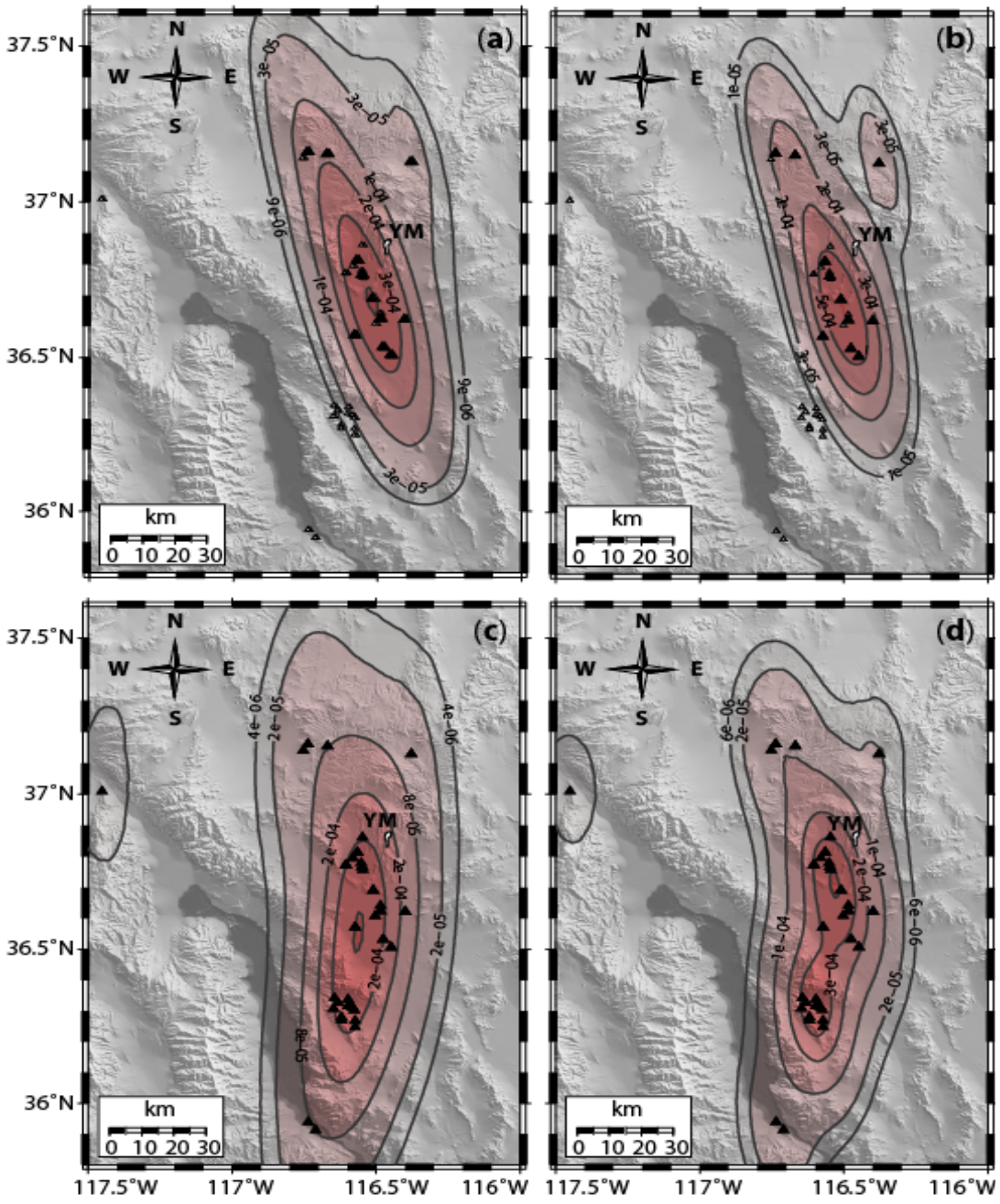

NOTE: I ran 1,200 simulations for each combination of bandwidth and data set: (a) YMR data set with SCV bandwidth estimator, (b) YMR data set with SAMSE estimator, (c) AVIP data set with SCV bandwidth estimator, and (d) AVIP data set with SAMSE estimator. The maps do not provide true probability density functions, because they do not integrate to one, but they show a degree of smoothing related to the amount of uncertainty. Contours represent the 25th, 50th, 75th, 95th, and 99th percentiles of increasing median spatial density. On map (d), for example, median values enclosed by the 99th percentile are greater than 5e-06 (5×10^{-6} km^{-2}).

Figure D.1-14. Four Spatial Density Maps Generated Using the Median Value at Each Grid Point (1-km spacing)

D.1.3.5 Weighting of Spatial Density Models

I weighted spatial density models based on the preceding analysis. The SCV and SAMSE models yield similar results, but the SAMSE model more effectively identifies the clusters that are a prominent feature of cinder cone volcanism. Therefore I use the SAMSE kernel bandwidth estimator. For the YMR data set (N = 11):

$$\mathbf{H} = \begin{bmatrix} 57.4 & -105.4 \\ -105.4 & 440.8 \end{bmatrix} \quad \text{(Eq. D.1-5)}$$

and for the AVIP data set (N = 34):

$$\mathbf{H} = \begin{bmatrix} 27.4 & -10.89 \\ -10.9 & 165.1 \end{bmatrix} \quad \text{(Eq. D.1-6)}$$

For the YMR data set, I also apply a model using the SAMSE bandwidth combined with the weighting of gravity data described above. Those models are weighted: 1/3 SAMSE YMR data set, 1/3 SAMSE AVIP data set, and 1/3 SAMSE YMR weighted by gravity data.

D.1.3.6 Other Data Sets Considered

I considered using both tomographic and extension data in my spatial analysis, but did not do so for the reasons presented below.

Tomographic Data

I considered but did not use the regional seismic tomographic data set in this analysis. Seismic tomography relies on regional earthquakes and seismic networks to identify areas of high or low compressional or shear-wave velocity in the subsurface. Slow-velocity regions have been mapped in many regions of active volcanism (e.g., Zhao, 2001). Velocity anomalies, which are attributed to areas of partial melting in the mantle, provide essential clues about the potential for eruptions, even in areas that lack surface manifestations (e.g., Martin et al., 2004; Umeda et al., 2006). As early as 1994, requests were made for detailed seismic tomographic studies in the YMR to assist with assessing volcanic hazards (Connor and Sanders, 1994). It is extremely unfortunate that no studies have been done. The seismic tomographic data that are available are low in resolution and open to interpretation (Biasi, oral communication at PVHA Workshop 1; Humphreys, personal communication). Although seismic tomographic anomalies appear to exist beneath Crater Flat and extend beneath Yucca Mountain, the DOE has not studied the YMR at the resolution available from, for instance, Northern Honshu, where such data are used in assessing potential sites for geologic high-level waste repositories (e.g., Martin et al., 2004). I include no tomographic data in this analysis because of the low quality of available data. If high-resolution seismic tomographic data were available, the results of this hazard assessment could change considerably.

Extension Data

Other data sets not used in my estimate of spatial density are related to extension across the YMR. Those data sets include GPS and structural models of the evolution of the Crater Flat basin and adjacent areas. The GPS data are of too low a resolution and too brief in duration to be useful in formulating a physical model for the distribution of potential future igneous events. The literature presents no successful geophysical model that directly relates GPS data to volcanic hazard on the scale of a few tens of kilometers (Wernicke et al., 1998; Connor et al., 1998). Some workers have interpreted strain estimates from structural models of the Crater Flat basin to suggest that extension is localized in southern Crater Flat (Fridrich, 1999). The details of those models, however, are open to interpretation (Ferrill et al., 1996, 1999). All the spatial density maps presented herein indicate that Crater Flat is the most likely locus of future volcanism. Nothing in the data regarding cumulative strain indicates any changes to the probability of future volcanism represented on those maps. As for GPS data, the literature provides no model to suggest that the distribution of volcanoes on the scale of a few tens of kilometers is related directly to strain rate.

D.1.4 TEMPORAL MODELS

Determining the timing of volcanism has been a central goal in the study of all monogenetic volcanic fields. The ages determined for individual volcanic features, such as lava flows and scoria cones, are used to estimate recurrence rates of volcanic events and to attempt to correlate rates of volcanic activity with other factors, such as plate motions, rates of crustal extension, or changes in petrogenesis.

Such studies, in the Yucca Mountain region (YMR) and other volcanic fields, reveal several characteristics of rates of volcanism in monogenetic volcanic fields that this hazard assessment must consider. First, in older volcanic systems, the number of vent-like bodies and dikes that ascend to the shallow subsurface far exceeds the number of vents that form at the surface. Worldwide, only extrusive events are used to estimate recurrence rates. To estimate a temporal recurrence rate for this hazard assessment, therefore, I assume that every igneous event of interest is associated with some extrusive feature. Although individual dikes may not vent at the surface (as commonly observed in eroded volcanic fields), they are grouped temporally with some extrusive feature. It is conceivable that the YMR contains only intrusive events that intrude to shallow depths, but such hypothetical events are not explicitly included in my estimate of recurrence rate.

Recurrence rates for volcanism change on geologic time scales, perhaps throughout periods of 10,000 to 100,000 years. In many of the world's monogenetic volcanic fields, rates of activity are observed to increase after long periods of steady-state or even waning activity. Examples include the Abu volcanic field, Japan (Figure D.1-15); the Cima volcanic field, California (Figures D.1-16 and D.1-17); and the Big Pine volcanic field, California (Figures D.1-18 and D.1-19). Unfortunately, no geologic explanation for these increases in volcanic activity has been identified. The changes do not correlate, for example, with plate tectonic reorganization, or even with the development of major fault systems. We must accept that, although YMR volcanism currently is waning in terms of eruptive volume on the time scale of the Pliocene-Quaternary,

this may not be a persistent characteristic of the volcanic field during the next 100,000 or 1,000,000 years.

Steady-state volcanism in these monogenetic volcanic fields usually is characterized on time scales of one to two million years or less. Several authors (e.g., Valentine and Perry, 2006) have noted that activity in the Pliocene-Quaternary indicates that the Crater Flat system is waning volumetrically, although the frequency of individual igneous events appears to be increasing. In all other volcanic fields I can document, or find documentation of, trends in activity are characterized on shorter time scales, for example the Quaternary. In other words, volcanism was more voluminous and less frequent in the Pliocene, and more frequent and less voluminous in the Quaternary. In forecasting activity during the next 10,000 to 100,000 years, the Quaternary rate is most relevant.

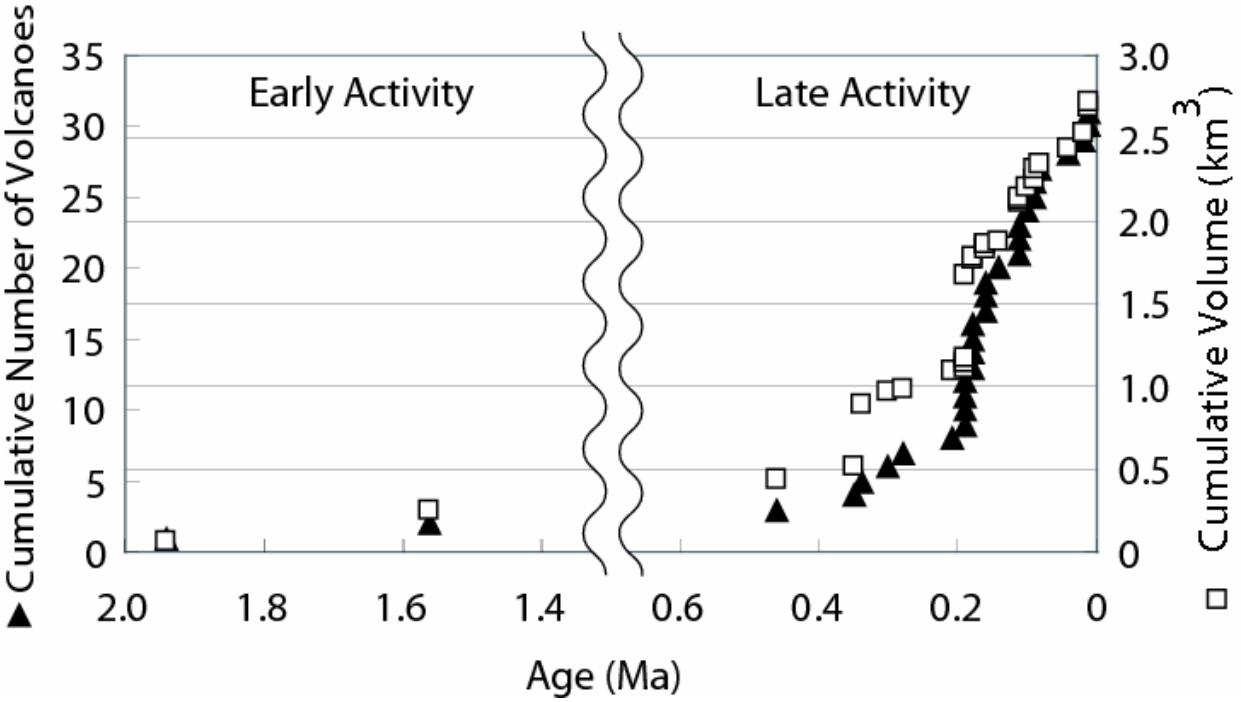

NOTE: From 2.0 Ma to approximately 0.2 Ma, rates of volcanism were less than those currently seen in the YMR. Since 0.2 Ma, rates of activity in the Abu volcanic field have accelerated greatly. This change in rate occurred on a time scale less than the resolution of radiometric age-dating methods, and likely less than 10 ky. The change in activity in the Abu volcanic field does not correspond with any known change in tectonic setting, plate reorganization, or similar phenomena. We cannot rule out the possibility of such changes in the rate of volcanic activity in the YMR over similar time scales. (Figure courtesy of Koji Kiyosugi.)

Figure D.1-15. Rates of Volcanism in the Abu Volcanic Field in Japan from 2.0 Ma to the Present

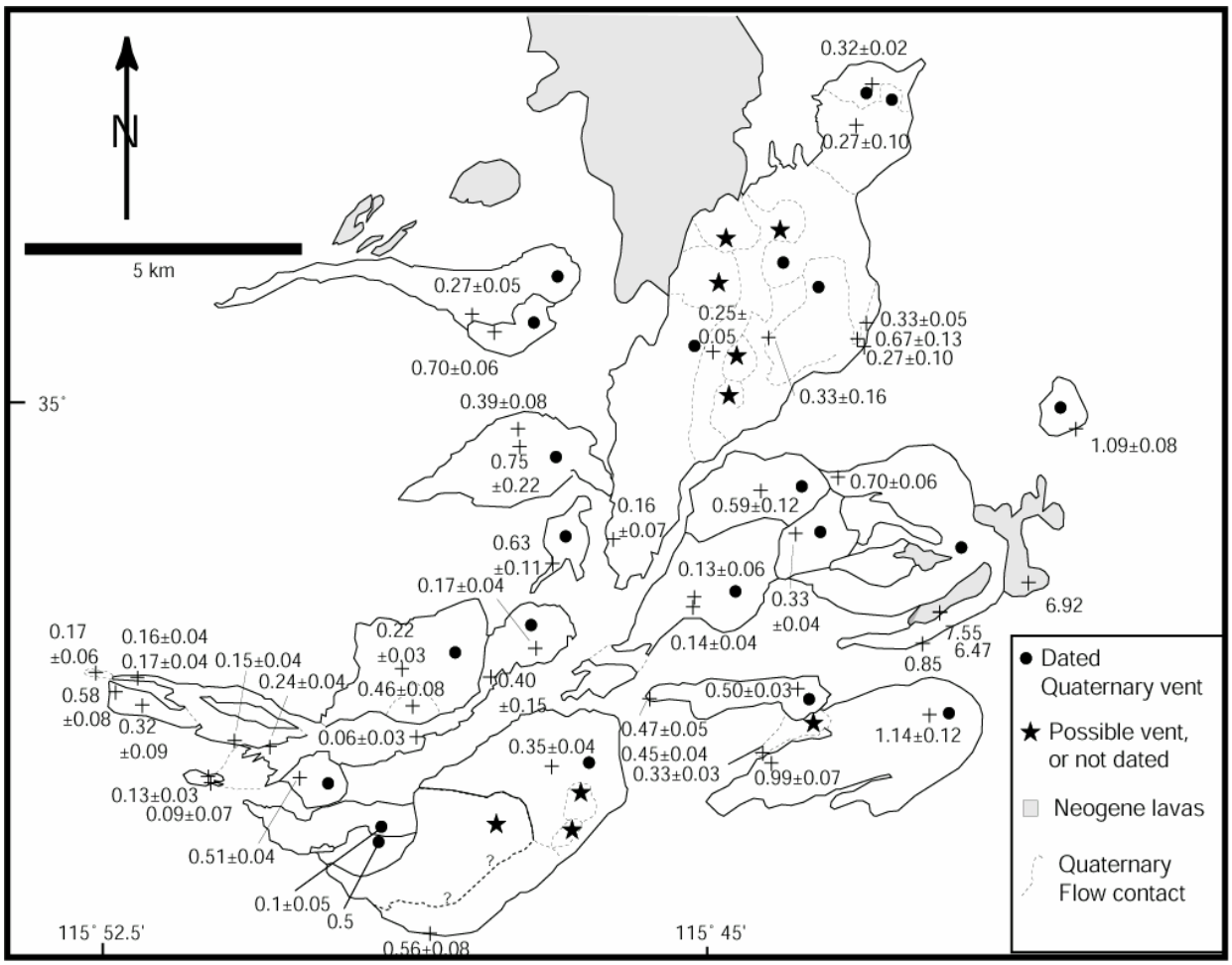

NOTE: Radiometric age determinations and uncertainties are shown (Ma) for specific sample localities. Data from Dohrenwend et al. (1986) and Turrin et al. (1985).

Figure D.1-16. Map Showing Locations of Lava Flow Fields, Vents, and Inferred Vents in the Southern Part of the Cima Volcanic Field, California

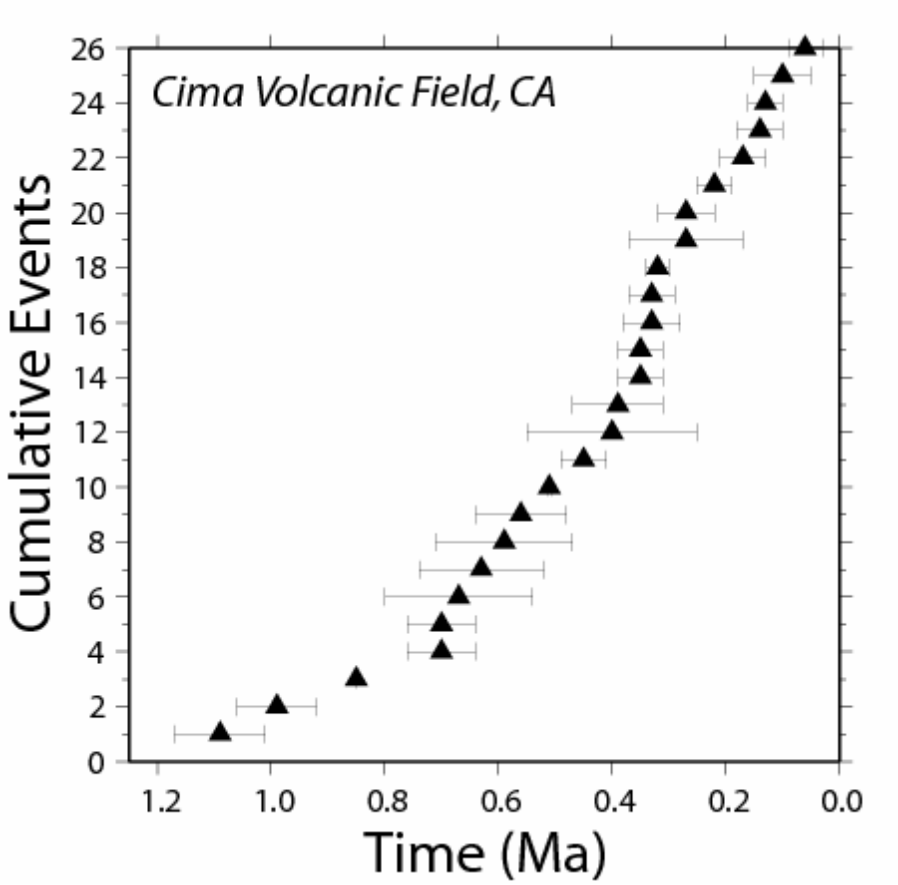

NOTE: Three events occurred between 1.2 Ma and approximately 0.7 Ma, after which time the rate of activity abruptly increased by approximately a factor of five. This change in activity does not correlate with any known change in the tectonic setting of the field.

Figure D.1-17. Number of Events over Time in the Cima Volcanic Field, California

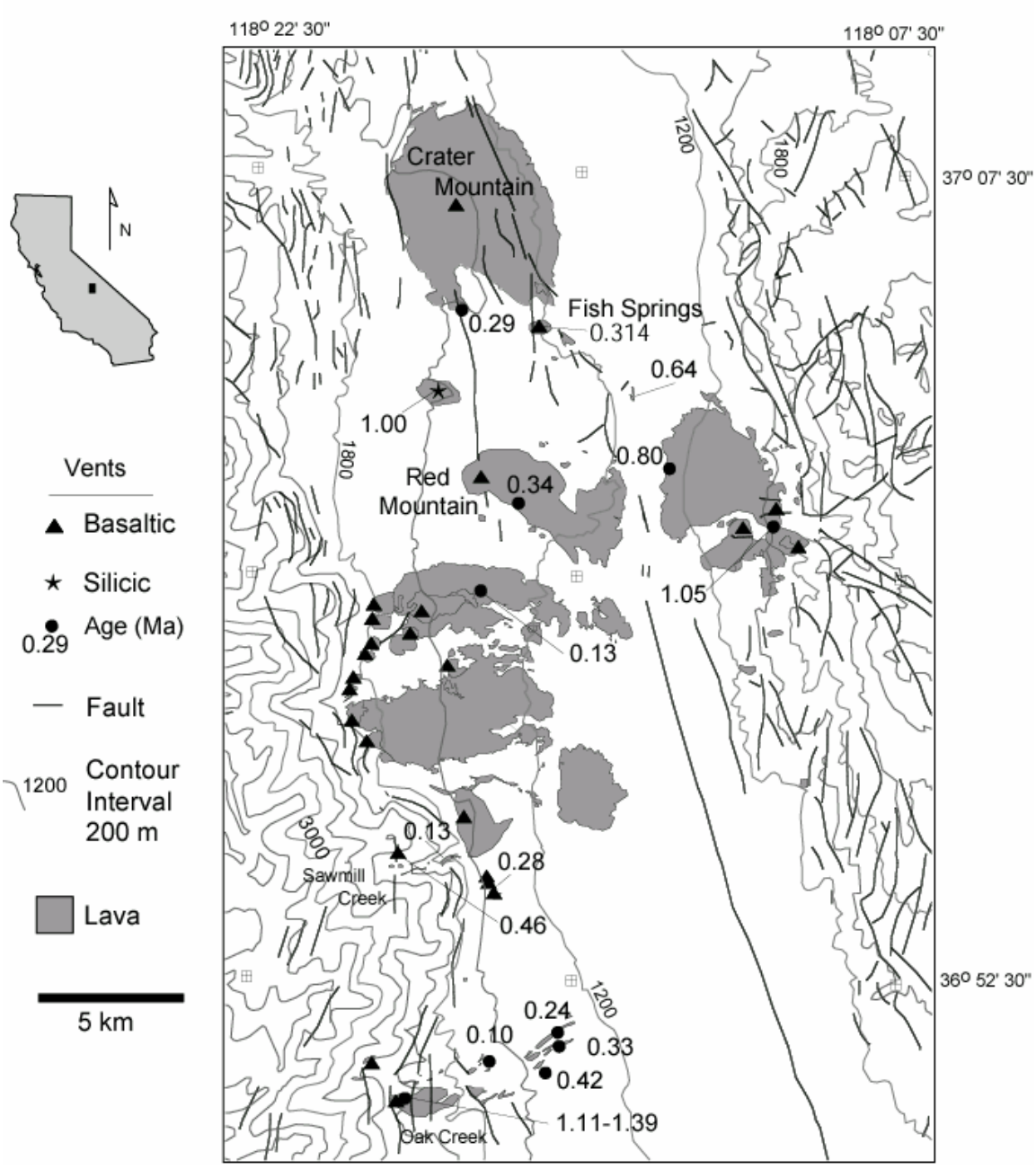

NOTE: Radiometric age determinations (Ma) are shown as solid circles [data from Ormerod et al. (1991) and Turrin and Gillespe (1986)]. Note the relationship between mapped faults and vents in this volcanic field and the concentration of 0.13-Ma vents (a single event) on the range-front fault of the Sierra Nevada Mountains. More vents occur at high elevations than in the topographic low of Owen's Valley. Water wells in the valley reveal that much of the valley consists of intercalated basalts and alluvium. Only the most recent volcanism crops out.

Figure D.1-18. Map Illustrating Distribution of Lavas, Vents (solid triangles), and Faults in the Big Pine Volcanic Field, California

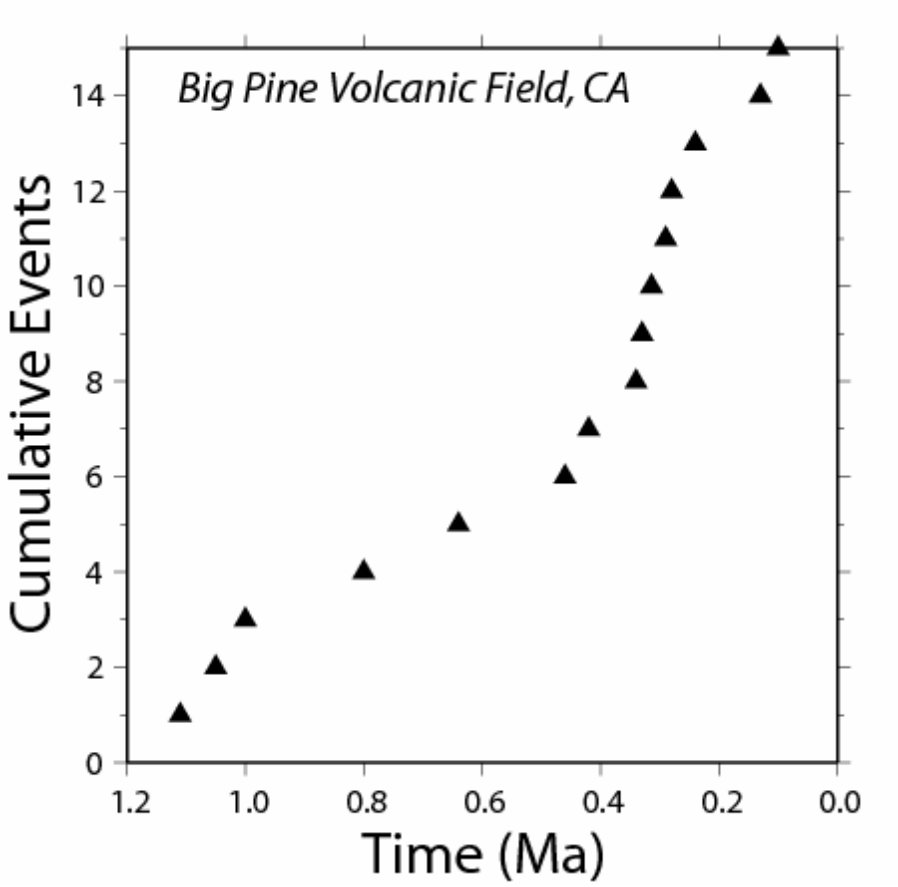

NOTE: The increase in rate at approximately 0.35 Ma does not appear to correlate with any change in tectonic setting of the volcanic field.

Figure D.1-19. Rates of Volcanism in the Big Pine Volcanic Field Appear to Have Fluctuated during the Past 1.2 Ma

Described below are three alternative conceptual models for the recurrence rate of volcanism in the YMR.

- A steady-state model. In this model, future volcanism is assumed to approximate the temporal pattern observed during the Quaternary. Because there are only three Quaternary events in the YMR data set and six Quaternary events in the AVIP data set, the uncertainty in the recurrence rate estimated using this model is relatively high.

- An increased-activity model. I believe it is possible that during the next 10 ky or 1 My, the rate of volcanism in the YMR will increase, so that the volcanic field comes to more closely resemble other fields in the western Great Basin, such as those at Cima and Coso. Changes in the rate of volcanism have occurred in many volcanic fields, as noted previously. To provide a basis for the rate estimate under this conceptual model, I gathered the following data about some of the most active Basin and Range volcanic fields.

- Cima: approximately 22 vents in the past 0.7 Ma = 3×10^{-5} per year.
- Coso: approximately 54 vents in 2 Ma = 3×10^{-5} per year.
- Big Pine: approximately 15 vents in 1.1 Ma = 1×10^{-5} per year.
- Camargo: approximately 308 vents in 3 Ma = 1×10^{-4} per year.
- Lunar Pancake: approximately 75 vents in 5.5 Ma = 1×10^{-5} per year.

It is difficult to use any of these rates directly. There is additional uncertainty in the event rate for each field because the vents (which are easy to count) may not represent separate events. I used the highest and lowest of the above rates as the bounds for a probability distribution on the recurrence rate for this conceptual model, and selected a minimally informative distribution to represent the uncertainty in that rate: log-uniform (10^{-4}; 10^{-5}).

- A "field extinction" model. Under this concept, activity in the YMR is assumed to be waning, so that the rate eventually drops to zero. There have been three relatively long hiatuses in volcanic activity in the region in the past 5 Ma, the longest of which is the gap between 2.9 Ma (Buckboard Mesa) and 1.1 Ma (Quaternary Crater Flat). To assess the best estimate of the recurrence rate under this conceptual model, I use a Poisson model for which the maximum likelihood recurrence interval is this 1.8-Ma gap (4×10^{-7} per year). Uncertainty in the recurrence rate can be estimated by finding the rates for which a 1.8-Ma interval is very unlikely or very likely (that is, 95th or 5th percentile).

I assign the three models different weights, depending on the performance period of interest. For a 10,000-year performance period, the Quaternary steady-state model and its accompanying uncertainty most likely capture the future recurrence rate. For the 10,000-year performance period, I assign weights of 80% steady-state, 10% increased-activity rate, and 10% reduced rate. I determined these weights subjectively, based on comparison with other volcanic fields. There is less reason to weight the models differently for a one-million-year performance period. Certainly other monogenetic volcanic fields commonly experience changes in the rate of activity on such a time scale. For the one-million-year performance period, I assign weights of 40% steady-state, 30% increased-activity rate, and 30% reduced rate. These weights also are determined subjectively, based on comparison with other volcanic fields.

For all three conceptual models, a homogenous Poisson model is considered most appropriate for the temporal distribution of future events. That is, I assume that the likelihood of an eruption in one time interval is independent of the number of eruptions during previous time intervals. The use of a Poisson model is related more to the paucity of events than to the belief that the Poisson model generally is the best model for predicting recurrence rates for volcanoes. Where sufficient data are available, it appears that other models, such as Weibull, log-logistic, Bayesian, or extreme value methods (e.g., Ho et al., 1991; Connor et al., 2003; Gelman et al., 2003; Coles and Sparks, 2006) can better model recurrence rates for volcanic activity.

D.1.5 REFERENCES

Abrahamson, N., 2006, Seismic hazard assessment—problems with current practice and future developments: Keynote Address at the First European Conference on Earthquake Engineering and Seismology, Geneva, Switzerland, September 3-8.

Aki, K., Fehler, M., and Das, S., 1977, Source mechanisms of volcanic tremors—fluid-driven crack models and their application to the 1963 Kilauea eruption: Journal of Volcanology and Geothermal Research, v. 2, p. 259-287.

Bergantz, G.W., and Dawes, R., 1994, Aspects of magma generation and ascent in continental lithosphere, in Ryan, M.P. (ed.), Magmatic Systems: Academic Press, San Diego, California, p. 291-317.

Coles, S.G., and Sparks, R.S.J., 2006, Extreme value methods for modeling historical series of large volcanic magnitudes, in Mader, H.M., Coles, S.G., Connor, C.B., and Connor, L.J. (eds.), Statistics in Volcanology: Special Publications of IAVCEI, 1, London Geological Society, p. 47-56.

Condit, C.D., and Connor, C.B., 1996, Recurrence rate of basaltic volcanism in volcanic fields—an example from the Springerville volcanic field, Arizona, USA: Geological Society of America Bulletin, v.108, p. 1225-1241.

Connor, C.B., 1990, Cinder cone clustering in the TransMexican volcanic belt: implications for structural and petrologic models: Journal of Geophysical Research, v. 95(B12), p. 19,395-19,405.

Connor, L.J., and Connor, C.B., in press 2008, Methods in kernel density estimation in geologic hazard assessment, in Connor, C.B., Chapman, N., and Connor, L.J. (eds.), Volcanism, Tectonism, and the Siting of Nuclear Facilities: London, Cambridge University Press.

Connor, C.B., and Conway, F.M., 2000, Basaltic volcanic fields, in Sigurdsson et al., Encyclopedia of Volcanology: Academic Press, p. 331-343.

Connor, C.B., and Hill, B.E., 1995, Three nonhomogeneous Poisson models for the probability of basaltic volcanism—application to the Yucca Mountain region: Journal of Geophysical Research, v. 100, p. 10,107-10,125.

Connor, C.B., and Sanders, C.O., 1994, Geophysics review topical report—application of seismic tomographic and magnetic methods to issues in basaltic volcanism: CNWRA Report 94-013. U.S. Nuclear Regulatory Commission Contract NRC-02-93-005.

Connor, C.B., R. S. J. Sparks, M. Diez, A. C. M. Volentik, S. Pearson. 2008. The nature of volcanism. In: Connor, C.B., Chapman, N., and Connor, L.J. (eds.), Volcanism, Tectonism, and the Siting of Nuclear Facilities: London, Cambridge University Press (in press).

Connor, C.B., Sparks, R.S.J., Mason, R.M., Bonadonna, C., and Young, S.R., 2003, Exploring links between physical and probabilistic models of volcanic eruptions—the Soufriere Hills Volcano, Montserrat: Geophysical Research Letters, v. 30, p. 1701, DOI:10.1029/2003GL017384.

Connor, C.B., Stamatakos, J., Ferrill, D., Hill, B.E., Ofoegbu, G., and Conway, F.M., 2000, Volcanic hazards at the proposed Yucca Mountain, Nevada, high-level radioactive waste repository: Journal of Geophysical Research, v. 105, p. 417-432.

Connor, C.B., J. Stamatakos, D. Ferrill, and B.E. Hill, 1998, Technical comment on article titled, "Anomalous strain accumulation in the Yucca Mountain region," by Wernicke, B., Davis, J.L., Bennett, R.A., Elosegui, P., Abolins, M.J., Brady, R.J., House, M.A., Niemi, N.A., and Snow, J.K. Technical comment in Science, v. 282, no. 5391, p. 1007. Original article in Science, v. 279, p. 2096-2100.

Connor, C.B., Magsino, S., Stamatakos, J., Martin, R., La Femina, P., Hill, B., and Lieber, S., 1997, Magnetic surveys help reassess volcanic hazards at Yucca Mountain: Eos, Transactions of the American Geophysical Union, v. 78, no. 7, p. 73 and 77-78.

Crowe, B.M., Vaniman, D.T., and Carr, W.J., 1983, Status of volcanic hazard studies for the Nevada nuclear waste storage investigations: Los Alamos National Laboratory Report LA-9325-MS.

D'Amato, A. and K. Engel (1988). State responsibility for the exportation of nuclear technology. Virginia Law Review, 74, 1011−1066.

Delaney, P.T., and Gartner, A.E., 1997, Physical processes of shallow dike emplacement near the San Rafael Swell, Utah: Geological Society of America Bulletin, v. 109, p. 1177-1192.

Díez, M., 2006, Solution and parametric sensitivity study of a coupled conduit and eruption column model, in Mader, H.M., Coles, S.G., Connor, C.B., and Connor, L.J. (eds.), Statistics in Volcanology. Special Publications of IAVCEI, 1, London, Geological Society, p. 185-200.

Diggle, P., 1985, A kernel method for smoothing point process data: Applied Statistics, v. 34, p. 138-147.

Diggle, P., and Marron, J.S., 1988, Equivalence of smoothing parameter selectors in density and intensity estimation: Journal of the American Statistical Association, v. 83, p. 793-800.

Dohrenwend, J.C., Wells, S.G., and Turrin, B.D., 1986. Degradation of Quaternary cinder cones in the Cima volcanic field, Mojave Desert, California: Geological Society of America Bulletin, v. 97, p. 421-427.

Doubik, P., and Hill, B.E., 1999, Magmatic and hydromagmatic conduit development during the 1975 Tolbachik eruption, Kamchatka, with implications for hazards assessment at Yucca Mountain, NV: Journal of Volcanology and Geothermal Research, v. 91, no. 1, p. 43-64.

Duong, T. 2007. ks: Kernel density estimation and kernel discriminant analysis for multivariate data in R, Journal of Statistical Software, 21(7): 1-16.

Duong, T., and Hazaelton, M.L., 2003, Plug-in bandwidth selectors for bivariate kernel density estimation: Journal of Nonparametric Statistics, v. 15, p. 17-30.

Efron, B., and Tibishrani, R., 1991, Statistical data analysis in the computer age: Science, v. 253, p. 390-394.

Einarsson, P., and Brandsdóttir, B., 1980, Seismological evidence for lateral magma intrusion during the July 1978 deflation of the Krafla volcano in NE Iceland: Journal of Geophysical Research, v. 47, p. 160-165.

Farmer, G.L., Perry, F.V., Semken, S., Crowe, B., Curtis, D., and DePaolo, D.J., 1989, Isotopic evidence on the structure and origin of subcontinental lithospheric mantle in southern Nevada: Journal of Geophysical Research, v. 94, p. 7885-7898.

Ferrill, D.A., Stamatakos, J.A., and Sims, D., 1999, Normal fault corrugation—implications for growth and seismicity of active normal faults: Journal of Structural Geology, v. 21, p. 1027-1038.

Ferrill, D.A., Stamatakos, J.A., Jones, S.M., Rahe, B., McKague, H.L., Martin, R.H., and Morris, A.P., 1996, Quaternary slip history of the Bare Mountain fault (Nevada) from the morphology and distribution of alluvial fan deposits: Geology, v. 24, p. 559-562.

Fridrich, C.J., 1999, Tectonic evolution of the Crater Flat basin, Yucca Mountain region, Nevada, in Wright, L.A., and Troxel, B.W. (eds.), Cenozoic Basins of the Death Valley Region: Boulder, Colorado, Geological Society of America Special Paper 333.

Gatrell, A.C., Bailey, T.C., Diggle, P.J., and Rowlingson, B.S., 1996, Spatial point pattern analysis and its application in geographical epidemiology: Transactions of the Institute of British Geography, NS 21, p. 256-274.

Gelman, A., Carlin, J.B., Stern, H.S., and Rubin, D.B., 2003, Bayesian Data Analysis, 2nd edition: New York, CRC Press.

Hall, P., Marron, J.S., and Park, B.U., 1992, Smoothed cross-validation: Probability Theory and Related Fields, v. 92, p. 1-20.

Hawkesworth, C.S., Turner, K., Gallagher, A., Hunter, T., Bradshaw, T., and Rogers, N., 1995, Calc-alkaline magmatism, lithospheric thinning and extension in the Basin and Range: Journal of Geophysical Research, v. 100, p. 10,271-10,286.

Ho, C.-H., Smith, E.I., Feuerbach, D.L., and Naumann, T.R., 1991, Eruptive probability calculation for the Yucca Mountain site—statistical estimation of recurrence rates: Bulletin of Volcanology, v. 54, p. 50-56.

Hornik, K., 2007, The R-FAQ, link on The R Project for Statistical Computing web page, http://www.r-project.org/, a free software environment for statistical computing and graphics hosted by the Department of Statistics and Mathematics, Vienna University of Economics and Business Administration. ISBN 3-900051-08-9.

Jaquet, O., and Carniel, R., 2006, Estimation of volcanic hazards using geostatistical methods, in Mader, H.M., Coles, S.G., Connor, C.B., and Connor, L.J. (eds.), Statistics in Volcanology: Special Publications of IAVCEI 1, London Geological Society, p. 89-103.

Jaquet, O., Connor, C.B., and Connor, L.J., in press 2008, Long-term volcanic hazard assessments for nuclear facilities: Nuclear Technology.

Jarvis, A., Reuter, H.I., Nelson, A., and Guevara, E., 2006, Hole-filled seamless SRTM data V3: International Centre for Tropical Agriculture (CIAT), available online from http://srtm.csi.cgiar.org.

Karakhanian, A., R. Djrbashian and V. Trifonov (2003). Volcanic hazards in the region of the Armenian nuclear power plant. Journal of Volcanology and Geothermal Research, 126, 31−62.

Lachenbruch, A.H., and Morgan, P., 1990, Continental extension, magmatism and elevation—formal relations and rules of thumb: Tectonophysics, v. 174, p. 39-62.

Langenheim, V.E., 1995, Magnetic and gravity studies of buried volcanic centers in the Amargosa Desert and Crater Flat, southwest Nevada: U.S. Geological Survey Open File Report 95-564.

Langenheim, V.E., Kirchoff-Stein, K.S., and Oliver, H.W., 1993, Geophysical investigations of buried volcanic centers near Yucca Mountain, southwest Nevada: Paper Presented at the Fourth Annual International Conference on High-Level Radioactive Waste Management, American Nuclear Society, La Grange Park, Illinois, April 26-30.

Leeman, W.P., and Fitton, J.G., 1989, Magmatism associated with lithospheric extension—introduction: Journal of Geophysical Research, v. 94, p. 7682–7684.

Lin, C. H., K. I. Konstantinou, W. T. Liang et al. (2005). Preliminary analysis of volcanoseismic signals recorded at the Tatun Volcano Group, northern Taiwan. Geophysical Research Letters, 32, L10313, doi:10.1029/2005GL022861.

Linde, A.T., Agustsson, I., Sacks, S., and Stefansson, R., 1993, Mechanism of the 1991 eruption of Hekla from continuous borehole strain monitoring: Nature, v. 365, p. 737-740.

Martin, A.J., Umeda, K., Connor, C.B., Weller, J.N., Zhao, D., and Takahashi, M., 2004, Modeling long-term volcanic hazards through Bayesian inference—example from the Tohoku volcanic arc, Japan: Journal of Geophysical Research, v. 109, p. B10208. DOI:10.1029/2004JB003201.

McKenzie, D., and Bickle, M.J., 1988, The volume and composition of melt generated by extension of the lithosphere: Journal of Petrology, v. 29, p. 625-679.

Musson, R.M.W., 1997, Seismic hazard studies in the U.K.—source specification problems of intraplate seismicity: Natural Hazards, v. 15, p. 105-119.

Omerod, D.S., Rogers, N.W., and Hawkesworth, C.J., 1991, Melting of the lithosphere mantle—inverse modeling of alkali-olivine basalts from the Big Pine volcanic field, California: Contributions to Mineralogy and Petrology, v. 108, p. 305-317.

Parsons, T., Thompson, G.A., and Cogbill, A.H., 2006, Earthquake and volcano clustering via stress transfer at Yucca Mountain, Nevada: Geology, v. 34, p. 785-788. DOI:10.1130/G22636.1.

Pedersen, T., and Ro, H.E., 1992, Finite duration extension and decompression melting: Earth and Planetary Science Letters, v. 113, p. 15-22.

Press, W.H., Flannery, B.P., Teukolsky, S.A., and Vetterling, W.T., 1992, Numerical Recipes in C, 2nd edition: Cambridge University Press, Cambridge.

Rogers, N.W., Hawkesworth, C.J., and Ormerod, D.S., 1995, Late Cenozoic basaltic magmatism in the western Great Basin, California and Nevada: Journal of Geophysical Research, v. 100, p. 10,287-10,301.

Silverman, B.W., 1986, Density estimation for statistics and data analysis: Monographs on Statistics and Applied Probability, No. 26, London, Chapman and Hall.

Silverman, B.W., 1978, Choosing the window width when estimating a density: Biometrika, v. 65, p. 1-11.

Smith, E.I., D.L. Feuerbach, T.R. Naumann, J.E. Faulds, 1990, The area of most recent volcanism about Yucca Mountain, Nevada: Implications for volcanic risk assessment. Paper presented at the International Nuclear Waste Symposium, American Nuclear Society, Las Vegas Nv., 1990.

Smith, E.I., Morikawa, S., and Sanchez, A., 1997, Volcanism studies related to the probabilistic volcanic hazard at Yucca Mountain for the period 1986-1996: available online at http://www.state.nv.us/nucwaste/yucca/volcan01.htm: Center for Volcanic and Tectonic Studies, University of Nevada, Las Vegas.

Spera, F.J., 1984, Carbon dioxide in petrogenesis III—Role of volatiles in the ascent of alkaline magma with special reference to xenolith-bearing mafic lavas: Contributions to Mineralogy and Petrology, v. 88, p. 217-232.

Stock, C., and Smith, E.G.C., 2002, Comparison of seismicity models generated by different kernel estimations: Bulletin of the Seismological Society of America, v. 92, p. 913-922.

Takahashi, E., and Kushiro, I., 1983, Melting of a dry peridotite at high pressures and basalt magma genesis: American Mineralogist, v. 68, p. 859-879.

Turrin, B.D., and Gillespie, A., 1986, K/Ar ages of basaltic volcanism of the Big Pine volcanic field, California—implications for glacial stratigraphy and neotectonics of the Sierra Nevada: Geological Society of America Abstracts with Programs, v. 18, no. 6, p. 777.

Turrin, B.D., Dohrenwend, J.C., Drake, R.E., and Curtis, G.H., 1985, Potassium-argon ages from the Cima volcanic field, eastern Mojave Desert, California: Isochron West, v. 44, p. 9-16.

Umeda, K., Asamori, K., Negi, T., and Ogawa, Y., 2006, Magnetotelluric imaging of crustal magma storage beneath the Mesozoic crystalline mountains in a non-volcanic region, northeast Japan: Geochemistry, Geophysics, Geosystems, v. 7, Q08005. DOI:10.1029/2006GC001247.

Valentine, G.A., and Perry, F.V., 2007, Tectonically controlled, time-predictable basaltic volcanism from a lithospheric mantle source (central Basin and Range Province, USA): Earth and Planetary Science Letters, v. 261, no. 1-2, p. 201-216.

Valentine, G.A., and Perry, F.V., 2006, Decreasing magmatic footprints of individual volcanoes in a waning basaltic field: Geophysical Research Letters, v. 33, no.14, p. L14305.

Wand, M.P., and Jones, M.C., 1995, Kernel smoothing: Monographs on Statistics and Applied Probability, No. 60, London, Chapman Hall.

Ward, S.N., 1994, A multidisciplinary approach to seismic hazard in Southern California: Bulletin of the Seismological Society of America, v. 84, p. 1293-1309.

Weller, J.N., Martin, A.W., Connor, C.B., Connor, L.J., and Karakhanian, A., 2006, Modelling the spatial distribution of volcanoes—an example from Armenia, in Mader, H.M., Coles, S.G., Connor, C.B., and Connor, L.J. (eds.), Statistics in Volcanology: Special Publications of IAVCEI 1, London Geological Society, p. 77-87.

Wernicke, B., Davis, J.L., Bennett, R.A., Elosegui, P., Abolins, M.J., Brady, R.J., House, M.A., Niemi, N.A., and Snow, J.K., 1998, Anomalous strain accumulation in the Yucca Mountain area, Nevada: Science, v. 279, p. 2096-2100.

Woo, G., 1996, Kernel estimation methods for seismic hazard area source modeling: Bulletin of the Seismological Society of America, v. 86, p. 353-362.

Yogodzinski, G.M., and Smith, E.I., 1995, Isotopic domains and the area of interest for volcanic hazard assessment in the Yucca Mountain area (abstract): EOS, Transactions of the American Geophysical Union, v. 76, no. 46, Fall Meeting Supplement, p. F669.

Yogodzinski, G.M., Naumann, T.R., Smith, E.I., and Bradshaw, T.R., 1996, Evolution of a mafic volcanic field in the central Great Basin, south central Nevada: Journal of Geophysical Research, v. 101, p. 17,425-17,445.

Zhao, D., 2001, New advances of seismic tomography and its applications to subduction zones and earthquake fault zones—a review: The Island Arc, v. 10, p. 68-84.

SUPPLEMENT A

DESCRIPTION OF AN EVENT SIMULATOR

A version of the event simulator discussed in the text was developed and implemented during the process of this elicitation.

The event simulator extracts geologic information about igneous features from an event library, and places those features in an event based on the expert-defined distributions and parameters described in the main text. The statistical distributions, and parameters for those distributions, are estimated subjectively using data from volcanic fields worldwide, but are especially influenced by observations in the Yucca Mountain region (YMR) and the San Rafael volcanic field.

For each grid point on the map area of the YMR (grid points are spaced at 1,000-m intervals), the event simulator is run 1,000 times. For each realization at each grid point, either no dikes intersect the repository (0), or one or more dikes intersect the repository (1). The results are tallied for each grid point and contoured as probabilities that a dike would intersect the repository, given that an event occurs at the grid point (see example in Figure D.1-20). Similarly, Monte Carlo simulations yield a probability that vent-like bodies or sills will intersect the repository. Only one node of the vent-like body or sill outline need fall within the repository boundary for intersection to occur. The stratigraphic level of the sill is not considered in this event simulator. The analysis is based on the observed frequency of sill formation at relatively shallow depths in the crust (<1 km). Although sills may lie within the boundary of the repository in map view, they may intrude a lower stratigraphic level.

Figures D.1-21 through D.1-23 show maps that represent three simulated igneous events. In each case the simulation output is located randomly on the digital elevation model of the YMR. This superposition on the digital elevation model provides a sense of the scale of the igneous events.

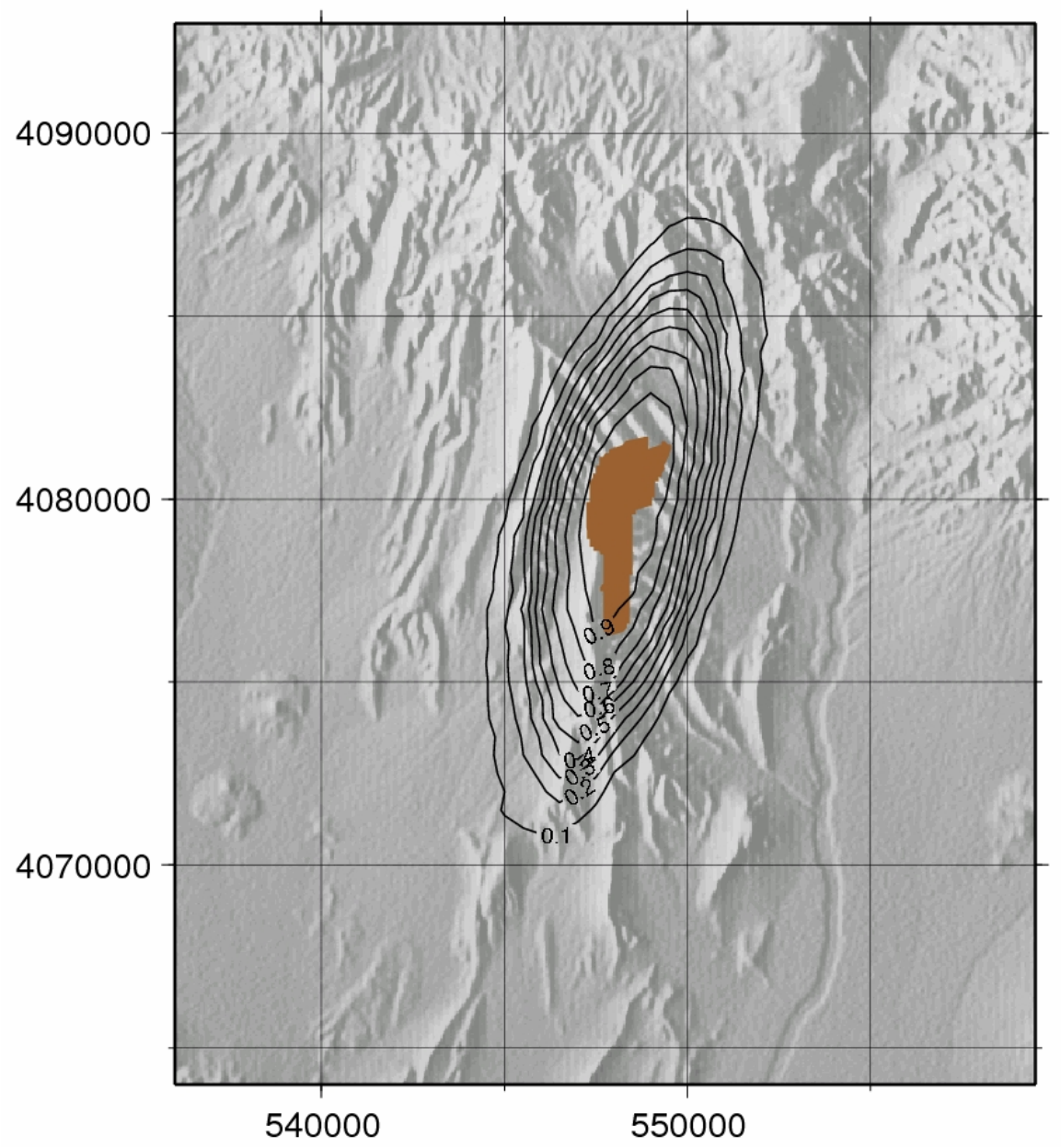

NOTE: Given that an igneous event is centered on a specific grid location, the contours indicate the probability that a dike associated with that event will intersect the repository. The brown area shows the approximate extent of the proposed repository. Exact parameter distributions used in the final model differ slightly from those shown.

Figure D.1-20. Map Illustrating One Output of the Event Simulator

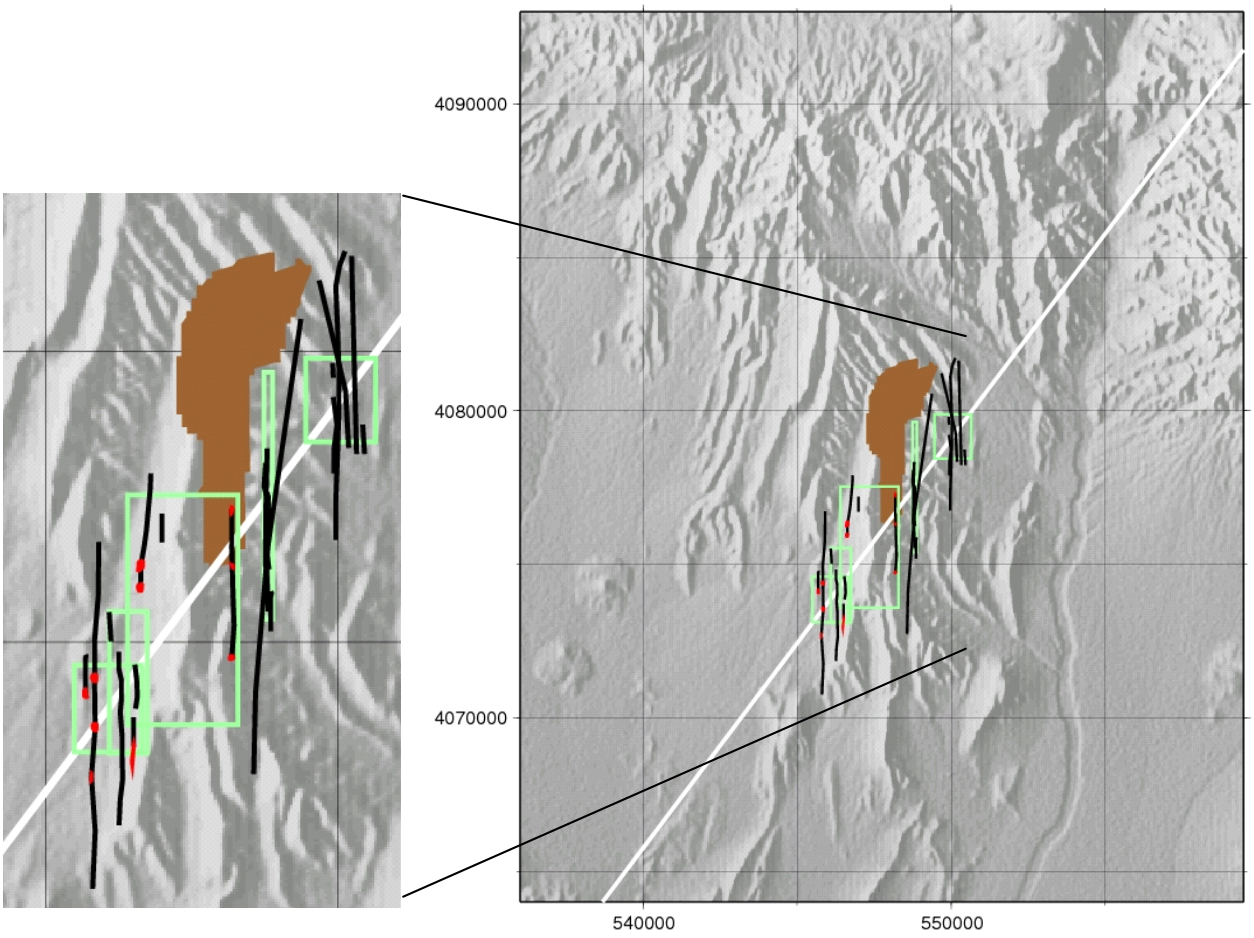

NOTE: This igneous event consists of 5 centers (indicated by green boxes), distributed along a N30°E trend (white line). Individual dikes (solid black lines) and vent or vent-like bodies (red zones) are distributed within each center. No sills are associated with this simulated event. The brown area shows the approximate extent of the proposed repository. For the purposes of illustration, this simulated event was placed randomly in the vicinity of the repository.

Figure D.1-21. Maps Showing One Realization of the Event Simulator for a Potential Future Event

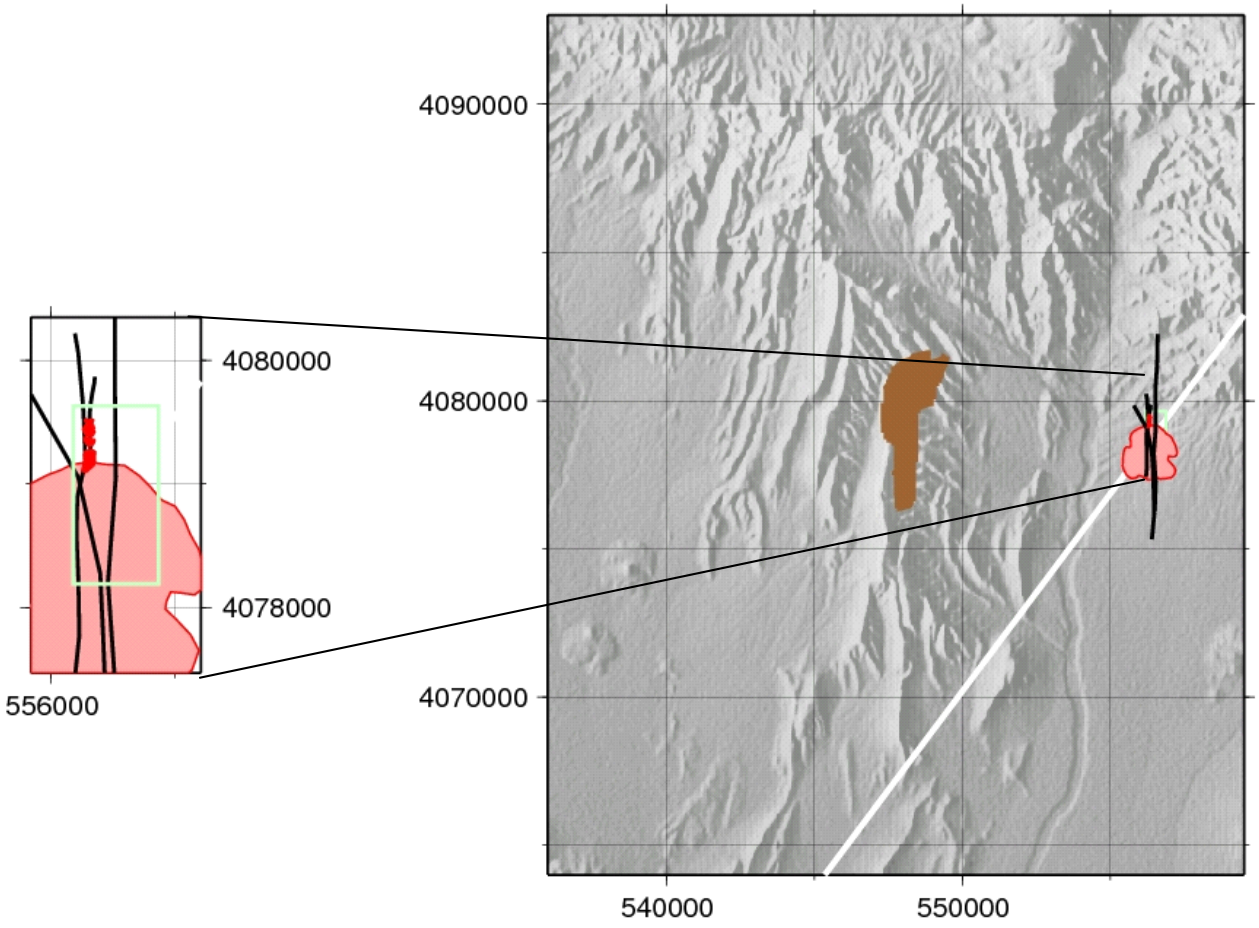

NOTE: This igneous event consists of one center (indicated by green box). Individual dikes (solid black lines) and vent or vent-like bodies (red zones) are distributed within the center. This event includes a sill (pink area), which has the dimensions of a sill mapped in the San Rafael volcanic field. The brown area shows the approximate extent of the proposed repository. For purposes of illustration, this simulated event was placed randomly in the vicinity of the repository.

Figure D.1-22. Maps Showing One Realization of the Event Simulator for a Potential Future Event

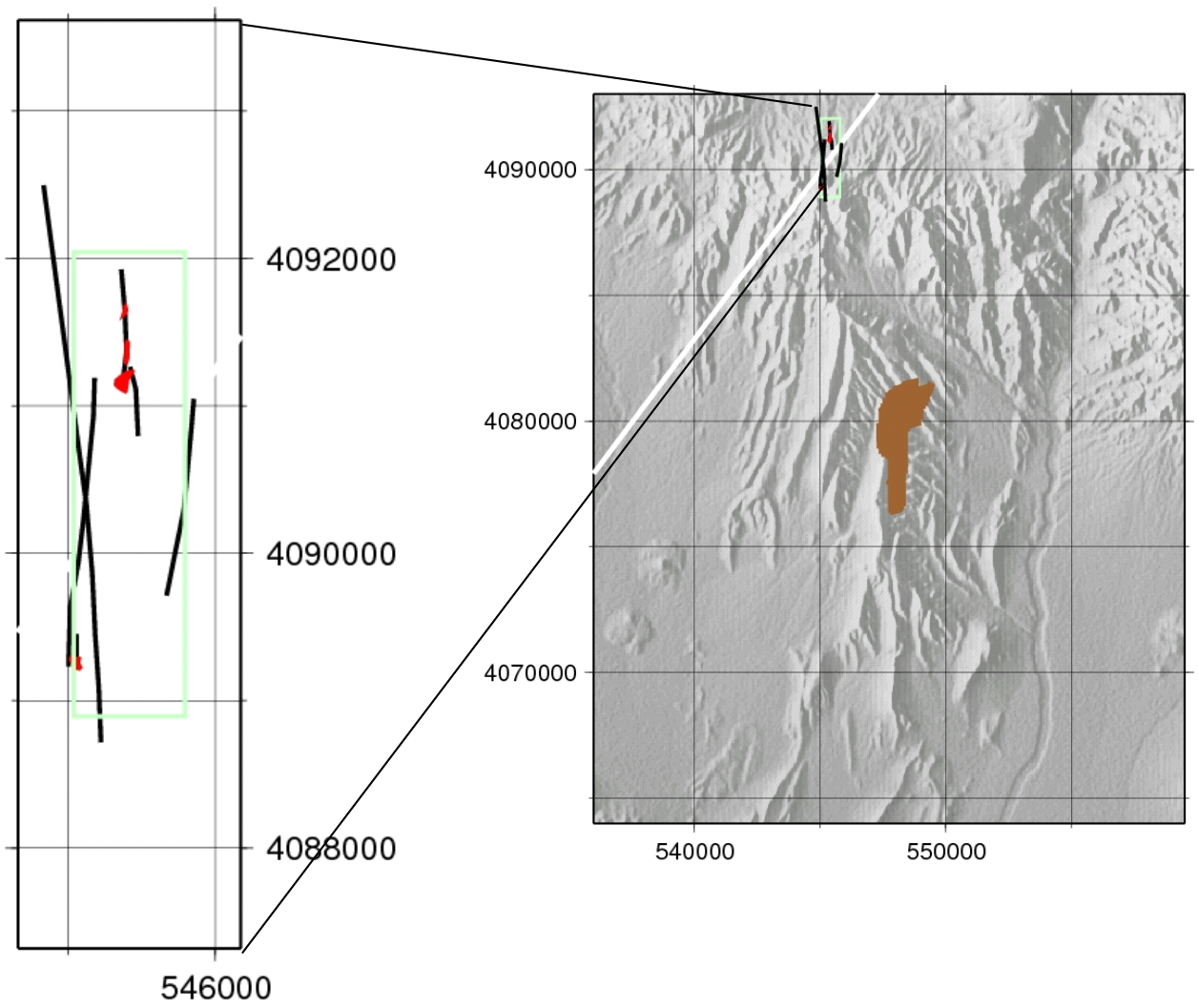

NOTE: This igneous event consists of one center (indicated by green box). Individual dikes (solid black lines) and vent or vent-like bodies (red zones) are distributed within the center. No sills are associated with this event. The brown area shows the approximate extent of the proposed repository. For purposes of illustration, this simulated event was placed randomly in the vicinity of the repository.

Figure D.1-23. Maps Showing One Realization of the Event Simulator for a Potential Future Event

SUPPLEMENT B

MATHEMATICAL DEFINITION OF SPATIAL DENSITY AND SPATIAL INTENSITY

The goal of estimating spatial density in the context of volcanic hazard assessment is to estimate the likely locations of potential future igneous events, or the probability of an igneous event at a specific location, *given that such events occur* within a region of interest. In this context, spatial intensity refers to the expected mean number of events per unit area defined at a point, **s** (Diggle, 1985; Diggle and Marron, 1988; Gatrell et al., 1996). Given a set of events (e.g., volcano locations) that occur within a region, *R,* these events can be designated $\{X_1, X_2, X_3 ... X_N\} \in R$, where N is the total number of events, and X_n is a matrix the elements of which provide the *x, y* location (e.g., given in easting and northing coordinates or latitude and longitude) of the n^{th} event. The events are realizations of a random variable, **X**, a function that describes the set of all possible realizations. In this case, **X** is the distribution of potential igneous events, from which are drawn a set of observed realizations (those volcanoes mapped in the Yucca Mountain region). The spatial intensity is written formally as follows (Gatrell et al., 1996):

$$\lambda(\mathbf{s}) = \lim_{ds \to 0} \left\{ \frac{E(X(d\mathbf{s}))}{d\mathbf{s}} \right\} \qquad \text{(Eq. D.1-7)}$$

where $E(X(d\mathbf{s}))$ is the expected number of events that fall within a small area $d\mathbf{s}$ about the point **s.** If the location, **s**, is given in easting and nothing (meters), the units of $\lambda(\mathbf{s})$ are m^{-2}. Although it may appear that the statistical definition of *intensity* is equivalent to the term *density* as used in the geosciences, this is not quite correct. The stochastic process that leads to the formation of volcanoes is unknown, so the true value of the local spatial intensity, $\lambda(\mathbf{s})$, is also unknown. That is, the observed distribution of events is only one realization of the underlying process that gives rise to those events. Our goal is to develop an estimate of the spatial intensity, $\hat{\lambda}(\mathbf{s})$, that approximates the true but unknown value of spatial intensity, $\lambda(\mathbf{s})$.

In hazard assessment, we can use estimates of spatial intensity to forecast the spatial distribution of potential future events. Here we are interested in spatial intensity in terms of the probable location of a future igneous event, given that one occurs within the region of interest. This conditional probability is estimated by dividing the estimate of local spatial intensity by the number of events used to make that estimate, as follows:

$$\hat{f}(\mathbf{s}) = \hat{\lambda}(\mathbf{s}) \Big/ N \qquad \text{(Eq. D.1-8)}$$

Integrating $\hat{f}(\mathbf{s})$ across the region of interest, *R*, gives unity if *R* is sufficiently large. Furthermore, all values of $\hat{f}(\mathbf{s})$ within this region are greater than or equal to zero, so $\hat{f}(\mathbf{s})$ is a probability density function that can be used in probabilistic hazard models, and we can refer to $\hat{f}(\mathbf{s})$ as an estimate of the spatial density.

SUPPLEMENT C

BIVARIATE GAUSSIAN KERNEL FUNCTION

This supplement describes my approach to utilizing a kernel function and observed event locations to estimate the spatial intensity of igneous events at any point in a region. I use a general approach here, applying a bivariate Gaussian kernel and a bandwidth matrix fit to past events.

For example:

$$\hat{\lambda}(\mathbf{s}) = \frac{1}{2\pi h^2} \sum_{i=1}^{N} \exp\left[-\frac{1}{2}\left(\frac{d_i}{h} \right)^2 \right] \qquad \text{(Eq. D.1-9)}$$

is a two-dimensional, radially symmetric kernel function in which spatial intensity decreases with distance from events based on a bivariate Gaussian function. The local spatial intensity estimate, $\hat{\lambda}(\mathbf{s})$, at point **s** depends on the distance, d_i, to the i^{th} event location and the bandwidth, h. The rate of change in spatial intensity with distance from events depends on the bandwidth, h, which in the case of a Gaussian kernel function is equivalent to the variance of the kernel. In this example, the kernel is radially symmetric; that is, h is constant in all directions. Nearly all kernel estimators used in geologic hazard assessment have been of this type (e.g., Woo, 1996; Stock and Smith, 2002; Connor and Hill, 1995; Condit and Connor, 1996). The bandwidth for calculating the spatial intensity function is selected based on some criterion, often visual smoothness of the resulting spatial intensity plots. Alternatively, in an adaptive kernel function, the bandwidth varies as a function of event spatial intensity (e.g., Stock and Smith, 2002; Weller et al., 2006).

Equation D.1-9 is a simplification of a more general case, in which h varies in magnitude depending on direction. Below is a two-dimensional elliptical kernel having a bandwidth that depends on direction, as given by Wand and Jones (1995).

$$\hat{\lambda}(\mathbf{s}) = \frac{1}{2\pi\sqrt{|\mathbf{H}|}} \sum_{i=1}^{N} \exp\left[-\frac{1}{2}\mathbf{b}^T\mathbf{b} \right] \qquad \text{(Eq. D.1-10)}$$

where:

$$\mathbf{b} = \mathbf{H}^{-1/2}\mathbf{x} \qquad \text{(Eq. D.1-11)}$$

and **H** is a 2-by-2 element bandwidth matrix that is positive and definite (important because the matrix must have a square root); $|\mathbf{H}|$ is the determinant of this bandwidth matrix; $\mathbf{H}^{-1/2}$ is read as the inverse of the square root of the matrix **H**; $\mathbf{b}^T$ is the transform of the matrix **b**; and **x** is a distance matrix comprised of distances between the set of points {**s**} (usually distributed on a grid) and event locations, $\{X_1, X_2, X_3 \ldots X_N\} \in R$. An example of a 2-by-2 bandwidth matrix is:

$$\mathbf{H} = \begin{bmatrix} 57.4 & -105.4 \\ -105.4 & 440.8 \end{bmatrix} \quad \text{(Eq. D.1-12)}$$

The value in the upper-left (diagonal) element represents the squared kernel bandwidth (km^2) in the east direction; the lower-right (diagonal) element represents the squared kernel bandwidth in the north direction; and the off-diagonal values represent rotation of the kernel in the NNW direction. Given the values shown for the elements in this example, the bandwidth matrix forms an elliptical kernel function that trends to the NNW.

SUPPLEMENT D

"LIBRARY" FOR DIKES, VENTS AND VENT-LIKE BODIES, AND SILLS USED IN THE EVENT SIMULATOR

For completeness, this supplement lists the data defining each dike, vent or vent-like body, and sill used in event simulation. This supplement was prepared by the MDT using the dike, vent, and sill databases provided by CC in ASCII files. The data in these files have been rounded to two decimal places. The dike data base consists of 93 sets of points, each representing a dike. Each dike is defined by the x and y coordinates of the points representing dike nodes, and a third field indicating the total length of the dike (in m). Dike node coordinates are given in m relative to an aribitrary dike "center."

The vent database consists of 38 sets of points, each representaing one vent or vent-like body, and the sill database consists of 3 sets of points, each representing on sill. Each of these individual features is described by the x and y coordinates of points that define a polygon representing the outline of the feature, and a third field representing the area of the polygon (in m^2). The coordinates of points on the perimeter of the feature are given in m relative to an aribrary "center" of the feature.

Dike 1		
10.82	-339.81	765
34.66	-130.02	765
25.12	146.52	765
1.28	423.06	765
Dike 2		
44.19	-501.91	1300
44.19	-277.82	1300
10.82	-72.8	1300
6.05	70.23	1300
1.28	332.47	1300
15.59	561.33	1300
10.82	794.96	1300
Dike 3		
1.28	-192	955
20.36	-6.05	955
29.89	170.36	955
-8.25	227.57	955
-36.86	351.54	955
-27.32	551.79	955
-22.56	690.06	955
-22.56	747.27	955
Dike 4		
10.82	-373.18	1365
34.66	-225.38	1365
15.59	-91.87	1365
-3.48	41.63	1365
-3.48	141.75	1365
-8.25	308.63	1365
6.05	499.35	1365
20.36	947.53	1365
1.28	1004.75	1365
Dike 5		
-17.79	-1579.4	3166
-22.56	-1436.4	3166
-22.56	-1264.7	3166
-13.02	-1112.2	3166
-22.56	-954.86	3166
10.82	-811.83	3166
6.05	-659.25	3166
20.36	-525.75	3166
15.59	-292.13	3166
25.12	-87.11	3166
15.59	94.07	3166
1.28	265.72	3166
6.05	518.42	3166
25.12	680.53	3166
29.89	918.92	3166
20.36	1100.1	3166
10.82	1262.21	3166
34.66	1386.18	3166
91.87	1567.36	3166
Dike 6		
2.73	-3356.3	6750
22.99	-3011.8	6750
2.73	-2596.4	6750
-17.54	-1948	6750
33.12	-1238.8	6750
33.12	-772.74	6750
63.52	-276.28	6750
33.12	270.83	6750
33.12	878.74	6750
73.65	1435.98	6750
63.52	1902.05	6750
53.39	2357.98	6750
2.73	2611.27	6750
-47.93	2905.1	6750
-118.85	3239.4	6750
-169.51	3361.03	6750
Dike 7		
-27.67	-1411.04	2988
2.73	-975.38	2988
43.26	-620.77	2988
33.12	-215.5	2988
33.12	118.85	2988
2.73	524.13	2988
22.99	767.29	2988
22.99	1071.24	2988
-17.54	1263.75	2988
-27.67	1567.7	2988
Dike 8		
1.29	-324.49	660
4.33	-260.66	660
0.27	-198.8	660
-0.74	-124	660
3.31	-44.85	660
-3.78	6.82	660
0.27	67.61	660
8.38	129.41	660
22.56	206.42	660
35.73	284.43	660
39.79	332.05	660
Dike 9		
2.3	-54.98	102
1.29	-21.54	102
2.3	5.81	102
0.27	26.06	102
1.29	47.35	102
Dike 10		
10.4	-87.41	132
6.35	-60.05	132
7.37	-24.59	132
4.33	-0.27	132
5.34	27.08	132
-1.75	43.29	132
Dike 11		
4.33	-335.64	679
-0.74	-312.3	679
2.3	-276.87	679
2.3	-236.34	679
-2.77	-212.02	679
2.3	-178.59	679
3.31	-136.04	679
3.31	-95.51	679
1.29	-37.76	679
-0.74	-1.28	679
4.33	45.32	679
2.3	66.6	679
3.31	108.14	679
3.31	146.64	679
1.29	194.26	679
3.31	256.06	679
7.37	313.81	679
1.29	340	679
Dike 12		
9.46	-1007.73	2644
16.91	-799.14	2644
16.91	-568.19	2644
31.8	-359.6	2644
46.7	-91.4	2644
31.8	132.09	2644
61.6	340.69	2644
69.05	512.03	2644
54.15	720.63	2644
54.15	824.93	2644

54.15	1003.73	2644
31.8	1152.72	2644
16.91	1316.62	2644
31.8	1450.72	2644
39.26	1629.51	2644
Dike 13		
2.01	-31.8	434
2.01	146.99	434
16.91	340.69	434
2.01	400.29	434
Dike 14		
-5.44	-2467.9	4990
-5.44	-2229.5	4990
-12.89	-1797.4	4990
2.01	-1491.97	4990
16.91	-992.84	4990
46.7	-300	4990
46.7	504.58	4990
16.91	1182.52	4990
-5.44	1890.25	4990
54.15	2240.4	4990
143.55	2500	4990
Dike 15		
2.01	-1253.5	2808
39.26	-903.43	2808
31.81	-441.54	2808
16.91	-76.5	2808
24.36	221.49	2808
91.4	504.58	2808
69.05	944.13	2808
31.81	1376.21	2808
2.01	1540.11	2808
Dike 16		
-12.89	-814.04	2257
9.46	-471.35	2257
46.7	-98.85	2257
39.26	430.09	2257
54.15	839.83	2257
24.36	1234.67	2257
-12.89	1435.81	2257
Dike 17		
-5.44	-54.15	186
9.46	132.09	186
Dike 18		
-5.44	-1506.87	2155
16.91	-1208.88	2155
2.01	-858.74	2155
24.36	-545.85	2155
76.5	-285.1	2155
54.15	-31.8	2155
46.7	214.04	2155
16.91	534.38	2155
9.46	638.68	2155
Dike 19		
-5.44	-113.75	254
16.91	139.54	254
Dike 20		
-154.44	-881.08	1775
-50.14	-448.99	1775
24.36	-113.75	1775
143.55	683.38	1775
173.35	862.18	1775
Dike 21		
-5.44	-76.5	223
9.46	146.99	233
Dike 22		
-5.44	-1521.77	2557
39.26	-970.49	2557
16.91	-426.65	2557
9.46	42.69	2557
-5.44	422.64	2557
-5.44	1033.52	2557
Dike 23		
2.01	-255.3	499
2.01	243.84	499
Dike 24		
2.01	-255.3	257
-5.44	-2.01	257
Dike 25		
-87.39	-977.94	1969
-72.49	-575.64	1969
-20.34	-270.2	1969
16.91	27.79	1969
83.95	720.63	1969
91.4	981.38	1969
Dike 26		
-72.49	-1246.13	2479
-57.59	-754.44	2479
-5.44	-9.46	2479
136.1	936.68	2479
158.45	1219.77	2479
Dike 27		
46.7	-173.35	415
-57.59	228.93	415
Dike 28		
24.36	-1410.02	3799
9.46	-1030.08	3799
-12.89	-679.94	3799
-35.24	-270.2	3799
-72.49	199.14	3799
-117.19	512.03	3799
-363.04	2367.04	3799
Dike 29		
-117.19	-300	605
54.15	281.08	605
Dike 30		
-258.74	-329.8	1008
-109.74	-24.36	1008
9.46	50.14	1008
113.75	243.84	1008
151	549.28	1008
Dike 31		
2.01	-61.6	193
2.01	132.09	193
Dike 32		
2.01	-61.6	105
16.91	42.69	105
Dike 33		
2.01	-61.6	371
-65.04	303.44	371
Dike 34		
2.01	-61.6	115
-27.79	50.14	115
Dike 35		
-132.09	-173.3	585
-5.44	-16.9	585
218.05	295.99	585
Dike 36		
54.15	-1067.33	3303
31.81	-545.85	3303
-5.44	5.44	3303
151	333.24	3303
538.4	1055.87	3303
600	2106.3	3303

Dike 37		
3.21	-3662.57	7642
27.05	-2577.87	7642
62.81	-682.64	7642
74.73	68.31	7642
241.6	1486.76	7642
-68.31	3095.93	7642
-402.06	3870.71	7642
Dike 38		
-235.19	-3889.05	7869
-199.43	-2494.44	7869
3.21	8.71	7869
408.48	2762.18	7869
575.36	3930.32	7869
Dike 39		
86.65	-3066.59	4647
158.17	-2220.28	4647
146.25	-1540.85	4647
110.49	-623.04	4647
86.65	-110.49	4647
-92.15	664.3	4647
-533.18	1439.08	4647
Dike 40		
-8.71	-110.49	203
27.05	92.15	203
Dike 41		
-8.71	-480	870
-8.71	-86	870
3.21	390.1	870
Dike 42		
15.13	-1528.9	3303
15.13	-718.39	3303
-8.71	56.39	3303
15.13	1260.28	3303
-235.19	1748.9	3303
Dike 43		
-557.02	-2625.5	5374
-56.39	139.83	5374
-32.55	557.02	5374
193.93	1093.41	5374
539.6	2619.14	5374
Dike 44		
-80.23	-122.41	364
98.57	199.43	364
Dike 45		
-80.23	-122.41	222
-20.63	92.15	222
Dike 46		
-282.87	-1624.29	3346
-199.43	-670.72	3346
-44.47	-38.97	3346
408.48	1689.4	3346
Dike 47		
38.97	-849.51	2947
-8.71	127.91	2947
-461.66	2023.15	2947
Dike 48		
-32.55	-480	990
62.81	509.34	990
Dike 49		
-390.14	-694.55	2154
15.13	139.83	2154
253.52	1343.72	2154
Dike 50		
74.73	-1564.69	3410
3.21	1319.88	3410
-8.71	1844.35	3410
Dike 51		
-20.63	-754.15	2389
-56.39	306.7	2389
-425.9	1582.12	2389
Dike 52		
-8.71	-515.75	539
3.21	-3.21	539
15.13	20.63	539
Dike 53		
-92.15	-313.1	697
62.81	366.3	697
Dike 54		
-20.63	-277.36	515
-68.31	235.19	515
Dike 55		
27.05	-968.71	2646
62.81	139.83	2646
74.73	1677.48	2646
Dike 56		
-56.39	-2029.5	2026
-44.47	-837.59	2026
-20.63	-3.21	2026
Dike 57		
-521.26	-1517.02	2739
-247.11	-575.36	2739
-68.31	270.95	2739
134.33	1141.09	2739
Dike 58		
3.21	-718.39	2197
15.13	235.19	2197
-80.23	1474.8	2197
Dike 59		
-20.63	-396.5	1478
3.21	1081.4	1478
Dike 60		
-521.26	-1004.47	
3.21	-27.05	
325.04	2476.1	
Dike 61		
-521.26	-1004.47	3633
3.21	-27.05	3633
325.04	2476.1	3633
Dike 62		
-15.47	-2988.3	5970
20.29	-1987.04	5970
-42.29	-1057.3	5970
20.29	-208.02	5970
11.35	641.26	5970
11.35	1275.99	5970
73.93	2035.87	5970
82.87	2974.55	5970
Dike 63		
20.29	-744.41	2569
11.35	104.87	2569
20.29	989.91	2569
100.75	1821.3	2569
Dike 64		
-5.44	-1506.87	2155
16.91	-1208.88	2155
2.01	-858.74	2155
24.36	-545.85	2155
76.5	-285.1	2155
54.15	-31.8	2155
46.7	214.04	2155
16.91	534.38	2155
9.46	638.68	2155

Dike 65		
29.23	-789.11	2059
-6.53	176.38	2059
38.17	730.66	2059
11.35	1267.04	2059
Dike 66		
-194.27	-2568.13	5265
-6.53	176.39	5265
38.17	730.66	5265
82.87	2688.48	5265
Dike 67		
-194.27	-2568.1	4076
-6.53	176.39	4076
38.17	730.66	4076
20.29	1499.48	4076
Dike 68		
-44.47	-3984.41	7997
-44.47	-2029.57	7997
3.21	-801.83	7997
3.21	-74.73	7997
-20.63	1307.97	7997
134.33	2309.23	7997
158.17	4000	7997
Dike 69		
1.6	-537.99	1311
7.56	-120.8	1311
55.24	284.47	1311
-4.36	767.22	1311
Dike 70		
13.52	-537.99	1268
19.48	-120.8	1268
67.16	284.47	1268
108.88	725.5	1268
Dike 71		
13.52	-537.99	825
19.48	-120.8	825
67.16	284.47	825
Dike 72		
-206.99	-388.99	951
-4.36	195.07	951
222.12	439.43	951
Dike 73		
1.6	-210.2	263
-22.23	52.03	263

Dike 74		
1.6	-454.55	507
-22.23	52.03	507
Dike 75		
251.92	-394.96	1700
-16.27	-55.24	1700
-236.79	552.66	1700
-218.91	1172.49	1700
Dike 76		
67.16	-186.36	313
-10.31	117.59	313
Dike 77		
-4.36	16.27	102
-10.31	117.59	102
Dike 78		
-4.36	-1038.6	2163
7.56	-537.99	2163
-22.23	-192.32	2163
-52.03	-43.32	2163
7.56	463.27	2163
67.16	957.94	2163
61.2	1112.89	2163
Dike 79		
-258.74	-2475.35	5009
-169.34	-1708.02	5009
-102.29	-1074.78	5009
-20.34	-255.3	5009
-12.89	-31.8	5009
98.85	966.48	5009
136.1	1510.32	5009
218.05	2024.36	5009
300	2500	5009
Dike 80		
69.05	-1894.26	3909
24.36	-1097.13	3909
9.46	243.84	3909
-117.19	1532.66	3909
-191.69	2002	3909
Dike 81		
-27.79	-367.04	926
24.36	102.29	926
16.91	556.73	926
Dike 82		
-27.79	-367.04	1299
24.36	102.29	1299

39.26	929.23	1299
Dike 83		
-27.79	-367	1886
24.36	102.29	1886
61.6	1517.76	1886
Dike 84		
-124.64	-583.09	1348
-5.44	5.44	1348
46.7	564.18	1348
61.6	750.43	1348
Dike 85		
69.05	-411.7	985
-5.44	5.44	985
46.7	564.18	985
Dike 86		
121.2	-508.5	992
31.81	-136.1	992
2.01	-16.9	992
-124.64	452.4	992
Dike 87		
-5.44	-292.5	1573
-12.89	117.19	1573
143.55	944.13	1573
113.75	1264.47	1573
Dike 88		
39.26	-277.65	1174
-20.34	132.09	1174
-5.44	891.98	1174
Dike 89		
-5.44	-188.25	474
-20.34	132.09	474
-57.59	281.09	474
Dike 90		
-130.09	-5000	10109
-100.29	-4131	10109
-130.09	-3088	10109
-85.39	-2268	10109
-25.79	-1434	10109
-10.89	-734	10109
4.01	10.89	10109
-130.09	651.5	10109
63.61	1173	10109
376.5	2543.8	10109
346.7	3199.4	10109
451	4078.5	10109

376.5	4734	10109
451	5000	10109
Dike 91		
-70.49	-3237.2	6824
-70.49	-2373	6824
-85.39	-1449.2	6824
4.01	-1002.29	6824
4.01	-644.7	6824
18.91	-123.21	6824
63.61	875.07	6824
123.21	2216.05	6824
227.51	2618.34	6824
212.61	3214.33	6824
272.21	3557.02	6824
Dike 92		
-5.44	-188.25	1010
-20.34	132.09	1010
-102.29	817.48	1010
Dike 93		
24.36	-98.85	756
-20.34	236.3	756
2.01	653.58	756

Vent 1		
-31.81	27.93	4566
-17.2	35.98	4566
8.13	34.79	4566
28.39	24.06	4566
39.12	-1.87	4566
26.3	-28.39	4566
-20.48	-36.44	4566
-41.94	-25.11	4566
-45.81	-2.46	4566
-35.38	6.77	4566
-31.81	16.31	4566
-31.81	27.93	4566
Vent 2		
-35.6	39.77	15141
-30.83	71.95	15141
-29.04	94	15141
-20.1	113.07	15141
-9.97	122.61	15141
3.74	121.42	15141
9.1	101.75	15141
8.5	76.13	15141
4.33	39.77	15141
3.74	2.22	15141
2.54	-23.4	15141
7.31	-43.67	15141
16.25	-71.68	15141
15.06	-108.03	15141
13.27	-135.45	15141
3.74	-161.67	15141
-15.93	-173.5	15141
-40.96	-171.2	15141
-53.48	-162.8	15141
-57.65	-143.7	15141
-58.84	-118.76	15141
-52.29	-101.4	15141
-46.33	-78.83	15141
-51.69	-56.18	15141
-47.52	-27.57	15141
-43.94	3.42	15141
-35.6	39.77	15141
Vent 3		
-35	60.63	6431
-2.82	63.61	6431
19.23	56.46	6431
29.36	33.21	6431
40.69	12.36	6431
31.75	-6.72	6431
24.6	-22.21	6431
10.29	-26.38	6431
-11.16	-23.4	6431
-29.64	-15.65	6431
-49.31	5.2	6431
-57.65	32.62	6431
-42.75	57.65	6431
-35	60.63	6431
Vent 4		
29.36	14.74	3343
27.58	-19.23	3343
1.95	-34.73	3343
-19.51	-18.64	3343
-23.68	14.14	3343
-18.32	33.21	3343
1.95	43.94	3343
28.17	37.39	3343
33.54	31.43	3343
31.15	20.7	3343
29.36	14.74	3343
Vent 5		
38.9	-7.91	3985
16.85	-27.58	3985
-8.78	-38.3	3985
-34.41	-33.54	3985
-20.7	-6.12	3985
-15.93	40.37	3985
-2.22	63.61	3985
10.89	37.39	3985
35.32	12.36	3985
40.69	-1.95	3985
38.9	-7.91	3985
Vent 6		
18.64	2.22	1591
14.46	-32.34	1591
-1.03	-27.57	1591
-7.59	-21.02	1591
-14.74	0.44	1591
-12.36	19.51	1591
-1.63	26.66	1591
8.5	32.62	1591
16.25	29.64	1591
15.66	20.1	1591
18.64	2.22	1591
Vent 7		
18.64	2.22	2392
14.46	-32.34	2392
-1.03	-27.58	2392
-7.59	-21.02	2392
-14.74	13.55	2392
-30.83	35	2392
-30.83	46.92	2392
6.12	43.94	2392
16.25	29.64	2392
15.66	20.1	2392
18.64	2.22	2392
Vent 8		
35.92	-0.76	6898
14.46	-32.34	6898
-1.03	-27.57	6898
-7.59	-21.02	6898
-14.74	13.55	6898
-4.01	107.11	6898
7.91	127.38	6898
17.44	135.72	6898
29.96	129.17	6898
43.07	29.04	6898
35.92	-0.76	6898
Vent 9		
77.04	-48.44	38050
31.15	-62.74	38050
-79.11	-27.58	38050
-121.42	31.43	38050
-95.79	148.84	38050
-81.49	160.75	38050
8.5	160.16	38050
40.69	164.93	38050
68.1	151.82	38050
88.96	42.75	38050
77.04	-48.44	38050
Vent 10		
25.19	-65.71	9035
18.04	-73.46	9035
-27.85	-45.46	9035
-52.88	-21.6	9035
-49.31	9.97	9035
-21.89	33.81	9035

15.06	57.05	9035
44.26	73.74	9035
73.47	68.97	9035
37.11	15.34	9035
25.19	-65.71	9035
Vent 11		
10.29	-18.64	8049
18.04	-73.47	8049
-27.85	-45.46	8049
-52.88	-21.62	8049
-49.31	9.97	8049
-21.89	33.81	8049
-23.08	60.63	8049
-11.16	78.51	8049
36.52	65.4	8049
49.63	56.46	8049
10.29	-18.64	8049
Vent 12		
8.5	-13.27	2992
-20.7	-35.32	2992
-31.43	-46.65	2992
-47.52	-53.8	2992
-43.94	-22.21	2992
-16.53	1.63	2992
-17.72	28.45	2992
6.12	36.19	2992
26.38	35	2992
27.58	18.91	2992
8.5	-13.27	2992
Vent 13		
22.21	-21.02	5628
-6.99	-43.07	5628
-17.72	-54.4	5628
-33.81	-61.54	5628
-30.24	-29.95	5628
-51.09	30.83	5628
-32.02	48.11	5628
-5.8	35.6	5628
40.09	27.25	5628
41.28	11.16	5628
22.21	-21.02	5628
Vent 14		
21.62	-25.79	4186
6.72	-21.62	4186
-2.82	-31.75	4186
-11.76	-29.36	4186
-27.25	-16.85	4186
-51.69	26.06	4186
-32.62	43.35	4186
-6.4	30.83	4186
39.5	22.49	4186
40.69	6.4	4186
21.62	-25.79	4186
Vent 15		
15.06	-28.77	2638
0.16	-24.59	2638
-9.38	-34.72	2638
-18.32	-32.34	2638
-25.47	-16.25	2638
-22.49	-5.52	2638
-22.49	8.78	2638
-12.95	27.85	2638
32.94	19.51	2638
34.13	3.42	2638
15.06	-28.77	2638
Vent 16		
-1.03	-69.89	6322
-15.93	-65.72	6322
-25.47	-75.85	6322
-34.41	-73.47	6322
-41.56	-57.38	6322
3.14	61.23	6322
28.77	75.53	6322
37.71	79.7	6322
42.48	71.95	6322
18.04	-37.71	6322
-1.03	-69.89	6322
Vent 17		
6.12	-38.9	13068
-8.78	-66.31	13068
-35	-132.46	13068
-72.55	-155.11	13068
-88.64	-146.17	13068
21.62	127.38	13068
29.96	136.92	13068
40.69	135.72	13068
49.63	102.95	13068
25.19	-6.72	13068
6.12	-38.9	13068
Vent 18		
43.07	-77.04	25655
3.14	-100.88	25655
-45.13	-100.88	25655
-76.13	-68.1	25655
-89.24	-11.48	25655
-73.74	62.42	25655
-20.7	93.41	25655
37.11	96.39	25655
69.89	63.01	25655
72.87	-16.85	25655
43.07	-77.04	25655
Vent 19		
60.36	-80.62	32593
20.42	-104.46	32593
-27.85	-104.46	32593
-58.84	-71.68	32593
-117.25	21.3	32593
-83.87	73.15	32593
-3.42	89.83	32593
74.06	114.27	32593
105.65	63.01	32593
90.15	-20.42	32593
60.36	-80.62	32593
Vent 20		
3.14	-48.44	2125
-11.16	-62.7	2125
-26.06	-72.8	2125
-19.51	-60.3	2125
-15.34	-44.2	2125
-9.97	-22.8	2125
13.27	38.58	2125
18.64	79.7	2125
26.98	56.46	2125
11.48	-26.98	2125
3.14	-48.44	2125
Vent 21		
7.31	-22.81	1225
-6.99	-37.11	1225
-21.89	-47.24	1225
-15.34	-34.73	1225
-11.16	-18.64	1225
-5.8	2.82	1225
-3.42	21.3	1225
5.52	33.81	1225

12.68	18.91	1225
15.66	-1.35	1225
7.31	-22.81	1225
Vent 22		
9.1	-11.48	1094
4.93	-20.42	1094
-6.4	-20.42	1094
-9.97	-14.46	1094
-14.74	-7.31	1094
-14.14	4.61	1094
-9.38	20.7	1094
6.12	29.64	1094
13.27	14.74	1094
16.25	-5.52	1094
9.1	-11.48	1094
Vent 23		
26.98	-25.19	4485
22.81	-34.13	4485
18.64	-48.44	4485
-2.82	-55.58	4485
-26.66	-37.7	4485
-29.04	-10.88	4485
-18.91	51.69	4485
7.31	35	4485
25.19	12.95	4485
34.13	-19.23	4485
26.98	-25.19	4485
Vent 24		
18.64	-14.46	1086
14.46	-23.4	1086
3.74	-16.25	1086
-9.97	-21.02	1086
-35	-26.98	1086
-21.3	-6.72	1086
-6.99	-4.93	1086
4.33	12.95	1086
14.46	9.97	1086
25.79	-8.5	1086
18.64	-14.46	1086
Vent 25		
37.71	-46.05	10356
27.58	-63.93	10356
6.72	-65.12	10356
-24.87	-62.14	10356
-48.71	-13.86	10356
-51.69	29.64	10356
-35.6	55.86	10356
0.16	63.61	10356
13.27	71.36	10356
44.26	48.71	10356
37.71	-46.05	10356
Vent 26		
37.71	-46.05	14024
27.58	-63.93	14024
-32.02	-115.19	14024
-63.01	-108.63	14024
-48.71	-13.87	14024
-51.69	29.64	14024
-35.6	55.86	14024
0.16	63.61	14024
13.27	71.36	14024
44.26	48.71	14024
37.71	-46.05	14024
Vent 27		
16.85	-47.84	4106
6.72	-65.72	4106
-8.18	-72.27	4106
-17.12	-60.95	4106
-13.55	-40.09	4106
-9.97	-4.33	4106
-6.4	39.77	4106
-33.81	78.51	4106
-17.72	74.34	4106
23.4	46.92	4106
16.85	-47.84	4106
Vent 28		
12.08	-57.38	2624
5.52	-77.04	2624
-5.8	-85.98	2624
-11.76	-76.45	2624
-5.2	-54.4	2624
-4.61	-16.25	2624
-6.4	6.4	2624
-1.03	55.86	2624
6.12	65.99	2624
16.25	54.07	2624
12.08	-57.38	2624
Vent 29		
12.08	-57.38	2992
5.52	-77.04	2992
-5.8	-85.98	2992
-11.76	-76.45	2992
-5.2	-54.4	2992
-18.91	-19.23	2992
-5.8	8.18	2992
-6.4	40.96	2992
5.52	48.71	2992
18.64	35	2992
12.08	-57.38	2992
Vent 30		
26.98	-39.49	7839
43.07	-73.47	7839
31.75	-82.41	7839
-4.61	-80.02	7839
-28.45	-66.91	7839
-35.6	-16.84	7839
-30.23	45.73	7839
-2.22	67.78	7839
19.83	48.11	7839
19.23	23.68	7839
26.98	-39.49	7839
Vent 31		
18.04	-1.95	3961
34.13	-35.92	3961
22.81	-44.86	3961
-13.55	-42.48	3961
-23.08	-14.46	3961
-44.54	20.7	3961
-37.39	35.6	3961
-12.36	24.87	3961
12.68	33.81	3961
26.98	27.25	3961
18.04	-1.95	3961
Vent 32		
25.79	-3.74	5008
41.88	-37.71	5008
30.56	-46.65	5008
-5.8	-44.26	5008
-39.17	-24.59	5008
-36.79	18.91	5008
-29.64	33.81	5008
-4.01	45.13	5008
20.42	32.02	5008
14.46	15.93	5008
25.79	-3.74	5008

Vent 33		
19.23	-11.48	1537
24.6	-22.81	1537
18.64	-28.76	1537
-11.76	-30.5	1537
-14.74	-7.9	1537
-1.03	5.2	1537
-14.74	22.48	1537
-1.63	29.63	1537
13.87	24.27	1537
12.68	6.4	1537
19.23	-11.48	1537
Vent 34		
15.06	-14.46	2929
20.42	-25.79	2929
14.46	-31.75	2929
-15.93	-33.53	2929
-26.66	-13.27	2929
-18.32	12.36	2929
-17.12	35.6	2929
-2.82	52.88	2929
22.21	31.43	2929
16.85	5.2	2929
15.06	-14.46	2929
Vent 35		
5.52	-3.74	2745
13.87	-20.42	2745
-9.38	-41.28	2745
-36.79	-44.85	2745
-19.51	-5.52	2745
-20.1	18.32	2745
-19.51	46.33	2745
-2.22	32.62	2745
23.4	26.66	2745
24	12.95	2745
5.52	-3.74	2745
Vent 36		
13.87	-1.35	3687
22.21	-18.04	3687
-1.03	-38.89	3687
-28.45	-42.47	3687
-32.62	2.22	3687
-30.23	34.41	3687
-12.36	29.04	3687
6.12	35	3687
31.75	29.04	3687
32.34	15.34	3687
13.87	-1.35	3687
Vent 37		
15.06	-2.54	8539
23.4	-19.23	8539
-15.93	-116.97	8539
-30.83	-100.29	8539
-31.43	1.03	8539
-8.18	39.77	8539
0.16	85.66	8539
12.08	122.61	8539
24	127.98	8539
33.54	14.14	8539
15.06	-2.54	8539
Vent 38		
7.31	-27.58	2891
15.66	-44	2891
-21.89	-410	2891
-33.81	-290	2891
-39.17	-240	2891
-2.82	11	2891
-4.61	27	2891
3.14	75.5	2891
10.89	27.2	2891
25.79	-10	2891
7.31	-27.58	2891

Sill 1		
-890.2	20	2622370
-872.32	94.5	2622370
-815.7	157	2622370
-750.14	139	2622370
-669.68	163.09	2622370
-657.76	228	2622370
-663.72	324	2622370
-687.56	443.21	2622370
-645.85	601	2622370
-577.31	669	2622370
-508.77	723.32	2622370
-368.71	797	2622370
-270.37	833.58	2622370
-177.99	881	2622370
-31.98	899	2622370
96.16	878.2	2622370
248.14	872.3	2622370
364.36	788.8	2622370
456.73	696.5	2622370
546.13	592.2	2622370
656.39	538.5	2622370
733.87	431.2	2622370
778.57	315	2622370
853.07	183.9	2622370
897.76	-21.6	2622370
888.83	-122	2622370
814.33	-176	2622370
704.07	-161.72	2622370
620.63	-152	2622370
584.87	-230	2622370
578.91	-289	2622370
665.33	-373	2622370
781.55	-498	2622370
850.09	-626	2622370
793.47	-781	2622370
704.07	-870.95	2622370
519.31	-915.64	2622370
346.48	-918.62	2622370
212.38	-897	2622370
60.4	-933	2622370
-91.58	-945	2622370
-195.87	-909	2622370
-267.39	-847	2622370
-401.49	-808	2622370
-499.83	-894.78	2622370
-654.78	-906	2622370
-809.74	-796	2622370
-911.06	-617.65	2622370
-940.86	-477.59	2622370
-928.94	-122	2622370
-890.2	20	2622370
Sill 2		
-633.93	-161.7	763831
-672.66	26.02	763831
-583.27	166.07	763831
-481.95	175.01	763831
-321.03	127.33	763831
-154.15	85.62	763831
-46.88	186.93	763831
33.58	350.83	763831
114.04	508.77	763831
307.74	580.29	763831
450.77	410.43	763831
417.99	201.83	763831
319.66	-200.45	763831
170.66	-450.77	763831
72.32	-605.73	763831
-103.5	-608.71	763831
-386.59	-513.3	763831
-613.07	-245.1	763831
-633.93	-161.7	763831
Sill 3		
-925.96	127.33	1913141
-878.28	288.25	1913141
-860.4	437.2	1913141
-711.4	607.11	1913141
-657.76	741.2	1913141
-541.55	860.4	1913141
-392.55	881.2	1913141
-270.37	726.3	1913141
-246.53	520.6	1913141
-29	368.7	1913141
117.02	273.35	1913141
245.16	356.79	1913141
432.89	344.87	1913141
608.71	109.45	1913141
718.97	-122.98	1913141
760.69	-364.36	1913141
775.59	-575.9	1913141
665.33	-820.2	1913141
432.89	-894.7	1913141
155.76	-930.5	1913141
-157.13	-879	1913141
-383.61	-790	1913141
-562.41	-632	1913141
-517.71	-388.19	1913141
-580.29	-268	1913141
-863.38	-54.4	1913141
-955.76	55.81	1913141
-925.96	127.33	1913141

D.2 BRUCE CROWE'S ELICITATION SUMMARY FOR PVHA-U PROJECT

This section summarizes and documents a volcanic hazard model prepared by Bruce Crowe as an expert panel member on the Probabilistic Volcanic Hazard Assessment Update (PVHA-U) for the Yucca Mountain Project. Because I assume that references to the literature provided to panel members will be included in the final PVHA-U report, I provide only those report-specific references critical to the elicitation model and/or not expected to be included in the final PHVA-U report. The nomenclature used for communicating uncertainty in the elicitation model is that recommended by the International Panel on Climate Change (IPCC) for quantifying uncertainty (Manning et al., 2004). Uncertainty comprises statistical components (natural variability, knowledge uncertainty) and structural components (uncertainty in models and conceptual framework). These and other aspects of model development are discussed in more detail in Supplement A. This report describes and is referenced to Microsoft Excel spreadsheets (Crowe, 2007) that contain additional discussion, documentation, and details of the model structure, measurements, and assessments (spreadsheets and worksheets are listed and briefly described in Supplement B). Tables in this report include key parts of the Excel spreadsheets.

D.2.1 OVERVIEW OF CONCEPTUAL MODEL

The model developed for this PVHA-U follows classic protocols defined in modeling textbooks (see Supplement A). All model information was updated to reflect the new mapping results for basaltic volcanoes in the Yucca Mountain region and the exploratory drilling and characterization of aeromagnetic anomalies. This new information is referenced in journal papers, reports, tables, and e-mail information that the PVHA-U Methodology Development Team provided to panel members.

The PVHA-U corresponds as closely as possible to constraints posed by the volcanic record of the Yucca Mountain region (YMR, defined as the region within a radius of about 50 km centered on Yucca Mountain). The uncertainty in model assumptions and parameter values are structured using information extracted from that volcanic record.

I followed two approaches in developing the elicitation model. First, components of uncertainty in the model were identified using uncertainty nomenclature and quantified using probability distribution functions and weighting of alternative models. Critical uncertainty components for my elicitation model include:

1. Boundary conditions and boundary assumptions
2. Alternative models of the structural framework of the model domain
3. Alternative models for regions used to predict sites of potential future volcanic activity
4. Natural variability in parameters
5. Knowledge/parameter uncertainty
6. Model uncertainty (expressed by using multiple permissive alternative models of future volcanic activity).

The second approach involves the concept of volcanic cycles. After identifying past volcanic cycles in the YMR, I use the patterns and characteristics of episodic cycles of basaltic volcanism to predict patterns of future volcanic activity.

My elicitation model is complicated, partly because it assembles alternative matrices for components of parameter and model uncertainty for two assessment periods (10,000 years and 1 My). Figure D.2-1 illustrates the model structure and lists the multiple alternative approaches used in the model. The figure is provided as a high-level guide to the logic of the elicitation model.

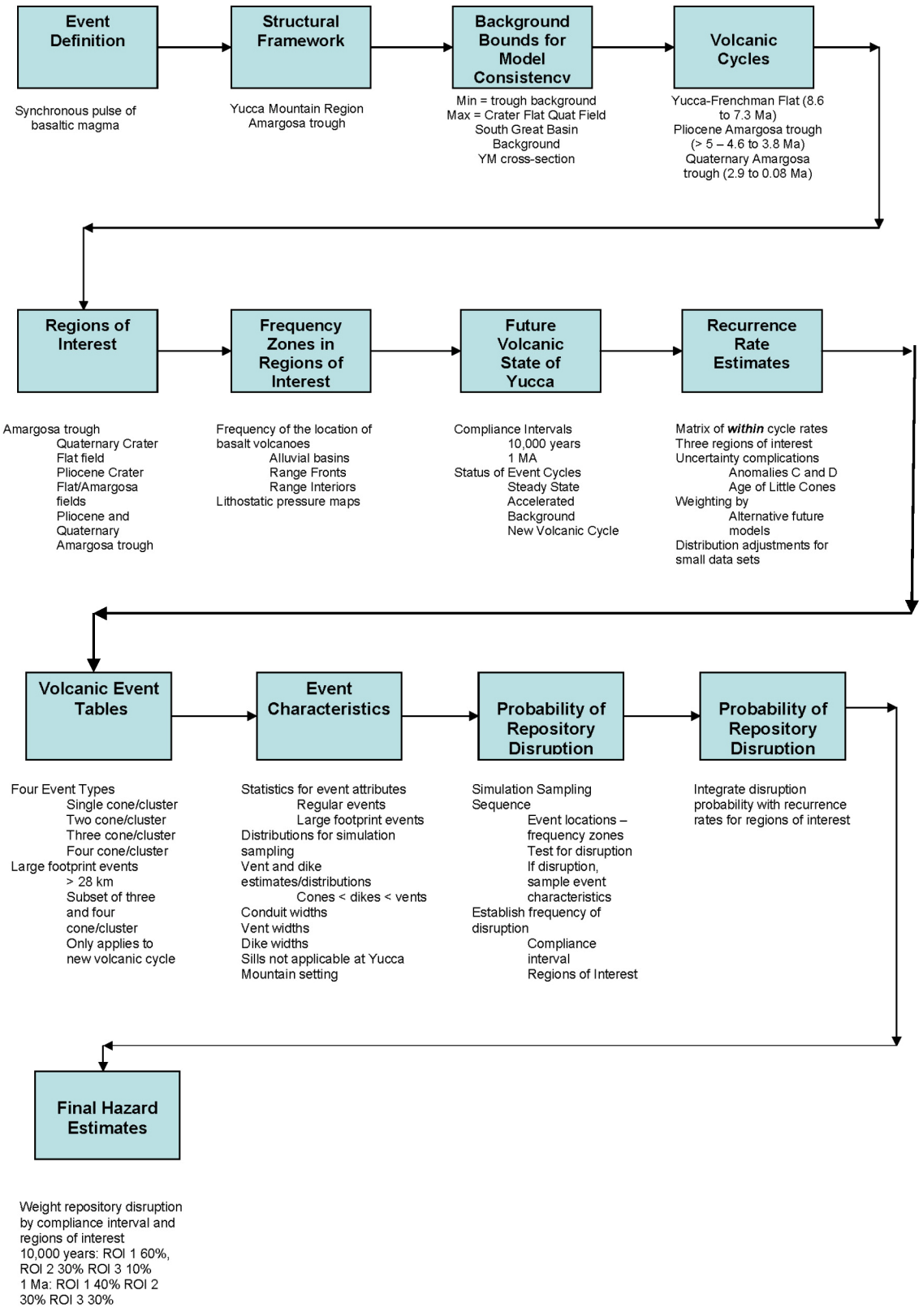

Figure D.2-1. Flow Diagram Showing Structure of the Elicitation Model